PHOTOCATALYTIC DEGRADATION OF AZODYES USING Ag@TiO$_2$ CORE-SHELL STRUCTURED NANOPARTICLES

Thesis

Submitted in partial fulfillment of the requirements for the degree of

DOCTOR OF PHILOSOPHY

by

ANKITA KHANNA

DEPARTMENT OF CHEMICAL ENGINEERING
NATIONAL INSTITUTE OF TECHNOLOGY
KARNATAKA
SURATHKAL, MANGALORE – 575 025
September, 2014

DECLARATION

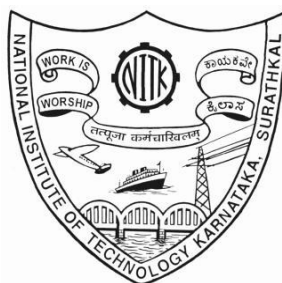I hereby *declare* that the Research Thesis entitled **"Photocatalytic degradation of azodyes using Ag@TiO₂ core-shell structured nanoparticles"** which is being submitted to the **National Institute of Technology Karnataka, Surathkal** in partial fulfillment of the requirements for the award of the Degree of **Doctor of Philosophy** in the Department of Chemical Engineering, is a *bonafide report of the research work carried out by me*. The material contained in this Thesis has not been submitted to any University or Institution for the award of any degree.

Place: NITK-Surathkal   Name   : ANKITA KHANNA

Date: Register Number : 090704CH09F01

                                             Department of Chemical Engineering

C E R T I F I C A T E

This is to certify that the Research Thesis entitled **"Photocatalytic degradation of azodyes using Ag@TiO₂ core-shell structured nanoparticles"** submitted by **Ms. Ankita Khanna (Register Number: 090704CH09F01)** as the record of the research work carried out by her, is *accepted as the Research Thesis submission* in partial fulfillment of the requirements for the award of degree of **Doctor of Philosophy**.

Chairman – DRPC/Research Guide

Dr. Vidya Shetty K
Associate Professor and Head
Dept. of Chemical Engineering
NITK, Surathkal

ACKNOWLEDGMENT

DEDICATED TO MY FAMILY

ABSTRACT

Wastewater released from textile industries consists of large volume of colored dye effluents and it needs to be treated before discharge to the environment by cost effective technologies. Heterogeneous photocatalysis is a promising technology for the treatment of dye wastewater. Ag@TiO$_2$ nanoparticle comprising of Ag core and TiO$_2$ shell is a promising photocatalyst. In the present study, Ag@TiO$_2$ nanoparticles were engineered to impart and enhance their UV and solar photocatalytic activity for efficient photocatalytic degradation of two azo dyes, namely: Acid Yellow-17(AY-17) and Reactive Blue-220 (RB-220). Ag@TiO$_2$ was found to be suitable as photocatalyst for UV and solar photocatalysis of these dyes. The engineered Ag@TiO$_2$ nanoparticles were characterized by different techniques. Ag@TiO$_2$ with an average crystallite size of around 39.33 nm, showed its ability to absorb both UV light and visible light. The band gap energy for these nanoparticles was estimated to be 1.85eV, which supported its high solar photocatalytic activity. Ag@TiO$_2$ exhibited better photocatalytic activity as compared to other conventional catalysts. Operational factors such as pH, catalyst loading and oxidant concentration were optimized for photocatalysis of these dyes. Kinetics of photocatalysis of the dyes obeyed modified Langmuir-Hinshelwood model. The rate of photocatalysis of the dyes was inhibited by the presence of salts like sodium chloride and sodium carbonate and was enhanced by increase in light intensity. Efficient decolorization and mineralization of AY-17 and RB-220 were achieved by photocatalysis using Ag@TiO$_2$. Optimum conditions obtained for AY-17 degradation were more favorable for the photocatalysis of water contaminated with mixture of these dyes. Degradation pathways for these dyes were proposed. Immobilized Ag@TiO$_2$ nanoparticles showed similar efficacy as free nanoparticles. Ag@TiO$_2$ was also found suitable for photocatalysis of other classes of dyes. Hence Ag@TiO$_2$ nanoparticles may be considered as effective catalysts for the photocatalytic degradation of dyes/textile wastewater. Solar energy utilization and fast kinetics feature of this process makes it an economical and favorable option for large scale treatment of dye/textile wastewater.

Keywords: Ag@TiO$_2$ core-shell nanoparticles; Azo dyes; Photocatalysis; Solar light; Wastewater

TABLE OF CONTENTS

LIST OF FIGURES

LIST OF TABLES

LIST OF ABBREVIATIONS

AANs	Artificial Neural Networks
AFM	Atomic Force Microscopy
Ag doped (PD)-CSTiO$_2$	Ag doped TiO$_2$ nanoparticles synthesized by photo deposition method
Ag doped(LI)-CSTiO$_2$	Ag doped TiO$_2$ nanoparticles synthesized by liquid impregnation method
Ag doped-SGTiO$_2$	Ag doped TiO$_2$ nanoparticles synthesized by sol-gel method
Ag@TiO$_2$	Ag core and TiO$_2$ shell
ANOVA	Analysis of Variance
AOPs	Advanced Oxidation Processes
APHA	American Public Health Association
AY-17	Acid Yellow-17
BET	Brunauer–Emmett–Teller
BOD	Biological Oxygen Demand
CB	Conduction Band
CCD	Central Composite Design
CCF	Central Composite Design Face-Centered
COD	Chemical Oxygen Demand
CPCB	Central Pollution Control Board
CSTiO$_2$	Combustion synthesized TiO$_2$ nanoparticles
CTAB	Cetyl Trimethyl Ammonium Bromide
CVD	Chemical Vapor Deposition
DMF	Dimethyl Formamide
DO	Dissolved Oxygen
DOE	Design of Experiment
DRS	Diffuse Reflectance Spectra
EDS	Energy Dispersive Spectra
EG	Ethylene Glycol

ESI	Electrospray Ionization
EWS	Engineered Wetland Systems
FAS	Ferrous ammonium sulphate
GC-MS	Gas Chromatography – Mass Chromatography
HPLC	High Performance Liquid Chromatography
LC-MS	Liquid Chromatography – Mass Chromatography
L-H	Langmuir-Hinshelwood
MO	Methyl Orange
MRA	Multiple regression analysis
ND	Not detected
NEDA	N-(1-Naphthyl)- ethylenediamine dihydrochloride
PFDF	Poly Vinylidene Flouride
PVC	Poly Vinyl Chloride
R6G	Rhodamine 6G
RB-220	Reactive Blue-220
RSM	Response Surface Methodology
SAED	Selected Area Electron Diffraction
SGTiO$_2$	Sol-gel synthesized TiO$_2$ nanoparticles
TBT	Tetrabutyl Titanate
TEM	Transmission Electron Microscopy
TG-DTA	Thermo Gravimetric-Differential Thermal Analysis
TOB	Titanium Ortho Butoxide
TOC	Total Organic Carbon
TTEAIP	Titanium Tetra Ethanolaminato Isopropoxide
TTIP	Titanium Tetra Isopropoxide
USEPA	U.S Environment Protection Agency
UV	Ultraviolet
VB	Valence Band
WHO	World Health Organization
XRD	X-Ray diffractogram

NOMENCLATURE

Adj MS	Adjusted mean square
Adj SS	Adjusted sum of squares
c	Speed of light
C	Concentration of dye at time 't'
$C_{(NH4)2S2O8}$	Initial concentration of $(NH_4)_2S_2O_8$
C_0	Initial concentration of dye
C_{AY-17}	Initial dye concentration of AY-17
C_{dye}	Concentration of the dye at time 't'
C_{H2O2}	Initial concentration of H_2O_2
C_{KBrO3}	Initial concentration of $KBrO_3$
C_{Na2CO3}	Initial concentration of Na_2CO_3
C_{NaCl}	Initial concentration of NaCl
$C_{pollutant}$	Concentration of pollutant
C_{RB-220}	Initial dye concentration of RB-220
DF	Degree of Freedom
eV	Electron volt
g	Gram
g/L	Gram per litre
h	Hour
h	Planck's constant
HU	Hazen Unit
k_{obs}	Constant related to adsorption
k_R	Reaction rate constant
LPM	Litre per minute
m/z	Mass to charge ratio
mg/L	Milligram per litre
min	Minute
mM	Millimolar
nm	Nanometer

r	Reaction rate of pollutants being degraded
R	Reflectance
r_0	Initial reaction rate
t_C	Calcinations time (in hours)
T_C	Calcination temperature (degree celcius)
λ	Wavelength
K	Reflectance transformed according to Kubelka Munk model
ν	Frequency

CHAPTER 1

INTRODUCTION

1.1 Background of research and motivation

The use of synthetic chemical dyes in various industrial processes like textiles, printing, plastics, paper and pulp manufacturing and leather treatment has increased considerably, resulting in the release of dye-containing industrial effluents into the aquatic ecosystems and soil (Aksu 2005). Among all the industrial sectors, wastewater from textile industries has become one of the major environmental concerns, in view of both the volume rejected and the composition of effluents (Reid 1996). Textile industries produce large volume of coloured dye effluents which are non-biodegradable and toxic (Reife and Fremann 1996).There are more than 10,000 types of commercial dyes and the global market demand has grown over 0.7 million tonnes in 2004-05 to 0.9 million tonnes in 2010-11 (Mangal 2010). In India, the dye and dyestuff production is over 0.17 million tonnes in the year 2011-2012 and 0.086 million tonnes upto September 2012-13 (Department of Chemicals and Petrochemicals, Ministry of Chemicals and Petrochemicals, Government of India 2013). Textile industries alone consume dyes in excess of 10^7 kg/year globally and approximately 90 % of this total end-up on fabric (Hameed et al. 2007). Consequently, textile industries discharge approximately 10^6 kg/year of dyes into the waste streams.

Since the colour associated with dye effluent is quite noticeable to the public, its discharge is an environmental concern. In the overall category of dyes, azo dyes constitute the most important and largest class of commercial dyes, characterized by the presence of an azo group ($-N=N-$) (Reid 1996). Chemical structures of azo dyes is characterized by highly substituted aromatic rings joined by one or more azo groups and among them, water soluble acid and reactive dyes are the most tricky, as they tend to pass through conventional treatment systems unaffected (Aksu 2005). Hence there is a necessity for new advanced technologies for their removal from wastewater. It is well known that azo dyes split into corresponding aromatic amines by liver enzymes and intestinal flora when incorporated into the body and can cause cancer in human.

According to WHO guidelines for drinking water quality, the maximum value for permissible colour is 15 Units (Binnie et al. 2002). Regulatory standard of colour

for industrial wastewater specified by Central Pollution Control Board, India is 400 Hazen unit (C P C B 2010). Tighter restrictions on effluent discharge and new ecolabels for textile products are forcing textile manufacturers to reuse chemicals and process water. In many industrialized countries, the introduction of ecolabels and new laws, in combination with international trade pressure is frightening the very survival of the textile industry. The textile industry quickly reacted to these new limitations with a broad range of drastic alterations and modernisms in the reuse, generation and treatment of textile effluent. Optimal wastewater treatment is a challenge faced by many textile industries throughout the world.

Among the most commonly used techniques are adsorption (on activated carbon, coal, alumina, china clay, red mud, flyash, silica etc.), chemical precipitation, flocculation, electrocoagulation, coagulation, chemical processes (chlorination, ozonation) and biological methods (aerobic and anaerobic) (Robinson et al. 2001).

Conventional wastewater treatment processes such as biological methods (aerobic and anaerobic) are commonly ineffective for the treatment of dye containing wastewater, due to non-biodegradable nature of the dyes. Other commonly used processes such as adsorption (on activated carbon, coal, alumina, china clay, red mud, flyash, silica etc.), chemical precipitation, flocculation, electrocoagulation, coagulation, chemical processes (chlorination, ozonation) etc. have disadvantages such as: only a transfer of dye from one phase to another with no mineralization; secondary sludge generation or high cost. To comply with today's demanding legislation, easy-operated and affordable technology is needed without the formation of sludge. These challenges have impelled intensive research in new advanced treatment technologies, some of which currently making their way to full-scale installations. Though several of these new technologies are promising in terms of performance and cost, they all serve drawbacks which need broader validation and further research.

Advanced oxidation processes (AOPs) have been proposed in recent years and among them, heterogeneous photocatalysis has been successfully employed for the degradation of organic pollutants of various families due to complete mineralization of effluents to carbon dioxide and water (Clark and Macquarrie 2002). Heterogeneous photocatalysis using titanium dioxide as a catalyst has proven to be an efficient process for elimination of a large number of dyes from textile wastewater

(Konstantinou and Albanis 2004). The advantage of using TiO_2 as a photocatalyst is that, it can be used under ambient conditions and may lead to total mineralization of dyes to CO_2 and H_2O (Gogate and Pandit 2004). The mechanism of photocatalytic degradation of dyes involves absorption of light by TiO_2 which causes the generation of electrons (e^-) and holes (h^+). For generation of e^- and h^+ to occur, TiO_2 should be irradiated with a light source, having energy greater than its band gap energy (Gupta et al. 2012 a,b). The photogenerated electron-hole pairs are powerful oxidizing and reducing agents. They either react with the dyes directly to form oxidation or reduction products (R^+) or lead to formation of superoxide radical anion ($O_2^{\cdot-}$) or hydroxyl ($OH^{\cdot}$) radicals. These radicals are powerful oxidants and are reported to be responsible for heterogeneous photocatalytic degradation of dyes.

However, the low quantum yields and large band gap of TiO_2 due to e^- and h^+ recombination prevent it from practical applications. The technological use of TiO_2 is largely impaired (Sakthivel and Kish 2003) due to these reasons. In photocatalytic processes various attempts have been made to reduce electron-hole recombination. Hence in recent times to increase the efficiency of AOPs, the research is focused on the advancement of modified semiconductor photocatalysts (Sobana et al. 2008).

Solar energy has the potential to provide for the future energy needs (Li et al. 2013) and exploitation of this alternate energy resource is the prime aim of 21st century engineers and scientists (Bokare et al. 2013). Solar light induced photocatalysis has attracted extensive attention due to its agreement with green chemistry concept in endorsing innovative technologies (Malato et al. 2003). Solar energy can be converted into chemical energy by photocatalysts which are used for degradation of dyes in wastewater (Sharma et al. 2012). The band gap energy of TiO_2 being 3.2eV, it can be excited only by UV light. It cannot be efficiently used as a photocatalyst in sunlight, which consists only 4–5% of UV irradiations (Dalrymple et al. 2010). Using UV irradiation for the treatment of industrial wastewater is not only costly but also not feasible, as UV light in bulk can be hazardous. In countries like India, which receives huge amount of solar light for almost 10 months in a year (Singh et al. 2011a), solar photocatalysis is preferable. So, there is a need of effective photocatalysts which can be excited by both UV and visible light of solar irradiation. While comparing degradation of organic compounds under artificial UV radiation and

by solar radiation, it has been found that the latter process demonstrates to be economically and technically feasible (Vineetha et al. 2013). Efforts are towards designing the photocatalysts which show very efficient UV and solar light induced photocatalytic activity, so that they find their application in continuous treatment of dye contaminated wastewaters, by their utilization as catalyst for solar light driven photocatalysis during day time and artificial UV light induced photocatalysis during night. Alternatively, wastewater generated during night may be stored and treated during daytime by batch photocatalysis.

In the composite systems photocatalytic efficiency can be enhanced by deposition of noble metals such as Au, Ag, Pd and Pt on a TiO_2 surface because they promote interfacial charge transfer processes by acting as electron trap (Behar and Rabani 2006). Though this type of catalyst structure is effective, it results in exposing noble metal to the surrounding medium and reactants (Subramanian et al. 2003; Hirakawa and Kamat 2004). Metals may get easily corroded on the surface of the semiconductor.

An efficient way to conquer these limitations is to develop a core–shell structure, in which the noble metal particles are introduced as core and the semiconductor dioxide such as TiO_2 as shell (Tom et al. 2003; Chan and Barteau 2005). The oxide shell is beneficial because it is an effective way to prevent corrosion and agglomeration of metals under extreme conditions. Among core-shell nanoparticles, Ag@TiO_2 with Ag core and TiO_2 shell has wider applications due to photoinduced charge separation, possibility to envisage electron storage and surface plasmon modulation using electron acceptor, band gap excitation and charge equilibration in the Fermi level (Hirakawa and Kamat 2005). These properties are suitable for photocatalysis by these core-shell structures. The nanosized core shell structures can also provide larger specific surface area and hence can exhibit enhanced photocatalytic activity, which is due to the fact that the specific surface area of small particles is greater than larger particles (Mercuri 2007) and it provides larger surface for photocatalytic reaction. The interesting properties exhibited due to an oxide shell on a metal nanoparticle, as reported by Hirakawa and Kamat (2004, 2005) is a motivation for the present research work, for the use of Ag@TiO_2 core-shell structures as photocatalysts for the degradation of dyes. It was hypothesized that, with

suitable modifications in the synthesis of these nanoparticles, solar photocatalytic activity can be imparted and UV photocatalytic activity can be enhanced. So, it was proposed to synthesize $Ag@TiO_2$ nanoparticles by one pot synthesis route of Hirakawa and Kamat, (2005) with suitable modifications to enhance their UV photocatalytic activity and to impart solar photocatalytic activity.

Among all the dyes, azo dyes represent upto 70 % of all the commercial dyes produced and among them water soluble Acid and Reactive dyes which consist of ionizable groups such as sulphonates ($-SO_3^-$), carboxylates ($-CO_2^-$) or sulphates ($-SO_4$) are the most problematic dyes because of their high molecular weight and complex structure. Azo dyes belonging to Acid and Reactive class have complex structure and their loss to the effluent during dyeing operation is high. So in the present study, two azo dyes namely Acid Yellow-17 (AY-17) and Reactive Blue-220 (RB-220) were chosen for studies on photocatalytic degradation by $Ag@TiO_2$ nanoparticles. AY-17 is a mono azo dye of acid class which is used for coloring foods. It is widely used in manufacturing of leather, silk, dyeing wool, cotton, paper, and hot stamping foil and also being used as an additive for manufacture of house hold products such as liquid soap, shampoo, alcohol based perfumes, shower gel and dishwashing liquids (Lackey et al. 2006). Reactive Blue-220 dye is used for colouring cotton fabric.

To the best of our knowledge, this is a first extensive report on the use of $Ag@TiO_2$ core-shell structured nanoparticles as photocatalysts for photocatalytic degradation of azo dyes under UV light irradiation. Cheng et al. (2010) have shown the photocatalytic property of $Ag@TiO_2$ core shell nanocomposite nanowires in terms of degradation of Rhodamine –B dye under UV light irradiation. Wang et al. (2008a) have used $Ag@TiO_2$ nanoparticles as catalysts for the photocatalytic degradation of Alizarin red under visible light irradiation. Their study was restricted to the comparison of photocatalytic activity of two steps synthesized $Ag@TiO_2$ nanoparticles with that of Degussa P25. In both the studies dyes used were not the azo dyes. Though there is a report by Wang et al. (2008b) on the examination of UV and visible photocatalytic activity of $Ag@TiO_2$ core-shell structured nanoparticles for degradation of methyl orange which is an azo dye, the study limited to the comparison of photocatalytic activity of two steps synthesized $Ag@TiO_2$ nanoparticles with that of Fe^{3+} doped $Ag@TiO_2$ nanoparticles. The energy consumption in the process was

very high, as very high power lamps were used for irradiation in their study. The current work not only presents the extensive study on UV photocatalysis of azo dyes but also reports the solar photocatalysis using Ag@TiO$_2$ nanoparticles synthesized by one pot route. To the best of our knowledge, there are no reports till date showing the solar photocatalytic activity of Ag@TiO$_2$ core-shell structured nanoparticles.

1.1 Organization of the Thesis

Thesis of the present work is divided into following five chapters:

Chapter 1 presents the **Introduction**. This chapter discusses the background of research, need for the study and problem statement.

Chapter 2 presents the detailed **Literature Review**. **This chapter summarizes the relevant literature review carried out during the current study, highlighting the research gaps in existing literature reports and the key research questions. Based on the extensive literature review, the objectives were specified for the currently reported research work and are presented at the end of this chapter.**

Chapter 3 presents the **Materials and Methods**. This chapter lists the materials used, followed by description of the experimental methodologies and the analytical procedures adopted to achieve the stated objectives.

Chapter 4 on **Results and Discussion** presents the results of the experiments on synthesis of Ag@TiO$_2$ nanoparticles, characterization, their efficacy for dye degradation, factors affecting dye degradation, optimization, kinetics, mineralization, degradation of mixture of dyes, use of immobilized Ag@TiO$_2$ nanoparticles and the efficacy of the nanoparticles to degrade other class of dyes etc. Results are presented in the form of Tables and Figures wherever necessary. Detailed discussion on the results with proper justification supported by the findings of this study, as well as other related research work reported in literature are presented in this chapter.

Chapter 5 presents the **Summary and Conclusions** of the present work along with the future cope for research.

CHAPTER 2

LITERATURE REVIEW

Following the background of this research work discussed in Chapter 1, an extensive review of literature on various relevant topics such as dyes present in wastewater from different industries, their toxicity, need for dye removal from wastewater, methods available and choice of photocatalysis as a favourable option, different types of photocatalysts available, modifications required in photocatalysts for improved performance, the advantages of various composite nanostructures such as core shell structures as photocatalysts, their dye degradation capacity, factors influencing and enhancing the degradation efficiency were undertaken. These literature analyses proved to be beneficial in problem definition and for setting the objectives of research. Review of literature was continued, in search of methodologies to be adopted to meet each of the specified objectives, as well as for comparing the results obtained in the current research with those obtained by other researchers in the field, wherever applicable. This chapter summarizes the relevant literature review carried out during the current study, highlighting the research gaps in existing literature reports and the key research questions. Based on the background of research and extensive literature review, the objectives were specified for the currently reported research work and are presented at the end of this chapter.

2.1 Dyes and their classification

The compounds which absorb light with wavelengths in the visible range (~350-700 nm) are colored. The first dye "Mauveine", a basic dye was discovered by W.H. Perkin in 1856 (Reid 1996), after which numerous dyes were discovered. Dyes contain chromophores and auxochromes that cause or intensify the colour of the chromophore by altering the overall energy of the electron system (Hunger 2003). Usual chromophores are -C=C-, -C=N-, -C=O, -N=N-, $-NO_2$, quinoidrings, and the auxochromes are $-NH_3$, -COOH, $-SO_3H$ and $-OH$ groups (Hunger 2003). Dyes can be classified according to their chemical structure or usage or method of application.

2.1.1 Classification by chemical structure

Dyes can be classified by chemical structure which has many advantages. It readily helps in identification of dyes belonging to a group, which has characterstic properties. Also this is the most widely used classification by both chemists and technologists, for example azo, anthraquinone, sulphur, indigoid, triphenylmethyl (trityl), and phthalocyanine derivatives. Among all the dyes, azo dyes constitute upto 70 % of all the commercial dyes produced. After azo dyes, anthraquinone dyes are the second largest class (~15%), followed by triarylmethanes (~3%) and phthalocyanines (~2%) (Hunger 2003). Table 2.1 shows the classification of dyes grouped according to their chemical structure.

Table 2.1 Classification of dyes according to chemical structure.
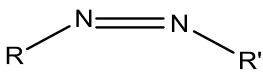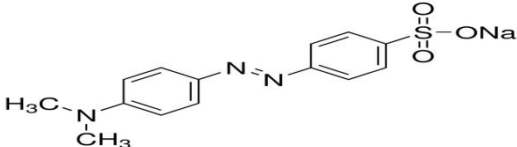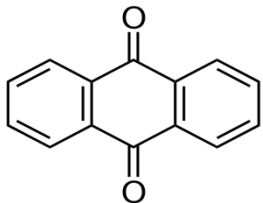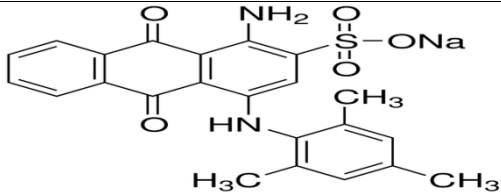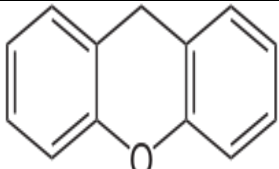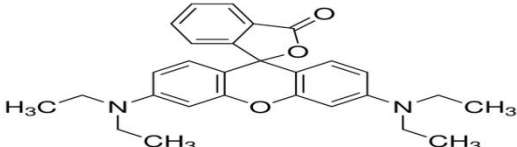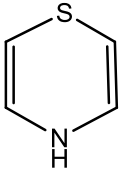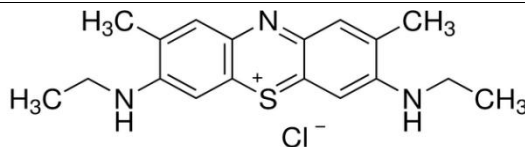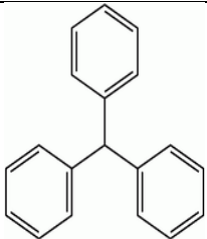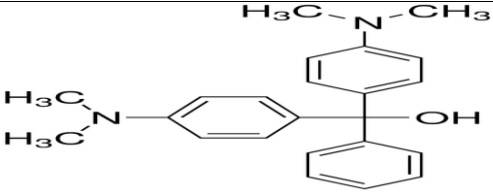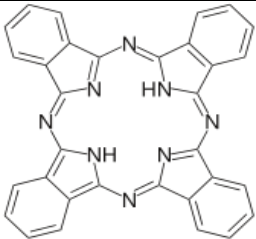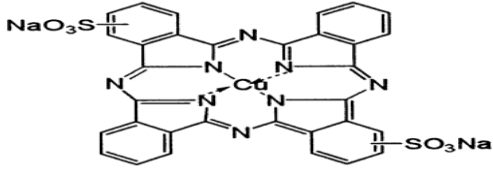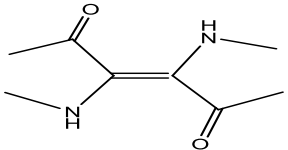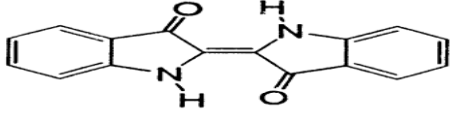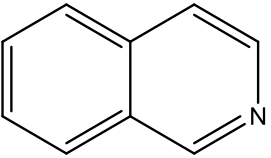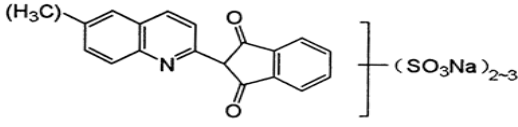
Class of dyes	Characterstic group	Example
Azo		Methyl Orange
Anthraquinone		Acid Blue-129
Xanthene		Rhodamine B
Thiazine		Methylene Blue

Table 2.1 Contd.

Class of dyes	Characterstic group	Example
Triphenylmeth ane		Malachite Green
Phthalocyanine		Direct Blue 86
Indigo		Vat Blue 1
Quinoline		Acid Yellow 3

2.1.2 Classification by properties for dye adhesion and application

It is advantageous to consider the classification of dyes based on the properties of the dyes which govern the mechanism of binding on the different materials and on their applications in detail due to nomenclature of the dye. This is the principal system adopted by the Colour Index (Anlinker 1979). The use or method of application of dye depends on the nature of the dye and the fiber on which it is applied. Fibers are of two types: synthetic and natural fibers. Table 2.2 shows the classification of dyes according to their properties, usage or method of application.

Table 2.2 Classification of dyes according to properties, use or application (Hunger 2003).

Class of dyes	Properties	Fiber	Chemical Class of dyes	Mechanism of attachment
Basic	Water soluble cationic	Paper, polyacrylnitrile, modified nylons and polyesters	diarymethane, triarylmethane, anthraquinone or azo compounds	Ionic bond
Acid	Anionic, highly water soluble, poor wet fastness	Nylon, wool, silks, modified acrylics, paper, leather, food, cosmetics	azo, anthraquinone or triarylmethane, azine, xanthene, nitro and nitroso compounds	Ionic bond
Disperse	Water insoluble non ionic dyes, good wet fastness	Polyester, nylon, acrylicfiber, cellulose and cellulose acetate	small azo/nitro compounds (yellow to red), anthraquinones (blue and green) metal complex azo compounds (all colors)	Colloidal impregnation and adsorption

Table 2.2 Contd.

Class of dyes	Properties	Fiber	Chemical Class of dyes	Mechanism of attachment
Vat dyes	Water insoluble	Cellulosic fibers	Anthraquinones or indigoids	Reduced dye impregnate the fabric followed by oxidation
Direct	Water soluble anionic, poor wet fastness	Cellulosic fibers	Polyazo, or phthalocyanine, stilbene or oxazine	Vander Wall forces
Sulphur	Colloidal after reaction in fiber, insoluble	cotton	Polymeric aromatics with heterocyclics containing rings	Dye precipitated in situ in fiber
Metalcomplex (Cr, Co, Cu)	Anionic, low water solubility, good wet fastness	Wood, Nylon	azo	Ionic bond
Reactive	Anionic, highly water soluble, good wet fastness	Cotton, Wool, nylon	Azo (metalized), anthraquinone, Phthalocyanine, formazan, triphendioxazine	Covalent bond

In ionic and nonionic dyes, chromophores are mostly azo or anthraquinone types. The reductive cleavage of azo bonds leads to the formation of amines which are highly toxic and among azo dyes; removal of sulphonated class is very difficult due to their high solubility in water. Owing to the fused aromatic structure and colour retaining capacity for longer time, anthraquinone dyes are mainly resistant to degradation.

2.1.3 Dye discharge statistics

On global scale over 0.9 million tons of dyes are produced each year. Discharge of dyes depends upon the nature of the dye and its chemical constituents. Table 2.3 shows the degree of fixation and percentage of dye lost to effluents. Among the azo dyes, water soluble acid and reactive dyes which consist of ionisable groups such as sulphonates ($-SO_3^-$), carboxylates ($-CO_2^-$) or sulphates ($-SO_4^-$) are the most problematic dyes because of their high molecular weight. So in the present study, two azodyes namely Acid Yellow-17 and Reactive Blue-220 were chosen for studies on photocatalytic degradation, due to their complexity in structure and high loss to the effluents.

Table 2.3 Percentage degree of dye fixation and its loss to effluents (Hunger 2003).

Class of dyes	Percentage degree of fixation	Percentage loss to effluents
Basic	95-100	0-5
Acid	80-95	5-20
Vat dyes	90-97	0-3
Direct	70-95	5-30
Reactive	50-90	10-50
Metalcomplex (Cr, Co, Cu)	90-98	2-10
Sulphur	60-90	10-40
Disperse	90-100	0-10

2.1.4 Environmental problems and adverse effects

The environmental issues associated with dye containing water are always a concern as dye concentration in water higher than 1 mg/L can be easily noticeable by public. It was found that high concentrations of dyes present in water can cause troubles in numerous ways (Pereira and Alves 2012):

(i)   Dyes can have acute and/or chronic effects on exposed organisms, depending on the exposure time and the dye concentration.

(ii)   Dye wastewater captures the attention of both the public and the authorities as the dyes are inherently highly visible and minor release itself can cause abnormal coloration of surface waters.

(iii)   Dyes can have drastic effects on the growth of bacteria as dyes absorb/reflect sunlight entering the water which may upset their biological activity.

(iv)   Dyes are difficult to treat due to their complicated and different molecular structures and therefore, interfere with municipal waste treatment operations.

(v)   Dye effluents undergo chemical and biological changes; destroy aquatic life by consuming dissolved oxygen from the stream.

(vi)   Dyes produce micro toxicity to fish and other organisms due to their tendency to sequester metal ions.

Due to the aromatic nature, most of the dyes are non-biodegradable, carcinogenic or cause allergies, dermatitis, skin irritation or different tissular changes (Carmen and Daniela 2012). Among various dyes, azo dyes are most dangerous as they try to pass conventional treatment process ineffectively and when incorporated into the body, it can split into corresponding aromatic amines by liver enzymes and intestinal flora, which can cause cancer in human (Carmen and Daniela 2012). The adsorption of azo dyes and their breakdown products (toxic amines) pose high potential health risk to human health through the gastrointestinal tract, skin, lungs, and also formation of hemoglobin adducts and disturbance of blood formation (Carmen and Daniela 2012). Also azo dyes can damage DNA which can lead to the genesis of malignant tumors. The carcinogenic potential can increase with electron-donating substituents in ortho and para position and diminishes with the protonation of amine groups (Carmen and Daniela 2012).

2.1.5 Regulations for dye containing wastewater

Presence of dyes in concentration more than the certain standard limit in water bodies causes many adverse effects to human beings, animals, plants etc. Hence, stringent regulations have been imposed by various organizations. World Health Organization (WHO) guidelines for drinking water quality, has set the maximum value for permissible colour at 15–20 units (Binnie et al. 2002). Color standard for drinking water specified by USEPA is 20 units (USEPA 2013). The Central Pollution Control Board (CPCB), India has prescribed the permissible colour level of 400 Hazen unit for the discharge of the effluent (CPCB 2010). Apart from regulatory standard for colour, these dyes contribute to Chemical Oxygen Demand (COD) and Biological Oxygen Demand (BOD) in wastewater. Hence removal of dyes from wastewater before discharge into surface waters is essential to meet the regulatory standards in terms of colour, COD and BOD.

2.2 Methods for removal of dyes from wastewater

Many tFreatment processes have been applied over last two decades in order to remove dyes from contaminated wastewater. Among the most commonly used techniques are adsorption on activated carbon (Rao et al. 1994), coal (Gupta et al. 1990), natural clay (Gupta et al. 1992), red mud (Ratnamala et al. 2012), flyash (Gupta et al. 1990), etc., electrocoagulation (Lopes et al. 2005), coagulation and precipitation (Kartikeyan, 1990), chemical processes such as chlorination (Namboodri et al. 1994 a,b) and ozonation (Xu and Lebrun 1999) and biological methods which include aerobic processes (Rai et al. 2005) and anaerobic processes (Delee et al. 1998). The classical or conventional method such as adsorption are not destructive but only transfer dye from one phase to another which creates other type of pollution (Khatee et al. 2009). Although some treatment processes, such as chemical coagulation, treatment with ozone and carbon adsorption, may remove certain categories of dye to about 90 % (Poon and Vittimberga 1981, Lorimer et al. 2001), each method has its own advantages and disadvantages. The main drawback of chemical coagulation, precipitation and electrocoagulation is the generation of a large

amount of sludge or solid waste, resulting in high operational costs for sludge treatment and disposal. Ozone treatment does not require sludge disposal but suffers from high cost. Many of the azo dyes are non-biodegradable and hence biological treatment options cannot be adopted. Even in the case of biodegradable dyes, biological treatment processes are slow and ineffective at high concentrations. Table 2.4 presents the available technologies for dye degradation with its advantages and disadvantages.

Therefore, it is necessary to find an effective method of wastewater treatment capable of removing dyes from industrial effluents. An affordable and easy-operated control technology without the formation of sludge is needed to comply with today's demanding legislation. These challenges have impelled serious research in new advanced treatment technologies, some of which are presently making their way to full-scale installations. Several new technologies in wastewater decolorization have emerged with improved performance and are more environmental friendly. Among them, advanced oxidation processes (AOP's) have been emerged as one of the promising technologies for the degradation of dyes due to their compliance with green chemistry concept. Due to the formation of highly reactive chemical species, the dye molecules degrade into biodegradable compounds, which further degrade to CO_2 and H_2O.

Table 2.4 Available technologies for dye degradation.

I PHYSICAL TREATMENTS		
Methods	**Advantages**	**Disadvantages**
Adsorption on different adsorbents such as Activated carbon (Raghavacharya 1997; Rao et al. 1994); Wood chips (Nigam et al. 2000); Barley Husks (Robinson et al. 2001); Corn cobs (El-Geundi 1990); natural clay (Gupta et al. 1992); Peat (Namasivayam and Kadirvelu 1998); Spent brewery grains (Silva et al. 2004); Cucurbituril (Karcher et al. 1999 a,b); Red mud (Ratnamala et al. 2012)	Widespread availability. Regeneration is not necessary Less investment in terms of both initial cost and land, simple design, easy operation, no effect by toxic substances and superior removal of organic waste constituents as compared to the conventional biological treatment processes (Gupta et al. 1999).	Required in bulk quantity It is not a destructive method. Transfers dyes from one phase to other phase.
Reverse osmosis (Al-Bastaki, 2004; Marcucci et al. 2001; Sostar-Turk et al. 2005)	Effective desalting and decolouring process Recycling of water possible	It cannot handle acid or base dyes and the molecules having molecular weight below 200 (Marcucci et al. 2001). Fouling of the membrane; high cost and slower process

Table 2.4 Contd.

Methods	Advantages	Disadvantages
Ion exchange (Slokar and Le Marechal 1998; Mishra and Tripathy 1993)	On regeneration no loss of ion exchange materials occur (Robinson et al. 2001).	It cannot accommodate a wide range of dyes (Slokar and Le Marechal 1998) High cost (Robinson et al. 2001)
Irradiation	Some dyes can be oxidized effectively (at a laboratory scale only) (Hosono et al. 1993).	Enough amount of dissolved oxygen is required (Robinson et al. 2001). Not all dyes can be degraded
II CHEMICAL TREATMENTS		
Chemical Oxidation process	Effective colour removal	Problem with sludge disposal High consumption of chemicals
Fenton's reagent	Effective in decolorizing both soluble and insoluble dyes (Pak and Chang 1999). A broad range of dyes can be decolourized (Namboodri and Walsh 1996).	It is generally effective within pH <3.5 (Cheng et al. 2004) Large amount of sludge production (Raghavacharya 1997) and hence associated sludge disposal problems.

Table 2.4 Contd.

Methods	Advantages	Disadvantages
Coagulation and precipitation, Electro coagulation	Short detention time Low capital cost Economically feasible method	The cost of chemicals for pH adjustment and precipitation is very high. Generate large amounts of sludge and waste which need further treatment for disposal. Troubles related with sludge disposal and dewatering, consequentially increase disposal costs (Gahr et al. 1994). In the supernatant, high amount of residual cation level remains. It can't be used for azo, acid, reactive and particularly the basic dyes (Hai et al. 2007) Poor results with acid dyes High coagulant cost
Ozonation	Treated effluent has no colour and low COD suitable for discharge (Xu and Lebrun 1999). No sludge formation (Ince and Gonene 1997). No toxic metabolites are produced (Gahr et al. 1994).	High cost, short half-life and continuous ozonation is required (Xu and Lebrun 1999).

Table 2.4 Contd.

Methods	Advantages	Disadvantages
Electrochemical oxidation	Little or no consumption of chemicals Non hazardous intermediates Efficient and economical removal of dyes High efficiency for colour removal and degradation of recalcitrant pollutants (Ogutveren and Kaparal 1994; Pelegrini et al. 1999). Applicable to a variety of contaminants.	High cost of electricity Sludge production
Treatment with Sodium hypochlorite	It can be used for water soluble dyes such as direct, acid, reactive and metal complex (Namboodri et al. 1994 a,b).	Unsuitable for water insoluble dyes such as vat and disperse (Namboodri et al. 1994 a,b). Not economically feasible due to the high dosages of Cl_2 High cost of the equipments, operating costs and the secondary pollution arising from the residual chlorine. Negative effects when released into waterways (Slokar and Le Marechal 1998)

Table 2.4 Contd.

III BIOLOGICAL TREATMENTS		
Methods	**Advantages**	**Disadvantages**
Biological treatments (aerobic (Rai et al. 2005) and anaerobic) (Rai et al. 2005; Delee et al. 1998)	Generally cheap and simple to apply	Complete mineralization may not occur Slower rate of degradation Nutrient addition can make the process cost intensive.
i) Aerobic	Colour removal is facilitated along with COD removal	Expensive aeration Problem with bulking sludge Most of the dyes are recalcitrant due to biological breakdown (Pagga and Brown 1986; Rai et al. 2005). Longer substarte removal and detention time.
ii) Anaerobic	Decolourization of soluble dyes. Biogas generation, Reduction in energy cost by reusing biogas which gives heat and power (Bras et al. 2005). Cheap No problem with bulking sludge	Insufficient BOD removal. No mineralization of dyes and other refractory organics. No removal of nutrients (N, P) and sulfate group converts into sulfide (Delee et al. 1998)

Table 2.4 Contd.

IV RECENT DEVELOPING TECHNOLOGIES		
Methods	**Advantages**	**Disadvantages**
Membrane filtration (Mishra and Tripathy 1993; Xu and Lebrun 1999).	Resistance to temperature, an adverse chemical environment, and microbial attack	Residual disposal problems High capital cost Possibility of clogging, and membrane replacement
Engineered wetland systems (EWS) (Mbuligwe 2003; Mbuligwe 2005)	Effective decolourization of dye Viable cost-effective technology to treat large volumes of wastewaters	High initial installation cost. Requires expertise and managing during monsoon becomes difficult
Sonication	Simplicity of its use.	Relatively new method and awaiting full scale application

2.2.1 Advanced Oxidation Processes (AOPs)

Due to the stringent environmental regulations set by governments and various organizations, research on water purification has been growing extensively for the last 25 years and has resulted in an intensive search for new and more efficient wastewater treatment technologies. AOPs are of ample interest currently for the effective oxidation of a wide variety of organics and dyes (Kang and Hoffmann, 1998; Boye et al. 2002; Stasinakis 2008). It is also being exploited for the purification and disinfection of drinking water (Andreozzi et al. 1999; Casero et al.1997; Benites et al. 1995; Masten and Davies 1994; Peyton et al. 1982; Legrini et al. 1993; Miller et al. 1988). Advanced oxidation technologies have been included by U.S. Environmental Protection Agency (USEPA) as one of the best available technology to meet the specification and standard that offer safe and ample pollution control (Bansal and Sud 2011). AOPs involve the formation of strong oxidizing radicals such as hydroxyl radicals (HO$^{.}$), superoxide anion etc. (O$_2^{.-}$) which further react with pollutants. These

highly reactive radicals have ability to oxidize almost all organic compounds to carbon dioxide (CO_2) and water (H_2O). Advanced oxidation processes can be divided into homogeneous and heterogeneous processes. Homogenous processes are further subdivided into two processes: photochemical and non-photochemical. Figure 2.1 shows the classification of homogenous and heterogeneous processes. Homogenous processes mainly need oxidant to generate hydroxyl radical and hydrogen peroxide is most frequently used. Heterogeneous processes use solid catalysts along with oxidants for degradation of dyes. It has been reported in literature that heterogeneous processes are more efficient and in the present study heterogeneous process has been used. Heterogeneous photocatalysis has emerged as an important destructive technology leading to the total mineralization of most of the organic pollutants including organic reactive dyes (Schiavello 1988; Guillard et al. 2003; Galindo et al. 2001; Serpone and Pelizzetti 1989; Fox and Dulay 1993; Kusvuran et al. 2005; Khodja et al. 2001; Neppolian et al. 2002a; Lathasree et al. 2004). Heterogeneous photocatalysis specially has several advantages, no reagent is used. The only chemical used is semiconductor photocatalyst such as TiO_2, SnO_2, ZrO_2, CdS and ZnO (Kansal et al. 2008; Daneshvar et al. 2006). Oxidants such as H_2O_2 may be added to enhance the rate of degradation.
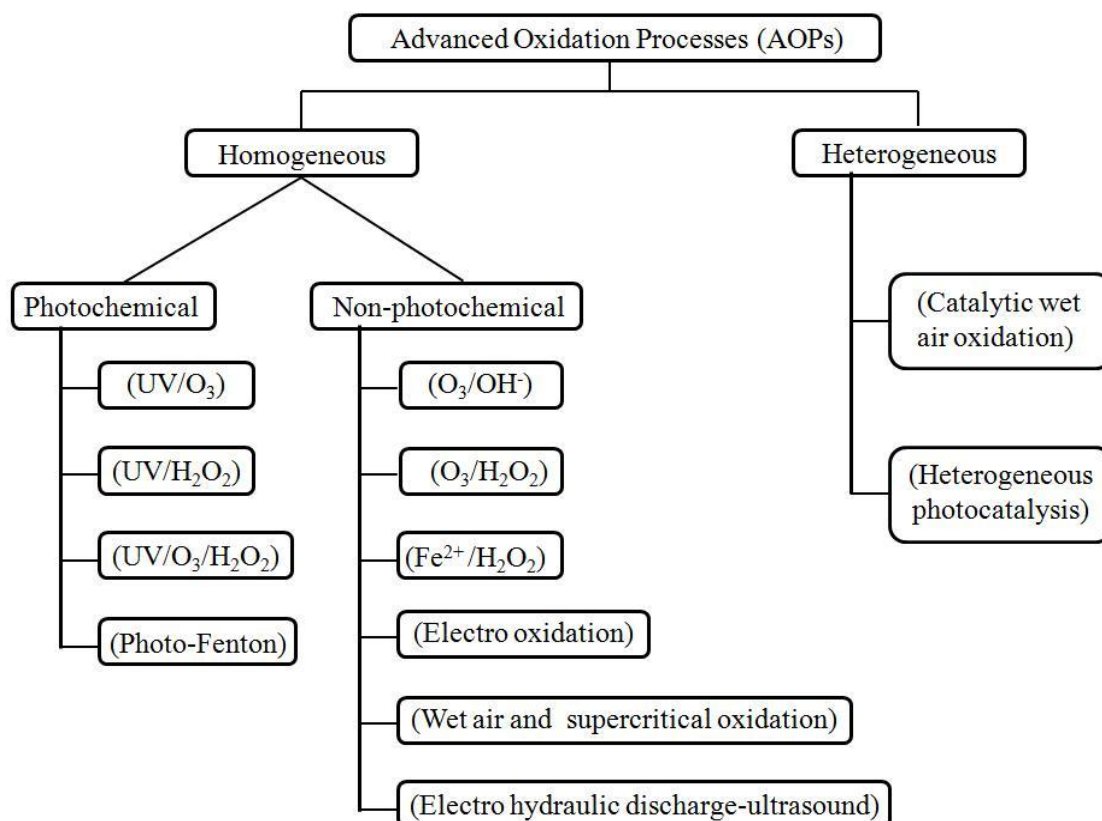
Figure 2.1 Classification of Advanced oxidation processes.

2.3 Basic principle of heterogeneous photocatalytic degradation of dyes

Photocatalysis in the presence of irradiated semiconducting oxides has been successfully used to oxidize many organic pollutants present in aqueous systems (Schiavello 1997; Fujishima and Tryk 1999). With the use of TiO_2 photocatalysts, the past two decades have witnessed serious studies associated with light stimulated mineralization of hazardous organic pollutants (Crittender et al. 1997; Yamashita et al. 2000; Di-Paola et al. 2002). Particularly, it has been also used to decolorate and mineralizes many kinds of azo-dyes in a bench scale by using both artificial irradiation (Goncalves et al. 1999; Kiriakidou et al. 1999) and also solar technology (Wang 2000). Photocatalysis usually happen with the attack of organic pollutants by the hydroxyl radical and super oxide radical, generated on TiO_2 catalyst surface due to oxidation of surface hydroxyl by TiO_2 and/or reduction of dissolved oxygen (Poulios and Aetopoulon 1999; Carlos et al. 2000). A large variety of organic pollutants can be broken down by photocatalysis to water, CO_2 and mineral salts as the degradation

products (Byrappa et al. 2000). The photocatalysis process can break down a large variety of organic compounds to CO_2, water and mineral salts, as the degradation products (Byrappa et al. 2000). The greatest advantage of photocatalysis over conventional treatment method is the complete mineralization of organic pollutants (Ding et al. 2000). Most of the photocatalytic studies use either synthetic or commercial TiO_2 as the photocatalyst (Grzechulska and Morawski 2002; Noorjahan et al. 2002). The TiO_2 semiconductor due to its comparatively high efficiency and low cost has been reported to be the most promising photocatalyst (Wang 2000; Ding et al. 2000; Neppolian et al. 2002b). Titanium dioxide has been widely used as photocatalyst because it has strong oxidizing power and nontoxic to human life. In recent years lot of reviews have been published (Ahmed et al. 2011; Akpan and Hameed 2009; Carmen and Daniela 2012; Gupta and Suhas 2009; Konstantinou and Albanis 2004) on photocatalysis with titanium dioxide.

The detailed mechanism of photocatalytic degradation of dyes involves absorption of light by the semiconductor (e.g., TiO_2 and ZnO) particle which causes the excitation of the semiconductor molecules from the valence band to the conduction band of the semiconductor and due to this, conduction band electrons (e^-) and valence band holes (h^+) are generated as shown in Eq.(2.1). General mechanism of photocatalytic degradation by TiO_2 is represented in Figure 2.2. For excitation to occur, semiconductor should be irradiated with light energy greater than its band gap energy (Akpan and Hameed 2009; Konstantinou and Albanis 2004).

$$TiO_2 + h\nu \ (UV) \rightarrow TiO_2(h^+_{(VB)} + e^-_{(CB)}) \tag{2.1}$$

These photogenerated electron-hole pairs are powerful oxidizing and reducing agents. The photogenerated electrons in the conduction band either reduce dye to form R^+ ,or react with oxygen adsorbed on the catalyst (TiO_2) surface and reducing it to superoxide radical anion ($O^{\cdot}_2$) whereas the photogenerated holes in valence band either oxidize the dye to form R^+, or react with OH^- or H_2O, oxidizing them into hydroxyl radicals. Highly oxidant species such as (Hydroxyl or peroxide radicals) are reported to be responsible for the heterogeneous photocatalytic degradation of dyes. According to this, the relevant oxidation and reduction reactions occurring at the semiconductor surface (TiO_2) can be expressed as follows:

$$TiO_2(h^+_{(VB)}) + H_2O \rightarrow TiO_2 + H^+ + HO^{\cdot} \tag{2.2}$$

$$TiO_2(h^+_{(VB)}) + OH^- \rightarrow TiO_2 + HO^{\cdot} \qquad (2.3)$$

$$TiO_2(e^-_{(CB)}) + O_2 \rightarrow TiO_2 + O_2^{\cdot -} \qquad (2.4)$$

$$O_2^{\cdot -} + H^+ \rightarrow HO_2^{\cdot} \qquad (2.5)$$

$$Dye + HO^{\cdot} \rightarrow Degradation\ produts \qquad (2.6)$$

$$Dye + (h^+_{(VB)}) \rightarrow Oxidation\ produts \qquad (2.7)$$

$$Dye + \left(e^-_{(CB)}\right) \rightarrow Reduction\ produts \qquad (2.8)$$
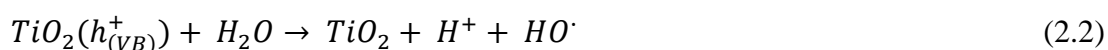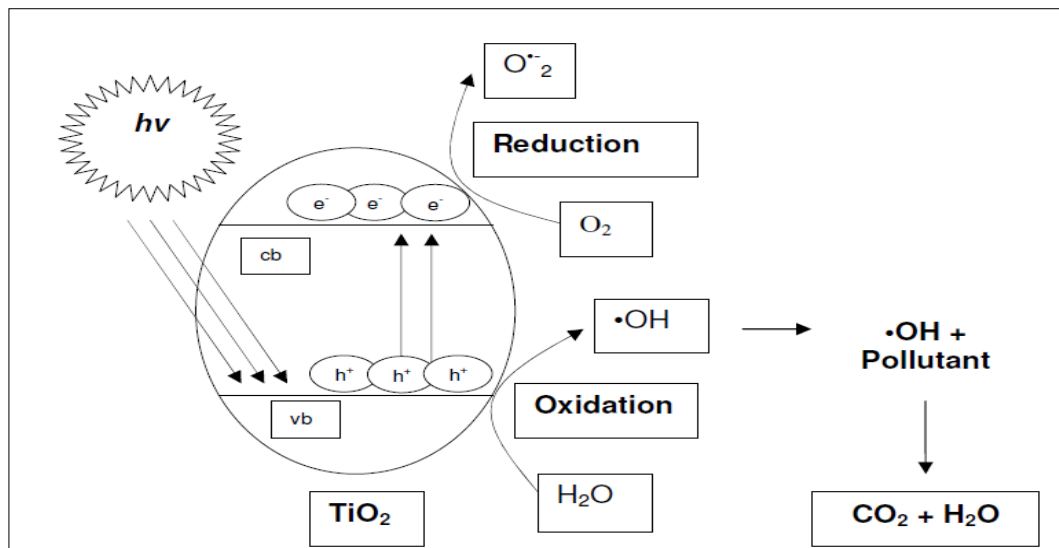
Figure 2.2 General mechanism of TiO$_2$ photocatalysis (as modified from Robert and Malato 2002; Dijkstra et al. 2001).

2.4 Photocatalysts

A wide variety of semiconductor photocatalysts have been employed for the photocatalysis of organic compounds (Daneshvar et al. 2004). Table 2.5 shows the band gap energy level of different semiconductors (Serpone 1995). Of all the photocatalysts, TiO$_2$ is found to be the most active catalyst for degradation of organic compounds. TiO$_2$ emerges to be a relatively economic, effectual, chemically stable and easily available (Zhao and Yang 2003; Zang et al. 1998). In the literature, abundant applications of this technique were cited and a number of outstanding reviews were published (Heglin 1989; Hegfeldt and Gratzel 1995; Fox and Dulay 1993; Kamat 1993). TiO$_2$ has three crystalline phase; anatase, rutile and brookite,

among which anatase and rutile form are frequently studied, as brookite is not stable and convert to rutile (Saepurahman et al. 2010). Anatase form of TiO_2 is found to be the most active form for photocatalysis (Ovenstone and Yanagisawa 1999).

Table 2.5 Band gap energy level of different semiconductors (Serpone 1995).

Semiconductor as photocatalyst	Band gap energy (eV)
TiO_2 anatase	3.23
TiO_2 rutile	3.02
ZnO	3.2
SiC	3
ZnS	3.7
SnO_2	3.5
$SrTiO_3$	3.4
Fe_2O_3	3.1
CdS	2.4
V_2O_5	2.7
WO_3	2.8

Special attention has been paid by researchers and engineers to TiO_2 nanoparticles as it has several advantages over bulk TiO_2: (i) It can reduce the recombination of photogenerated electron-hole pair. (ii) Surface area of catalyst can be increased which further enhance the rate of photocatalysis. (iii) It can lead to quantum size effect.

Various authors have used commercially available TiO_2 photocatalysts such as Degussa P25, PC500, TTP and UV100 for the photocatalytic degradation of dyes. P25 has been found to be effective in most of cases because P25 consist of 75% anatase and 25% rutile with a specific BET-surface area of 50 m^2 g^{-1} and primary particle size of 20 nm (Bickley et al. 1991). Hombikat UV100 consists of 100% anatase with a specific BET surface area >250 m^2 g^{-1} and primary particle size of 5 nm (Lindner et al. 1997). The photocatalyst PC500 has a BET-surface area of 287 m^2 g^{-1} with 100% anatase and primary particle size of 5-10 nm (Saquib et al. 2003). The commercially available TTP, India photocatalyst, has a BET surface area of 9.82 m^2/g. Various authors have reported that Degussa P25 shows better photocatalytic activity as

compared to other commercially available photocatalysts for the photocatalytic degradation of dyes (Faisal et al. 2007, Muruganandham and Swaminathan 2006a, 2004; Qamar et al. 2005 a,b).

Faisal et al. (2007) tested the photocatalytic activity of three different commercially available TiO_2 powders (namely Degussa P25, Hombikat UV100 and PC500) on the degradation kinetics of model pollutants (Acridine Orange and Ethidium Bromide) at different concentrations such as 0.5, 1, 2 and 3 g L^{-1}. Degussa P25 was found to be more efficient for the degradation of both the dyes at all concentrations.

Saquib and Muneer (2002) tested the activity of three different commercially available photocatalysts (Degussa P25, Hombikat UV100 and PC500) for photocatalytic degradation of an anthraquinone dye, Remazol Brilliant Blue R under UV light. It was observed that the degradation of dye proceeds much more rapidly in the presence of P25. Saquib and Muneer (2003a) checked the activity of these three different commercially available photocatalysts on the degradation kinetics of gentian violet. It was observed that the mineralization and degradation of dye proceeds much more rapidly in the presence of P25 as compared with other photocatalysts. The order of decolorization efficiency of various photocatalysts was found to be P25> PC500> UV100 for gentian violet. Saquib and Muneer (2003b) checked the activity of four different commercially available photocatalysts (Degussa P25, Hombikat UV100, PC500 and TTP) on the degradation kinetics of Acid orange 8. It was observed that the mineralization and degradation of dye proceeds rapidly in the presence of P25 as compared with other photocatalysts. The order of decolorization efficiency of various photocatalysts was found to be P25> UV100> PC500> TTP. Saquib et al. (2008) have also found that in the degradation of two selected dye derivatives, Fast Green and Acid Blue 1, the order of decolorization efficiency of various photocatalysts was P25>PC500>UV100. The photocatalytic activity of these three commercially available photocatalysts were examined on the degradation of Xylenol orange (Tariq et al. (2008), Amarnth and Bismark brown (Tariq et al. 2005) and it was found that Degussa P25 has a highest photocatalytic activity as compared to others.

Many earlier studies have reported that Degussa P25 shows a better activity for the photocatalytic degradation of a large number of organic compounds (Muneer

et al. 2001; Muneer et al. 1999). Muruganandham and Swaminathan, (2006 a,b) and Kansal et al. (2006) have also observed the higher efficacy of Degussa P25 as compared to TiO_2 anatase as a photocatalyst in both the degradation and decolorization of dyes.

Qamar and Muneer (2009) explained that, the higher photocatalytic activity of Degussa P25 is due to its mixed phase (75% anatase and 25% rutile). Degussa P25 composed of small nano-crystallites of rutile disperses within an anatase matrix. It is explained by Qamar and Muneer (2009) that, the excited electrons get trapped in the rutile phase thus inhibiting the electron–hole pair recombination (a major energy wasting step) which in turn increases the photocatalytic efficiency of P25. Another reasoning reported was that, the smaller band gap of rutile catches the photons, generating electron/hole pairs. The electron transfer, from the rutile conduction band (CB) to electron traps in anatase phase, takes place. Recombination is thus inhibited, allowing the hole to move to the surface of the particle and react (Hurum et al. 2003).

In certain cases, 100 % anatase TiO_2 showed better photocatalytic activity, than the mixture of rutile and anatase TiO_2.

Saquib and Muneer (2002) had found that Hombikat UV100 was slightly better under sunlight as compared with Degussa P25 for photocatalytic degradation of an anthraquinone dye, Remazol Brilliant Blue. Saquib et al. (2008) have also found that in the degradation of Fast Green, UV100 was better than P25. Similar results were observed by Tariq et al. (2008) in the degradation of Acid blue 45. The order of decolorization efficiency of various photocatalysts was found to be UV100 > P25 > PC500.

TiO_2 as photocatalyst have been used in numerous studies. However, the TiO_2 photocatalyst has its limitations,

i) Owing to its large band gap energy, only UV light can be used as a radiation source, as natural solar radiation encompasses only about 4–5 % of UV rays (Heller 1995; Linesbigler et al. 1995).

ii) Low quantum yields of TiO_2 due to recombination of photogenerated electron and hole pairs (Rothenberger et al. 1985; Tributsch et al. 1989).

Several attempts have been performed to improve the photocatalytic activity of TiO_2 such as, combination of TiO_2 with other semiconductors (Wu 2004), covering

of the surface with dyes in order to extend the light absorption to the visible range, doping metal ions into the TiO_2 lattice (Behpour et al. 2010; Sakthivel et al. 2004; Subba Rao et al. 2003; Hoffmann et al. 1995) and partially coating with noble and transition metals (Sajjad et al. 2010; Siemon et al. 2002; Liu et al. 2004). Amongst them, the noble metal deposition on the surface of TiO_2, such as, silver, gold, platinum and palladium (Vamathevan et al. 2002) can be cited. Most of the deposited metals that have been previously studied belong to group VIII. A considerable increase of the photocatalytic activity has been reported in particular with platinum deposited on TiO_2 particles (Hufschmidt and Bahnemann 2002; Klare et al. 2000). The photocatalytic activity with silver deposit was much less enhanced than that with Pt deposit. Nevertheless, silver is most suitable for industrial applications due to its lower cost and easy preparation (Vamathevan et al. 2002). In photocatalytic oxidations, the reaction rate is controlled by charge transfer to O_2 (Sclafani and Herrmann 1998) and silver has special behavior for oxygen adsorption. Kondo and Jardim (1991) have shown that the Ag-loaded TiO_2 was more effective than the pure TiO_2 in the degradation of chloroform and urea. Also, Sahoo et al. (2006) found that Ag^+ doped TiO_2 is slightly more efficient than the undoped TiO_2 in the photocatalytic degradation of C.I. Basic Violet 3. It was reported by Behnajady et al. (2008) that, silver doped TiO_2 is more efficient than undoped TiO_2 in photocatalytic degradation of Acid Red-88. Rupa et al. (2007) investigated the photocatalytic degradation of Reactive Yellow 17 using Ag doped TiO_2 nanoparticles and found enhancement in photocatalytic activity under both UV and visible light irradiations for Ag doped TiO_2 nanoparticles. The increase in efficacy of Ag doped TiO_2 as compared to bare TiO_2 is owing to the accumulation of electrons, small size of Ag nanoparticles on TiO_2 surface and better charge separation which reduces the recombination of electron and hole pairs.

Thus it is well-known that noble metal nanoparticles (e.g. Ag and Au) can tune the catalytic properties of metal oxides such as TiO_2 (Hirakawa and Kamat 2005).The combination of two nanomaterials (Ag and TiO_2) may be properly designed to yield improved catalytic and optical properties.

In recent years, several research groups have synthesized metal core and TiO_2 shell (metal@TiO_2) (Hirakawa and Kamat 2005) and TiO_2 core and metal shell

(TiO$_2$@metal) (Vıctor et al. 2008; Zhang et al. 2003; Mirkhani et al. 2009; Rupa et al. 2007) nanocomposites. The presence of co catalytic noble metal deposits on metal oxide particles is often employed to enhance the photocatalytic oxidation efficiency of processes through achievement of a more efficient charge separation (Hidaka et al. 2007). Ag-TiO$_2$ modified photocatalysts and their potential applications with enhanced photocatalytic efficacy have been reported. The core-shell structures have the ability to store photogenerated electrons which make them suitable for light energy conversion and storage. Although noble metals such as gold and silver are poor catalysts in bulk form, nano-sized counterparts with a passivating shell show excellent catalytic activity as a result of the high surface area and interface dominated properties (Zhang et al. 2006). In most of the catalytic studies, metal particles are usually deposited on the oxide surface (Dawson and Kamat 2001; Ohko et al. 2001). The presence of Ag deposits on TiO$_2$ surface can help to efficiently separate the electron-hole pairs by attracting the conduction band photoelectrons. This process has been shown to improve the overall efficiency for a number of photocatalytic reactions (Tran et al. 2006).The deposited metal, on the one hand, can suppress the electron-hole recombination, beneficial to the photocatalytic oxidation (Sclafani and Herrmann 1998; Fox 1992). However, corrosion or dissolution of the metal nanoparticles after their extended exposure to reactants and the surrounding medium may pose a concern for their photocatalytic activities (Subramanian et al. 2001, 2003; Lahiri et al. 2003).The oxide shell is important because it is an effective way to prevent metal nanoparticles from agglomerating under extreme conditions, whereas uncoated particles coagulate easily resulting from the Van der Waals' force (Zhang et al. 2006). To address this problem, a composite structure of metal nanoparticle core and oxide shell is considered a better design, because the oxide shell can protect the metal core and stabilize it against chemical attack.

Hirakawa and Kamat (2005) found that, photoexcitation of TiO$_2$ shell results in accumulation of the electrons in the Ag core in Ag@TiO$_2$ nanoparticle. Their results showed that the stored electrons are discharged when an electron acceptor such as O$_2$ is introduced into the system. Charge equilibration with redox couple showed the ability of these core shell structures to carry out photocatalytic reduction reactions. With electron acceptor it is also possible to envisage surface plasmon modulation and

electron storage in Ag@TiO_2 nanoparticles (Hirakawa and Kamat 2004). Cheng et al. (2010) have shown the photocatalytic property of Ag@TiO_2 core-shell nanocomposite nanowires in terms of degradation of Rhodamine – B dye under UV light irradiation. Their results confirmed that Ag@TiO_2 core-shell nanowires exhibited excellent photocatalytic activity as compared to Degussa P25 and TiO_2. Wang et al. (2008a) have used Ag@TiO_2 nanoparticles as catalysts for the photocatalytic degradation of Alizarin red under visible light irradiation. The study was restricted to the comparison of photocatalytic activity of two steps synthesized Ag@TiO_2 nanoparticles with that of Degussa P25. In both the studies, dyes used were not the azo dyes. Though there is a report by Wang et al. (2008b) on the examination of UV and visible photocatalytic activity of Ag@TiO_2 core-shell structured nanoparticles for degradation of methyl orange which is an azo dye, the study limited to the comparison of photocatalytic activity of two steps synthesized Ag@TiO_2 nanoparticles with that of Fe^{3+} doped Ag@TiO_2 nanoparticles. The energy consumption in the process was very high, as very high power lamps were used for irradiation. The interface between Ag and TiO_2 can attract light-induced electrons from the semiconductor TiO_2 to reduce electron–hole recombination. Since it is reported in literature that Ag@TiO_2 nanoparticles have unique properties of interfacial charge transfer and high visible light absorption, it was proposed to study the efficacy of Ag@TiO_2 nanoparticles for the UV and solar photocatalysis of azo dyes.

To the best of our knowledge, there are no reports till date showing the solar photocatalytic activity of Ag@TiO_2 core-shell structured nanoparticles.

2.4.1 Preparation of Ag@TiO_2 nanoparticles

Many people have reported on the synthesis of metal@TiO_2 nanoparticles or composites (Hirakawa and Kamat 2005; Dawson and Kamat 2001; Hyun-Woo et al. 2007; Du et al. 2006; Young et al. 2004; Zhang et al. 2005). The combination Ag and TiO_2 nanomaterials may be suitably designed by proper synthesis method and conditions, to yield enhanced optical and catalytic properties that utilize the characteristics of photoexcitation of the electron from the TiO_2 shell to the metal core (Hirakawa and Kamat 2005).

There are two reported methods for the preparation of Ag@TiO$_2$ nanoparticles. They are one pot synthesis method and two step synthesis method.

(i) One pot synthesis

Pastoriza-Santos et al. (2000) have tried to synthesize the Ag@TiO$_2$ nanoparticles by high temperature reduction of Ag by dimethyl formamide (DMF)/ethanol mixture in the presence of titanium tetraoxybutyl and acetylacetone. Similar nanoparticles were synthesized by refluxing a mixture of silver and TiO$_2$ colloids (from Ti (IV) butoxide) at 90°C (Kim et al. 2004). Tom et al. (2003) synthesized nanostructures by reduction of silver nitrate with DMF and titanium isopropoxide was used as the shell-forming reagent on silver nanoparticles n. The colloidal material was precipitated by the addition of toluene. Du et al. (2006) prepared Ag@TiO$_2$ nanostructures by one pot synthesis. In this method, tetrabutyl titanate (TBT) was added dropwise to ethylene glycol (EG) containing the desired amount of AgNO$_3$. Solution was loaded into a 20 mL stainless steel cell and maintained at 240 °C or 270 °C for 14 h. Zhang et al. (2006) and Dang et al. (2010) synthesized Ag@TiO$_2$ by a simple one-pot chemical reaction procedure using dimethyl formamide reduction of AgNO$_3$ and titanium isopropoxide with heating and stirring for 90 min. Hirakawa and Kamat (2005) also used the same one pot synthesis using dimethyl formamide reduction of AgNO$_3$ and titanium tetra ethanolaminato isopropoxide (TTEAIP) with heating at 85 °C and continuous refluxing, stirring for 90 min.

(ii) Two step synthesis

Zeena et al. (2004) synthesized Ag@TiO$_2$ nanoparticles by two step method. First, the formation of silver core takes place by the reduction of trisodium citrate and then formation of TiO$_2$ shell take place by heating and refluxing at 60 °C. Zhang et al. (2005) prepared Ag@TiO$_2$ nanoparticles by two step method. First the formation of the silver core takes place by the reduction of Tollen's reagent with glucose in the water phase of the water-in-oil emulsions, and the hydrolysis of Titanium ortho butoxide (TOB) at the water/oil interface for the formation of the amorphous TiO$_2$

shell. Wang et al. (2008a) synthesized Ag@TiO$_2$ core–shell nanoparticles using silver acetate, dodecylamine, oleic acid and titanium tetraisopropoxide. First, silver acetate was dissolved in dodecylamine and then oleic acid was added. After this titanium tetra isopropoxide was slowly added and stirring was continued for 15 min. Finally, the solution was transferred into autoclave. The autoclave was first kept at 120 ºC for 5 h, then increased to 150 ºC and kept for another 47 h. To precipitate the nanoparticles, isopropanol was added. Wang et al. (2008b) made Ag@TiO$_2$ core–shell nanoparticles by two step method, wherein, the formation of silver core takes place by reduction of hydrazine with cetyl trimethyl ammonium bromide (CTAB) followed by addition of titanium tetra isopropoxide (TTIP) to the Ag solution under vigorous stirring for 10min at ambient temperature, which forms a TiO$_2$ shell. To obtain uniform core–shell structures of Ag@TiO$_2$, Vaidya et al. (2010) developed a two step based reverse-micelle tactic using titanium hydroxyacylate as the shell forming agent. Abdulla-Al-Mamun et al. (2011) prepared the Ag@TiO$_2$ core–shell nanoparticles by two step citrate reduction method. Ag@TiO$_2$ was prepared by adding AgNO$_3$ and titanium tetraethanolaminato isopropoxide (TTEAIP) with heating at 60 °C and continuous refluxing and stirring for 90 min. Solution was then purged with N$_2$ gas and irradiated with ultraviolet light (15 mW/cm^2) to reduce any unreacted Ag$^+$ in solution to Ag^0. Angkaew and Limsuwan (2012) prepared Ag@TiO$_2$ nanoparticles by reduction method using hydrazine as reducing agent and CTAB as a stabilizer. First, Ag nanoparticles were prepared by adding hydrazine to CTAB solution and followed by addition of silver nitrate dropwise to hydrazine and CTAB solution. After this various TTIP concentration were added to Ag nanoparticles.

One pot synthesis is less time consuming and reported to produce better core shell structures than two step synthesis routes. So in the present study, it was proposed to use the one pot synthesis route followed by Hirakawa and Kamat (2005) for the synthesis of Ag@TiO$_2$ photocatalyst. It was proposed to modify the synthesis procedure suitably to get enhanced photocatalytic activity.

To test the efficacy of Ag@TiO$_2$ photocatalyst, its photocatalytic activity need to be compared with other common photocatalysts such as commercial TiO$_2$, synthesized TiO$_2$ and Ag doped TiO$_2$ photocatalysts under both UV and solar light

irradiation conditions. So a review of literature on synthesis of TiO_2 and Ag doped TiO_2 nanocatalysts was carried out and is presented in the following section.

2.4.2 Synthesis of TiO$_2$ and Ag doped TiO$_2$ nanocatalysts

2.4.2.1 Synthesis of TiO$_2$

There are many methods available for the synthesis of TiO_2 nanoparticles. The synthesis of TiO_2 can be classified as solution phase and gas phase techniques. Solution phase synthesis is the most preferred technique for the preparation of TiO_2 in the form of powders and thin films. Some of the solution phase techniques are precipitation method (Jing et al. 2009), hydrothermal synthesis (Jeong et al. 2008), sol-gel method (Rupa et al. 2009), combustion synthesis (Nagaveni et al. 2004), electrochemical synthesis (Kumar et al. 2008) and sonochemical synthesis (Arami et al. 2007). Gas phase technique is widely employed for the synthesis of thin film samples. Some of the gas phase techniques include chemical vapor deposition (CVD) (Mills et al. 2002) and spray pyrolysis deposition (Okuya et al. 2002). In all the above methods combustion synthesis has been reported to yield TiO_2, which have 100% anatase without any rutile impurity (Sivalingam et al. 2003). It is because, during combustion, the temperature reaches about 650 $^\circ$C for a short period of time (1-2 minutes) making the material crystalline (Nagaveni et al. 2004). Since the time is too short, particle growth of TiO_2 and phase transition to rutile is hindered. This technique involves the combustion of a stoichiomeric mixture of titanyl nitrate with the fuel, glycine at 350 $^\circ$C in a muffle furnace. Titanyl nitrate is synthesized by the hydrolysis and subsequent nitration of the precursor compound, titanium tetra-isopropoxide. The stoichiomeric reaction can be represented as (Addamo et al. 2004) shown in Eq.(2.9).

$$9\,TiO(NO_3)_2 + 10C_2H_5O_2N \rightarrow 9TiO_2 + 14N_2 + 20CO_2 + H_2O \qquad (2.9)$$
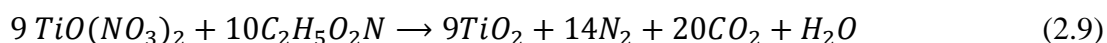
The above reaction indicates that 9 moles of titanyl nitrate reacts with 10 moles of glycine to yield 9 moles of TiO_2 and nearly 60 moles of gaseous products. The evolution of such high amounts of gases results in high porosity and hence, high surface area of TiO_2. Moreover, low overall temperature results in the formation of anatase phase TiO_2. In the present study, TiO_2 nanoparticles were prepared by

different methods and photocatalytic activity of as synthesized TiO_2 nanoparticles was compared with Ag@TiO_2 photocatalyst.

2.4.2.2 Preparation of Ag doped TiO_2

Catalyst modification by doping with metal or transition metal ion is an approach to enhance the photocatalytic activity. Since 1980s, catalyst has been modified mainly by metal loading to achieve a better photocatalytic activity (Morikawa et al. 2004). Besides, a successful doping by transition metal ion also showed improvement in the photocatalytic system (Davydov et al. 2003). There are many methods available for the preparation of doped TiO_2 which includes sol gel (Rupa et al. 2009; Zhang et al. 2008), hydrothermal (Jeong et al. 2008), liquid impregnation (Sahoo et al. 2005, Behnajady et al. 2008) and photodeposition (Behnajady et al. 2008).So in the present study, Ag doped TiO_2 nanoparticles were prepared by different methods and photocatalytic activity of as synthesized Ag doped TiO_2 nanoparticles was compared with Ag@TiO_2 photocatalyst.

2.5 Characterization of nanoparticles

In nanotechnology, materials show unique properties as compared to bulk counterparts when size are reduced to nano level. To understand the potential application of nanoparticles, a deeper knowledge of properties and characteristics is needed. For engineered nanoparticles to be useful in photocatalysis applications, it is very important to characterize them. Careful investigation of characterization is crucial in order to find the properties of the engineered nanoparticles.

For nanoparticle characterization, large number of techniques can be employed and common techniques are Transmission Electron Microscopy (TEM), Scanning Electron Microscopy (SEM), Atomic Force Microscopy (AFM), Energy dispersive Analysis (EDS), X-ray diffraction (XRD), Diffuse Reflectance Spectroscopy (DRS), Thermal properties and surface area analysis (Tiede et al. 2008). Structural characterization of nanoparticles is usually done with TEM (Pradeep 2010), AFM (Dror 1994), and XRD (Pradeep 2010) to determine the morphology (structure

and shape), size and crystallinity of engineered nanoparticles. For optical characterization of powder samples, DRS (Reddy et al. 2002) is usually preferred. Band gap energy can be determined using DRS (Murphy 2007). Thermo gravimetric-differential thermal analysis (TG-DTA) can be used to study thermal stability of materials at different temperature, construction of phase diagram and phase transition (Skoog et al. 2005). Surface area evaluation is very important in photocatalysis and BET surface area analysis method is used to find specific surface area of nanoparticles.

2.6 Factors affecting the photocatalytic degradation of dyes

Photocatalytic degradation of dyes depends upon the intrinsic and extrinsic (operational) factors. Intrinsic factors include the type and composition of catalyst used, calcination temperature and time.

Extrinsic (operational) factors include pH, catalyst loading, concentration, oxidant, light intensity and presence of interfering substances. Both these parameters affect the degradation of dyes and hence affect the efficiency. So understanding the effect of all these operational parameters on the photocatalytic efficiency is important from the operational and design point of view when selecting sustainable and efficient method for treatment of dyes.

2.6.1 Effects of intrinsic parameters on the photocatalytic degradation of dyes

2.6.1.1 Effect of catalyst composition

Photocatalytic activity of TiO_2 is dependent on the catalyst composition. Catalyst compositions play an important role in the photocatalytic degradation of dyes. In case of doping, dopant concentrations play an important role in the photocatalytic degradation. Behnajady et al. (2008) prepared silver doped TiO_2 nanoparticles by liquid impregnation and photo deposition methods with different amounts of silver (0.5-2.5% mole ratio) deposited on TiO_2 surface for determining optimum metal loading and also to compare the activity of the silver doped TiO_2 prepared with

different methods for the photocatalytic degradation of Acid Red 88. He found that rate of degradation increased with an increase in the silver loading up to optimum loading of 2 % in Liquid impregnation and 0.5 % in photodeposition beyond which the rate decreased, which was due to, (i) the formation of number of photogenerated e^- and h^+ pairs reduce due to the limitation of amount of light reaching the catalyst surface with too much coverage of TiO_2 and consequently reduce the photocatalytic efficacy of TiO_2 (Carp et al. 2004). (ii) the active sites for the desired photocatalysis on the TiO_2 surface may be occupied by metal deposits which results in decrease in photocatalytic activity (Coleman et al. 2005). (iii) high Ag loadings results in recombination, as negatively charged Ag start attracting holes and consequently holes recombine with electrons (Carp et al. 2004). (iv) with excessive concentration of Ag, the possibility of the hole capture increases as a result possibility of holes reacting with adsorbed species at the TiO_2 surface reduces (Sobana et al. 2006).

Liu et al. (2003) studied the effect of silver content (0-0.46 atomic %) on doping of TiO_2 for the photocatalysis of Methyl Orange and found that 0.05 atomic % Ag doped TiO_2 exhibited the highest rate of degradation, while further increase in Ag content decreased the rate of degradation. Sobana et al. (2006) investigated the effect of (0-2 atomic %) in Ag doped TiO_2 on photocatalytic degradation of Direct Red 23 and found that 1.5 % of Ag was optimum to achieve the highest photocatalytic efficiency.

In case of core-shell structures, by varying the ratio of core diameter and shell thickness, large shift in the optical emission and absorption has been reported (Chen et al. 2004). Rayford et al. (2005) studied the optical properties of gold nanospheres and observed when the shell thickness of a core/shell particle is decreased; the plasmon resonance shifts to longer wavelengths (red) and become more intense. Increasing the ratio of core radius to total radius causes the peak to shift towards red. Thinning the shell layer produces a large increase in polarization at the sphere boundary, which yields the more intense extinction peaks. The same general trends are observed when the nanoparticle size was increased. Catalyst composition helps in the formation of uniform core-shell structures (Vaidya et al. 2010). To obtain uniform core-shell structures, Vaidya et al. (2010) synthesized Ag@TiO_2 core–shell structures utilizing two step method, by varying shell thickness and controlling the size of the

core by changing [H_2O] to [surfactant] ratio and found Ag:Ti::1:0.67 ratio optimum for uniform core–shell nanostructures. Dang et al. (2010) studied the effect of shell-layer thickness on dielectric properties in Ag@TiO_2 core-shell nanoparticles filled with ferroelectric poly (vinylidene fluoride) composites (PVDF) and discovered that the shell-layer thickness of the Ag@TiO_2 core-shell nanoparticles had a crucial effect on the dielectric properties of Ag@TiO_2/PVDF nanocomposites. The variation of dielectric properties of the nanocomposites with temperature also depended on the shell-layer thickness of Ag@TiO_2 core-shell nanoparticles. Angkaew and Limsuwan (2012) studied the effect of Ti to Ag molar ratio on preparation of two step synthesized Ag@TiO_2 nanoparticles. They reported that at low concentration of titanium tetraisopropoxide (TTIP) precursor salt for Ti, TiO_2 can be effectively formulated on Ag nanoparticles which lead to the formation of core-shell structure but higher concentration lead to formation of core-shell particles with larger shell thickness. However, in their studies, too high concentration of TTIP lead to the composite structure with Ag nanoparticles embedded in TiO_2 matrix. According to them, the effect of Ag-Ti mole ratio on the morphology of nanoparticles can be explained in terms of the available nucleation sites and growth of titania particles on the pre-existing surface of silver nanoparticles. Since it was found that catalyst composition has a profound effect on the optical, photocatalytic properties and in controlling the morphology of photocatalyst, it was proposed to vary the concentration of TTEAIP and $AgNO_3$ in the synthesis mixture for optimization of Ag to Ti molar ratio to facilitate the formation of Ag core and TiO_2 shell and to achieve high photocatalytic activity.

2.6.1.2 Effect of calcination temperature and time

Calcination temperature is important in shaping and in improving the activity of catalyst. It affects the catalytic efficiency of photocatalyst. Decolorization and degradation of pollutants increase if the calcination temperature of catalyst increased. It is well known from the literature that calcination temperature is an important factor that perhaps influences the crystallinity, morphology, and surface area of catalyst nanoparticles. Photocatalytic activity can be affected by calcination temperature

(Sathish et al. 2007; Li et al. 2005). Enhancing calcination temperature improves the crystallization of TiO_2 (Wang et al. 2005; Kominami et al. 2003) which helps in the improvement of photocatalytic activity of TiO_2 (Yu et al. 2003; Wang et al. 2005; Ovenstone 2001; Kominami et al. 2003). A better crystallization means, decrease of crystal defects, which are the recombination centers of photo-induced charge carries (Yu et al. 2007 a,b; Yu et al. 2005; Mrowetz et al. 2004; Jung et al. 2005; Liqang et al. 2006). Phase transformation of TiO_2 depends on the calcination temperature and catalyst composition (Zhang and Reller 2002). Jian-Hua and Hai-Jun (2009) noticed the effect of calcination temperature (300-500 ˚C) on the photocatalytic degradation of Congo Red dye using TiO_2 coated on coal cinder. They found that, as the calcination temperature increased, degradation increased but further increase in the calcination temperature decreased the photocatalytic efficiency. They reported that it was due to the increase in content of anatase in TiO_2 arrays, with increasing heat treatment temperature. According to Tao et al. (2005), near 500 °C the rutile phase emerges, and the content of rutile increases as the temperature increases. It is widely accepted that the anatase phase of titania is a relatively ideal photocatalytic material among its three crystalline phases (Ovenstone and Yanagisawa 1999). In addition, the anatase with a small fraction of rutile shows enhanced photocatalytic activity compared to the pure anatase due to the electron and hole transfer between the two phases (Ozawa et al. 2005). Bickley et al. (1991) presented that the mixed crystal has higher catalytic activity compared to the pure anatase and rutile. So, catalyst calcined at 500 °C showed better photocatalytic efficiency. They reasoned it as, the mixed crystal facilitating the separation and preventing the recombination of holes with electrons. Saepurahman et al. (2010) studied the effect of calcination temperature (450-850 ºC) on the photocatalytic degradation of Methyl Orange, Methyl Violet and Methylene Blue dye using tungsten loaded TiO_2 and compared with unmodified TiO_2. With increasing temperatures, the anatase fraction of unmodified TiO_2 was decreasing rapidly from 650 ºC onwards. In unmodified TiO_2 with increase in calcination temperature from 450-650 ºC the ratio of anatase fraction reduced from 0.82 to 0.06 which confirmed that anatase to rutile phase transformation took place at around 500–650 ºC. Their results were comparable to the earlier reported range for phase transformation from anatase to rutile at 500–600 ºC (Fernandes-Machado and Santana

2005). Above 550 ºC calcination temperature, the photocatalytic activity decreased and further increase in temperature to 650 ºC or higher resulted in more reduction with unmodified TiO_2. Anatase phase of TiO_2 was detected with 1 mol % of tungsten loaded TiO_2 at calcination temperature of 750 ºC, but above this temperature no anatase phase was observed due to transformation process. High photocatalytic activity was observed with 1 mol % of WO_3 at calcination temperature of 550 ºC and only slight decrease occurred at 650 ºC but above this temperature significant reduction was seen with calcination temperature of 750 and 850 ºC. With 6.5 mol % of WO_3, major anatase phase was observed at calcination temperature as high as 850 ºC, which may be due to increase in tungsten loading stabilize the transformation process of conversion of anatase phase into rutile (Saepurahman et al. 2010). Huang et al. (2008) investigated the effect of calcination temperature on the UV photocatalytic degradation of Methyl Orange dye using Pt doped TiO_2 and found with increase in calcination temperature from 110 °C to 500 °C, the rate of decolourization decrease from around 73 to 31 %. With 1.5 % Pt loading, rate of decolorization decreases from around 88 to 43 % with increase in temperature from 110 °C to 500 °C. Authores explained that this phenomenon was due to conversion of anatase phase of TiO_2 and accumulation of catalyst particles which decreased the specific surface areas of catalyst, resulting in the reduction of photocatalytic activity. Ubonchonlakat et al. (2008) examined the effect of calcination temperature (400-600 ºC) on the degradation of Methylene blue dye using Ag doped TiO_2 coated on tile substrate. In the presence of Ag doped TiO_2 optimum calcination temperature was 500 °C for the degradation of Methylene blue. Behnajady et al. (2008) studied the effect of calcination temperature (500-900 ˚C) on the degradation of Acid red 88 dye using Ag doped TiO_2 catalyst. They found that the rate constant decreases with increase in the calcination temperature. They also attributed this behavior to the transformation of anatase to the rutile phase, which has a little photocatalytic activity. Mozia (2008) examined the effect of calcination temperature (600-800 ºC) on the degradation of mono and poly azo dyes using TiO_2 catalyst. The high rate of degradation of dyes were observed with catalyst calcined at 700 ºC for 1 h and rate of degradation decreased when calcined at 700 ºC for 2 to 4 h. With catalyst calcined at 700 ºC lowest rate of degradation was observed. They explained that, increase in calcination

temperature results in increase in crystallite size of anatase phase and decrease in specific surface area; but further increase in temperature results in phase transformation from anatase to rutile followed by a considerable decrease of the specific surface area (Mozia 2008). The rate of photocatalysis depends upon the anatase content and crystallite size. The photocatalyst calcined at 700 ℃ for 1 h, consisted 97 % of anatase content with crystallite size of 27 nm and samples calcined at 700 °C for 2 to 4 h consisted 94 % of anatase with crystallites of 28 – 30 nm (Mozia 2008). Photocatalytic activity was found to be higher with the catalyst containing higher anatase content and lower crystallite size. The photocatalyst calcined at 800 °C showed lowest rate due to the presence of rutile phase. Yang et al. (2008) tested the effect of calcination temperature (573-873 K) on the photocatalytic degradation of Rhodamine B and methyl ter-butyl ether using Silver and Indium Oxide codoped TiO_2 nanocomposites. According to their studies, the UV–photocatalytic activity was enhanced as the calcination temperature increased from 573 to 723 K. Further increasing the temperature to 873 K resulted in the decreased activity. Periyat et al. (2009) investigated the effect of calcination temperature (700-900 °C) on the UV and visible light induced photocatalytic degradation of Rhodamine 6G using N and S codoped TiO_2. All the samples calcined at different temperatures showed significantly higher photocatalytic efficiency compared to the control titania prepared under identical condition. The photocatalytic activities of these codoped samples were also compared with that of the Degussa P25 photocatalyst. The highest photocatalytic activity was obtained for sample calcined at 850 °C. This sample showed higher photocatalytic activity than the Degussa P25 sample, both under UV/visible and visible light. Wang et al. (2008c) examined the effect of calcination temperature (400-900 °C) on the visible light driven photocatalytic degradation of indigo carmine using Bi and S codoped TiO_2. They observed a decrease in catalytic activity with increase in calcination temperature. They have reported that, the trend was because of higher calcination temperature, which gave rise to blue-shifted absorption and the reduced oxygen vacancies caused by higher crystallinity. Consequently, the photocatalytic activity declined because of the limited utilization of visible light. Wang et al. (2008d) tested effect of calcination temperature on the photocatalytic degradation of Basic Violet 10 using TiO_2 catalysts supported by Y

Zeolite under UV light. It was found that photodegradation efficiency increased with increasing calcination temperature and optimum temperature was found to be 600 °C. According to these authors, the sharp decrease in photocatalytic degradation rate for the catalyst treated at 700 °C may have two causes: one is overgrowth of the TiO_2 crystallite size and the other the existence of a rutile phase in the TiO_2 crystal. You et al. (2005) investigated the effect of calcination temperature (573-973 K) on the photocatalytic degradation of Methyl Orange using TiO_2 as catalyst. The photocatalytic activity increased as the calcination temperature was increased from 573 K to 673 K and reached a maximum at a calcination temperature of 673 K, but further increase in calcination temperature then decreased the photocatalytic activity significantly. The low activity shown at 573 K was reported to be due to low crystallinity, though it had a smaller particle size. On the other hand, above 673 K, lower photocatalytic activity is due to the phase transformation of TiO_2 and increased crystallite size. Thus calcination temperature of 673 K was found to be optimum.

Calcination time affects the catalytic efficiency of photocatalyst. Hua et al. (2009) found the effect of calcination time (3-7 h) on the photocatalytic degradation of Methyl Orange dye by cobalt doped titania. He found that as the calcination time increased, the photocatalytic activity was higher. However, the optimum time was 5 h by considering energy resource. Mozia (2008) investigated the effect of calcination time (1-4 h) on the degradation of mono and poly azo dyes using TiO_2 catalyst. The anatase crystallite size slightly increased with increase in the calcination time and ranged from 19 to 21 nm. As per their studies, as calcination time increases anatase to rutile ratio increases and degradation decreases. Optimum time was found to be 1 h. Wang et al. (2010) studied the effect of calcination time on photocatalytic activity of an Er^{3+}:$YAlO_3$/ZnO–TiO_2composite for the degradation of Acid Red B after 30.0 min solar light irradiation. Along with the increase of heat-treatment time at 500 ºC, descending adsorption ratio was observed and the degradation ratio was ascending. This shows that the crystallization grade of ZnO–TiO_2 composite and integration between Er^{3+}:$YAlO_3$ and ZnO–TiO_2 is intensified with the increase of heat-treatment time. You et al. (2005) studied the effect of calcination time (1-10 h) on the photocatalytic degradation of Methyl Orange using TiO_2 as catalyst. It was found as calcination time increased the photocatalytic activity increased and reaches a

maximum at 2 h, but further increase in time decreased the photocatalytic activity. It may be due to the high crystallinity of TiO_2 at 2 h but with increase in time crystallite size increases there by reducing surface area. Therefore 2 h was found to be optimum time for the photocatalytic activity. Since it was found that calcination temperature and time has a profound effect on the crystallinity and phase conversion, it was proposed to carry out the catalyst optimization in the currently reported study to enhance photocatalytic efficacy, by varying the calcination temperature and time.

2.6.2 Effect of extrinsic (operational) factors

Rate of photocatalysis of dyes and hence the photocatalysis process efficiency is influenced by various factors such as pH, catalyst loading, concentration of dyes, types of oxidants and their concentration and light intensity.

2.6.2.1 Effect of pH

pH can play an important role in photocatalysis because rate of degradation of dyes can be enhanced by increasing or decreasing pH of the reaction mixture. This is due to the fact that pH influences the adsorption of dye molecules on the TiO_2 surface, which is an important step in photodegradation (Neppolian et al. 2002b; Akpan and Hameed 2009). The point of zero charge (pzc) of the TiO_2 is 6.8 (Muruganandham and Swaminathan 2004). Due to the amphoteric nature of TiO_2, its surface remains positively charged in acidic medium (pH<6.8) and negatively charged in alkaline medium (pH>6.8), as shown in the following equations (Muruganandham and Swaminathan 2004).

$$pH < pzc: Ti - OH + H^+ \rightarrow TiOH_2 \qquad (2.10)$$

$$pH > pzc: Ti - OH + OH^- \rightarrow TiO^- + H_2O \qquad (2.11)$$
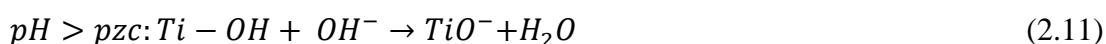
The pH change also effects the formation of the hydroxyl radicals by the reaction between hydroxide ions and positive holes. At low pH, the positive holes act as the predominant oxidation species whereas at neutral or high pH levels hydroxyl radicals act as the major species (Sakthivel et al. 2003). Hydroxyl radicals are easily generated in alkaline pH by oxidizing more hydroxyl ions available on TiO_2 surface,

thus the efficiency of the process is logically enhanced (Galindo et al. 2000). Similar results have been shown in the photocatalysed degradation of acidic azo dyes and triazine containing azo dyes (Neppolian et al. 2002a) although it should be noted that in alkaline pH there is columbic repulsion between the negative charged surface of photocatalyst and the hydroxide anions. This would prevent the generation of hydroxyl radicals and thus decrease the photodegradation. Very high pH has been found favorable even when anionic azo dyes should hamper adsorption on the negatively charged surface (Mills et al. 1993). Reduction by electrons in conduction band may play a very important role in the dye degradation at low pH due to the reductive cleavage of azo bonds. The surface area available for dye adsorption and photon absorption would be reduced due to agglomeration of TiO_2 particles under acidic pH (Bahnemann et al. 1994). Rupa et al. (2007) tested the effect of pH in the range of 2-13; on the photocatalytic degradation of Reactive Yellow-17 using Ag doped TiO_2 under UV and visible light and found that degradation of dye increased up to neutral pH and decreased thereafter for both visible and UV light. pH of 7 and 8 was found to be optimum owing to maximum degradation of dye under UV and visible light, respectively. At highly acidic conditions decrease in degradation was attributed to the dissolution of TiO_2. However, they found that above pH 9 reduction in degradation efficacy is due to columbic repulsion between the negatively charged dye surface and the hydroxyl anions. Sohrabi et al. (2009) tested the effect of pH in the range of 2-11, on the photocatalytic degradation of Benzidien Yellow. 100 % degradation after 60 min was obtained at pH of 2. It was explained that if carbonyl groups of the dye have negative and positive charged groups in its structure, the acidic solution favours adsorption of dye onto the photocatalyst surface. Maximum degradation was reported at pH of 3 by Sobana and Swaminathan (2007) and Wang et al. (2009) in their studies on the photocatalytic degradation of Direct Blue 53 and Acid Red B respectively under solar light. They explained that, it is due to the surface chemical state of TiO_2 and the ionization state of organic dye molecules at a certain pH. A summary of photocatalytic degradation of various dyes studied at different pH is given in Table 2.6. The review of literature supports the influence of pH on photocatalytic degradation of dyes and hence it is important to optimize the pH conditions.

Table 2.6 Effect of initial pH on the photocatalysis of dyes.

Dyes	Illumination Source	Catalyst used	Range of pH used	Optimum initial pH	References
Acid Red 14	UV	TiO_2	1-11	3	Abo-Farha (2010)
Acid Orange 10	UV	TiO_2	1-11	3	Abo-Farha (2010)
Acid Red 1	UV	Ca ion doped TiO_2	3-10	3	Akpan and Hameed (2011)
Methyl Orange	UV	TiO_2	1-12	3	Bouanimba et al. (2013)
Malachite green	UV	TiO_2	3-9	9	Chen et al. (2007)
Acridine Orange	UV	TiO_2	3-10	10	Faisal et al. (2007)
Ethidium Bromide	UV	TiO_2	3-10	4.6	Faisal et al. (2007)
Remazol Red 133	UV	TiO_2	3-9.5	3	Gumus and Akbal (2011)
Tartrazine	UV	TiO_2	2.2-11	11	Gupta et al. (2011)
Amaranth	UV	TiO_2	2.4-9.6	2.4	Gupta et al. (2012b)
Quinoline yellow	UV	TiO_2	3.8-11.5	11.5	Gupta et al. (2012a)
Reactive Yellow-125	UV/Vis	Zeolite modified with N-doped TiO_2	3-9	3	Ilinoiu et al. (2013)
Amido Black-10B	UV	TiO_2	2-10	5.6	Joice et al. (2012)
Acid Yellow 17	UV	TiO_2	3-11	3	Liu et al. (2006)
Reactive Orange 4	Solar	TiO_2	1-9	9	Muruganandham and Swaminathan (2004)
Reactive Orange 4	UV	TiO_2	1-12	10	Muruganandham and Swaminathan (2006a)

Table 2.6 Contd.

Dyes	Illumination Source	Catalyst used	Range of pH used	Optimum initial pH	References
Reactive Black 5	Solar	TiO$_2$	3-9	9	Muruganandham et al. (2006)
Rhodamine B	UV-LED	TiO$_2$	2.05-8.02	4.33	Natarajan et al. (2011)
Disperse Yellow 23	UV	TiO$_2$ on Clinoptilolite	6-11	11	Nikazar et al. (2007)
Chrysoidine Y	UV	TiO$_2$	3-9	9	Qamar et al. (2004)
Chromotrope 2B	UV	TiO$_2$	3-9	9	Qamar et al. (2005a)
Amido black 10B	UV	TiO$_2$	3-9	9	Qamar et al. (2005a)
Chrysoidine R	UV	TiO$_2$	3-11	8.3	Qamar et al. (2005b)
Acid red 29	UV	TiO$_2$	3-11	10.5	Qamar et al. (2005b)
Acridine Orange	UV	Pt doped TiO$_2$	3.8-11.6	11.6	Qamar (2010)
Reactive Yellow-17	UV and Vis	Ag doped TiO$_2$	2-13	7 and 8	Rupa et al. (2007)
Methylene Blue	UV	W loaded TiO$_2$	3-10	5.1	Saepurahman et al. (2010)
Remazol Brilliant Blue R	UV	TiO$_2$	3-11	9	Saquib and Muneer (2002)
Remazol Brilliant Blue R	Sunlight	TiO$_2$	3-11	3	Saquib and Muneer (2002)
Gentian Violet	UV	TiO$_2$	3-11	3	Saquib and Muneer (2003a)
Acid Orange 8	UV	TiO$_2$	3-11	9	Saquib and Muneer (2003b)
Fast Green	UV	TiO$_2$	3-11	4.4	Saquib et al. (2008)
Acid Blue 1	UV	TiO$_2$	3-11	11	Saquib et al. (2008)
Direct Red 23	UV	Ag doped TiO$_2$	4-10	6	Sobana et al. (2006)

Table 2.6 Contd.

Dyes	Illumination Source	Catalyst used	Range of pH used	Optimum initial pH	References
Direct Red 23	UV	TiO_2	2-9	2	Sohrabi and Ghavami (2008)
Benzidien Yellow	UV	TiO_2	2-11	2	Sohrabi et al. (2009)
Direct Yellow 12	UV	TiO_2	2-11	3	Sohrabi and Ghavami (2010)
Direct Blue 78	Sunlight	TiO_2	3-9	3	Song et al. (2010)
Amaranth	UV	TiO_2	3-10	7.73	Tariq et al. (2005)
Bismarck Brown	UV	TiO_2	3-10	3.25	Tariq et al. (2005)
Acid Blue 45	UV	TiO_2	2-10	5.8	Tariq et al. (2008)
Direct Yellow 12	UV	TiO_2	4.5-11	4.5	Toor et al. (2006)
Basic Violet 10	UV	TiO_2 supported by Y zeolite	4-10	9	Wang et al. (2008d)
Acid Red B	Solar	$Er^{3+}:YAlO_3/ZnO-TiO_2$	3-11	3	Wang et al. (2010)

2.6.2.2 Effect of catalyst loading

It is observed from reported literature, the rate of photocatalytic reaction increases with the catalyst loading, but after certain loading of the catalyst rate decreases and become independent of catalyst loading. Many authors have investigated the reaction rate as a function of catalyst loading under different experimental conditions (San et al. 2001; Gouvea et al. 2000; Saquib and Munner 2002). Qamar et al. (2005a) investigated the effect of catalyst loading (0.5-5 g/L) on the photocatalytic degradation of two selected dye derivatives, Chromotrope 2B and Amido Black 10B, using titanium dioxide as catalyst. They have found increase in the degradation rate for the mineralization and decomposition of the model compounds, increase with the

increase in catalyst loading. Soutsas et al. (2010) studied the effect of catalyst loading (0.5-1.5 g/L) on decolorization and degradation of reactive azo dyes via heterogeneous photocatalytic processes. However, they found that, further increase in catalyst loading (>1 g/L) does not lead to significantly higher decolorization efficiency. The catalyst amount has both positive and negative impact on the photodecomposition rate. The enhancement of the degradation rate with increase in catalyst loading has been attributed to (i) increase in the number of dye molecules adsorbed, with the increase in the amount of catalyst loading. Catalyst addition increases the active sites for dye adsorption on the photocatalyst surface as well as the free hydroxyl radical ($^{.}$OH) generation (Soutsas et al. 2010)   (ii) increase in the density of particles in the area of illumination (Muruganandham and Swaminathan 2004).

Higher amount of catalyst may not be useful both in view of possible aggregation as well as reduced irradiation field due to increase in light scattering (Wei and Wan 1991). Furthermore, rate may decrease as a result of loss in surface area available for light-harvesting occasioned by agglomeration (particle-particle interactions) at high solid concentration. These two opposite phenomena results in an optimum catalyst loading for the photocatalysis process (Adesina 2004). In order to avoid excess catalyst (Hermann 1999) and to increase absorption capacity of photons the optimum catalyst loading is necessary. Soutsas et al. (2010) studied the effect of catalyst loading (0.5-1.5 g/L) on decolorization and degradation of reactive azo dyes via heterogeneous photocatalytic processes. They reported that decolorization efficiency increases with increase in TiO_2 loading, especially up to 1 g/L and further increase in catalyst loading (>1 g/L) does not lead to significantly higher decolorization efficiency. A summary of photocatalytic degradation of various dyes studied at different catalyst loading is given in Table 2.7. The review of literature supports the influence of catalyst loading on photocatalytic degradation of dyes and hence it is important to optimize catalyst loading in order to avoid excess catalyst and to have maximum possible rate.

Table 2.7 Effect of catalyst loading on the photocatalytic degradation of dyes.

Dyes	Illumination Source	Photocatalyst			References
		Type	Range used (g/L)	Optimum loading (g/L)	
Acid Orange 10	UV	TiO_2	0.05- 0.2	0.2	Abo-Farha (2010)
Acid Red 14	UV	TiO_2	0.05-0.2	0.2	Abo-Farha (2010)
Procion Blue HERD	UV	TiO_2	0.5-2	1.5	Bansal and Sud (2011)
Procion Blue HERD	UV	ZnO	0.5-2	1	Bansal and Sud (2011)
Rhodamine B	Solar	ZnO	0.05-0.4	0.3	Byrappa et al. (2006)
Malachite green	UV	TiO_2	0.1-0.5	0.25	Chen et al. (2007)
Reactive Violet 5	UV	TiO_2	.01-0.1	.08	Chung and Chen (2009)
Acid Red 14	UV	ZnO	0-0.1	.04	Daneshvar et al. (2004)
Remazol Red 133	UV	TiO_2	0.5-3	3	Gumus and Akbal (2011)
Acridine Orange	UV	TiO_2	0.5-3	10	Faisal et al. (2007)
Ethidium Bromide	UV	TiO_2	0.5-3	2	Faisal et al. (2007)
Tartrazine	UV	TiO_2	0.02-0.2	0.18	Gupta et al. (2011)
Amaranth	UV	TiO_2	0.04-0.2	0.16	Gupta et al. (2012b)
Quinoline yellow	UV	TiO_2	0.02-0.12	0.1	Gupta et al. (2012a)
Reactive Yellow-125	UV/Vis	Zeolite modified with N-doped TiO_2	0.5-2	1	Ilinoiu et al. (2013)
Reactive Black 5	UV	ZnO	0.25 to 1.25	1.25	Kansal et al. (2009)
Reactive Orange 4	UV	ZnO	0.25 to 1.25	1	Kansal et al. (2009)

Table 2.7 Contd.

Dyes	Illumination Source	Photocatalyst			References
		Type	Range used (g/L)	Optimum loading (g/L)	
Biebrich Scarlet	UV	ZnO	0.25-1.25	0.75	Kansal et al. (2010)
Reactive Red 22	UV	$La_2Ti_2O_7$	0.5-3	2	Ku et al. (2011)
Reactive Orange 4	Solar	TiO_2	1-6	4	Muruganandham and Swaminathan, (2004
Reactive Yellow 14	Solar	TiO_2	1-6	4	Muruganandham and Swaminathan (2006b)
Reactive Orange 4	UV	TiO_2	1-6	4	Muruganandham and Swaminathan (2006a)
Reactive Black 5	Solar	TiO_2	1-3	2	Muruganandham et al. (2006)
Rhodamine B	UV-LED	TiO_2	0.4-2.8	1.6	Natarajan et al. (2011)
Disperse Yellow 23	UV	TiO_2 on Clinoptil-olite	-	.04	Nikazar et al. (2007)
Congo Red	UV and Vis	ZrO_2	0.2-1	0.7	Pouretedal and Hosseini (2010)
Chrysoidine Y	UV	TiO_2	0.5-5	5	Qamar et al. (2004)
Chrysoidine Y	UV	ZnO	0.5-5	5	Qamar et al. (2004)
Chromotrope 2B	UV	TiO_2	0.5-5	5	Qamar et al. (2005a)
Amido black 10B	UV	TiO_2	0.5-5	5	Qamar et al. (2005a)
Chrysoidine R	UV	TiO_2	0.5-5	5	Qamar et al. (2005b)
Acid red 29	UV	TiO_2	0.5-5	5	Qamar et al. (2005b)
Acridine Orange	UV	TiO_2	0.5-5	3	Qamar (2010)
Methylene Blue	UV	W loaded TiO_2	0-2	1	Saepurahman et al. (2010)

Table 2.7 Contd.

Dyes	Illumination Source	Photocatalyst			References
		Type	Range used (g/L)	Optimum loading (g/L)	
Remazol Brilliant Blue R	UV	TiO_2	0.5-5	2	Saquib and Muneer (2002)
Gentian Violet	UV	TiO_2	0.5-5	5	Saquib and Muneer (2003a)
Acid Orange 8	UV	TiO_2	0.5-5	2	Saquib and Muneer (2003a)
Fast Green	UV	TiO_2	0.5-4	4	Saquib et al. (2008)
Acid Blue 1	UV	TiO_2	0.5-4	4	Saquib et al. (2008)
Direct Red 23	UV	Ag doped TiO_2	1-5	3	Sobana et al. (2006)
Benzidien Yellow	UV	TiO_2	0.5-3	2	Sohrabi et al. (2009)
Direct Yellow 12	UV	TiO_2	1-6	5	Sohrabi and Ghavami (2010)
Direct Blue 78	Sunlight	TiO_2	0.2-2	1	Song et al. (2010)
Acid Blue 80	Sunlight	TiO_2	0.3-4	2	Su et al. (2009)
Amaranth	UV	TiO_2	0.5-6	4	Tariq et al. (2005)
Bismarck Brown	UV	TiO_2	0.5-6	1	Tariq et al. (2005)
Xylenol	UV	TiO_2	0.5-3	3	Tariq et al. (2006)
Acid Blue 45	UV	TiO_2	0.5-3	2	Tariq et al. (2008)
Direct Yellow 12	UV	TiO_2	0.5-3.5	2	Toor et al. (2006)
Acid Red B	Solar	$Er^{3+}:YAlO_3/ZnO–TiO_2$	0-12.5	12.5	Wang et al. (2010)

2.6.2.3 Effect of concentration of dyes

Initial concentration of a dye is an important parameter in the photocatalytic degradation of dyes. It was found that as the concentration increases rate of degradation decreases. A possible explanation for this is that as the initial concentration of the dye increases, the path length of the photons entering the solution decreases due to impermeability of the dye solution (Pare et al. 2008); a considerable quantity of light can be absorbed by the dye molecules rather than the catalyst and this may also decrease the catalytic efficiency because the concentrations of $OH^{\cdot}$ and $O_2^{\cdot-}$ decrease (Daneshvar et al. 2004; Tang and An 1995; Mills et al. 1993) which leads to a decreased photodegradation rate (Song et al. 2010). Another reason is with increase in dye concentration, adsorption of dye on catalyst surface also occur and hence the formation of $OH^{\cdot}$ radicals decreases because active sites of catalyst are covered by ions of dye and thus affects the catalytic activity of the catalyst. Hence, it was concluded by Neppolian et al. (2002a) that as initial concentration of the dye increases, the requirement of catalyst surface needed for the degradation also increase. Soutsas et al. (2010) studied the effect of dye concentration (50-250 mg/L) on heterogeneous photocatalytic decolorization and degradation of Reactive azo dyes and found that the decolorization efficiency (as %) decreases, while the amount of dye actually removed from the solution increases, with increase in the initial dye concentration from 50-250 mg/L. Kansal et al. (2006) investigated the effect of concentration (5-200 mg/L) of dyes on Methyl Orange (MO) and Rhodamine 6G (R6G). As the concentration of the dye was increased, the rate of photo decolorization decreased which indicated either to increase the catalyst dose or time span for the complete removal. A summary of photocatalytic degradation of various dyes studied at different concentrations is given in Table 2.8. Initial concentration of dye is an important parameter to be studied in photocatalytic degradation, so as to obtain the optimum concentration for a given catalyst loading or to obtain the catalyst loading required for the given initial concentration.

Table 2.8 Effect of concentration of dyes on the photocatalytic degradation of dyes.

Dyes	Light Source	Photocatalyst	Concentration range (mg/L)	Optimum dye concentration (mg/L)	References
Acid Orange 10	UV	TiO_2	452.37-45.23	4.52	Abo-Farha (2010)
Acid Red 14	UV	TiO_2	502.42-50.242	5.02	Abo-Farha (2010)
Procion Blue HERD	UV	ZnO	10-100	25	Bansal and Sud (2011)
Procion Blue HERD	UV	TiO_2	10-100	25	Bansal and Sud (2011)
Malachite green	UV	TiO_2	5-25	15	Chen et al. (2007)
Reactive Violet 5	UV	TiO_2	10-50	10	Chung, (2009)
Acid Orange 7	UV	ZnO	20-60	20	Daneshvar et al. (2007)
Acridine Orange	UV	TiO_2	26.53-132.67	66.33	Faisal et al. (2007)
Ethidium Bromide	UV	TiO_2	39.43-197.15	39.43	Faisal et al. (2007)
Tartrazine	UV	TiO_2	10.69-42.75	32.06	Gupta et al. (2011)
Amaranth	UV	TiO_2	12.09-60.46	48.37	Gupta et al. (2012b)
Quinoline yellow	UV	TiO_2	13.9-41.70	37.07	Gupta et al. (2012a)
Reactive Yellow-125	UV/Vis	Zeolite modified with N-doped TiO_2	25-100	25	Ilinoiu et al. (2013)
Rhodamine 6G	UV	ZnO	5-200	25	Kansal et al. (2006)
Rhodamine 6G	UV	ZnO	0.25-2	0.5	Kansal et al. (2006)
Reactive Black 5	UV	ZnO	10-100	25	Kansal et al. (2009)

Table 2.8 Contd.

Dyes	Light Source	Photocatalyst	Concentration range (mg/L)	Optimum dye concentration (mg/L)	References
Biebrich Scarlet	UV	ZnO	5-100	25	Kansal et al. (2010)
Reactive Red 22	UV	$La_2Ti_2O_7$	5-30	10	Ku et al. (2011)
Reactive Orange 4	Solar	TiO_2	63.1-694.53	315.7	Muruganandham and Swaminathan (2004)
Reactive Orange 4	UV	TiO_2	63.1-694.53	315.7	Muruganandham and Swaminathan (2006a)
Reactive Black 5	Solar	TiO_2	76.37-687.33	381.85	Muruganandham et al. (2006)
Rhodamine B	UV	ZnO	10-30	10	Nagaraja et al. (2011)
Disperse Yellow 23	UV	TiO_2 on Clinoptilolite	20-80	20	Nikazar et al. (2007)
Basic Blue 9	UV	CoS/AlMCM-41	0.25-3.5	3.2	Pourahmad et al. (2010)
Chrysoidine Y	UV	ZnO	31.08-248.71	186.53	Qamar et al. (2004)
Chromotrope 2B	UV	TiO_2	128.34-385.02	179.67	Qamar et al. (2005a)
Amido black 10B	UV	TiO_2	154.13-462.39	154.13	Qamar et al. (2005a)
Chrysoidine R	UV	TiO_2	28.96-203.65	101.82	Qamar et al. (2005b)
Acid red 29	UV	TiO_2	117.09-351.29	117.09	Qamar et al. (2005b)
Acridine Orange	UV	TiO_2	39.8-132.67	66.33	Qamar (2010)
Reactive Yellow17	UV/Vis	Ag doped TiO_2	6.83-34.15	6.83	Rupa et al. (2007)
Methylene Blue	UV	W loaded TiO_2	10-60	10	Saepurahman et al. (2010)

Table 2.8 Contd.

Dyes	Light Source	Photocatalyst	Concentration range (mg/L)	Optimum dye concentration (mg/L)	References
Remazol Brilliant Blue R	UV	TiO_2	75.18-313.27	156.63	Saquib and Muneer (2002)
Remazol Brilliant Blue R	Sunlight	TiO_2	75.18-313.27	75.18	Saquib and Muneer (2002)
Gentian Violet	UV	TiO_2	73.43-203.98	101.99	Saquib and Muneer (2003a)
Acid Orange 8	UV	TiO_2	43.72-182.17	91.08	Saquib and Muneer (2005a)
Fast Green	UV	TiO_2	25.07-101.11	25.07	Saquib et al. (2008)
Acid Blue 1	UV	TiO_2	36.26-101.99	36.26	Saquib et al. (2008)
Direct Red 23	UV	TiO_2	2-5	4	Sohrabi and Ghavami (2008)
Acid Blue 80	Sunlight	TiO_2	20.36-135.73	20.36	Su et al. (2009)
Amaranth	UV	TiO_2	148.34-296.69	247.24	Tariq et al. (2005)
Bismarck Brown	UV	TiO_2	125.79-251.59	251.59	Tariq et al. (2005)
Acid Blue 45	UV	TiO_2	142.99-284.59	142.99	Tariq et al. (2008)
Xylenol	UV	TiO_2	201.80-403.60	336.33	Tariq et al. (2008)
Direct Yellow 12	UV	TiO_2	100-500	100	Toor et al. (2006)
Basic Violet 10	UV	TiO_2 supported by Y zeolite	10-100	10	Wang et al. (2008d)
Acid Red B	UV	Er^{3+}:$YAlO_3$/ZnO–TiO_2	5-25	5	Wang et al. (2010)

2.6.2.4 Effect of Oxidants

UV photocatalytic process suffers from a relatively low apparent quantum yield due to the rapid recombination of photogenerated electrons and holes. In irradiated photocatalyst suspensions, oxygen on the TiO_2 surface provides a natural sink for the electrons generated. OH radicals form via the oxidation of H_2O adsorbed on TiO_2 surface or hydroxyl ions by the surviving holes (Jung et al. 2009).

Addition of oxidants can enhance the degradation rate in several ways (Muruganandham and Swaminathan 2004; Muruganandham and Swaminathan 2006a; Muruganandham and Swaminathan 2006b; Qamar et al. 2005a; Qamar et al. 2005b; Faisal et al. 2007; Rupa et al. 2007; Su et al. 2009): (i) When O_2 is used as an oxidant, it was found that the rate of photocatalysis increases. The increase in degradation in presence of O_2 is due to decrease in rate of electron–hole recombination by adsorption of O_2 on the catalyst surface (Paola et al. 2003; Silva and Faria 2003). (ii) O_2 is the source of hydroxyl radicals and organic peroxides which are significant species for the degradation of dyes and intermediates and hence formation of these radicals depends on O_2. (iii) By preventing oxygen reduction. Molecular oxygen is most commonly used in heterogeneous catalysis. When O_2 is used as an oxidant, it was found that the rate of photocatalysis increases.

Mirkhani et al. (2009) investigated photocatalytic degradation of dyes in the presence of different flow rates of oxygen and results indicated that the presence of O_2 is necessary. Gupta et al. (2006) investigated the photocatalytic degradation of a mixture of Crystal Violet (Basic Violet 3) and Methyl Red dye. The degradation of dyes decreased under limited supply of O_2 which indicated O_2 is essential for the photocatalysis process to occur.

The introduction of a more effective electron acceptor than oxygen may be beneficial (Jung *et al*. 2009). As hydroxyl radicals play an important role, besides the addition of molecular oxygen, many authors have studied the effect of other oxidants such as H_2O_2, $(NH_4)_2S_2O_8$ and $KBrO_3$ on the photocatalytic degradation of different dyes

(Muruganandham and Swaminathan 2004 and 2006 a, b; Qamar et al. 2005a; Rupa et al. 2007; Su et al. 2009; Faisal et al. 2007).

Muruganandham and Swaminathan (2004) studied the effect of addition of H_2O_2 (5-20 mM) on the photocatalytic degradation of Reactive Orange 4 using TiO_2 nanoparticles and found as concentration of H_2O_2 (5-15 mM) was increased, degradation rate increased, but rate of degradation started decreasing with further increase in concentration of H_2O_2 to 20 mM. They proposed that the increase of degradation is due to an increase in the hydroxyl radical concentration and decrease is due to scavenging effect of hydroxyl radical as shown by the following equations:

$$H_2O_2 + e^-_{(CB)} \xrightarrow{h\upsilon} HO^{\cdot} + OH^- \qquad\qquad (2.12)$$

$$H_2O_2 \rightarrow 2HO^{\cdot} \qquad\qquad (2.13)$$

H_2O_2 can also react with superoxide anion to form $^{\cdot}OH$ radical

$$H_2O_2 + O_2^- \rightarrow HO^{\cdot} + OH^+ + O_2^{\cdot} \qquad\qquad (2.14)$$

$$H_2O_2 + HO^{\cdot} \rightarrow HO_2^{\cdot} + H_2O \qquad\qquad (2.15)$$

$$HO_2^{\cdot} + HO^{\cdot} \rightarrow H_2O + O_2^{\cdot} \qquad\qquad (2.16)$$

Table 2.9 shows the summary of effect of H_2O_2 concentration on the photocatalytic degradation of dyes.

Table 2.9 Effect of H_2O_2 concentration on the photocatalytic degradation of dyes.

Dyes	Light Source	Catalyst used	Range of C_{H2O2} used (mM)	Optimum C_{H2O2} (mM)	References
Remazol Black 5	UV	TiO$_2$	5-20	15	Chen et al. (2012)
Remazol Brilliant Orange 3R	UV	TiO$_2$	5-20	15	Chen et al. (2012)
Amaranth	UV	TiO$_2$	1-3	2.25	Gupta et al. (2012b)
Tartrazine	UV	TiO$_2$	0.2-1.5	1.5	Gupta et al. (2011)
Rhodamine B	UV	TiO$_2$	1-5	5	Natrajan et al. (2011)
Acid Red 14	UV	TiO$_2$	5-100	50	Abo-Farha (2010)
Acid Orange 10	UV	TiO$_2$	5-100	50	Abo-Farha (2010)
Acid Blue 80	Solar	TiO$_2$	1-7	5	Su et al. (2009)
Direct Red 23	UV	Ag doped TiO$_2$	5-20	10	Sobana et al. (2008)
Reactive Yellow17	UV/ Vis	Ag doped TiO$_2$	5-20	10	Rupa et al. (2007)
Reactive Orange 4	UV	TiO$_2$	5-20	10	Muruganandham and Swaminathan (2006a)
Acid Orange 7	UV	ZnO	4-20	10	Daneshvar et al. (2006)
Methyl Orange	UV	Pelagite	2-12	6	Chen et al. (2006)
Reactive Orange 4	Solar	TiO$_2$	5-20	15	Muruganandham and Swaminathan (2004)
Reactive Yellow 17	UV	TiO$_2$	10-40	30	Neppolian et al. (2003)
Acid Red 14	UV	ZnO	1-15	10	Daneshvar et al. (2003)

When $(NH_4)_2S_2O_8$ was used as an oxidant by Muruganandham and Swaminathan (2004 and 2006b) for the photocatalytic degradation of Reactive Orange 4 and Reactive Yellow 14 using TiO_2 nanoparticles, it was found that the rate of degradation increased with the increase in concentration of $(NH_4)_2S_2O_8$ upto certain level and then decreased with the increase in its concentration. They hypothesized that, the increase in degradation is attributed to the inhibition of electron–hole recombination and production of other oxidizing species such as sulphate radical anion (Chen et al. 2007). The sulphate radical anion (SO_4^{-}) is a very strong oxidant and it may react with photogenerated electron and with water molecule which results in production of hydroxyl radical as shown by the following equations:

$$S_2O_8^{2-} + e^-{}_{(CB)} \rightarrow SO_4^{\bullet-} + SO_4^{2-} \qquad (2.17)$$

$$SO_4^{\bullet-} + e^-{}_{(CB)} \rightarrow SO_4^{2-} \qquad (2.18)$$

$$SO_4^{\bullet-} + H_2O \rightarrow SO_4^{2-} + HO^{\bullet} + H^+ \qquad (2.19)$$

At high concentration of $(NH_4)_2S_2O_8$ rate of degradation of dyes decreases due to the adsorption of sulphate anion (SO_4^{2-}) on catalyst surface. Also SO_4^{2-} may react with photogenerated holes and hydroxyl radical which results in formation of SO_4^{-}. Since SO_4^{-} is less reactive than $^{\bullet}OH$ radical and h^+ and hence decrease the degradation of the dye as explained by following equations:

$$SO_4^{2-} + h^+{}_{(VB)} \rightarrow SO_4^{\bullet-} \qquad (2.20)$$

$$SO_4^{2-} + HO^{\bullet} \rightarrow SO_4^{\bullet-} + OH^- \qquad (2.21)$$

Increase in the rate of degradation with increase in addition of $(NH_4)_2S_2O_8$ upto a certain value and then a decrease in degradation with further increase in addition of $(NH_4)_2S_2O_8$ was also observed by Sobana et al. (2008) in their studies on the photocatalytic degradation of Direct Red 23 using nano Ag doped TiO_2 under UV irradiation. They found that $(NH_4)_2S_2O_8$ concentration of 3 g/L is the optimum.

Increase in the rate of degradation of dyes with increase in concentration of persulfate has been reported for the photocatalytic degradation of Reactive Yellow17 using Ag doped TiO_2 (Rupa et al. 2007); Reactive Yellow 17 using TiO_2 (Neppolian et al. 2003), Acid Blue 80 using TiO_2 under solar light irradiation and during the photocatalytic degradation of Remazol Black 5 and Remazol Brilliant Orange 3R using mesoporous TiO_2 under UV irradiation (Chen et al. 2012).

KBrO$_3$ is an efficient electron acceptor and it has been exploited as an additive to enhance rate of photocatalytic degradation (Gratzel et al. 1990; Sanchez et al. 1998; Poulios and Tsachpinis 1999). When KBrO$_3$ was added degradation rate was found to increase with the increase in concentration of KBrO$_3$ upto certain level but further increase in concentration of KBrO$_3$, then leads to decrease in the rate of degradation. Increase in the degradation of dyes with increased addition of KBrO$_3$ and then a decrease in degradation with its further increases has been reported by Muruganandham and Swaminathan (2004) in their studies on the photocatalytic oxidation of Reactive Orange 4 under solar light and in studies by Sobana et al. (2008) on the photocatalytic degradation of Direct Red 23 using nano Ag doped TiO$_2$ under UV irradiation. Increase in degradation of the dyes with increased addition of KBrO$_3$ upto a certain concentration and then almost a constant value of degradation with further increase in KBrO$_3$ addition was reported by Muruganandham and Swaminathan (2006) in their studies on UV photocatalytic degradation of Reactive Yellow 14 and by Su et al. (2009) in the photocatalytic degradation of Acid Blue 80 using TiO$_2$ nanoparticles under solar light. Chen et al. (2012) examined the effect of KBrO$_3$ (5-20 mM) on the photocatalytic degradation of Remazol Black 5 and Remazol Brilliant Orange 3R using mesoporous TiO$_2$ under UV irradiation and found rate of degradation of both dyes increased with increase in concentration of KBrO$_3$ from 5 to 20 mM.

The enhancement of degradation rate is due to reduction of electron–hole recombination and formation of other radicals which helps in increasing the degradation rate as shown in equation (2.22).

$$BrO_3^- + 6e_{(CB)}^- + 6H^+ \rightarrow Br^- + 3H_2O \tag{2.22}$$
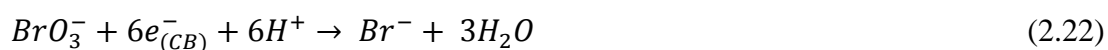
Further decrease is due to adsorption effect of Br$^-$ ion on catalyst surface which affects the catalytic activity (Muruganandham and Swaminathan 2004; Muruganandham and Swaminathan 2006 and Sobana et al. 2008).

2.6.2.5 Comparison of various oxidants

Various authors compared the effect of oxidants on the photocatalytic degradation of dyes. A summary of comparison of various oxidants on the photocatalytic degradation of dyes is given in Table 2.10.

Table 2.10 Comparison of various oxidants on the photocatalytic degradation of dyes.

Dye	Catalyst used	Oxidants used	Light Source	Activity	References
Remazol Black 5	TiO_2	H_2O_2, $KBrO_3$, $(NH_4)_2S_2O_8$	UV	$KBrO_3$>H_2O_2>$(NH_4)_2S_2O_8$	Chen et al. (2012)
Remazol Brilliant Orange 3R	TiO_2	H_2O_2, $KBrO_3$, $(NH_4)_2S_2O_8$	UV	$KBrO_3$>H_2O_2>$(NH_4)_2S_2O_8$	Chen et al. (2012)
Acridine Orange	TiO_2	H_2O_2, $KBrO_3$,	UV	H_2O_2>$KBrO_3$	Faisal et al. 2007
Ethidium Bromide	TiO_2	H_2O_2, $KBrO_3$, $(NH_4)_2S_2O_8$	UV	$(NH_4)_2S_2O_8$>$KBrO_3$>H_2O_2	Faisal et al. 2007
Chrysoidine Y	TiO_2	H_2O_2, $KBrO_3$,	UV	H_2O_2>$KBrO_3$	Qamar et al. 2004
Chrysoidine Y	ZnO	H_2O_2, $KBrO_3$,	UV	$KBrO_3$>H_2O_2	Qamar et al. 2004
Chromotrope 2B	TiO_2	H_2O_2, $KBrO_3$, $(NH_4)_2S_2O_8$	UV	$KBrO_3$>H_2O_2>$(NH_4)_2S_2O_8$	Qamar et al. 2005a
Amido Black 10B	TiO_2	$KBrO_3$	UV	$KBrO_3$	Qamar et al. 2005a
Chrysoidine R	TiO_2	H_2O_2	UV	H_2O_2	Qamar et al. 2005b
Acid Red 29	TiO_2	H_2O_2, $(NH_4)_2S_2O_8$	UV	$(NH_4)_2S_2O_8$>H_2O_2	Qamar et al. 2005b
Remazol brilliant blue R	TiO_2	H_2O_2, $KBrO_3$, $(NH_4)_2S_2O_8$	UV	$KBrO_3$>$(NH_4)_2S_2O_8$>H_2O_2	Saquib and Muneer 2002
Remazol brilliant blue R	TiO_2	H_2O_2, $KBrO_3$, $(NH_4)_2S_2O_8$	Solar	$(NH_4)_2S_2O_8$>H_2O_2>$KBrO_3$	Saquib and Muneer 2002
Acid Orange 8	TiO_2	H_2O_2, $KBrO_3$	UV	H_2O_2>$KBrO_3$	Saquib and Muneer 2003

Table 2.10 Contd.

Dye	Catalyst used	Oxidants used	Light Source	Activity	References
Fast Green	TiO_2	H_2O_2, $KBrO_3$, $(NH_4)_2S_2O_8$	UV	$KBrO_3 > (NH_4)_2S_2O_8 > H_2O_2$	Saquib et al. 2008
Acid Blue 1	TiO_2	H_2O_2, $KBrO_3$, $(NH_4)_2S_2O_8$	UV	$H_2O_2 > KBrO_3 > (NH_4)_2S_2O_8$	Saquib et al. 2008
Acid blue 45	TiO_2	H_2O_2, $KBrO_3$	UV	$H_2O_2 > KBrO_3$	Tariq et al. 2008
Xylenol orange	TiO_2	H_2O_2, $KBrO_3$	UV	$KBrO_3 > H_2O_2$	Tariq et al. 2008
Amaranth	TiO_2	H_2O_2, $KBrO_3$, $(NH_4)_2S_2O_8$	UV	$KBrO_3 > H_2O_2 > (NH_4)_2S_2O_8$	Tariq et al. 2005
Bismarck brown	TiO_2	H_2O_2, $KBrO_3$,	UV	$KBrO_3 > H_2O_2$	Tariq et al. 2005

It can be seen from literature, activity of different oxidants and their concentrations may play an important role in improving the rate of photocatalytic degradation process. Thus in the current study, to increase the rate of degradation of dyes, photocatalysis was attempted with the addition of H_2O_2, $(NH_4)_2S_2O_8$, and $KBrO_3$ as oxidants.

2.7 Optimization of photocatalysis process

Feasibility of commercialization of any process depends on the economics of the process. Drive is towards decreasing the cost of the process. Fixed cost of photocatalysis process may be reduced, if the rate of photocatalysis is enhanced to a considerable extent. Higher rate results in requirement for smaller size reactor for a given operation if the process is continuous or reduction in time needed for operation for a batch process. Rate of photocatalysis may be enhanced by operating the process at optimum conditions of pH, catalyst loading and oxidant concentration. Similarly the operating cost may be reduced if the amount of catalyst requirement and the concentration of oxidant are optimized to yield maximum rate of degradation, so that no excess chemicals or catalyst are used in the process.

The knowledge on interactions between the operational factors is important, particularly for optimizing the performance and minimizing the operation cost for an

industrial photocatalytic treatment processes. The conventional technique for optimization is very often by one-factor-at-a time approach, while keeping other factors as constant. In this technique, the knowledge of the interaction between operational factors was often neglected. However, this approach leads to inadequate optimization results. Moreover, one factor at a time approach is time consuming; efficiency of process is very less and they require many experiments to validate and correlate the interactions between the operational factors involved. Though development of mathematical models based on first principles with process validation has been a common practice associated with many studies on modeling and optimization, it has serious limitations of availability of model parameter values. These parameter values need to be determined experimentally by independent experimentation. Accurate determination of model parameters may often be difficult, due to non availability of experimental methods.

Recently a number of statistical design of experiments (DOE) and data analysis techniques have been employed in various fields of process optimization (Levin et al. 2008; Chen et al. 2008a; Yu et al. 2008). In order to make out the effect of individual factors and to find the neighborhood of the optimum response, these designs include blocking and factorial experiments for determining the path of steepest ascent, (Box et al. 1978). In addition to that, Response Surface Methodology (RSM) is described as suitable method for illustrating a near optimum region and thus for exactly finding conditions for a multifactorial system. According to the observations of Myers et al. (2006), the response surface framework has become the standard approach for much of the experimentation carried out in industrial research, development, manufacturing, and technology commercialization.

It is clear that RSM can play a crucial role in obtaining optimum photocatalytic reaction conditions. RSM is often based on statistically designed set of experiments. RSM involves the design of experiments to describe the response as a function of several factors, the fitting of experimental result data to the empirical or theoretical models, the explanation of the nature of the fitted response and the judgment of the adequacy of the model. RSM results in reduction of number of experiments without neglecting the interaction among the factors. The use of multivariate experimental design technique is becoming increasingly widespread in

applied catalysis. Multivariate designs, which allow the simultaneous study of several control variables, are faster to implement and more cost effective than traditional univariate approaches (Montgomery 1997). But before going for experimental design models, experiments to screen the factors are most important. This helps in determination of important factors which can influence the rate of photocatalysis. It is well known from literature review that, in photocatalysis, the factors that affect the degradation (response) are dye concentration, catalyst loading, initial pH, electron acceptors and light intensity. As the factors influencing photocatalytic process are well documented, screening is not necessary in the current study. But to fix a proper range of operational factors for designing the experiments and for optimization, preliminary studies are always essential.

Several experimental design models could be employed to reduce the number of experiments under different conditions. The most commonly used designs are 3^k factorial, Doehlert, Box–Behnken and Central Composite Design (CCD) (Sakkas et al. 2010). Table 2.11 shows the application of DOE in RSM for optimization of photocatalysis of dyes. A very useful experimental design for fitting second-order models is the CCD. It consists of three types of points: cube, axial and centre points. The number of experiments required (N) is given by

$$N = 2^k + 2k + C_0 \tag{2.23}$$

Where k is the number of variables, 2^k is the number of cube points, $2k$ is the number of axial points and C_0 is the number of center points (Sakkas et al. 2010). In CCD, central point is often used to find error. This design has been most widely used for the optimization of parameters affecting photocatalysis of dyes as it provides almost as much information as a multilevel factorial design, fewer experiments are needed as compared to full factorial design (Kasiri and Khatee 2011). So in the presently reported study, Central Composite Design was chosen for the optimization of operational factors for UV and solar photocatalysis of the dyes.

Table 2.11 Application of DOE in RSM for optimization of photocatalysis of dyes.

Dyes	Photocatalyst used	Irradiation source	Selected factors	DOE technique	References
Basic Red-2	H_2O_2	UV	dye concentration, pH and H_2O_2 concentration	D-optimal design	Bahadir et al. (2008)
Reactive Red-120	TiO_2	UV	TiO_2 loading, dye concentration and UV intensity	Central composite design (CCD)	Cho and Zoh (2007)
Azo Pyridone	TiO_2	UV	H_2O_2 concentration, irradiation time and pH	CCD	Dostanic et al. (2013)
Acid Blue-7	TiO_2	UV	pH, light intensity, TiO_2 loading	Box-Behnken design	Fu and Wu (2008)
Acid-Red 14	Fe-ZSM5/H_2O_2	UV	Catalyst loading, molar ratio of initial concentration of H_2O_2 to that of the dye (H value), concentration of dye and pH	CCD, artificial neural networks (ANNs)	Kasiri et al. (2008)
Acid Green-25	Immobilized TiO_2	UV	Dye concentration, light intensity, flow rate and time	CCD	Khatee et al. (2011)
Dyeing wastewater	TiO_2/H_2O_2	UV	TiO_2 loading and H_2O_2 concentration	CCD	Lee et al. (2005)
Reactive Red-239	TiO_2	UV	UV light intensity, TiO_2 loading, pH, stirring speed	2^4 full-factorial CCD design	Liu and Chiou, (2005)

Table 2.11 Contd.

Dyes	Photocatalyst used	Irradiation source	Selected factors	DOE technique	References
Reactive Blue- 19	TiO$_2$/ZnO	UV	pH, catalyst loading, dye concentration	Factorial design	Lizama et al. (2002)
Indole	TiO$_2$	UV	dye concentration, TiO$_2$ loading, temperature, flow rate	Central composite experimental design (CCD)	Merabet et al. (2008)
Methyl Blue	Ag ion doped TiO$_2$	UV	Dye concentration, catalyst loading and pH	Box-Behnken design	Sahoo and Gupta (2012)
Methylene blue	Ag ion doped TiO$_2$	UV	Dye concentration, catalyst loading and pH	Box-Behnken design	Sahoo and Gupta (2013)
Congo Red	TiO$_2$	UV	TiO$_2$ loading and H$_2$O$_2$ concentration	Central composite design (CCD)	Sakkas et al. (2010)
Metanil-Yellow	TiO$_2$	UV	Dye concentration, TiO$_2$ loading, pH, light flux	Central composite design face-centered (CCF)	Sleiman et al. (2007)

2.8 Reaction kinetics for dye degradation

The photocatalytic process efficiency is one of the most critical factor that determines whether photocatalytic technique will be of any practical significance. From the reactor design point of view, for large scale application of photocatalysis of dyes in wastewater, determination of the rate equation governing photocatalytic process and the evaluation of the parameters of the rate equation are important. Kinetic studies of degradation helps in the prediction of rate equation. For semiconductor photocatalysis, to describe the rate of degradation of organic compounds a variety of models have been derived. Most kinetic models used in photocatalysis are based on the Langmuir-Hinshelwood (L-H) mechanism confirming the heterogeneous catalytic

characteristics of the system (Ollis and Serpone 1989; Fox and Dulay 1993; Hoffmann et al. 1995; Mills and Le Hunte 1997).). Many studies on the photocatalysis of organic pollutants have reported that the rate (r) of photodegradation of the pollutant fits a Langmuir-Hinshelwood model (Equation 2.24) (Turchi et al. 1989; Chen et al. 1998).

$$(-r) = \frac{k_{obs}k_R[C_{pollutant}]}{1+k_R[C_{pollutant}]} \qquad (2.24)$$

Where $(-r)$ is the reaction rate of the pollutant being degraded, $C_{pollutant}$ is the concentration of the pollutant, k_{obs} is the constant related to adsorption and k_R is the reaction rate constant. Both k_{obs} and k_R depend on the catalyst utilized and the nature of the pollutant.

A photocatalytic reaction proceeds on the surface of semiconductors via several steps: (i) generation of electron–hole pairs by irradiation of the semiconductor with light energy content higher than the band gap energy of the semiconductor; (ii) separation of the photogenerated electrons and holes due to trapping by species, that are adsorbed on the semiconductor; (iii) redox reactions between the trapped electrons and holes and the adsorbents; (iv) desorption of reaction products and reconstruction of the surface (Fu et al. 1996; Li et al. 2011; Khezrianjoo and Revanasiddappa 2012).

In Langmuir-Hinshelwood models, the surface of the catalyst is assumed as being energetically uniform, and it is assumed that there is no energetic interaction between species adsorbed on the surface. Each reactant is assumed to adsorb on a surface site. Products are generated at the surface by surface reaction between adsorbed reactants and the products desorb from the surface. It is assumed that the surface reaction step is irreversible and the adsorption/desorption steps are reversible. In the simplest form, L-H approach assumes one relatively rapid reaction achieving adsorption equilibrium (quasi-equilibrated) followed by a single slow surface reaction step (Murzin 2006) The free energy change associated with the quasi-equilibrated adsorption step is negligible compared to that of the surface reaction step. The surface reaction is thus called the *rate determining step* (RDS), since nearly all of the free energy change for the overall reaction is associated with that step (Davis and Davis 2003).

To estimate the parameters of L-H kinetic model, it has been customary to write (Equation 2.24) in reciprocal form and then to plot the reciprocal initial reaction rate, $1/(r_0)$, versus the reciprocal initial concentration, $1/C_0$, as shown in Equation (2.25).

$$-\frac{1}{r_o} = \frac{1}{k_{obs}.k_R[C_{pollutant}]} + \frac{1}{k_{obs}} \qquad (2.25)$$

This method is called the method of initial rates (Levenspiel 1972). The constants k_{obs} and k_R may be determined from a plot of $1/r_0$ versus $1/C_{pollutant}$. If a catalytic system obeys the Langmuir-Hinshelwood (L-H) model, the plot should be linear. The intercept of the line with the y-axis provides $1/k_{obs}$ with the slope equal to $1/k_{obs}k_R$. Hence the parameters of the kinetic model can be evaluated.

This law successfully explains the kinetics of heterogeneous surface reactions as, it makes use of both reaction rate constant and adsorption equilibrium constant. At low pollutant concentration the catalyst surface will not be saturated with pollutant, and then L-H kinetic model follows first order reaction equation. Several researchers have reported the validity of Langmuir Hinshelwood kinetic model to describe the kinetics of photocatalysis of dyes (Gupta et al. 2011; Gupta et al. 2012 a, b; Muruganandham and Swaminathan 2006 a, b).

2.9 Effect of light intensity

Light intensity is an important parameter as absorption of light by the catalyst and formation of electron–hole which is the initiation step in photocatalysis depends on it (Cassano and Alfano 2000). Distribution of light intensity determines the degradation efficiency and pollutant conversion (Pareek et al. 2008). Ollis et al. (1991) reviewed the studies reported by different researchers on effect of light intensity on rate of photocatalysis and stated that:

i) At lower light intensities (0–20 mW/cm^2), the rate of degradation would increase linearly with increasing light intensity (Daneshvar et al. 2004; Muruganandham and Swaminathan 2006b).

(ii) At intermediate light intensities (~ 25 mW/cm^2), the rate of degradation would depend on the square root of the light intensity (Daneshvar et al. 2004; Muruganandham and Swaminathan 2006b).

(iii) At high light intensities the rate of degradation is independent of light intensity (Daneshvar et al. 2004; Muruganandham and Swaminathan 2006b).

This is because at lower light intensity, photocatalysis process involves the formation of electron–hole which is the predominant step and electron–hole recombination is insignificant. Hence the rate increases with the increase in light intensity. With further increase in intensities, the rate of degradation increases with the square root of the light intensity, as electron hole recombination can compete with charge carrier transfer due to high intensity and lowers the effect on the reaction rate (Konstantinou and Albanis 2004).

Rashed and El-Amin (2007) investigated the effect of UV light intensity on Methyl Orange dye using TiO_2 nanoparticles and found, as the light intensity increases the rate of degradation increases. Similar results were reported by Konstantinou and Albanis (2004) and Hermann (1999) for the photocatalytic degradation of dyes. Muruganandham and Swaminathan (2006b) examined the effect of UV light power on the degradation of Reactive Yellow 14. Results showed that the degradation of dye increases with the increase in UV power from 16 to 32 W, but no considerable increase was observed between 32 to 48 W. Further increase in light intensity from 48 to 64 W, showed independent behavior on degradation. Liu et al. (2006) studied the effect of UV light intensity on the photocatalytic degradation of Acid Yellow 17 and found that increase in light intensity increases the dye removal. Ku et al. (2011) examined the effect of UV light intensity (6.3 to 10.5 mW/cm^2) on the photocatalytic degradation of Reactive Red 22 dye. It was observed, degradation of dye increased linearly with the increase in UV light intensity. Bouanimba et al. (2011) examined the effect of UV light intensity (2 to 10 mW/cm^2) on the photocatalytic degradation of Bromophenol Blue dye. Results showed, with increase in light intensity rate of degradation increases and linear relationship was observed. Gupta et al. (2011) investigated the effect of UV light intensity (8 to 14 mW/cm^2) on the photocatalytic degradation of Tartrazine dye using TiO_2 and found a linear relationship between rate of dye degradation and light intensity. The increased rate of degradation with increase in light intensity is attributed to the formation of more hydroxyl radical as more radiations fall on the catalyst surface. Neppolian et al. (2002b) studied the effect of solar light intensity at various time intervals on

photocatalytic degradation of textile dye Reactive Blue 4 using TiO_2. The maximum degradation of dye was observed during April–June; peak summer period of the year in Chennai, India. Park et al. (2004) investigated the effect of UV light intensity on solar light induced degradation of Reactive Dye (Red120) using photocatalysis. Three experiments were conducted on; clear sky, partly cloudy and thick cloudy sky. It was observed dye decolourisation on clear sky day was about three and thirteen times higher than partly cloudy and thick cloudy sky. The rate of decolorisation of dye increased linearly with increase in UV light intensity. Jeni and Kanmani (2011) examined the effect of solar UV light intensity on photocatalytic decolorisation of reactive dyes using TiO_2. Results showed that with increase in solar UV light intensity, decolorisation of both dyes increased and maximum is observed with UV light intensity of 31 W/m^2.

As the light intensity plays a very important role in photocatalysis, it was proposed to study the effect of light intensity on rate of photocatalysis.

2.10 Effect of addition of salts (NaCl, Na$_2$CO$_3$)

Presence of interfering substances plays an important role in the degradation of dyes. In textile industries, NaCl and Na$_2$CO$_3$ play an important role in transferring dye to fabric and in adjusting pH of dye bath which is necessary in fixing dye on the fabrics (Arslan et al. 1991). Large amount of these salts get wasted during dyeing process and therefore, the dye industry wastewater contains a considerable amount of carbonate and chloride ions. Waste water containing anions (Cl^-, CO_3^{2-}) decrease the rate of the reaction and affect the water transmittance. Hence, it is important to study the influence of CO_3^{2-} and Cl^- ions on the photocatalytic degradation of dyes.

Neppolian et al. (2003) studied the effects of NaCl and Na$_2$CO$_3$ on the photocatalytic degradation of Reactive Yellow 17 dye; the percentage degradation of dye decreased gradually with increase in carbonate ion concentration. The decrease in degradation of the dye in the presence of carbonate ions is attributed to the hydroxyl scavenging property of carbonate ions as explained in following reactions (Behar *et al*. 1970; Neppolian et al. 2003).

$$OH + CO_3^{2-} \rightarrow OH^- + CO_3^{-} \tag{2.26}$$

$$OH + HCO_3^- \rightarrow H_2O + CO_3^{\cdot -} \tag{2.27}$$
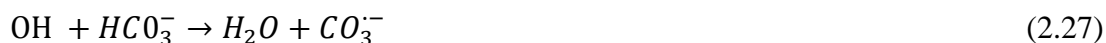
It can be seen from the above reactions, carbonate radical which is very less active than $\cdot OH$ radical, is produced and hence results in lower degradation. Also with increase in CO_3^{2-} concentration, $\cdot OH$ which is a primary source responsible for photocatalysis of dyes decreases, and as a result percentage degradation of dyes decreases. In the photocatalytic degradation of Reactive Dyes, similar trend was observed (Nansheng et al. 1996).

With the increase in concentration of Cl^-, degradation of dye decreases. The decrease in degradation of dye with increase in Cl^- concentration is attributed to the hole scavenging property of Cl^- ion as explained in the following reactions (Bockelmann et al. 1996).

$$Cl^- + h_{(VB)}^+ \rightarrow Cl^{\cdot} \tag{2.28}$$

$$Cl^{\cdot} + Cl \rightarrow Cl^{2\cdot -} \tag{2.29}$$

It can be seen from theabove reactions, chloride radical anion is produced which blocks the active surface sites available at the catalyst surface. These chloride radical anions are not readily oxidizable and hence results in decrease in the degradation of dyes.

Muruganandham and Swaminathan (2004) investigated the effect of Cl^- and CO_3^{2-} on the photocatalytic degradation of Reactive Orange 4. Rate of degradation of dye was found to decrease with the addition of Cl^- and CO_3^{2-}. Addition of Cl^- and CO_3^{2-} from 1 to 4 g/L resulted in decrease in degradation of dye and around 60 % and 55 % (after 60 min irradiation time) degradation of dye was observed with the addition of Cl^- and CO_3^{2-} respectively. Bouanimba et al. (2013) investigated the effect of Cl^- and CO_3^{2-} on the photocatalytic degradation of Methyl Orange dye. Results showed that in presence of Cl^- and CO_3^{2-}, rate of degradation is hindered. Sohrabi et al. (2009) investigated the effect of Cl^- on the photocatalytic degradation of Benziden Yellow and found decrease in degradation in the presence of Cl^-. Decrease in degradation of dyes with increase in Cl^- (0.02 mol) was also reported by Mahmoodi, (2013) during the photocatalytic degradation of Direct Red 23 and Direct Red 31 dyes using carbon nanotube and TiO_2 nanoparticles as photocatalysts.

Since the presence of different salts in textile effluents may interfere with the degradation of dyes, it is necessary to study the effect of the presence of these salts on photocatalytic degradation of dyes.

2.11 Photocatalytic mineralization of dyes

The degradation of dyes leads to the conversion of organic carbon into harmless gaseous CO_2 and that of nitrogen and sulfur heteroatoms into inorganic ions, such as nitrate, nitrite, sulfate, chloride etc. During photocatalysis process extent of mineralization reached is generally assessed by the formation of inorganic ions and further mineralization to CO_2 and H_2O (Bianco-Prevot et al. 2001; Zhang et al. 1998; Liu et al. 1999; Stylidi et al. 2003; Tanaka et al. 2000; Spadaro et al. 1994). However, in textile effluents information on the real decay of pollutant is not provided and monitoring of inorganic ions, only offers a global estimation on the well-functioning of the treatment. So in textile industries, estimation of mineralization of dyes is generally done by measuring total organic carbon (TOC), chemical oxygen demand (COD) and biological oxygen demand (BOD) (Neppolian et al. 2002 a, b; Zhang et al. 1998; Sakthivel et al. 2003; So et al. 2002; Tanaka et al. 2000; Hu et al. 2003; Chun and Yizhong 1999). Until now, most of photocatalysis studies showed mineralization of azo dyes as evidenced by decrease in TOC and COD with increase in irradiation time (Sakthivel et al. 2003; Stylidi et al. 2003; Tanaka et al. 2000; Gouvea et al. 2000). The COD is widely used as an effective technique to measure the organic strength of wastewater. The test allows the measurement of wastes in terms of the total quantity of oxygen required for oxidation of organic matter to CO_2 and water. The reduction in COD and TOC values of the treated dye solution indicates the mineralization of dye molecules along with color removal. Usually exponential or sigmoidal shapes were observed with COD or TOC curves which mean small decrease in COD or TOC values when solution is still colored and sharp decrease when solution becomes colourless (Stylidi et al. 2003; So et al. 2002; Chun and Yizhong 1999). According to these researchers a small decrease in TOC or COD values is due to the decomposition of dye molecules to lower molecular weight compounds and sharp decrease corresponds to oxidation of most stable compounds

which indicates the complete mineralization of intermediates. So in the present study TOC and COD measurement were carried out in order to check for mineralization of dyes.

Inorganic ions such as chlorides, sulphates, nitrates and nitrites are formed by mineralization from the chlorine, nitrogen and sulphur containing heteroatoms in dyes. It was reported by Sakthivel et al. (2003) that, for chlorinated dye molecules, chloride ions are first to appear during photocatalysis. Wang et al. (2000) studied the photocatalytic degradation of dyes with chloride substitute and reported that the release product of chlorinated dye depends upon the position in which it is attached to molecular structure. Nitrogen containing groups are mineralized to nitrate, nitrite and ammonium ions and the proportion mainly depends on the irradiation time, structure of dye and oxidation of nitrogen groups (Nohara et al.1997; Puzenat et al. 2003). It was reported by Stylidi et al. (2003) at the end of experiment the total amount of nitrogen containing ions is usually lower than the stoichiometry. It may be due to adsorption on photocatalyst surface or production of nitrogen and ammonia gas. The dyes containing sulphonic groups or sulphur atoms are mineralized into sulphate ions and in most studies stoichiometry were observed (So et al. 2002).

So in the presently reported study, it was proposed to analyze COD removal, TOC removal and formation of sulphate, nitrate, nitrite and chloride ions in order to check mineralization of dyes.

2.12 Photocatalytic degradation of mixture of dyes

In the application of photocatalysis for treatment of wastewater from textile industries, the effluent will normally consist of a mixture of many dyes rather than a single dye and their interaction may mutually improve or reduce photocatalysis process. Numerous papers have been published for dye degradation with single component system but very limited studies have been reported for mixture of dyes.

Ong et al. (2013) investigated solar photocatalytic degradation of mono azo Methyl Orange and diazo Reactive Green 19 in single and binary dye solutions using TiO_2 nanoparticles. Their studies showed removal efficiency of 56 and 98 % for Methyl Orange and Reactive Green 19, respectively in binary dye solution. The

photocatalytic degradation of both dyes were found to be less in binary dye solution as compared to single dye solution which may be due to competitive nature of dyes towards reactive sites on TiO_2 nanoparticles. Also no interactions of dyes were observed and hence analysis of dyes was done at their corresponding λ_{max} values.

Sahel et al. (2010) studied the photocatalytic degradation of a mixture of two anionic dyes: Procion Red MX-5B and Remazol Black 5 using TiO_2 nanoparticles under UV light. Their studies showed, at lower concentration (3 µmol/L) of mixture of dyes rate of degradation was similar to rate of degradation of individual dye but at higher concentration (10 µmol/L) rate of degradation decreased due to limited number of available sites on TiO_2 surface. No complex formation was observed with mixture of dyes hence concentrations of each dye were measured at their λ_{max} values.

Damodar et al. (2009) examined the photocatalytic degradation of a mixture of Acid Yellow and Reactive Red (25 and 50 mg/L each) dyes using immobilized TiO_2 under UV light irradiation and observed rate of removal of mixture of dyes decreased as compared to individual dye solution. This proves the inhibition of degradation of a dye due to the presence of other dyes in mixture due to competition for reactive sites on catalyst surface. Also the absorption spectra of mixture of dyes did not show any change in λ_{max} values and hence the degradation was studied by dye analysis separately at their corresponding λ_{max} values.

Gupta et al. (2006) studied photocatalytic degradation of a mixture of Crystal Violet (Basic Violet 3) and Methyl Red dye using Ag ion doped TiO_2 nanoparticles under UV light irradiation. Their studies showed no interaction effect of dyes with each other and analysis of dyes was done at their corresponding λ_{max} values. With different proportions of Crystal Violet (Basic Violet 3) and Methyl Red dye, almost 99 % degradation of both dyes occurred within 90 min of UV irradiation.

Since the presence of one or more of the dyes in wastewater, may interfere with the degradation of a specific dye, it is necessary to study the effect of mixture of dyes on photocatalysis. The optimum conditions obtained for maximum degradation of one of the dyes in a mixture may prove to be sub optimal for other dyes and hence choosing the conditions favorable for the degradation of all the dyes in the wastewater contaminated with several dyes may be a challenging task. There are no studies reported so far on choice of optimal conditions for wastewater containing two or more

dyes. An attempt has been made in the present study to suggest a suitable methodology to choose an appropriate optimal condition for treatment of wastewater containing mixture of dyes.

2.13 Identification of degradation products, their intermediates and the degradation pathway

The photocatalytic degradation of dyes to simpler compounds is not a one step reaction. In order to improve our knowledge about degradation pathway and to determine which specific compounds are produced in the effluent (Konstantinou and Albanis 2004), it is necessary to identify the intermediates and degradation products. This may also reveal which step is crucial for the large-scale application of photocatalysis process and help in evaluation of kinetics of formation and decomposition of the byproducts. To maximize the overall efficiency of the photocatalysis process, identification of intermediates is one of the main key factors. A variety of intermediates are produced during photocatalysis due to non-selective reaction of hydroxyl radical and various analytical techniques such as high performance liquid chromatography (HPLC) (Galindo et al. 2000; Bandara et al. 1999; Baiocchi et al. 2002), gas chromatography–mass spectrometry (GC–MS) (Liu et al. 1999; Stylidi et al. 2003; Daneshvar et al. 2003; Galindo et al. 2000), liquid chromatography–mass spectrometry (LC–MS) (Meetani et al. 2010; Bansal and Sud 2010; Bansal and Sud 2012) and FT-IR (Stylidi et al. 2003; Galindo et al. 2001; Lucarelli et al. 2000; Hu et al. 2003; Nasr et al. 1996) were used for the determination of organic intermediates.

Hisaindee et al. (2013) reviewed application of LC-MS to find the intermediate products and reaction mechanisms of dye degradation during advanced oxidation process (AOP). Rajeshwar et al. (2008) reviewed the degradation mechanism of azo dyes (Congo Red, Acid Orange 7, Disperse Red 13, Reactive Black 5, Acid Orange 52, Reactive Yellow 145, and Disperse Red 1 etc.) and non azo dyes (Acid Blue 80, Methylene Blue, Reactive Blue 4, Rhodamine B, Alizarine Red, Eosin etc) during heterogeneous photocatalysis and reported the formation of various reaction intermediates.

Photocatalytic degradation products of Acid Orange 7 dye were identified using GC-MS by Stylidi et al. (2003). Karkmaz et al. (2004) proposed the degradation pathway of Amaranth dye for the evaluation of aliphatic organic acids during TiO_2 mediated photocatalysis. Hasnat et al. (2005) compared the photocatalytic degradation pathway of Methylene Blue (cationic dye) and Procion Red (anionic dye) using TiO_2 as catalyst under visible light and found degradation pathway of Procion Red to be somewhat different from Methylene Blue. Bansal et al. (2010) examined the photocatalytic degradation and mineralization extent of Acid Orange 7 dye in aqueous suspension of TiO_2. To judge the degradation pathway of Acid Orange 7 dye, mechanism of formation of intermediates and final products were monitored by LC/MS. Meetani et al. (2010) studied the photocatalytic degradation of diazo dye (Amido Black) using UV/H_2O_2 and detailed study was carried out to establish degradation pathway and intermediates produced. The dye degradation proceeded with the attack of hydroxyl radical at electron deficient nitrogen and further pathway included radical denitration, radical desulfonation and radical diazotization of Amido Black dye. Fabbri et al. (2010) examined the degradation of Acid Violet 7 (azo dye) and Acid Green 25 (anthraquinone) dye using TiO_2 as photocatalyst. In their studies, dye degradation, mineralization and identification of intermediates were done by LC-MS and degradation pathway was reported. Complete mineralization of both dyes and conversion of sulfonic groups into sulphate ion and nitrogen into nitrate and ammonium ions were observed. Natarajan et al. (2011) studied the photocatalytic mineralization, identification of intermediates and degradation pathway of photocatalysis of Rhodamine B dye with TiO_2 catalyst under UV/LED light irradiation. Kalsoom et al. (2012) investigated the degradation mechanism of Remazol Turquoise Blue dye with LC-MS during photolysis with UV/H_2O_2 and found after 120 min of irradiation time, dye was broken down and new products were formed. Bansal and Sud (2013) studied the photocatalytic degradation of Reactive Red 35 in aqueous suspension of TiO_2 under UV light and found degradation pathway and identified the intermediates by LC/MS.

The review of literature suggested the importance of degradation pathway and mechanism of dye degradation. Several researchers have successfully established the degradation pathway by analysis and identification of intermediates and products of

degradation using LC/MS. So in the presently reported study, identification of intermediates and products produced during photocatalysis was carried out using LC/MS.

2.14 Immobilized photocatalysts

Photocatalyst can be employed either in a colloidal form or in an immobilized form (Chun et al. 2001; You et al. 2001; Chai et al. 2000). Most of the experimental work on aqueous systems has been carried out using photocatalysts in the form of fine particles suspended in the liquid phase, but the main drawback of this process is that the separation of photocatalyst from the solution is expensive. The separation process is more challenging when the photocatalyst is nanosized. Use of suspended nanoparticles as photocatalysts in continuous photocatalytic reactor has drawbacks in terms of retainment of nanoparticles in the reactor, as these catalyst nanoparticles may get washed away with the reactor effluents. In photoreactors operated with catalyst particles as slurry, the use of suspensions requires the separation and recycling of the nanosized catalyst from treated liquid and it can be an inconvenient, time consuming and expensive process. The requirement of separation of ultra fine catalyst particles from treated liquid hinders the wide application of slurry photocatalytic reaction systems. Attention is also given to the development of reactor configurations which allow the debottlenecking of typical problems related to the use of slurry photocatalytic reactors, such as the separation of the catalyst powders from the product stream. For instance, Chin et al. (2006; 2007) developed a submerged membrane photocatalytic reactor using membrane to separate TiO_2 from the effluent; however, the problem of membrane fouling happened occasionally. The above problems can be avoided in photocatalytic reactors where the catalyst particles are immobilized on a support or carrier. Hence, to avoid the cost of separation of small catalyst particles from treated water and also to retain constant catalyst loading in the reactor throughout the operation, methods of fixing the catalyst on the support within the reactor has also been investigated which in many cases showed higher photocatalytic activity than the parent TiO_2 (Xu and Langford 1997; Chun et al. 2001). It is promising to employ the immobilized photocatalysts in photocatalytic

reactors. Puttamraju and Ray (2008) found that the removal rates of Methyl Ethyl Ketone in gas phase was higher for the catalysts supported on different adsorbents as compared to bare TiO_2 (Degussa P25 and sol-gel TiO_2) due to both improved adsorption and photocatalytic degradation. Recently, the photoreactor design oriented to developing immobilized forms. Thus, various materials such as activated carbon (Torimoto et al. 1997), silica gel (Belhekar et al. 2002) and zeolite (Reddy et al. 2003) were selected as photocatalyst support to condense pollutants in bulk solution for degradation. Usually supports are classified by their chemical nature to organic and inorganic supports. Whatever the support is, it plays an important role in immobilizing active catalyst. Principally, the support has three main functions: (i) to increase the surface area of catalytic material, (ii) to decrease sintering and to improve hydrophobicity and thermal, hydrolytic, and chemical stability of the catalytic material, and (iii) to govern the useful lifetime of the catalyst (Matatov-Meytal and Sheintuch 1998). Support may also improve the activity of the catalyst by acting as a co-catalyst. Surface bound-conjugated TiO_2/SiO_2 was prepared by means of impregnation method for photocatalysis of azo dyes by Chun et al. (2001). This TiO_2 fixed on silica gel showed three times higher photoactivity for the degradation of reactive dye. Noorjahan et al. (2003) reported the photodegradation of H-acid over a novel TiO_2 thin film fixed bed reactor by immobilized TiO_2 Degussa P-25 on inert cuddapah stone. Gopalkrishnan and Mohan (1997) carried out photodegradation of few textile dyes using TiO_2 in fixed mode i.e. by coating TiO_2 on sand and hollow glass beads. Subramanyam et al. (1998) have studied photocatalytic degradation of textile dyes: Vat Blue, Fast Orange GC Base by immobilizing TiO_2 on ceramic beads and SiO_2. TiO_2 has been affixed to a variety of surfaces like glass, silica, metals, ceramics, polymers etc. (Lei et al. 1999; Liu et al. 2000; Miller et al. 1999; Shchukin et al. 1999; Sirisuk et al. 1999; Rao et al. 2003; Fernandez et al. 2004). Photocatalytic degradation of various dyes using solar light as an irradiation source and immobilized TiO_2 as a photocatalyst showed the potential application for the decolorization of wastewater (Cangcang and Dewan 1998). Photocatalytic degradation of a few dyes has been successfully carried out using immobilized ZnO films (Roselin et al. 2002; Comparelli et al. 2004; Yoshida et al. 2002). Robert et al. (1999) have presented the preparation of TiO_2 supported on glass-fibre by sol-gel method. The supported

catalysts showed a good photocatalytic activity towards benzamide. However, the reduction of total organic carbon (TOC) with supported TiO_2 was very slow. This observation carries out that the degradation process is not the same as that with the classical TiO_2-P25. Mills et al. (2002) have prepared a novel chemical vapor deposition (CVD) film of titanium (IV) oxide on glass via the reaction of titanium (IV) chloride and ethyl acetate, using a CVD technique. The film was reported to be active photocatalytically and was able to destroy a deposited layer of stearic acid upon exposure to UV light. Neppolian et al. (2003) examined the photocatalytic degradation of common textile dye, Reactive Yellow 17 by photocatalysis over TiO_2 (Degussa P25) photocatalyst coated on the glass plates (reactor) using cement as a binder employing solar energy and found that it is a suitable technique for removal of colored wastewater from textile industries. Lim and Kim (2005) used TiO_2 coated on silica gel for photocatalytic degradation of trichloroethylene in fluidized bed reactor. Na et al. (2005) showed that the photocatalytic fluidized bed reactor with the hollow ceramic ball coated with TiO_2, effectively photocatalyzed the degradation of Rhodamine B dye. Behnajady et al. (2007) investigated the photocatalytic degradation of Acid Red 27 with immobilized TiO_2 on glass plates in a tubular continuous-flow photoreactor under UV light. Damodar et al. (2009) examined the photocatalytic degradation of a mixture of Acid Yellow and Reactive Red (25 and 50 mg/L each) dyes using TiO_2 nanoparticles immobilized on poly vinyl chloride(PVC) tube under UV light irradiation. Fathinia et al. (2010) compared photocatalytic degradation of two dyes having different structure using TiO_2 nanoparticles immobilized on glass plates. Many techniques have been devised to fix TiO_2 to a substrate, and research is ongoing. Immobilization techniques have been used successfully to fix TiO_2 to many supports, such as glasses (Fernandez et al. 1995; Rachel et al. 2002; Mills et al. 2002; Takeda et al. 2001), Quartz (Fernandez et al. 1995; Harizanov and Harizanova 2000), ceramics (Na et al. 2005, Mills et al. 2002), Optical fibres (Wang and Ku 2003; Peill et al. 1997), fabrics (Park and na 2008; Bottcher et al. 2010), polymers (Langlet et al. 2002), silica gel (Ding et al. 2001), activated carbon (Ding et al. 2001) and zeolite (Zainudin et al. 2008). Essentially the immobilization matrix needs to be mechanically robust, and must maintain a high level of photoactivity. One important drawback in application of immobilized catalysts is the mass transfer limitations.

When the catalyst particles are coated on to a support, the organic pollutants in water should transfer from the bulk liquid phase to the surface of the catalyst film and also to its interiors for effective utilization of the available catalyst surface. Even when the catalyst particles are entrapped in a support matrix, the organic molecules from water should diffuse through the matrix to reach the entrapped catalyst particles. This may offer diffusional mass transfer limitations to photocatalytic process and the overall photocatalytic degradation rate may become mass transfer limited. The research drive is to choose suitable immobilization matrix which are simple, cheap and which offer no mass transfer limitations on the process, which implies that the rate of photocatalysis with immobilized system should at least be similar to that with free nanoparticles.

In recent years, polymers such as chitosan (Singh et al. 2011b), cellulose acetate (Wu et al. 2005), PVA (Lei et al. 2012) and sodium alginate (Kim et al. 2010) have been used as support materials for nanoparticle immobilization due to their biodegradable nature. So in the present study cellulose acetate and chitosan matrices were used for immobilization of the nanoparticles.

2.15. Scope and objectives of research work

Based on extensive review of literature, it was hypothesized that, with suitable modifications in the synthesis of Ag@TiO_2 nanoparticles, solar photocatalytic activity can be imparted and UV photocatalytic activity can be enhanced. It was proposed to synthesize Ag@TiO_2 nanoparticles by one pot synthesis route of Hirakawa and Kamat (2005) with suitable modifications to enhance their UV photocatalytic activity and to impart solar photocatalytic activity. Research work was planned and designed based on the key research questions driven by the hypothesis mentioned above. The key research questions were: (i) whether or not, by properly engineering the Ag@TiO_2 nanoparticles through optimization of Ag to Ti molar ratio during synthesis, calcination temperature and calcination time, good UV and solar photocatalytic activity can be imparted to the nanoparticles (ii) what characteristics of these nanoparticles are responsible for imparting the photocatalytic activity? (iii) whether these nanoparticles can be used for removal of complex azo dyes such as Acid

yellow-17 and Reactive Blue-220 by photocatalytic degradation under UV light and solar light? (iv) whether these nanoparticles have better photocatalytic activity than, the other conventional photocatalysts? (v) which factors influence the photocatalysis process catalyzed by these nanoparticles and how? (vi) whether optimization of operational factors improve the rate of photocatalysis? (vii) whether the photocatalytic activity of $Ag@TiO_2$ nanoparticles better under UV light irradiation or solar light irradiation? (vii) whether these nanoparticles can be recycled and reused as photocatalysts? (viii) how does light intensity affect the rate of photocatalysis? (x) whether the presence of salts like NaCl and Na_2CO_3 in effluents, which are added during dyeing operation in textiles, influence the photocatalysis rate? (xi) what is the kinetic model governing the rate of photocatalysis of the dyes? (xii) what is the extent of mineralization of AY-17 and RB-220 during photocatalysis?, (xiii) what is the mechanism of degradation and the degradation pathway for these dyes?, (xiv) how efficiently the optimum conditions devised for the degradation of single dye solution can be used for degradation of dyes in an aqueous solution containing mixture of dyes? (xv) Photocatalyst can be employed either in a colloidal form or in an immobilised form. In photoreactors operated with catalyst particles as slurry, the use of suspension requires the separation and recycling of the nanosized catalyst from the treated liquid and can be an inconvenient, time consuming and expensive process. Catalysts can be immobilized on supports to overcome these limitations. But immobilized nano photocatalysts may lead to mass transfer limitations. So the research question was, how efficient are nanoparticles immobilized on biodegradable polymeric matrix such as cellulose acetate and chitosan beads, in comparison with free nanoparticles in terms of degradation of the dyes? (xvi) whether these engineered $Ag@TiO_2$ nanoparticles can be used for the photocatalytic degradation of other class of dyes?

Based on the critical understanding of the problem, extensive review of literature, key research questions raised and the need for research in this area the following objectives were formulated for the research work.

OBJECTIVES

The main objective of the present work is to study the efficacy of Ag@TiO$_2$ core shell structured nanoparticles as a photocatalyst, for the removal of two azo dyes: AY-17 and RB-220 from contaminated water by batch photocatalytic degradation.

The specific objectives are

- To synthesize Ag@TiO$_2$ core-shell structured nanoparticles by one pot synthesis route and to engineer them by optimization of Ag to Ti ratio in the synthesis mixture and the calcination conditions to impart and enhance the UV and solar photocatalytic activity in terms of degradation of the dyes.

- To assess the suitability of Ag@TiO$_2$ as a photocatalyst for degradation of the dyes by   photocatalysis under UV and solar light irradiation.

- To characterize the nanoparticles.

- To compare the photocatalytic activity of Ag@TiO$_2$ nanoparticles with those of commercial TiO$_2$, synthesized TiO$_2$ and Ag doped TiO$_2$ nanoparticles, in terms of degradation of the dyes under UV and solar light irradiation.

- To study the effect of factors which affect UV and solar photocatalytic degradation of the dyes; to obtain optimum conditions of pH and ratio of dye to catalyst loading and to choose an effective oxidant with the optimum concentration for maximum degradation of the dyes.

- To compare the UV and solar photocatalytic activity of Ag@TiO$_2$ in terms of degradation of the dyes.

- To test for the loss of activity of the catalyst after multiple uses and find its suitability for reuse.

- To determine kinetic models for UV and solar photocatalytic degradation of the dyes under optimum conditions.

- To study the effect of light intensity and the presence of salts on photocatalytic degradation of the dyes under UV and solar light irradiation.

- To test for photocatalytic mineralization of the dyes under UV and solar light irradiation.

- To study degradation of each of the dyes in water contaminated with mixture of two dyes by photocatalysis.

- To propose the reaction pathway by identification of the degradation products and intermediates.

- To compare the activity of free and immobilized nanoparticles in terms of degradation of the dyes.

A complimentary objective is

- To test for the efficacy of Ag@TiO$_2$ as a photocatalyst for degradation of other class of dyes.

CHAPTER 3
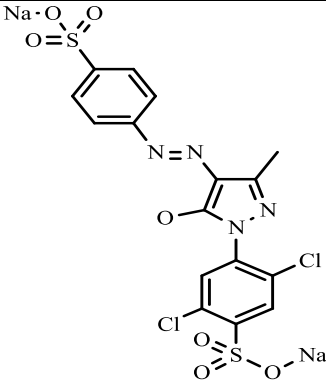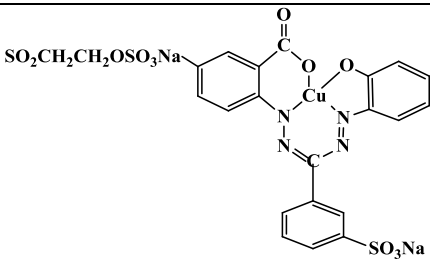
MATERIALS AND METHODS

This chapter deals with the materials used, the description of the experimental methodologies and the analytical procedures adopted to achieve the stated objectives.

3.1 Materials

AY-17 dye was purchased from Sigma-Aldrich, Chemicals Pvt. Ltd., Bangalore and RB-220 dye was purchased from DyStar India Ltd., Mumbai and was used without further purification. Table 3.1 presents the structure and characteristics such as molecular formula, molecular weight and wavelength corresponding to maximum absorbance (λ_{max}) of AY-17 and RB-220 dyes. Titanium-(triethanolaminato) isopropoxide ($N((CH_2)_2O)_3TiOCH(CH_3)_2$) (TTEAIP), titanium tetra isopropoxide (TTIP), chitosan and cellulose acetate were purchased from Sigma-Aldrich Chemicals Pvt. Ltd., Bangalore; 2-Propanol (GR grade), dimethyl formamide (DMF), glycine, mercuric sulphate (Hg_2SO_4), potassium dichromate ($K_2Cr_2O_7$), hydrochloric acid (HCl), ferrous ammonium sulphate ($Fe(NH_4)_2SO_4$), gluteraldehyde, acetone, potassium chromate, glycerol, barium chloride ($BaCl_2$), sulfanilamide, N-(1-Naphthyl)- ethylenediamine dihydrochloride (NEDA), nitric acid (HNO_3), acetic acid, silver nitrate ($AgNO_3$), sodium chloride (NaCl), sodium carbonate (Na_2CO_3), sodium hydroxide (NaOH) and sulphuric acid (H_2SO_4) were purchased from Merck India Pvt. Ltd., Mumbai and were used as received. Degussa P25 was obtained as a gift pack from Evonik Degussa India Pvt. Ltd. It consists of 75% anatase and 25% rutile TiO_2 with Brunauer–Emmett–Teller (BET) - specific surface area of 50 m^2/g and primary particle size of 20 nm. Care was taken while handling toxic solvents such as DMF and hygroscopic materials such as TTEAIP.

Table 3.1 Structure and characteristics of AY-17 and RB-220 dye.

Dye name	Molecular structure and formula	Molecular weight (g/mol)	λ_{max} (nm)
AY-17	$C_{16}H_{10}Cl_2N_4Na_2O_7S_2$	551.29	418
RB-220	$C_{22}H_{15}CuN_4Na_2O_{12}S_3$	733.10	609

3.2 Preparation of Ag@TiO$_2$

To synthesize Ag@TiO$_2$ core-shell structured nanoparticles, one pot synthesis method of hydrolysis of TTEAIP and the reduction of metal ions in dimethyl formamide, as has been followed by Hirakawa and Kamat (2005) was used, but with modification in terms of Ag to Ti ratio used during synthesis. 8.3 mM TTEAIP solution was prepared in 2-propanol and 15 mM of AgNO$_3$ solution was prepared in distilled water. Two mL of 15 mM AgNO$_3$ solution was mixed with 18 mL of TTEAIP solution. The molar concentration ratio of Ag$^+$ and TTEAIP in the reaction mixture was then 1:5. The molar concentration ratio of AgNO$_3$ and TTEAIP, and hence the molar ratio of Ag to

Ti in the reaction mixture was varied as 1:5, 1:3.1, 1:2.2, 1:1.67 and 1:0.8 by suitably varying the volumes of AgNO$_3$ and TTEAIP solution added, keeping the total volume constant. Table 3.2 presents the volume of AgNO$_3$ and TTEAIP solutions mixed to make a synthesis mixture with the desired Ag to Ti molar ratios. The solution was placed in a three necked flask with magnetic stirrer and equipped with a reflux condenser. Figure 3.1 shows the schematic diagram of laboratory scale reactor used for the synthesis of Ag@TiO$_2$ nanoparticles. The mixture was stirred for 15 min at room temperature and ten mL of DMF was then added into TTEAIP-Ag solution. The mixture was heated with reflux in a temperature controlled thermostatic heating mantle with continued stirring. With continued heating of the solution at 85 ℃, the colour slowly changed from colourless to light brown. After 90 min, the colour of the suspension turned to dark brown. At this point, the heating was stopped and the suspension was stirred until it was cooled to room temperature. The cluster suspension of Ag@TiO$_2$ was kept for settling in a beaker for 1 h and then centrifuged at 10000 rpm at 10 ℃ for 10 min. Ag@TiO$_2$ particles were separated and resuspended in ethanol solution. The procedure of suspension in ethanol and centrifugation was repeated at least 3-times to minimize the content of water and DMF in the suspension. After repeated ethanol washing and centrifugation, the particles were dried in a hot air oven at 100 °C for two hours. The particles were then calcined at a temperature ranging from 150 °C to 550 °C as desired, in a muffle furnace for a calcination time of 3 h. To study the effect of calcination time, the calcination was carried out for different time periods of 1 to 5 h as desired. After the calcination, the particles were stored as suspension in ethanol until further use. Prior to use, the particles were separated from ethanol by centrifugation and dried.

Table 3.2 Volume of AgNO$_3$ and TTEAIP solutions mixed to make a synthesis mixture with desired Ag to Ti molar ratios.

S. No.	Volume of TTEAIP (mL)	Volume of AgNO$_3$ (mL)	Ag to Ti molar ratio in synthesis mixture
1	18	2	1:5
2	17	3	1:3.1
3	16	4	1:2.2
4	15	5	1:1.7
5	12	8	1:0.8
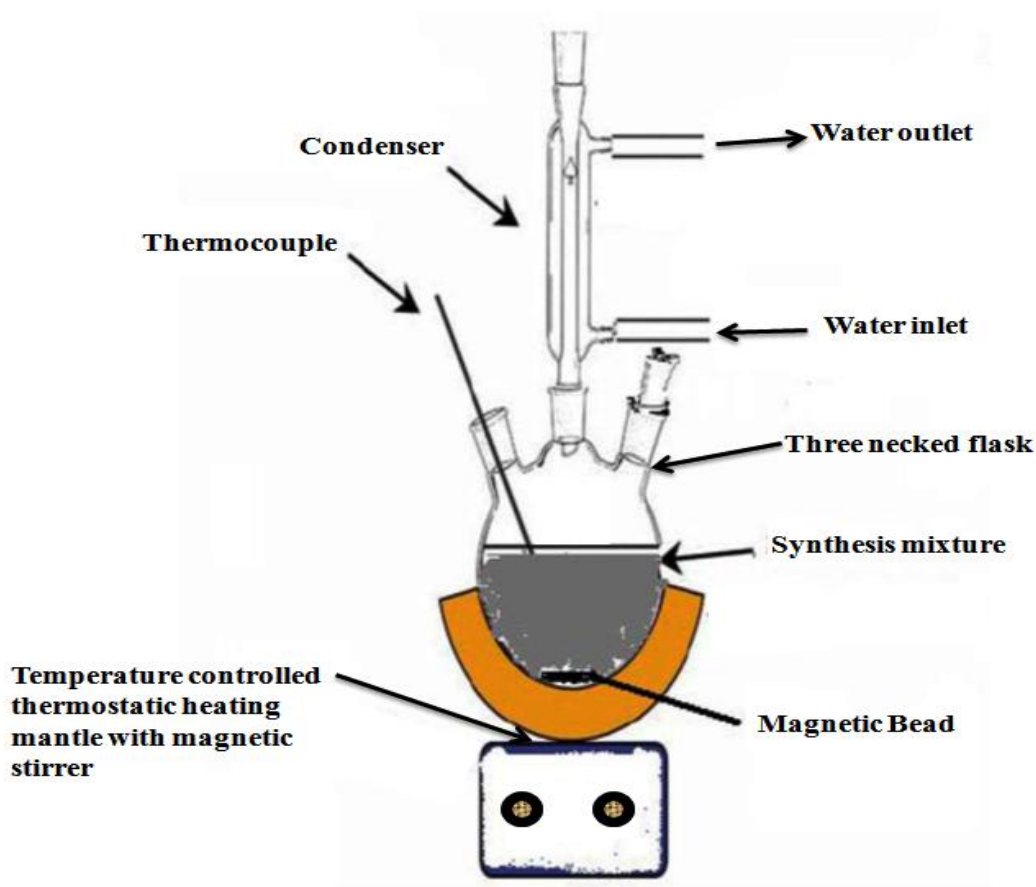
Figure 3.1 Schematic diagram of laboratory scale reactor for nanoparticle synthesis.

3.3.1 Synthesis of TiO_2 nanoparticles using combustion synthesis ($CSTiO_2$) method

To synthesize TiO_2 using combustion synthesis method, the methodology followed by Nagaveni et al. (2004) was adopted. A beaker containing 100 mL of distilled water was kept in a water bath at room temperature. 8.8 mL of TTIP solution was added drop wise to the distilled water. The mixture was stirred continuously using a magnetic stirrer for twenty minutes until a curdy white precipitate of titanyl hydroxide was obtained. 100 mL of concentrated HNO_3 was added very slowly to the above suspension. A clear light yellow solution of titanyl nitrate was obtained. Then 2.5024 g of glycine was added to the solution. The solution was transferred to silica crucible and kept in a muffle furnace at 350 °C for 15 min. At the end of 15 min, a white powder of TiO_2 was obtained. TiO_2 was then calcined at 450 °C in a muffle furnace for 3 h.

3.3.2 Synthesis of TiO_2 nanoparticles using sol gel ($SGTiO_2$) method

TiO_2 was synthesized using sol gel method as per the methodology explained by Rupa et al. (2009). 17 mL of TTIP was mixed with 40 mL of 2-propanol. This mixture was added drop wise into a mixture consisting of 5 mL water, 15 mL acetic acid and 60 mL 2-propanol with vigorous stirring for 2 h. The gel obtained was then dried in an oven at
105 °C for 12 h until it turns into white block crystals. Then these particles were calcined in a muffle furnace at 450 °C for 3 h.

3.4 Synthesis of Ag doped TiO_2 nanoparticles

In the synthesis of Ag doped TiO_2 nanoparticles, Ag to Ti molar ratio of 1:1.7 was used. This ratio was the optimum ratio obtained for core shell nanoparticles for maximum degradation of the dyes. Ag doped TiO_2 nanoparticles were synthesized by three different methods: sol gel method, liquid impregnation method and photodeposition method described below.

3.4.1 Synthesis of Ag doped TiO$_2$ nanoparticles by sol gel (Ag doped-SGTiO$_2$) method

The synthesis of Ag doped TiO$_2$ using sol gel method was carried out using the methodology followed by Zhang et al. (2008). 17 mL of TTIP was mixed with 40 mL of 2-propanol by magnetic stirring and the mixture was marked as solution A. 3.53 g of AgNO$_3$ was added to a mixture consisting of 10 mL water, 10 mL acetic acid, and 40 mL of 2-propanol and marked as solution B. Solution A was added drop-wise into solution B with vigorous stirring at room temperature. After addition, the solution was further stirred for about 1 h and then dried in an oven at 105 °C for 12 h. Then these particles were calcined in a muffle furnace at 450 °C for 3 h.

3.4.2 Synthesis of Ag doped TiO$_2$ nanoparticles by liquid impregnation (Ag doped (LI) - CSTiO$_2$) method

Ag doped TiO$_2$ nanoparticles were synthesized by liquid impregnation method as per the methodology explained by Sahoo et al. (2005) and Behnajady et al. (2008). In the liquid impregnation method, silver ion (Ag$^+$) doped TiO$_2$ was prepared according to the following steps. 3 g of TiO$_2$ powder prepared by combustion synthesis method explained in Section 3.3.1 were added to 100 mL of deionized water. Then 3.923 g of AgNO$_3$ was added to TiO$_2$ suspension for doping such that Ag to Ti ratio on molar basis was 1:1.7 as per the requirement. The slurry was stirred well and allowed to rest for 24 h and then dried in a hot air oven at 100 °C for 12 h. The dried solids were ground in an agate mortar and calcined at 450 °C for 3 h in a muffle furnace.

3.4.3. Synthesis of Ag doped TiO$_2$ nanoparticles by photodeposition (Ag doped (PD) - CSTiO$_2$) method

To synthesize Ag doped TiO$_2$ using photodeposition method, the procedure given by Behnajady et al. (2008) was followed. In the photodeposition method, Ag metal doped on TiO$_2$ was prepared by photo reducing Ag$^+$ ions to Ag metal on the TiO$_2$ surface according to the following steps: 3.0 g of TiO$_2$ synthesized by combustion

synthesis method as explained in Section 3.3.1 was added to 100 mL distilled water. The pH of the TiO_2 suspension was adjusted to 3, by addition of perchloric acid. Then, 3.923 g of $AgNO_3$ for doping was added to the TiO_2 suspension such that Ag to Ti ratio on molar basis was 1:1.7 as per the requirement. The mixture was then irradiated with UV light (36 W) for 3 h and then dried in a hot air oven at 100 $^{\circ}$C for 12 h. The dried solids were ground in an agate mortar and calcined at 450 $^{\circ}$C for 3 h in a muffle furnace.

3.5 Characterization of Ag@TiO$_2$ nanoparticles

In order to be able to tailor the properties of any engineered nanoparticles, careful investigation of the produced particles is crucial. If characterization is performed on the nanoparticles, it is easy to determine what improvement in the properties of nanoparticles has been brought about and how these changes contribute to targeted application. In the current study characterization was essential to determine the size and shape of the nanoparticles, to ensure the formation of core-shell structure, to determine the composition, crystallinity, band gap energy, thermal stability and light absorption characteristics. Ag@TiO_2 nanoparticles synthesized were characterized using various well documented techniques such as Transmission Electron Microscopy (TEM), Selected Area Electron diffraction (SAED), Energy Dispersive Spectra (EDS), Atomic Force Microscopy (AFM), X-Ray diffraction (XRD), Thermo gravimetric-differential thermal analysis (TG-DTA), Diffuse Reflectance Spectra (DRS) and Brunauer-Emmett-Teller (BET) surface area analysis. Knowledge on these characteristics has helped in understanding the photocatalytic activity of Ag@TiO_2 nanoparticles.

3.5.1. Transmission Electron Microscopy (TEM)

TEM is a microscopic technique in which a beam of electrons is transmitted through an ultra-thin specimen, interacting with the specimen as it passes through. An image is formed from the interaction of the electrons transmitted through the specimen; the image is magnified and focused (Pradeep 2010). TEM analysis of Ag@TiO_2

nanoparticles was done to obtain information about morphology, composition and crystallography. The TEM, SAED and EDS measurements were performed with a JEOL-JEM-2100 F microscope operating at an acceleration potential of 200 kV. For TEM measurements, the sample was prepared by dispersing the colloids in ethanol by sonication, followed by drying on a carbon film.

3.5.2 Atomic Force Microscopic (AFM) analysis

For nearly 20 years, Scanning Probe Microscopy (SPM) has been routinely employed as a surface characterization technique and AFM is the most widely used subset of SPM. AFM is ideally suited for characterization of nanoparticles, as it offers the capability of 3D visualization and both qualitative and quantitative information on many physical properties including size, morphology, surface texture and roughness. Statistical information, including size, surface area, and volume distributions, can be determined as well (Dror 1994). AFM consist sharp tip mounted on tiny cantilever spring attached with mechanical scanner which move over the surface to be characterized (Bonnell 2001). Surface height variation helps in variation of acting force on tip which further varies the bending of the cantilever. At the base of the cantilever spring, an integrated stress sensor measure bending which gets recorded in the electronic memory line by line (Bonnell 2001). AFM analysis of Ag@TiO$_2$ nanoparticles was done to obtain information about morphology and particle size distribution. AFM–measurements and imaging were carried out using a scanning probe microscope (model: NT-MDT, NTEGRA) and all the images were obtained in a contact mode. Software-based image processing of AFM data was done from groups of particle to generate quantitative information about particle size distribution. The statistics on groups of particles was carried out with image analysis and data processing which resulted in determination of particle size distribution of Ag@TiO$_2$ nanoparticles.

3.5.3 X-Ray diffraction (XRD) analysis

XRD is one of the powerful techniques for the characterization of nanoparticles. When X-rays interact with a crystalline substance (phase), diffraction pattern is obtained. The X-ray diffraction pattern of a pure substance is like a fingerprint of the substance. The powder diffraction method is thus ideally suited for characterization and identification of polycrystalline phases. The main use of powder diffraction is to identify components in a sample by a search/match procedure. Size of nanoparticles can also be determined using XRD. XRD analysis of Ag@TiO$_2$ nanoparticles was carried out to obtain information about crystalline structure and size. In the case of materials where the core and the shell are crystalline, diffraction patterns from the prominent lattice planes can be seen in the diffractograms (Pradeep 2010). The X-ray diffractograms of the dried samples of Ag@TiO$_2$ core-shell structured nanoparticles were obtained using JEOL X-ray Diffractometer (XRD); using CuK-alpha radiation ($\lambda = 1.5425$ Å, V = 40 KV, I = 20 mA) which allowed the determination of crystallite size of Ag@TiO$_2$ nanoparticles. The average crystallite size was obtained using the Scherrer's equation and is given by Eq.(3.1) (Spurr and Myers 1957; Harold and Leroy 1974)

$$D = k \times \lambda / (\beta \times cos\,\theta) \tag{3.1}$$

where D is the crystallite size, k is the constant dependent on crystallite shape (0.89), λ is the X-ray wavelength, β is the FWHM (full width at half max) or integral breadth, θ is the Bragg's angle, and β is the difference in angles at half max $[(2\theta\ High) - (2\theta\ Low)]$ (Spurr and Myers 1957; Klug and Alexander 1974).

3.5.4 Thermo gravimetric-differential thermal analyzer (TG-DTA)

TGA is an analytical technique used to determine a material's thermal stability and its fraction of volatile components by monitoring the weight change that occurs, as a specimen is heated. The measurement is normally carried out in air or in an inert atmosphere and the weight is recorded as a function of increasing temperature. DTA is an analytical technique used to determine a material's thermal stability and the energy released or absorbed via chemical reactions during the heating process (Skoog

et al. 2003). In the present study, the weight changes in the catalyst were measured using thermo gravimetric-differential thermal analyzer (TG-DTA) (model: 6000 TG-DTA 6300, Exstar, Japan) under nitrogen gas flow of 50 mL/min. The temperature was raised from room temperature to 600 ºC using a linear programmer at heating rate of 10 ºC/min. The sample weight was between 5 and 10 mg.

3.5.5 Diffuse Reflectance Spectra (DRS) analysis and determination of band gap energy

DRS is a frequently used technique for obtaining information about the optical properties of powder sample. The method utilizes spectral difference between incident and backscattered light intensity for quantifying the underlying absorption and scattering processes that affects the light-medium interaction (Masuda et al. 2007). Optical absorption characterization of the Ag@TiO$_2$ nanoparticles was done using diffuse reflectance spectroscopy (DRS) (Varian Cary 5000 Spectrometer) within the wavelength range of 200-800 nm. The incident beam is collimated, and reflected light is captured by an integrating sphere. To provide a nominal 100 % reflectance measurement, teflon reference was used. For diffuse reflectance measurement, the incident light is diffusely scattered on the surface of finely powdered sample and then scattered light is concentrated on reflectance sphere. Diffuse reflectance spectra provides information about the band gap energy of powder sample i.e. minimum energy required for an electron to be excited from valance band to conduction band. Band gap measurement is very important for a photocatalyst. Band gap was calculated using Kubelka Munk's model i.e. a two-flux model which means, only diffused light is considered. Process for obtaining the band gap was based on Tauc's plot (Tauc et al. 1966; Tauc 1972; Davis and Mott 1970). Kubelka Munk's transformation of measured reflectance was performed using Eq.(3.2).

$$k = \frac{(1-R)^2}{2R} \hspace{6cm} (3.2)$$

where k is reflectance transformed according to Kubelka Munk and R is the reflectance (%).

The reflectance data were fitted to equations for both indirect Eq.(3.3) and direct band gap transitions Eq.(3.4), to find the type of band to band transition in Ag@TiO$_2$ nanoparticles. The indirect and direct band gap transitions can be expressed by Kubelka –Munk's model as follows:

For indirect band gap transition (Reddy et al. 2002)

$$(k \times h\nu)^{1/2} = f(h\nu) \tag{3.3}$$

For direct band gap transition (Reddy et al. 2002)

$$(k \times h\nu)^{2} = f(h\nu) \tag{3.4}$$

Where h= Plank's constant = 6.626×10^{-34} J/s, $\nu = \frac{c}{\lambda}$ where c = Speed of light = 3×10^{8} m/s and λ= wavelength (nm= 10^{-9} m)

The indirect and direct band gap equations were used to construct the plots. $f(h\nu)$ was plotted against the photon energy E$_g$ = $h\nu$ in eV for both direct and indirect band gap transition. Then band gap of Ag@TiO$_2$ core-shell nanoparticles was calculated from linear portion of the plot by drawing tangent and the value associated with the intersection of the tangent to the plotted curve inflection point with the horizontal axis gives the band gap energy (Tauc 1966). The Tauc's plot for transition mode which shows a perfect fit of corresponding equation and realistic values of band gap energy was considered. Based on the fit of the equation, the transition mode was selected and corresponding band gap energy was obtained.

3.5.6 Surface area analysis by Brunauer-Emmett-Teller (BET)

BET analysis provides precise specific surface area evaluation of materials by nitrogen multilayer adsorption measured as a function of relative pressure using a fully automated analyser. The technique encompasses external area and pore area evaluations to determine the total specific surface area in m^2/g yielding important information in studying the effects of surface porosity and particle size in many applications. Surface area analysis of nanoparticles was carried out by BET method (Quanta chrome, USA). The sample weights used was 0.02 g.

3.6. Preparation of aqueous dye solutions and analysis of the dyes

3.6.1. Preparation of aqueous dye solutions

Aqueous dye solutions at the required concentrations were prepared by dissolving appropriate quantity (considering the purity) of the dyes in 100 mL distilled water. For example, 100 mg/L of AY-17 dye solution was prepared by dissolving 0.0166 g of AY-17 (purity 60 %) in 100 mL of distilled water and 100 mg/L of RB-220 solution was prepared by dissolving 0.011 g of RB-220 (90 % pure) in 100 mL of distilled water.

3.6.2. Analysis of dyes

The dye concentrations in the aqueous samples were analyzed by measurement of the absorbance of the solutions at the corresponding wavelengths (at 418 nm for AY-17 and at 609 nm for RB-220) using Hitachi UV-160A spectrophotometer and then by obtaining the corresponding concentration from the calibration equation. The procedure for calibration of the spectrophotometer, calibration data and calibration plot with the corresponding calibration equation for both the dyes are presented in Appendix I. Whenever the concentrations of the samples were beyond the calibration concentration limits, the samples were suitably diluted before the measurement of absorbance and the concentration obtained from the calibration equation were multiplied by the dilution factors.

3.7. Photocatalysis experiments

Batch photocatalysis experiments were conducted to study the efficacy of the nanoparticles as photocatalysts both under UV and solar light irradiation. Core-shell structured Ag@TiO$_2$ nanoparticles were used as photocatalysts for the degradation of AY-17 and RB-220 dyes. The efficacy of these nanoparticles was also compared with commercial Degussa-P25 catalyst and other synthesized TiO$_2$ and Ag doped TiO$_2$

nanoparticles. The experimental set up used for these experiments and the experimental procedures are explained in the following sections.

3.7.1. Experimental setup

The experimental setup for UV photocatalysis is shown in Figure 3.2. It consisted of an aluminium chamber of 40 cm $\times$ 70 cm $\times$ 70 cm dimensions equipped with two numbers of 18 W UV lamps (wavelength, λ = 365 nm, Philips), placed vertically as shown in Figure 3.2. The UV lamps are placed 22 cm apart. The lamps are specified to radiate 80 % UV-A and 20 % UV-B light. A borosilicate glass reactor was placed equidistant from both the UV lamps. The reaction mixture in the reactor was magnetically stirred. Air was continuously bubbled through the reactor contents, at a flow rate of 2 LPM. Figure 3.3 shows the photographic image of the experimental UV photocatalytic reactor set up used in the current study. Light intensity was measured using a UV light intensity meter (model: UV-340A, Lutron) and an average light intensity of 5.85 mW/cm^2 was found at the reactor walls. To maintain a constant temperature in the reactor, an exhaust fan was fitted on top of the chamber to drive out the heated air. The temperature of the reaction mixture during the entire irradiation period of 360 min was 31.5 $\pm$ 1.5° C for UV photocatalysis.

Similar reactor was used for experiments on solar photocatalysis (Figure 3.4) and experiments were done in an open terrace between 10:00 a.m. and 4:00 p.m. Figure 3.5 shows the photographic image of the reactor used for solar photocatalysis. The reaction mixture was magnetically stirred. The intensity of solar light was measured using UV light intensity meter (UV-340A, Lutron) and lux meter (KM-LUX-100K) respectively for UV and visible light intensity. The temperature of the reaction mixture was measured and found to be 33 $\pm$ 3 °C during the entire irradiation period of 360 min.

To study the effect of light intensity, an immersion well photochemical reactor (Figure 3.6) supplied by Scientific Aids and Instruments Corporation, Chennai, India was used. It consists of a double walled immersion well made of quartz (IWQ1), which houses the lamp. Inlet and outlet tubes are provided into the annular space between the double walls of the immersion well for circulation of water for cooling.

The immersion well is placed inside a borosilicate cylindrical reaction flask of 150 mL volume (Model A/150), with flattened bottom for placing the magnetic stirring bead. It is provided with one angle socket and one vertical socket made of glass. The reaction mixture containing the dye solution and the catalyst was placed in the reaction flask and continuously stirred with magnetic stirrer. Cooling water was circulated through the annular space in immersion well. Tubing for air supply was inserted into the reaction flask through one of the sockets on the wall of the reaction flask. Samples from reaction mixture were withdrawn using a peristaltic pump through a tube inserted into another socket on the reaction flask wall. Figure 3.7 shows the photographic image of the immersion well photoreactor. The reactor content was irradiated with 80 or 125 W medium pressure mercury vapor lamps that radiate pre-dominantly 365-366 nm radiation with smaller amounts in the wavelength of 265, 297, 303, 313 nm, as well as small amounts in the visible region. The lamps are housed inside the immersion well. The immersion well photoreactor was housed in an aluminium chamber so as to protect the personnel from UV radiations and to avoid radiation loss.
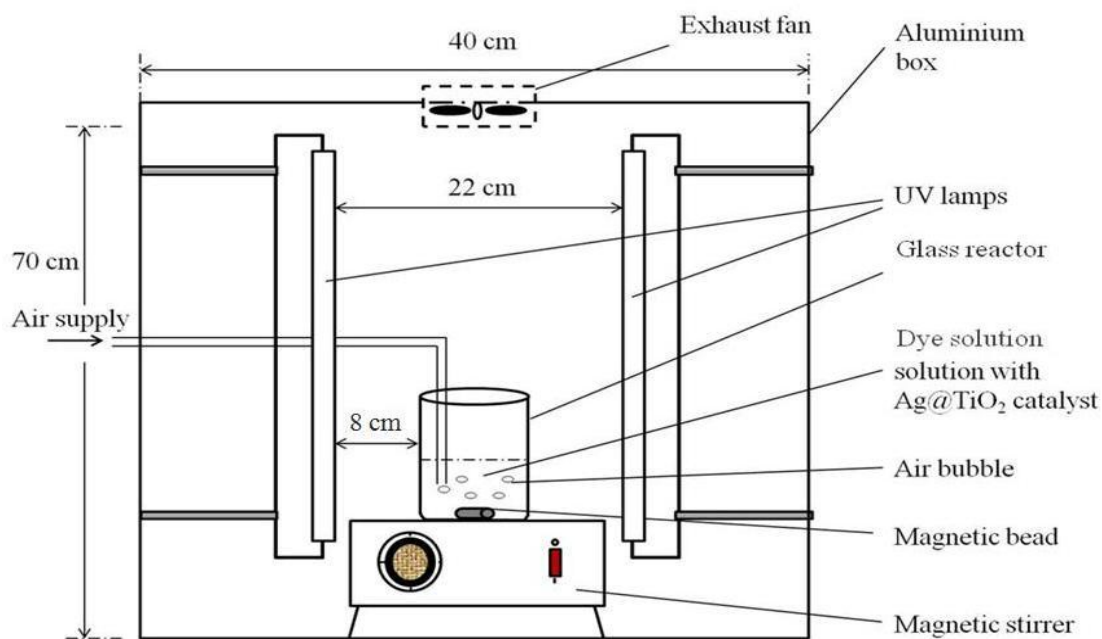
Figure 3.2 Schematic diagram of the laboratory-scale batch stirred reactor for UV photocatalysis.

Figure 3.3 Photographic image of the batch stirred reactor experimental set-up for UV photocatalysis.
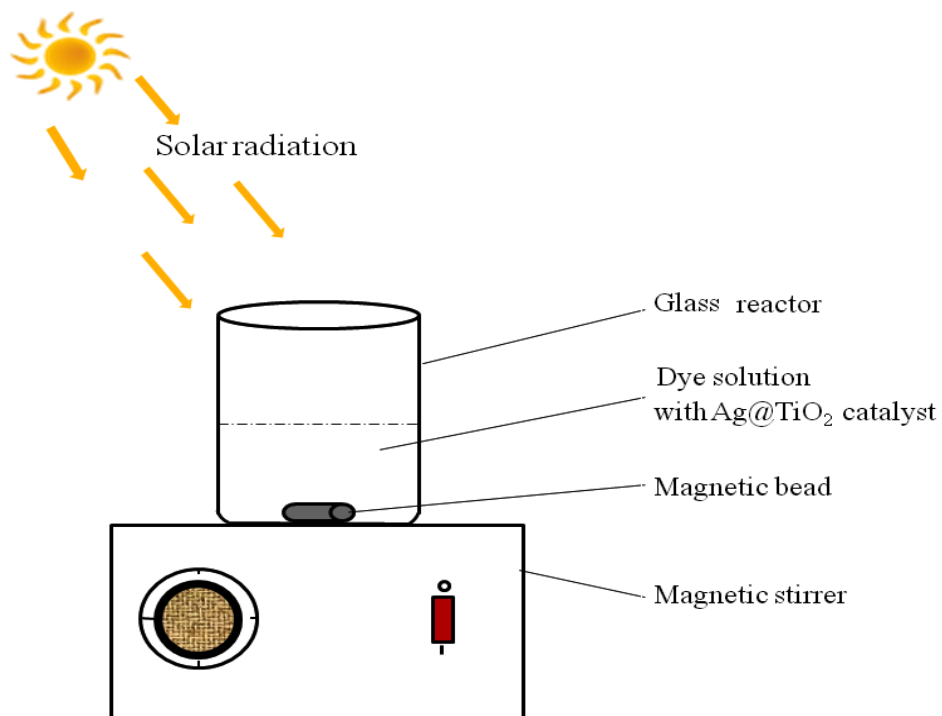
Figure 3.4 Schematic diagram of the batch stirred reactor experimental set-up for solar photocatalysis.

Figure 3.5 Photographic image of the batch stirred reactor experimental set-up for solar photocatalysis.
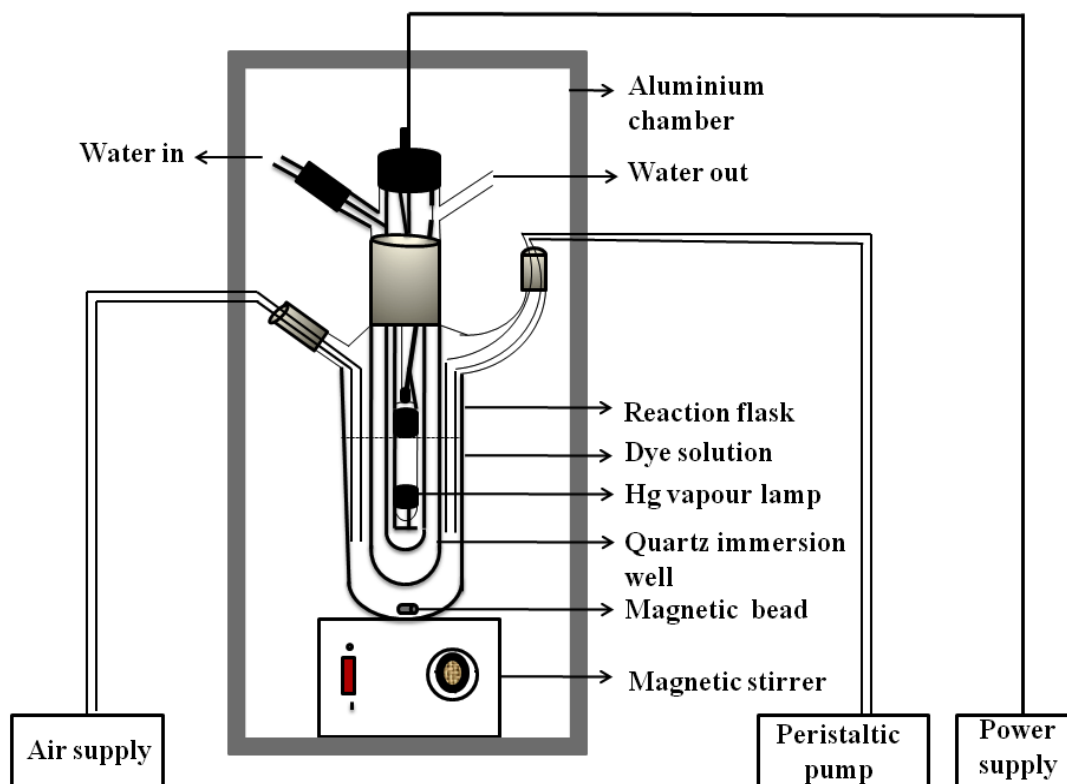
Figure 3.6 Schematic diagram of quartz immersion well photoreactor.

Figure 3.7 Photographic image of quartz immersion well photoreactor.

3.8 Experimentation

3.8.1 Photocatalysis experiments in batch stirred reactor

Batch photocatalytic degradation experiments were performed in a batch stirred reactor for photocatalytic degradation of the dyes with Ag@TiO$_2$ core shell structured nanoparticles or other photocatalysts, as per requirement of the experimental studies under UV or solar light irradiation. In all the experiments 100 mL aqueous dye solution with the required concentration of the dye, containing appropriate quantity of the photocatalyst was used. Initial pH of the solution was adjusted to a required value by adding 0.01 N NaOH or 0.01 N H$_2$SO$_4$ and by measuring the pH with a pH meter (Equip-Tronics model no.EQ-610). Aqueous dye solutions were magnetically stirred. In the absence of other oxidants, air was bubbled through the reaction mixture continuously at a flow rate of 2 LPM for UV photocatalysis. For experiments with other oxidants, appropriate quantities of oxidants (H$_2$O$_2$, (NH$_4$)$_2$S$_2$O$_8$, KBrO$_3$) were added to the reaction mixture. In experiments for solar photocatalysis, where these oxidants were not used, only the dissolved oxygen present in the reaction mixture acted as the oxidant. No additional air supply was provided for solar photocatalysis. At regular time intervals, 3 mL of the samples were withdrawn and centrifuged at

10000 rpm for 5 min to separate the catalyst. The absorbance of the dye solution at λ_{max} (418 nm for AY-17 and 609 nm for RB-220) was measured by a UV–Vis spectrophotometer (Hitachi model no.U-2000) and corresponding dye concentration in the solution was measured. The percentage of degradation of the dye was calculated by using Eq.(3.5)

$$\% \, degradation = \frac{(C_0 - C)}{C_0} \times 100 \tag{3.5}$$

where C_0 is the initial dye concentration and C is the dye concentration in the reactor at any time. All the experiments were performed in triplicates, and at each sampling time, average values are reported.

Various experimental studies were conducted in batch stirred reactor and are listed below.

(i) Batch photocatalysis experiments were conducted with Ag@TiO$_2$ nanoparticles synthesized with different Ag to Ti molar ratio followed by calcination at different temperatures. The experiments were conducted for the degradation of both AY-17 and RB-220 using Ag@TiO$_2$ synthesized with varying Ag to Ti molar ratio range of 1:5, 1:3.1, 1:2.2, 1:1.7,1:0.8, calcined at temperature range of 150-550 ºC for 3 h under the following conditions: (a) for AY-17 dye with initial pH=3, catalyst loading= 100 mg/L, initial dye concentration= 10 mg/L, (b) for RB-220 dye at initial pH=3, catalyst loading= 1 g/L for UV photocatalysis and 500 mg/L for solar photocatalysis, initial dye concentration= 50 mg/L. Effect of Ag to Ti molar ratio and calcination temperature on photocatalytic degradation was studied. These experimental results were also analyzed to select optimum Ag to Ti molar ratio and calcination temperature based on maximum degradation of the dyes.

(ii) Ag@TiO$_2$ nanoparticles were synthesized with optimum Ag to Ti molar ratio (1:1.7) and calcined at optimum temperature for different calcination times ranging from 1-5 h. Batch photocatalysis experiments under UV and solar light irradiation were conducted with these nanoparticles calcined for different time periods, to study the effect of calcination time on photocatalytic degradation of both the dyes. The conditions used for these studies were: (a) for AY-17 dye: initial pH=3, catalyst loading=100 mg/L, initial dye concentration=10 mg/L. (b) for RB-220 dye: initial pH=3, catalyst loading=1 g/L for UV photocatalysis and 500 mg/L for solar

photocatalysis, initial dye concentration=50 mg/L. These experiments were conducted to select optimum calcination time and the optimum values were selected, based on maximum degradation of the dyes.

(iii) Batch experiments were then conducted in order to confirm that the removal of AY-17 and RB-220 from contaminated water, in the presence of light and $Ag@TiO_2$ nanoparticles is due to photocatalysis. Batch experiments were conducted for removal of AY-17 and RB-220 dyes (a) under UV or solar light irradiation and in the absence of the catalyst, (b) under dark conditions with $Ag@TiO_2$ nanoparticles, and (c) with $Ag@TiO_2$ under UV and solar light irradiations. In all the experiments 100 mL of dye solution was used. Experiments were conducted at following conditions under UV and solar light irradiation (a) for AY-17: pH=3, initial dye concentration=10 mg/L and catalyst loading=100 mg/L (wherever applicable), (b) for RB-220 dye: pH=3, initial dye concentration=50 mg/L and catalyst loading=1 g/L (UV) and 500 mg/L (solar) (wherever applicable). Similar conditions were used for experiments under dark.

(iv) Further batch photocatalysis experiments were conducted under UV and solar light irradiation, with $Ag@TiO_2$ nanoparticles synthesized with optimum Ag to Ti molar ratio and calcined at optimum temperature for optimum period of time. Experiments were also conducted with commercial TiO_2 (Degussa P25) and other catalysts such as $SGTiO_2$, $CSTiO_2$, Ag doped-$SGTiO_2$, Ag doped (LI)-$CSTiO_2$ and Ag doped (PD)-$CSTiO_2$. Ag doped TiO_2 nanoparticles used in these experiments were synthesized with optimum Ag to Ti molar ratio chosen for $Ag@TiO_2$ nanoparticles and were calcined at 450 ºC for 3h. Conditions used for these experiments were: (a) for AY-17 dye: initial pH=3, catalyst loading=100 mg/L, initial dye concentration=10 mg/L. (b) for RB-220 dye: initial pH=3, catalyst loading=1 g/L for UV photocatalysis and 500 mg/L for solar photocatalysis, initial dye concentration=50 mg/L. The photocatalytic activity of these nanoparticles in terms of photocatalytic degradation of AY-17 and RB-220 dyes was compared with that of $Ag@TiO_2$ core shell structured nanoparticles by UV and solar photocatalysis.

(v) Batch photocatalysis experiments were then conducted with $Ag@TiO_2$ nanoparticles synthesized with optimum Ag to Ti molar ratio and calcined at optimum temperature for optimum period of time, to study the effect of pH ranging from 1-9

for UV and solar photocatalysis of AY-17; 2-7 for UV photocatalysis of RB-220 and 2-9 for solar photocatalysis of RB-220. The conditions used for these studies were: (a) for AY-17 dye: catalyst loading=100 mg/L, initial dye concentration=10 mg/L. (b) for RB-220 dye: catalyst loading=1 g/L for UV photocatalysis and 500 mg/L for solar photocatalysis, initial dye concentration=50 mg/L. These experiments were conducted to select the optimum pH and the optimum values were selected based on maximum degradation of the dyes. Batch photocatalysis experiments were also conducted at different pH under the light source (UV or solar) and in the absence of catalyst in order to confirm the sole effect of pH on the degradation of AY-17 and RB-220 dyes. Optimum pH was chosen based on 'one factor at a time' analysis.

(vi) Batch photocatalysis experiments were then conducted with Ag@TiO$_2$ nanoparticles synthesized with optimum Ag to Ti molar ratio and calcined at optimum temperature for optimum period of time, to study the effect of catalyst loading ranging from 50-1000 mg/L for UV and 50-500 mg/L for solar photocatalysis of AY-17 and 500-2000 mg/L for UV and 250-2000 mg/L for solar photocatalysis of RB-220. Experiments were conducted at optimized pH values for both the dyes. The conditions used for these studies were: (a) for AY-17 dye: initial pH=3, initial dye concentration=10 mg/L. (b) for RB-220 dye: initial pH=3, initial dye concentration=50 mg/L. These experiments were conducted to select the optimum catalyst loading and the optimum values were selected, based on maximum degradation of the dyes. Optimum catalyst loading was chosen based on 'one factor at a time' analysis. Optimum dye to catalyst ratio was selected based on optimum catalyst loading obtained.

(vii) Batch photocatalysis experiments were also conducted by varying the dye concentration and catalyst loading individually, while keeping the dye to catalyst ratio constant, to study whether, initial dye concentration acts as an independent parameter affecting the degradation. Initial dye concentration was varied from 10-200 mg/L for UV and 10-500 mg/L for solar photocatalysis of AY-17; 50-200 mg/L for UV and 50-500 mg/L for solar photocatalysis of RB-220. Experiments were conducted by keeping dye to catalyst ratio constant at 1:30 (g/g) for UV and 1:10 (g/g) for solar photocatalysis of AY-17 and 1:20 (g/g) for UV and 1:10 (g/g) for solar photocatalysis of RB-220. Initial pH was adjusted to 3. These experiments were conducted to select

optimum dye to catalyst ratio and the optimum values were selected based on maximum degradation of the dyes.

(viii) Batch photocatalysis experiments were conducted with different oxidants such as H_2O_2, $(NH_4)_2S_2O_8$ and $KBrO_3$ under UV and solar light irradiation at the following conditions: (a) for AY-17 dye: pH=3, initial dye concentration= 100 mg/L, optimum dye to catalyst ratio=1:30 (g/g)(from one factor at a time analysis) for UV photocatalysis and pH=3, initial dye concentration= 100 mg/L, optimum dye to catalyst ratio=1:10 (g/g) (from one factor at a time analysis) for solar photocatalysis (b) for RB-200 dye: pH=3, initial dye concentration= 100 mg/L, dye to catalyst ratio=1:20 (g/g) for UV photocatalysis and pH=3, initial dye concentration= 100 mg/L, dye to catalyst ratio=1:10 (g/g) for solar photocatalysis. These experiments were conducted with oxidants in the following concentration range: H_2O_2 (5 to 20 mM), $(NH_4)_2S_2O_8$ (1 to 4 g/L) and $KBrO_3$ (1 to 4 g/L) for UV and solar photocatalysis of AY-17 and H_2O_2 (10 to 40 mM), $(NH_4)_2S_2O_8$ (0.5 to 2.5 g/L) for UV and solar, $KBrO_3$ (2 to 6 g/L) for UV and $KBrO_3$ (1 to 4 g/L) for solar photocatalysis of RB-220. Batch photocatalysis experiments were also conducted at different concentrations of oxidants under the light source (UV or solar) and in the absence of catalyst in order to confirm the sole effect of oxidants (H_2O_2, $(NH_4)_2S_2O_8$, and $KBrO_3$) on the degradation of AY-17 and RB-220 dyes. Effect of concentrations of each of the oxidants on photocatalytic degradation of the dyes was studied and optimum concentration of each of the oxidants was obtained. Then the degradation of the dyes with optimum concentration of different oxidants were compared. Based on these studies, the best oxidant among those studied in the current work, was chosen.

Optimum values of pH, optimum dye to catalyst ratio and optimum oxidant concentration were thus obtained by crude optimization method based on 'One factor at a time' set of experimental results. The range of pH, catalyst loading and oxidant concentration for RSM based optimization studies were also chosen based on these initial set of 'One factor at a time' experimental result analysis.

(ix) Batch photocatalysis experiments were conducted under UV and solar light to check the feasibility of reuse of Ag@TiO$_2$ catalyst for repeated photocatalysis. In all the experiments 100 mL of dye solution was used. Experiments were conducted under following conditions (a) for AY-17: pH=3, catalyst loading=1.5 g/L, initial dye

concentration=50 mg/L for UV photocatalysis and pH=3, catalyst loading=1 g/L, initial dye concentration=100 mg/L for solar photocatalysis (b) for RB-220 dye: pH=3, catalyst loading=1g/L, initial dye concentration=50 mg/L for UV and pH=3, catalyst loading=500 mg/L, initial dye concentration=50 mg/L for solar photocatalysis. After performing an experiment with freshly prepared catalyst, it was reused thrice for further experiments. The regeneration of catalyst for the next cycle was done by centrifugation at 10,000 rpm for 10 min to separate the particles from the reaction mixture and then by suspending the separated particles in ethanol for washing. The particles were further separated from ethanol by centrifugation. The process of ethanol washing and centrifugation was repeated thrice. To remove ethanol from the particles after centrifugation, the particles were dried in an oven at 100 ^{0}C for 2 h. These particles were then used for next cycle of batch experiment. Same experimental conditions were used for all the four cycles (with fresh catalyst and for three cycles of reuse).

3.9 Optimization of factors affecting the degradation of AY-17 and RB-220 dyes

3.9.1 Optimization of conditions for photocatalytic process

The methodical optimization of factors affecting the photocatalytic process namely, pH, catalyst loading and the oxidant concentration were carried out by conducting batch experiments under UV and solar light radiation, in accordance with the experiments designed as per Design of Experiments (DOE) strategy. The oxidant which yielded maximum degradation and highest rate of degradation of the dyes during the initial set of experiments (One factor at a time) conducted to screen a suitable oxidant was selected for optimization. The selected factors for optimization were pH (X_1), catalyst loading (X_2) and the oxidant concentration (X_3). These three factors were chosen at five different levels. The selected oxidant was ammonium persulfate for degradation of both the dyes. Experiments were designed as per Central Composite Design (CCD). DOE based on CCD needed twenty experimental runs with three factors and five levels. Twenty sets of experimental conditions obtained through CCD are presented in Table 3.4 and Table 3.5 respectively for UV and solar

photocatalysis of AY-17 and RB-220 dyes. Twenty sets of batch photocatalysis experiments were conducted for each of the dyes and both under UV and solar light irradiation. For statistical calculations, the variables Xi were coded as x_i according to the following relationship:

$$x_i = \frac{X_i - X_0}{\delta X} \qquad\qquad (3.6)$$

where X_0 is the value of X_i at the center point and δX represents the step change (Khatee et al. 2009) . x_i is the coded factor for the actual value of the factor *Xi* (Uncoded). Table 3.3 and Table 3.4 show the various levels of pH, catalyst loading and ammonium persulfate concentration used for design of experiments for UV and solar photocatalysis of AY-17 and RB-220 dyes respectively in coded (x_i) and uncoded (*Xi*) form. Batch experimental trials were conducted as described in Section 3.8.1, at experimental conditions specified by the experimental design matrix through CCD, which is presented in terms of coded and uncoded levels in Table 3.5 and Table 3.6 for UV and solar photocatalysis of AY-17 and RB-220 dyes respectively. In all the experiments, initial dye concentration of 100 mg/L was used. Concentration of the dye (AY-17 or RB-220) was measured by spectrophotometric analysis as described in Section 3.8.1. Percentage degradation of AY-17 dye obtained at the end of 15 min for UV and solar photocatalysis were subjected to analysis using Response Surface Methodology (RSM). Percentage degradation of RB-220 dye obtained at the end of 20 min for UV photocatalysis and 10 min for solar photocatalysis were subjected to analysis using RSM.

3.9.2 Multiple regression analysis and optimization using RSM

The results of the experiments conducted under conditions based on Central Composite design set were analyzed using RSM. The effects of three factors (pH, catalyst loading and ammonium persulfate concentration) as individuals and in combination with interacting effect on the response [% degradation of AY-17 or RB-220] were evaluated using RSM. Multiple regression analysis (MRA) on the experimental input-output data was performed using MINITAB 14 software. The results were fitted into the regression equation and the effects of factors on the response were analyzed by RSM. The analysis included the linear and quadratic

effects of the three factors and their interactions. Thus, the equations giving percentage degradation of the dyes as a function of the factors fitted onto second-order polynomial model with 10 coefficients ($b_0, b_1,\ b_{12}\ ...... \ b_{23}$), is presented in Eq.(3.7).

$$Y = b_o + b_1X_1 + b_2X_2 + b_3X_3 + b_{11}X_1^2 + b_{22}X_2^2 + b_{33}X_3^2 + b_{12}X_1X_2 + b_{13}X_1X_3 + b_{23}X_2X_3 \qquad (3.7)$$

where Y is the response (percentage degradation of the dye). X_1, X_2 and X_3 are the uncoded values of the factors pH, catalyst loading and ammonium persulphate concentration respectively. b_0 is the constant ; b_1, b_2 and b_3 are the regression coefficients for linear effects; b_{11}, b_{22} and b_{33} are regression coefficients for quadratic effects; b_{12}, b_{13} and b_{23} are the regression coefficients for interaction effects. The coefficients were estimated using MRA with MINITAB 14 software. The significance of the terms in the model were evaluated by using Analysis of Variance (ANOVA) based upon the *F*-test with unequal variance ($P<0.05$) (Liu et al. 2005a). The optimum values of the pH, catalyst loading, and ammonium persulfate concentration were obtained by using response optimizer of MINITAB 14 for UV and solar photocatalysis of AY-17 and RB-220 dyes.

Table 3.3 The coded and uncoded values of levels for pH, catalyst loading and ammonium persulfate concentration selected for design of experiments using CCD for AY-17 degradation under UV light and solar light irradiation.

Irradiation type	Coded levels (x_i)	-2	-1	0	1	2
	Factors	Uncoded levels (Xi)				
UV light	pH	1	2	3	4	5
	Catalyst loading (g/L)	0.5	2.0	3.5	5	6.5
	Ammonium persulfate concentration (g/L)	0.5	1.5	2.5	3.5	4.5
Solar light	pH	1	2.2	3.4	4.6	5.8
	Catalyst loading (g/L)	0.3	1.2	2.1	3	3.9
	Ammonium persulfate concentration (g/L)	0.5	1.5	2.5	3.5	4.5

Table 3.4 The coded and uncoded values of levels for pH, catalyst loading and ammonium persulfate concentration selected for design of experiments using CCD for RB-220 degradation under UV light and solar light irradiation.

Irradiation type	Coded levels (x_i)	-2	-1	0	1	2
	Factors	Uncoded levels (Xi)				
UV light	pH	2.2	2.7	3.2	3.7	4.2
	Catalyst loading (g/L)	1	1.4	1.8	2.2	2.6
	Ammonium persulfate concentration (g/L)	0.5	1	1.5	2	2.5
Solar light	pH	2.5	3	3.5	4	4.5
	Catalyst loading (g/L)	0.2	0.7	1.2	1.7	2.2
	Ammonium persulfate concentration (g/L)	0.5	1	1.5	2	2.5

Table 3.5 Central Composite design matrix represented in coded and uncoded units for the photocatalysis of AY-17 under UV and solar light irradiation.

Exp. No.	Values of factors (coded) for UV photocatalysis						Values of factors (coded) for solar photocatalysis					
	pH		Catalyst loading		Ammonium persulfate		pH		Catalyst loading		Ammonium persulfate	
	(x_1)	(X_1)	(x_2)	(X_2)	(x_3)	(X_3)	(x_1)	(X_1)	(x_2)	(X_2)	(x_3)	(X_3)
1	0	3	2	6.5	0	2.5	-2	1.0	0	2.1	0	2.5
2	0	3	-2	0.5	0	2.5	2	3.4	0	2.1	0	2.5
3	-2	1	0	3.5	0	2.5	0	3.4	0	2.1	0	0.5
4	0	3	0	3.5	2	4.5	0	3.4	-2	3.9	0	2.5
5	0	3	0	3.5	0	2.5	0	5.8	0	2.1	-2	2.5
6	0	3	0	3.5	0	2.5	0	3.4	0	2.1	2	2.5
7	0	3	0	3.5	-2	0.5	0	3.4	0	0.3	0	2.5
8	2	5	0	3.5	0	2.5	0	3.4	2	2.1	0	4.5
9	1	4	-1	2.0	-1	1.5	0	4.6	0	3.0	0	1.5
10	0	3	0	3.5	0	2.5	1	4.6	-1	1.2	-1	1.5
11	-1	2	1	5.0	1	3.5	1	4.6	1	1.2	-1	3.5
12	-1	2	1	5.0	-1	1.5	-1	4.6	-1	3.0	1	3.5
13	1	4	-1	2.0	1	3.5	1	2.2	-1	3.0	1	3.5
14	-1	2	-1	2.0	1	3.5	-1	2.2	1	3.0	-1	1.5
15	-1	2	-1	2.0	-1	1.5	-1	3.4	1	2.1	1	2.5
16	0	3	0	3.5	0	2.5	0	2.2	0	1.2	0	3.5
17	1	4	1	5.0	-1	1.5	-1	3.4	-1	2.1	-1	2.5
18	0	3	0	3.5	0	2.5	1	3.4	1	2.1	1	2.5
19	0	3	0	3.5	0	2.5	0	3.4	0	2.1	0	2.5
20	1	4	1	5.0	1	3.5	0	2.2	0	1.2	0	1.5

Table 3.6 Central Composite design matrix represented in coded and uncoded units for the photocatalysis of RB-220 under UV and solar light irradiation.

| Exp. No. | Values of factors (coded) for UV photocatalysis | | | | | | Values of factors (coded) for solar photocatalysis | | | | | |
| | pH | | Catalyst loading | | Ammonium persulfate | | pH | | Catalyst loading | | Ammonium persulfate | |
	(x_1)	(X_1)	(x_2)	(X_2)	(x_3)	(X_3)	(x_1)	(X_1)	(x_2)	(X_2)	(x_3)	(X_3)
1	-2	2.2	0	1.8	0	1.5	1	4.0	1	1.7	1	2.0
2	2	4.2	0	1.8	0	1.5	-1	3.0	-1	0.7	1	2.0
3	0	3.2	0	1.8	0	1.5	0	3.5	0	1.2	0	1.5
4	0	3.2	-2	1.0	0	1.5	1	4.0	1	1.7	-1	1.0
5	0	3.2	0	1.8	-2	0.5	0	3.5	0	1.2	0	1.5
6	0	3.2	0	1.8	2	2.5	0	3.5	0	1.2	0	1.5
7	0	3.2	0	1.8	0	1.5	0	3.5	0	1.2	0	1.5
8	0	3.2	2	2.6	0	1.5	-1	3.0	-1	0.7	-1	1.0
9	0	3.2	0	1.8	0	1.5	-1	3.0	1	1.7	1	2.0
10	1	3.7	-1	1.4	-1	1.0	1	4.0	-1	0.7	-1	1.0
11	1	3.7	1	2.2	-1	1.0	-1	3.0	1	1.7	-1	1.0
12	-1	2.7	-1	1.4	1	2.0	1	4.0	-1	0.7	1	2.0
13	1	3.7	-1	1.4	1	2.0	-2	2.5	0	1.2	0	1.5
14	-1	2.7	1	2.2	-1	1.0	0	3.5	0	1.2	-2	0.5
15	-1	2.7	1	2.2	1	2.0	2	4.5	0	1.2	0	1.5
16	0	3.2	0	1.8	0	1.5	0	3.5	2	2.2	0	1.5
17	-1	2.7	-1	1.4	-1	1.0	0	3.5	0	1.2	2	2.5
18	1	3.7	1	2.2	1	2.0	0	3.5	0	1.2	0	1.5
19	0	3.2	0	1.8	0	1.5	0	3.5	0	1.2	0	1.5
20	0	3.2	0	1.8	0	1.5	0	3.5	-2	0.2	0	1.5

3.9.3 Experiments at optimized conditions

Batch experiments were conducted at RSM based methodical optimized values of initial pH, catalyst loading and ammonium persulfate concentration. The optimum values obtained from the response optimizer of MINITAB 14 were used to verify the effectiveness of DOE and optimization strategy, as well as to validate the regression equation. Dye solution of 100 mg/L was prepared. Catalyst and ammonium persulphate were added such that their optimum concentrations were obtained. Initial pH was adjusted to the optimum value. Batch experiments were conducted under optimized conditions for UV and solar photocatalysis of AY-17 and RB-220 dyes. The percentage degradation obtained from the model and by experiments was compared to validate the model. The percentage degradations obtained under RSM based methodically optimized conditions were compared with those obtained under crude optimized conditions by "one factor at a time' analysis, to determine the effectiveness of RSM based optimization strategy.

3.10 Experiments to study effect of initial dye concentration

The effect of initial concentration on photocatalytic degradation of dyes was studied, as it is important from both mechanistic and application point of view. Batch photocatalysis experiments were carried out in a batch stirred reactor to study the effect of initial dye concentration on degradation of AY-17 and RB-220 dyes using $Ag@TiO_2$ core shell structured nanoparticles as the photocatalyst under UV and solar light irradiation. In all the experiments 100 mL aqueous dye solution in water was used and experiments were done at RSM based methodically optimized conditions. The effect of initial concentration of AY-17 on the UV and solar photocatalytic degradation was investigated over the concentration range from 100 mg/L to 700 mg/L. For RB-220, effect of initial concentration was investigated over the concentration range from 100 mg/L to 500 mg/L for UV and 100 mg/L to 700 mg/L for solar photocatalytic degradation. The experiments were conducted by keeping the catalyst loading at the optimum obtained for 100 mg/L dye concentration. So when the initial dye concentration was varied, the dye to catalyst ratio also varied. Samples

were withdrawn at regular intervals of time and analyzed for dye concentrations using UV–Vis spectrophotometer as described in Section 3.8.1 and percentage degradation were calculated.

3.11 Experiments to study the effect of light intensity

3.11.1 Batch experiments in immersion well reactor to study the effect of light intensity on UV photocatalysis

Batch photocatalysis experiments were carried out in an immersion well reactor shown in Figure3.6 to study the effect of light intensity on photocatalysis of AY-17 and RB-220 dyes using Ag@TiO$_2$ core shell structured nanoparticles as a photocatalyst under UV light irradiation. In all the experiments, 100 mL dye solution was used. The experiments were conducted for AY-17 dye degradation under the following experimental conditions: initial pH=3, catalyst loading= 3 g/L, initial dye concentration= 100 mg/L. Experiments were also conducted for RB-220 dye degradation under the following conditions: initial pH=3, catalyst loading= 2 g/L, initial dye concentration= 100 mg/L. Experiments were conducted with continuous supply of air into the reactor, which served as a source of oxidant. Experiments were conducted at two different light intensities provided by irradiation with 80 W or 125 W medium pressure Hg lamps. The UV light intensities with 80 W and 125 W lamps on the reactor wall surface were 11.2 and 13.5 mW/cm^2 respectively as measured by UV light intensity meter (UV-340A, Lutron). Air was bubbled through the reaction mixture continuously at a flow rate of 2 LPM. Aqueous dye solutions were magnetically stirred. The temperature of the reaction mixture during the entire irradiation period remained almost constant due to continuous water circulation around the lamps. At regular time intervals, 3 mL of the samples were withdrawn using peristaltic pump and centrifuged at 10000 rpm for 5 min to separate the catalyst. Concentration of the dye (AY-17 or RB-220) was measured by spectrophotometric analysis as described in Section 3.8.1.

3.11.2 Batch experiments in stirred reactor to study the effect of light intensity on solar photocatalysis

Batch photocatalysis experiments were carried out in stirred reactor to study the effect of light intensity on solar photocatalysis of AY-17 and RB-220 dyes using Ag@TiO$_2$ core shell structured nanoparticles as a photocatalyst on a sunny day, semi cloudy day and a cloudy day. The UV and visible light intensities were measured on the reactor walls at regular time periods during the experimental runs and at four different locations on the reactor walls, using UV intensity meter (UV-340A, Lutron) and lux meter (KM-LUX-100K) respectively. The light intensities were averaged over different locations on the reactor walls and over different time periods of experimental run. Three experiments were performed at different conditions of illumination; on a full sunny day (clear sky), on a semi cloudy day, and on full cloudy day. In all the experiments 100 mL aqueous dye solution was used. The experiments were conducted for AY-17 and RB-220 dye degradation under the following experimental conditions: initial pH=3, catalyst loading= 1 g/L, initial dye concentration= 100 mg/L, oxidant used= atmospheric air, average UV and visible light intensities on a full sunny, semi and full cloudy day were 3.56, 2.65 and 1.25 mW/cm^2 (UV) respectively and 13×10^4, 92×10^3 and 45×10^3 lux (visible) respectively. At regular time intervals, samples were withdrawn and the concentration of the dye (AY-17 or RB-220) was measured by spectrophotometric analysis as described in Section 3.8.1.

3.12 Effect of presence of salts on UV and solar photocatalytic degradation of dyes

Batch photocatalysis experiments were carried out in a batch stirred reactor to study the effect of salts such as NaCl, and Na$_2$CO$_3$ present in dye contaminated water, on degradation of AY-17 and RB-220 dyes using Ag@TiO$_2$ core shell structured nanoparticles as the photocatalyst under UV and solar light irradiation. All the experiments were performed under RSM based methodically optimized conditions. Samples were withdrawn at regular intervals of time and analyzed for dye concentrations using UV–Vis spectrophotometer as described in Section 3.8.1.

3.13 Mineralization of AY-17 and RB-220 dyes

To study the extent of mineralization of the dyes by UV and solar photocatalysis, batch experiments were conducted in a batch stirred reactor under RSM based methodically optimized conditions. Samples withdrawn from the reactor at various intervals of time were analyzed for COD, TOC, nitrate concentration, nitrite concentration, chloride concentration and sulphate concentration. The protocols for these analyses are presented in the following sub sections.

3.13.1 Determination of Chemical Oxygen Demand in aqueous dye solutions

Chemical Oxygen Demand (COD) measures the oxygen requirement equivalent of organic matter that is susceptible to oxidation with the help of a strong chemical oxidant. It is important, rapidly measured parameter as a means of measuring organic strength for streams and polluted water bodies. Measurement of COD was done with standard reflux method (APHA 1995). 0.4 g of mercuric sulphate ($HgSO_4$), 20 mL of sample or an aliquot of sample diluted to 20 mL with distilled water and 10 mL of 0.25 N potassium dichromate ($K_2Cr_2O_7$) solution was added to reflux flask and mixed well. 30 mL of concentrated sulphuric acid was added slowly to reflux flask and mixed properly. Then reflux flask was placed in a COD-digester and refluxed for minimum of 2 h at 150 ºC. After 2 h, heating and refluxing was stopped and solution was cooled to room temperature. The solution was then diluted to about twice its volume with distilled water and titrated against ferrous ammonium sulphate (FAS) with ferroin as the indicator. The sharp colour change observed from blue green to reddish brown indicates the endpoint or completion of the titration. Volume of FAS added was noted and titration was repeated three times to get concordant readings. Blank sample was prepared in similar way by substituting sample with distilled water and volume of FAS consumed for blank sample was also analyzed in the similar manner. COD was determined using Eq.(3.8).

$$COD \left(\frac{mg}{L}\right) = \frac{(a-b) \times N \times 8000}{mL \, of \, sample \, used}$$ (3.8)

Where, a= mL of FAS used for blank, b= mL of FAS used for sample, N= Normality of FAS.

3.13.2 Determination of Total Organic Carbon in aqueous dye solutions

Total Organic Carbon (TOC) measurement is the standard method for the evaluation of organic matter content in domestic and industrial wastes, as well as in surface and ground waters. The amount of organic matter present in water is an important criterion for its quality. TOC measurement was carried out with Shimadzu TOC-V$_{CSH}$ Carbon Analyzer.

3.13.3 Estimation of nitrate in aqueous dye solutions

In organic pollutants, nitrate ions are important indicators of pollution, as nitrogen from dye molecules often decompose as nitrate ions (APHA 1995). Estimation of nitrate ion was carried out with spectroscopic method (APHA 1995). 25 mL of sample and 1 mL of 2N hydrochloric acid (HCl) were added to 100 mL standard flask and solution was made upto the mark with distilled water. Blank sample was prepared in similar way by substituting sample with distilled water. Absorbance of the solution was measured at 220 nm using Hitachi U2000 model spectrophotometer against blank and the nitrate concentration was measured using the calibration equation. Calibration plot and calibration equation for nitrate ion analysis along with the detailed procedure of calibration is given in Appendix II.

3.13.4 Estimation of nitrite in aqueous dye solutions

For the determination of nitrite ion in surface water, sea water and wastewater, spectrophotometric method is the most useful (ISSO 6777:1984). It is based on the reaction of nitrite ions with sulfanilamide which result in formation of diazo compound. This compound further react with naphthylethylenediamine (NEDA)

yielding a red colour (ISSO 6777:1984). Estimation of nitrite ion was carried out with spectrophotometric method (ISSO 6777:1984). 50 mL of clear sample and 1mL of sulfanilamide solution was added to 100 mL standard flask and made upto the mark with distilled water. After 2-8 min, 1.0 mL of NEDA solution was added and mixed. Blank sample was prepared in similar way by substituting sample with distilled water. Absorbance of the solution against blank was measured at 540 nm using Hitachi U2000 model spectrophotometer and the nitrite concentration was measured using the calibration equation. Calibration plot and calibration equation for nitrite ion analysis along with the detailed procedure of calibration is given in Appendix III.

3.13.5 Estimation of sulphate in aqueous dye solutions

For the determination of sulphate ion in surface water, sea water and wastewater, turbidimetric method is the most useful (APHA 1995). In this method sulphate ion is precipitated in acidic medium with barium chloride and as a result barium sulphate crystals are formed. The absorbance is then measured by spectrophotometer and sulphate ion concentration is determined by comparison of reading with standard curve. In the present study, the estimation of sulphate ion was carried out with turbidimetric method (APHA 1995). 75 g of NaCl, 30 mL of concentrated HCl and 100 mL of 95% ethyl alcohol were added to 300 mL of distilled water. Then 50 mL of glycerol was added to the above solution and mixed well. 25 mL of sample, 10 mL of the above solution and 10 mL of 10 % $BaCl_2$ solution were added to 100 mL standard flask and solution was made upto the mark with distilled water. Blank sample was prepared in the similar way by substituting the sample with distilled water. Absorbance of the solution was measured at 420 nm using Hitachi U2000 model spectrophotometer and the sulphate ion concentration was measured using the calibration equation. Calibration plot for sulphate ion along with the detailed procedure for calibration and analysis is given in Appendix IV.

3.13.6 Estimation of chloride in aqueous dye solutions

Chloride ion in water and wastewater is one of the major inorganic anions. The amount of chloride present in water can be easily determined by titrating with silver nitrate solution which easily reacts with chloride and as a result, red silver chromate is formed (APHA 1995). In the current study, the estimation of chloride ion was carried out with the APHA standard method (APHA 1995). 50 mL of the sample was taken in a conical flask and 2-3 drops of potassium chromate indicator was added into the flask to get yellow colour and the solution was titrated against silver nitrate solution until the colour changed from yellow to brick red. Volume of silver nitrate added was noted and titration was repeated three times to get concordant readings. Blank sample was prepared in the similar way by substituting sample with distilled water. Chloride concentration was determined using Eq.(3.9).

$$Chloride \left(\frac{mg}{L}\right) = \frac{(a-b) \times N \times 35.45 \times 1000}{mL \ of \ sample \ taken} \tag{3.9}$$

Where a = Volume of silver nitrate for sample, b = Volume of silver nitrate for blank, N = Normality of silver nitrate (0.0282N), 35.45 = Equivalent weight of chlorine.

3.14 Treatment of mixture of dyes in contaminated water

Batch photocatalysis experiments were conducted under UV and solar light irradiation and degradation of each of the dyes in mixed dye solution was studied. These experiments were carried out in a batch stirred reactor for photocatalysis of mixture of dyes in aqueous solution using Ag@TiO$_2$ core shell structured nanoparticles as the photocatalyst. Experiments were conducted with 100 mL of the aqueous dye solution and with the dye concentration combination specified in Table 3.7. All the experiments for the treatment of mixture of dyes were conducted under RSM based methodically optimized conditions obtained for both AY-17 and RB-220 dye degradation, in order to check the applicability of optimized conditions for degradation of one of the dyes, to degradation of both the dyes simultaneously in mixed dye solution. Concentrations of the dyes (AY-17 or RB-220) were measured at regular time intervals by spectrophotometric analysis as described in Section 3.15.2.

Percentage degradation was then determined for each of the dyes in a mixed dye solution and compared with that in single dye solution.

Table 3.7 Combination of dye concentrations of each dye in aqueous solution of mixture of dyes.

S. No.	Dye Concentration (mg/L) of each dye in mixture of dyes	
	AY-17 (mg/L)	RB-220 (mg/L)
1	100	100
2	400	100
3	300	200
4	200	300
5	100	400

3.14.1 Preparation of mixture of dye stock solution

The stock solutions of 1000 mg/L concentration of AY-17 and RB-220 dyes were prepared separately. The aqueous solutions of mixture of the dyes containing desired combinations of AY-17 and RB-220 were prepared by mixing the required volumes of the stock solutions and diluting the mixture suitably with distilled water.

3.14.2 Analysis of mixture of dyes (AY-17 and RB-220) solution

When a mixture of two or more dyes are present in water, there may be a possibility of physical and chemical bond formation between them, which causes interference in analysis of the dyes. In such cases, the wavelengths used for absorbance measurement for single dyes using UV/Vis spectrophotometer, may not be suitable for the analysis of single dyes in mixed dye solution. So, to study whether any interference of the dyes in mixture occurs during analysis, the zero order absorption spectra of aqueous solutions of AY-17 (35 mg/L) and RB-220 (35 mg/L) individually and mixture of AY-17 and RB-220 (each 35 mg/L) were recorded using UV-Visible spectrophotometer (Hitachi UV-160A) and shown in Figure 3.8. It can be seen from Figure 3.8 that the λ_{max} values of both the dyes (AY-17 and RB-220) do not change

with mixture of dyes and two different peaks for AY-17 and RB-220 dyes were observed. Figure 3.8 shows no overlapping of AY-17 and RB-220 dyes spectra and at the wavelength corresponding to the maximum absorbance for one dye, the absorbance due to other dye was nearly zero. The absorbance values for mixtures at λ_{max} corresponding to AY-17 coincided with that for aqueous solution of AY-17. Similarly, the absorbance values for mixtures at λ_{max} corresponding to RB-220 coincided with that for aqueous solution of RB-220. So their concentrations in mixtures can be determined by direct absorbance measurement at their corresponding λ_{max}. No overlapping of absorption spectra of single dye solutions with each other and overlapping of the mixture absorbance with the particular single dye absorbance at its λ_{max} or zero absorbance for the other dye at this λ_{max}, indicates that both the dyes (AY-17 and RB-220) are not linked with physical or chemical bond and hence no interference effects were observed. So in the study on the degradation of each of the dyes in aqueous mixed dye solution of AY-17 and RB-220, the absorbance was measured at their corresponding λ_{max} values of 418 and 609 nm respectively. Concentrations were then measured using the corresponding calibration plots shown in Appendix V.
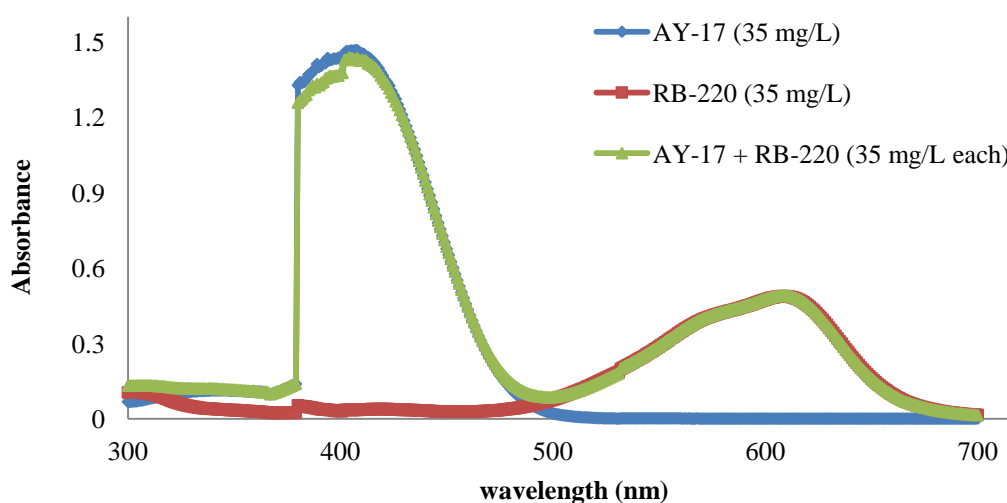
Figure 3.8 Absorption spectra for mixed dye solution and single dye solution (AY-17 + RB-220).

3.15 Determination of colour in Hazen unit

Batch photocatalysis experiments were conducted with single and mixed dye solutions at optimized conditions for each of the dyes. Samples withdrawn at different intervals of time and those before treatment were analyzed for colour in terms of Hazen unit. This method is based on the optical comparison of the liquid with a platinum cobalt reference solution. Today the Platinum/cobalt colour also named as APHA colour is one of the most common standards for the colour measurement of liquids.

3.15.1 Preparation of a calibration standard stock solution with 500 mg/L Pt/Co (500 Hazen)

Estimation of colour in terms of Hazen unit was carried out with spectroscopic method (APHA 1995). 1.245 g of potassium hexachloroplatinate and 1.0 g of cobalt (II) - chloride hexahydrate was dissolved in 100 mL of concentrated HCl. The solution was further transferred to 1 L standard flask and diluted with distilled water to make upto the mark. Different standards of colour of 100, 200, 300 and 400 Hazen were prepared by diluting 10, 20, 30 and 40 mL of stock colour standard with distilled water and by making upto the mark to 100 mL. The values of colour for AY-17 and RB-220 in standard solutions and treated solution were measured at 340 nm using Thermo Electron Corporation (Aquamate) model spectrophotometer against distilled water blank. Analysis of all samples for colour in terms of Hazen unit was done in BASF, India Ltd., Katipalla, Mangalore. Calibration plot for Hazen colour analysis is given in Appendix VI.

3.16 Identification of intermediates by Liquid Chromatography-Mass Spectrophotometer (LC-MS) to propose the degradation pathway for the dyes

To study the mineralization and mechanism of degradation of the dyes, the samples withdrawn from the reactor at various time periods during solar photocatalysis, were

subjected to Liquid chromatography and mass spectroscopy (LC-MS), to identify the intermediates and products formed by photocatalysis of the dyes.

LC-MS (Thermo Surveyor) was used for the identification of intermediates and products formed during solar photocatalysis of the dyes. Aqueous samples collected after every 15 min, during photocatalysis experiments were analyzed by LC-MS. For separation of intermediates, capillary column Terra C-18 and a mixture of acetonitrile–water (70/30, v/v) mobile phase was used. The flow rate was maintained at 0.08 mL min^{-1} and the injection volume was 20 μL. From the chromatographic column eluent consecutively enter the UV–Vis diode array detector, the Electrospray ionization (ESI) interface and the quadruple ion trap mass analyzer. Mass spectrometer equipped with an ESI ion source was used to carry out MS analysis. The ESI probe tip and capillary potentials were set at 2.5 kV and 25 V, respectively and 50–800 m/z was used. The mass-to-charge ratio of an ion is the unitless ratio of its mass number to the number of fundamental charges on the ion (Skoog et al. 2003). In mass spectrometer, most of the formed ions have single charge so m/z ratio is equivalent to exact mass (Skoog et al. 2003). When the charge of the formed ions is two then m/z ratio is equivalent to exact mass divided by two (Skoog et al. 2003). If peak of fragmented ions have m/z ratio greater then the exact mass, then that peak is attributed to the ions having the same chemical formula, but different isotopic compositions (Skoog et al. 2003). So the possible intermediates were identified manually based on their fragment ions mass to charge (m/z) ratio in the mass spectra. The chemical names of intermediate products of dyes formed during solar photocatalysis were found using Chem Draw Ultra 12 software.

3.17 Photocatalysis with immobilized Ag@TiO$_2$ nanoparticles

Batch photocatalysis experiments were conducted using Ag@TiO$_2$ nanoparticles immobilized in chitosan beads or cellulose acetate film for the degradation of AY-17 and RB-220 dyes under solar light irradiation. Experiments were conducted with 100 mL of the dye solution with initial dye concentration of 100 mg/L and under RSM based methodically optimized conditions. Optimum quantity of the catalyst nanoparticles were immobilized in chitosan beads and cellulose acetate film using the

methods described in Section 3.17.1.1 and 3.17.1.2 respectively. These immobilized nanoparticles were used for batch photocatalysis in a batch stirred reactor. Samples were withdrawn at regular intervals of time and analyzed for dye concentrations using UV –VIS spectrophotometer as described in Section 3.8.1 and percentage degradation was calculated.

3.17.1. Immobilization of Ag@TiO$_2$ nanoparticles

Ag@TiO$_2$ nanoparticles were immobilized in chitosan beads or in cellulose acetate films as described in the following sub sections.

3.17.1.1. Immobilization of Ag@TiO$_2$ nanoparticles in chitosan beads

Chitosan beads were prepared according to the method described by Wan Ngah et al. (2006) with a few modifications. The method used by Wan Ngah et al. (2006) for preparation of chitosan beads yielded beads with low strength. So in the present work, in order to increase the strength of chitosan beads, cross linking with gluteraldehyde was attempted (Singh et al. 2011b). Ag@TiO$_2$ loaded chitosan beads were prepared according to the protocol explained below.

Chitosan solution was prepared by dissolving 2 g of chitosan flakes in 60 mL of 5% (v/v) acetic acid solution. 500 mL of 1 mol/L NaOH solution was prepared. Magnetic stirrer was used to dissolve the NaOH pellets; the solution was cooled to room temperature. 1mL gluteraldehyde was added to the NaOH solution. Optimized amount (0.18 g for AY-17 and 0.1 g for RB-220 to yield 1.8 g/L and 1 g/L of optimum catalyst loading in the reactor) of Ag@TiO$_2$ nanoparticles (as obtained from RSM based optimized conditions) was added to the chitosan solution and was mixed well to obtain uniform solution. (Ag@TiO$_2$ nanoparticles were prepared with Ag to Ti molar ratio of 1:1.7 according to the procedure mentioned in section 3.2 and calcined at 450 ºC for 3 h). The viscous Chitosan-Ag@TiO$_2$ solution was added drop wise using syringe into precipitation bath containing NaOH solution. This ensures that the acetic acid within the chitosan gel is neutralized and there by coagulates the chitosan gel to spherical uniform chitosan gel bead. Gluteraldehyde which is present in the

NaOH solution acts as cross linking agent for chitosan and adds mechanical strength to the beads formed. The viscous solution was added slowly in order to obtain beads of uniform size and shape (average size of the beads were 3 mm as measured using vernier callipers). The beads were left in the solution for about 3 h for hardening. The hardened beads were removed and washed with distilled water to remove NaOH residues. Ag@TiO$_2$ immobilized in chitosan beads is hereinafter referred as Chitosan-Ag@TiO$_2$ beads.

3.17.1.2. Preparation of Cellulose Acetate-Ag@TiO$_2$ film

Cellulose acetate films were prepared according to the solvent Casting Method (Wu et al. 2005).

2 g of cellulose acetate solution in acetone was prepared. The solution was mixed well to obtain uniform solution. Optimized amount (0.18 g for AY-17 and 0.1 g for RB-220 to yield 1.8 g/L and 1 g/L of optimum catalyst loading in the reactor) of Ag@TiO$_2$ nanoparticles (as obtained from RSM based optimized conditions) was added to the Cellulose acetate - acetone solution. (Ag@TiO$_2$ particles were prepared with Ag to Ti molar ratio of 1:1.7 according to the procedure mentioned in Section 3.2 and calcined at 450 ºC for 3 h). The mixture was stirred well using glass rod and was casted on clean and dry glass plate. The film was exposed to air for complete evaporation of Acetone for around 15 to 20 minutes. Once the acetone was evaporated, the film was peeled off slowly. The resulting film was cut into small flakes (approximately to 3mm×3mm square flakes) using scissors. Then these flakes were kept in oven for about 15-20 min at 60 °C for further drying. Cellulose acetate - Ag@TiO$_2$ flakes were stored in ethanol until use. Ag@TiO$_2$ immobilized in cellulose acetate film is here in after referred as Cellulose Acetate-Ag@TiO$_2$ film.

3.18 Batch experiments for degradation of other class of dyes

Batch photocatalytic degradation experiments were performed in a batch stirred reactor for photocatalytic degradation of the other class of dyes with Ag@TiO$_2$ core shell structured nanoparticles under solar light irradiation. Batch experiments were

performed in order to check the photocatalytic efficacy of Ag@TiO$_2$ nanoparticles for the degradation of other dyes belonging to different classes, like: Basic Blue-41 (basic azo dye), Malachite Green (triarylmethane dye), Acid Blue-129 (anthraquinone dye), Congo red (diazo dye), Reactive Red-120 (reactive diazo dye), methyl orange (acid azo dye), methyl red (acid azo dye), and methylene blue (thi- azine dye). In all the experiments 100 mL dye solution in water was used. The conditions used for these studies were: catalyst loading=100 mg/L, initial dye concentration=10 mg/L. Experiments were done at different initial pH, depending upon the nature of dyes. For Malachite Green, Acid Blue-129, Congo red, Reactive Red-120, Methyl Orange and Methyl Red dyes experiments were done at initial pH=3 as all these dyes are acidic in nature and for Methylene Blue and Basic Blue-41 experiments were done at initial pH=9 as both of these dyes are basic in nature.

CHAPTER 4

RESULTS AND DISCUSSIONS

Experiments were performed as per the methodologies presented in Chapter 3, to fulfill the objectives of the present research work. This chapter presents the results of the experiments which include synthesis of Ag@TiO$_2$ nanoparticles, its characterization, efficacy for degradation of two azo dyes namely, AY-17 and RB-220 by UV and solar photocatalysis, factors affecting dye degradation, optimization of conditions for photocatalytic degradation of the dyes, kinetics of degradation of the dyes, mineralization of the dyes, degradation of mixture of dyes, use of immobilized Ag@TiO$_2$ nanoparticles and the efficacy of the nanoparticles to degrade other class of dyes etc. Results are presented in the form of tables and figures wherever necessary. Detailed discussion on the results with proper justification supported by the findings of this study, as well as other related research work reported in literature are also presented in this chapter.

4.1 Engineering Ag@TiO$_2$ nanoparticles by optimization of Ag to Ti molar ratio during synthesis, calcination temperature and calcination time for enhancement in UV and solar photocatalytic activity for degradation of AY-17 and RB-220 dyes

In the present study, Ag@TiO$_2$ nanoparticles were synthesized on the basis of one pot synthesis route reported by Hirakawa and Kamat (2005) with certain modification as described in Section 3.2. It is necessary to engineer the nanoparticles for better photocatalytic activity. It can be done by varying the composition of the nanoparticles, calcination temperature and calcination time. The current investigation focuses on engineering Ag@TiO$_2$ nanoparticles by optimization of Ag to Ti molar ratio during the synthesis, calcination temperature and calcination time for enhancement in UV and solar photocatalytic activity and hence its utilization as a photocatalyst in treatment of dye contaminated wastewater. Molar ratio of Ag to Ti may play an important role in the structure of the catalyst. Size of the core and shell of Ag@TiO$_2$ depends on the molar ratio of Ag to Ti (Angkaew and Limsuwan 2012), which in turn may affect the photocatalytic activity. Calcination is important in shaping and in improving the activity of catalyst. It affects the efficiency of the photocatalyst. Calcination temperature and time affect the crystalline nature and size

of the catalyst. Enhancing calcination temperature improves the crystallization of photocatalyst (Wang et al. 2005; Kominami *et al*. 2003), which in turn helps in the improvement of photocatalytic activity of TiO_2 (Ovenstone 2001; Yu et al. 2003). A better crystallization means the decrease of crystal defects, which are the recombination centers of photo-induced charge carriers (Yu et al. 2007a, b; Yu et al. 2005; Mrowetz et al. 2004; Jung and Park 2001; Liqang et al. 2006). It is well known from literature that calcination temperature not only influences the crystallinity, but also the morphology and surface area of the catalyst, which can clearly affect the photocatalytic activity (Sathish et al. 2007; Li et al. 2005). Calcination is a thermal treatment that also helps in the phase transformation. Phase transformation of TiO_2 depends on the calcination temperature (Zhang and Reller 2002). So the effect of calcination temperature and the composition of the catalyst synthesis mixture as Ag to Ti molar ratio, on the photocatalytic activity of $Ag@TiO_2$ in terms of degradation of AY-17 and RB-220 dyes by UV and solar photocatalysis were studied. $Ag@TiO_2$ catalysts were prepared with the Ag to Ti molar ratio of 1:5, 1:3.1, 1:2.2, 1:1.7 and 1:0.8 in the synthesis mixture. The synthesized catalysts were calcined at different temperatures ranging from 150 to 550 ºC for a time period of 3h and then evaluated for their photocatalytic activity under UV and solar light irradiation for degradation of AY-17 and RB-220 dyes.

4.1.1 Effect of Ag to Ti molar ratio during synthesis and the calcination temperature of the catalyst on photocatalytic activity of $Ag@TiO_2$ in terms of photocatalytic degradation of AY-17 under UV and solar light irradiation

To study the effect of Ag to Ti molar ratio during synthesis and the calcination temperature of the catalyst, on the degradation of AY-17, batch photocatalysis experiments were carried out under UV and solar light irradiations in stirred reactor at initial concentration of 10 mg/L of the dye in aqueous solution with an initial pH of 3.Experiments were conducted with $Ag@TiO_2$ catalysts synthesized with different Ag to Ti molar ratios (1:5, 1:3.1, 1:2.2, 1:1.7 and 1:0.8) and calcined at temperatures ranging from 150-550 °C. In all the experiments, catalyst loading of 100 mg/L was used. For UV photocatalysis, air at a flow rate of 2 LPM was supplied as an oxidant

whereas, for solar photocatalysis, oxygen from atmospheric air transferred to the solution and being present as dissolved oxygen in the dye solution, itself acted as the oxidant. The data on time course variations of AY-17 dye concentration during UV and solar photocatalysis are presented in Table 4.1 and Table 4.2 respectively and the corresponding percentage degradation are presented in Table 4.3 and Table 4.4 respectively. Figure 4.1 and Figure 4.2 show the representative plots of time course variations of percentage degradation by UV and solar photocatalysis with Ag@TiO$_2$ calcined at different temperatures. These Figures are presented for photocatalysis with Ag@TiO$_2$ synthesized with Ag to Ti molar ratio of 1:2.2 and 1:1.7 respectively. It is observed from the trend of the plots that the rate of degradation with uncalcined catalyst is very low and as the calcination temperature of the catalyst increases from 150 ℃ to 450 ℃, the rate of degradation increases. But the rate of degradation with the catalyst, calcined at 550 °C is lesser than or almost equal to the rate achieved with the uncalcined catalyst. Similar results are also observed in case of UV and solar photocatalysis by catalysts prepared with other Ag to Ti molar ratios. Under UV photocatalysis, the time course variation of percentage degradation with Ag@TiO$_2$ calcined at 550 °C showed initial increase in percentage dye removal with increase in irradiation time and then a decrease. Though the phenomena of decrease in removal of dyes at later times cannot be explained with confirmation, it may be hypothesized that at calcination temperature of 550 °C, Ag core may not have an even coating of TiO$_2$ on its surface. There may be a week binding (adsorption) of the dye on Ag surface or on TiO$_2$ film initially, which may further release into the solution on continued stirring conditions or by the turbulence created with air bubbling. Or due to the coating of TiO$_2$ on Ag surface being uneven, lead to crevices on the surface of nanoparticles. Dye molecules may get trapped in these crevices initially, but released to the solution at later times due to continued stirring or by the turbulence created with air bubbling. These are only the hypothesis put forward, and further research is needed in this regard, which is beyond the scope of the current research work. But such a phenomena is not observed in solar photocatalysis, due to lower turbulence level in the absence of air bubbling.

Figure 4.3a shows that, as Ag to Ti molar ratio increases from 1:5 to 1:0.8 the degradation of AY-17 in 360 min of UV irradiation increases from 0.09 % to 10.3 %,

with uncalcined Ag@TiO$_2$ nanoparticles. As the Ag to Ti molar ratio was increased from 1:5 to 1:0.8, the degradation of AY-17 in 360 min of UV irradiation increased from 0.98 % to 25.2 %, with Ag@TiO$_2$ nanoparticles calcined at 150 ºC; 3.1 % to 30.5 % with the nanoparticles calcined at 250 ºC; 6.43 % to 83.8 % with the nanoparticles calcined at 350 ºC. With the nanoparticles calcined at 450 ºC, as Ag to Ti molar ratio was increased from 1:5 to 1:1.7, the degradation of AY-17 in 360 min of UV irradiation increased from 9.8 % to 99.2 %, but further increase in molar ratio to 1:0.8, decreased the degradation and was only around 42.1 %. With the nanoparticles calcined at 550 ºC, as Ag to Ti molar ratio was increased from 1:5 to 1:1.7, the degradation of AY-17 in 360 min of UV irradiation increased from 0.14 % to 2.8 %, but further increase in molar ratio to 1:0.8 decreased the degradation to only around 0.22 % (at 360 min). So, highest percentage degradation was achieved with nanoparticles calcined at a temperature of 450 ºC with all Ag to Ti molar ratios studied. But percentage degradation obtained using nanoparticles synthesized with Ag to Ti molar ratio of 1:1.7 was much higher than those obtained with other Ag to Ti molar ratios.

Similar observations were made for solar photocatalysis of AY-17 dye. Figure 4.3b shows that, as Ag to Ti molar ratio increases from 1:5 to 1:0.8, the degradation of AY-17 in 360 min of solar irradiation increases from 1.67 % to 13.7 % with uncalcined Ag@TiO$_2$ nanoparticles; 4.11 % to 32.27 % with Ag@TiO$_2$ nanoparticles calcined at 150 ºC; 8.21 % to 34.81 % with those calcined at 250 ºC. Figure 4.3b also shows that, with Ag@TiO$_2$ nanoparticles calcined at 350 ºC, as Ag to Ti molar ratio increases from 1:5 to 1:1.7 the degradation of AY-17 in 360 min of solar irradiation increases from 23.52 % to 99.46 %. But further increase in composition ratio to 1:0.8, did not result in any significant change in degradation. Similarly with Ag@TiO$_2$ nanoparticles calcined at 450 ºC, as shown in Figure 4.3b, as Ag to Ti molar ratio was increased from 1:5 to 1:1.7 the degradation of AY-17 in 360 min of solar irradiation increased from 51.16 % to almost 100 %, but further increase in molar ratio to 1:0.8 decreased the degradation to around 96.24 % (at 360 min). Highest rate of degradation was found with nanoparticles synthesized with 1:1.7 molar ratio of Ag to Ti and calcined at 450 ºC as observed in Figure 4.2b. Almost complete degradation can be achieved within 60 min of irradiation time by solar photocatalysis with those

nanoparticles synthesized with Ag to Ti molar ratio of 1:1.7 and calcined at 450 ºC, as shown in Figure 4.2b. Figure 4.3b shows that, as Ag to Ti molar ratio increases from 1:5 to 1:0.8, the degradation of AY-17 in 360 min of solar irradiation decreases from 25.96 % to 11.72 %, with Ag@TiO$_2$ nanoparticles calcined at 550 ºC. So, highest percentage degradation was achieved with the nanoparticles calcined at a temperature of 450 ºC. This was observed with nanoparticles synthesized with all Ag to Ti molar ratios. But highest percentage degradation and rate of degradation were obtained using nanoparticles synthesized with 1:1.7 Ag to Ti molar ratio.

Increase in percentage degradation with calcination temperature is attributed to the formation of crystalline phase of TiO$_2$, which increases with increasing calcination temperature, as reported by other researchers during degradation of Congo red dye (Jian-Hua and Hai-Jun 2009; Bickley et al. 1991) with TiO$_2$ as a catalyst under UV light and Acid red B dye (Wang et al. 210) with Er^{3+}:YAlO$_3$/ZnO–TiO$_2$composite under sunlight. Increase in calcination temperature improves the crystallization and hence increases the activity of catalyst. TiO$_2$ has three crystalline phases: anatase, rutile and brookite, among which anatase is more reactive than rutile and reported to be responsible for the photocatalysis. It is reported, as calcination temperature increases the content of anatase phase increases but further increase in calcination temperature leads to change from anatase to rutile phase and rutile content increases as the temperature is increased (Ovenstone and Yanagisawa 1999; Behnajady et al. 2008; Wang et al. 2010).

In the present study, with nanoparticles calcined at 550 °C, decreased degradation was observed as compared to that with 450 °C, which may be due to phase conversion from anatase to rutile phase. TG-DTA analysis of the synthesized nanoparticles with Ag to Ti ratio of 1:1.7 presented later in Section 4.4.5, showed a releasing peak at around 514 °C indicating the possible phase conversion of TiO$_2$ from anatase to rutile which supports the decrease in photocatalytic degradation with nanoparticles calcined at 550 °C. Similar observation was also made by Zhang et al. (2005). It is widely accepted that the anatase phase of titania is a relatively ideal photocatalytic material among its three crystalline phases (Ovenstone and Yanagisawa 1999). It is also reported by other researchers (Sivalingam et al. 2003; Nagaveni et al. 2004; Aarthi et al. 2007) that, TiO$_2$ containing only anatase phase

show better photocatalytic activity as compared to the commercial Degussa P-25 catalyst which consists of 75 % anatase and 25 % rutile phase. It is observed, as calcination temperature increases photocatalytic activity increases but further increase in calcination temperature leads to decrease in activity due to rutile phase formation. Decreased activity with nanoparticles calcined at 550 °C may also be due to increase in silver content. It has also been observed that after calcination at 550 °C, the Ag@TiO$_2$ nanoparticles turned to grey lustrous surface, characteristic of Ag, instead of the blackish brown film of TiO$_2$ on the surface as was found in the catalyst after calcination at other temperatures. It was found that for catalysts prepared with all Ag to Ti molar ratios, as the calcination temperature was increased, degradation increased but further increase in calcination temperature to above 450 ºC lead to decrease in degradation. Hence, highest degradation was found at 450 °C and it can be considered as the optimum calcination temperature.

Optimization of composition plays a very important role in the structure and morphology of the catalyst. Angkaew and Limsuwan (2012) studied the effect of Ti to Ag molar ratio on two step synthesized Ag@TiO$_2$ nanoparticles. They reported that at low concentration of titanium tetraisopropoxide (TTIP) as a precursor salt for Ti, TiO$_2$ can be effectively formulated on Ag nanoparticles which lead to the formation of core-shell structure but higher concentration lead to formation of core-shell particles with larger shell thickness. However, in their studies, too high concentration of TTIP lead to the composite structure with Ag nanoparticles embedded in TiO$_2$ matrix. According to them, the effect of Ag-Ti mole ratio on the morphology of nanoparticles can be explained in terms of the available nucleation sites and growth of titania particles on the pre-existing surface of silver nanoparticles. Since it was found that molar ratio is an important parameter in controlling the morphology of the resulting Ag@TiO$_2$ nanoparticles, optimization of Ag to Ti molar ratio was carried out in the present study by varying the concentration of TTEAIP and AgNO$_3$ in the synthesis mixture for the formation of Ag core and TiO$_2$ shell.

As it is evident from Figure 4.3, with the increase in Ag to Ti molar ratio from 1:5 to 1:1.7 the percentage degradation increases. But further increase in the ratio to 1:0.8 has lead to decrease in the degradation. The maximum degradation occurred with nanoparticles synthesized with Ag to Ti molar ratio of 1:1.7. In order to

understand the reason for maximum photocatalytic activity by nanoparticles synthesized with 1:1.7 Ag to Ti ratio, XRD of the nanoparticles were obtained for the nanoparticles synthesized with different Ag to Ti molar ratios (1:5, 1:3.1, 1:2.2, 1:1.7; 1:0.8) and calcined at 450 ℃ for 3 h and are shown in Figure 4.4.

Table 4.5 shows the presence of different crystal planes of Ag and TiO_2 in nanoparticles synthesized with different Ag to Ti molar ratio and calcined at a temperature of 450 ℃ for 3 h, where (A) and (R) correspond to the anatase and rutile planes of TiO_2 respectively and (111), (200), (220), and (311) correspond to the different crystal planes of Ag^0.

Average crystallite size of Ag@TiO_2 nanoparticles prepared with different Ag to Ti molar ratio (1:5, 1:3.1, 1:2.2, 1:1.7; 1:0.8) were calculated based on the Scherrer's formula and are presented in Table 4.6. X-Ray diffractogram of Ag@TiO_2 catalysts synthesized with different composition ratios of Ag to Ti and which were calcined at temperature of 450 ℃ for 3 h, as shown in Figure 4.4a to Figure 4.4e and as summarized in Table 4.5 reveal that, as the Ag to Ti molar ratio increases, increase in crystallinity is observed and it also resulted in increase in anatase phase of TiO_2. Decrease in particle size (Table 4.6) of Ag@TiO_2 nanoparticles was observed as the Ag to Ti molar composition ratio was increased from 1:5 to 1:0.8. Smaller the size of particles, larger is the specific surface area and the rate of photocatalysis increases with the increase in specific surface area. As shown in Figure 4.3, as Ag to Ti molar ratio increases till 1:1.7, the percentage degradation of the dye at a particular irradiation time increases as an evidence of increase in rate of photocatalysis. Although smallest crystallite size was found with 1:0.8 Ag to Ti molar ratio as seen in Table 4.6, percentage degradation is lower than that obtained with the nanoparticles synthesized with 1:1.7 molar ratio. The X-Ray diffractogram of Ag@TiO_2 synthesized with 1:0.8 Ag to Ti molar ratio, presented in Figure 4.4e showed only one anatase phase peak. But many anatase peaks were observed in nanoparticles synthesized with 1:1.7 Ag to Ti molar ratio as shown in Figure 4.4d. In case of particles with 1:5, 1:3.1, 1:2.2 Ag to Ti molar ratios, presence of both anatase and rutile phase were observed in XRD presented in Figure 4.4a to Figure 4.4c and peak for AgO was also found. Wang et al. (2008b) have reported that the presence of AgO in Ag@TiO_2 nanoparticles result in decrease in photocatalytic property. But in case of

nanoparticles with 1:1.7 molar ratio of Ag to Ti (Figure 4.4d), three peaks of anatase phase of TiO_2 and well defined crytalline structure were found as compared to nanoparticles synthesized with other molar ratios and no peaks of rutile TiO_2 and AgO were found. These are the main reasons of high photocatalytic activity shown by nanoparticles with 1:1.7 molar ratio of Ag to Ti. Highest photocatalytic activity with nanoparticles synthesized with Ag to Ti molar ratio of 1:1.7, can also be contributed to a Schottky energy barrier formed by the combination of Ag core and TiO_2 shells. The interface can attract light-induced electrons from the semiconductor TiO_2 to reduce electron–hole recombination. Presence of AgO which resulted due to oxidation of Ag, can be verified by the appearance of AgO diffraction peaks in Figure 4.4a to Figure 4.4c at lower Ag to Ti molar ratios. The AgO cannot serve as a Schottky energy barrier (Wang et al. 2008b). But no AgO peak was observed with nanoparticles synthesized with 1:1.7 molar ratio. Hence lower photocatalytic activity was observed at Ag to Ti ratios of 1:5 to 1:2.2. From the results of photocatalytic degradation, the least Ag content sample (1:5) showed the least photocatalytic activity. This may also be because of the thicker TiO_2 shell which inhibits light-induced electrons from arriving at the interface between the Ag cores and the TiO_2 shells at low Ag to Ti ratio used during synthesis (Wang et al. 2008b).

With 1:0.8 Ag to Ti molar composition ratio, in the XRD shown in Figure 4.4.e, there was no AgO peak and though anatase phase peak observed. Ag (1, 1, 1) peak showed the highest intensity for these nanoparticles, as compared to nanoparticles synthesized with other ratios, indicating that the silver content is predominant. So lower photocatalytic activity shown by particles with 1:0.8 Ag to Ti molar ratio, may be due to high Ag content and very less TiO_2. Owing to high Ag and less Ti, not enough TiO_2 may be formed during the synthesis process, to grow as a film around all the Ag nuclei surface. Surface coverage of Ag core with TiO_2 may be very less and the decreasing content of TiO_2 means that fewer electrons were generated to take part in the photodegradation of dyes, hence leading to lower photocatalytic activity.

Due to the presence of more anatase phase TiO_2, formation of well defined crystalline structure with core shell morphology and absense of AgO, Ag@TiO_2 nanoparticles synthesized with Ag to Ti molar ratio of 1:1.7 and calcination

temperature of 450 °C were found to be the optimum conditions for maximum photocatalytic activity in terms of photocatalytic degradation of AY-17 dye under UV and solar light irradiation. Hence Ag@TiO$_2$ nanoparticles synthesized with Ag to Ti molar ratio of 1:1.7 and calcined at 450 °C were used for further experiments.

Table 4.1 Time course variation of concentration of AY-17 during batch photocatalysis under UV light irradiation, using Ag@TiO$_2$catalyst synthesized with different Ag to Ti molar ratio, calcined at different calcination temperatures.

Ag to Ti molar ratio	Time (min)	$C_{AY\text{-}17}$ (mg/L) during photocatalysis with Ag@TiO$_2$calcined at different temperatures T_c					
		uncalcined	150ºC	250ºC	350ºC	450ºC	550ºC
	0	10	10	10	10	10	10
	60	10	9.99	9.97	9.94	9.89	9.68
	120	10	9.98	9.86	9.80	9.76	9.44
1:5	180	9.99	9.96	9.77	9.74	9.68	9.09
	240	9.99	9.93	9.69	9.52	9.40	9.77
	300	9.99	9.92	9.69	9.42	9.29	9.93
	360	9.99	9.90	9.69	9.36	9.02	9.99
	10	10	10	10	10	10	10
	60	9.99	9.99	9.91	9.80	9.68	9.61
	120	9.98	9.93	9.86	9.71	9.41	9.54
1:3.1	180	9.95	9.89	9.62	9.42	9.22	9.49
	240	9.94	9.87	9.59	9.22	8.84	9.41
	300	9.93	9.86	9.51	9.11	8.56	9.77
	360	9.91	9.86	9.49	9.09	8.03	9.99
	10	10	10	10	10	10	10
	60	9.99	9.97	9.82	9.73	9.43	9.62
	120	9.96	9.93	9.66	9.61	9.06	9.28
1:2.2	180	9.93	9.88	9.38	9.21	8.44	9.21
	240	9.91	9.83	9.10	8.79	7.81	9.32
	300	9.89	9.75	9.10	8.75	7.13	9.55
	360	9.84	9.72	9.10	8.70	6.18	9.98
	10	10	10	10	10	10	10
	60	9.82	9.71	9.61	8.48	7.38	9.59
	120	9.65	9.44	9.16	6.09	5.92	9.52
1:1.7	180	9.51	9.28	8.60	4.32	4.36	9.35
	240	9.47	9.07	8.02	3.58	2.41	9.32
	300	9.41	8.84	7.72	2.88	1.22	9.53
	360	9.34	8.78	7.50	2.16	0.08	9.72
	10	10	10	10	10	10	10
	60	9.76	9.67	9.33	8.46	9.18	9.56
	120	9.45	9.05	8.66	5.82	7.32	9.56
1:0.8	180	9.29	8.33	8.02	3.89	6.86	9.56
	240	9.11	7.87	7.59	2.93	6.41	9.74
	300	9.04	7.61	7.18	2.04	5.98	9.83
	360	8.97	7.48	6.95	1.62	5.79	9.98

Table 4.2 Time course variation of concentration of AY-17 during batch photocatalysis under solar light irradiation, using Ag@TiO$_2$ catalyst synthesized with different Ag to Ti molar ratio, calcined at different calcination temperatures.

Ag to Ti molar ratio	Time (min)	C_{AY-17} (mg/L) with Ag@TiO$_2$calcined at different temperatures T_c					
		uncalcined	150 ºC	250 ºC	350 ºC	450 ºC	550 ºC
	0	10	10	10	10	10	10
	60	9.97	9.65	8.68	8.02	8.8	9.85
	120	9.94	9.52	8.26	6.91	8.53	9.71
1:5	180	9.92	9.44	8.17	5.81	8.35	9.64
	240	9.90	9.3	8.1	5.51	8.16	9.53
	300	9.89	9.22	7.81	5	7.86	9.57
	360	9.83	9.18	7.65	4.88	7.40	9.59
	10	10	10	10	10	10	10
	60	9.90	9.52	9.39	8.02	5.45	8.72
	120	9.83	9.32	8.97	6.02	3.39	8.21
1:3.1	180	9.79	9.21	8.48	4.37	2.48	8.14
	240	9.70	9.11	7.97	3.56	1.98	8.02
	300	9.66	9.04	7.53	2.66	1.35	7.87
	360	9.6	8.99	7.05	2.03	1.01	7.6
	10	10	10	10	10	10	10
	60	9.98	9.65	9.22	5.98	0.95	9.46
	120	9.87	8.92	8.75	3.86	0.15	9.16
1:2.2	180	9.69	8.17	8.02	2.00	0.15	8.58
	240	9.51	7.62	7.39	1.03	0.15	8.16
	300	9.44	7.34	6.71	0.51	0.15	7.99
	360	9.31	7.11	6.49	0.31	0.13	7.79
	10	10	10	10	10	10	10
	60	9.86	9.36	9.17	2.79	0.08	9.76
	120	9.64	8.65	8.45	1.13	0.05	9.56
1:1.7	180	9.45	7.95	7.75	0.08	0.05	9.38
	240	9.29	7.45	7.27	0.08	0.05	9.26
	300	9.11	7.18	6.55	0.08	0.05	9.04
	360	8.97	6.80	6.23	0.05	0.05	8.77
	10	10	10	10	10	10	10
	60	9.85	9.25	9.04	1.80	4.18	9.41
	120	9.77	8.74	8.36	0.38	2.25	9.31
1:0.8	180	9.55	7.47	7.77	0.15	0.96	9.18
	240	9.35	6.92	6.94	0.08	0.77	8.96
	300	9.03	6.92	6.80	0.08	0.59	8.77
	360	8.83	6.77	6.52	0.08	0.38	8.56

Table 4.3 Time course variation of percentage degradation of AY-17 during batch photocatalysis under UV light irradiation, using Ag@TiO$_2$catalyst synthesized with different Ag to Ti molar ratio, calcined at different calcination temperatures.

Ag to Ti molar ratio	Time (min)	% degradation of AY-17 with Ag@TiO$_2$ calcined at different temperatures T_c					
		uncalcined	150 ºC	250 ºC	350 ºC	450 ºC	550 ºC
	0	0	0	0	0	0	0
	60	0.03	0.09	0.3	0.65	1.1	3.2
	120	0.05	0.24	1.4	1.98	2.4	5.6
1:5	180	0.07	0.41	2.3	2.57	3.2	9.06
	240	0.07	0.67	3.1	4.83	6	2.3
	300	0.09	0.83	3.1	5.85	7.1	0.69
	360	0.09	0.98	3.1	6.43	9.8	0.14
	0	0	0	0	0	0	0
	60	0.09	0.15	0.92	1.97	3.17	3.89
	120	0.24	0.75	1.39	2.93	5.91	4.65
1:3.1	180	0.48	1.1	3.83	5.77	7.82	5.14
	240	0.65	1.32	4.08	7.85	11.62	5.91
	300	0.72	1.4	4.89	8.87	14.37	2.33
	360	0.89	1.43	5.09	9.07	19.66	0.15
	0	0	0	0	0	0	0
	60	0.15	0.31	1.8	2.7	5.7	3.76
	120	0.41	0.72	3.4	3.9	9.4	7.2
1:2.2	180	0.75	1.25	6.25	7.9	15.6	7.9
	240	0.92	1.69	9	12.1	21.9	6.8
	300	1.08	2.5	9	12.52	28.7	4.5
	360	1.6	2.79	9	13	38.2	0.16
	0	0	0	0	0	0	0
	60	1.78	2.9	3.92	15.2	26.24	4.1
	120	3.5	5.57	8.4	39.1	40.82	4.8
1:1.7	180	4.9	7.21	14	56.8	56.4	6.5
	240	5.34	9.31	19.8	64.2	75.93	6.8
	300	5.93	11.57	22.8	71.2	87.8	4.74
	360	6.6	12.2	25	78.4	99.2	2.8
	0	0	0	0	0	0	0
	60	2.41	3.3	6.7	15.4	8.2	4.4
	120	5.5	9.5	13.4	41.8	26.8	4.4
1:0.8	180	7.1	16.7	19.8	61.1	31.4	4.4
	240	8.93	21.3	24.1	70.7	35.9	2.56
	300	9.64	23.9	28.2	79.6	40.2	1.67
	360	10.3	25.2	30.5	83.8	42.1	0.22

Table 4.4 Time course variation of percentage degradation of AY-17 during batch photocatalysis under solar light irradiation, using Ag@TiO$_2$ catalyst synthesized with different Ag to Ti molar composition ratio, calcined at different calcination temperature.

Ag to Ti molar ratio	Time (min)	% degradation of AY-17 with Ag@TiO$_2$ calcined at different temperatures T_c					
		uncalcined	150 ºC	250 ºC	350 ºC	450 ºC	550 ºC
	0	0	0	0	0	0	0
	60	0.32	1.47	3.55	13.18	19.83	12.06
	120	0.57	2.95	4.79	17.4	30.9	14.72
1:5	180	0.76	3.58	5.64	18.35	41.87	16.53
	240	0.98	4.75	7.02	19.09	44.83	18.4
	300	1.23	4.34	7.83	21.88	50	21.4
	360	1.67	4.11	8.21	23.52	51.16	25.96
	0	0	0	0	0	0	0
	60	0.98	4.77	6.14	19.83	45.53	12.82
	120	1.7	6.81	10.34	39.8	66.13	17.93
1:3.1	180	2.09	7.93	15.2	56.31	75.25	18.61
	240	2.98	8.88	20.3	64.36	80.22	19.82
	300	3.4	9.56	24.7	73.39	86.51	21.31
	360	4.01	10.14	29.5	79.71	89.9	24.01
	0	0	0	0	0	0	0
	60	0.22	3.5	7.83	40.16	90.46	5.36
	120	1.3	10.8	12.46	61.4	98.48	8.37
1:2.2	180	3.1	18.3	19.8	80.05	98.48	14.18
	240	4.9	23.78	26.09	89.75	98.48	18.38
	300	5.6	26.65	32.94	94.92	98.48	20.08
	360	6.9	28.9	35.09	96.86	98.7	22.12
	0	0	0	0	0	0	0
	60	1.4	6.43	8.31	72.11	99.16	2.45
	120	3.6	13.49	15.48	88.73	99.49	4.38
1:1.7	180	5.52	20.51	22.48	99.24	99.49	6.21
	240	7.14	25.54	27.34	99.24	99.49	7.45
	300	8.9	28.21	34.46	99.24	99.49	9.62
	360	10.34	32.01	37.7	99.46	99.49	12.26
	0	0	0	0	0	0	0
	60	1.49	7.52	9.58	81.98	58.17	5.9
	120	2.35	12.61	16.41	96.22	77.46	6.94
1:0.8	180	4.5	19.34	22.35	98.48	90.39	8.22
	240	6.47	25.3	30.58	99.24	92.33	10.43
	300	9.66	30.78	32.04	99.24	94.15	12.27
	360	11.72	32.27	34.81	99.24	96.24	14.4
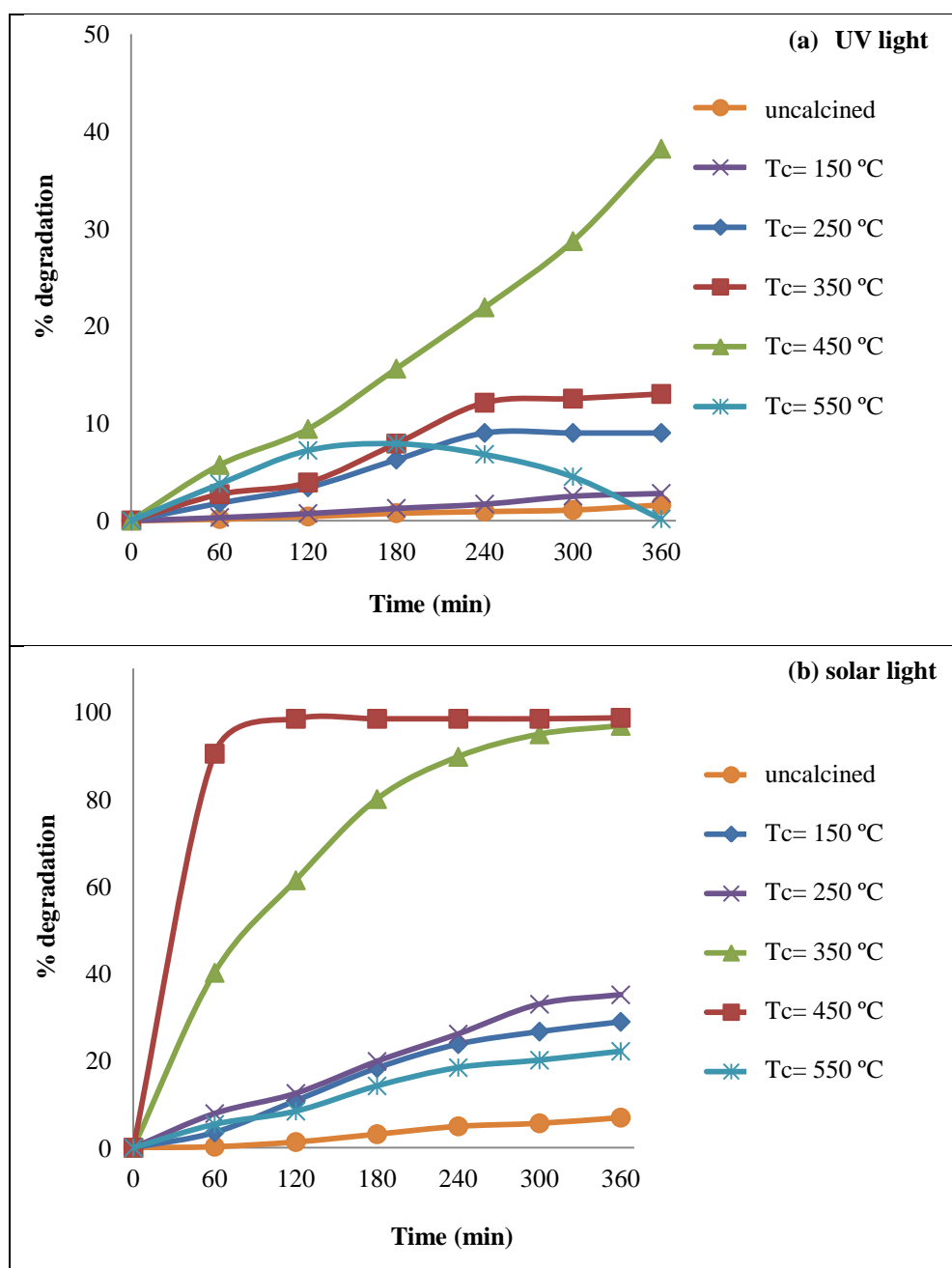
Figure 4.1 Representative plots showing the effect of calcination temperature on time course variation of photocatalytic degradation of AY-17 dye under a) UV light; (b) solar light: average UV and visible light intensity of solar light= 3.52 mW/cm^2 and 1198×100 lux respectively from 10 a.m. to 4 p.m. Conditions: Catalyst used=Ag@TiO$_2$; Ag to Ti molar ratio=1:2.2; pH=3; Catalyst loading= 100 mg/L; C$_0$= 10 mg/L.
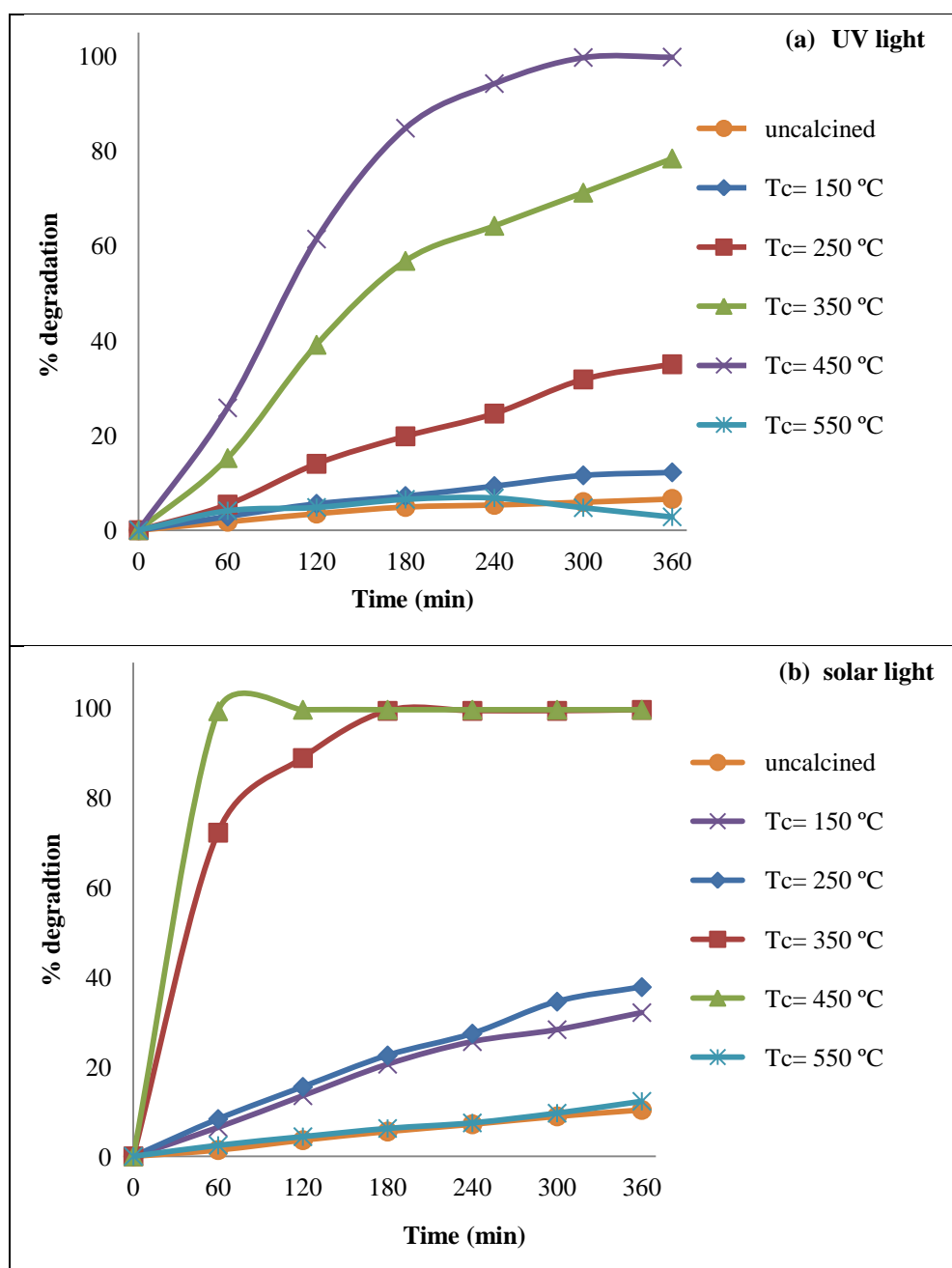
Figure 4.2 Representative plot showing the effect of calcination temperature on time course variation of photocatalytic degradation of AY-17 dye under a) UV light; b) solar light: average UV and visible light intensity of solar light= 3.50 mW/cm^2 and 1191×100 lux respectively from 10 a.m. to 4 p.m. Conditions: Catalyst used=Ag@TiO$_2$; Ag to Ti molar ratio=1:1.7; pH=3; Catalyst loading= 100 mg/L; C$_0$= 10 mg/L.
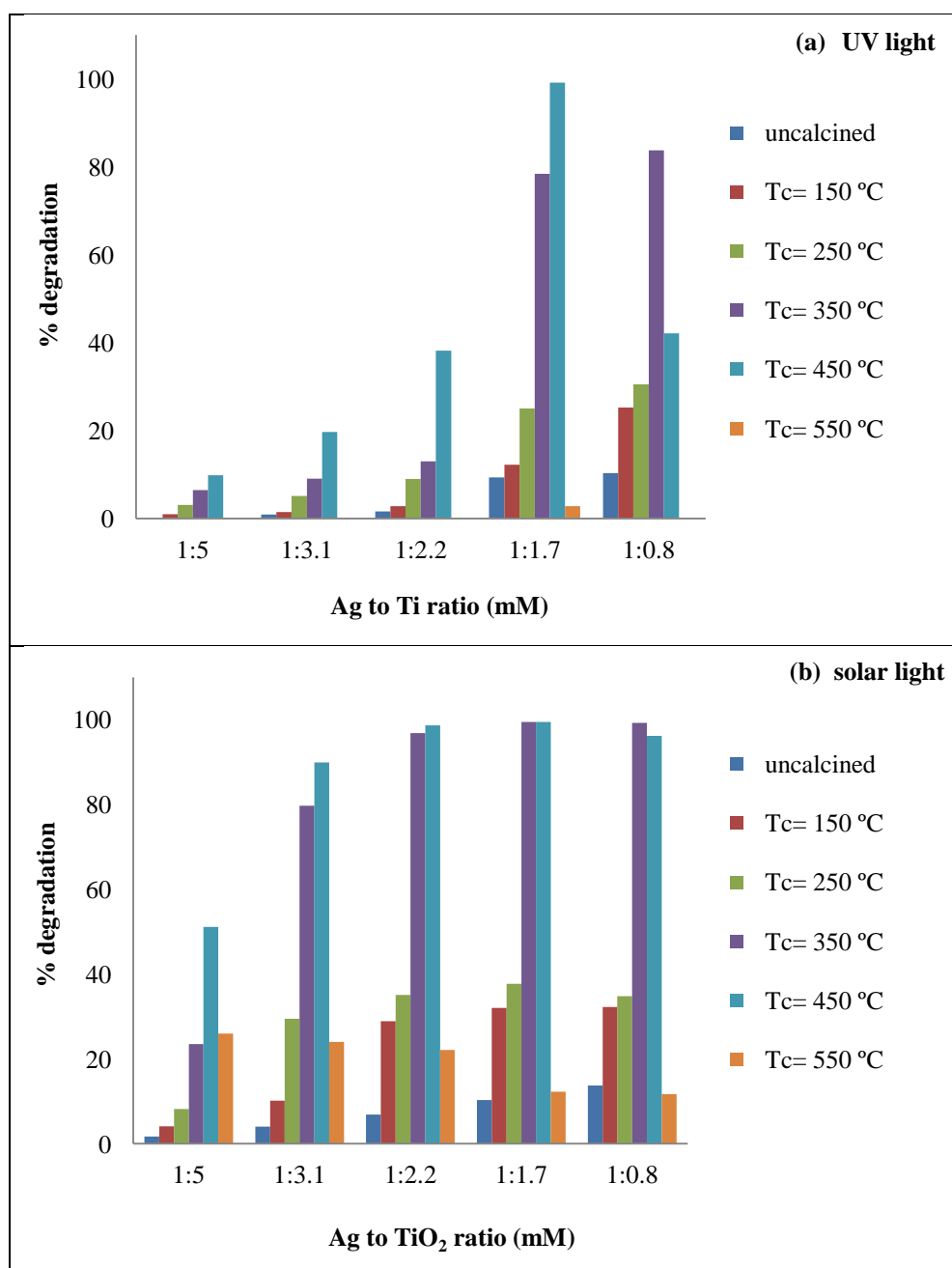
Figure 4.3 Effect of Ag to Ti molar composition ratio and calcination temperature on percentage degradation of AY-17 dye during photocatalysis using Ag@TiO$_2$ under a) UV light; b) solar light. Conditions: Ag@TiO$_2$ loading= 100 mg/L; C$_0$=10 mg/L; Irradiation time =360 min; pH=3.

Table 4.5 Presence of different crystal planes of Ag and TiO$_2$ in nanoparticle synthesized with different Ag to Ti molar ratio (1:5, 1:3.1, 1:2.2, 1:1.7; 1:0.8) and calcined at 450 ºC for 3 h.

Crystal planes of Ag and TiO$_2$ with different Ag to Ti molar ratios at calcination temperature of 450ºC					
Ag to Ti ratio / Planes	1:5 (Figure 4.4a)	1:3.1 (Figure 4.4b)	1:2.2 (Figure 4.4c)	1:1.7 (Figure 4.4d)	1:0.8 (Figure 4.4e)
Ag 2θ (crystal plane)	37.63 (111)	37.90 (111)	37.90 (111)	37.94 (111)	37.98 (111)
	44.13 (200)	44.11 (200)	44.11 (200)	44.20 (200)	44.38 (200)
	64.30 (220)	64.20 (220)	64.14 (220)	64.30 (220)	64.50 (220)
	77.21 (311)	77.40 (311)	77.14 (311)	77.10 (311)	77.50 (311)
TiO$_2$ 2θ (crystal phase)	25.10 (A)	25.72 (A)	25.10 (A)	25.30 (A)	25.50 (A)
	55.13 (R)	55.17 (R)	48.01 (A)	48.14 (A)	
				54.02 (A)	

A:Anatase and
R:Rutile

Table 4.6 Size of nanoparticles obtained with nanoparticles synthesized with different Ag to Ti molar ratio and calcined at 450 ºC for 3 h

Ag to Ti molar ratio	1:5	1:3.3	1:2.2	1:1.7	1:0.8
Crystallite size (nm)	68.70	60.11	56.61	39.40	27.46
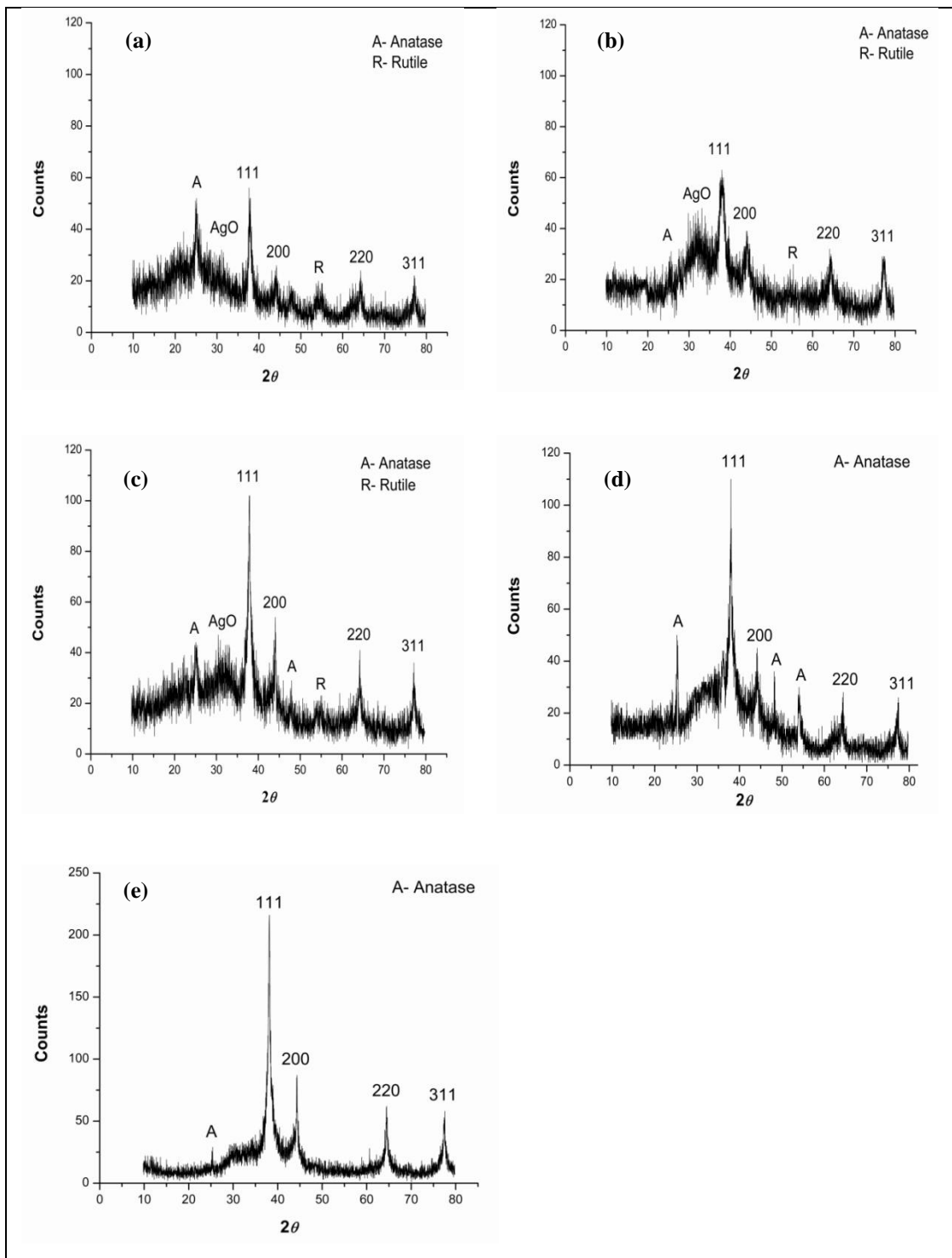
Figure 4.4 X-Ray diffractogram of Ag@TiO₂nanoparticles synthesized with different Ag to Ti molar ratio of (a) 1:5 (b) 1:3.1 (c) 1:2.2 (d) 1:1.7 (e) 1:0.8 and calcined at 450 ºC for 3 h.

4.1.2 Effect of calcination temperature and Ag to Ti molar ratio on photocatalytic activity of Ag@TiO$_2$ in terms of photocatalytic degradation of RB-220 under UV and solar light irradiation

To study the effect of Ag to Ti molar ratio used during synthesis and the calcination temperature of the catalyst on the degradation of RB-220, batch photocatalysis experiments were carried under UV and solar light irradiations in stirred reactor at initial dye concentration of 50 mg/L in aqueous solution and at initial pH=3 with Ag@TiO$_2$ catalysts synthesized with different Ag to Ti molar ratios (1:5, 1:3.1, 1:2.2, 1:1.7 and 1:0.8) and calcined at temperatures ranging from 150-550 °C. In all the experiments, catalyst loading of 1 g/L for UV photocatalysis and 500 mg/L for solar photocatalysis were used. For UV photocatalysis, air at a flow rate of 2 LPM was supplied to provide oxygen as an oxidant whereas for solar photocatalysis, atmospheric air transferred to the solution and being present as dissolved oxygen in the dye solution itself acted as an oxidant.

The data on time course variations of RB-220 dye concentration during UV and solar photocatalysis are presented in Table 4.7 and Table 4.8 respectively and the corresponding percentage degradation are presented in Table 4.9 and Table 4.10 respectively. Figure 4.5 and Figure 4.6 show the representative plots of time course variations of percentage degradation by UV and solar photocatalysis of RB-220 with Ag@TiO$_2$ calcined at different temperatures. These Figures are presented for photocatalysis with Ag@TiO$_2$ synthesized with Ag to Ti molar ratio of 1:2.2 and 1:1.7 respectively. It is observed from the trend of the plots, the rate of degradation with uncalcined catalyst is very low and as the calcination temperature of the catalyst increases from 150 ºC to 450 ºC, the rate of degradation increases. But the rate of degradation with the catalyst, calcined at 550 °C is lesser than or almost equal to the rate achieved with the uncalcined catalyst. Similar results were also observed in case of UV and solar photocatalysis by catalysts prepared with other Ag to Ti molar ratios.

Figure 4.7a and Figure 4.7b show that the maximum percentage degradation of RB-220 dye is obtained with the nanoparticles synthesized with Ag to Ti molar ratio of 1:1.7 and that calcined at a temperature of 450 °C both for UV and solar photocatalysis, as the case with AY-17 dye degradation. The percentage degradation

obtained using nanoparticles synthesized with Ag to Ti molar ratio of 1:1.7 is much higher than those obtained with other Ag to Ti molar ratios. 98.92 % degradation of RB-220 occurred in 240 min of irradiation with UV light and nearly 100 % degradation occurred in 180 min of solar light irradiation with the Ag@TiO$_2$ catalyst synthesized with 1:1.7 Ag to Ti molar ratio and calcined at 450 °C. The rate of degradation obtained using nanoparticles synthesized with 1:1.7 Ag to Ti molar ratio was much higher than those synthesized with other ratios.

Increase in degradation with calcination temperature is attributed to the formation of crystalline phase of TiO$_2$ and the effect of calcination temperature and Ag to Ti molar ratio on photocatalytic activity of Ag@TiO$_2$ in terms of photocatalytic degradation of RB-220 can be explained on similar grounds as it is explained for the degradation of AY-17 dye in Section 4.1.1.

Hence Ag to Ti molar ratio of 1:1.7 in synthesis mixture and calcination temperature of 450 °C were found to be the optimum conditions for maximum photocatalytic activity in terms of photocatalytic degradation of RB-220 dye under UV and solar light irradiation. So Ag@TiO$_2$ nanoparticles synthesized with Ag to Ti molar ratio of 1:1.7 and calcined at 450 °C were used for further experiments.

Table 4.7 Time course variation of concentration of RB-220 during batch photocatalysis under UV light irradiation, using Ag@TiO$_2$ catalyst synthesized with different Ag to Ti molar composition ratio, calcined at different calcination temperatures.

Ag to Ti molar ratio	Time (min)	$C_{RB\text{-}220}$ (mg/L)during photocatalysis with Ag@TiO$_2$calcined at different temperatures T_c					
		uncalcined	150 ºC	250 ºC	350 ºC	450 ºC	550 ºC
	0	50	50	50	50	50	50
	30	50	49.58	49.37	48.94	48.17	48.87
	60	49.65	49.08	48.45	47.75	46.55	47.25
1:5	90	49.30	48.17	47.46	46.62	45.28	46.34
	120	48.80	47.25	46.27	45.56	43.10	45.42
	180	48.24	46.06	44.72	43.03	41.13	44.08
	240	47.46	44.93	42.82	40.49	37.18	42.75
	0	50	50	50	50	50	50
	30	49.98	49.64	49.35	48.75	46.79	49.79
	60	49.69	48.31	47.58	47.26	43.48	48.84
1:3.1	90	49.22	47.57	46.36	45.47	41.50	48.11
	120	48.86	46.72	45.25	44.23	39.22	46.75
	180	48.52	45.34	43.18	41.38	36.49	45.24
	240	47.02	44.01	41.04	38.05	32.03	43.07
	0	50	50	50	50	50	50
	30	49.44	48.31	47.54	46.83	44.72	49.44
	60	48.87	47.32	46.48	42.61	40.14	48.87
1:2.2	90	48.31	46.34	45.07	40.49	36.62	48.31
	120	47.75	45.28	42.96	35.92	34.15	47.75
	180	46.97	43.94	40.14	30.63	27.46	46.97
	240	45.85	42.39	38.87	23.94	14.79	45.85
	0	50	50	50	50	50	50
	30	49.30	47.68	46.34	41.83	29.30	49.15
	60	48.52	46.69	45.00	39.23	20.56	48.38
1:1.7	90	47.61	45.70	42.61	36.13	12.96	47.82
	120	46.41	44.79	41.20	32.54	7.61	47.04
	180	44.93	43.52	39.01	27.82	1.55	46.20
	240	43.94	41.97	37.25	16.48	0.54	45.42
	0	50	50	50	50	50	50
	30	48.10	46.83	43.94	41.83	43.17	49.86
	60	47.75	45.85	42.11	36.69	40.42	49.44
1:0.8	90	46.97	44.93	41.34	30.49	38.80	49.01
	120	45.92	43.94	39.65	23.59	36.27	48.24
	180	44.44	42.39	37.96	13.94	32.54	47.39
	240	43.52	40.70	36.48	4.58	28.52	46.48

Table 4.8 Time course variation of concentration of RB-220 during batch photocatalysis under solar light irradiation, using Ag@TiO$_2$ catalyst synthesized with different Ag to Ti molar composition ratio, calcined at different calcination temperatures.

Ag to Ti molar ratio	Time (min)	C_{RB-220} (mg/L) during photocatalysis with Ag@TiO$_2$calcined at different temperatures T_c					
		uncalcined	150 ºC	250 ºC	350 ºC	450 ºC	550 ºC
	0	50	50	50	50	50	50
	15	49.30	47.75	46.83	43.10	42.68	46.83
	30	48.73	46.48	46.27	41.76	39.93	45.56
1:5	45	47.89	45.35	44.93	39.30	35.42	44.65
	60	47.04	44.65	43.73	37.46	34.30	43.73
	120	45.28	42.11	40.56	34.08	28.10	41.90
	180	43.66	40	38.10	30.99	22.82	37.61
	0	50	50	50	50	50	50
	15	49.15	46.76	46.20	44.01	41.83	47.89
	30	48.52	45.49	45.35	41.48	38.80	47.04
1:3.1	45	47.61	44.30	44.08	39.72	35.42	45.56
	60	46.83	43.17	42.61	37.61	32.75	44.65
	120	45.07	40.70	40.07	34.37	26.34	41.83
	180	43.45	37.68	37.11	29.37	19.15	38.87
	0	50	50	50	50	50	50
	15	49.15	46.76	45.42	42.75	39.15	47.75
	30	48.31	45.49	44.15	40.00	35.28	46.41
1:2.2	45	47.25	44.30	42.32	38.10	31.90	45.56
	60	46.41	43.17	41.69	36.83	29.08	44.79
	120	44.44	40.70	39.01	32.46	17.46	42.89
	180	42.54	37.68	36.34	27.18	4.44	40.28
	0	50	50	50	50	50	50
	15	48.94	45.14	44.23	41.27	20.21	48.52
	30	47.75	44.93	41.76	38.31	8.73	47.54
1:1.7	45	46.06	42.54	39.79	35.42	1.48	46.55
	60	44.93	41.20	37.39	32.96	0.49	45.70
	120	42.11	38.31	34.30	26.34	0.28	43.80
	180	40.56	35.70	31.06	15.99	0.14	41.69
	0	50	50	50	50	50	50
	15	48.38	47.04	45.21	39.72	41.90	48.52
	30	47.54	45.28	43.87	36.41	39.01	47.54
1:0.8	45	46.55	43.24	42.39	33.38	36.06	46.55
	60	45.63	42.04	41.20	30.00	32.96	45.70
	120	42.82	38.87	37.96	21.34	25.49	43.80
	180	40.49	35.21	32.96	5.28	20.00	42.11

Table 4.9 Time course variation of % degradation of RB-220 during batch photocatalysis under UV light irradiation, using Ag@TiO$_2$ catalyst synthesized with different Ag to Ti molar composition ratio, calcined at different calcination temperatures.

Ag to Ti molar ratio	Time (min)	% degradation of RB-220 during photocatalysis with Ag@TiO$_2$calcined at different temperatures T$_c$					
		uncalcined	150 ºC	250 ºC	350 ºC	450 ºC	550 ºC
1:5	0	0	0	0	0	0	0
	30	0	0.85	1.27	2.11	3.66	2.25
	60	0.70	1.83	3.10	4.51	6.90	5.49
	90	1.41	3.66	5.07	6.76	9.44	7.32
	120	2.39	5.49	7.46	8.87	13.80	9.15
	180	3.52	7.89	10.56	13.94	17.75	11.83
	240	5.07	10.14	14.37	19.01	25.63	14.51
1:3.1	0	0	0	0	0	0	0
	30	0.6	2.1	2.8	4.1	8.5	2.8
	60	1.7	4.1	5.1	6.6	14	3.9
	90	2.8	5.8	7.5	9.6	18	4.9
	120	4.1	7.7	9.7	11	22	7.9
	180	4.9	9.6	14	19	28	10
	240	6.1	11	18	24	37	13
1:2.2	0	0	0	0	0	0	0
	30	1.13	3.38	4.93	6.34	10.56	2.82
	60	2.25	5.35	7.04	14.79	19.72	4.08
	90	3.38	7.32	9.86	19.01	26.76	5.35
	120	4.51	9.44	14.08	28.17	31.69	7.18
	180	6.06	12.11	19.72	38.73	45.07	9.15
	240	8.31	15.21	22.25	52.11	70.42	10.85
1:1.7	0	0	0	0	0	0	0
	30	1.41	4.65	7.32	16.33	41.41	1.69
	60	2.96	6.62	10	21.55	58.87	3.24
	90	4.79	8.59	14.79	27.75	74.08	4.37
	120	7.18	10.42	17.61	34.93	84.79	5.92
	180	10.14	12.96	21.97	44.37	96.90	7.61
	240	12.11	16.06	25.49	67.04	98.92	9.15
1:0.8	0	0	0	0	0	0	0
	30	3.80	6.34	12.11	16.33	13.66	0.28
	60	4.51	8.31	15.77	26.62	19.15	1.13
	90	6.06	10.14	17.32	39.01	22.39	1.97
	120	8.17	12.11	20.70	52.82	27.46	3.52
	180	11.13	15.21	24.08	72.11	34.93	5.21
	240	12.96	18.59	27.04	90.85	42.96	7.04

Table 4.10 Time course variation of % degradation of RB-220 during batch photocatalysis under solar light irradiation, using Ag@TiO$_2$ catalyst synthesized with different Ag to Ti molar composition ratio, calcined at different calcination temperatures.

Ag to Ti molar ratio	Time (min)	% degradation of RB-220 during photocatalysis with Ag@TiO$_2$ calcined at different temperatures					
				T$_c$			
		uncalcined	150 ºC	250 ºC	350 ºC	450 ºC	550 ºC
	0	0	0	0	0	0	0
	15	1.41	4.51	6.34	13.80	14.65	7.46
	30	2.54	7.04	7.46	16.48	20.14	9.86
1:5	45	4.23	9.3	10.14	21.41	29.15	12.11
	60	5.92	10.70	12.54	25.07	31.41	13.24
	120	9.44	15.77	18.87	31.83	43.80	19.86
	180	12.68	20	23.80	38.03	54.37	24.79
	0	0	0	0	0	0	0
	15	1.69	6.48	7.61	11.97	16.34	4.23
	30	2.96	9.01	9.3	17.04	22.39	5.92
1:3.1	45	4.79	11.41	11.83	20.56	29.15	8.87
	60	6.34	13.66	14.79	24.79	34.51	10.70
	120	9.86	18.59	19.86	31.27	47.32	16.34
	180	13.10	24.65	25.77	41.27	61.69	22.25
	0	0	0	0	0	0	0
	15	1.69	6.48	9.15	14.51	21.69	4.51
	30	3.38	9.01	11.69	20	29.44	7.18
1:2.2	45	5.49	11.41	15.35	23.80	36.2	8.87
	60	7.18	13.66	16.62	26.34	41.83	10.42
	120	11.13	18.59	21.97	35.07	65.07	14.23
	180	14.93	24.65	27.32	45.63	91.13	19.44
	0	0	0	0	0	0	0
	15	2.11	9.72	11.55	17.46	59.58	2.96
	30	4.51	10.14	16.48	23.38	82.54	4.93
1:1.7	45	7.89	14.93	20.42	29.15	97.04	6.90
	60	10.14	17.61	25.21	34.08	99.01	8.59
	120	15.77	23.38	31.41	47.32	99.44	12.39
	180	18.87	28.59	37.89	68.03	99.72	16.62
	0	0	0	0	0	0	0
	15	3.24	5.92	9.58	20.56	16.2	2.96
	30	4.93	9.44	12.25	27.18	21.97	4.93
1:0.8	45	6.90	13.52	15.21	33.24	27.89	6.90
	60	8.73	15.92	17.61	40	34.08	8.59
	120	14.37	22.25	24.08	57.32	49.01	12.39
	180	19.01	29.58	34.08	89.44	60	15.77
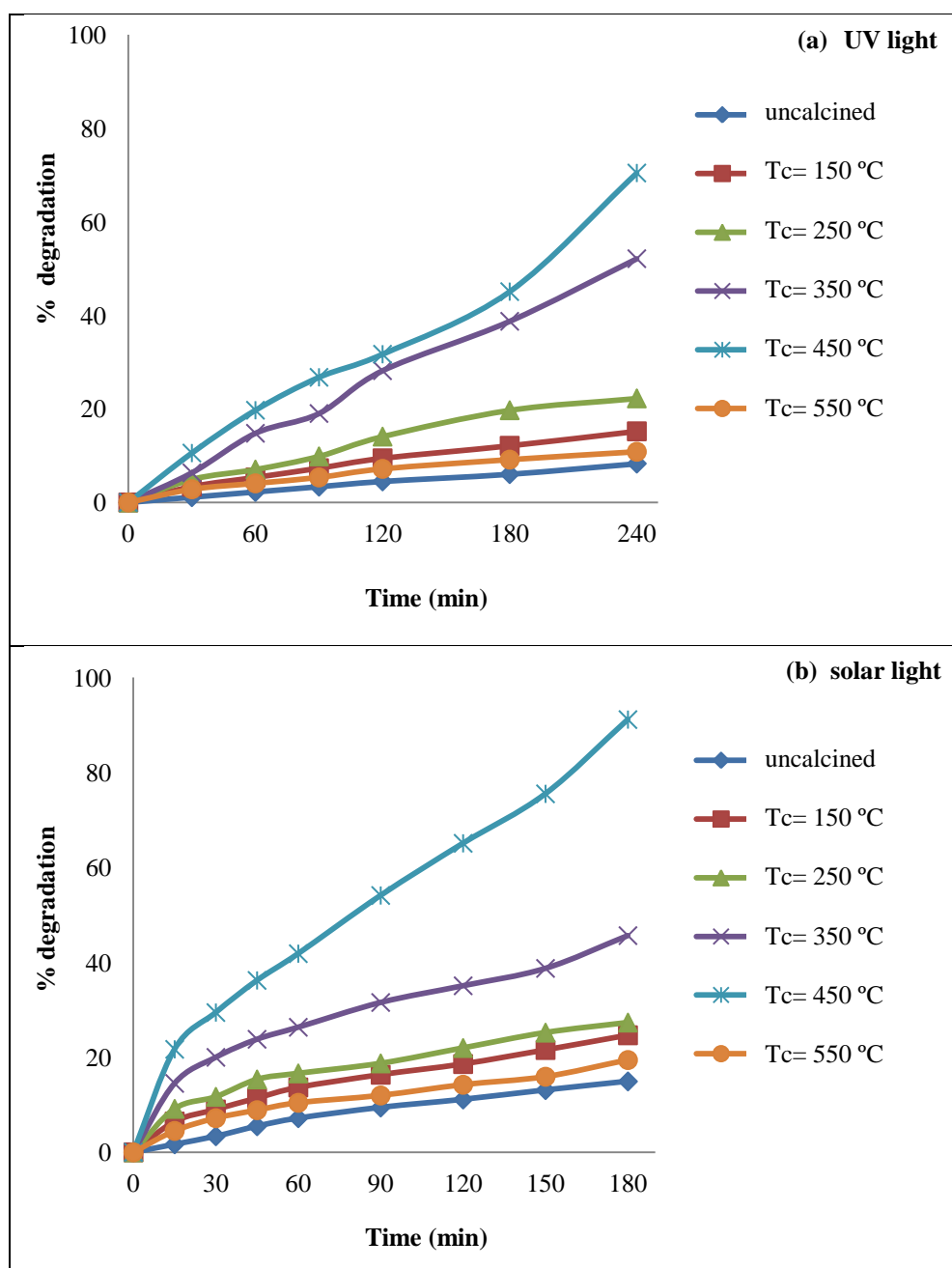
Figure 4.5 Representative plots showing the effect of calcination temperature on time course variation of photocatalytic degradation of RB-220 dye; a) UV light; b) solar light: average UV and visible light intensity of solar light= 3.61 mW/cm^2 and 1215×100 lux respectively from 11 a.m. to 2 p.m. Conditions: Catalyst used=Ag@TiO$_2$; Ag to Ti ratio=1:2.2; pH=3; C$_0$= 50 mg/L; Catalyst loading= 1 g/L (UV photocatalysis) and 500 mg/L (solar photocatalysis).
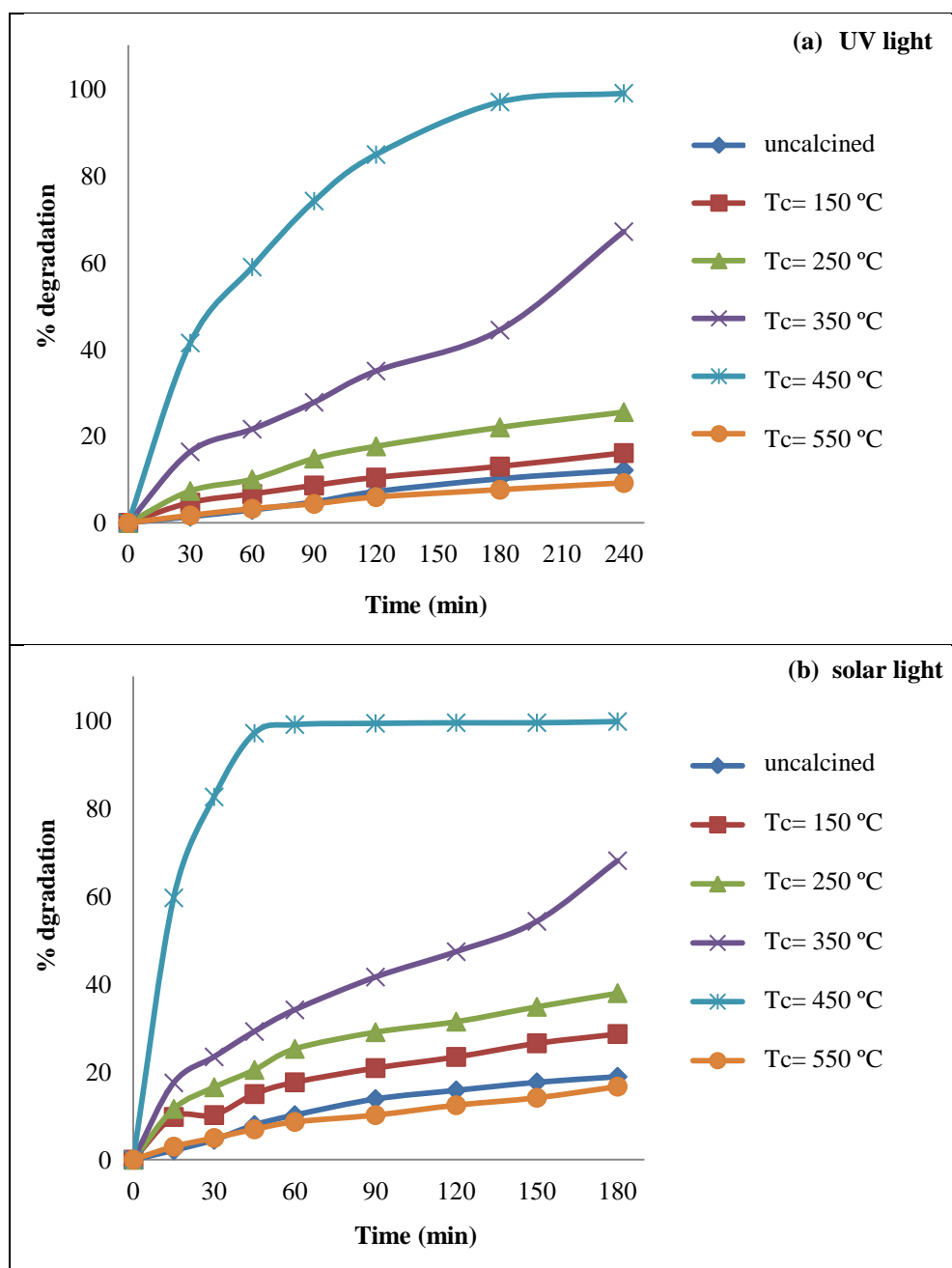
Figure 4.6 Representative plot showing the effect of calcination temperature on time course variation of photocatalytic degradation of RB-220 dye; a) UV light; b) solar light: average UV and visible light intensity of solar light= 3.6 mW/cm^2 and 1209×100 lux respectively from 11 a.m. to 2 p.m. Conditions: Catalyst used=Ag@TiO$_2$; Ag to Ti ratio=1:1.7; pH=3; C$_0$= 50 mg/L; Catalyst loading= 1 g/L (UV photocatalysis) and 500 mg/L (solar photocatalysis).
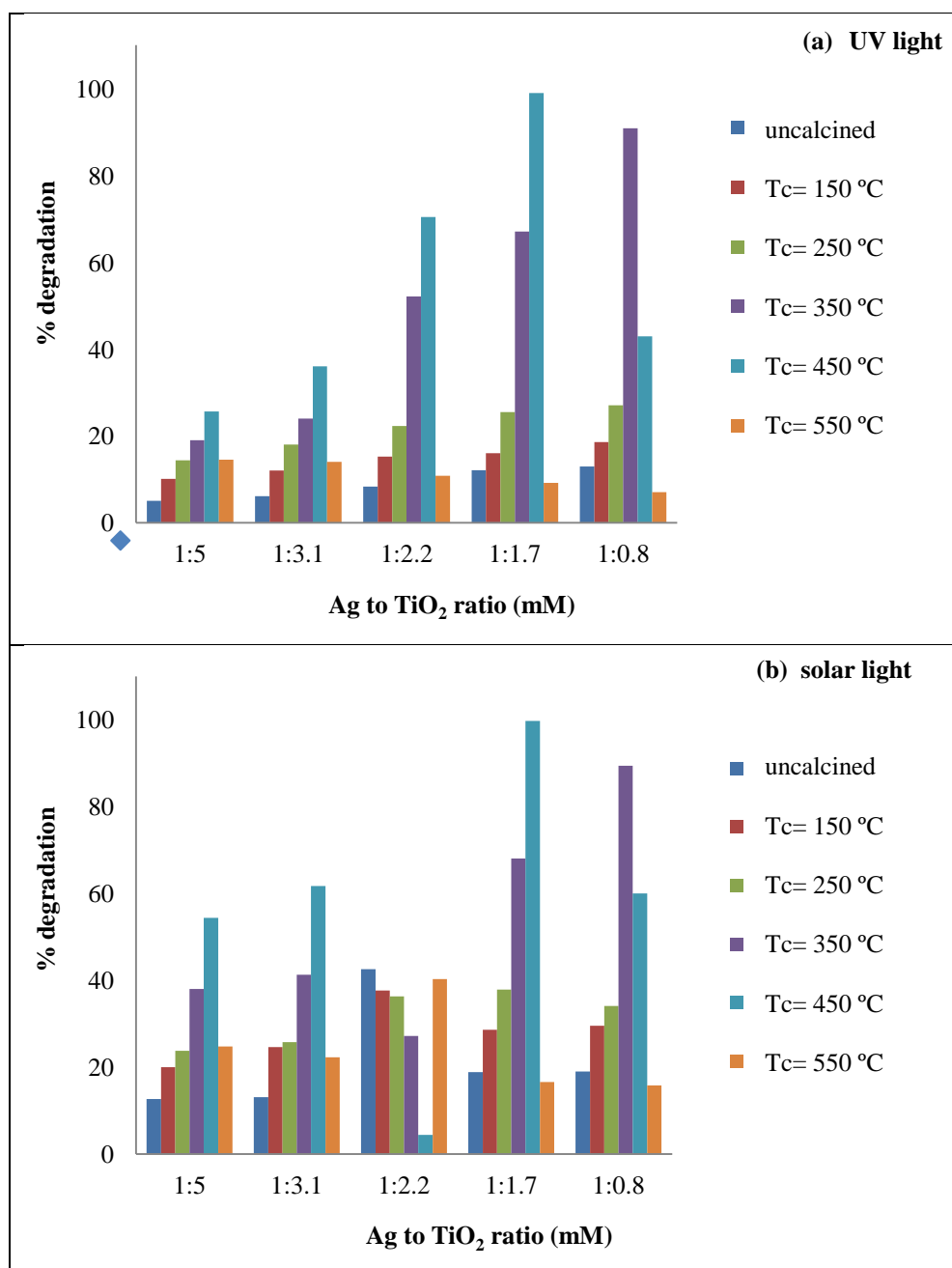
Figure 4.7 Effect of Ag to Ti molar composition ratio and calcination temperature on percentage degradation of RB-220 dye during photocatalysis using Ag@TiO$_2$ under a) UV light : Ag@TiO$_2$ loading= 1 g/L; Irradiation time =240 min; b) solar light: Ag@TiO$_2$ loading= 500 mg/L; Irradiation time =180 min. Conditions: C$_0$=50 mg/L; pH=3.

4.2 Effect of catalyst calcination time on the photocatalytic activity of Ag@TiO$_2$ in terms of photocatalytic degradation of AY-17 and RB-220 dye under UV and solar light irradiation

Calcination time affects the photocatalytic activity by determining the existence of crystalline phases present in the photocatalyst. So, the photocatalytic degradation of AY-17 and RB-220 in aqueous solution under UV and solar light irradiation at initial pH=3 was studied using Ag@TiO$_2$ catalysts synthesized with the Ag to Ti molar ratio of 1:1.7 and calcined at 450ºC for different calcination time periods ranging from 1 to 5 h. Experiments were performed with initial dye concentration of 10 mg/L and catalyst loading of 100 mg/L for both UV and solar photocatalysis of AY-17 dye. Similarly the degradation of RB-220 dye was studied with the initial concentration of 50 mg/L; catalyst loading of 1 g/L for UV photocatalysis and 500 mg/L for solar photocatalysis. For UV photocatalysis experiments, air at a flow rate of 2 LPM was supplied as an oxidant whereas for solar photocatalysis, atmospheric air transferred to the solution and being present as dissolved oxygen in the dye solution itself acted as an oxidant.

The data on time course variations of AY-17 dye concentration during UV and solar photocatalysis are presented in Table 4.11. Figure 4.8a shows the time course variation of percentage degradation of AY-17 dye during UV photocatalysis experiments carried out with Ag@TiO$_2$ nanoparticles calcined at 450 ºC for different calcination times. Time course variations have shown that, the rate of degradation of the dye increases with increase in calcination time from 1 to 3 h, but further increase in calcination time to 4 and 5 h, results in decreased rate of degradation. Effect of catalyst calcination time on percentage degradation of AY-17 dye (at 360 min irradiation time) with the catalyst calcined at different times is shown in Figure 4.9a. Figure 4.9a shows that, as the calcination time increases from 1 to 3 h the degradation in 360 min of irradiation time increases from 80.65 % to 99.2 %, but further increase in calcination time from 4 to 5 h leads to decreased degradation and it reached to only around 0.018 % (at 360 min). Therefore, the highest degradation with UV photocatalysis was observed with the nanoparticles calcined for 3 h.

Figure 4.8b shows the time course variation of percentage degradation of AY-17 dye and Figure 4.9b shows the effect of catalyst calcination time on percentage degradation of AY-17 dye (at 360 min irradiation time) during solar photocatalysis experiments carried out with Ag@TiO$_2$ nanoparticles calcined at 450 ℃ for different calcinations times. Time course variations have shown that, the rate of degradation of the dye increases with increase in calcination time as discussed previously for UV photocatalysis. As evident from Figure 4.9b, highest degradation (≈100 %) with solar photocatalysis occurred with the nanoparticles calcined for 3 h.

The data on time course variations of RB-220 dye concentration during UV and solar photocatalysis are presented in Table 4.12. Figure 4.10a shows the time course variation of percentage degradation of RB-220 dye during UV photocatalysis experiments carried out with Ag@TiO$_2$ nanoparticles calcined for different calcination times. Time course variations have shown that, the rate of degradation of the dye increases with increase in calcination time. Effect of catalyst calcination time on percentage degradation of RB-220 dye (at 240 min irradiation time) presented in Figure 4.11a, shows that, as calcination time increased from 1 to 3 h the degradation of RB-220 in 240 min of irradiation time increased from 82.54 % to 98.92 %, but further increase in calcination time from 3 to 5 h decreased the degradation, which reached to only around 16.05 % (at 240 min). Similar observations on effect of calcination time were made from Figure 4.10b and 4.11b for solar photocatalysis of RB-220 dye. Figure 4.11b shows that, as calcination time increases from 1 to 3 h the degradation in 180 min of irradiation time increased from 93.66 % to around 100 %, but further increase in calcination time from 3 to 5 h decreases the degradation, which reached to only around 27.88 % (at 180 min). Therefore, the highest degradation was observed at calcination time of 3 h for UV and solar photocatalysis of RB-220 dye.

Increase in degradation of the dyes with increase in calcination time may be attributed to increase in content of anatase TiO$_2$, which increases with increasing calcination time. It is reported by You et al. (2005), Mozia (2008) and Wang et al. (2010) that, as calcination time increases, formation of anatase phase increase but further increase in time lead to conversion of anatase phase to rutile phase which decreases the photocatalytic activity. As seen from XRD (Figure 4.4d) at calcination time of 3 h, anatase TiO$_2$ was found, so catalyst calcined at 450 ℃ for 3 h showed

better photocatalytic efficiency for photocatalytic degradation of AY-17 and RB-220 dyes. As the calcination time increased degradation increased, but further increase in the calcination time to above 3h decreased the degradation. Therefore calcination time of 3 h was found to be the optimum.

Thus the $Ag@TiO_2$ nanoparticles synthesized with Ag to Ti molar ratio of 1:1.7 and calcined at 450 ºC for 3 h was found to be optimum for maximum photocatalytic activity in terms of degradation of AY-17 and RB-220 under UV and solar light irradiation.

Table 4.11 Time course variation of concentration of AY-17 during batch photocatalysis under UV and solar light irradiation, using $Ag@TiO_2$ nanoparticles calcined for different time periods. Conditions: Catalyst used=$Ag@TiO_2$; Ag to Ti molar ratio=1:1.7; calcination temperature=450 °C; pH=3; C_0=10 mg/L; Catalyst loading= 100 mg/L.

Time (min)	C_{AY-17} (mg/L) with $Ag@TiO_2$ calcined at different time during									
	UV photocatalysis					Solar photocatalysis				
	t_c					t_c				
	1 h	2 h	3 h	4 h	5 h	1 h	2 h	3 h	4 h	5 h
0	10	10	10	10	10	10	10	10	10	10
60	8.82	8.31	7.38	9.34	9.81	8.37	6.55	0.08	7.69	9.51
120	7.11	6.46	5.92	8.56	9.64	6.75	4.27	0.05	5.79	9.21
180	5.65	4.94	4.36	7.81	9.61	4.32	2.08	0.05	4.32	8.68
240	3.99	3.28	2.41	7.73	9.60	2.72	1.25	0.05	3.63	8.32
300	2.82	1.98	1.22	7.62	9.78	1.81	0.75	0.05	3.55	8.25
360	1.94	1.20	0.08	7.58	9.99	1.12	0.42	0.05	3.20	8.12
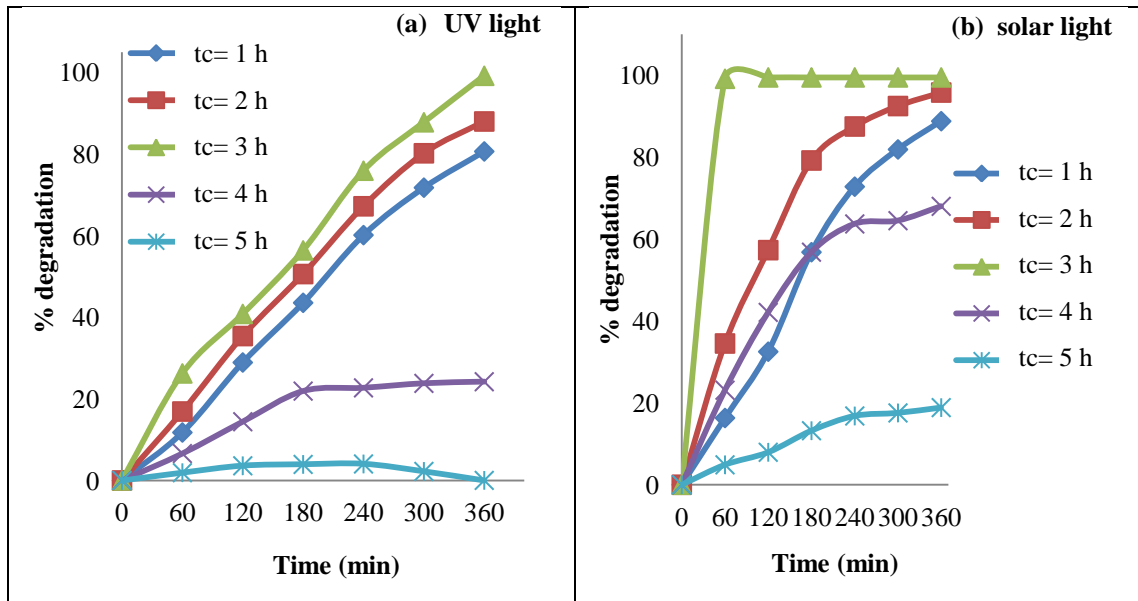
Figure 4.8 Effect of calcination time on time course variation of photocatalytic degradation of AY-17 dye under a) UV light; b) solar light: average UV and visible light intensity of solar light= 3.55 mW/cm^2 and 1206×100 lux respectively from 10 a.m. to 4 p.m. Conditions: Catalyst used=Ag@TiO$_2$; Ag to Ti molar ratio=1:1.7; Calcination temperature= 450 ºC; pH=3; C$_0$=10 mg/L; Catalyst loading= 100 mg/L.

Figure 4.9 Effect of calcination time on percentage degradation of AY-17 dye under a) UV light; b) solar light. Conditions: Ag@TiO$_2$ loading= 100 mg/L; C$_0$=10 mg/L; pH=3; Irradiation time =360 min; Calcination temperature= 450ºC.

Table 4.12 Time course variation in concentration of RB-220 during batch photocatalysis under UV and solar light irradiation, using Ag@TiO$_2$ nanoparticles calcined for different times. Conditions: Catalyst used=Ag@TiO$_2$; Ag to Ti molar ratio=1:1.7; calcination temperature=450° C; pH=3; C$_0$=50 mg/L; Catalyst loading= 1 g/L (UV photocatalysis) and 500 mg/L (solar photocatalysis).

Time (min)	C$_{RB-220}$ (mg/L) with Ag@TiO$_2$ calcined for different times									
	UV photocatalysis					Solar photocatalysis				
	t$_c$					t$_c$				
	1 h	2 h	3 h	4 h	5 h	1 h	2 h	3 h	4 h	5 h
0	50	50	50	50	50	50	50	50	50	50
30	45.21	42.54	29.30	48.17	48.80	38.59	29.44	8.73	42.75	45.92
60	41.27	36.27	20.56	43.17	47.96	29.08	9.44	0.49	34.37	42.32
90	36.20	31.97	12.96	40.28	46.83	21.48	6.69	0.35	29.15	40.85
120	30.70	25.85	7.61	36.90	45.35	13.31	2.25	0.28	24.51	39.93
180	20.70	18.03	1.55	32.54	43.87	3.17	0.85	0.14	16.62	36.06
240	8.73	4.72	0.54	29.72	41.97	-	-	-	-	-
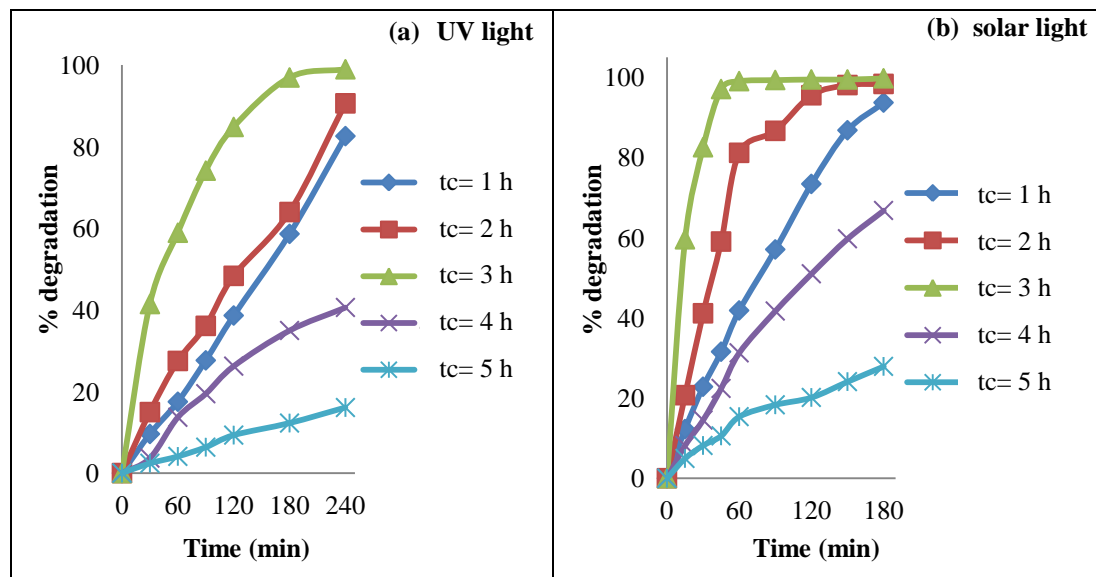
Figure 4.10 Effect of calcination time on time course variation of photocatalytic degradation of RB-220 dye under a) UV light; b) solar light: average UV and visible light intensity of solar light= 3.51 mW/cm^2 and 1201×10 lux respectively from 11 a.m. to 2 p.m. Conditions: Catalyst used=Ag@TiO$_2$; Ag to Ti molar ratio=1:1.7; pH=3; C$_0$=50 mg/L; Catalyst loading= 1g/L (UV photocatalysis) and 500 mg/L (solar photocatalysis).
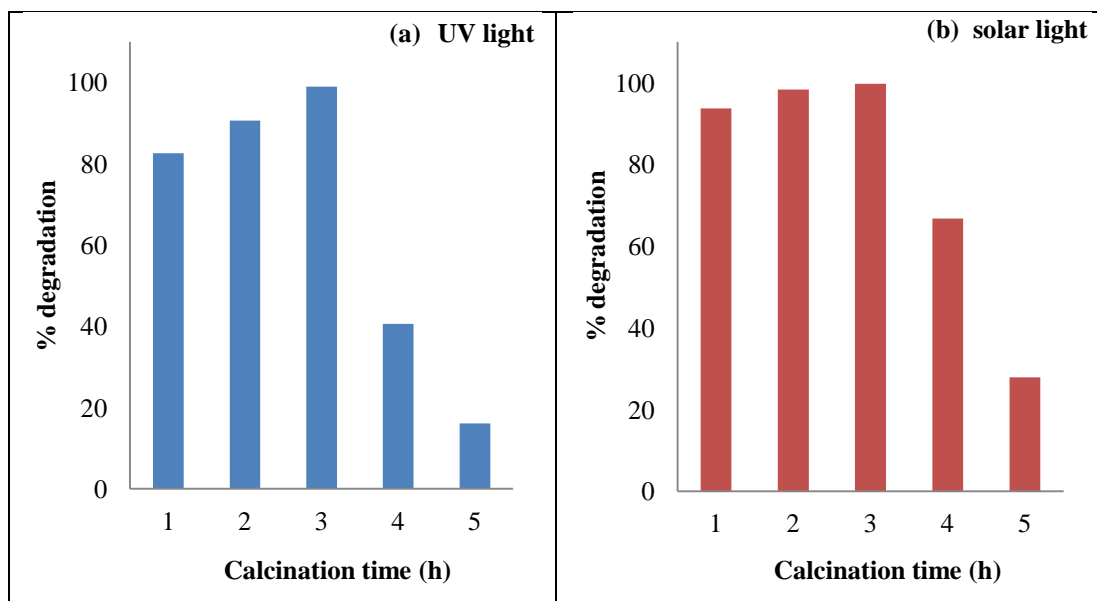
Figure 4.11 Effect of calcination time on percentage degradation of RB-220 dye under a) UV light: Ag@TiO$_2$ loading= 1g/L; Irradiation time =240 min; b) solar light: Ag@TiO$_2$ loading= 500 mg/L; Irradiation time =180 min. Conditions: C$_0$=50 mg/L; pH=3; Calcination temperature= 450 ºC.

4.3 Photocatalytic efficacy of Ag@TiO$_2$ nanoparticles and its suitability as a photocatalyst in degradation of AY-17 and RB-220 dyes

When photocatalysis experiments were performed with Ag@TiO$_2$ nanoparticles synthesized with Ag to Ti molar ratio of 1:1.7, calcined at 450°C for 3 h, good degradation of the dyes occurred. In order to confirm the role of Ag@TiO$_2$ nanoparticles as photocatalysts in degradation of AY-17 and RB-220 dyes and to confirm their suitability as photocatalysts, the photodegradation of AY-17 and RB-220 dyes were studied (a) under a light source (UV and solar) and in the absence of any catalyst, (b) under dark conditions with Ag@TiO$_2$ nanoparticles, and (c) with Ag@TiO$_2$ under UV and solar light irradiations. Figure 4.12a and 4.12b show the comparison of degradation of AY-17 as the function of time for control experiments (under light in the absence of Ag@TiO$_2$) or with Ag@TiO$_2$ (under dark) with the results obtained when UV and solar light was used with Ag@TiO$_2$. The initial concentration of AY-17 used was 10 mg/L. Figure 4.13a and 4.13b show the comparison of degradation of RB-220 as a function of time for control experiments

(under light (absence of Ag@TiO$_2$) or with Ag@TiO$_2$ (under dark)) with the results obtained when UV and solar light was used with Ag@TiO$_2$. The initial concentration of RB-220 used was 50 mg/L. No significant dye degradation occurred in the absence of catalyst and AY-17 or RB-220 solutions were found to be stable on irradiation with UV and solar light irradiation, indicating that no photolysis occurs. Under dark conditions and in the presence of Ag@TiO$_2$, around 25 % degradation of AY-17 dye occurred in 60 min and % degradation remained constant after 60 min. Under dark conditions and in the presence Ag@TiO$_2$, around 7 % degradation of RB-220 dye occurred in 60 min and around 8 % degradation occurred after 240 min of irradiation. It is because of the adsorption of dye molecules on the surface of Ag@TiO$_2$ nanoparticles (Gupta et al. 2007). On the other hand degradation of AY-17 dye increased drastically and almost complete degradation of dye occurred within 360 min under UV irradiation and within 60 min under solar light irradiation when Ag@TiO$_2$ at loading of 100 mg/L was used as catalyst. Similarly, degradation of RB-220 increased continuously at a fast rate and almost complete degradation occurred within 240 min under UV irradiation and within 60 min under solar light irradiation when Ag@TiO$_2$ at loading of 1 g/L (UV) and 500 mg/L (solar) were used as catalyst.

The rates of degradation of AY-17 or RB-220 with the catalyst under solar light were tremendously faster as compared to those with the catalyst under UV light. As Ag@TiO$_2$ nanoparticles get illuminated by light (UV or solar), reactive species such as H$_2$O$_2$, O$_2^-$ and ˙OH are produced. The azo bond of the dyes would have been attacked by these reactive species which lead to cleavage of azo bond and thus causes degradation. This confirms that the cause of degradation of AY-17 and RB-220 dyes is photocatalysis by Ag@TiO$_2$ under UV and solar light irradiation. Hence it is concluded that Ag@TiO$_2$ nanoparticles are effective photocatalysts for the degradation of azo dyes such as AY-17 and RB-220 both for UV and solar photocatalysis and hence are suitable for treatment of water contaminated with these dyes by photocatalysis.
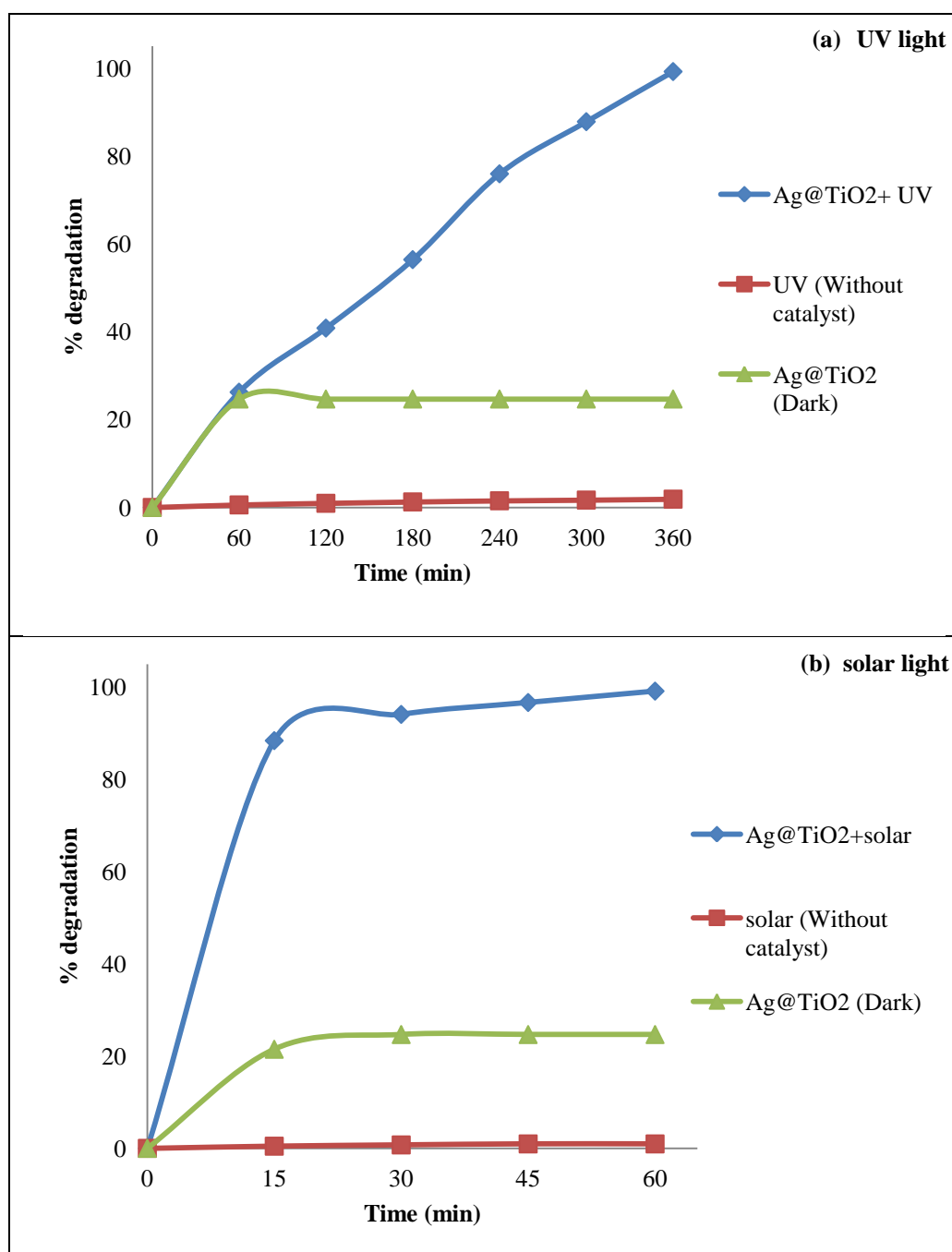
Figure 4.12 Photocatalytic degradation of AY-17 dye under a) UV light; b) solar light: average UV and visible light intensity of solar light= 3.57 mW/cm^2 and 1208×100 lux respectively from 11 a.m. to 12 p.m. Conditions: pH=3; C$_0$= 10 mg/L; catalyst loading = 100 mg/L.
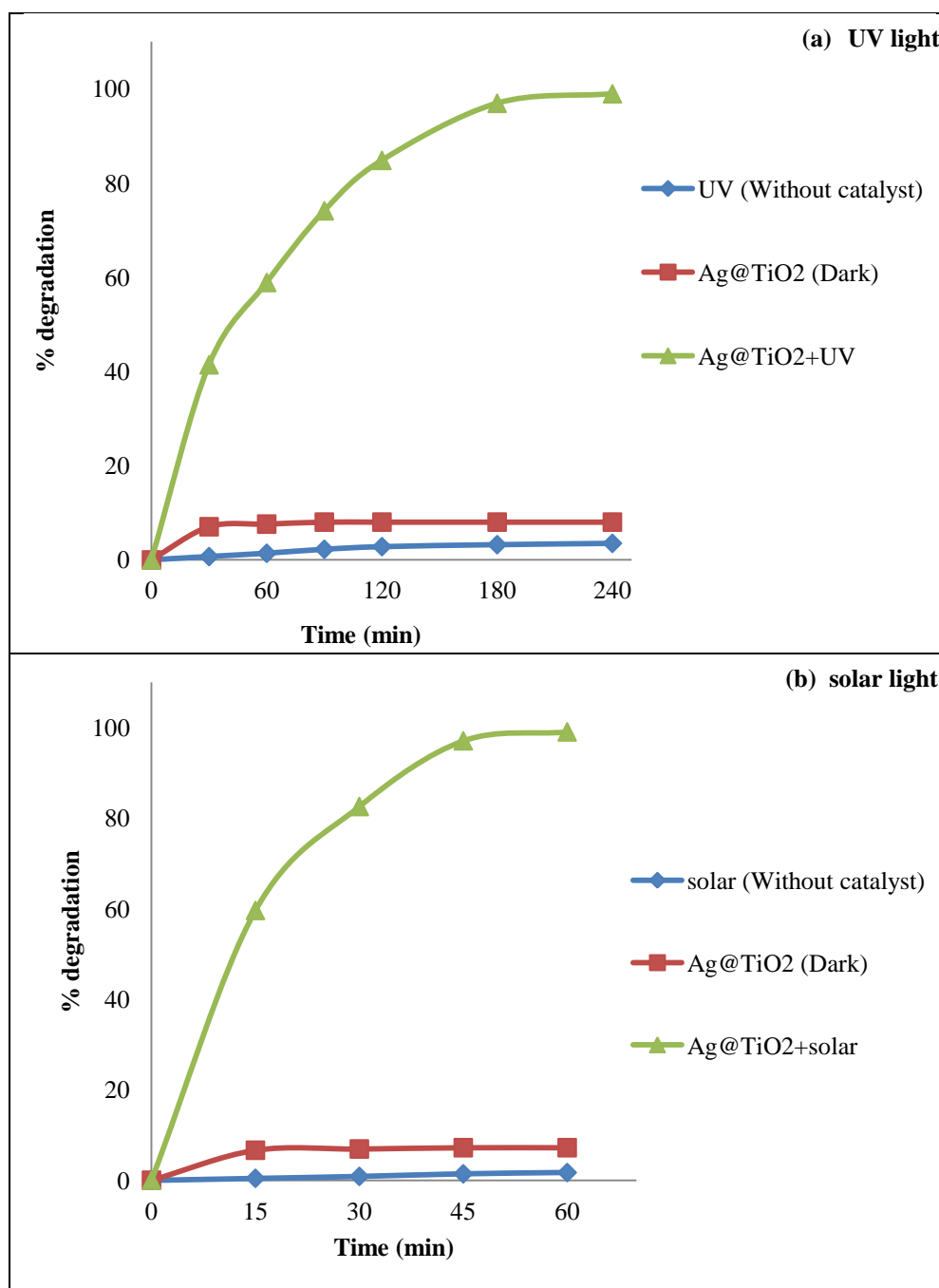
Figure 4.13 Photocatalytic degradation of RB-220 dye under a) UV light; b) solar light: average UV and visible light intensity of solar light= 3.62 mW/cm^2 and 1120×100 lux respectively from 11 a.m. to 12 p.m. Conditions: pH=3; C_0= 50 mg/L; catalyst loading = 1 g/L (UV photocatalysis) and 500 mg/L (solar photocatalysis).

4.4 Characterization of Ag@TiO$_2$ nanoparticles

It was concluded from the results discussed in Section 4.1-4.2 that, Ag@TiO$_2$ catalyst synthesized with Ag to Ti molar ratio of 1:1.7 and calcined at a temperature of 450 ℃ for 3 h exhibited highest photocatalytic activity for UV and solar photocatalysis of AY-17 and RB-220 dyes. They were found to be effective photocatalysts for the degradation of azo dyes such as AY-17 and RB-220. Further these Ag@TiO$_2$ nanoparticles were characterized using TEM, SAED, EDS, AFM, XRD, TG-DTA, DRS and BET to determine their size, shape, crystalline nature, light absorption behavior, band gap, thermal characteristics, surface area etc, in order to understand their behavior as photocatalysts for UV and solar photocatalysis.

4.4.1 Transmission Electron Microscopy (TEM)

Figure 4.14 and Figure 4.15 present the TEM images of the Ag@TiO$_2$ nanoparticle synthesized with Ag to Ti molar ratio of 1:1.7 and calcined at 450 $^\circ$C for 3h, at different magnifications. These images show the formation of core-shell structure. Figure 4.15a and b; show the TEM images of a single Ag@TiO$_2$ core-shell nanoparticle at high magnifications. These images confirm the formation of core-shell structure and the visible crystal lattice in the structure in Figure 4.15b confirms the crystallinity of the nanoparticle. The black central portion indicates the presence of Ag core and the white outer layer around the Ag core is the TiO$_2$ shell as seen from Figure 4.14b, 4.15a and 4.15b. Also in bulk portion of the image in Figure 4.14a, several particles are shown with Ag core covered by TiO$_2$ shell. The particles were slightly oval in shape. The core of the particle is of average diameter of 33.63 nm and TiO$_2$ shell has the average thickness 3.7 nm. The size of core-shell structure was found to be around 37.33 nm. The corresponding SAED pattern of Ag@TiO$_2$ is also shown in inset of Figure 4.14c. Each diffraction rings correspond to the crystal planes of Ag and TiO$_2$. Hence SAED analysis and the XRD shown in Figure 4.4d of Section 4.1.1 confirmed the crystallinity of core-shell structures and are in good agreement with each other.

4.4.2 Energy Dispersive spectra (EDS)

Figure 4.16 illustrates the EDS spectra of Ag@TiO$_2$ nanoparticles. The presence of Cu in the spectra is due to the copper grid used in the TEM measurement. The EDS analysis showed the presence of O, Ti, and Ag elements in Ag@TiO$_2$.

4.4.3 Atomic Force Microscopic (AFM) analysis

The AFM image (Figure 4.17) reveals the formation of Ag@TiO$_2$ nanoparticles. As it can be seen in Figure 4.17, silver core is in the form of well-defined oval nanoparticle and is covered by TiO$_2$ shell. This analysis is in good agreement with the TEM analysis. The analyses confirmed the formation of core-shell structure. Kim et al. (2004) and Zhang et al. (2005) synthesized Ag@TiO$_2$ nanoparticles by two pot synthesis method. They had shown the presence of core shell structure through a TEM image before calcination, but had not shown any evidence on the retainment of core shell structure after calcination. But in the present study, the TEM and AFM analysis of Ag@TiO$_2$ nanoparticles confirms the presence of core shell structure in the calcined nanoparticle. Figure 4.18 presents the particle size distribution curve of Ag@TiO$_2$ nanoparticles and it shows that the nanoparticles are polydispersed and the size varied in the range of 10-50 nm with the average particle size of approximately 30nm. This result is in good agreement with TEM results. The double peaks corresponding to particles of size 26 and 32 nm in the size distribution curve indicate that these two particle sizes are found more frequently in the distribution.

4.4.4 X-Ray diffraction (XRD) analysis

XRD analysis of Ag@TiO$_2$ nanoparticles was carried out to check the crystalline nature of core-shell nanoparticles. The discussions on the XRD of Ag@TiO$_2$ nanoparticles synthesized with Ag to Ti molar composition ratio of 1:1.7, calcined at 450°C for 3h has already been presented in Section 4.1.1 and the XRD shown in Figure 4.4d confirmed the crystalline nature of both Ag core and TiO$_2$ shell. The XRD revealed the presence of anatase phase TiO$_2$.No peaks of rutile phase TiO$_2$ or AgO

reflection peak (2θ=30.2) were observed in the diffraction pattern. Absence of AgO indicates that Ag core exist as Ag^0 in Ag@TiO$_2$ and there is no possibility of lowering of photocatalytic activity which would have occurred if AgO was present, as reported by Wang et al. (2008b).

The average crystallite size of these nanoparticles was calculated using Scherrer's formula and presented in Table 4.6. The average crystallite size calculated by Scherrer's formula being 39.40 nm, is in close agreement with the average particle size of 37.33 nm obtained by TEM and reasonably matches with the particle size range obtained with particle size distribution by AFM analysis.

4.4.5 Thermo gravimetric-differential thermal (TG-DTA) analysis

To study the thermal characteristics of Ag@TiO$_2$ nanoparticles, TG-DTA analysis was performed. The TG-DTA curve for the synthesized Ag@TiO$_2$ nanoparticles is shown in Figure 4.19. The temperature - weight loss course can be divided into three stages in TG curve. The first stage between 0 and 100 °C corresponds to desorption or release of solvent and water in the sample, second stage between 100 and 350 °C corresponds to combustion and decomposition of organic matter, produced from the hydrolysis of TTEAIP, and the third correspond to weight loss in the range of 350 − 600 °C, which is not very obvious and may be due to the dissociation of hydroxyl groups from the surface of TiO$_2$ nanoparticles. DTA results indicate the appearance of a decalescence peak at 61.9 °C on the curve, which corresponds to desorption or release of solvent and water in the nanoparticles. As the temperature increases, two releasing peaks at 262.1 and 345.2 °C corresponding to combustion and decomposition of organic matter are observed. In the range of 350 − 600 °C, few decalescence and releasing peaks are also present, which may be due to the phase conversion of TiO$_2$ from amorphous to anatase (around 350 °C), surface hydroxyl groups dissociation (350–600 °C) and phase conversion of TiO$_2$ from anatase to rutile (around 514 °C). Similar observations were made by Zhang et al. (2005). These discussions on TG-DTA results, presenting the possible phase conversion of TiO$_2$ from amorphous to anatase phase at around 350°C and from anatase to rutile at temperatures of around 514 °C is supported by the experimental results on effect of

calcination temperature on photocatalytic degradation of AY-17 and RB-220 dyes which are presented in Figure 4.3 and Figure 4.7 respectively. These Figures show increase in photocatalytic activity with increase in calcination temperature upto 450 °C and decrease in the activity with further increase in calcination temperature to 550 °C. So, decreased activity at 550 °C may be owing to conversion of anatase to rutile phase of TiO_2 at temperatures greater than 514 °C as indicated by TGA results.

4.4.6 Diffuse Reflectance Spectra (DRS) analysis

The DRS of the $Ag@TiO_2$ nanoparticles (Figure 4.20) showed a sharp reflectance peak at 320 nm in the UV region which is the characteristic of TiO_2 corresponding to the charge transfer process from the valence band to conduction band in TiO_2 (Li et al. 2008). The $Ag@TiO_2$ also shows strong visible light absorption in the range of 398 - 509 nm and maximum is seen at 509 nm. It shows that, $Ag@TiO_2$ is able to absorb both UV light and portion of visible light, maximum visible light absorption being at 509 nm. The visible light absorption of $Ag@TiO_2$ particles, as seen by the occurrence of red shift is due to the surface plasmon resonance of Ag core and it is strongly influenced by the oxide shell (Rodriguez-Gattorno et al. 2002). The high dielectric constant of TiO_2 shell causes a red shift in the plasmon absorption of the silver core (Chan and Barteau 2005; Mulvaney 1996; Liz-Marzán and Mulvaney 2003; Kreibig and Vollmer 1995). The ability of these core-shell nanoparticles to absorb both UV and visible light shall enhance their photocatalytic activity in solar light, which constitutes small portion of UV and majority being the visible light. The DRS analysis hence supports the solar photocatalytic activity of these nanoparticles as observed in Figure 4.12 and Figure 4.13 in terms of solar photocatalytic degradation of AY-17 and RB-220 dyes respectively.

4.4.7 Band gap determination

The band gap energy which is the minimum energy required for an electron to be excited from valance band to conduction band is an important characteristic of any photocatalyst. The band gap energy of $Ag@TiO_2$ nanoparticles was determined from

DRS using Kubelka Munk's model. Firstly the reflectance data were fitted to Kubelka Munk's model for direct Eq.(3.4) and indirect Eq.(3.3) band gap transition to establish the type of band to band transition in Ag@TiO$_2$ nanoparticles. It was seen, when reflectance data was fitted to indirect band gap transition, band gap energy with negative value was obtained which is not realistic. So the data was fitted to direct transition and Figure 4.21 shows the Tauc's plot of $(k \times h\nu)^2$ versus hν for Ag@TiO$_2$ nanoparticles. The data fitted well into Kubelka Munk's model for direct transition. The band gap energy was estimated from linear portion of the plot by drawing tangent and intersection of the tangent to the plotted curve inflection point with the horizontal axis resulted in the band gap energy value of 1.85eV. Direct band gap transition is found to be favorable with Ag@TiO$_2$ nanoparticles in the present study. Since in the present study Ag@TiO$_2$ nanoparticles consist of anatase phase TiO$_2$ and it is reported in literature by Reddy et al. (2002) that direct band gap transition is more favourable when anatase phase of TiO$_2$ is present. In direct band gap materials, the electronic transition is electrical dipole allowed and in indirect band gap materials, it is electrical dipole forbidden and photon assisted. Both energy and momentum are changed during indirect transition. In direct band gap transition absorption and emission is much stronger as compared to indirect band gap transition. So a direct band gap transition can result in a more efficient absorption of solar energy (Reddy et al. 2002) and hence much better photocatalytic properties. The band gap energy of Ag@TiO$_2$ nanoparticles was found to be around 1.85eV, which is much lesser than the band gap energy for TiO$_2$ (3.2eV), indicating that Ag@TiO$_2$ nanoparticles have all the potential to be excited by longer wavelength radiations in visible range and hence can be used effectively for solar photocatalysis. Lower band gap energy value justifies the solar photocatalytic activity of these nanoparticles as observed in Figure 4.12 and Figure 4.13 in terms of solar photocatalytic degradation of AY-17 and RB-220 dyes respectively.
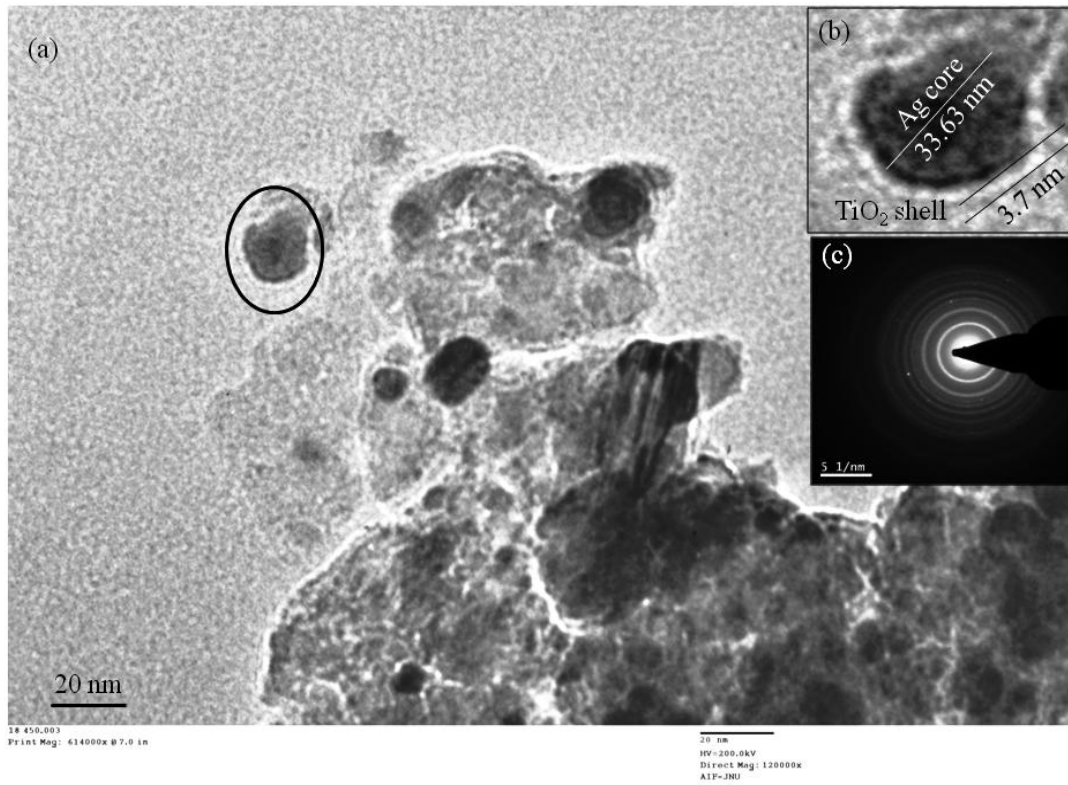
Figure 4.14 TEM image (a) of Ag@TiO$_2$ nanoparticles calcined at 450$^°$C and Inset (b) magnified image of particle (c) SAED pattern of Ag@TiO$_2$.
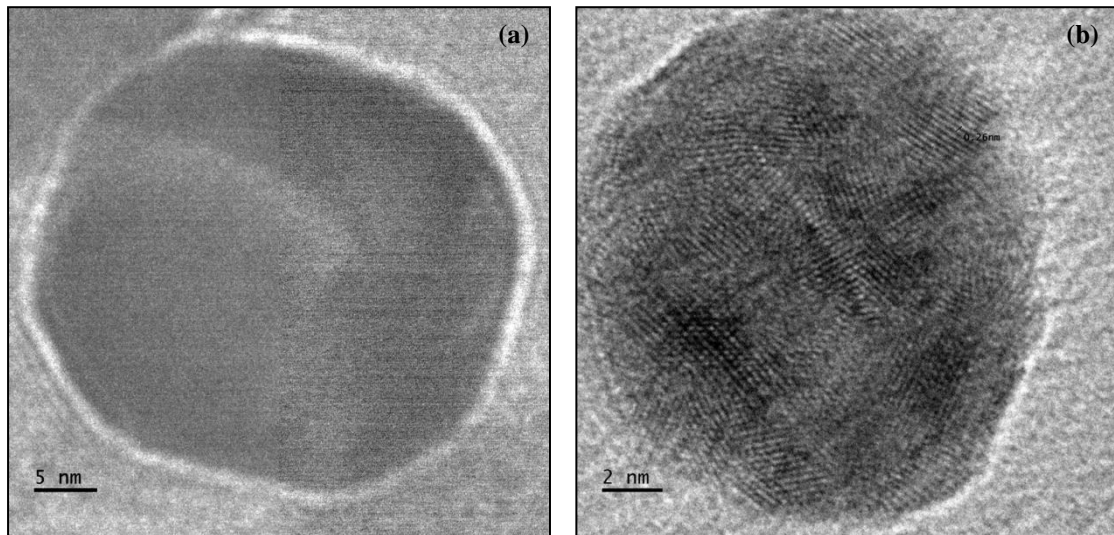
Figure 4.15 TEM image of Ag@TiO$_2$ nanoparticle calcined at 450$^°$C (a) at 5nm scale (b) magnified image at 2 nm scale.
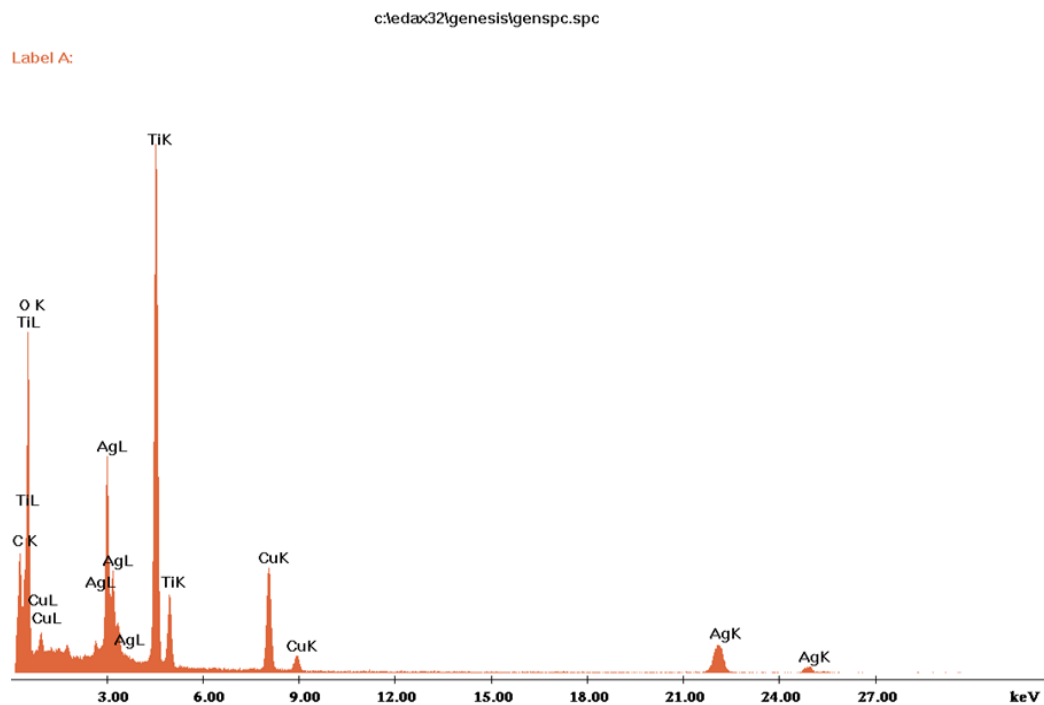
Figure 4.16 EDS spectra of Ag@TiO₂ nanoparticles.
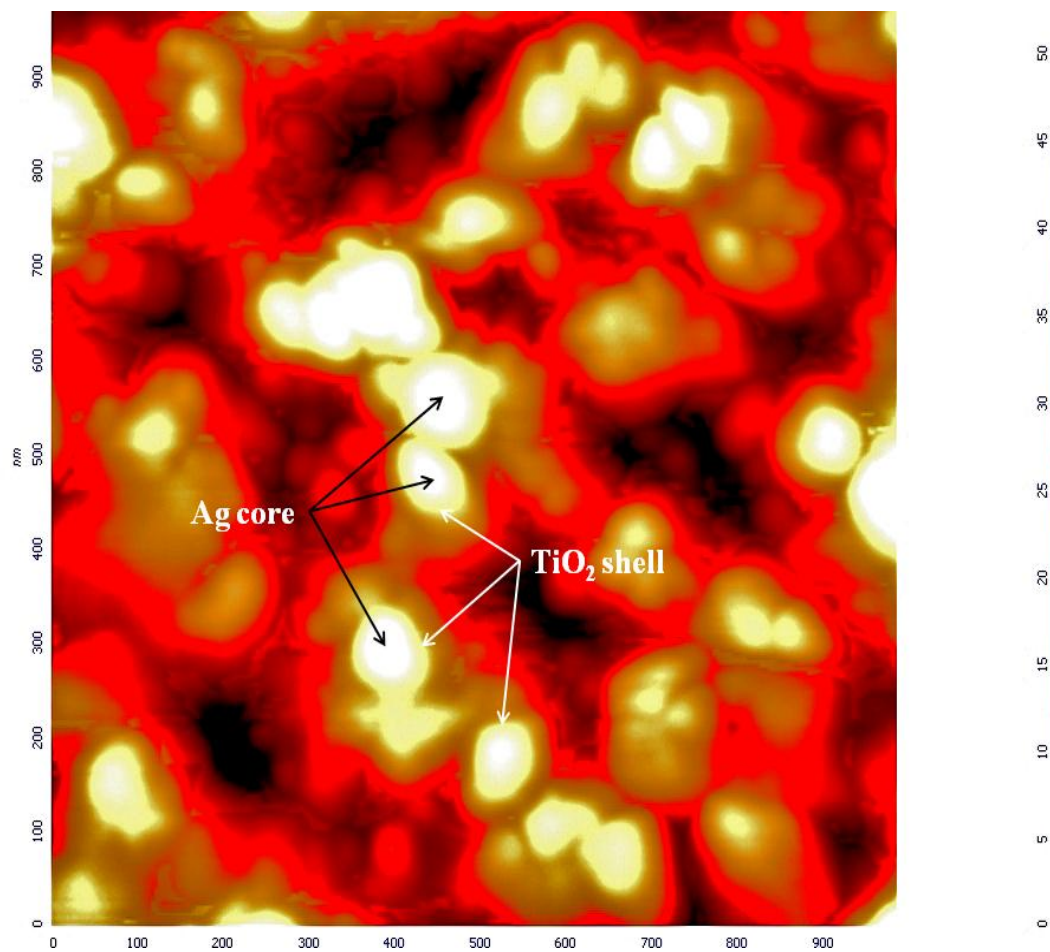
Figure 4.17 AFM image of Ag@TiO$_2$ nanoparticles calcined at 450 ºC.

Figure 4.18 Particle size distribution of Ag@TiO₂ nanoparticles calcined at 450 ºC.
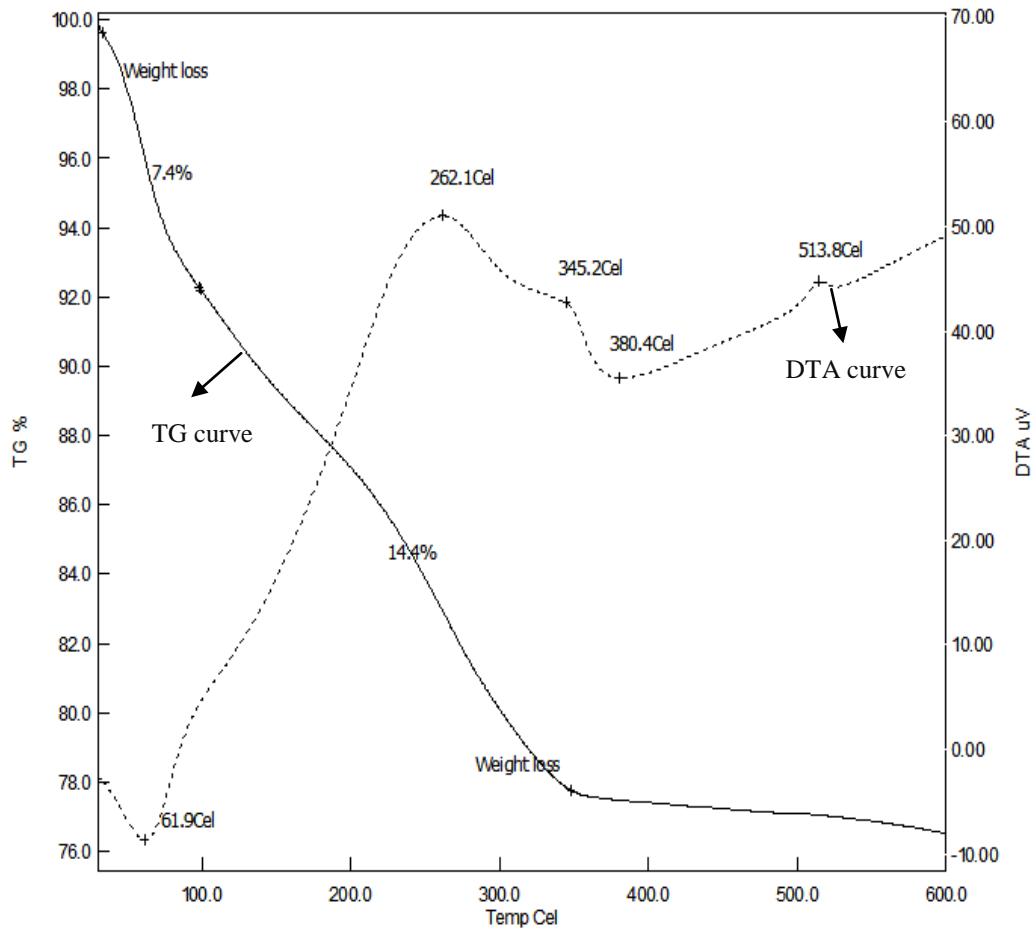
Figure 4.19 TG-DTA curve of Ag@TiO$_2$ nanoparticles.
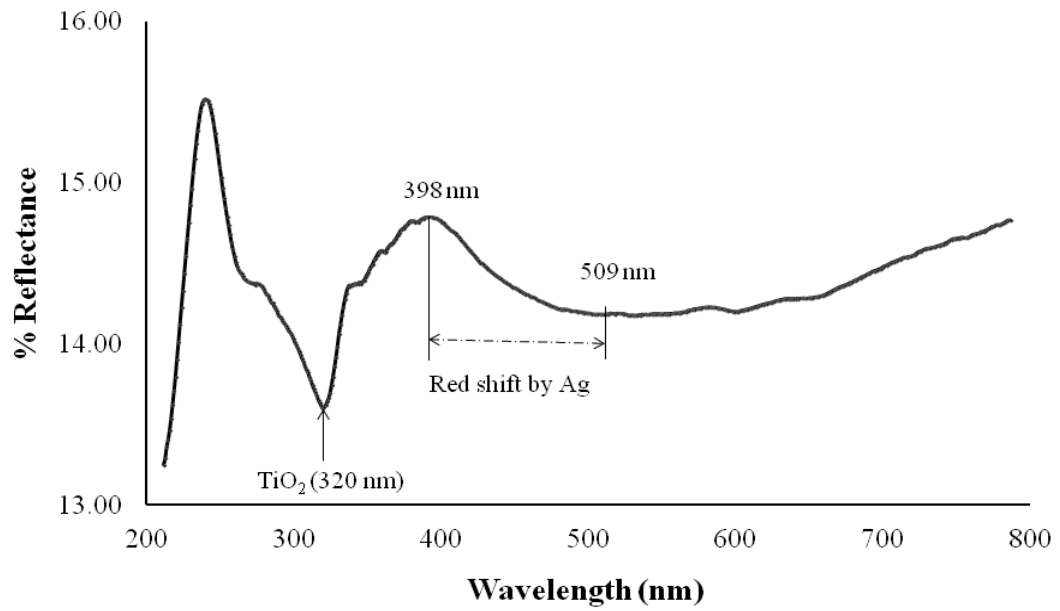
Figure 4.20 DRS spectrum of Ag@TiO$_2$ nanoparticles calcined at 450 ºC.
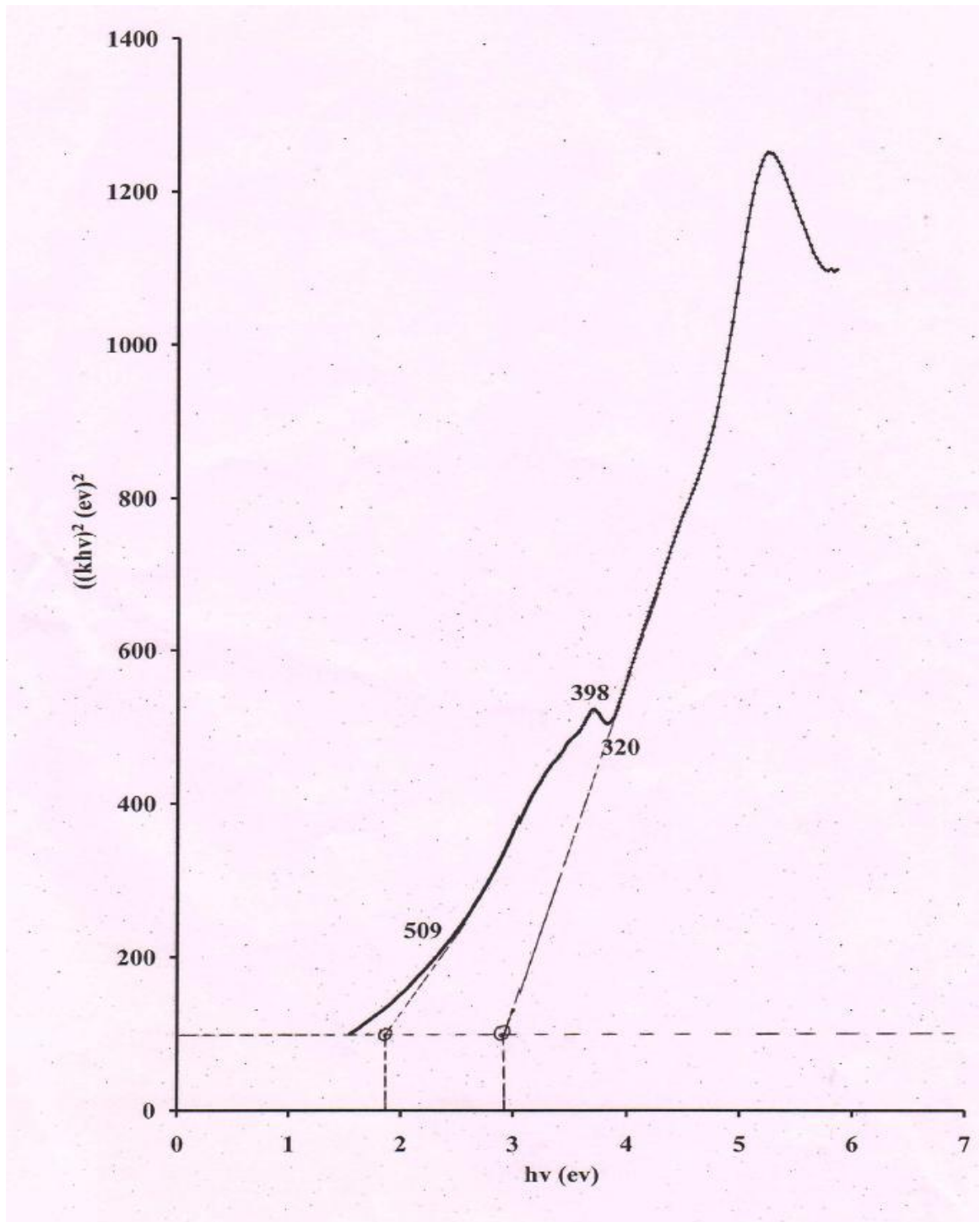
Figure 4.21 Tauc's plot of (khν)^2 versus hν for direct band gap transition of Ag@TiO$_2$ nanoparticles.

4.4.8 Surface area analysis (BET)

The surface area of the catalyst is an important factor affecting the rate of photocatalysis. The specific surface area of nanoparticles is the sum of the areas of the exposed surfaces of the particles per unit mass (Akbari et al. 2011). Smaller the particles, larger will be the specific surface area and hence rate of photocatalysis will be higher with smaller sized particles due to higher availability of more active sites per unit mass. The specific surface area of $Ag@TiO_2$ nanoparticles was determined by nitrogen gas adsorption BET method and found to be $22.93 m^2/g$.

4.5 Comparison of photocatalytic activity of $Ag@TiO_2$ core shell structured nanoparticles with other photocatalysts for degradation of AY-17 and RB-220 dyes under UV and solar light irradiation

The efficacy of $Ag@TiO_2$ nanoparticles as a photocatalyst was compared with other catalysts such as TiO_2 and Ag doped TiO_2 based on the degradation of AY-17 and RB-220 dyes under UV and solar light irradiations. In case of UV photocatalysis, air was bubbled through the solution continuously to act as an oxidant. In case of solar photocatalysis, continuous bubbling of air was found not necessary as the results obtained in the presence and absence of air bubbling matched with each other, indicating that dissolved oxygen (DO) present in the reaction mixture initially and subsequent dissolution from atmospheric air during the experiments, itself was sufficient to serve as an oxidant, for the reaction duration.

4.5.1 Comparison of photocatalytic activity in terms of degradation of AY-17 dye under UV and solar light irradiation

The photocatalytic efficacy of $Ag@TiO_2$ for the degradation of AY-17 dye with initial concentration of 10 mg/L, catalyst loading of 100 mg/L, and at initial pH 3 was compared with commercially available Degussa P-25 catalyst, $SGTiO_2$, $CSTiO_2$, Ag doped-$SGTiO_2$, Ag doped (LI)-$CSTiO_2$, and Ag doped (PD)-$CSTiO_2$. Photocatalytic degradation of AY17 by different catalysts at various irradiation times

are shown in Figure 4.22a and 4.22b for UV and solar light irradiations respectively. These Figures clearly show that $Ag@TiO_2$ nanoparticles are the most efficient photocatalysts in degradation of AY-17 dye as compared to other catalysts under study and photocatalytic activity in terms of degradation of AY-17 dye is in the order of $Ag@TiO_2$ > Degussa P25 > Ag doped-$SGTiO_2$> Ag doped (LI)-$CSTiO_2$> $SGTiO_2$> $CSTiO_2$> Ag doped (PD)-$CSTiO_2$ under UV light. Under solar irradiation, the activities are rated as $Ag@TiO_2$> Ag doped-$SGTiO_2$> Degussa P25 > $SGTiO_2$> Ag doped (LI)-$CSTiO_2$> $CSTiO_2$> Ag doped (PD)-$CSTiO_2$. Though the specific surface area of $Ag@TiO_2$ nanoparticles ($22.93m^2/g$) is lesser than that of Degussa P25 ($50m^2/g$), high photocatalytic activity is exhibited by $Ag@TiO_2$ both under UV and solar light irradiations, which might be due to their ability to inhibit electron-hole recombination, by storage of electron in Ag core and subsequent discharge on provision of electron acceptor such as O_2 (Hirakawa and Kamat 2005), owing to their capability to absorb both UV and visible light radiations of solar light and also due to low band gap energy. In case of solar light with $Ag@TiO_2$ catalyst, almost 100 % degradation of the dye occurred in 60 min and around 89 % degradation occurred within 15 min; whereas with UV light, it took around 360 min for around 100 % degradation. It is found that catalyst loading and irradiation time required for solar photocatalysis is much lesser than that used in UV photocatalysis. In comparison to UV photocatalysis, under solar light rate of photocatalysis was very high with $Ag@TiO_2$ catalyst, due to its potential to absorb both UV and visible light portions of solar radiation, as indicated by DRS spectrum shown in Figure 4.19 and also due to low band gap energy of 1.85eV. As discussed in Section 4.3.7, direct band gap transition can result in a more efficient absorption of solar energy, so this may be another reason of high photocatalytic activity observed by $Ag@TiO_2$ nanoparticles under solar photocatalysis.

Lower photocatalytic efficacy exhibited by Degussa P25, $SGTiO_2$, and $CSTiO_2$ may be due to the electron-hole recombination, leading to low quantum yield and due to higher band gap energy of 3.2eV for TiO_2. However, less photocatalytic efficacy exhibited by Ag doped-$SGTiO_2$, and Ag doped (LI)-$CSTiO_2$ may be due to loss of activity of TiO_2, as metal deposits occupy the active sites on the TiO_2 surface (Coleman et al. 2005). Less activity was shown by Ag doped (PD)-$CSTiO_2$ as the

negative charge on silver may start to attract holes and then recombine with electrons leading to recombination of electron-hole (Carp et al. 2004) thus lowering the photocatalytic activity.

4.5.2 Comparison of photocatalytic activity in terms of degradation of RB-220 under UV and solar light irradiation

The photocatalytic efficacy of $Ag@TiO_2$ in terms of degradation of RB-220 dye with initial concentration of 50 mg/L, and at initial pH of 3 was compared with commercially available Degussa P-25 catalyst, $SGTiO_2$, $CSTiO_2$, Ag doped-$SGTiO_2$, Ag doped(LI)-$CSTiO_2$, and Ag doped (PD)-$CSTiO_2$. In all the experiments, catalyst loading of 1 g/L for UV photocatalysis and 500 mg/L for solar photocatalysis were used. The photocatalytic degradation of RB-220 using different catalysts at various irradiation times are shown in Figure 4.23a and 4.23b for UV and solar light irradiations respectively. These Figures clearly show that $Ag@TiO_2$ nanoparticles are more efficient photocatalysts in the degradation of RB-220 dye as compared to other catalysts and photocatalytic activity is rated in the order of $Ag@TiO_2$> Degussa P25> Ag doped-$SGTiO_2$> $SGTiO_2$> $CSTiO_2$> Ag doped (PD)-$CSTiO_2$> Ag doped (LI)-$CSTiO_2$ under UV light and the activity under solar irradiation is rated as $Ag@TiO_2$> Ag doped-$SGTiO_2$> Degussa P25 > $SGTiO_2$> $CSTiO_2$>Ag doped (PD)-$CSTiO_2$>Ag doped (LI)-$CSTiO_2$. High photocatalytic efficacy is exhibited by $Ag@TiO_2$ under UV and solar light irradiations. The reason for higher activity of $Ag@TiO_2$ in terms degradation of RB-220 dye are similar to those discussed in Section 4.5.1 for photocatalysis of AY-17 dye. In case of solar photocatalysis with $Ag@TiO_2$ catalyst, almost 100 % degradation of RB-220 occurred within 60 min, whereas with UV photocatalysis, it took around 240 min. It can also be noted that, the catalyst loading and irradiation time required for solar photocatalysis is much lesser than that used in UV photocatalysis. Rate of photocatalysis under solar light is much higher than that under UV photocatalysis, due to the potential of $Ag@TiO_2$ to absorb both UV and visible light portions of solar radiation, low band gap energy and due to direct band gap transition, as already discussed in Section 4.5.1. The   reasons   for   lower photocatalytic efficacy of Degussa P25, $SGTiO_2$, $CSTiO_2$, Ag doped-$SGTiO_2$ and Ag

doped (LI)-CSTiO$_2$ are already explained in Section 4.5.1 for photocatalytic degradation of AY-17 dye and are as well valid for the degradation of RB-220 dye.

Ag@TiO$_2$ catalyst showed appreciably better UV photocatalytic activity and it excels in terms of its solar photocatalytic activity for the degradation of both AY-17 and RB-220 dyes, in comparison to other commercial and synthesized catalysts. So Ag@TiO$_2$ can be effectively used as a photocatalyst for the degradation of dyes by both UV and solar photocatalytic process for the treatment of dye contaminated wastewaters. Further optimization of process conditions is necessary for exploitation of the process into industrial scale operations.
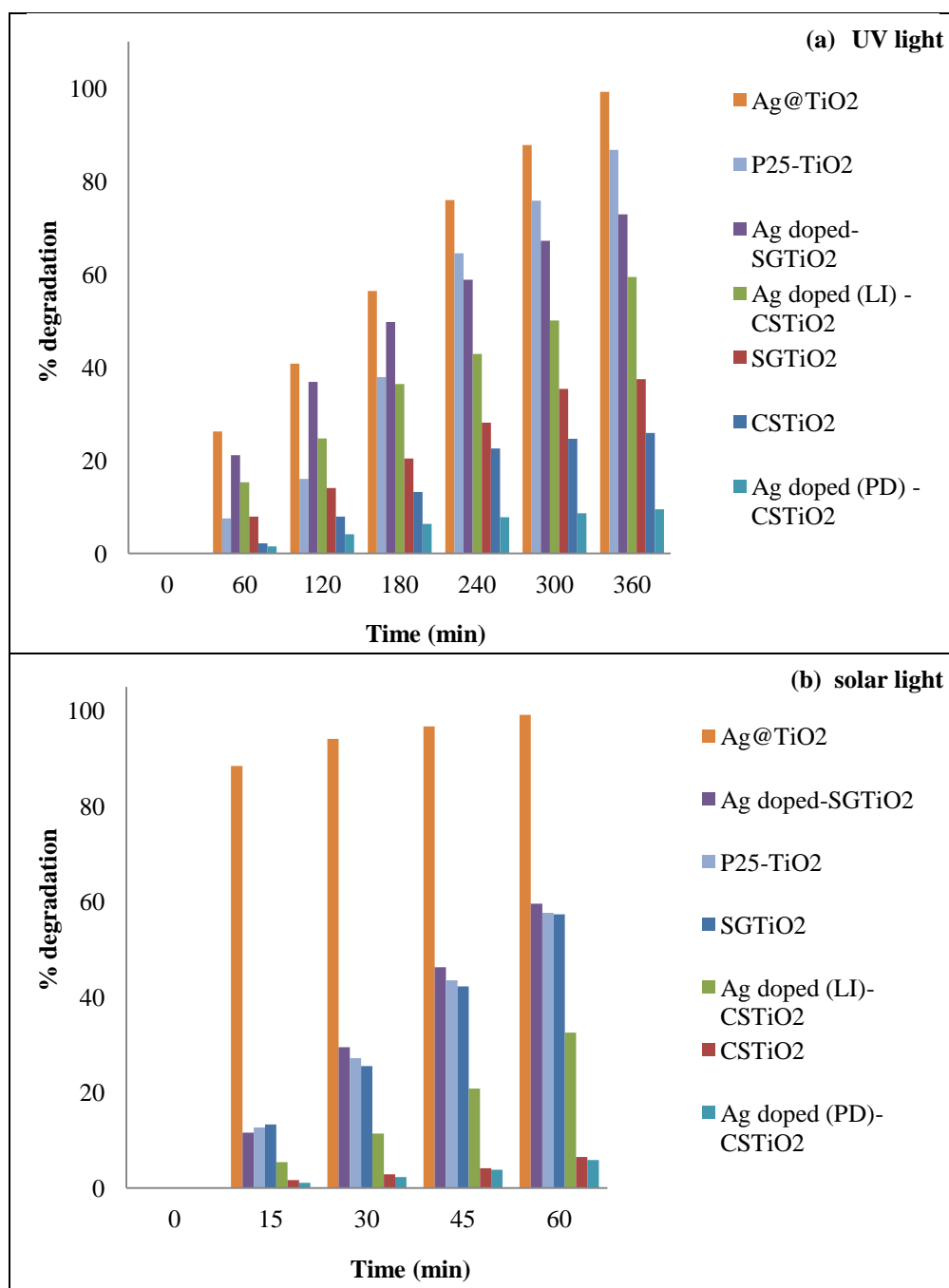
Figure 4.22 Comparison of photocatalytic activity of different photocatalysts in terms of degradation of AY-17 dye under a) UV light; b) solar light: average UV and visible light intensity of solar light= 3.57 mW/cm^2 and 1208×100 lux respectively from 11 a.m. to 12 p.m. Conditions: initial pH=3; catalyst loading = 100 mg/L; C_0 =10 mg/L.
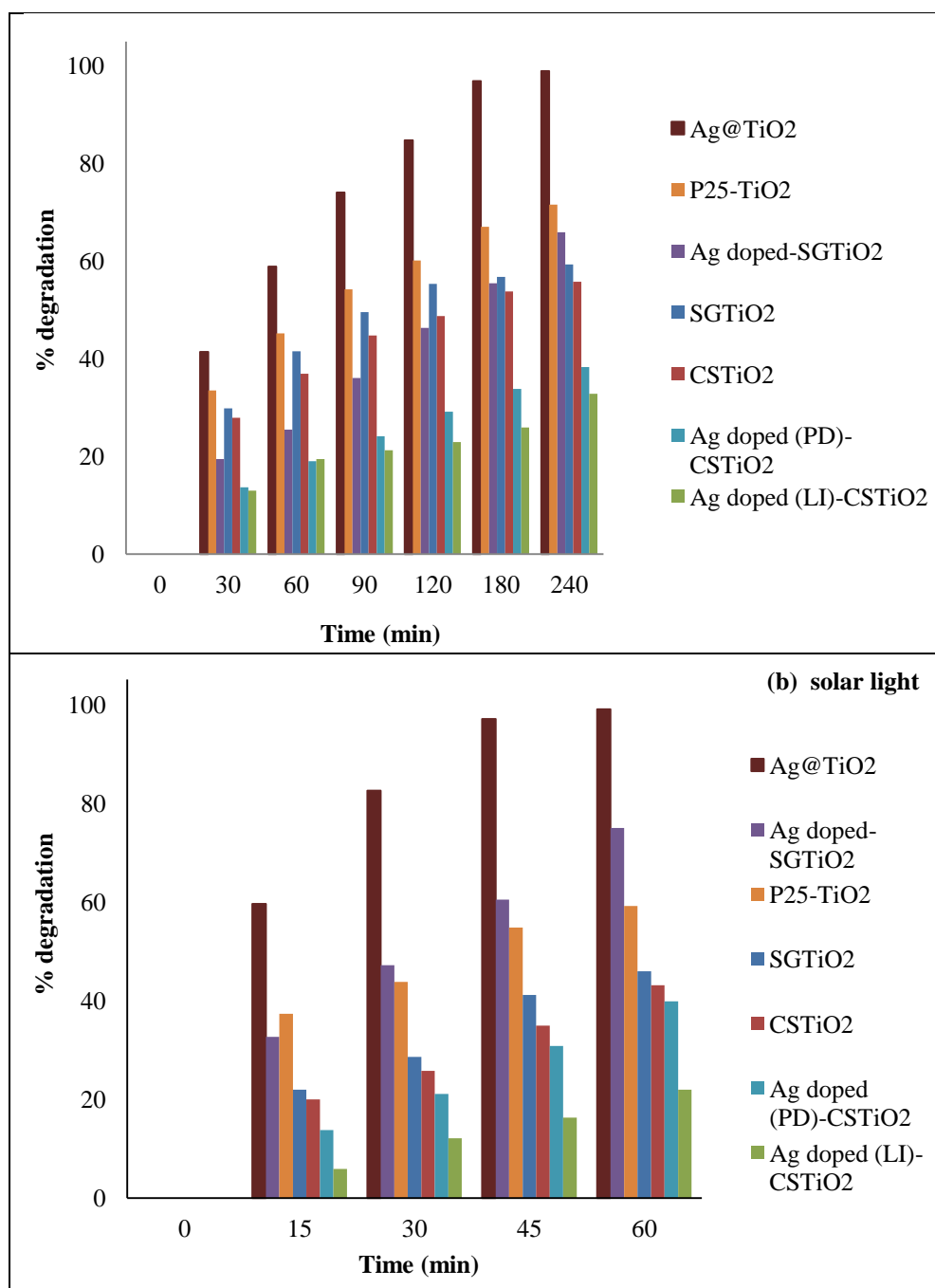
Figure 4.23 Comparison of photocatalytic activity of different photocatalysts in terms of degradation of RB-220 dye under a) UV light: catalyst loading = 1 g/L; b) solar light: catalyst loading = 500 mg/L; average UV and visible light intensity of solar light= 3.62 mW/cm^2 and 1120×100 lux respectively from 11 a.m. to 12 p.m. Conditions: initial pH=3; C_0=50 mg/L.

4.6. Effect of operational factors on the UV and solar photocatalysis of AY-17 and RB-220 dyes

In the earlier Sections it is reported that Ag@TiO$_2$ catalyst is very effective for UV and solar photocatalysis of azo dyes such as AY-17 and RB-220. If the photocatalysis process is to be exploited in industrial scale operations for the treatment of dye contaminated wastewaters, there is a necessity to look for different ways by which rate of photocatalysis may be improved. If the rate needs to be enhanced, then it is very important to determine the various operational factors that influence the rate of photocatalysis and then to optimize the process. From extensive review of literature reported in Section 2.6, it was noted that factors such as pH, catalyst loading, initial dye concentration and oxidants influence the rate of photocatalysis and hence the effect of these factors were studied and the results are discussed in the present section.

4.6.1 Effect of pH on the photocatalytic degradation of AY-17 and RB-220 under UV and solar light irradiation

The pH of wastewater contaminated with dyes varies largely according to the type of dyes present in it. The pH of the solution dominantly affects the photocatalytic degradation process because change in pH affects the surface charge property of TiO$_2$, charge of dye molecule, adsorption of dye on to TiO$_2$ surface and hydroxyl radical concentration. So, it is necessary to study the effect of pH on photocatalytic degradation of AY-17 and RB-220 under UV and solar light irradiation. To study the effect of pH, batch photocatalysis experiments were conducted in a stirred reactor under UV and solar light irradiation with AY-17 and RB-220 dyes. In case of UV photocatalysis experiments, air at a flow rate of 2 LPM was supplied continuously and it acted as an oxidant. But for solar photocatalysis no additional air was supplied and the dissolved oxygen in the reaction mixture itself acted as an oxidant.

4.6.1.1 Effect of pH on the photocatalytic degradation of AY-17 under UV and solar light irradiation

To study the effect of pH, photocatalytic degradation experiments with AY-17 at concentration of 10 mg/L in aqueous solution were performed under UV and solar light irradiation, by varying the initial pH from 2 to 9. The catalyst loading of 100 mg/L was used in all the experiments under UV and solar light irradiation. Time course variations of AY-17 dye concentrations obtained with different initial pH conditions are shown in Table 4.13-4.14 respectively for UV and solar photocatalysis. In order to confirm the effect of initial pH, control experiments at different initial pH were also done under a light source (UV or solar) and in the absence of catalyst. No significant degradation of dye occurred in the absence of catalyst with different initial pH and AY-17 solution was found to be stable on irradiation with UV and solar light irradiation.

Figure 4.24a presents the effect of pH on time course variation of percentage degradation of AY-17 dye under UV light irradiation. Figure 4.25a shows that, as the pH of AY-17 dye solution increases from 1 to 3, the degradation in 360 min of irradiation time increases from 41.63 to 99.2 %, but further increase in pH to 4 and higher, decreases the degradation, which reached to only around 0.23 % (at 360 min) at a pH of 9. Therefore, the highest degradation of AY-17 was observed at pH 3. Similar observations have been reported by other researchers in their studies on UV photocatalysis with TiO_2 as a photocatalyst, during the degradation of AY-17 (Liu et al. 2006) with maximum degradation at pH of 3 and in the degradation of Acid Orange 7 (Tanaka et al. 2000) with maximum degradation at pH of 2.

Figure 4.24b presents the effect of pH on time course variation of percentage degradation of AY-17 dye under solar light irradiation. Figure 4.25b shows that, as pH of the dye solution increases from 1 to 3, the degradation increases from 71 % to almost 100 %. But further increase in pH to 4 and higher results in decreased degradation. Negligible reduction was observed at pH above 6. The highest degradation was observed at pH 3. Sakthivel et al. (2003a) also reported similar trends in their studies on effect of pH on photocatalytic degradation of Acid brown 14 using TiO_2 under solar light irradiation. They found that pH of 3 yields maximum

percentage degradation and at lower pH values, positively charged TiO_2 surface adsorbed more dye and hence more degradation was achieved.

pH plays multiple roles on the photocatalytic process by affecting the sorption–desorption processes on the surface of the catalyst particles, electrostatic interactions between the catalyst surface, dye molecules, and charged radicals formed during the reaction process. In acidic suspensions, the adsorption of dye on the TiO_2 surfaces is significantly higher than the extent of adsorption in neutral or alkaline suspensions. This is attributed to the fact that TiO_2 shows an amphoteric character so that either a positive or a negative charge can be developed on its surface (Sohrabi and Ghavami 2010). Therefore, below the point of zero charge (pzc) of TiO_2 which is 6.8 (pH_{pzc}), the surface of the particles is positively charged (pH $<pH_{pzc}$), above this value it is negatively charged (pH $>pH_{pzc}$) whereas it is neutral when pH $= pH_{pzc}$ (Chiou et al. 2008). Since, AY-17 is an anionic dye with a good solubility; the sodium ion is easily dissociated in water and leaves the dye molecule with negative charges (Liu et al. 2006). Due to the charge difference between negatively charged dye molecules and positively charged TiO_2 shell on the catalyst, coupling between dye and catalyst molecules increases at lower pH, which in turn increases the electrostatic interactions between the photocatalyst surface and dye anions which lead to adsorption. Density of hydroxyl radicals increases at lower pH values; hence catalyst easily gets adsorbed and facilitates the reaction to proceed at lower pH value (Sohrabi and Ghavami 2010). In contrast, under alkaline and neutral conditions, little adsorption occurs on the surface of catalyst due to columbic repulsion between the negatively charged catalyst and dye molecule which decreases the generation of hydroxyl radicals and hence decrease the photocatalytic degradation (Chiou et al. 2008). Therefore pH of 3 is considered as the optimum for the photocatalytic degradation of AY-17 under UV and solar light irradiation using Ag@TiO_2 nanoparticles as catalyst.

4.6.1.2 Effect of pH on the photocatalytic degradation of RB-220 dye under UV and solar light irradiation

To study the effect of pH on degradation of RB-220 dye, photocatalytic degradation experiments were performed under UV and solar light irradiation with RB-220 at concentration of 50 mg/L in aqueous solution by varying the initial pH. Experiments were performed under UV light with different initial pH ranging from 2 to 7 and under solar light, pH ranging from 2 to 9. The catalyst loading of 1 g/L for UV photocatalysis and 500 mg/L for solar photocatalysis was used. Time course variations of RB-220 dye concentrations obtained with different initial pH conditions are shown in Table 4.15-4.16 respectively for UV and solar photocatalysis. In order to confirm the effect of initial pH, control experiments at different initial pH were also conducted under a light source (UV and solar) and in the absence of catalyst. No significant degradation of RB-220 dye occurred in the absence of catalyst at different initial pH and RB-220 solution was found to be stable on irradiation with UV and solar light irradiation.

Figure 4.26a presents the time course variation of effect of pH on percentage degradation of RB-220 dye under UV light irradiation, which shows a maximum rate of degradation at pH of 3. Figure 4.27a shows that, as pH of the dye solution increases from 2 to 3 the degradation in 240 min of irradiation time increases from 23.09 % to 98.92 %, but further increase in pH to 4 and higher decreases the degradation, which reaches to only around 2.53 % (at 240 min) at pH of 7. The highest degradation was observed at a pH of 3. Soustas et al. (2009) in their studies on photocatalytic degradation of reactive azo dyes using TiO_2 under UV light irradiation have also observed that higher degradation are achieved at low and acidic pH values, and maximum degradation occurs at pH of 3.

Similarly Figure 4.26b and Figure 4.27b present the effect of pH on time course variation of percentage degradation of RB-220 dye and on percentage degradation at 180min irradiation time respectively, under solar light irradiation. It is observed from Figure 4.27b, the highest rate of degradation and percentage degradation (after 120 min irradiation time) occurs at a pH of 3. Maximum percentage degradation which occurred by solar photocatalysis at initial pH of 3 was 99.44 %.

Effect of pH on photocatalysis of RB-220 dye can be explained on similar grounds as it is explained for the degradation of AY-17 dye in Section 4.6.1.1. pH of 3 is the optimum for the photocatalytic degradation of RB-220 under UV and solar light irradiation using Ag@TiO$_2$ nanoparticles as catalyst, as is the case with AY-17dye.

Table 4.13 Time course variation of concentration of AY-17 obtained with different initial pH conditions during UV photocatalysis. Conditions: Ag@TiO$_2$ loading= 100 mg/L; C$_0$= 10 mg/L.

Time (min)	C$_{AY-17}$ (mg/L) with different initial pH						
	pH=1	pH=2	pH=3	pH=4	pH=5	pH=7	pH=9
0	10	10	10	10	10	10	10
60	6.07	6.21	7.38	9.54	9.60	9.95	9.98
120	5.84	4.07	5.92	8.37	8.97	9.95	9.98
180	5.84	3.14	4.36	7.68	8.54	9.95	9.98
240	5.84	2.21	2.41	7.33	7.62	9.65	9.98
300	5.84	1.84	1.52	6.49	7.13	9.44	9.98
360	5.84	1.71	0.08	5.55	6.66	9.10	9.98

Table 4.14 Time course variation of concentration of AY-17 obtained with different initial pH conditions during solar photocatalysis. Conditions: Ag@TiO$_2$ loading= 100 mg/L; C$_0$= 10 mg/L.

Time (min)	C$_{AY-17}$ (mg/L) with different initial pH						
	pH=1	pH=2	pH=3	pH=4	pH=5	pH=7	pH=9
0	10	10	10	10	10	10	10
60	2.90	0.78	0.08	6.89	9.58	9.88	9.91
120	0.74	0.21	0.05	5.48	9.18	9.59	9.75
180	0.27	0.14	0.05	3.89	8.57	9.04	9.27
240	0.14	0.07	0.05	2.93	7.73	8.97	8.93
300	0.14	0.07	0.05	2.39	7.26	8.64	8.58
360	0.14	0.07	0.05	1.68	7.05	8.36	8.44

Table 4.15 Time course variation of concentration of RB-220 obtained with different initial pH conditions during UV photocatalysis. Conditions: Ag@TiO$_2$ loading= 1 g/L; C$_0$= 50 mg/L.

Time (min)	C$_{RB-220}$ (mg/L) with different initial pH				
	pH=2	pH=3	pH=4	pH=5	pH=7
0	50	50	50	50	50
30	42.96	29.30	48.10	49.15	49.65
60	41.06	20.56	44.44	48.38	49.65
90	40	12.96	40.07	48.17	48.94
120	38.94	7.61	35.35	47.89	48.73
180	38.66	1.55	29.65	47.68	48.73
240	38.45	0.54	22.75	47.54	48.73

Table 4.16 Time course variation of concentration of RB-220 obtained with different initial pH conditions during solar photocatalysis. Conditions: Ag@TiO$_2$ loading= 500 mg/L; C$_0$= 50 mg/L.

Time (min)	C$_{RB-220}$ (mg/L) with different initial pH					
	pH=2	pH=3	pH=4	pH=5	pH=7	pH=9
0	50	50	50	50	50	50
15	40	20.21	29.01	33.73	43.52	46.62
30	32.61	8.73	24.51	30.70	41.13	45.85
45	25.63	1.48	17.96	27.11	40.63	45.00
60	20.77	0.49	13.94	23.52	40	43.80
90	15.99	0.35	8.66	20.21	39.01	42.89
120	12.25	0.28	6.41	17.11	38.45	42.39
150	8.38	0.28	5.28	15.35	37.89	42.11
180	5.77	0.14	3.94	12.39	37.61	41.83
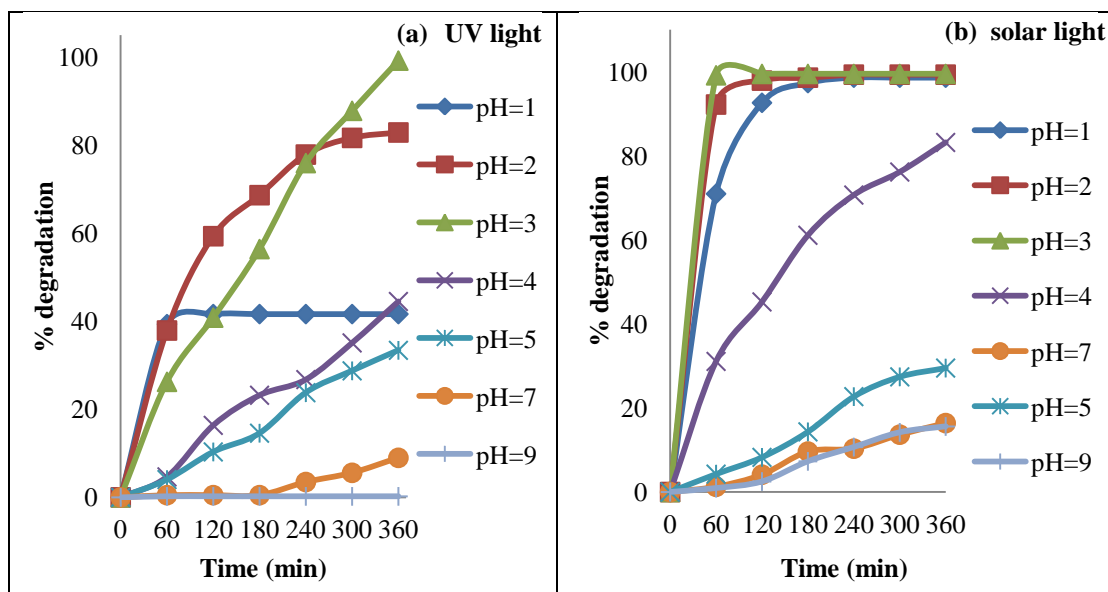
Figure 4.24 Effect of initial solution pH on time course variation of photocatalytic degradation of AY-17 dye under a) UV light; b) solar light: average UV and visible light intensity of solar light= 3.52 mW/cm^2 and 1189×100 lux respectively from 10 a.m. to 4 p.m. Conditions: Ag@TiO$_2$ loading= 100 mg/L; C$_0$= 10 mg/L.
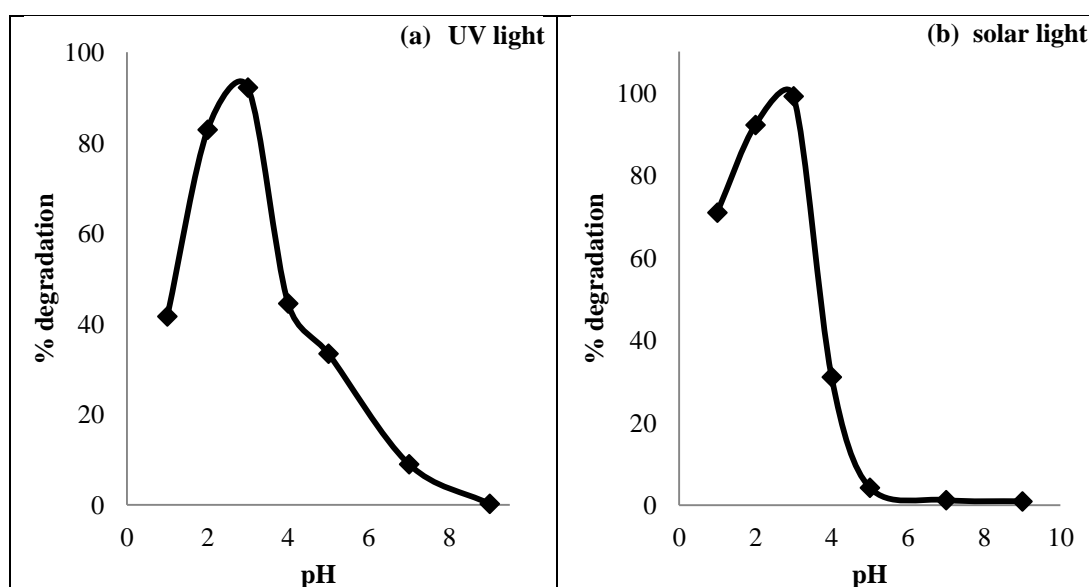
Figure 4.25 Effect of initial solution pH on percentage degradation of AY-17 dye under a) UV light: Irradiation time =360 min; b) solar light: Irradiation time =60 min. Conditions: Ag@TiO$_2$ loading= 100 mg/L; C$_0$=10 mg/L.
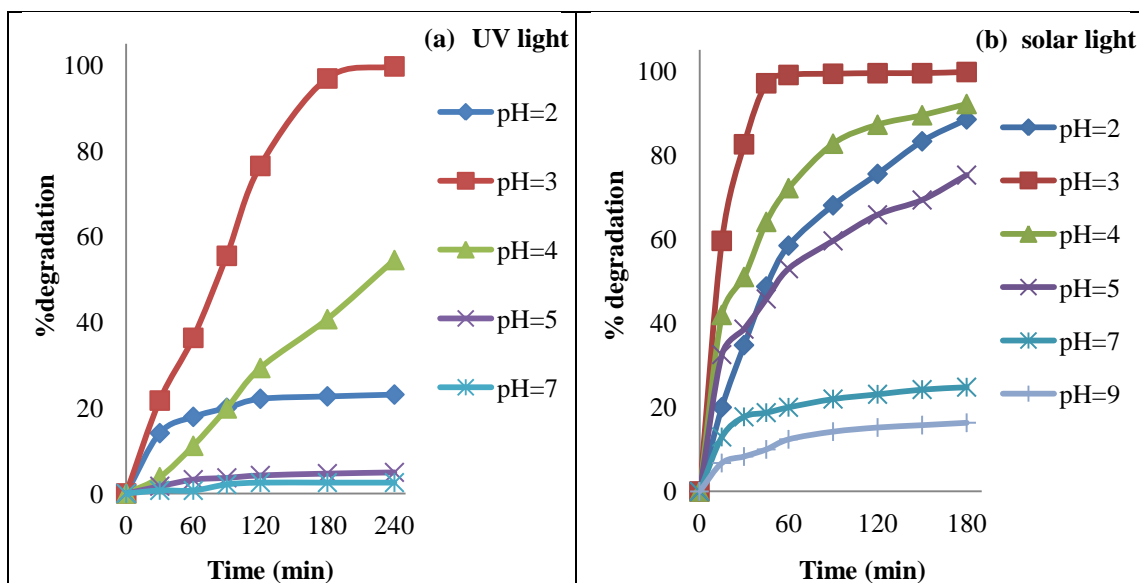
Figure 4.26 Effect of initial solution pH on time course variation of photocatalytic degradation of RB-220 dye under a) UV light: Ag@TiO$_2$ loading= 1 g/L; b) solar light: Ag@TiO$_2$ loading= 500 mg/L; average UV and visible light intensity of solar light= 3.55 mW/cm^2 and 1202×100 lux respectively from 11 a.m. to 2 p.m. Condition: C$_0$= 50 mg/L.
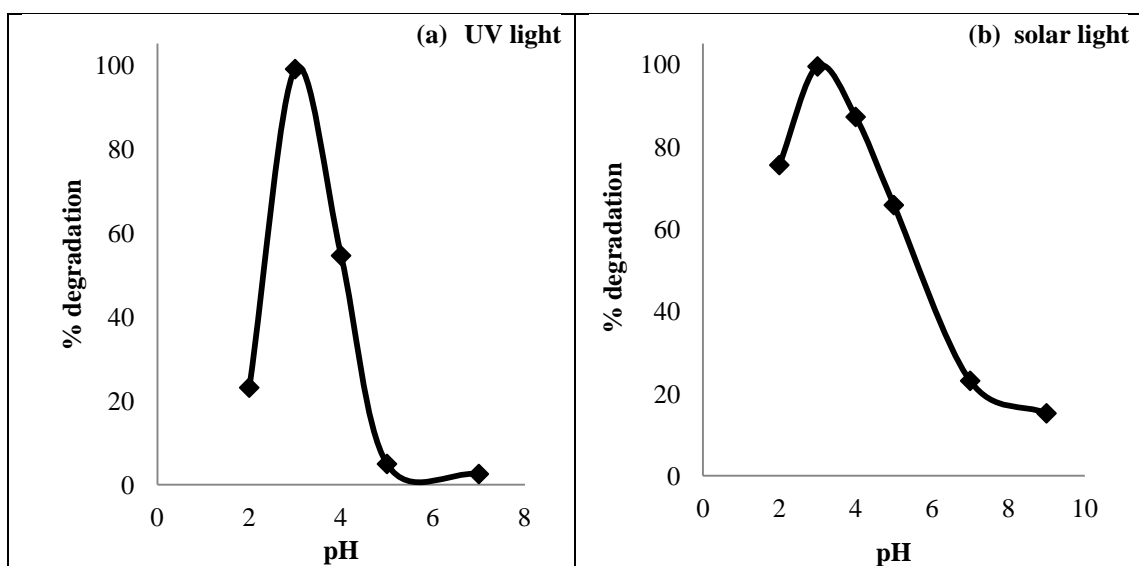
Figure 4.27 Effect of initial solution pH on percentage degradation of RB-220 dye under a) UV light: Irradiation time =240 min; Ag@TiO$_2$ loading= 1 g/L; b) solar light: Irradiation time =120 min; Ag@TiO$_2$ loading= 500 mg/L. Conditions: C$_0$=50 mg/L.

4.6.2 Effect of catalyst loading on photocatalytic degradation of AY-17 and RB-220 dyes under UV and solar light irradiation

The efficiency of photocatalytic degradation depends on the type and concentration of photocatalyst and the pollutant concentration (Habibi et al. 2005), therefore it is necessary to find the optimum catalyst loading for the photocatalytic process since in photocatalysis rate of reaction is a function of catalyst loading (San et al. 2002; Saquib and Munner 2002). Optimum catalyst loading will not only enhance the degradation efficiency, but also limit the excess usage of the catalyst and hence making the process economically friendlier. As a first step to determine the optimum catalyst loading, the effect of catalyst loading on photocatalytic degradation of AY-17 and RB-220 under UV and solar light irradiation were studied. For UV photocatalysis; air was continuously supplied at a flow rate of 2 LPM. For solar photocatalysis atmospheric air served as a source for oxidant as explained in Section 4.6.1.

4.6.2.1 Effect of catalyst loading on photocatalytic degradation of AY-17

To study the effect of catalyst loading, batch experiments on photocatalytic degradation of AY-17 with initial concentration of 10 mg/L in aqueous solution were performed in   a stirred reactor at optimum pH obtained from earlier Sections (pH=3), under UV and solar light irradiation, by varying the catalyst loading. Experiments were performed under UV light by varying the amount of catalyst from 50 mg/L to 1 g/L and under solar light by varying the amount of catalyst from 50 to 500 mg/L. Time course variations of AY-17 dye concentrations obtained with different catalyst loadings are shown in Table 4.17-4.18 respectively for UV and solar photocatalysis.

Figure 4.28a presents the effect of catalyst loading on time course variation of percentage degradation of AY-17 dye under UV light irradiation and maximum rate of degradation is observed at catalyst loading of 300 mg/L. It can be seen from Figure 4.29a, as the loading of the catalyst increases from 50 to 300 mg/L the percentage degradation (after 300 min irradiation time), increases from 10 to 99.94 %. The increase in the degradation may be attributed to the fact that, as the loading of

Ag@TiO$_2$ increases, the active sites for the adsorption of dye molecules also increase, which in turn increases the formation of electron and hole pairs; thus increasing the formation of hydroxyl radicals and hence an enhancement in the photocatalytic reaction rate occurs. On the other hand, with further increase in catalyst loading from 300 to 1000 mg/L, the percentage degradation has decreased to as low as around 49.18 % (after 300 min irradiation). This may be due to agglomeration (particle–particle interaction) of particles at a higher loading, resulting in the decrease in surface area available for light absorption and hence, a decrease in photocatalytic degradation rate. Although with increase in catalyst loading the number of active sites in solution increases, a saturation point occurs; beyond which light penetration is hindered as a result of shielding effect of suspended catalyst particles. The relation between these two opposite phenomena results in an optimum catalyst loading for the photocatalytic degradation (Adesina 2004; Ahmed et al. 2011). The optimum amount of catalyst loading was found to be 300 mg/L for the degradation of AY-17 with initial dye concentration of 10 mg/L. Optimum catalyst loading is a function of initial dye concentration. Hence dye to catalyst ratio is the more appropriate parameter in photocatalytic degradation applications. The optimum catalyst loading of 300 mg/L for 10 mg/L of dye concentration corresponds to dye to catalyst ratio of 1:30 (g/g). Hence the optimum dye to catalyst ratio for UV photocatalytic degradation of AY-17 using Ag@TiO$_2$ core-shell structured nanoparticles is 1:30 on weight basis.

Figure 4.28b presents the effect of catalyst loading on the time course variation of percentage degradation of AY-17 dye and Figure 4.29b presents the effect on percentage degradation after 60 min irradiation time, under solar light irradiation. It can be seen from Figure 4.28a and Figure 4.29b that, the rate of degradation and hence the percentage degradation (after 60 min irradiation time) is the maximum at the catalyst loading of 100 mg/L. As the catalyst loading was increased from 50 to 100 mg/L the percentage degradation (after 60 min irradiation), increased from around 76 to 100 %. On the other hand, with further increase in catalyst loading from 100 to 500 mg/L, the percentage degradation has decreased to around 91 % (after 60 min). The observed effect of catalyst loading on the dye degradation by solar photocatalysis is similar to that for UV photocatalysis and the reason for the trend is as explained for UV photocatalysis of the dye. The optimum amount of catalyst

loading for solar photocatalysis is found to be 100 mg/L for the degradation of AY-17 with initial dye concentration of 10 mg/L. The optimum catalyst loading of 100 mg/L for 10 mg/L initial dye concentration corresponds to dye to catalyst ratio of 1:10 (g/g). Hence the optimum dye to catalyst ratio for solar photocatalytic degradation of AY-17 using Ag@TiO$_2$ core-shell structured nanoparticles is 1:10 (g/g).

4.6.2.2 Effect of catalyst loading on photocatalytic degradation of RB-220

To study the effect of catalyst loading on photocatalytic degradation of RB-220, experiments were performed with initial concentration of 50 mg/L in aqueous solution at optimum pH as obtained in Section 4.6.1 (pH=3), under UV and solar light irradiation, by varying the catalyst loading. Experiments were performed in a batch stirred reactor under UV light by varying the amount of catalyst from 500 mg/L to 2 g/L and under solar light, amount of catalyst ranging from 250 mg/L to 2 g/L. Time course variations of RB-220 dye concentrations obtained with different catalyst loadings are shown in Table 4.19-4.20 respectively for UV and solar photocatalysis. Figure 4.30a presents the effect of catalyst loading on time course variation of percentage degradation of RB-220 dye under UV light irradiation. It can be seen from Figure 4.31a that, as the concentration of catalyst increases from 500 mg/L to 1 g/L the degradation after 240 min of UV irradiation, increases from 38.17 to 98.92 %. On the other hand, with further increase in catalyst loading from 1 g/L to 2 g/L, the percentage degradation has decreased to as low as 45.91 % (after 240 min). The optimum amount of catalyst loading is found to be 1 g/L for the UV photocatalytic degradation of RB-220 with initial dye concentration of 50 mg/L. 1 g/L optimum catalyst loading for 50 mg/L dye concentration correspond to dye to catalyst ratio of 1:20 (g/g). Hence the optimum dye to catalyst ratio for UV photocatalytic degradation of RB-220 using Ag@TiO$_2$ core-shell structured nanoparticles is 1:20.

Figure 4.30b presents the effect of catalyst loading on time course variation of percentage degradation of the RB-220 dye under solar light. As the concentration of the catalyst was increased from 250 to 500 mg/L the degradation (after 120 min irradiation)   increased from 88.02 % to 99.44 % (Figure 4.31b). On the other hand, with further increase in catalyst loading from 500 mg/L to 2 g/L, the percentage

degradation (after 120 min irradiation) decreased to around 91.97 %. So the optimum amount of catalyst loading for solar photocatalysis is 500 mg/L for the degradation of RB-220 with initial dye concentration of 50 mg/L. Optimum catalyst loading of 500 mg/L for 50 mg/L dye concentration corresponds to dye to catalyst ratio of 1:10 (g/g). Hence the optimum dye to catalyst ratio for solar photocatalytic degradation of RB-220 using $Ag@TiO_2$ core-shell structured nanoparticles is 1:10 (g/g).

The trend showing the effect of catalyst loading on UV and solar photocatalysis of RB-220 dye is similar to that for AY-17 dye and the reason for this trend is already explained in Section 4.6.2.1.

Table 4.17 Time course variation of concentration of AY-17 obtained with different catalyst loading (mg/L) during UV photocatalysis. Conditions: pH=3; C_0= 10 mg/L.

Time (min)	C_{AY-17} (mg/L) with different catalyst loading						
	Catalyst loading (mg/L)						
	50	100	200	300	400	500	1000
0	10	10	10	10	10	10	10
60	9.84	7.38	7.20	6.78	6.47	6.12	9.34
120	9.64	5.92	5.40	4.27	1.88	2.99	8.25
180	9.42	4.36	3.76	2.04	0.77	1.56	7.59
240	9.28	2.41	1.56	0.83	0.77	1.28	6.33
300	9.00	1.52	0.65	0.01	0.51	1.05	5.08
360	8.72	0.08	0.05	0.002	0.44	0.88	3.70

Table 4.18 Time course variation of concentration of AY-17 obtained with different catalyst loading (mg/L) during solar photocatalysis. Conditions: pH=3; C_0= 10 mg/L.

Time (min)	C_{AY-17} (mg/L) with different catalyst loading					
	Catalyst loading (mg/L)					
	50	100	200	300	400	500
0	10	10	10	10	10	10
15	5.52	1.16	0.93	0.81	0.74	0.94
30	4.35	0.59	0.61	0.77	0.74	0.94
45	2.86	0.33	0.53	0.54	0.74	0.94
60	2.43	0.08	0.47	0.54	0.74	0.94
75	2.21	0.05	0.47	0.54	0.74	0.94
90	2.02	0.05	0.41	0.54	0.74	0.94
105	1.78	0.05	0.41	0.54	0.74	0.94
120	1.41	0.05	0.41	0.54	0.74	0.94
180	0.87	0.05	0.41	0.54	0.74	0.94
240	0.68	0.05	0.41	0.54	0.74	0.94
300	0.47	0.05	0.41	0.54	0.74	0.94
360	0.36	0.05	0.41	0.54	0.74	0.94

Table 4.19 Time course variation of concentration of RB-220 obtained with different catalyst loading (mg/L) during UV photocatalysis. Conditions: pH=3; C_0= 50 mg/L.

Time (min)	C_{RB-220} (mg/L) with different catalyst loading				
	Catalyst loading (mg/L)				
	500 mg/L	750 mg/L	1000 mg/L	1500 mg/L	2000 mg/L
0	50	50	50	50	50
30	43.80	40.21	29.30	42.54	45.00
60	41.06	33.94	20.56	36.69	40.42
90	37.89	27.75	12.96	31.41	37.89
120	35.21	20.99	7.61	26.90	34.15
180	31.76	10.70	1.55	19.23	31.06
240	30.92	5.99	0.54	15.49	27.04

Table 4.20 Time course variation of concentration of RB-220 obtained with different catalyst loading (mg/L) during solar photocatalysis. Conditions: pH=3; C_0= 50 mg/L.

Time (min)	C_{RB-220} (mg/L) with different catalyst loading				
	Catalyst loading (mg/L)				
	250 mg/L	500 mg/L	750 mg/L	1000 mg/L	2000 mg/L
0	50	50	50	50	50
15	39.72	20.21	19.79	19.58	10.70
30	33.45	8.73	7.75	6.48	4.01
45	26.90	1.48	3.24	3.66	4.01
60	19.15	0.49	2.75	3.17	4.01
90	11.41	0.35	2.11	2.54	4.01
120	5.99	0.28	1.83	2.54	4.01
150	4.79	0.28	1.34	2.11	4.01
180	3.73	0.14	1.34	2.11	4.01
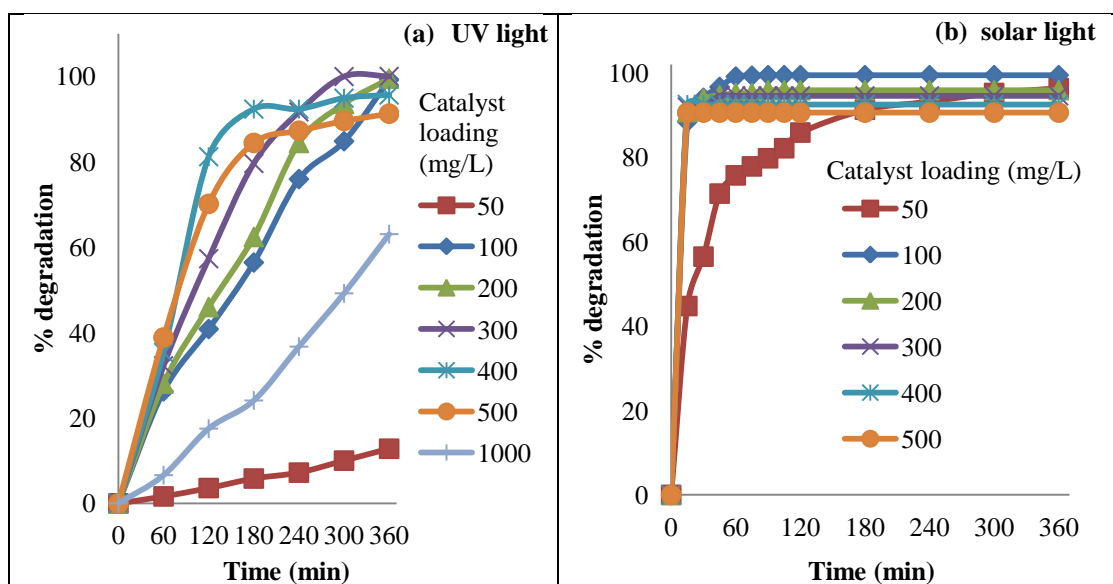
Figure 4.28 Effect of catalyst loading on time course variation of photocatalytic degradation of AY-17 dye under a) UV light; b) solar light: average UV and visible light intensity of solar light= 3.57 mW/cm^2 and 1204×100 lux respectively from 10 a.m. to 4 p.m. Conditions: pH=3; C_0= 10 mg/L.
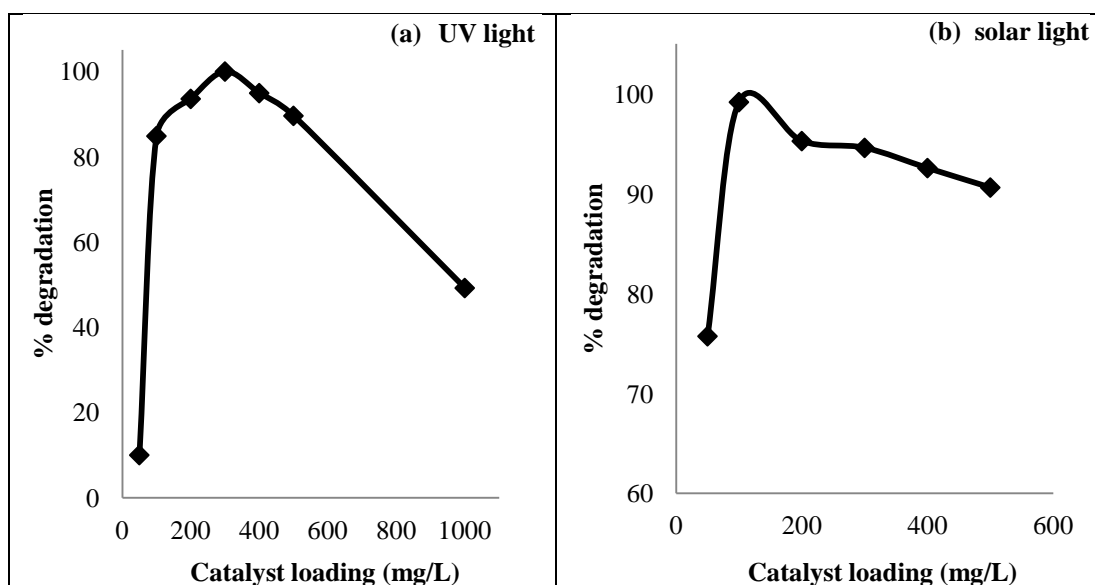
Figure 4.29 Effect of catalyst loading on percentage degradation of AY-17 dye under a) UV light: Irradiation time =300 min b) solar light: Irradiation time =60 min. Conditions: pH=3; C_0= 10 mg/L.
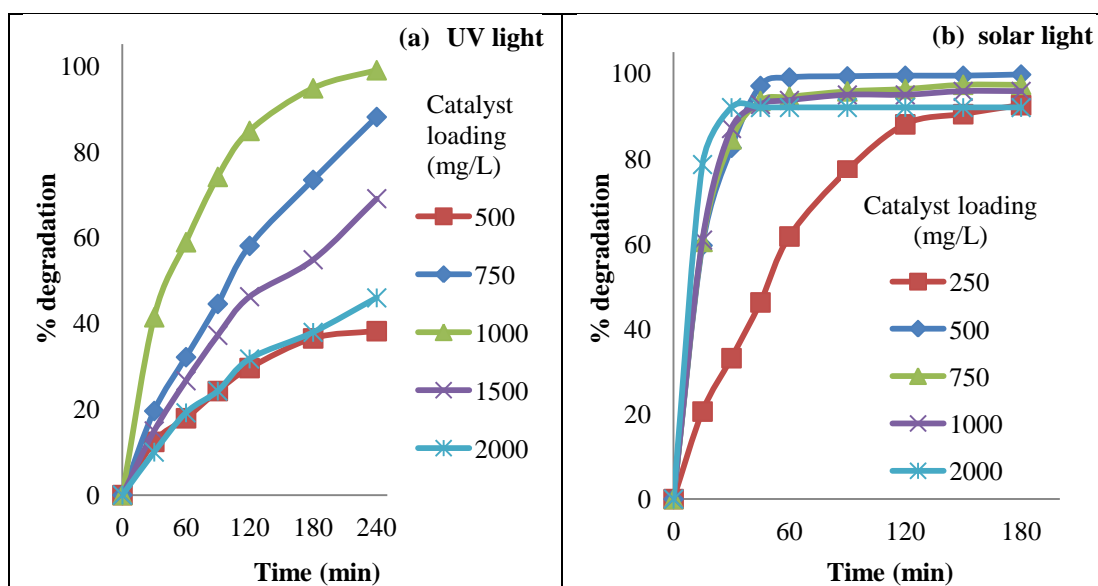
Figure 4.30 Effect of catalyst loading on time course variation of photocatalytic degradation of RB-220 dye under a) UV light; b) solar light: average UV and visible light intensity of solar light= 3.61 mW/cm^2 and 1209×100 lux respectively from 11 a.m. to 2 p.m. Conditions: pH=3; C_0= 50 mg/L.
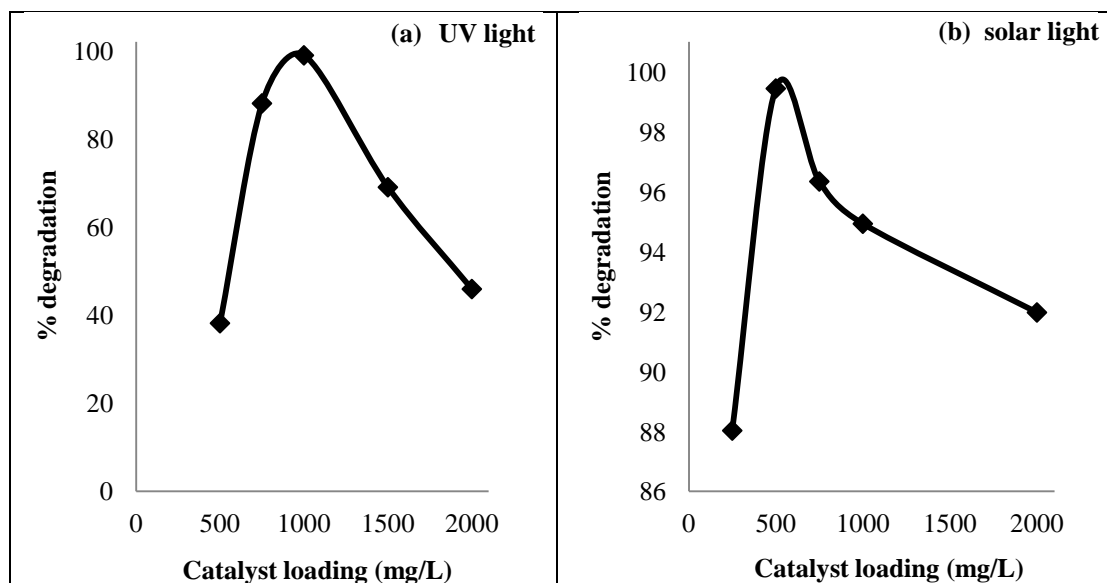
Figure 4.31 Effect of catalyst loading on percentage degradation of RB-220 dye under a) UV light: Irradiation time =240 min b) solar light: Irradiation time =120 min. Conditions: pH=3; C_0= 50 mg/L.

4.6.3 Effect of initial dye concentration on photocatalytic degradation of AY-17 and RB-220 under UV and solar light irradiation

Though dye to catalyst ratio is an important parameter governing the photocatalytic degradation of dyes, the initial dye concentration may act as an independent factor governing the rate of photocatalytic degradation of dyes. So in order to study the influence of initial dye concentration as an independent factor, photocatalytic degradation experiments of AY-17 and RB-220 were performed under UV and solar light irradiation, by varying the initial dye concentrations and keeping the ratio of dye to catalyst loading constant at optimum values obtained from Section 4.6.2.

4.6.3.1 Effect of initial dye concentration on photocatalytic degradation of AY-17 under UV and solar light irradiations

Experiments were performed under UV light with different initial dye concentrations ranging from 10 to 200 mg/L and under solar light with dye

concentrations ranging from 10 to 500 mg/L. In case of experiments under UV irradiation, dye to catalyst loading ratio was kept constant at 1:30 (g/g) whereas in solar photocatalysis it was kept constant at 1:10 (g/g). For example, when the initial concentration was 200 mg/L, the catalyst loading was 6 g/L (0.6 g/100 mL). The dye to catalyst loading chosen in these experiments were the optimum values as obtained by crude optimization method based on "one factor at a time" experiments presented in Section 4.6.2. The time course variations of AY-17 dye concentrations obtained with different initial concentrations of the dye are presented in Table 4.21-4.22 respectively for UV and solar photocatalysis.

Figure 4.32 presents the effect of initial dye concentration on time course variation of photocatalytic degradation of the dye, under constant dye to catalyst ratio of 1:30. It is observed, as the concentration increases from 10 mg/L to 200 mg/L, the percentage degradation (after 360 min irradiation time) decreases drastically from 99.98 to 18.6 %, though the dye to catalyst ratio was kept constant. Constant dye to catalyst ratio indicates that the numbers of available active sites are appropriate for the given dye loading. In spite of enough active sites being present, the degradation decreased as the initial concentration was increased. Higher dye concentration may hinder the photocatalytic degradation in several ways: (i) at higher dye concentration, increased numbers of dye molecules present in the reactor increases the colour intensity of the reaction mixture, thereby hindering light penetration into the interior parts of the reactor. This slows down the activation of the catalysts in the interior parts, in spite of provision of mixing. (ii) solubility of oxygen in the reaction mixture may decrease by the presence of dyes at higher concentrations, hence decreasing the available dissolved oxygen (DO). The stored electrons in Ag core are discharged when an electron acceptor such as O_2 is available. Deficiency of dissolved oxygen at high dye concentration may slow down the release of electrons and hence the rate of photocatalytic process may be reduced. The decrease in DO was observed in the present study at high concentrations and the DO variations are presented in Table 4.23. (iii) Table 4.23 also shows an increase in pH of the reaction mixture with the progress of the reaction. Large increase in pH was observed with 200 mg/L initial dye concentration. When the initial concentrations are high, the reduced DO may lead to incomplete mineralization, which results in buildup of intermediates in the reaction

mixture. The presence of intermediates would have increased the pH. As discussed in Section 4.6.1, acidic pH of 3 favors the photocatalytic degradation and at pH values above 3, decrease in dye degradation was observed. At higher pH of above 6.8 (pzc), adsorption of dye is not favored and hence the rate of photocatalysis slows down. The reduced photocatalytic degradation with increased dye concentration may be attributed also to increased pH during the reaction. Time course variations of percentage degradation, shown in Figure 4.32 indicates that as the initial concentration is increased, the rate of photocatalysis slows down, as indicated by reduction in slopes of time course plots. Gradual decrease in slopes with time in the time course plots, indicate reduced rates, with the progress of reaction. As it is evident from Figure 4.32, dye to catalyst ratio of 1:30 is not favorable at high initial dye concentrations. So it may be concluded that dye to catalyst ratio of 1:30 may not be valid throughout the wide range of concentrations. Only 66 % degradation of 100 mg/L of dye could be attained within 360 min, with 1:30 dye to catalyst ratio and the ratio is not favorable even for 50 mg/L dye concentration.

Figure 4.33 presents the effect of initial dye concentration on time course variation of solar photocatalytic degradation of AY-17 dye, under constant dye to catalyst ratio of 1:10. As observed from the Figure, almost 100 % degradation of 10 and 50 mg/L dye is achieved within 120 minutes indicating the faster rates of degradation at low concentrations. Time course variations of percentage degradation, shown in Figure 4.33 indicate that as the initial concentration increases, the rate of photocatalysis slows down, as observed from the time course plots. As the concentration was increased from 10 mg/L to 500 mg/L, the percentage degradation (after 360 min irradiation time) decreased considerably from 99.49 to 20.42 %, though the dye to catalyst ratio was kept constant. Higher dye concentration may hinder the photocatalytic degradation as discussed previously in this section on UV photocatalysis of AY-17 dye. Large decrease in DO and increase in pH of the reaction mixture observed during the progress of the reaction is presented in Table 4.24. When the initial concentrations are high, the reduced DO may lead to incomplete mineralization as discussed earlier in this section on UV photocatalysis. The reduced photocatalytic degradation with increased dye concentration may also be attributed to increased pH during the reaction. Almost 100 % degradation of 100 mg/L of dye

could be achieved in 360 min. But at higher concentrations above 100 mg/L, rate of degradation was slower and the percentage degradations were much lesser. So it may be concluded that dye to catalyst ratio of 1:10 is not valid to concentrations above 100 mg/L of initial dye concentration. Time taken to achieve almost 100 % degradation of 100 mg/L of dye was 360 min, but for 10 and 50 mg/L, almost 100 % degradation with 1:10 dye to catalyst ratio could be achieved within 120 min.

The rates of degradation obtained with different initial concentrations using catalyst loading which provides dye to catalyst ratio at the optimum obtained for 10 mg/L of the dye, from crude optimization method based on "one factor at a time analysis" were very low. So to check whether rate of UV and solar photocatalysis of AY-17 can be improved by the addition of other oxidants, further experiments were performed with initial dye concentration of 100 mg/L and dye to catalyst ratio of 1:30 for UV photocatalysis and 1:10 for solar photocatalysis with different oxidants.

Table 4.21 Time course variation of concentration of AY-17 obtained with different initial concentration during UV photocatalysis. Conditions: Dye to catalyst ratio=1:30 (g/g); pH=3.

Time (min)	C_{AY-17} (mg/L) with different initial concentration and with fixed dye to catalyst ratio					
	Initial concentration of dye (mg/L)					
	10	50	75	100	150	200
0	10	50	75	100	150	200
60	6.78	42.32	63.84	87.20	134.91	179.88
120	4.27	35.86	58.18	80.93	123.71	164.94
180	2.04	28.12	46.20	69.08	117.57	156.76
240	0.83	20.23	35.55	57.11	112.79	150.38
300	0.006	11.79	25.91	46.69	111.98	149.30
360	0.002	7.32	20.31	34.41	111.15	148.20

Table 4.22 Time course variation of concentration of AY-17 obtained with different initial concentration (mg/L) during solar photocatalysis. Conditions: Dye to catalyst ratio=1:10 (g/g); pH=3.

Time (min)	C_{AY-17} (mg/L) with different initial concentrations and with fixed dye to catalyst ratio						
	Initial concentration of dye (mg/L)						
	10	50	100	200	300	400	500
0	10	50	100	200	300	400	500
60	0.08	4.93	39.95	119.54	236.16	337.80	442.60
120	0.05	1.05	23.88	91.14	205.44	308.76	425.70
180	0.05	0.90	14.32	79.42	182.34	290.20	417.85
240	0.05	0.69	8.55	69.66	170.94	272.92	409.35
300	0.05	0.37	5.85	63.58	160.71	261.44	399.70
360	0.05	0.04	3.10	59.70	153.96	253.44	397.90

Table 4.23 Time course variation of dissolved oxygen (DO) and pH during UV photocatalysis with different initial concentrations of AY-17 dye. Conditions: Dye to catalyst ratio=1:30 (g/g).

Time (min)	DO (mg/L)			pH		
	Initial concentration of dye (mg/L)			Initial concentration of dye (mg/L)		
	50	100	200	50	100	200
60	6.96	6.22	5.54	3.17	3.69	4.33
120	6.58	5.5	4.71	3.38	4.18	5.36
180	6.39	4.89	4.28	3.52	4.83	6.24
240	6.14	4.47	3.93	3.88	4.92	6.81
300	5.93	4.13	3.62	4.24	4.97	7.04
360	5.74	3.86	3.58	4.75	5.05	7.12

Table 4.24 Time course variation of dissolved oxygen (DO) and pH during solar photocatalysis with different initial concentrations of AY-17 dye. Conditions: Dye to catalyst ratio=1:10 (g/g).

Time (min)	DO (mg/L)			pH		
	Initial concentration of dye (mg/L)			Initial concentration of dye (mg/L)		
	100	300	500	100	300	500
60	6.79	6.40	6.11	3.38	3.56	3.82
120	6.18	5.89	5.63	3.51	3.88	4.16
180	5.71	5.41	5.06	4.02	4.14	4.48
240	5.47	4.97	4.54	4.46	4.57	4.69
300	5.16	4.35	3.96	4.46	4.89	5.04
360	4.98	3.82	3.33	4.46	5.08	5.25
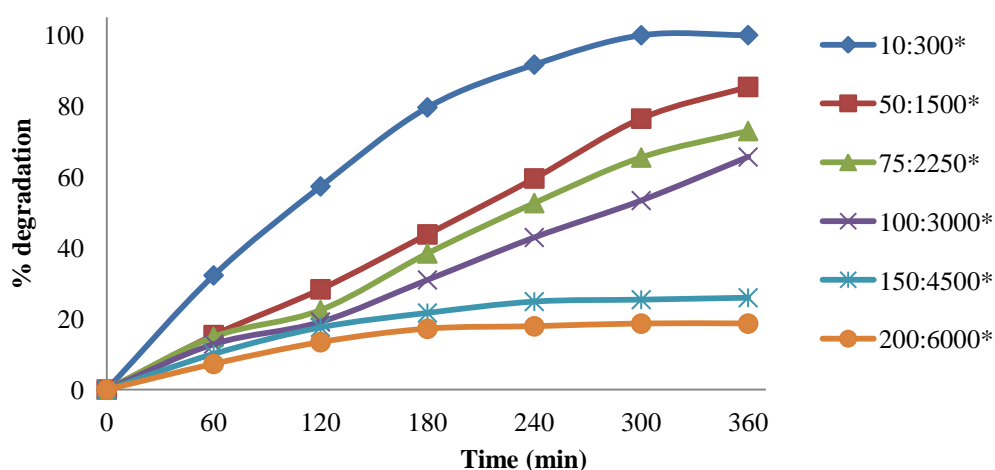
Figure 4.32 Effect of initial dye concentration on time course variation of UV photocatalytic degradation of AY-17 dye. Conditions: Catalyst used=Ag@TiO$_2$; dye to catalyst ratio=1:30 (g/g); pH=3. *(dye (mg/L): catalyst (mg/L)).
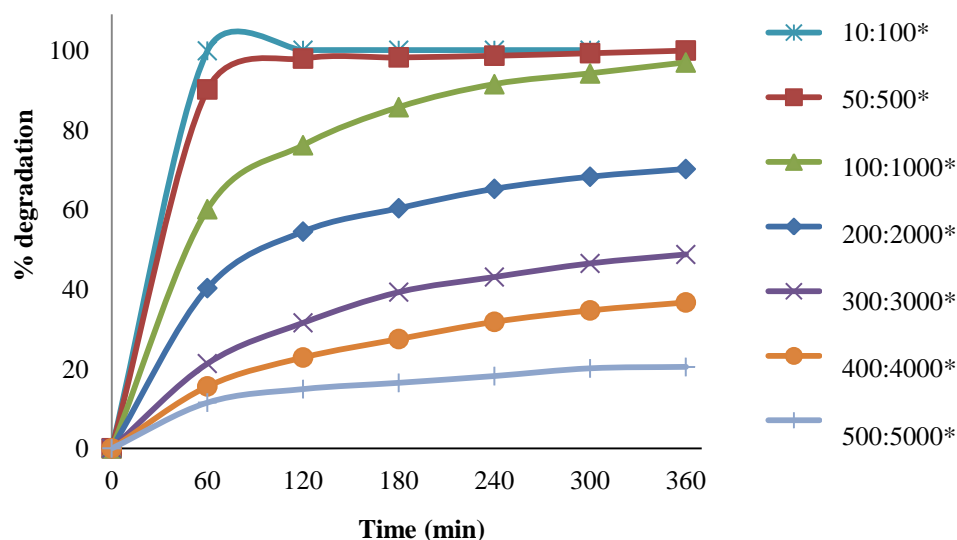
Figure 4.33 Effect of initial dye concentration on time course variation of solar photocatalytic degradation of AY-17 dye. Conditions: Catalyst used=Ag@TiO$_2$; dye to catalyst ratio=1:10 (g/g); pH=3; average UV and visible light intensity of solar light= 3.52 mW/cm^2 and 1172×100 lux respectively from 10 a.m. to 4 p.m. *(dye (mg/L): catalyst (mg/L)).

4.6.3.2 Effect of initial dye concentration on photocatalytic degradation of RB-220 under UV and solar light irradiations

Experiments were performed under UV light with different initial dye concentrations of RB-220 ranging from 50 to 200 mg/L and under solar light with dye concentrations ranging from 50 to 500 mg/L. In case of experiments under UV irradiation, dye to catalyst loading ratio was kept constant at 1:20 (g/g) whereas in solar photocatalysis it was kept constant at 1:10 (g/g). The dye to catalyst loading ratio chosen in these experiments were the optimum values as obtained by crude optimization method based on "one factor at a time" experiments presented in Section 4.6.2. The time course variations of RB-220 dye concentrations obtained with different initial concentrations of the dye are presented in Table 4.25-4.26 respectively, for UV and solar photocatalysis.

Figure 4.34 presents the effect of initial dye concentration on time course variation of UV photocatalytic degradation of the dye, under constant dye to catalyst

ratio of 1:20. Almost 100 % degradation of 50 mg/L dye was achieved within 180 min indicating faster rates of degradation at low concentrations. Time course variations of percentage degradation, shown in Figure 4.34 indicate that as the initial concentration is increased, the rate of photocatalysis slows down. As the concentration was increased from 50 to 200 mg/L, the percentage degradation (after 360 min irradiation time) has decreased considerably from almost 100 % to 45 %, though the dye to catalyst ratio was kept constant. Higher dye concentration may hinder the photocatalytic degradation as discussed previously in section 4.6.3.1. Large decrease in DO and increase in pH of the reaction mixture observed during the progress of the reaction are presented in Table 4.27. Decrease in DO and increase in pH during the course of reaction causes decrease in degradation of RB-220 dyes, as explained in Section 4.6.3.1 for photocatalysis of AY-17. Around 91% degradation of 100 mg/L of dye could only be achieved in 360 min. But at higher concentrations of above 100 mg/L, degradation was much lesser. So it may be concluded that dye to catalyst ratio of 1:20 is not favorable to concentrations of 100 mg/L or more initial dye concentration. So, further experiments were performed with the addition of oxidants other than oxygen, with initial dye concentration of 100 mg/L and dye to catalyst loading of 1:20, to test whether the photocatalytic degradation rate can be enhanced by the presence of additional oxidants during the reaction.

Figure 4.35 presents the effect of initial dye concentration on time course variation of solar photocatalytic degradation of RB-220 dye under solar light irradiation, with constant dye to catalyst ratio of 1:10. Time course variations of percentage degradation, shown in Figure 4.35 indicate that as the initial concentration is increased, the rate of photocatalysis slows down. As the concentration was increased from 50 to 500 mg/L, the percentage degradation (after 360 min irradiation time) decreased considerably from almost 100 % to 39 %, though the dye to catalyst ratio was kept constant. It can be observed, almost 100 % degradation of 50 mg/L of dye is achieved within 120 min indicating faster rates of degradation at low concentrations. Higher dye concentration may hinder the photocatalytic degradation as discussed previously in section 4.6.3.1. Large decrease in DO and increase in pH of the reaction mixture observed during the progress of the reaction as presented in Table 4.28 also lead to decrease in photocatalytic degradation and the reason for this

trend is explained in Section 4.6.3.1. Almost 100 % degradation of 100 mg/L of dye could be achieved in 120 min and dye at concentration of 200 mg/L could be degraded to more than 98 % in 360 min. But at higher concentrations of 300 mg/L or above, degradations were much lesser. So it may be concluded that dye to catalyst ratio of 1:10 is not valid to concentrations above 200 mg/L. Time taken to achieve almost 100 % degradation of 100 mg/L of dye was 120 min, but for 200 mg/L, it took around 360 min for around 98 % degradation with the same dye to catalyst ratio. So, further experiments were performed with initial dye concentration of 100 mg/L and dye to catalyst loading of 1:10, to test whether the photocatalytic degradation rate can be enhanced by the presence of additional oxidants during the reaction.

Table 4.25 Time course variation of concentration of RB-220 obtained with different initial concentration (mg/L) during UV photocatalysis. Conditions: Dye to catalyst ratio = 1:20 (g/g); pH=3.

Time (min)	C_{RB-220} (mg/L) with different initial concentration and with fixed dye to catalyst ratio						
	Initial concentration of dye (mg/L)						
	50	75	100	125	150	175	200
0	50	75	100	125	150	175	200
30	29.30	53.94	77.46	104.75	130.70	161.62	190.85
60	20.56	45.14	67.68	93.84	121.27	151.23	182.63
120	7.61	34.51	53.87	81.34	107.18	138.03	169.72
180	1.55	24.08	41.69	66.90	93.94	127.64	157.75
240	0.54	15.28	30.35	54.58	79.58	112.85	142.72
300	0.14	8.03	19.44	41.73	64.79	96.83	126.53
360	0.14	1.55	9.44	30.81	48.31	77.11	109.86

Table 4.26 Time course variation of concentration of RB-220 obtained with different initial concentration (mg/L) during solar photocatalysis. Conditions: Dye to catalyst ratio = 1:10 (g/g); pH=3

Time (min)	C_{RB-220} (mg/L) with different initial concentration and with fixed dye to catalyst ratio					
	Initial concentration of dye (mg/L)					
	50	100	200	300	400	500
0	50	100	200	300	400	500
30	8.73	31.34	146.20	245.92	347.82	463.24
60	1.27	10.28	107.11	223.10	316.06	429.93
120	0.28	0.63	28.87	196.62	295.14	410.56
180	0.14	0.63	4.08	168.17	275.77	385.77
240	0.14	0.42	4.08	129.93	244.01	351.69
300	0.07	0.28	3.66	91.13	224.65	330.77
360	0.07	0.21	3.66	87.04	204.51	305.99

Table 4.27 Time course variation of dissolved oxygen (DO) and pH during UV photocatalysis for different initial concentrations of RB-220 dye. Conditions: Dye to catalyst ratio = 1:20 (g/g).

Time (min)	DO (mg/L)			pH		
	Initial concentration of dye (mg/L)			Initial concentration of dye (mg/L)		
	50	100	200	50	100	200
60	6.94	6.58	6.03	3.15	3.49	4.62
120	6.67	6.12	5.5	3.32	3.97	4.98
180	6.21	5.75	4.92	3.76	4.28	5.36
240	6.03	5.26	4.18	4.05	4.56	5.74
300	5.86	4.74	3.65	4.58	4.89	6.15
360	5.43	4.26	2.47	5.03	5.36	6.89

Table 4.28 Time course variation of dissolved oxygen (DO) and pH during solar photocatalysis for different initial concentrations of RB-220 dye. Conditions: Dye to catalyst ratio = 1:10 (g/g).

Time (min)	DO (mg/L)			pH		
	Initial concentration of dye (mg/L)			Initial concentration of dye (mg/L)		
	100	300	500	100	300	500
60	6.85	6.59	6.25	3.29	3.48	3.71
120	6.29	6.12	5.92	3.64	3.72	4.04
180	5.97	5.85	5.36	4.15	4.21	4.59
240	5.58	5.27	4.84	4.52	4.74	4.86
300	5.24	4.78	4.12	4.65	4.93	5.31
360	5.03	4.04	3.61	4.71	5.18	5.78
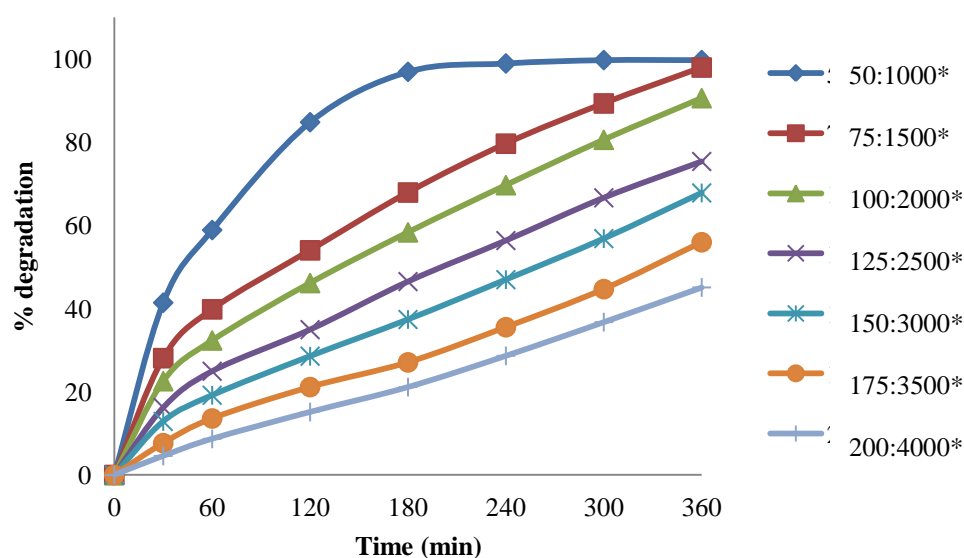
Figure 4.34 Effect of initial dye concentration on time course variation of UV photocatalytic degradation of RB-220 dye. Catalyst used=Ag@TiO$_2$; dye to catalyst ratio=1:20 (g/g); pH=3; *(dye (mg/L): catalyst (mg/L)).
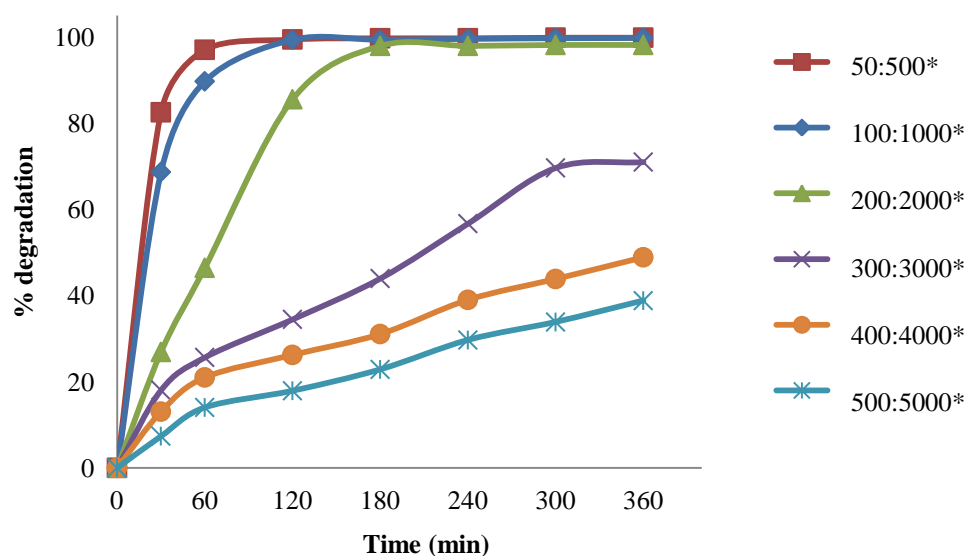
Figure 4.35 Effect of initial dye concentration on time course variation of solar photocatalytic degradation of RB-220 dye. Conditions: Catalyst used=Ag@TiO$_2$; dye to catalyst ratio=1:10 (g/g); pH=3; average UV and visible light intensity of solar light= 3.55 mW/cm^2 and 1198×100 lux respectively from 10 a.m. to 4 p.m. *(dye (mg/L): catalyst (mg/L)).

4.6.4 Effect of oxidants on photocatalytic degradation of AY-17 and RB-220 dye under UV and solar light irradiation

Use of additional oxidants other than dissolved oxygen can have several effects on the photocatalytic degradation rate:

(i) It can help in release of electrons from the Ag core, (ii) it can produce more radicals and other oxidizing species, hence increasing the degradation rate of intermediate compounds produced during the photocatalytic process, and (iii) it can prevent problems caused by decrease in oxygen concentration (Bahnemann et al. 2007)

As oxidants play an important role, many researchers have studied the effect of oxidants such as H$_2$O$_2$, (NH$_4$)$_2$S$_2$O$_8$, and KBrO$_3$ on the photocatalytic degradation of different dyes (Neppolian et al. 2002a; Qamar et al. 2005a; Qamar et al. 2005b; Muruganandham and Swaminathan 2006a; Muruganandham and Swaminathan, 2006b; Akyol et al. 2007; Faisal et al. 2007). So the effect of addition of oxidants

such as H_2O_2, $(NH_4)_2S_2O_8$, and $KBrO_3$ on the UV and solar photocatalytic degradation of AY-17 and RB-220 using $Ag@TiO_2$ core-shell structured nanoparticles were studied. In order to check if the oxidants (H_2O_2, $(NH_4)_2S_2O_8$, and $KBrO_3$) themselves can lead to photolysis of the dyes, control experiments were also done at different concentrations of oxidants under the light source (UV and solar) and in the absence of catalyst. Degradation of dyes achieved with different concentrations of oxidants in the absence of catalyst were insignificant as compared to those obtained with oxidants in the presence of catalyst indicating direct photolysis is not significant.

4.6.4.1 Effect of oxidants on photocatalytic degradation of AY-17 dye

(i) Effect of addition of H_2O_2 on UV and solar photocatalysis of AY-17

Hydroxyl radical is responsible for the photocatalytic degradation of dyes, so hydrogen peroxide as an oxidant in concentration range of 5-20 mM, was added initially to the aqueous dye solution of 100 mg/L concentration and with initial pH of 3, for UV and solar photocatalysis. In case of UV photocatalysis, catalyst loading of 3 g/L and for solar photocatalysis, catalyst loading of 1 g/L was used. These catalyst loadings provided dye to catalyst ratio of 1:30 (g/g) and 1:10 (g/g) respectively for UV and solar photocatalysis. The experiments with H_2O_2 addition were conducted in the absence of air supply. The time course variations of AY-17 dye concentrations obtained with different concentrations of H_2O_2 are presented in Table 4.29-4.30 respectively for UV and solar photocatalysis.

Figure 4.36a presents the time course variation of percentage degradation of AY-17 during UV photocatalysis in the presence of H_2O_2 as an oxidant. Less than around 77 % degradation could only be achieved in 360 min irradiation time with any concentration of H_2O_2. Figure 4.37a shows the comparison of the percentage degradation (after 60 min irradiation) achieved using only air and different concentrations of H_2O_2 as oxidants. The results showed that the percentage degradation achieved using H_2O_2 as an oxidant was higher than that achieved with air. The percentage degradation increased from 20.5 to 23.6 % as the concentration of H_2O_2 increased in the range of 5-10 mM, but further increase in H_2O_2 concentration to

20 mM decreased the degradation to about 10.59 %. It was also observed from Figure 4.36a, rate of degradation of AY-17 is the highest when 10 mM H_2O_2 was added as compared to addition of H_2O_2 at other concentrations. So 10 mM H_2O_2 was found to be the optimum for the photocatalytic degradation of AY-17 under UV light irradiation.

Similar experiments were conducted using hydrogen peroxide in concentration range of 10-20 mM as oxidant for solar photocatalysis of dye solution of 100 mg/L concentration with catalyst loading of 1 g/L and with initial pH of 3. Figure 4.36b presents the time course variation of percentage degradation of AY-17, with the addition of H_2O_2 during solar photocatalysis. Almost 100 % degradation could be achieved in 360 min irradiation time with 10 mM H_2O_2, but with addition of H_2O_2 at other concentrations, complete degradation was not possible in 360 min. Figure 4.37b shows percentage degradation (after 60 min irradiation time) achieved by using H_2O_2 as an oxidant at different concentrations. The results show that the percentage degradation achieved with H_2O_2 as an oxidant is higher than that achieved without the addition of H_2O_2. Further it is observed, as the concentration of H_2O_2 increases from 5 to 10 mM, degradation increases from around 68.7 % to 73.23 %, but further increase in H_2O_2 concentration to greater than 10 mM causes decrease in degradation, reaching to about 34.73 % at 20 mM. It is observed from the Figure 4.36b, rate of degradation of AY-17 is the highest with 10 mM H_2O_2 addition, as compared to addition of H_2O_2 at other concentrations. So 10 mM H_2O_2 is the optimum for the photocatalytic degradation of AY-17 under solar light irradiation.

The increase in degradation by addition of H_2O_2 is due to increase in the hydroxyl radical concentration by the following ways (Muruganandham and Swaminathan, 2004, 2006 a,b):
(i) Direct reaction with conduction band (CB) electrons and thus inhibiting the electron–hole recombination (ii) indirect reaction with superoxide radical anion (Pichat et al. 1995).

But at high H_2O_2 concentration of above 10 mM, the percentage degradation decreases with increase in H_2O_2 concentration due to:(i) Scavenging effect of hydroxyl radical (Sarthy and Mohseni 2006). Excess of H_2O_2 reacts with hydroxyl radical ($^\bullet$OH) and forms hydroperoxy radical ($HO_2^\bullet$). These hydroperoxy radicals

($HO_2^{\bullet}$) are very less reactive than the hydroxyl radical ($^{\bullet}OH$) and do not contribute to oxidative degradation of dye (ii) when H_2O_2 is present in excess quantity, it may act as hole scavenger (Pichat et al. 1995). In photocatalytic degradation, the positive hole either oxidizes dye directly or it reacts with water to produce hydroxyl radical. Hence, the degradation of hole decreases the dye degradation rate.

In the present study, maximum dye degradation occurred with the addition of 10 mM (340 mg/L) H_2O_2. Hence, 10 mM H_2O_2 was found to be the optimum concentration for photocatalytic degradation of AY-17 using Ag@TiO_2 core shell structured nanoparticles under UV and solar light irradiation.

Table 4.29 Time course variation of concentration of AY-17 obtained with different initial concentration of H_2O_2 during UV photocatalysis. Conditions: Dye to catalyst ratio=1:30 (g/g); pH=3; C_0= 100 mg/L.

Time (min)	C_{AY-17} (mg/L) with air as oxidant source	C_{AY-17} (mg/L) obtained with different initial concentration of H_2O_2			
		$C_{H2O2= 5mM}$	$C_{H2O2=10mM}$	$C_{H2O2= 15mM}$	$C_{H2O2= 20mM}$
0	100	100	100	100	100
60	87.20	79.5	76.4	81.26	89.41
120	80.93	66.3	62.98	72.8	79.5
180	69.08	52.5	49.5	57.5	69.1
240	57.11	43.5	39.3	44.7	52.8
300	46.69	35.1	30.6	34.2	39.65
360	34.41	28.2	23.8	27.66	31.05

Table 4.30 Time course variation of concentration of AY-17 obtained with different initial concentration of H$_2$O$_2$ during solar photocatalysis. Conditions: Dye to catalyst ratio=1:10 (g/g); pH=3; C$_0$= 100 mg/L.

Time (min)	C$_{AY-17}$ (mg/L) with air as oxidant source	C$_{AY-17}$ (mg/L) obtained with different initial concentration of H$_2$O$_2$			
		C$_{H2O2= 5mM}$	C$_{H2O2=10mM}$	C$_{H2O2= 15mM}$	C$_{H2O2= 20mM}$
0	100	100	100	100	100
60	39.95	31.3	26.77	50.6	65.27
120	23.88	20.45	17.35	40.6	47.5
180	14.32	11.7	9.44	23.2	36.3
240	8.55	7.88	5.4	16.85	19.86
300	5.85	4.4	2.24	11.3	13.5
360	3.10	2.11	1.17	7.56	9.8
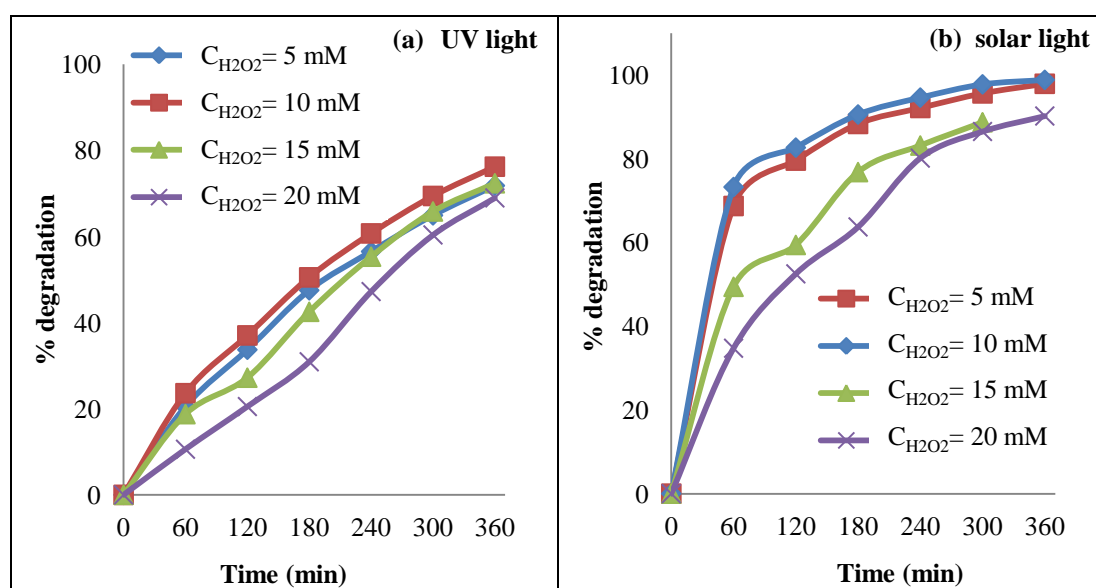
Figure 4.36 Effect of H$_2$O$_2$ on time course variation of photocatalytic degradation of AY-17 dye under a) UV light: Dye to catalyst ratio=1:30 (g/g); b) solar light: Dye to catalyst ratio=1:10 (g/g); average UV and visible light intensity of solar light= 3.57 mW/cm^2 and 1212×100 lux respectively from 10 a.m. to 4 p.m. Conditions: pH=3; C$_0$= 100 mg/L.
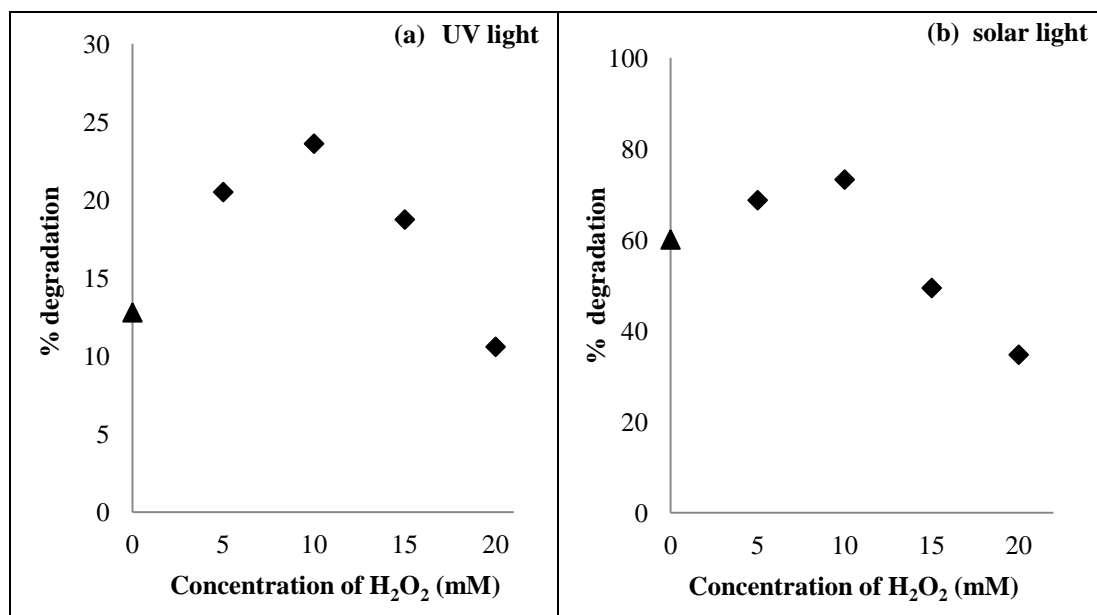
Figure 4.37 Effect of addition of H_2O_2 on photocatalysis of AY-17 dye under; a) UV light: ◆ H_2O_2 as the oxidant; ▲supplied air as the source of oxidant; dye to catalyst ratio= 1:30; b) solar light:◆H_2O_2 as the oxidant;▲ atmospheric air as the source of oxidant; dye to catalyst ratio= 1:10. Conditions: pH=3; C_0=100 mg/L; Irradiation time =60 min.

(ii) Effect of addition of ammonium persulphate [$(NH_4)_2S_2O_8$] as an oxidant for UV and solar photocatalysis of AY-17

Effect of addition of $(NH_4)_2S_2O_8$ as an oxidant was studied with dye solution of 100 mg/L concentration and with initial pH = 3 by varying the concentration of $(NH_4)_2S_2O_8$ from 1 to 4 g/L for the photocatalytic degradation of AY-17 under UV and solar light irradiation. In case of UV photocatalysis, catalyst loading of 3 g/L and for solar photocatalysis, a catalyst loading of 1 g/L was used. The dye to catalyst ratio was hence maintained at 1:30 for UV and 1:10 for solar photocatalysis. The experiments with $(NH_4)_2S_2O_8$ addition were conducted in the absence of air supply. The time course variations of AY-17 dye concentrations obtained with different concentrations of $(NH_4)_2S_2O_8$ are presented in Table 4.31-4.32 respectively for UV and solar photocatalysis.

Figure 4.38a presents the time course variation of percentage degradation of AY-17 during UV photocatalysis with addition of $(NH_4)_2S_2O_8$ at different concentrations. Almost 100 % degradation of AY-17 could be achieved in 30 min irradiation with the addition of 2 g/L and 3 g/L of $(NH_4)_2S_2O_8$. But with other concentrations of $(NH_4)_2S_2O_8$, complete degradation could not be achieved even after 120 min of irradiation. The effect of addition of $(NH_4)_2S_2O_8$ (1-4 g/L) on photocatalytic degradation of the dye after 60 min irradiation time is shown in Figure 4.39a. As seen from the results, higher degradation was achieved with $(NH_4)_2S_2O_8$, as compared to that with air as an oxidant. Tremendous increase in the rate of degradation was observed on the addition of $(NH_4)_2S_2O_8$. As the concentration of $(NH_4)_2S_2O_8$ was increased from 1 to 2 g/L, degradation at the end of 60 min increased from 92.4 to 98.96 %, whereas only around 12.8 % (degradation) was achieved using air as the source of oxidant. Though degradation remained almost constant, when $(NH_4)_2S_2O_8$ was increased from 2 to 3 g/L, further increase in its concentration to 4 g/L resulted in reduction in degradation from 97.6 to 95.54 %. It is observed from Figure 4.38a, 2 g/L $(NH_4)_2S_2O_8$ is the optimum for the photocatalytic degradation of AY-17 under UV light, owing to achievement of maximum degradation of the dye.

Similar experiments were conducted using $(NH_4)_2S_2O_8$ in concentration range of 1-4 g/L as an oxidant with AY-17 dye solution of 100 mg/L concentration and catalyst loading of 1 g/L with initial pH of 3 under solar light irradiation. Figure 4.38b presents the time course variation of percentage degradation of AY-17 with addition of $(NH_4)_2S_2O_8$ during solar photocatalysis. Almost 100 % degradation of AY-17 could be achieved in 30 min irradiation with the addition of 2 g/L and 3 g/L of $(NH_4)_2S_2O_8$. But with other concentrations of $(NH_4)_2S_2O_8$, complete degradation could not be achieved even after 120 min of irradiation. The effect of addition of $(NH_4)_2S_2O_8$ (1-4 g/L) on photocatalytic degradation of dye after 60 min irradiation time is shown in Figure 4.39b. Results show that higher degradation could be achieved with the addition of $(NH_4)_2S_2O_8$. The rate of degradation has increased considerably on the addition of $(NH_4)_2S_2O_8$. By the addition of $(NH_4)_2S_2O_8$ as oxidant at concentration of 1 g/L, the percentage degradation at 60 min irradiation time has increased to 94.5 %, whereas only 60.05 % degradation was achieved without the addition of $(NH_4)_2S_2O_8$. As the concentration of $(NH_4)_2S_2O_8$ increased from 1 to 2 g/L, degradation after 60

min of irradiation time has increased from 94.5 % to almost 99.29 %. Further increase in its concentration to 3 and 4 g/L, did not alter the percentage degradation. It is observed from Figure 4.38b, 2 g/L $(NH_4)_2S_2O_8$ is the optimum for the photocatalytic degradation of AY-17 under solar light.

The increase in degradation in the presence of persulphate ion is due to the following facts:

Persulphate ion can trap the conduction band electron and results in the formation of sulphate radical ion $(SO_4^{.-})$ which is a powerful oxidizing agent, can add hydrogen to the unsaturated carbon, subtracts hydrogen from the saturated carbon or it can remove electrons from the carboxylate anion and from certain neutral molecules of dye (Nasr et al.1997; Neppolian et al. 2002b). In addition, $SO_4^{.-}$ can trap the conduction band electrons and/or generate hydroxyl radical (Pelizzetti et al. 1991; Minero et al. 1993; Nasr et al. 1997). This unique nature of $SO_4^{.-}$ increases the fragmentation of the dye molecules by attacking at various positions (Neppolian et al. 2002b) and can result in the enhancement of degradation rate.

At a high concentration of persulphate, excess of sulphate radical anion $(SO_4^{2.-})$ may get adsorbed on Ag@TiO$_2$ surface and deactivate a section of catalyst there by inhibiting the degradation process or may also react with photogenerated holes and with hydroxyl radicals (Muruganandham and Swaminathan 2006b). $SO_4^{2.-}$ being less reactive than $^{\bullet}OH$ radical and h^+, thus in excess may reduce the photodegradation of the dye. But in the present studies, the excess persulphate did not yield significant reduction in percentage degradation, indicating that inhibition effect is negligible in the concentration range studied. As high rate and almost complete degradation of AY-17 was observed with 2 g/L of $(NH_4)_2S_2O_8$, it may be considered as the optimum for UV and solar photocatalysis of AY-17.

Table 4.31 Time course variation of concentration of AY-17 obtained with different initial concentration of $(NH_4)_2S_2O_8$ during UV photocatalysis. Conditions: Dye to catalyst ratio=1:30 (g/g), pH=3, C_0= 100 mg/L.

Time (min)	C_{AY-17} (mg/L) with air as oxidant source	C_{AY-17} (mg/L) obtained with different initial concentration of $(NH_4)_2S_2O_8$			
		$C_{(NH4)2S2O8=}$ 1 g/L	$C_{(NH4)2S2O8=}$ 2 g/L	$C_{(NH4)2S2O8=}$ 3 g/L	$C_{(NH4)2S2O8=}$ 4 g/L
0	100	100	100	100	100
15	95.42	41.25	23.46	9.9	4.46
30	92.96	19.62	3.56	2.4	4.46
45	90.18	9.45	2.58	2.4	4.46
60	87.2	7.6	1.04	2.4	4.46
75	85.04	6.2	0.79	2.4	4.46
90	83.42	5.26	0.54	2.4	4.46
105	81.91	4.78	0.42	2.4	4.46
120	80.93	4.02	0.33	2.4	4.46

Table 4.32 Time course variation of concentration of AY-17 obtained with different initial concentration of $(NH_4)_2S_2O_8$ during solar photocatalysis. Conditions: Dye to catalyst ratio=1:10 (g/g), pH=3, C_0= 100 mg/L.

Time (min)	C_{AY-17} (mg/L) with air as oxidant source	C_{AY-17} (mg/L) obtained with different initial concentration of $(NH_4)_2S_2O_8$			
		$C_{(NH4)2S2O8=}$ 1 g/L	$C_{(NH4)2S2O8=}$ 2 g/L	$C_{(NH4)2S2O8=}$ 3 g/L	$C_{(NH4)2S2O8=}$ 4 g/L
0	100	100	100	100	100
15	81.75	31.8	17.2	5.4	6.9
30	65.53	14.6	1.8	3.2	4.5
45	51.06	7.3	1.02	1.6	2
60	39.95	5.5	0.71	0.96	1.31
75	34.65	3.8	0.32	0.96	1.31
90	31.11	2.33	0.25	0.96	1.31
105	27.32	1.97	ND	0.19	1.31
120	23.88	1.1	ND	0.19	1.31
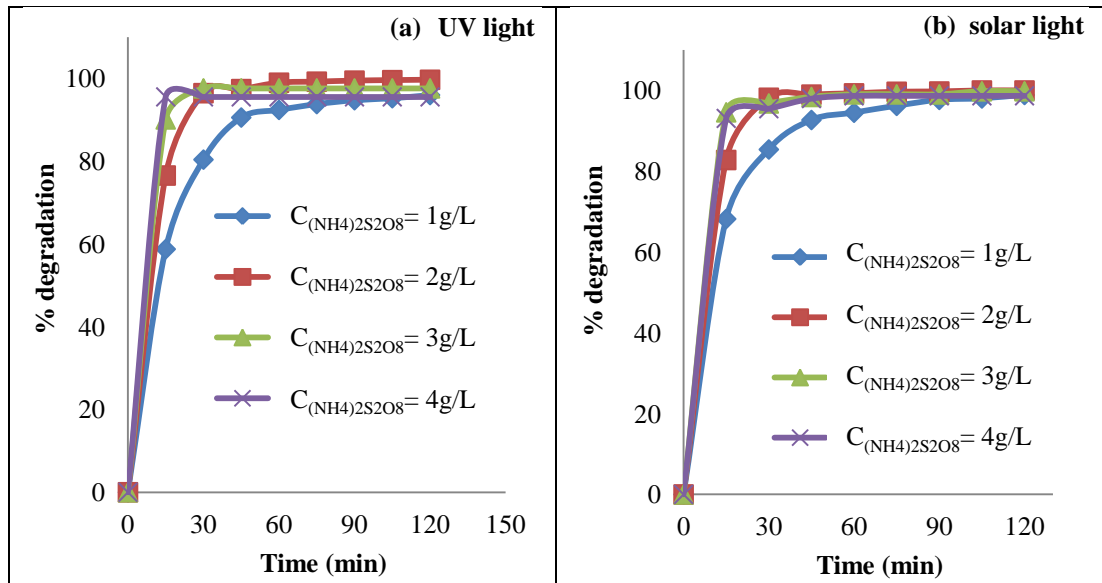
Figure 4.38 Effect of (NH$_4$)$_2$S$_2$O$_8$ addition on time course variation of photocatalytic degradation of AY-17 dye under a) UV light: Dye to catalyst ratio=1:30 (g/g) b) solar light: Dye to catalyst ratio=1:10 (g/g); average UV and visible light intensity of solar light = 3.56 mW/cm^2 and 1213×100 lux respectively from 11 a.m. to 12 p.m. Conditions: pH=3; C$_0$= 100 mg/L.
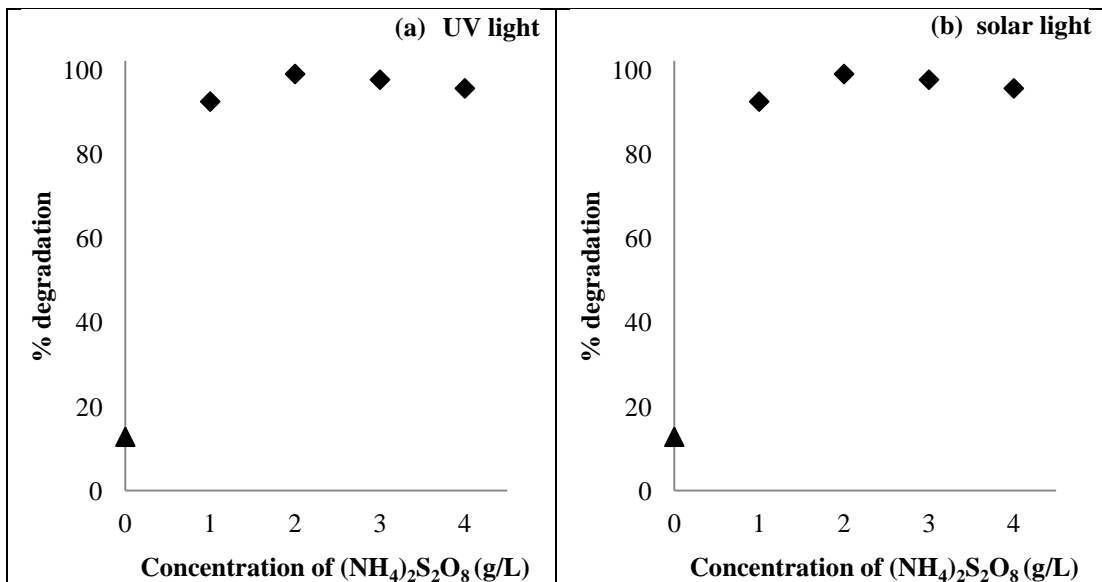
Figure 4.39 Effect of addition of (NH$_4$)$_2$S$_2$O$_8$ on the photocatalysis of AY-17 dye under a) UV light: ◆(NH$_4$)$_2$S$_2$O$_8$ as the oxidant; ▲supplied air as the source of oxidant; dye to catalyst ratio= 1:30; b) solar light: ◆(NH$_4$)$_2$S$_2$O$_8$ as the oxidant;▲ atmospheric air as the source of oxidant; dye to catalyst ratio= 1:10. Conditions: pH=3; C$_0$=100 mg/L; Irradiation time =60 min.

(iii) Effect of addition of KBrO$_3$ as oxidant for UV and solar photocatalysis of AY-17

Effect of addition of KBrO$_3$ as an oxidant for photocatalytic degradation of AY-17 under UV and solar light irradiation was studied with the dye solution of 100 mg/L concentration and initial pH = 3 by varying the concentration of KBrO$_3$ from 1 to 4 g/L. In case of UV photocatalysis, catalyst loading of 3 g/L and in solar photocatalysis, catalyst loading of 1 g/L was used. The experiments with KBrO$_3$ addition were conducted in the absence of air supply. The time course variations of AY-17dye concentrations obtained with different concentrations of KBrO$_3$ are presented in Table 4.33-4.34 respectively for UV and solar photocatalysis.

Figure 4.40a presents the effect of addition of KBrO$_3$ on the time course variation of percentage degradation of AY-17 during UV photocatalysis. Complete degradation of AY-17 could not be achieved with any concentration of KBrO$_3$. The effect of addition of KBrO$_3$ (1-4 g/L) on UV photocatalytic degradation of AY-17 after 60 min irradiation time, is shown in Figure 4.41a. Figure 4.41a also shows the data point indicating the percentage degradation achieved after 60 min, with air as the source of oxidant. Addition of KBrO$_3$ resulted in higher degradation as compared to that with air as the source of oxidant. As the KBrO$_3$ concentration was increased from 1 to 2 g/L, the degradation (after 60 min of irradiation time) was found to increase from 28.2 to 34.56 %, but further increase in KBrO$_3$ concentration to 3 g/L or above, decreased the degradation. So, 2 g/L of KBrO$_3$ is the optimum for the photocatalytic degradation of AY-17 under UV light irradiation.

Similar experiments were conducted using KBrO$_3$as an oxidant in concentration range of 1-4 g/L for solar photocatalysis of dye solution of 100 mg/L concentration with catalyst loading of 1 g/L and with initial pH of 3. Figure 4.40b presents the time course variation of percentage degradation of AY-17 with addition of KBrO$_3$ under solar light irradiation. Almost 100 % degradation of AY-17 could be achieved in 360 min irradiation with the addition of 2 g/L of KBrO$_3$, whereas with other concentrations of KBrO$_3$, complete degradation could not be achieved even after 360 min of irradiation. The effect of addition of KBrO$_3$ (1-4 g/L) on photocatalytic degradation of AY-17 after 60 min irradiation time is shown in Figure 4.41b. The

Figure also presents the percentage degradation without the addition of $KBrO_3$. As shown in Figure 4.41b, the addition of $KBrO_3$ leads to higher degradation of the dye. As the concentration of $KBrO_3$ was increased from 1 to 2 g/L, degradation after 60 min of irradiation time increased from around 70.72 % to 78.06 %, but further increase in concentration of $KBrO_3$ to 3 g/L and above, has decreased the degradation. So, 2 g/L of $KBrO_3$ was found to be optimum for the photocatalytic degradation of AY-17 under solar light irradiation.

The increase in degradation rate with the addition of $KBrO_3$ is owing to its electron scavenging effect by the reaction between conduction band electron and BrO_3^- ion as shown in Eq.(4.1).

$$BrO_3^- + 6e^-_{(CB)} + 6H^+ \rightarrow Br^- + 3H_2O \qquad (4.1)$$

The decrease in the degradation rate with further increase in concentration of $KBrO_3$ may be due to the adsorption of Br^- ion on $Ag@TiO_2$ surface, which affects the catalytic activity of $Ag@TiO_2$ (Muruganandham and Swaminathan 2004, 2006 a, b).

In the present study, maximum dye degradation occurred with the addition of 2 g/L $KBrO_3$. Hence 2 g/L $KBrO_3$ concentration is found to be the optimum for photocatalytic degradation of AY-17 using $Ag@TiO_2$ core shell structured nanoparticles under UV and solar light irradiation.

Table 4.33 Time course variation of concentration of AY-17 obtained with different initial concentration of $KBrO_3$ during UV photocatalysis. Conditions: Dye to catalyst ratio=1:30 (g/g); pH=3; C_0=100 mg/L.

Time (min)	C_{AY-17} (mg/L) with air as oxidant source	C_{AY-17} (mg/L) obtained with different initial concentration of $KBrO_3$			
		$C_{KBrO3=1\ g/L}$	$C_{KBrO3=2\ g/L}$	$C_{KBrO3=3\ g/L}$	$C_{KBrO3=4\ g/L}$
0	100	100	100	100	100
60	87.20	71.8	65.44	77.4	80.4
120	80.93	59.83	52.3	62.6	64.17
180	69.08	49.18	43.2	50.1	53.75
240	57.11	41.57	35.1	41.15	44.3
300	46.69	34.6	27.4	32.7	35.08
360	34.41	27.62	20.52	24.46	29.49

Table 4.34 Time course variation of concentration of AY-17 obtained with different initial concentration of KBrO$_3$ during solar photocatalysis. Conditions: Dye to catalyst ratio=1:10 (g/g); pH=3; C$_0$=100 mg/L.

Time (min)	C$_{AY-17}$ (mg/L) with air as oxidant source	C$_{AY-17}$ (mg/L) obtained with different initial concentration of KBrO$_3$			
		C$_{KBrO3=1\ g/L}$	C$_{KBrO3=2\ g/L}$	C$_{KBrO3=3\ g/L}$	C$_{KBrO3=4\ g/L}$
0	100	100	100	100	100
60	39.95	29.28	21.94	48.3	63.14
120	23.88	20.9	12.52	35.65	46.5
180	14.32	12.5	5.03	23.87	35.85
240	8.55	6.46	3.21	12.5	22.7
300	5.85	4.06	1.96	6.2	11.6
360	3.10	2.46	1.24	3.77	7.42
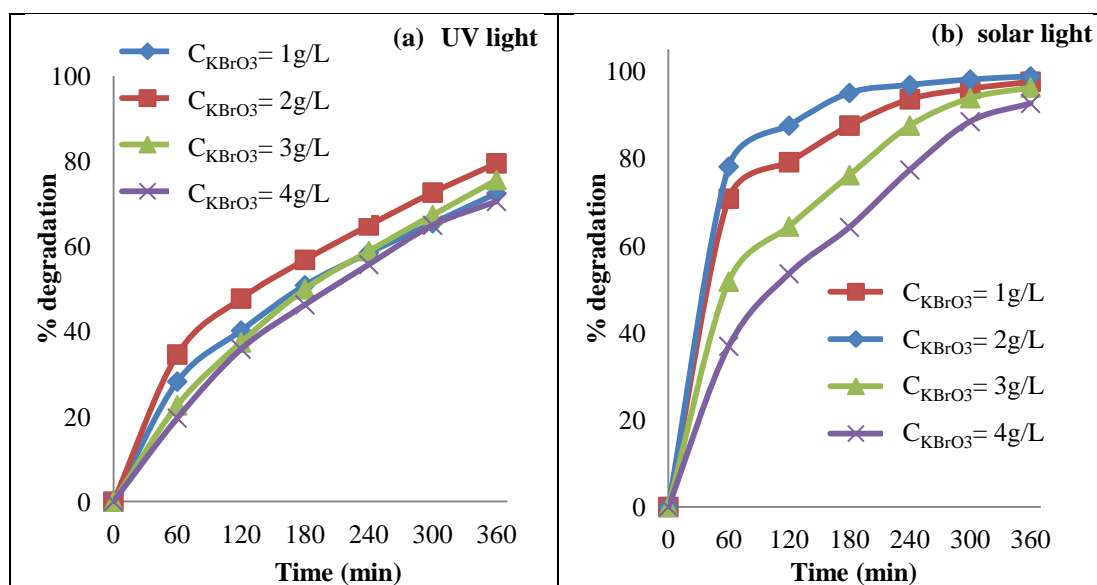
Figure 4.40 Effect of KBrO$_3$ addition on time course variation of photocatalytic degradation of AY-17 dye under a) UV light: Dye to catalyst ratio=1:30 (g/g); b) solar light: Dye to catalyst ratio=1:10 (g/g); average UV and visible light intensity of solar light = 3.54 mW/cm^2 and 1198×100 lux respectively from 10 a.m. to 4 p.m. Conditions: pH=3; C$_0$= 100 mg/L.
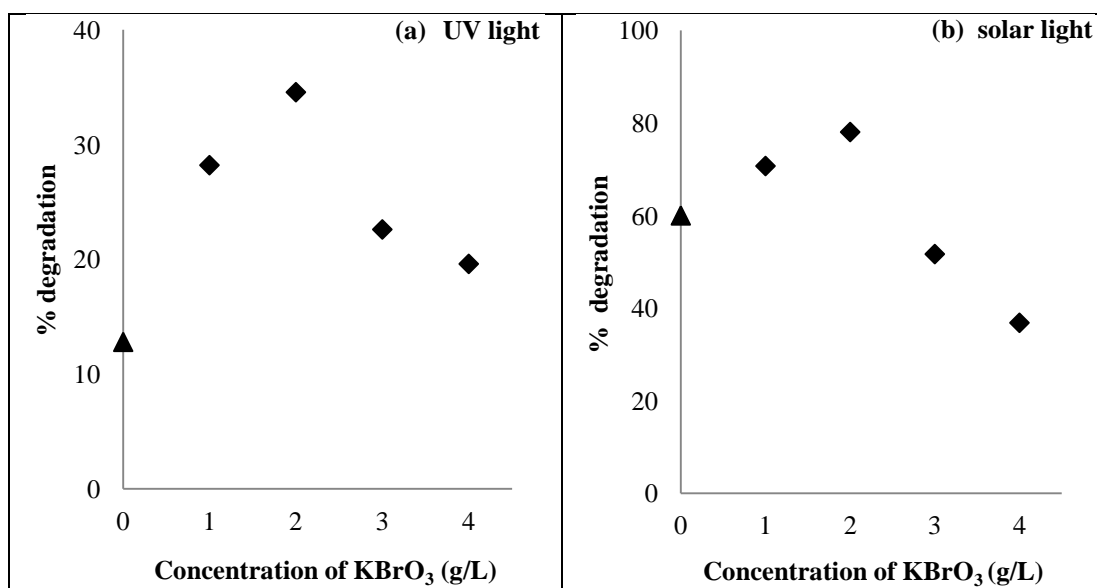
Figure 4.41 Effect of addition of KBrO$_3$ on the photocatalysis of AY-17 dye under a) UV light: ◆ KBrO$_3$ as the oxidant; ▲supplied air as the source of oxidant; dye to catalyst ratio= 1:30; b) solar light:◆KBrO$_3$ as the oxidant;▲ atmospheric air as the source of oxidant; dye to catalyst ratio= 1:10 Conditions: pH=3; C$_0$=100 mg/L; Irradiation time =60 min.

(iv) Comparison of the oxidants on UV and solar photocatalysis of AY-17

It is evident from the results on effect of oxidants discussed in earlier parts of this Section that the optimum concentration of oxidants on UV and solar photocatalysis of AY-17 dye are 10 mM (0.34 g/L) of H$_2$O$_2$, 2 g/L of (NH$_4$)$_2$S$_2$O$_8$ and 2 g/L of KBrO$_3$ when these compounds are used as oxidants. Figure 4.42 shows the time course variation of percentage degradation of AY-17 dye with different oxidants at their optimum concentrations obtained by UV and solar photocatalysis. It is evident that the rate of photocatalysis is the maximum when (NH$_4$)$_2$S$_2$O$_8$ is used as the oxidant and is the least when air is used as a source of oxygen to serve as an oxidant, as is evident from the slopes of time course plots. Rate of degradation and maximum degradation are lower with H$_2$O$_2$ and KBrO$_3$ as compared to (NH$_4$)$_2$S$_2$O$_8$. When air was used as the oxidant for UV photocatalysis, only around 7.34 %, 12.8 % and 19.07 % of degradation of dye could be achieved after 30, 60 or 120 min, respectively, indicating the least rate of reaction as compared to photocatalysis with other oxidants.

In case of solar light, when atmospheric air was used as the source of oxidant, only around 34.47 % and 60.05 % of degradation of dye could be achieved after 30 or 60 min, respectively, indicating the least rate of reaction as compared to photocatalysis with other oxidants. Figure 4.43 shows the comparison of different oxidants in UV and solar photocatalysis of AY-17. $(NH_4)_2S_2O_8$ is a very effective oxidant as compared to others used in this study. Maximum degradation of almost around 100 % was achieved within 60 min both under UV and solar light, when $(NH_4)_2S_2O_8$ was used as the oxidant at an optimum concentration of 2 g/L. Percentage degradations achieved with optimum concentration of H_2O_2 (10 mM or 0.34 g/L) and $KBrO_3$ (2 g/L) as oxidants were only around 23.6 % and 34.56 % respectively after 60 min of irradiation time under UV light. In solar light, percentage degradations achieved with optimum concentration of H_2O_2 (10 mM or 0.34 g/L) and $KBrO_3$ (2 g/L) as oxidants were only around 73.23 % and 78.06 % respectively after 60 min of irradiation time. Although the optimum concentration of H_2O_2 (10 mM or 340 mg/L) is much lower than that for $(NH_4)_2S_2O_8$, the rate of reaction is very slow with H_2O_2. The order of activity of oxidants is $(NH_4)_2S_2O_8 > KBrO_3 > H_2O_2 >$ air for UV and solar photocatalysis. The difference in their activities is due to the differences in the absorption of light which depends on the one-electron reduction potentials of different species (Irmak et al. 2004; Sobana et al. 2008). The one-electron reduction potentials for O_2, H_2O_2, $KBrO_3$, and $(NH_4)_2S_2O_8$ are: E $(O_2/O_2^{\bullet-})$ = - 155 mV, E $(H_2O_2/OH^{\bullet})$ = 800 mV, E $(BrO_3^-/BrO_2^{\bullet})$ = 1150 mV and E $(S_2O_8^{2-}/SO_4^-)$ = 1100 mV (Wardman 1989; Faisal et al. 2007) respectively. So from the thermodynamic point of view, all the oxidants should be more efficient than molecular oxygen. Experimental observations showed that $(NH_4)_2S_2O_8$ may increase the release of stored electrons from Ag core and also lead to generation of sulphate radicals along with hydroxyl radicals, which played a great role in increasing the photocatalytic degradation of AY-17 both under UV and solar light irradiation, and hence $(NH_4)_2S_2O_8$ (2 g/L) was found to be the best oxidant as compared to other oxidants studies here, for the photocatalytic degradation of AY-17 under UV and solar light irradiation.
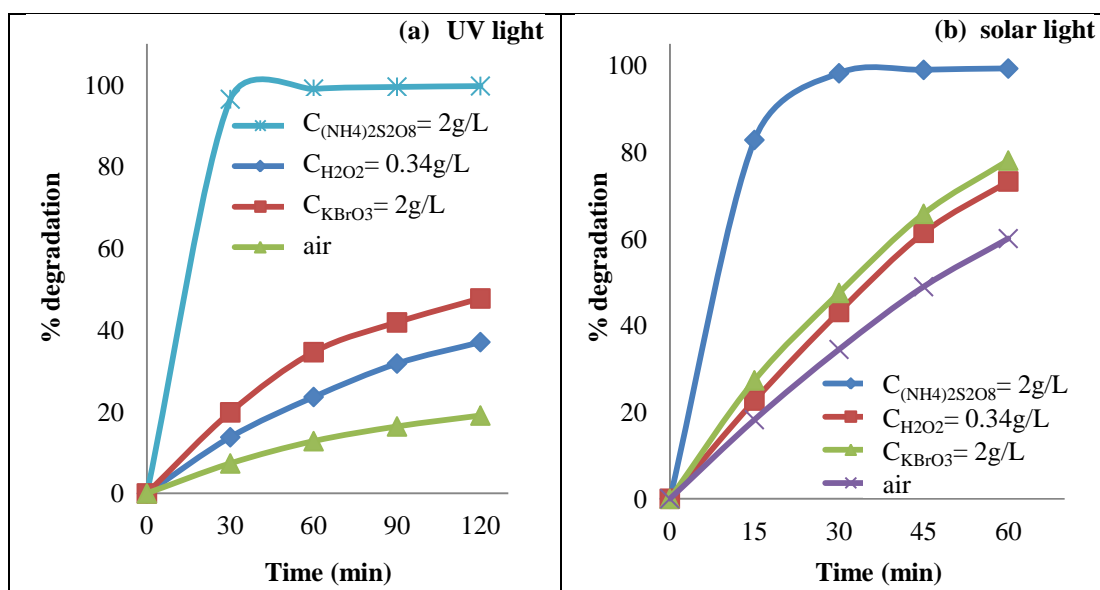
Figure 4.42 Time course variation of comparison of different oxidants at their optimum concentrations for the photocatalytic degradation of AY-17 under a) UV light: Catalyst loading=3 g/L; b) solar light: Catalyst loading=1 g/L. Conditions: pH=3; C_0=100 mg/L.
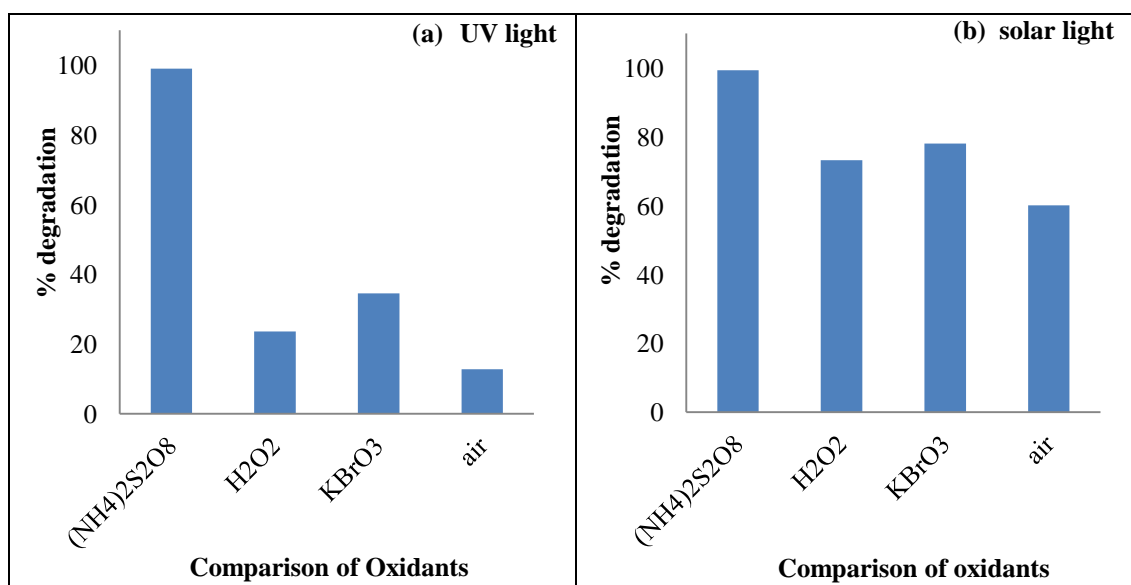
Figure 4.43 Comparison of different oxidants (at their optimum concentrations) in terms of percentage degradation of AY-17 under a) UV light: Catalyst loading=3 g/L b) solar light: Catalyst loading=1 g/L. Conditions: $(NH_4)_2S_2O_8$= 2 g/L; H_2O_2= 10 mM (0.34g/L); $KBrO_3$= 2 g/L; pH=3; C_0=100 mg/L; Irradiation time= 60 min.

4.6.4.2 Effect of oxidants on photocatalytic degradation of RB-220 dye

(i) Effect of addition of H_2O_2 as an oxidant on UV and solar photocatalysis of RB-220

To study the effect of addition of H_2O_2 as an oxidant for photocatalytic degradation of RB-220 dye, hydrogen peroxide in concentration range of 10-40 mM, was added to the dye solution of 100 mg/L concentration, with initial pH of 3 and batch experiments were conducted under UV light and solar light irradiation. In case of UV photocatalysis, catalyst loading of 2 g/L and for solar photocatalysis, catalyst loading of 1 g/L was used. This has provided dye to catalyst ratio of 1:20 and 1:10 for UV and solar photocatalysis respectively. The experiments with H_2O_2 addition were conducted in the absence of air supply. The time course variations of RB-220 dye concentrations obtained with different concentrations of H_2O_2 are presented in Table 4.35-4.36 respectively for UV and solar photocatalysis.

Figure 4.44a presents the time course variation of percentage degradation of RB-220 with H_2O_2 as an oxidant for photocatalysis under UV light. Figure 4.45a shows the comparison of the percentage degradation (after 30 min irradiation) achieved by using air as the oxidant, with that achieved by using H_2O_2 at different concentrations as the oxidant. The results show that the percentage degradation achieved by photocatalysis aided by H_2O_2 as an oxidant was higher (68.17 %) than that achieved with air (22.54 %) as the oxidant. Further, as the concentration of H_2O_2 increased from 10 to 20 mM, degradation increased from 68.17 to 77.75 %, but further increase in H_2O_2 concentration to greater than 20 mM lead to decrease in degradation, which reached to about 61.69 % at 40 mM. The rate of degradation of RB-220 was the highest when 20 mM H_2O_2 was added as compared to addition of H_2O_2 at other concentrations. Almost 100 % degradation occurred in 180 min with 20 mM H_2O_2, whereas with other concentrations of H_2O_2, complete degradation could not be achieved in 180 min. So 20 mM H_2O_2 was found to be the optimum for the photocatalytic degradation of RB-220 under UV light irradiation.

Similar experiments were conducted using hydrogen peroxide in concentration range of 10-40 mM as oxidant for solar photocatalysis of the dye solution of 100

mg/L concentration with catalyst loading of 1 g/L and with initial pH of 3. Figure 4.44b presents the time course variation of percentage degradation of RB-220 by solar photocatalysis with H_2O_2 as oxidant. The percentage degradation (after 30 min irradiation time) achieved by using H_2O_2 as an oxidant at different concentrations are shown in Figure 4.45b. The results show that the percentage degradation achieved with H_2O_2 as an oxidant is higher than that achieved without the addition of H_2O_2. Further it is observed , with the increase in concentration of H_2O_2 from 10-20 mM, degradation increased from 81.06 % to 90 %, but further increase in H_2O_2 concentration to greater than 20 mM lead to decrease in degradation, reaching about 65.63 % at 40 mM. As observed in Figure 4.44b, the rate of degradation of RB-220 is the highest with 20 mM H_2O_2 addition, as compared to addition of H_2O_2 at other concentrations. With the addition of 20 mM H_2O_2, almost 100 % degradation occurred within 45 min, but with other concentrations of H_2O_2, it took more than 90 min to achieve the similar degradation. So 20 mM H_2O_2 is the optimum for the photocatalytic degradation of RB-220 under solar light irradiation.

The increase in degradation by addition of H_2O_2 upto 20 mM is due to increase in the   hydroxyl radical concentration as explained in Section 4.6.4.1. But at high H_2O_2 concentration of above 20 mM, the percentage degradation decreased with increase in H_2O_2 concentration and the reason for the same is already discussed in Section 4.6.4.1(i).

In the present study, maximum dye degradation and faster rate of degradation occurred with the addition of 20 mM (0.68 g/L) H_2O_2. Hence, 20 mM H_2O_2 was found to be the optimum concentration for photocatalytic degradation of RB-220 using $Ag@TiO_2$ core shell structured nanoparticles under UV and solar light irradiation.

Table 4.35 Time course variation of concentration of RB-220 obtained with different initial concentration of H_2O_2 during UV photocatalysis. Conditions: Dye to catalyst ratio=1:20 (g/g), pH=3, C_0= 100 mg/L.

Time (min)	C_{RB-220} (mg/L) with air as oxidant source	C_{RB-220} (mg/L) obtained with different initial concentration of H_2O_2			
		$C_{H2O2=10mM}$	$C_{H2O2=20mM}$	$C_{H2O2=30mM}$	$C_{H2O2=40mM}$
0	100	100	100	100	100
30	77.46	31.83	22.25	31.62	38.31
60	67.68	26.13	12.54	25.07	33.45
90	59.41	20.63	4.51	16.97	27.04
120	53.87	12.96	2.96	13.03	18.38
150	47.96	6.76	0.99	7.32	13.24
180	41.69	3.73	0.14	6.13	8.80

Table 4.36 Time course variation of concentration of RB-220 obtained with different initial concentration of H_2O_2 during solar photocatalysis. Conditions: Dye to catalyst ratio=1:10 (g/g), pH=3, C_0= 100 mg/L.

Time (min)	C_{RB-220} (mg/L) with air as oxidant source	C_{RB-220} (mg/L) obtained with different initial concentration of H_2O_2			
		$C_{H2O2=10mM}$	$C_{H2O2=20mM}$	$C_{H2O2=30mM}$	$C_{H2O2=40mM}$
0	100	100	100	100	100
15	45.70	35.77	28.94	48.31	56.83
30	31.34	18.94	10	27.25	34.37
45	17.46	8.10	0.42	13.03	19.65
60	10.28	4.51	0.14	8.94	13.52
90	2.39	0.70	0.14	4.51	6.55
120	0.63	0.28	0.14	1.48	3.94
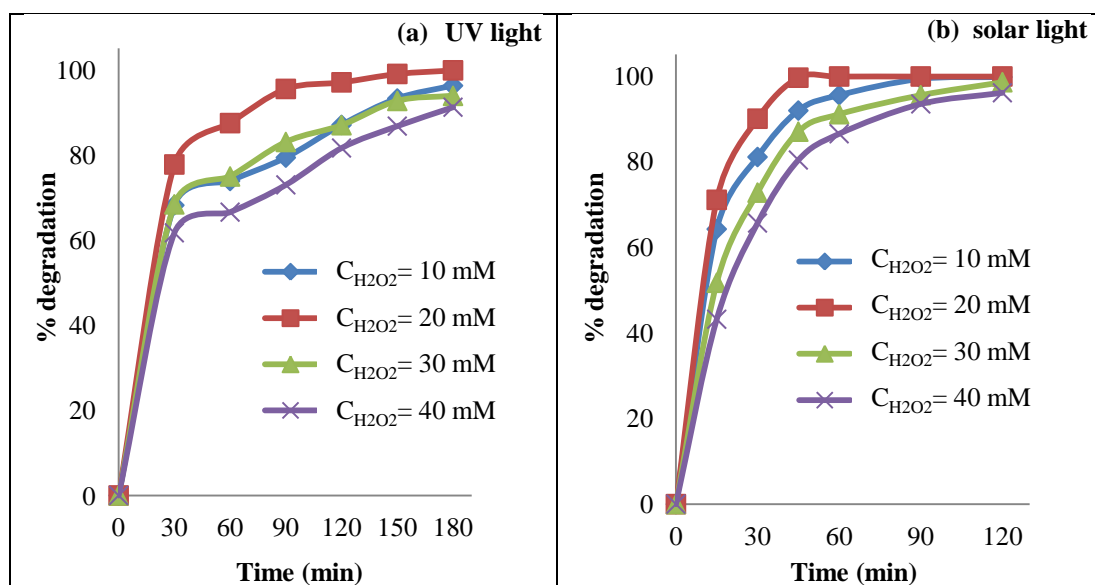
Figure 4.44 Effect of H$_2$O$_2$ addition on time course variation of photocatalytic degradation of RB-220 under a) UV light: Dye to catalyst ratio=1:20 (g/g) b) solar light: Dye to catalyst ratio=1:10 (g/g); average UV and visible light intensity of solar light = 3.56 mW/cm^2 and 1210×100 lux respectively from 11 a.m. to 1 p.m. Conditions: pH=3; C$_0$= 100 mg/L.
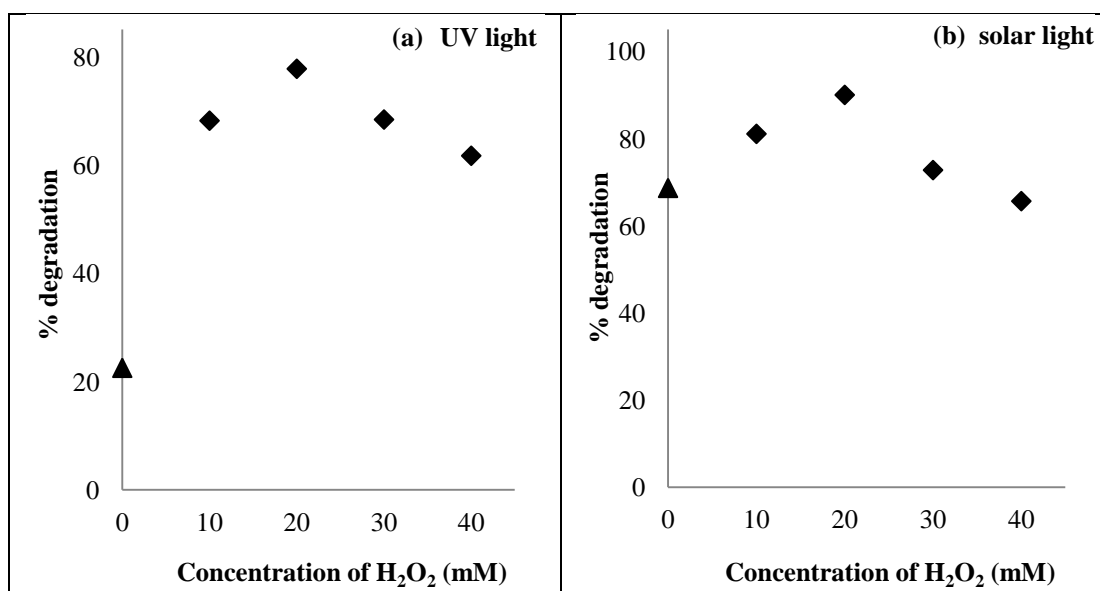
Figure 4.45 Effect of addition of H$_2$O$_2$ on photocatalysis of RB-220 dye under a) UV light: ◆ H$_2$O$_2$ as the oxidant; ▲ supplied air as the source of oxidant; dye to catalyst ratio= 1:20; b) solar light: ◆ H$_2$O$_2$ as the oxidant ▲ atmospheric air as the source of oxidant; dye to catalyst ratio= 1:10. Conditions: pH=3; C$_0$=100 mg/L; Irradiation time =30 min.

(ii) Effect of addition of ammonium persulphate [$(NH_4)_2S_2O_8$] as an oxidant on UV and solar photocatalysis of RB-220

Effect of addition of $(NH_4)_2S_2O_8$ as an oxidant was studied with RB-220 dye solution of 100 mg/L concentration and with initial pH = 3, by varying the concentration of $(NH_4)_2S_2O_8$ from 1 to 2.5 g/L for the photocatalytic degradation of RB-220 under UV and solar light irradiation. In case of UV light experiments, catalyst loading of 2 g/L and for solar light experiments, catalyst loading of 1 g/L was used. The dye to catalyst ratio was hence maintained at 1:20 for UV and 1:10 for solar experiments. The experiments with $(NH_4)_2S_2O_8$ addition were conducted in the absence of air supply. The time course variations of RB-220 dye concentrations obtained with different concentrations of $(NH_4)_2S_2O_8$ are presented in Table 4.37 and 4.38 respectively for UV and solar photocatalysis.

Figure 4.46a presents the time course variation of percentage degradation of RB-220 under UV light, with addition of $(NH_4)_2S_2O_8$. Almost 100 % degradation of RB-220 occurred in 30 min with the addition of 1.5 g/L of $(NH_4)_2S_2O_8$, but to achieve similar degradations more than 60 min were required with other concentrations of $(NH_4)_2S_2O_8$. The effect of addition of $(NH_4)_2S_2O_8$ (1-2.5 g/L) on photocatalytic degradation of the dye after 30 min irradiation time is shown in Figure 4.47a. Results show that higher percentage degradation of the dye could be achieved with $(NH_4)_2S_2O_8$ as the oxidant, as compared to air as the oxidant. The rate of degradation has increased tremendously on the addition of $(NH_4)_2S_2O_8$. 88.45 % degradation was achieved with $(NH_4)_2S_2O_8$, whereas only around 22.54 % degradation was achieved with air as the oxidant. As the concentration of $(NH_4)_2S_2O_8$ increased from 1 to 1.5 g/L, degradation (after 30 min of irradiation time) has increased from 88.45 to 99.01 %. Further increase in its concentration from 2 to 2.5 g/L resulted in decrease in dye degradation from 83.94% to 76.83 %. As observed from Figure 4.46a, the addition of 1.5 g/L $(NH_4)_2S_2O_8$ resulted in maximum degradation of the dye and hence 1.5 g/L $(NH_4)_2S_2O_8$ is the optimum for the photocatalytic degradation of RB-220 under UV light, owing to achievement of maximum degradation of the dye.

Similar experiments were conducted using $(NH_4)_2S_2O_8$ in concentration range of 1 to 2.5 g/L as the oxidant with dye solution of 100 mg/L concentration and

catalyst loading of 1 g/L with initial pH of 3 under solar light irradiation. Figure 4.46b presents the time course variation of percentage degradation of RB-220 with addition of $(NH_4)_2S_2O_8$ during solar photocatalysis. Almost 100 % degradation of RB-220 occurred in 15 min with the addition of 1.5 g/L of $(NH_4)_2S_2O_8$, but to achieve similar degradations more than 30 min were required with other concentrations of $(NH_4)_2S_2O_8$. The effect of addition of $(NH_4)_2S_2O_8$ (1-2.5 g/L) on photocatalytic degradation of the dye after 30 min irradiation time is shown in Figure 4.47b. Results show that higher dye degradation could be achieved on addition of $(NH_4)_2S_2O_8$, as compared to that without its addition. The rate of degradation has increased tremendously on the addition of $(NH_4)_2S_2O_8$. 99.72 % degradation was achieved with $(NH_4)_2S_2O_8$, whereas only around 68.66 % degradation was achieved in the absence of $(NH_4)_2S_2O_8$. As the concentration of $(NH_4)_2S_2O_8$ increased from 1 to1.5 g/L, degradation of RB-220 (after 30 min of irradiation time) increased from 99.72 to 99.79 %. Further increase in its concentration to 2 g/L and above has resulted in decrease in degradation. As observed from Figure 4.47b, 1.5 g/L $(NH_4)_2S_2O_8$ is the optimum for the photocatalytic degradation of RB-220 under solar light. The reasons for increase in degradation in the presence of persulphate ion have been discussed previously in Section 4.6.4.1.

At a high concentration of persulphate, excess of sulphate radical anion (SO_4^{2-}) may get adsorbed on Ag@TiO$_2$ surface and deactivate a section of catalyst leading to decreased dye degradation as explained in Section 4.6.4.1. As high rate and almost complete degradation of RB-220 was observed with 1.5 g/L of $(NH_4)_2S_2O_8$, it may be considered as the optimum for UV and solar photocatalysis of RB-220.

Table 4.37 Time course variation of concentration of RB-220 obtained with different initial concentration of $(NH_4)_2S_2O_8$ during UV photocatalysis. Conditions: Dye to catalyst ratio=1:20 (g/g), pH=3, C_0= 100 mg/L.

Time (min)	C_{RB-220} (mg/L) with air as oxidant source	C_{RB-220} (mg/L) obtained with different initial concentration of $(NH_4)_2S_2O_8$			
		$C_{(NH4)2S2O8}$ = 1 g/L	$C_{(NH4)2S2O8}$ 1.5 g/L	$C_{(NH4)2S2O8}$ = 2 g/L	$C_{(NH4)2S2O8}$ 2.5 g/L
0	100	100	100	100	100
10	91.63	33.17	24.30	36.83	45
20	83.72	22.68	15.63	28.45	33.94
30	77.46	11.55	0.99	16.06	23.17
40	73.24	6.27	0.35	12.32	15.85
50	70.36	2.82	0.14	6.48	8.24
60	67.68	0.70	0.14	4.15	6.27

Table 4.38 Time course variation of concentration of RB-220 obtained with different initial concentration of $(NH_4)_2S_2O_8$ during solar photocatalysis. Conditions: Dye to catalyst ratio=1:10 (g/g), pH=3, C_0= 100 mg/L.

Time (min)	C_{RB220} (mg/L) with air as oxidant source	C_{RB-220} (mg/L) obtained with different initial concentration of $(NH_4)_2S_2O_8$			
		$C_{(NH4)2S2O8}$ 1 g/L	$C_{(NH4)2S2O8}$ 1.5 g/L	$C_{(NH4)2S2O8}$ = 2 g/L	$C_{(NH4)2S2O8}$ 2.5 g/L
0	100	100	100	100	100
5	80.41	34.37	25.07	36.27	43.87
10	62.36	24.30	13.24	27.61	33.66
15	45.70	13.17	0.99	16.55	23.73
20	39.47	4.72	0.35	10.42	14.93
25	34.79	1.41	0.21	5.99	7.18
30	31.34	0.28	0.21	3.31	5.28
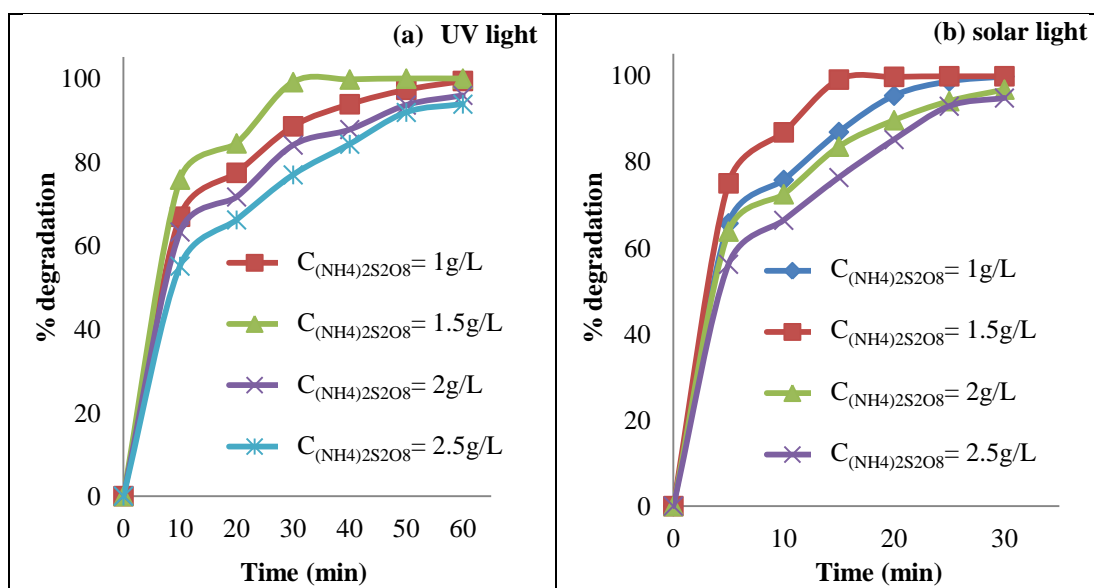
Figure 4.46 Effect of (NH$_4$)$_2$S$_2$O$_8$ addition on time course variation of photocatalytic degradation of RB-220 dye under a) UV light: Dye to catalyst ratio=1:20 (g/g); b) solar light: Dye to catalyst ratio=1:10 (g/g); average UV and visible light intensity of solar light = 3.55 mW/cm^2 and 1202×100 lux respectively from 11 to 11.30 a.m. Conditions: pH=3; C$_0$= 100 mg/L.
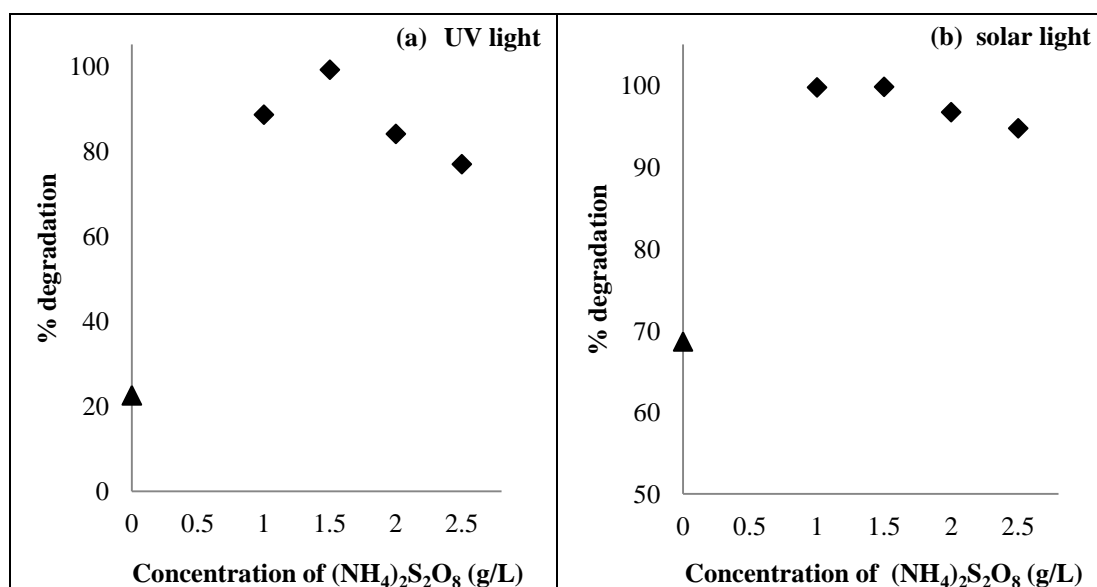
Figure 4.47 Effect of addition of (NH$_4$)$_2$S$_2$O$_8$ on the photocatalysis of RB-220dye under; a) UV light:◆(NH$_4$)$_2$S$_2$O$_8$ as the oxidant; ▲supplied air as the source of oxidant; dye to catalyst ratio= 1:20; b) solar light:◆(NH$_4$)$_2$S$_2$O$_8$ as the oxidant;▲ atmospheric air as the source of oxidant; dye to catalyst ratio= 1:10. Conditions: pH=3; C$_0$=100 mg/L; Irradiation time =30 min.

(iii) Effect of addition of KBrO$_3$ as an oxidant on UV and solar photocatalysis of RB-220

Effect of addition of KBrO$_3$ as an oxidant for photocatalytic degradation of RB-220 was studied with the dye solution of 100 mg/L concentration and with initial pH = 3, by varying the concentration of KBrO$_3$ from 2 to 6 g/L under UV light and 1 to 4 g/L under solar light irradiation. In case of UV photocatalysis, catalyst loading of 2 g/L and in solar photocatalysis, catalyst loading of 1 g/L was used. The time course variations of RB-220 dye concentrations obtained with different concentrations of KBrO$_3$ are presented in Table 4.39-4.40 respectively, for UV and solar photocatalysis.

Figure 4.48a presents the effect of addition of KBrO$_3$ on the time course variation of percentage degradation of RB-220. 100 % degradation could not be achieved with the addition of KBrO$_3$ at any concentrations, even after 180 min irradiation time. The effect of addition of KBrO$_3$ (2-6 g/L) on photocatalytic degradation of RB-220 after 30 min irradiation time is shown in Figure 4.49a. Figure 4.49a also shows the data point indicating the percentage degradation achieved after 30 min, with air as the oxidant. As observed from Figure 4.49a, the addition of KBrO$_3$ leads to higher degradation of the dye, as compared to that with air as an oxidant. As the concentration of KBrO$_3$ increased from 2 to 4 g/L, degradation (after 30 min of irradiation time) has increased from 26.9 to 34.51 %, but further increase in concentration of KBrO$_3$ from 4 to 6 g/L, has decreased the degradation to around 8.45 %. So, 4 g/L of KBrO$_3$ was found to be the optimum for the photocatalytic degradation of RB-220 under UV light irradiation.

Similar experiments were conducted using KBrO$_3$ as an oxidant in concentration range of 1-4 g/L for photocatalysis of RB-220 dye solution of 100 mg/L concentration with catalyst loading of 1 g/L and with initial pH of 3 under solar light. Figure 4.48b presents the time course variation of percentage degradation of RB-220 with addition of KBrO$_3$ under solar light irradiation. Almost complete degradation could be achieved in 45 min irradiation time when 2 g/L of KBrO$_3$ was added. But with the addition of KBrO$_3$ in other concentrations, irradiation for 60 min or higher was required, depending on the concentration of KBrO$_3$ added. The effect of addition of KBrO$_3$ (1-4 g/L) on photocatalytic degradation of RB-220 after 30 min irradiation

time is shown in Figure 4.49b. It can be observed from Figure 4.49b, addition of $KBrO_3$ lead to higher degradation of dye. As the concentration of $KBrO_3$ increased from 1 to 2 g/L, degradation (at 30 min of irradiation time) has increased from 78.94 to 87.04 %, but further increase in concentration of $KBrO_3$ from 2 to 4 g/L, decreased the degradation from 58.38 to 38.10 %. So 2 g/L of $KBrO_3$ was found to be optimum for the photocatalytic degradation of RB-220 under solar light irradiation.

The increase of the degradation rate by the addition of $KBrO_3$ upto 2 g/L is due to its electron scavenging effect as explained in Section 4.6.4.1. The decrease in the degradation rate at higher concentrations of $KBrO_3$ may be due to the adsorption of Br^- ion on $Ag@TiO_2$ surface as mentioned previously in Section 4.6.4.1.

In the present study, in case of UV photocatalysis maximum dye degradation occurred with the addition of 4 g/L $KBrO_3$ and in case of solar photocatalysis, maximum dye degradation oc curred with the addition of 2 g/L $KBrO_3$. Hence 4 g/L and 2 g/L $KBrO_3$ concentrations were found to be the optimum for photocatalytic degradation of RB-220 using $Ag@TiO_2$ core shell structured nanoparticles under UV and solar light irradiation respectively.

Table 4.39 Time course variation of concentration of RB-220 obtained with different initial concentration of $KBrO_3$ during UV photocatalysis. Conditions: Dye to catalyst ratio=1:20 (g/g); pH=3; C_0=100 mg/L.

Time (min)	C_{RB-220} (mg/L) with air as oxidant source	C_{RB-220} (mg/L) obtained with different initial concentrations of $KBrO_3$		
		$C_{KBrO3= 2 g/L}$	$C_{KBrO3= 4 g/L}$	$C_{KBrO3= 6 g/L}$
0	100	100	100	100
30	77.46	73.10	65.49	91.55
60	67.68	61.48	49.27	87.04
90	59.41	50.56	37.49	83.87
120	53.87	41.06	26.06	80.70
150	47.96	35.63	19.65	76.69
180	41.69	31.06	14.93	71.65

Table 4.40 Time course variation of concentration of RB-220 obtained with different initial concentration of KBrO$_3$ during solar photocatalysis. Conditions: Dye to catalyst ratio=1:10 (g/g); pH=3; C$_0$=100 mg/L.

Time (min)	C$_{RB220}$ (mg/L) with air as oxidant source	C$_{RB-220}$ (mg/L) obtained with different initial concentration of KBrO$_3$			
		C$_{KBrO3= 1 g/L}$	C$_{KBrO3= 2 g/L}$	C$_{KBrO3= 3 g/L}$	C$_{KBrO3= 4 g/L}$
0	100	100	100	100	100
15	45.70	49.15	36.20	70.42	86.20
30	31.34	21.06	12.96	41.62	61.90
45	17.46	2.96	0.21	13.73	34.08
60	10.28	1.41	0.21	4.37	16.55
90	2.39	1.13	0.21	2.25	7.96
120	0.63	0.85	0.21	1.27	3.59
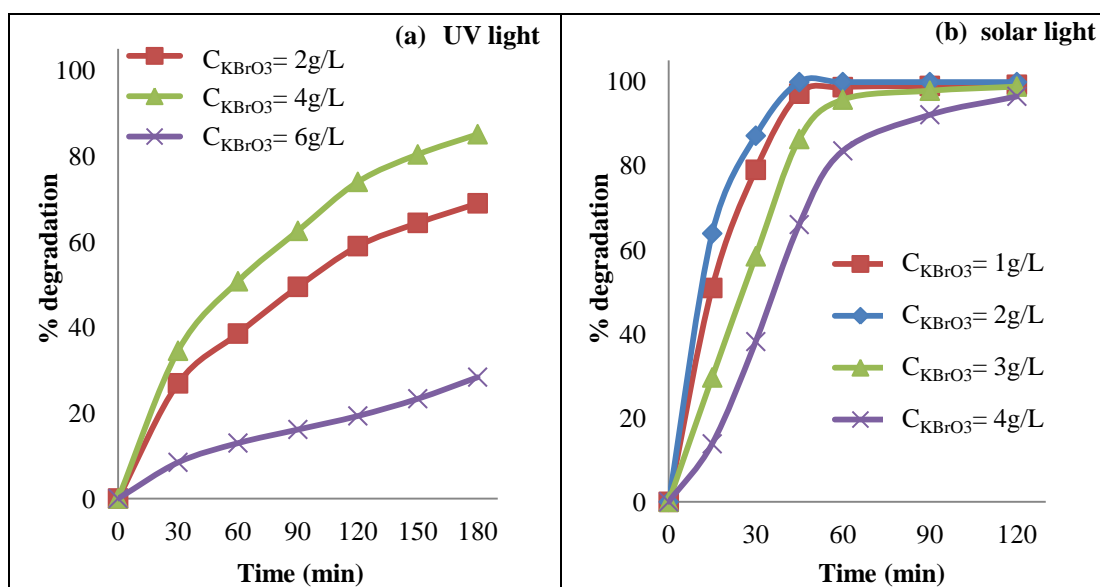
Figure 4.48 Effect of KBrO$_3$ addition on time course variation of photocatalytic degradation of RB-220 dye under a) UV light: Dye to catalyst ratio=1:20 (g/g); b) solar light: Dye to catalyst ratio=1:10 (g/g); average UV and visible light intensity of solar light = 3.53 mW/cm^2 and 1202×100 lux respectively from 11 a.m. to 1 p.m. Conditions: pH=3; C$_0$= 100 mg/L.
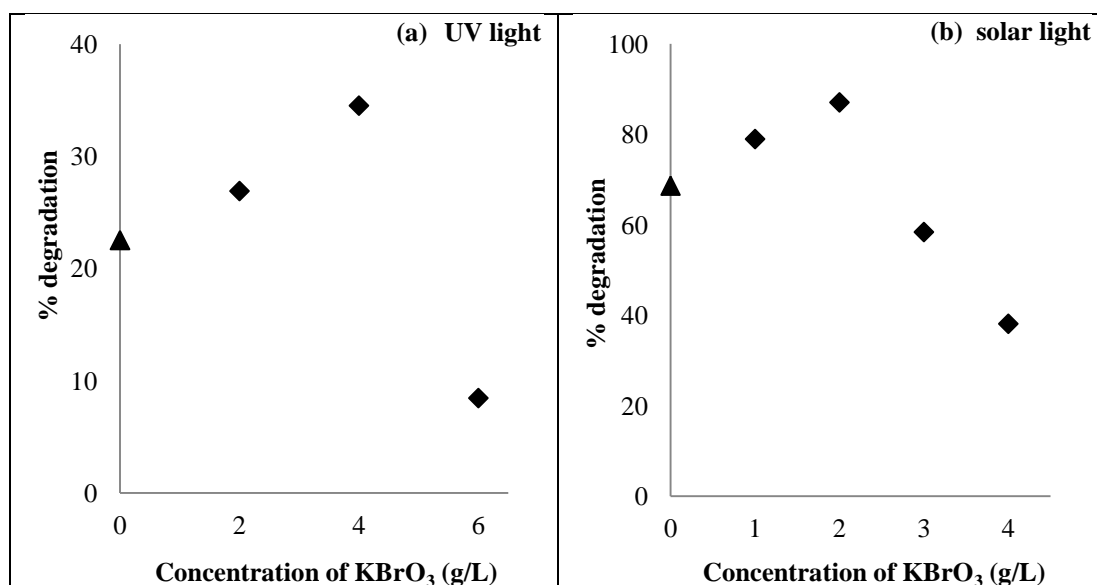
Figure 4.49 Effect of addition of KBrO$_3$ on the photocatalysis of RB-220 dye under; a) UV light: ◆KBrO$_3$ as the oxidant; ▲ supplied air as the source of oxidant; dye to catalyst ratio= 1:20; b) solar light: ◆KBrO$_3$ as the oxidant;▲ atmospheric air as the source of oxidant; dye to catalyst ratio= 1:10. Conditions: pH=3; C$_0$=100 mg/L; Irradiation time =30 min.

(iv) Comparison of the effect of oxidants for UV and solar photocatalysis of RB-220

It is evident from the results on effect of oxidants discussed in previous part Section 4.6.4.2 that, the optimum concentration of oxidants for UV photocatalysis of RB-220 dye are 20 mM (0.68 g/L) of H$_2$O$_2$, 1.5 g/L of (NH$_4$)$_2$S$_2$O$_8$ and 4 g/L of KBrO$_3$ and for solar photocatalysis *viz.* 20 mM (0.68 g/L) of H$_2$O$_2$, 1.5 g/L of (NH$_4$)$_2$S$_2$O$_8$ and 2 g/L of KBrO$_3$ when these compounds are used as oxidants. Figure 4.50 shows the time course variation of percentage degradation of RB-220 dye with different oxidants at their optimum concentrations obtained by UV and solar photocatalysis. The rate of photocatalysis is the maximum when (NH$_4$)$_2$S$_2$O$_8$ was used as the oxidant and was the least when air was used as a source of oxygen as oxidant, as is evident from the slopes of time course plots. Rate of degradation and maximum degradation are lower with H$_2$O$_2$ and KBrO$_3$ as compared to (NH$_4$)$_2$S$_2$O$_8$. When air was used as the oxidant under UV light, only around 22.54 %, 32.32 % and 46.13 % of degradation of dye could be achieved after 30, 60 or 120 min, respectively, indicating the least rate of reaction as

compared to photocatalysis with other oxidants. In case of solar light, when atmospheric air was used as the oxidant source, only around 54.30 %, 68.66 % and 89.71 % of degradation of dye could be achieved after 15, 30 or 60 min, respectively, indicating the least rate of reaction as compared to photocatalysis with other oxidants. Figure 4.51 shows the comparison of different oxidants in UV and solar photocatalysis of RB-220. $(NH_4)_2S_2O_8$ is a very effective oxidant as compared to others used in this study. Maximum degradation of almost around 100 % was achieved within 30 min in case of UV light and 15 min in case of solar light, when $(NH_4)_2S_2O_8$ was used as the oxidant at an optimum concentration of 1.5 g/L. Percentage degradations achieved with optimum concentration of H_2O_2 (20 mM) and $KBrO_3$ (4 g/L) as oxidants were only around 77.75 % and 34.51 % respectively after 30 min of irradiation time under UV light. In solar light, percentage degradations achieved with optimum concentration of H_2O_2 (20 mM) and $KBrO_3$ (2 g/L) as oxidants were only around 71.06 % and 63.80 % respectively after 15 min of irradiation time. Although the optimum concentration of H_2O_2 (20 mM or 680 mg/L) is much lower than that for $(NH_4)_2S_2O_8$, the rate of reaction is very slow with H_2O_2. The order of activity of oxidants is $(NH_4)_2S_2O_8 > H_2O_2 > KBrO_3 >$ air under UV and solar light. The difference in their activities is due to the differences in the absorption of light as discussed in Section 4.6.4.1. Experimental observations showed that $(NH_4)_2S_2O_8$ may increase the release of stored electrons from Ag core and also lead to generation of sulphate radicals as explained in Section 4.6.4.1. Hence $(NH_4)_2S_2O_8$ (1.5 g/L) was found to be the best oxidant as compared to other oxidants studies here, for the photocatalytic degradation of RB-220 under UV and solar light irradiation.
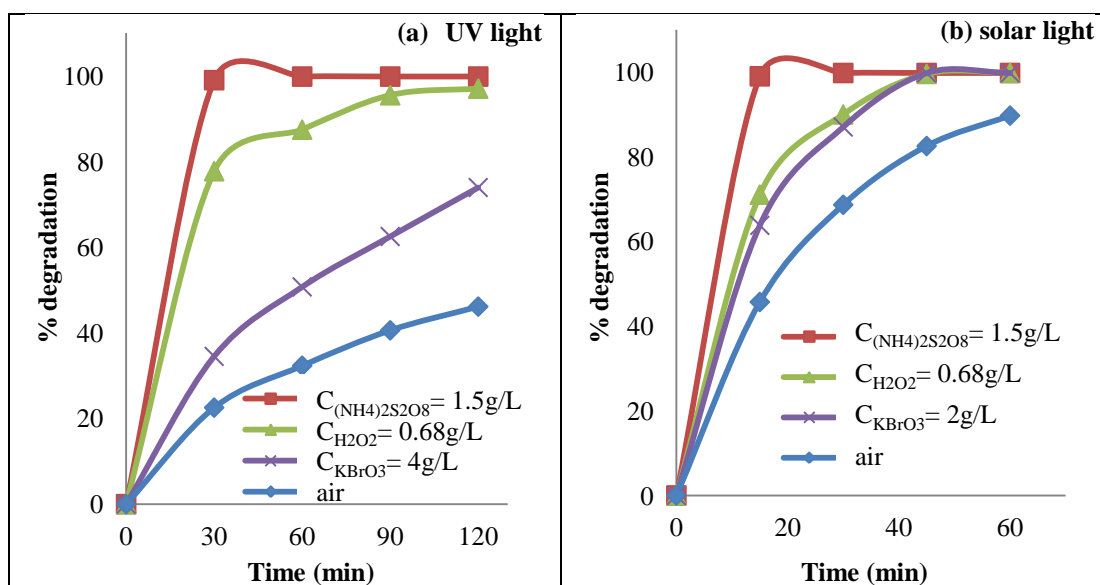
Figure 4.50 Time course variation of comparison of different oxidants at their optimum concentrations for the photocatalytic degradation of RB-220 under; a) UV light: Catalyst loading=2 g/L b) solar light: Catalyst loading=1 g/L. Conditions: pH=3; C_0=100 mg/L.
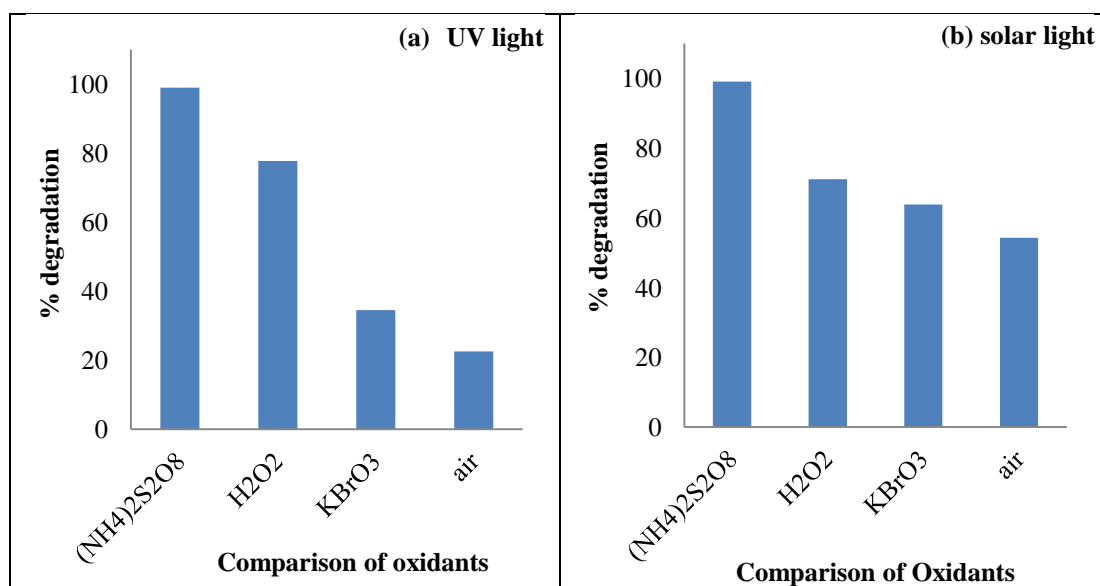
Figure 4.51 Comparison of different oxidants (at their optimum concentrations) in terms of percentage degradation of RB-220 under a) UV light: Catalyst loading=2 g/L; Irradiation time= 30 min; $(NH_4)_2S_2O_8$= 1.5 g/L; H_2O_2= 20 mM (0.68 g/L); $KBrO_3$= 4 g/L b) solar light: Catalyst loading=1 g/L; Irradiation time= 15 min; Conditions: $(NH_4)_2S_2O_8$= 1.5 g/L; H_2O_2= 20 mM (0.68 g/L); $KBrO_3$= 2 g/L; pH=3; C_0=100 mg/L.

4.7 Feasibility of reuse of Ag@TiO$_2$ catalyst for repeated photocatalysis of AY-17 and RB-220 dyes

In order to check for any loss of activity of the catalyst and feasibility of reuse of Ag@TiO$_2$ catalyst for repeated photocatalysis, experiments were carried out with aqueous dye solution containing 50 mg/L AY-17, catalyst loading of 1.5 g/L and at pH 3 under UV irradiation with air as an oxidant. For solar photocatalysis, AY-17 dye concentration of 100 mg/L, catalyst loading of 1 g/L and pH of 3 were used. Similarly for photocatalysis of RB-220 dye, experiments were carried out with aqueous dye solution containing 50 mg/L of RB-220 with a catalyst loading of 1 g/L, at initial pH 3 under UV irradiation, with air as an oxidant and in case of solar photocatalysis, experiments were carried out with 50 mg/L concentration of RB-220, with a catalyst loading of 500 mg/L and initial pH=3. After completion of experiment with a fresh catalyst (cycle I), the Ag@TiO$_2$ nanoparticles at the end of cycle I was collected, regenerated and then utilized for the next set of experiments. So Ag@TiO$_2$ was reused thrice and totally four experiments were done for each dye, out of which the first cycle was with the fresh catalyst and the remaining three cycles were with the recycled catalyst. Similar experimental conditions were used for all the four cycles. The method for regeneration of catalyst for the next cycle is presented in Section 3.8.1.

The % degradation of AY-17 by UV and solar photocatalysis after 360 min of irradiation, using fresh catalyst particles (Cycle I), particles of single prior use (Cycle II), particles of two prior uses (Cycle III), and particles of three prior uses (Cycle IV) are presented in Table 4.41. After three cycles of reuse, decrease in photocatalytic activity from around 85.36 to 81.50 % was observed under UV light irradiation and from 96.90 to 93.35 % under solar light irradiation. The reduction in activity was found to be only around 5 % by UV photocatalysis and 3 % in case of solar photocatalysis after three cycles of reuse in terms of the degradation of AY-17.

The % degradation of RB-220 using fresh particles (Cycle I), particles of single prior use (Cycle II), particles of two prior uses (Cycle III), and particles of three prior uses (Cycle IV) after 240 min of irradiation for UV and 60 min of irradiation for solar photocatalysis are given in Table 4.42. After three cycles of reuse,

decrease in photocatalytic activity from around 98.92 to 96.36 % was observed under UV light irradiation (240 min) and from 99.02 to 97.14 % under solar light irradiation (60 min). The reduction in activity in terms of RB-220 degradation was found to be less than 4 % by UV photocatalysis and less than 2 % by solar photocatalysis after three cycles of reuse. So it can be concluded that Ag@TiO$_2$ can be recycled without much decline in activity and can be used for the photocatalysis of dyes using UV and solar irradiation. So it can be concluded that Ag@TiO$_2$ can be recycled without much decline in activity.

Table 4.41 Effect of catalyst recycling on percentage degradation of AY-17 dye under UV light: pH=3; Ag@TiO$_2$ loading= 1.5 g/L; C$_0$= 50 mg/L; solar light: pH=3; Ag@TiO$_2$ loading= 1 g/L; C$_0$= 100 mg/L.

Cycle number	UV light	solar light
	% degradation of AY-17 after 360 min	% degradation of AY-17 after 360 min
Fresh (I)	85.36	96.90
II	84.22	95.72
III	82.68	94.64
IV	81.50	93.35

Table 4.42 Effect of catalyst recycling on percentage degradation of RB-220 dye under UV light: pH=3; Ag@TiO$_2$ loading= 1 g/L; C$_0$= 50 mg/L; solar light: pH=3; Ag@TiO$_2$ loading= 500 mg/L; C$_0$= 50 mg/L.

Cycle number	UV light	solar light
	% degradation of RB-220 after 240 min	% degradation of RB-220 after 60 min
Fresh (I)	98.92	99.02
II	98.09	98.47
III	97.11	98.02
IV	96.36	97.14

4.8 Optimization of parameters for AY-17 and RB-220 dye degradation by photocatalysis using Ag@TiO₂ under UV and solar light irradiation using Response surface methodology (RSM) based on Central Composite Design (CCD)

The most common goals for optimization of dye degradation process are, minimizing the cost (Fu et al. 2007). This will eliminate the blind usage of unnecessary components and therefore ease the process and thereby reduce the cost of the process. Most important of all these is that, optimization will enhance the efficiency of the process by increasing the rate. It was reported that the complexities and uncertainties associated with large-scale processes usually come from a lack of knowledge of the sophisticated interactions among various factors affecting the process (Liu et al. 2005b). Unfortunately, classical 'one factor at a time' method for optimization frequently fails to locate the region of optimum response because the joint effects of factors on the response are not taken into account in such approach. These approaches are also time consuming and require many a number of experiments to determine optimum levels, which may be unreliable. These limitations of a classical method can be eliminated by optimizing all the process parameters collectively by Response Surface Methodology (RSM) using statistical experimental design. In the current study, once the variables having the greatest influence on the AY-17 and RB-220 dye degradation were identified based on literature, classical 'one factor at a time" method was followed as discussed in Section 4.6.1 to 4.6.4 to determine the effects of these variables. Section 4.6.1 to 4.6.4 presented the studies on effect of different variables on photocatalytic degradation of two dyes (AY-17 and RB-220) by UV and solar photocatalysis. As pH, catalyst loading and oxidant concentration are the important factors affecting the AY-17 and RB-220 degradation by Ag@TiO₂ nanoparticles, these variables were selected as the factors for optimization of photocatalytic process under UV and solar light irradiation. The optimum conditions were selected based on "one factor at a time" analysis. But these optimum conditions were obtained by crude optimization methodology and the interaction effects among the variables were not taken into account. In order to account for interaction effect among the variables, methodical optimization is

required. So in the current study, process optimization was carried out by using Response Surface Methodology (RSM). Central Composite experimental design was used to design the experiments needed for optimization of the values of these variables (factors) by RSM, for enhancing the percentage degradation of the dyes (response). Based on the preliminary studies the best oxidant for photocatalysis and the effective range of factors (pH, catalytic loading, and oxidant concentration) to be used in the Central Composite Design was fixed for UV and solar photocatalysis of each of the two dyes.

Ammonium persulphate was chosen as the oxidant for the degradation of AY-17 and RB-220 dye both for UV and solar photocatalysis, based on discussions presented in Section 4.6.4.The main parameter affecting the photocatalytic degradation process is the initial pH of the reaction mixture. The effect of pH of reaction mixture on percentage degradation of AY-17 under UV and solar light was studied in the pH range of 1-9 as discussed in Section 4.6.1 and the results are presented in Figure 4.24 and Figure 4.25 respectively. Similarly the effect of pH on percentage degradation of RB-220 under UV light was studied in the pH range 2-7 and in case of solar light in the pH range 2-9 as discussed in Section 4.6.1 and the results is presented in Figure 4.26 and Figure 4.27 respectively. The degradation of AY-17 and RB-220 were more in acidic pH range and almost no degradation was observed in the basic pH range in case of both irradiation sources. So for methodical optimization using RSM with CCD set of experiments, pH range was chosen only in acidic range of 1 to 5.

The percentage degradation of AY-17 by UV and solar photocatalysis at different catalyst loading were carried out with the dye solution of concentration 10 mg/L as discussed in Section 4.6.2 and crude optimization resulted in 1:30 as the optimum dye to catalyst loading ratio for UV and 1:10 for solar photocatalysis, with air as the oxidant. Similarly the percentage degradation of RB-220 by UV and solar photocatalysis at different catalyst loading were carried out with the dye solution concentration of 50 mg/L as discussed in Section 4.6.2 and crude optimization resulted in 1:20 as the optimum dye to catalyst loading ratio for UV and 1:10 for solar photocatalysis, with air as the oxidant. So for methodical optimization using RSM with CCD experimental data set, the range of catalyst loading chosen for AY-17 were

0.5 to 6.5 g/L for UV and 0.3 to 3.9 g/L for solar. These ranges cover the dye to catalyst ratio of 1:5 to 1:65 for UV photocatalysis and 1:3 to 1:39 for solar photocatalysis. Similarly the range of catalyst loading for photocatalysis of RB-220 dye were 1 to 2.6 g/L for UV and 0.2 to 2.2 g/L for solar photocatalysis. These ranges cover the dye to catalyst ratio of 1:10 to 1:26 (g/g) for UV and 1:2 to 1:22 (g/g) for solar.

The effect of the next important parameter, ammonium persulphate (oxidant) concentration, on the percentage degradation of AY-17 by UV and solar photocatalysis was investigated as discussed in Section 4.6.4 and the results are presented in Figure 4.38 and Figure 4.39 respectively. Maximum rate of degradation was observed with 2 g/L of ammonium persulphate concentration under UV and solar light irradiation. Similarly the effect of ammonium persulphate concentration, on the percentage degradation of RB-220 under UV and solar light were investigated as discussed in Section 4.6.4 and the results are presented in Figure 4.46 and Figure 4.47 respectively. Maximum rate of degradation was observed with 1.5 g/L of ammonium persulphate concentration under UV and solar light irradiation. So the ammonium persulphate concentration range of 0.5 to 4.5 g/L for UV and solar photocatalysis of AY 17; 0.5 to 2.5 g/L for UV and solar photocatalysis of RB-220 were selected for CCD.

The various levels selected in this study for these factors are presented in Table 3.3 and Table 3.4 respectively for UV and solar photocatalysis of AY-17 and RB-220 dyes. For three variables with five levels, a set of 20 experiments is required as per CCD. 15 experiments are equidistant from a central experiment having the coded values (0, 0, 0) and are distributed on a sphere with a radius of 1. One Central experiment point with four replicates was also taken for high efficiency of the design. Therefore, a total of 20 experiments each, were conducted under both UV and solar light irradiation. The experimental conditions in uncoded form as per CCD for UV and solar photocatalysis of AY-17 are presented in Table 4.43 and those for RB-220 are presented in Table 4.44. Catalyst loading, oxidant concentration and the initial pH were to be optimized by RSM, using the results of experiments conducted as per Central Composite design matrix. Batch photocatalytic experiments were conducted under conditions specified by CCD and the percentage degradation of AY-17 were

obtained for each experiment at the end of irradiation time of 15 min both for UV and solar photocatalysis and are presented as responses in Table 4.43. For solar photocatalysis of AY-17 dye, average UV and visible light intensity of solar light= 3.61 mW/cm^2 and 1226×100 lux respectively from 12 a.m. to 12.15 p.m. Similarly the percentage degradation of RB-220 were obtained at the end of 20 min of irradiation for UV photocatalysis and 10 min of irradiation for solar photocatalysis for each experiment of CCD matrix conducted to optimize the RB-220 degradation process and are presented as responses in Table 4.44. For solar photocatalysis of RB-220 dye, average UV and visible light intensity of solar light= 3.63 mW/cm^2 and 1221×100 lux respectively from 12 a.m. to 12.10 p.m.

4.8.1 Process Analysis and optimization using response surface methodology (RSM)

The experimental input-output data (factors and response data) presented in Table 4.43 for UV and solar photocatalysis of AY-17; Table 4.44 for UV and solar photocatalysis of RB-220 were analyzed by response surface methodology using the software MINTAB 14. The input-output data for each case were fitted by a nonlinear regression equation (multiple regression analysis (MRA) models) of the form given in Eq.(3.7) and were used to describe the relationship between the response and predictor variables (factors).

Recalling Eq.(3.7),

$$Y = b_o + b_1 X_1 + b_2 X_2 + b_3 X_3 + b_{11} X_1^2 + b_{22} X_2^2 + b_{33} X_3^2 + b_{12} X_1 X_2 + b_{13} X_1 X_3 + b_{23} X_2 X_3 \quad (3.7)$$

The regression coefficients were obtained. Table 4.45 shows the MRA models in uncoded form for UV and solar photocatalysis of AY-17 and RB-220. Statistical testing of the regression models was done in the form of analysis of variance (ANOVA) on the coded equation, to test the significance and adequacy of the model. The results of ANOVA on the MRA models for AY-17 and RB-220 are presented in Table 4.46 for UV and solar photocatalysis. The P values are used as a tool to check the significance of each of the coefficients, which, in turn, may indicate the pattern of interactions between the variables. The smaller the P value for a given term in the

model (generally less than 0.05), indicates that the null hypothesis can be rejected and the term is significant in the model. In this work, the ANOVA of the regression model demonstrates that the model is highly significant, as is evident from the calculated F value with a very low P values ($P < 0.05$) for linear, quadratic and combined effects of factors and for regression. Hence, the regression models given in Eq.(3.7) with the corresponding regression coefficient values as shown in Table 4.45 for UV and solar photocatalysis of AY-17 and RB-220 dyes are the good prediction of the experimental results.

The goodness of fit of the models was verified by the determination coefficient (R^2) and the values of the adjusted determination coefficient (*Adj R^2*). It is also the proportion of the variability in the response variables, which is accounted for by the regression analysis. Table 4.46 shows the R^2 and adj R^2 values for the MRA models representing the degradation of AY-17 and RB-220 dyes under UV and solar light irradiation. Table 4.43 to Table 4.44 also show the model predicted responses of AY-17 and RB-220 dye degradation by UV and solar photocatalysis respectively. The observed values are the experimentally obtained values and the predicted values were calculated based on the respective model equation. Figure 4.60 and Figure 4.61 show the plot of model predicted vs. experimentally determined values of % degradation of AY-17 and RB-220 under UV and solar light irradiation with the R^2 values. The R^2 values being greater than 0.99 for both the dyes (AY-17 and RB-220) in both cases of UV and solar photocatalysis, indicate the goodness of fit for the models to represent the experimental data and hence these models are accurate enough for the prediction of % degradation at the given set of predictor variables for UV and solar photocatalysis.

The MRA models were subjected to optimization using *"Response optimizer"* of MINITAB 14, so as to obtain the optimum values of the variables (factors) which maximize the dye degradation. The optimum values of the variables for degradation of AY-17 and RB-220 dyes by UV and solar photocatalysis are presented in Table 4.47. Batch photocatalysis experiments under UV and solar light were conducted for AY-17 and RB-220 at their corresponding RSM based methodically optimized conditions and the percentage degradation at the specified irradiation time were obtained and are presented in Table 4.47. The MRA model predicted values at these

optimum conditions are also presented in the corresponding tables. It is observed that the experimental values obtained under optimum conditions match well with the model predicted values and hence the MRA model is validated and RSM based optimization method is found to be very effective.

4.8.2 Effect of predictor variables

To understand the effect of predictor variables (factors) as individuals (main effect) and in interaction with the other predictor variables (interaction effect) on AY-17 and RB-220 dye degradation, 3D response surface plots were generated from MRA models using MINITAB 14 . Evaluating interactions is extremely important, because an interaction can magnify or cancel out main effects. At all the response surfaces, while the effects of two factors to each other were being inspected, the remaining one variable was held constant at zero (middle) level. The surface plots for % degradation of AY-17 by UV and solar photocatalysis are presented in Figure 4.52 and Figure 4.53 respectively. The surface plots for % degradation of RB-220 by UV and solar photocatalysis are presented in Figure 4.54 and Figure 4.55 respectively.

4.8.2.1. Effect of predictor variables on UV and solar photocatalysis of AY-17 dye

Figure 4.52 shows the surface plots for interaction between the variables with the response (% degradation of AY-17) for UV photocatalysis. The surface plot as observed from Figure 4.52 (i), shows the interaction of variables: pH and catalyst loading on % degradation of AY-17 by UV photocatalysis. As the pH was increased from 2 to around 3, percentage degradation increased marginally, but further increase in pH to values greater than 3, led to a sharp decrease in percentage degradation. Highly acidic pH favors the dye degradation. As the catalyst loading was increased upto a certain level, percentage degradation increased. But with further increase in catalyst loading, percentage degradation has decreased. The catalyst loading at which maximum percentage degradation occurred, has varied with the pH, which implies that pH and catalyst loading are the interacting factors in UV photocatalytic

degradation of AY-17 dye. Similar observations are made for solar photocatalysis of AY-17 dye as shown in Figure 4.53 (i), which implied the interaction effect of pH and catalyst loading in solar photocatalytic degradation of AY-17 dye. Figure 4.52 (ii), shows the interaction of variables: pH and ammonium persulphate concentration in UV photocatalysis of AY-17. The plot shows an increase in percentage dye degradation as the ammonium persulfate concentration increases to a certain level, beyond which the percentage degradation decreases. The concentration of ammonium persulphate at which maximum degradation occurs is found to decrease with the increase in pH. It indicates the interaction effect between pH and ammonium persulphate concentration on UV photocatalytic degradation of AY-17 dye. Similar observations are made in the case of solar photocatalysis of AY-17 dye, as presented in Figure 4.53 (ii), with the indication of interaction effect of pH and ammonium persulphate concentration. Figure 4.52 (iii) shows the interaction of variables: catalyst loading and ammonium persulphate concentration in UV photocatalysis of AY-17 dye. The plot shows an increase in the percentage dye degradation as the catalyst loading increases to a certain level, beyond which the percentage degradation decreases. Ammonium persulphate concentration at which maximum percentage degradation occurred has varied with the catalyst loading. Interaction between catalyst loading and ammonium persulphate concentration is significant. Similar is the case of AY-17 dye degradation under solar light, as shown in Figure 4.53 (iii), where in ammonium persulphate concentration at which maximum percentage degradation of AY-17 dye occurred has varied with the catalyst loading. Significant interaction between pH and catalyst loading; pH and oxidant concentration; catalyst loading and oxidant concentration were observed for UV and solar photocatalysis of AY-17dye.

A contour plot is a graphical representation of the relationships among three numeric variables in two dimensions. Two variables are for X and Y axes, and a third variable Z is for contour levels. The response surfaces having circular contour plots indicate that the interaction between the corresponding variables is negligible. An elliptical or saddle nature of the contour plots indicates the significance of the interactions between the corresponding variables. In the case of saddle contour plots, the optimum values are obtained at the point of intersection of lines which are formed by joining the locus (Murthy et al. 2000).

The contour plots for % degradation of AY-17 by UV and solar photocatalysis are presented in Figure 4.56 and Figure 4.57 respectively. From the contour plots shown in Figure 4.56, for % degradation of AY-17 under UV light it can be seen that the plots being elliptical indicate the significance of the interactions between the variables, catalyst loading and ammonium persulfate; pH and ammonium persulfate; pH and catalyst loading. It can be observed, each factor influenced the other. Similar observations were made in case of photocatalysis of AY-17 dye under solar light, as shown in Figure 4.57. It can be seen that each factor has an interactive influence with the other on percentage degradation.

4.8.2.2 Effect of predictor variables on UV and solar photocatalysis of RB-220 dye

Figure 4.54 and Figure 4.55 illustrate the surface plots for interaction between the variables with % degradation of RB-220 (response) for UV and solar photocatalysis respectively. Figure 4.54 shows the surface plots for interaction between variables with % degradation of RB-220 for UV photocatalysis. The surface plot as observed from Figure 4.54 (i), shows the interaction of variables: pH and catalyst loading. As the pH is increased from 2 to around 3.2, percentage degradation has increased marginally, but further increase in pH above 3.2, has led to sharp decrease in percentage degradation. Highly acidic pH favors the dye degradation. As the catalyst loading increased upto a certain level, percentage degradation has increased. But with further increase in catalyst loading, the percentage degradation has decreased. The catalyst loading at which maximum percentage degradation has occurred, varied with the pH, which implies that pH and catalyst loading are the interacting factors in UV photocatalytic degradation. Similar observations are made with solar photocatalysis as shown in Figure 4.55 (i), which implied the interaction effect of pH and catalyst loading in solar photocatalytic degradation of RB-220. Figure 4.54 (ii), shows the interaction of variables: pH and ammonium persulphate concentration. The plot shows an increase in percentage dye degradation as the ammonium persulfate concentration increases to a certain level, beyond which the percentage degradation decreases. At higher pH of around 4.2, maximum percentage

degradation of the dye occurred at low ammonium persulphate concentration. The concentration of ammonium persulphate at which maximum degradation occurs is found to decrease with the increase in pH. It indicates the interaction effect between pH and ammonium persulphate concentration on UV photocatalytic degradation of RB-220 dye. Similar observations are made in the case of solar photocatalysis, as presented in Figure 4.55 (ii), with the indication of interaction effect of pH and ammonium persulphate concentration on solar photocatalytic degradation of RB-220. Figure 4.54 (iii) shows the interaction of variables: catalyst loading and ammonium persulphate concentration on UV photocatalysis of RB-220. The plot shows increase in percentage dye degradation as the catalyst loading increases to a certain level, beyond which the percentage degradation decreases. Ammonium persulphate concentration at which maximum percentage degradation occurred has changed with the catalyst loading, indicating the interaction between catalyst loading and ammonium persulphate concentration to be considerable. Similar is the case with solar photocatalysis, as shown in Figure 4.55 (iii), wherein ammonium persulphate concentration at which maximum percentage degradation occurred has varied with the catalyst loading.

The contour plots for % degradation of RB-220 for UV and solar photocatalysis are presented in Figure 4.58 and Figure 4.59 respectively. From the contour plots for % degradation of RB-220 under UV light and solar light, it can be seen that the plots being elliptical indicate the significance of the interactions between the variables, catalyst loading and ammonium persulfate; pH and ammonium persulfate; pH and catalyst loading. Each factor interacted with the other in influencing the percentage degradation of RB-220.

Table 4.43 Experimental and model predicted percentage degradation of AY-17 (response) obtained by UV and solar photocatalysis for CCD set of experiments. Conditions: C_0=100 mg/L; Irradiation time = 15 min.

Exp No.	For UV photocatalysis					For solar photocatalysis				
	Uncoded values			Response (% degradation of AY-17)		Uncoded values			Response (% degradation of AY-17)	
	pH (X_1)	Catalyst loading (g/L) (X_2)	$C_{(NH4)2S2O8}$ (g/L) (X_3)	Experimental	Model predicted	pH (X_1)	Catalyst loading (g/L) (X_2)	$C_{(NH4)2S2O8}$ (g/L) (X_3)	Experimental	Model predicted
1	3	6.5	2.5	66.00	65.16	1.0	2.1	2.5	96.22	96.89
2	3	0.5	2.5	47.00	47.66	3.4	2.1	2.5	92.98	93.20
3	1	3.5	2.5	74.00	75.41	3.4	2.1	0.5	77.00	77.50
4	3	3.5	4.5	85.00	84.41	3.4	3.9	2.5	75.71	76.06
5	3	3.5	2.5	98.60	98.95	5.8	2.1	2.5	63.10	62.26
6	3	3.5	2.5	98.74	98.95	3.4	2.1	2.5	92.91	93.20
7	3	3.5	0.5	74.00	74.41	3.4	0.3	2.5	76.90	76.38
8	5	3.5	2.5	33.00	31.41	3.4	2.1	4.5	88.70	88.03
9	4	2.0	1.5	51.00	50.22	4.6	3.0	1.5	72.10	71.86
10	3	3.5	2.5	98.38	98.50	4.6	1.2	1.5	67.80	68.38
11	2	5.0	3.5	85.00	85.97	4.6	1.2	3.5	75.30	76.09
12	2	5.0	1.5	82.00	80.47	4.6	3.0	3.5	77.60	78.33
13	4	2.0	3.5	53.00	54.72	2.2	3.0	3.5	91.21	90.80
14	2	2.0	3.5	85.00	83.22	2.2	3.0	1.5	88.60	87.98
15	2	2.0	1.5	81.00	80.72	3.4	2.1	2.5	92.58	92.58
16	3	3.5	2.5	98.89	98.50	2.2	1.2	3.5	94.20	94.61
17	4	5.0	1.5	63.00	64.97	3.4	2.1	2.5	92.94	92.58
18	3	3.5	2.5	98.60	98.50	3.4	2.1	2.5	92.89	92.58
19	3	3.5	2.5	98.89	98.50	3.4	2.1	2.5	92.60	92.58
20	4	5.0	3.5	72.00	72.47	2.2	1.2	1.5	91.10	90.54

Table 4.43 Experimental and model predicted percentage degradation of RB-220 (response) obtained by UV and solar photocatalysis for CCD set of experiments. Conditions: C_0=100 mg/L; Irradiation time = 20 min (UV photocatalysis) and Irradiation time = 10 min (solar photocatalysis).

Exp No.	For UV photocatalysis					For solar photocatalysis				
	Uncoded values			Response (% degradation of RB-220)		Uncoded values			Response (% degradation of RB-220)	
	pH (X_1)	Catalyst loading (g/L) (X_2)	$C_{(NH4)2S2O8}$ (g/L) (X_3)	Experimental	Model predicted	pH (X_1)	Catalyst loading (g/L) (X_2)	$C_{(NH4)2S2O8}$ (g/L) (X_3)	Experimental	Model predicted
1	2.2	1.8	1.5	96.86	96.21	4.0	1.7	2.0	51.74	52.46
2	4.2	1.8	1.5	40.29	39.34	3.0	0.7	2.0	92.15	92.40
3	3.2	1.8	1.5	97.66	99.02	3.5	1.2	1.5	94.15	94.19
4	3.2	1.0	1.5	98.26	98.44	4.0	1.7	1.0	67.23	67.28
5	3.2	1.8	0.5	97.23	96.43	3.5	1.2	1.5	94.62	94.19
6	3.2	1.8	2.5	80.78	80.58	3.5	1.2	1.5	94.34	94.19
7	3.2	1.8	1.5	97.38	99.02	3.5	1.2	1.5	94.85	94.19
8	3.2	2.6	1.5	85.42	84.24	3.0	0.7	1.0	98.98	98.56
9	3.2	1.8	1.5	96.97	96.24	3.0	1.7	2.0	85.23	85.40
10	3.7	1.4	1.0	82.17	82.57	4.0	0.7	1.0	70.74	70.87
11	3.7	2.2	1.0	71.79	72.53	3.0	1.7	1.0	96.58	96.09
12	2.7	1.4	2.0	99.58	99.84	4.0	0.7	2.0	59.78	60.57
13	3.7	1.4	2.0	68.65	68.42	2.5	1.2	1.5	98.42	98.81
14	2.7	2.2	1.0	96.16	97.39	3.5	1.2	0.5	97.74	98.25
15	2.7	2.2	2.0	95.08	95.68	4.5	1.2	1.5	38.87	38.18
16	3.2	1.8	1.5	96.82	96.24	3.5	2.2	1.5	57.95	57.88
17	2.7	1.4	1.0	98.98	99.20	3.5	1.2	2.5	78.08	77.27
18	3.7	2.2	2.0	55.26	56.04	3.5	1.2	1.5	94.15	94.79
19	3.2	1.8	1.5	97.42	96.24	3.5	1.2	1.5	94.54	94.79
20	3.2	1.8	1.5	97.75	96.24	3.5	0.2	1.5	68.70	68.47

Table 4.45 MRA models for % degradation of AY-17 and RB-220 by UV and solar photocatalysis with uncoded factors.

For AY-17 by UV photocatalysis

$$\% \, degradation = -41.28 + 47.32 \, X_1 + 27.063 \, X_2 + 23.68 \, X_3 - 11.39 \, X_1{}^2 - 4.73 \, X_2{}^2 - 4.89 \, X_3{}^2 + 2.5 \, X_1 X_2 + 0.5 \, X_1 X_3 + 0.5 \, X_2 X_3 \quad (4.2)$$

For AY-17 by solar photocatalysis

$$\% \, degradation = 58.90 + 4.03 \, X_1 + 18.03 \, X_2 + 13.82 \, X_3 - 2.37 X_1{}^2 - 5.24 \, X_2{}^2 - 2.61 \, X_3{}^2 + 1.4 \, X_1 X_2 + 0.75 \, X_1 X_3 - 0.35 \, X_2 X_3 \quad (4.3)$$

For RB-220 by UV photocatalysis

$$\% \, degradation = 97.63 - 14.07 \, X_1 - 3.56 \, X_2 - 3.96 \, X_3 - 7.74 \, X_1{}^2 - 1.92 \, X_2{}^2 - 2.63 \, X_3{}^2 - 2.06 \, X_1 X_2 - 3.7 \, X_1 X_3 - 0.59 \, X_2 X_3 \quad (4.4)$$

For RB-220 by solar photocatalysis

$$\% \, degradation = 94.49 - 15.16 \, X_1 - 2.65 \, X_2 - 5.25 \, X_3 - 6.57 \, X_1{}^2 - 7.90 \, X_2{}^2 - 1.76 \, X_3{}^2 - 0.28 \, X_1 X_2 - 1.03 \, X_1 X_3 - 1.13 \, X_2 X_3 \quad (4.5)$$

Table 4.46 Analysis of Variance of the MRA models for % degradation of AY-17 and RB-220 by UV and solar photocatalysis.

For photocatalysis of	Sources	DF	Seq SS	Adj SS	Adj MS	F	P
AY-17 under UV light	Regression	9	7132.35	7132.35	792.48	341.82	0.000
	Linear	3	2342.25	2342.25	780.75	336.76	0.000
	Square	3	4671.10	4671.10	1557.03	671.59	0.000
	Interaction	3	119.00	119.00	39.67	17.11	0.000
	Residual Error	9	20.87	20.87	2.32		
	Lack of Fit	5	20.67	20.67	4.13	85.24	0.000
	Pure Error	4	0.19	0.19	0.05		
	Total	19	7501.72				
Goodness of fit	R-Sq				0.997		
	R-Sq(adj)				0.994		
AY-17 under solar light	Regression	9	1910.58	1910.58	215.62	374.74	0.000
	Linear	3	1310.69	1310.69	436.89	759.31	0.000
	Square	3	604.20	604.20	201.40	350.03	0.000
	Interaction	3	25.69	25.69	8.563	14.88	0.001
	Residual Error	9	5.18	5.18	0.575		
	Lack of Fit	5	5.07	5.07	1.014	37.02	0.002
	Pure Error	4	0.11	0.11	0.027		
	Total	19	1983.48				
Goodness of fit	R-Sq				0.997		
	R-Sq(adj)				0.994		
RB-220 under UV light	Regression	9	5213.91	5213.91	579.32	346.58	0.000
	Linear	3	3618.92	3618.92	1206.31	721.67	0.000
	Square	3	1449.12	1449.12	483.04	288.98	0.000
	Interaction	3	145.87	145.87	48.62	29.09	0.000
	Residual Error	9	15.04	15.04	1.67		
	Lack of Fit	5	14.46	14.46	2.89	19.91	0.006
	Pure Error	4	0.58	0.58	0.15		
	Total	19	5237.29				
Goodness of fit	R-Sq				0.997		
	R-Sq(adj)				0.994		
RB-220 under solar light	Regression	9	6324.40	6324.40	702.71	1435.93	0.000
	Linear	3	4229.58	4229.58	1409.86	2880.93	0.000
	Square	3	2075.41	2075.41	691.80	1413.64	0.000
	Interaction	3	19.41	19.41	6.47	13.22	0.001
	Residual Error	9	4.22	4.22	0.49		
	Lack of Fit	5	4.04	4.04	0.81	8.97	0.027
	Pure Error	4	0.36	0.36	0.09		
	Total	19	6439.84				
Goodness of fit	R-Sq				0.999		
	R-Sq(adj)				0.999		
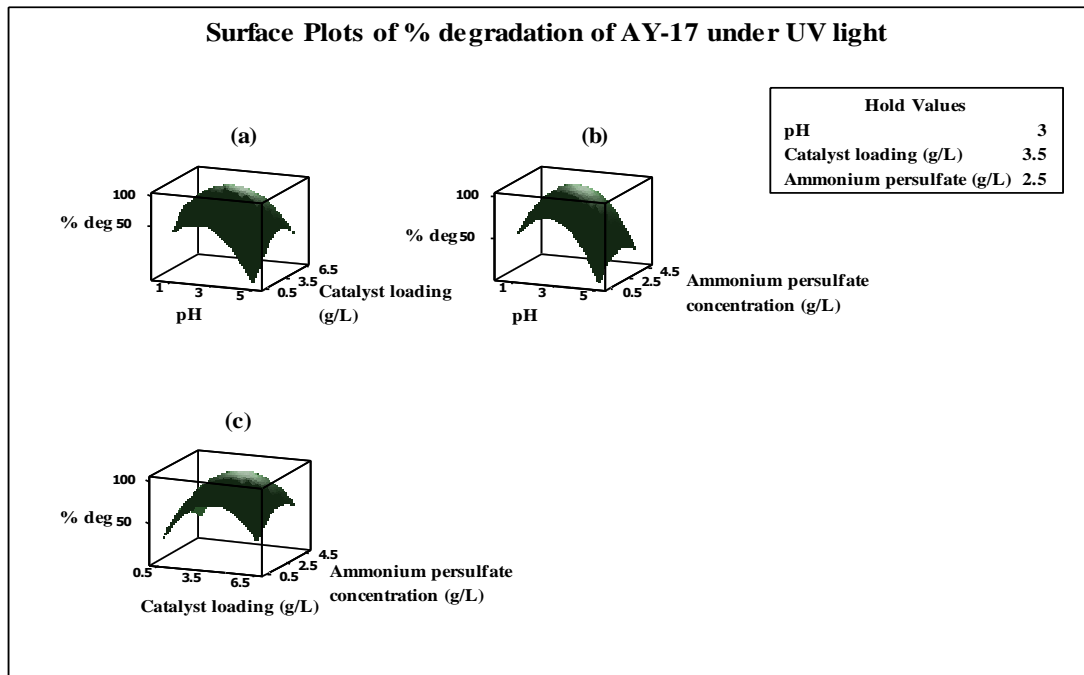
Figure 4.52 Surface plots of percentage degradation of AY-17 by UV photocatalysis.
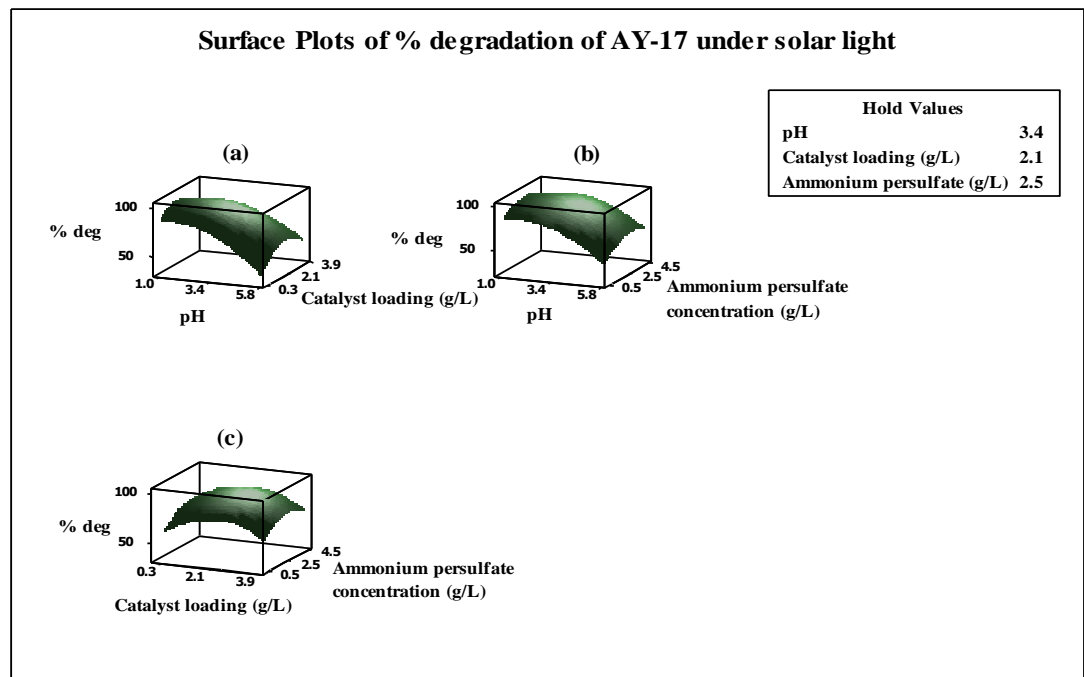
Figure 4.53 Surface plots of percentage degradation of AY-17 by solar photocatalysis.
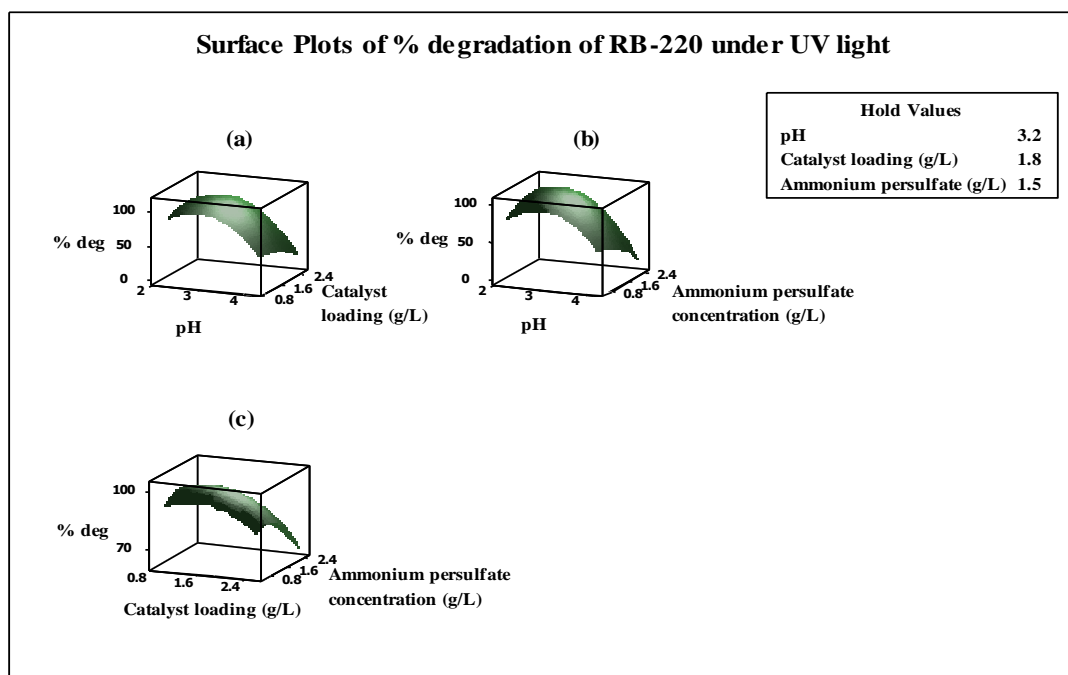
Figure 4.54 Surface plots of percentage degradation of RB-220 by UV photocatalysis.
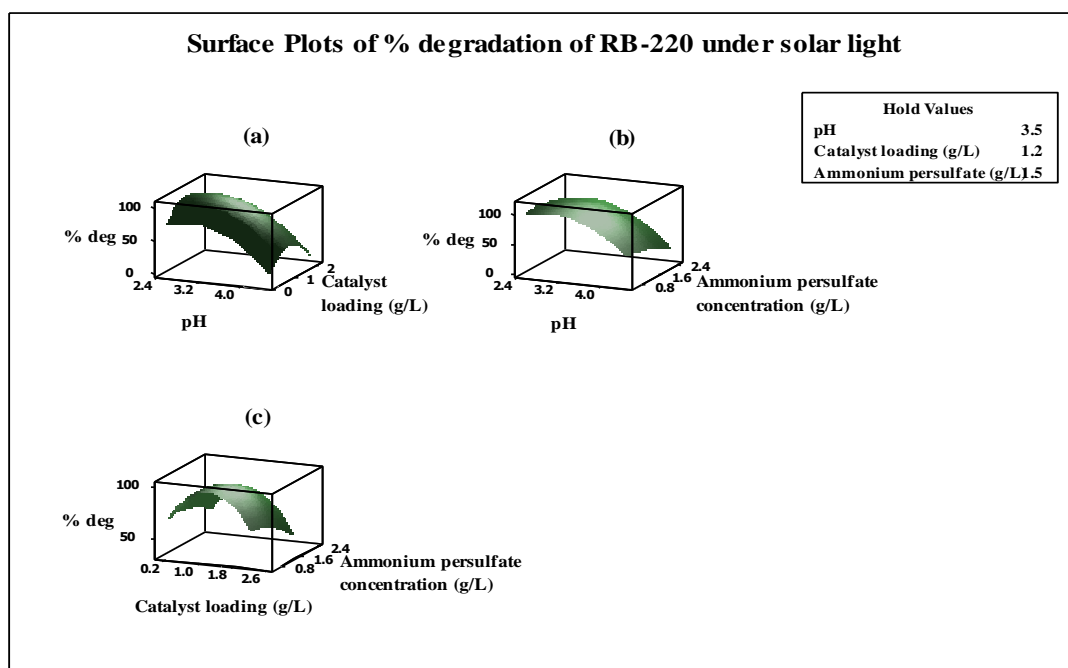
Figure 4.55 Surface plots of percentage degradation of RB-220 by solar photocatalysis.
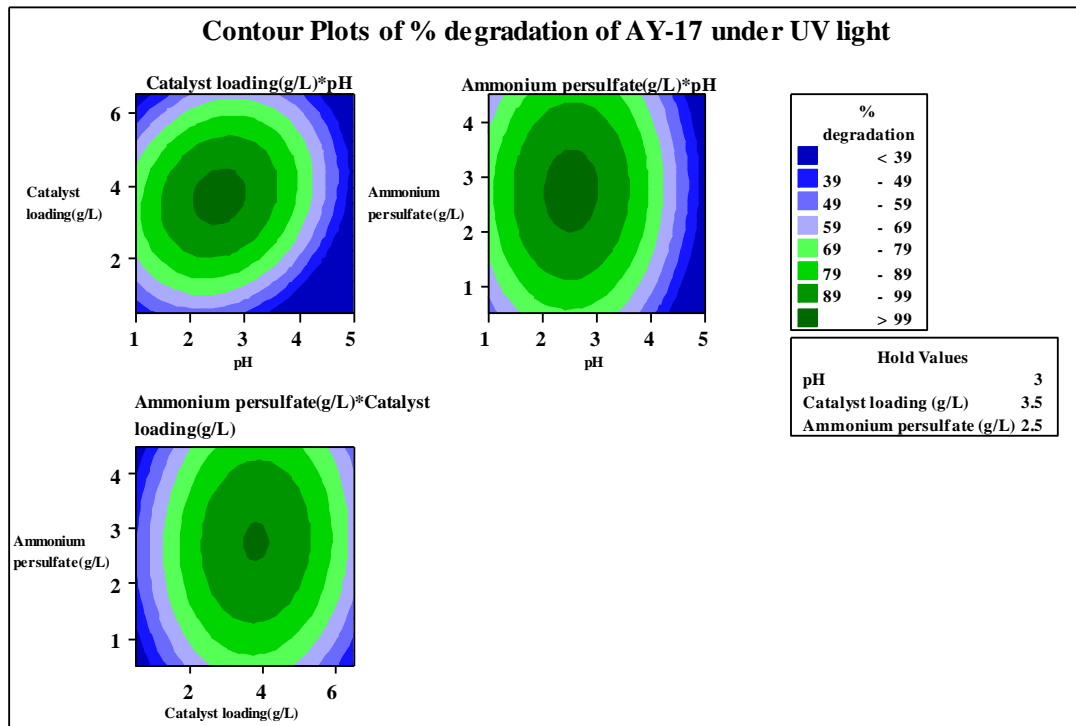
Figure 4.56 Contour plots for percentage degradation of AY-17 by UV photocatalysis.
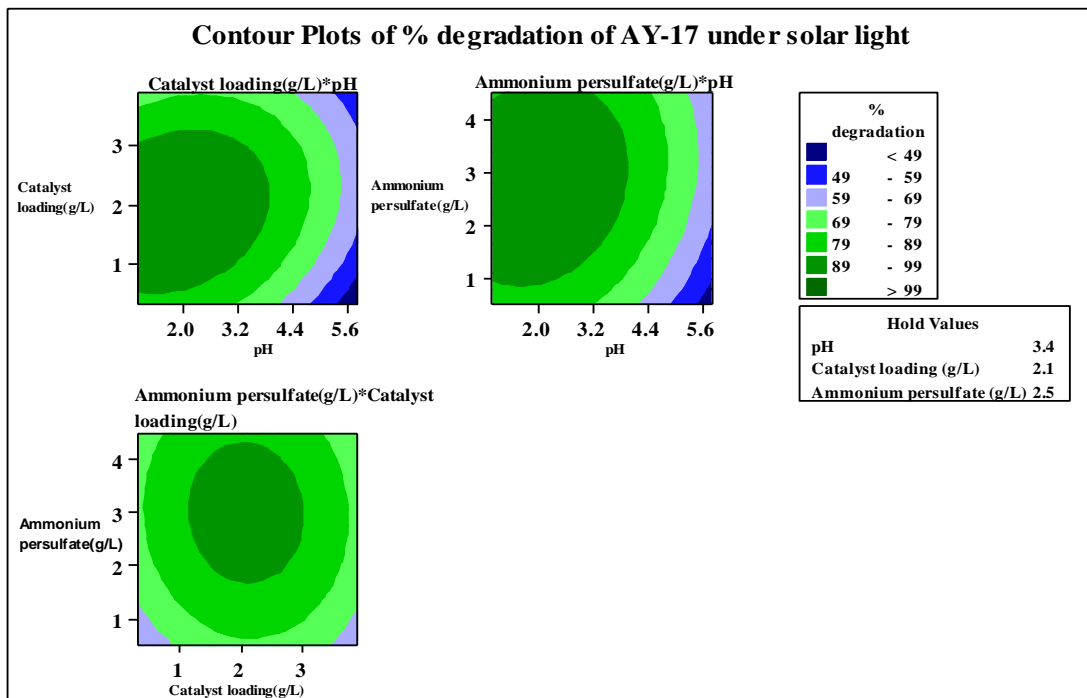
Figure 4.57 Contour plots for percentage degradation of AY-17 by solar photocatalysis.
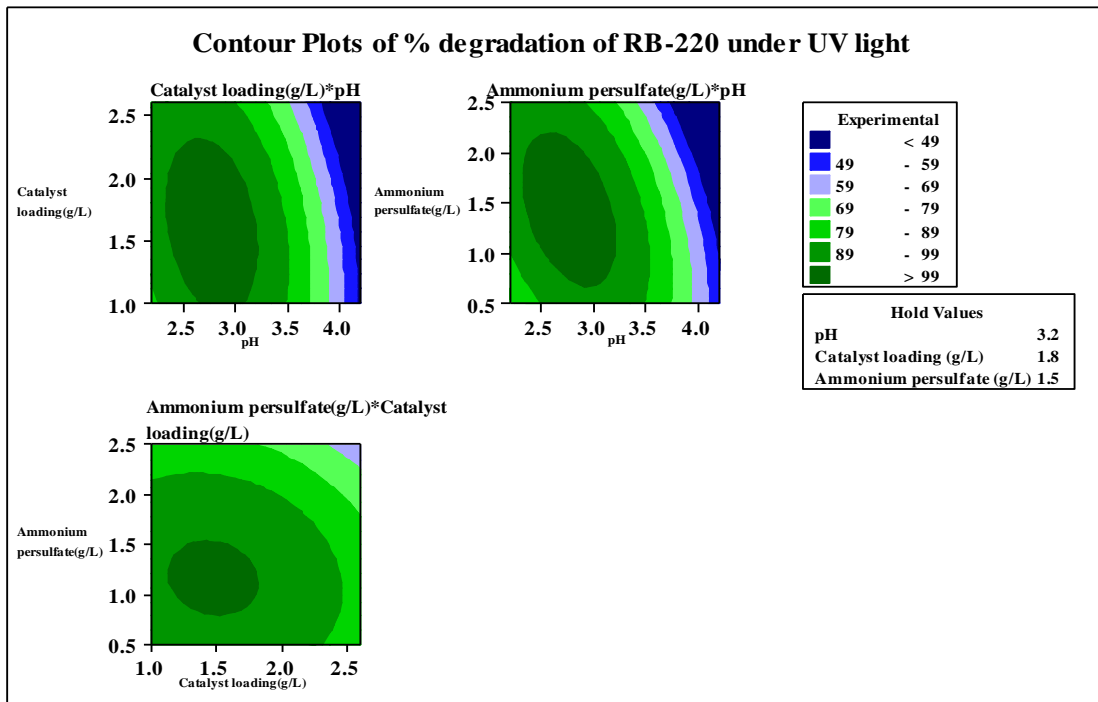
Figure 4.58 Contour plots of percentage degradation of RB-220 by UV photocatalysis.
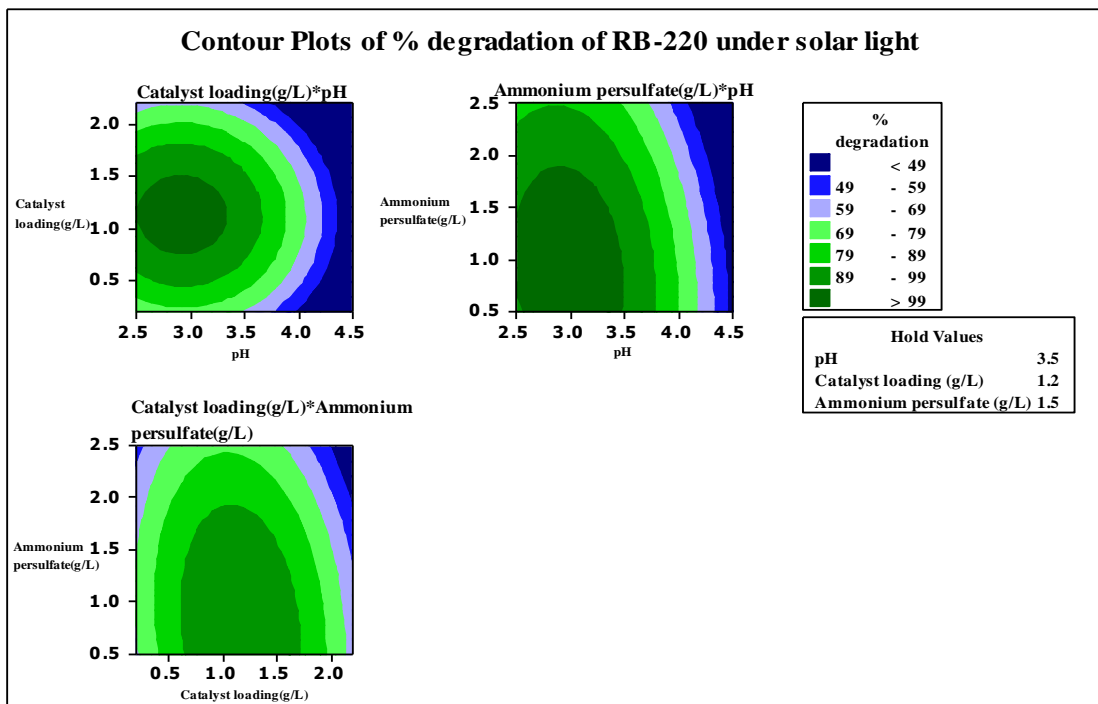
Figure 4.59 Contour plots of percentage degradation of RB-220 by solar photocatalysis.
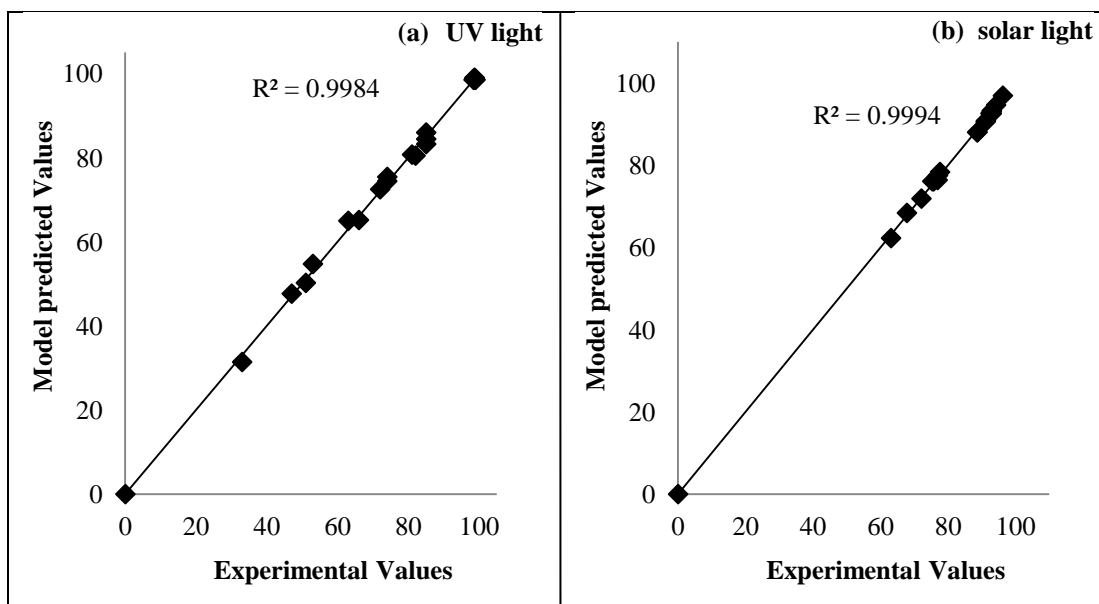
Figure 4.60 Plot of model predicted vs. experimentally determined values of % degradation of AY-17 under a) UV light; b) solar light.
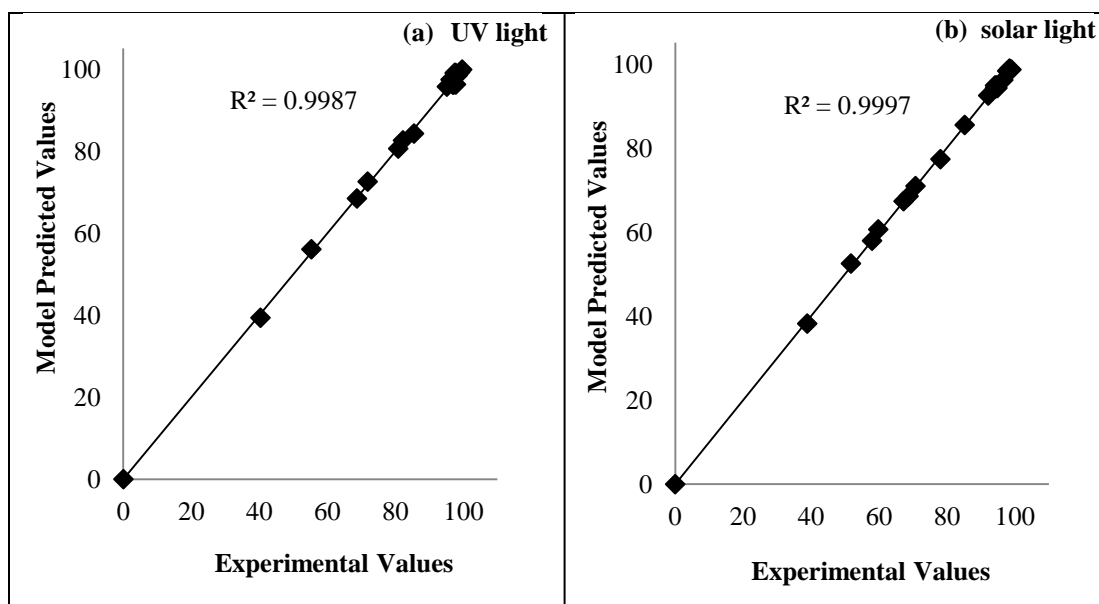
Figure 4.61 Plot of model predicted vs. experimentally determined values of % degradation of RB-220 under a) UV light; b) solar light.

Table 4.47 Optimum values of each variable (factor) determined by RSM based methodical optimization and crude optimization for UV and solar photocatalysis of AY-17 and RB-220 and corresponding percentage degradation. Initial dye concentration= 100 mg/L.

Variable	Optimum values of the variables							
	Crude optimization for UV photocatalysis		Methodical optimization (RSM) for UV photocatalysis		Crude optimization for solar photocatalysis		Methodical optimization (RSM) for solar photocatalysis	
	AY-17	RB-220	AY-17	RB-220	AY-17	RB-220	AY-17	RB-220
pH	3	3	2.9	3.2	3	3	2.1	3.3
Catalyst loading in g/L (dye to catalyst ratio, g/g)	3 (1:30)	2 (1:20)	3.4 (1:34)	1.8 (1:18)	1 (1:10)	1 (1:10)	1.8 (1:18)	1.1 (1:11)
Ammonium persulfate concentration(g/L)	2	1.5	2.25	1.3	2	1.5	2.71	1.36
% degradation (irradiation time, min) *Experimental*	76.54 (15)	82.25 (20)	98.78 (15)	98.62 (20)	82.80 (15)	86.76 (10)	99.34 (15)	99.49 (10)
% degradation (irradiation time,min) *Model Predicted*	-	-	99.89 (15)	99.78 (20)	-	-	98.62 (15)	99.53 (10)

4.8.3 Validation of RSM based methodical optimization and its comparison with crude optimization of the factors for UV and solar photocatalysis of AY-17 and RB-220

Batch photocatalysis experiments were conducted under methodically optimized conditions of pH, catalyst loading and ammonium persulfate concentration as obtained from RSM using the results of experiments conducted as per Central Composite design. The RSM based methodically optimized conditions and the crude optimized conditions (based on one factor at a time analysis) explained in Section 4.6, at which the batch experiments were performed for the photocatalytic degradation of AY-17 and RB-220 under UV and solar light are presented in Table 4.47. The initial dye concentration used was 100 mg/L. The methodically optimized conditions showed highly efficient UV and solar photocatalytic process for both the dyes (AY-17 and RB-220). In other words, time for dye degradation reduced, showing complete reduction of the dye at a shorter time period as compared to that under crude optimization conditions. It shows that under methodically optimized conditions, rate of reduction has enhanced tremendously. It can be observed that percentage degradation of AY-17 dye was 98.78 % and more than 99 % in 15 min of irradiation with UV and solar light respectively under methodically optimized conditions, whereas under crude optimization conditions the degradations were only around 76 % and 82 % respectively at similar irradiation time periods.

Percentage degradation of RB-220 dye was 98.62 % in 20 min and more than 99 % in 10 min with UV and solar photocatalysis respectively under methodically optimized conditions, whereas only around 82 % and 86 % degradation were obtained at similar irradiation time periods under crude optimization conditions. The time course variations of AY-17 and RB-220 dye concentrations obtained with methodically optimized conditions as compared to the crude optimization conditions are presented in Table 4.48 to Table 4.49 respectively for UV and solar photocatalysis. Figure 4.62 and Figure 4.63 show the reduction in time for complete degradation of the dyes with methodically optimized conditions as compared to the crude optimization conditions, which indicate that the rate of dye degradation by Ag@TiO$_2$ can be greatly increased by using the RSM based methodically optimized

conditions. These results indicate the effectiveness of RSM based optimization. The knowledge on optimum conditions is advantageous especially in large-scale dye degradation processes where factors such as cost and time are of extreme importance. The increase in rate will eventually result in lowering the size of reactor to be used for continuous dye degradation from industrial effluents, thereby reducing the capital cost. Operating cost can as well be reduced due to minimum requirement of the catalyst and the oxidant. The time of operation can be reduced in the case of batch reactors.

Table 4.48 Time course variation of concentration of AY-17 obtained with methodically optimized conditions as compared to the crude optimization conditions during UV and solar photocatalysis.

Time (min)	For UV photocatalysis		For solar photocatalysis	
	C_{AY-17} (mg/L) with		C_{AY-17} (mg/L) with	
	Crude optimization	Methodical optimization	Crude optimization	Methodical optimization
0	100	100	100	100
15	23.46	1.22	17.2	0.66
30	3.56	0.28	1.8	0.15
45	2.58	0.1	1.02	ND
60	1.04	0.03	0.71	ND

Table 4.49 Time course variation of concentration of RB-220 obtained with methodically optimized conditions as compared to the crude optimization conditions during UV and solar photocatalysis.

Time (min)	For UV photocatalysis		Time (min)	For solar photocatalysis	
	C_{RB-220} (mg/L) with			C_{RB-220} (mg/L) with	
	Crude optimization	Methodical optimization		Crude optimization	Methodical optimization
0	100	100	0	100	100
10	24.3	11.52	5	25.07	20.14
20	15.63	1.38	10	13.24	0.51
30	0.99	0.46	15	0.99	0.09
40	0.35	0.03	20	0.35	0.02
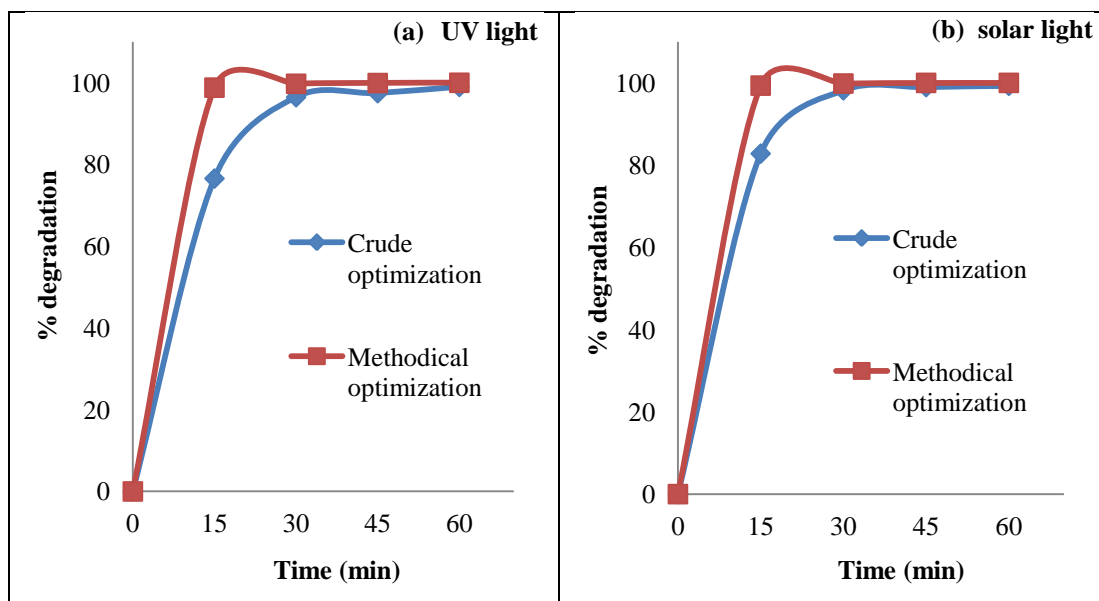
Figure 4.62 Time course variation of percentage degradation of AY-17 dye under crude optimization and RSM based methodical optimization conditions by photocatalysis under a) UV light; b) solar light.
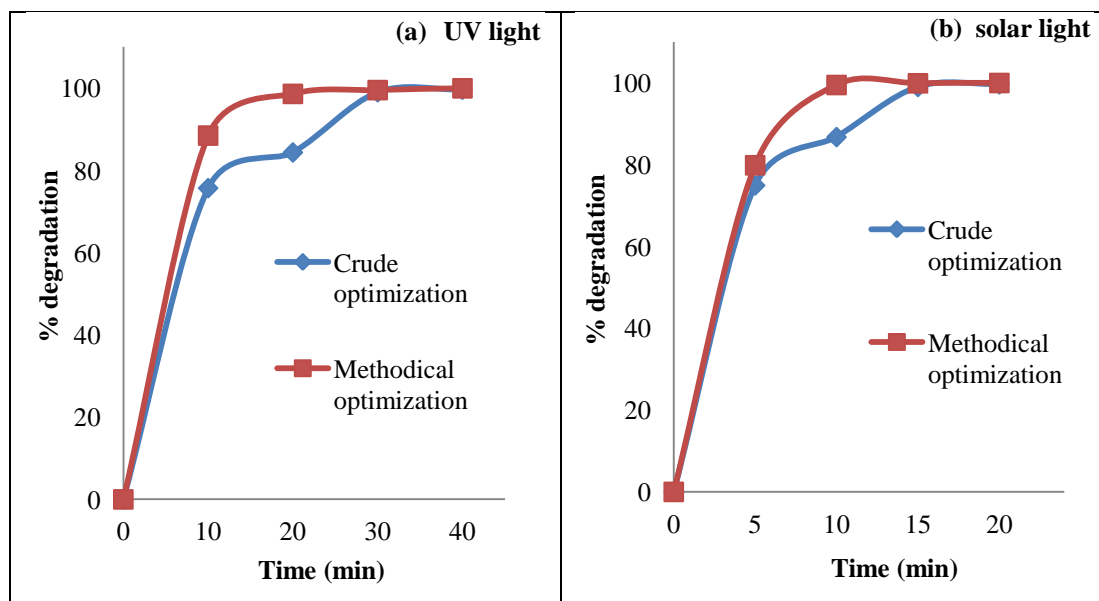
Figure 4.63 Time course variation of percentage degradation of RB-220 dye under crude optimization and RSM based methodical optimization conditions by photocatalysis under a) UV light; b) solar light.

4.9 Effect of initial concentration of the dyes on UV and solar photocatalytic degradation of AY-17 and RB-220 under optimized conditions

4.9.1 Effect of initial concentration of AY-17 on the UV and solar photocatalytic degradation under optimized conditions

The effect of initial concentration of AY-17 on its photocatalytic degradation was studied, as it is important from both mechanistic and application point of view. Generally industrial wastewater treatment plants are designed to handle effluents of specified quality corresponding to normal conditions. Catalyst loading for the photocatalytic treatment process is selected based on optimum dye to catalyst ratio, so as to be adequate for the concentration of dyes in the industrial effluent under normal conditions. The reactor for the said operation will be designed based on the rate of photocatalysis with this optimum catalyst loading for the given dye concentration corresponding to normal conditions of effluent. But sometimes the concentration of dye in the effluent may vary owing to variation in process operation. If the concentration increases, then the catalyst loading used may be inadequate for photocatalysis and hence longer time of irradiation may be needed in batch photocatalytic reactor or the volume of continuous reactor may be inadequate to obtain the effluent that meets the environmental standards. Studies on effect of initial concentration of the dye on photocatalytic degradation is very important to understand the unsteady state behavior of the process under abnormal conditions, which will in turn help in understanding the dynamics and control of the process. In the present work, the effect of initial concentration of AY-17 on the photocatalytic degradation was investigated over the concentration range from 100 mg/L to 700 mg/L at optimized conditions of pH=2.9; Catalyst loading= 3.4 g/L; $(NH_4)_2S_2O_8$= 2.25 g/L for UV photocatalysis and pH=2.1; Catalyst loading= 1.8 g/L; $(NH_4)_2S_2O_8$= 2.71 g/L for solar photocatalysis as mentioned in Table 4.47, under UV and solar light irradiation. The experiments were conducted by keeping the catalyst loading at the optimum obtained for 100 mg/L dye concentration. So when the initial dye concentration was varied, the dye to catalyst ratio also varied. Hence in these cases dye to catalyst loading ratio is not the optimum. Time course variations of AY-17 dye concentrations

obtained with different initial dye concentration are shown in Table 4.50 and Table 4.51 respectively for UV and solar photocatalysis.

Figure 4.64a depicts the effect of initial dye concentration on time course variation of photocatalytic degradation of AY-17 dye under UV light irradiation. As revealed in Figure 4.65a as the dye concentration increases from 100 to 400 mg/L, the percentage degradation at the end of 360 min irradiation time decreases marginally from 99.97 to 95.49 %. But further increase in concentration above 400 mg/L upto 700 mg/L, resulted in decrease in percentage degradation to around 61 %. It was observed, for dye solutions of 100 mg/L almost 100 % degradation occurred within 60 min, in case of 200 mg/L almost 96 % degradation occurred within 60 min and in case of 300 mg/L, almost 95 % degradation was observed in 60 min. For 400 mg/L of the dye solution degradation was 86.22 % in 60 min and it gets further decreased on increasing the concentration of dye. High rates of degradation were observed within 60 min of irradiation time with concentration less than 400 mg/L.

Figure 4.64b shows the effect of initial dye concentration on time course variation of photocatalytic degradation of AY-17 dye under solar light irradiation. The experiments were conducted by keeping the catalyst loading at the optimum obtained for 100 mg/L dye concentration. So when the initial dye concentration was varied, the dye to catalyst ratio varied. As observed in Figure 4.65b, as the concentration increases from 100 mg/L to 400 mg/L, the percentage degradation (at the end of 360 min irradiation time) decreases marginally from 100 to 97.83 %. But further increase in concentration above 400 mg/L upto 700 mg/L, resulted in decrease in percentage degradation to around 67 %. For dye solutions of 100 mg/L almost complete degradation occurred within 30 min, almost 97 % in case of 200 mg/L and 95 % degradation in case of 300 mg/L were observed in 60 min. For 400 mg/L of the dye solution degradation was 89 % in 60 min and it gets further decreased on increasing the concentration of dye. As in UV photocatalysis As in UV photocatalysis, high rates of degradation were observed within 60 min of irradiation time with concentration of less than 400 mg/L.

The possible explanation for this behavior is that, when the initial dye concentration in the reaction mixture is low, the ratio of dye to catalyst loading is lower. As the dye concentration is increased, the ratio increases. If the dye to catalyst

ratio increases, then the number of dye molecules present per unit surface area of catalyst increases. The increase in dye concentration also decreases the path length of photon entering the dye solution and the opposite effect is observed in low concentration, thus at lower concentration the number of photon absorption by the catalyst increases (Davis et al. 1994). At high dye concentration a significant amount of light may be absorbed by the dye molecules rather than the catalyst and this may also reduce the catalytic efficiency (Mills et al. 1993). Also the degradation rate is directly proportional to the probability of formation of hydroxyl radicals ($OH^{.}$) on the catalyst surface and the probability of hydroxyl radicals reacting with the dye molecules (Tang and An 1995). As the initial concentration of the dye increases, the interaction of $^{.}OH$ radical with dye decreases. Further, increase in concentration also reduces the light penetration and the relative formation of hydroxyl radicals; superoxide radical anions decreases leading to the decreased photodegradation efficiency. The results also indicate the effectiveness of the catalyst to degrade the dye solution at concentration upto 300 mg/L, to an extent of above 96 % in UV photocatalysis and 97 % in solar photocatalysis within 120 min of irradiation time and 400 mg/L dye solution to above 95 % in 360 min of UV light irradiation and 180 min of solar light irradiation. Greater than 98 % degradation of upto 300 mg/L AY-17 dye was possible within 360 min of UV and solar light irradiation. So if there is a possibility of large deviations from normal conditions of dye concentration in the industrial effluent, then proper control measures are to be taken in the treatment process to keep the treated effluent quality within the standard. It is always advisable to design the reactor based on most probable maximum dye concentration in the industrial effluent and its corresponding optimum catalyst loading, so that the treated effluent quality will always meet the standard.

Table 4.50 Time course variation of concentration of AY-17 obtained with different initial concentration (mg/L) during UV photocatalysis. Conditions: pH=2.9; Catalyst loading= 3.4 g/L; $(NH_4)_2S_2O_8$= 2.25 g/L.

Time (min)	C_{AY-17} (mg/L) with different initial concentrations					
	C_0= 100 mg/L	C_0=200 mg/L	C_0=300 mg/L	C_0=400 mg/L	C_0=500 mg/L	C_0=700 mg/L
0	100	200	300	400	500	700
15	1.22	23.14	56.86	98.48	183.44	319.72
30	0.28	14.63	40.33	78.14	176.19	304.42
45	0.23	10.65	30.69	63.72	170.05	298.88
60	0.03	8.26	15.63	55.12	163.72	293.02
120	0.03	6.60	9.12	41.63	156.65	288.47
180	0.03	4.16	8.06	33.26	153.67	283.26
240	0.03	2.65	6.43	25.00	147.53	279.02
300	0.03	1.30	5.86	20.12	141.77	275.12
360	0.03	0.23	5.95	18.02	140.28	272.84

Table 4.51 Time course variation of concentration of AY-17 obtained with different initial concentration (mg/L) during solar photocatalysis. Conditions: pH=2.1; Catalyst loading= 1.8 g/L; $(NH_4)_2S_2O_8$= 2.71 g/L.

Time (min)	C_{AY-17} (mg/L) with different initial concentration					
	C_0= 100 mg/L	C_0=200 mg/L	C_0=300 mg/L	C_0=400 mg/L	C_0=500 mg/L	C_0=700 mg/L
0	100	200	300	400	500	700
15	0.66	20.26	46.28	87.72	160.37	289.33
30	0.16	16.93	29.67	69.02	145.86	277.23
45	ND	11.63	21.02	55.07	138.05	269.07
60	ND	5.21	16.56	44.30	133.02	262.72
120	ND	3.44	8.28	31.74	125.21	254.56
180	ND	2.05	6.51	20.02	120.74	247.00
240	ND	1.30	5.40	13.19	116.28	242.47
300	ND	0.56	4.74	10.81	111.81	237.02
360	ND	0.09	4.19	8.65	110.51	232.79
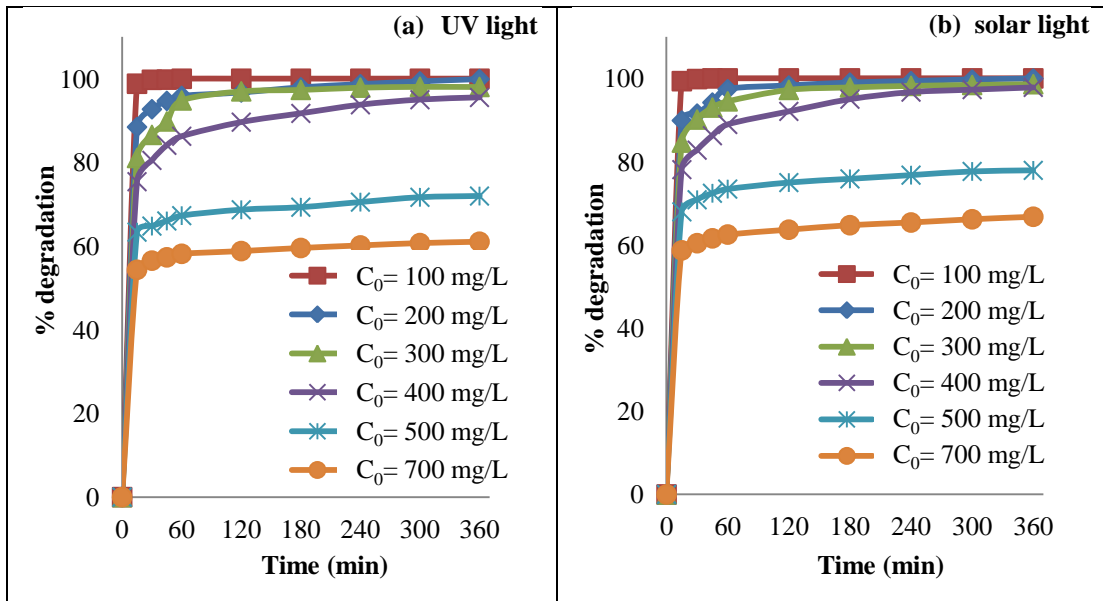
Figure 4.64 Effect of initial dye concentration on time course variation of photocatalytic degradation of AY-17 dye under a) UV light (pH=2.9; catalyst loading= 3.4 g/L; $(NH_4)_2S_2O_8$= 2.25 g/L); b) solar light (pH= 2.1; catalyst loading= 1.8 mg/L; $(NH_4)_2S_2O_8$= 2.71 g/L). Average UV and visible light intensity of solar light= 3.54 mW/cm^2 and 1218×100 lux respectively from 10 a.m. to 4 p.m.
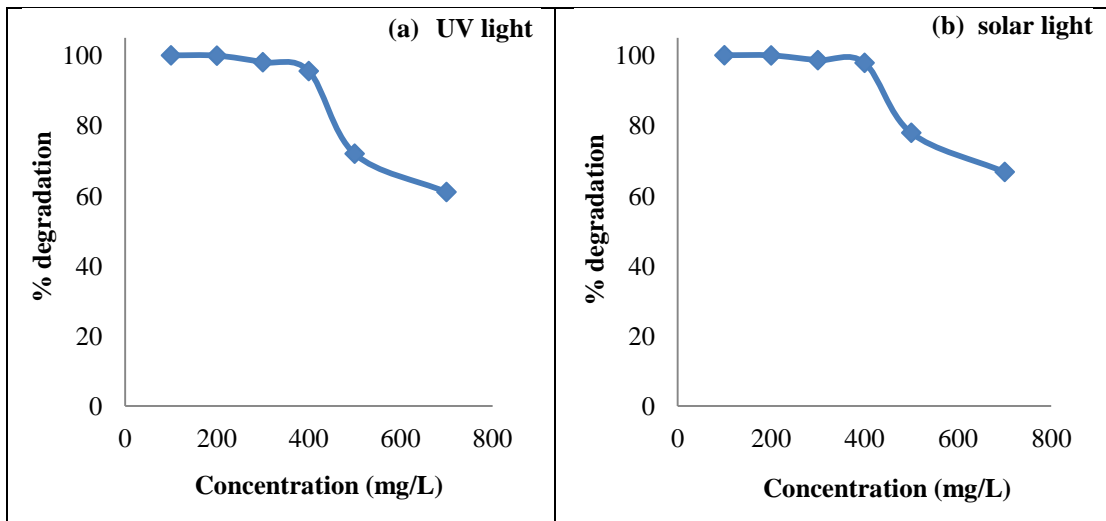
Figure 4.65 Effect of initial dye concentration on percentage degradation of AY-17 dye a) UV light (Catalyst used= Ag@TiO$_2$ (3.4 g/L); pH=2.9; Oxidant used= $(NH_4)_2S_2O_8$ (2.25 g/L); Irradiation time =360 min); b) solar light (Catalyst used= Ag@TiO$_2$ (1.8 g/L); pH=2.1; Oxidant used= $(NH_4)_2S_2O_8$ (2.71 g/L); Irradiation time =360 min).

4.9.2 Effect of initial concentration on the UV and solar photocatalytic degradation of RB-220 under optimized conditions

The effect of initial concentration of RB-220 on the photocatalytic degradation was investigated over the concentration range from 100 mg/L to 500 mg/L at optimized conditions [pH=3.2, Catalyst loading= 1.8 g/L, $(NH_4)_2S_2O_8$= 1.3 g/L] under UV light irradiation. In case of solar light irradiation effect of initial concentration of RB-220 was investigated over the concentration range from 100 mg/L to 700 mg/L at optimized conditions [pH=3.3, Catalyst loading= 1.11 g/L, = $(NH_4)_2S_2O_8$= 1.36 g/L]. The experiments were conducted by keeping the catalyst loading at the optimum obtained for 100 mg/L dye concentration. Hence dye to catalyst loading ratio is not the optimum. Time course variations of RB-220 dye concentrations obtained with different initial dye concentration are shown in Table 4.52-4.53 respectively for UV and solar photocatalysis.

Figure 4.66a which presents the effect of initial dye concentration on time course variation of photocatalytic degradation of RB-220 dye under UV light irradiation, reveals that as the initial dye concentration increases, rate of degradation reduces. As seen in Figure 4.67a, as the concentration increases from 100 mg/L to 500 mg/L, the percentage degradation at the end of 240 min of irradiation time decreases from 100 % to 92.25 %. For dye solutions of 100 mg/L, almost 100 % degradation occurred, almost 96 % degradation in case of 200 mg/L and almost 93 % degradation in case of 300 mg/L were achieved in 60 min of irradiation time. For 400 mg/L of the dye solution degradation was 90 % in 60 min and the percentage degradation further decreased on increasing the concentration of the dye. High rates of degradation were observed within 60 min of irradiation time.

Figure 4.66b shows the effect of initial dye concentration on time course variation of photocatalytic degradation of RB-220 dye under solar light irradiation. As the initial dye concentration increased, rate of degradation reduced. Figure 4.67b shows that as the concentration increases from 100 mg/L to 700 mg/L, the percentage degradation at the end of 120 min irradiation time decreases from 100 to 93.87 %. It was observed from Figure 4.66b, for dye solutions of 100 mg/L almost complete degradation occurred within 10 min, almost 87 % degradation in case of 200 mg/L,

and almost 68 % degradation in case of 300 mg/L could be achieved in 10 min. For 400 mg/L of the dye solution degradation was 57 % in 10 min and it was further decreased on increasing the concentration of the dye. High rates of degradation were observed within 10 to 15 min of irradiation time with concentrations of 100 mg/L and 200 mg/L.

The possible explanation for this behavior has already been discussed in Section 4.10.1. The results also indicate the effectiveness of the catalyst to degrade the dye solution at concentration upto 500 mg/L, to an extent of above 92 % within 240 min of UV light irradiation time and 700 mg/L dye solution to above 94 % in 120 min of solar light irradiation time. Greater than 99 % degradation of (i) upto 500 mg/L RB-220 could be achieved within 45 min of irradiation by solar photocatalysis and (ii) upto 300 mg/L could be achieved within 240 min of irradiation by UV photocatalysis. So, as discussed in Section 4.10.1, it is always advisable to design the reactor based on most probable maximum dye concentration in the industrial effluent and its corresponding optimum catalyst loading, so that the treated effluent quality will always meet the standard.

Table 4.52 Time course variation of concentration of RB-220 obtained with different initial concentration during UV photocatalysis. Conditions: pH=3.2, Catalyst loading= 1.8 g/L, $(NH_4)_2S_2O_8$= 1.3 g/L.

Time (min)	C_{RB-220} (mg/L) with different initial concentration				
	C_0= 100 mg/L	C_0=200 mg/L	C_0=300 mg/L	C_0=400 mg/L	C_0=500 mg/L
0	100	200	300	400	500
5	34.23	79.58	135.21	203.52	284.15
10	11.52	41.69	87.46	132.75	216.97
20	1.38	27.32	60.92	99.01	160.14
30	0.46	15.70	41.55	69.08	121.48
40	0.08	10.63	29.01	52.25	97.18
60	0.06	7.96	21.76	39.08	69.65
120	0.04	3.45	13.17	22.82	49.65
180	ND	0.99	8.38	20.99	43.17
240	ND	0.42	3.38	17.25	38.73

Table 4.53 Time course variation of concentration of RB-220 obtained with different initial concentration (mg/L) during solar photocatalysis. Conditions: pH=3.3, Catalyst loading= 1.11 g/L, = $(NH_4)_2S_2O_8$= 1.36 g/L.

Time (min)	C_{RB-220} (mg/L) with different initial concentration					
	C_0= 100 mg/L	C_0=200 mg/L	C_0=300 mg/L	C_0=400 mg/L	C_0=500 mg/L	C_0=700 mg/L
0	100	200	300	400	500	700
5	20.14	75.63	122.54	191.62	262.25	479.58
10	0.51	26.41	97.18	148.73	214.23	422.54
15	0.09	3.87	64.23	118.31	185.07	374.65
20	0.02	2.18	45.56	90	141.55	322.89
25	0.02	1.27	5.00	38.10	70.07	283.10
30	0.02	0.70	3.66	17.89	32.89	258.17
45	ND	0.28	2.32	3.52	5.56	189.30
60	ND	0.07	1.62	2.54	3.17	120.17
90	ND	ND	0.21	0.70	1.06	64.93
120	ND	ND	0.21	0.42	0.70	42.89
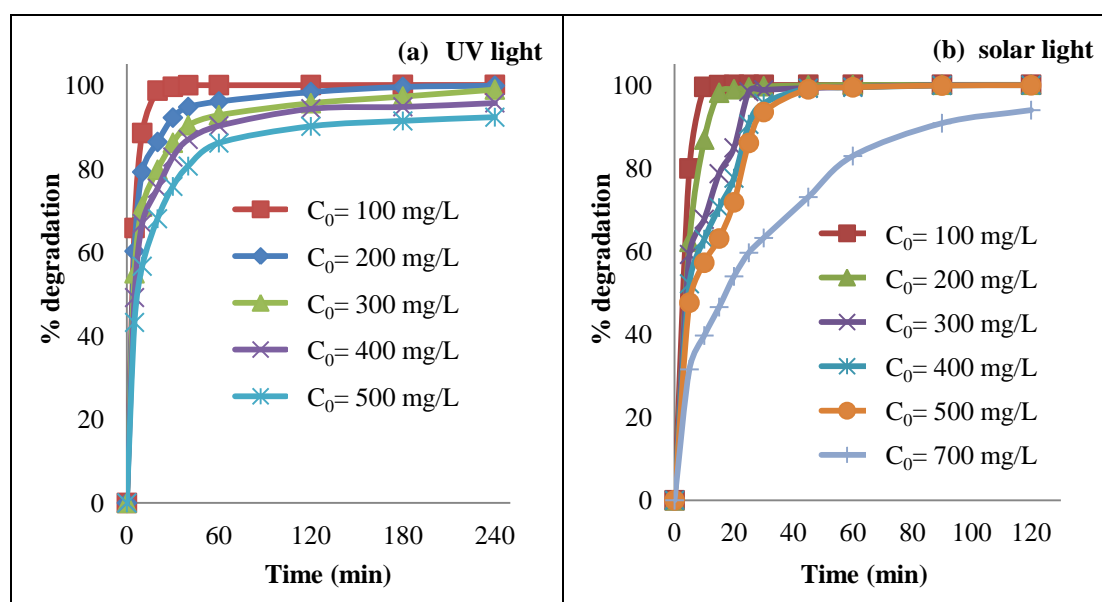
Figure 4.66 Effect of initial dye concentration on time course variation of percentage degradation of RB-220 dye under a) UV light (pH=3.2; Ag@TiO$_2$= 1.8 g/L; $(NH_4)_2S_2O_8$= 1.3 g/L); b) solar light (pH= 3.3; Ag@TiO$_2$= 1.11 g/L; $(NH_4)_2S_2O_8$= 1.36 g/L). Average UV and visible light intensity of solar light= 3.54 mW/cm^2 and 1218×100 lux respectively from 11 a.m. to 1 p.m.
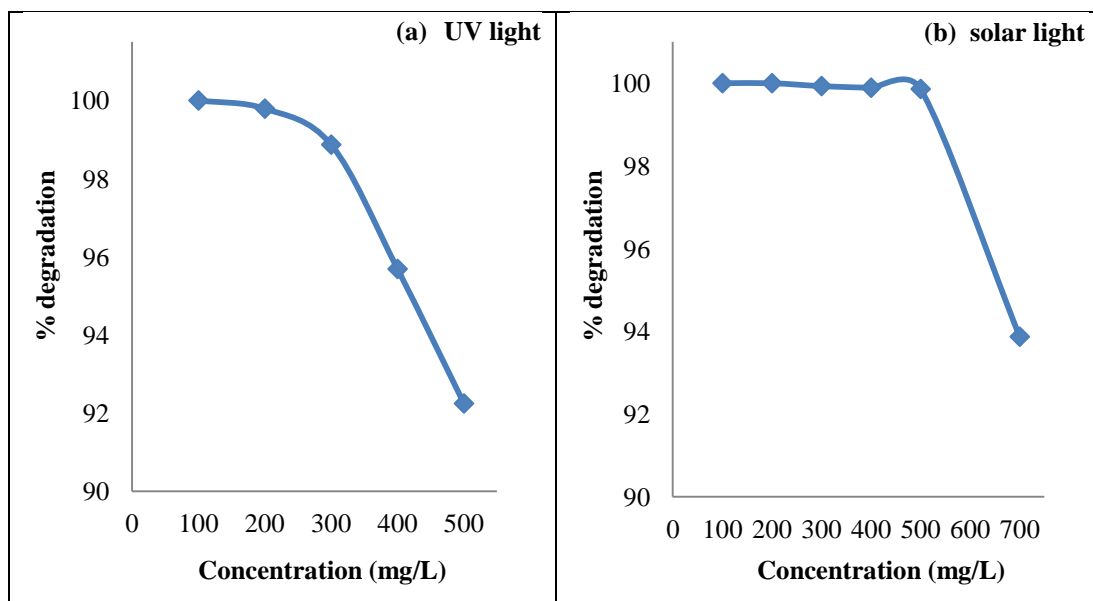
Figure 4.67 Effect of initial dye concentration on percentage degradation of RB-220 dye under a) UV light (Catalyst used= Ag@TiO$_2$ (1.8 g/L); pH=3.2; (NH$_4$)$_2$S$_2$O$_8$=1.3 g/L; Irradiation time =240 min; b) solar light (Catalyst used= Ag@TiO$_2$ (1.11 g/L); pH=3.3; Oxidant used= (NH$_4$)$_2$S$_2$O$_8$ (1.36 g/L); Irradiation time =120 min).

4.10 Kinetics of degradation of AY-17 and RB-220 under UV and solar light irradiation

Determination of rate equation governing photocatalytic process and the evaluation of the parameters of the rate equation are important for the design of photoreactors which are used for photocatalysis of dyes in wastewater. Rate kinetics is important to determine the volume of continuous reactors for photocatalysis or to determine the time to be provided for photocatalytic reaction in batch reactor. Studies on kinetics of degradation help in the prediction of rate equation. To analyze the heterogeneous photocatalytic reaction kinetics successfully, many researchers (Chen and Ray 1998; Wenhua et al. 2000; Galindo et al. 2001) have used the modified Langmuir–Hinshelwood (L–H) kinetic expression.

The data obtained by conducting UV and solar photocatalysis experiments at optimum reaction conditions of pH, catalyst loading and (NH$_4$)$_2$S$_2$O$_8$ concentration, by varying the initial dye concentration has been rationalized in terms of the modified

form of L–H kinetic model to describe the solid–liquid reaction successfully. The L-H model assumes that the reaction on the surface governs the rate, with one of the elementary steps in the reaction sequence constituting a rate determining step, thus all the adsorption/desorption steps are quasi-equilibrated. It is assumed that dyes are strongly adsorbed on the catalyst surface, than the intermediate products and the rate of degradation of AY-17 and RB-220 dye by surface reaction is proportional to the surface coverage of dye on Ag@TiO$_2$ nanoparticles (Al-Ekabi and Serpone 1988). The effect of dye concentration on the rate of degradation is given in the form of Eq.(4.6) (Matthews 1987)

$$(-r) = \frac{k_{obs}k_R[C_{dye}]}{1 + k_R[C_{dye}]} \tag{4.6}$$

where (–r) is the reaction rate of AY-17 or RB-220 dye being degraded, C_{dye} is the concentration of the dye, k_{obs} is the constant related to adsorption and k_R is the reaction rate constant. To estimate the parameters, it has been customary to write Eq.(4.6) in linear form using the reciprocals as shown in Eq.(4.7) and then to plot the reciprocal of initial reaction rate, 1/(r), versus the reciprocal of initial concentration, $1/C_{dye}$

$$\frac{-1}{r} = \frac{1}{k_{obs}} \frac{1}{k_R[C_{dye}]} + \frac{1}{k_{obs}} \tag{4.7}$$

This method is called the method of initial rates (Levenspiel 1972). To estimate the parameters in Eq.(4.7), rates of AY-17 and RB-220 dye degradation were obtained by drawing tangents at time t=0, on plots of dye concentration vs. time data obtained by batch experiments with different initial dye concentrations under UV and solar light. The initial dye concentrations and their corresponding rates by UV and solar photocatalysis, calculated manually for AY-17 and RB-220 are given in Table 4.54 and Table 4.55 respectively. 1/(r) versus $1/C_{dye}$ was plotted for AY-17 and RB-220 as shown in Figure 4.68 and Figure 4.69. The linearity of the plots show the applicability of L-H kinetics and the values of kinetic parameters were estimated from the slope and intercept. The values of k_{obs} and k_R are presented in Table 4.56 for degradation of AY-17 and RB-220 dye by UV and solar photocatalysis. The applicability of L–H equation for the degradation of AY-17 and RB-220 has been confirmed by the linear nature of the plot. This indicates that the rate of degradation of the dye is determined mainly by the reaction occurring on the surface of Ag@TiO$_2$.

Table 4.54 Initial dye concentrations and their corresponding rates for AY-17 degradation by UV and solar photocatalysis.

S. No.	UV photocatalysis			solar photocatalysis		
	C_{0AY-17} (mg/L)	C_{0AY-17} (mM)	Rate (mM/min)	C_{0AY-17} (mg/L)	C_{0AY-17} (mM)	Rate (mM/min)
1	100	0.18	0.018	100	0.18	0.02
2	200	0.36	0.04	200	0.36	0.04
3	300	0.54	0.05	300	0.54	0.05
4	400	0.73	0.06	400	0.73	0.06
5	500	0.91	0.06	500	0.91	0.082
6	700	1.27	0.073	700	1.27	0.10

Table 4.55 Initial dye concentrations and their corresponding rates for RB-220 degradation by UV and solar photocatalysis.

S. No.	UV photocatalysis			solar photocatalysis		
	$C_{0RB-220}$ (mg/L)	$C_{0RB-220}$ (mM)	Rate (mM/min)	$C_{0RB-220}$ (mg/L)	$C_{0RB-220}$ (mM)	Rate (mM/min)
1	100	0.14	0.023	100	0.14	0.027
2	200	0.27	0.045	200	0.27	0.045
3	300	0.41	0.055	300	0.41	0.068
4	400	0.55	0.068	400	0.55	0.091
5	500	0.68	0.082	500	0.68	0.11
6	-	-	-	700	0.95	0.123

Table 4.56 Values of k_{obs} and k_R for UV and solar photocatalysis AY-17 and RB-220 dyes.

AY-17 under UV light		AY-17 under solar light		RB-220 under UV light		RB-220 under solar light	
k_{obs} (mM. min^{-1})	k_R (mM)$^{-1}$	k_{obs} (mM. min^{-1})	k_R (mM)$^{-1}$	k_{obs} (mM. min^{-1})	k_R (mM)$^{-1}$	k_{obs} (mM. min^{-1})	k_R (mM)$^{-1}$
0.10	1.55	0.12	1.82	0.19	1.20	0.21	1.5
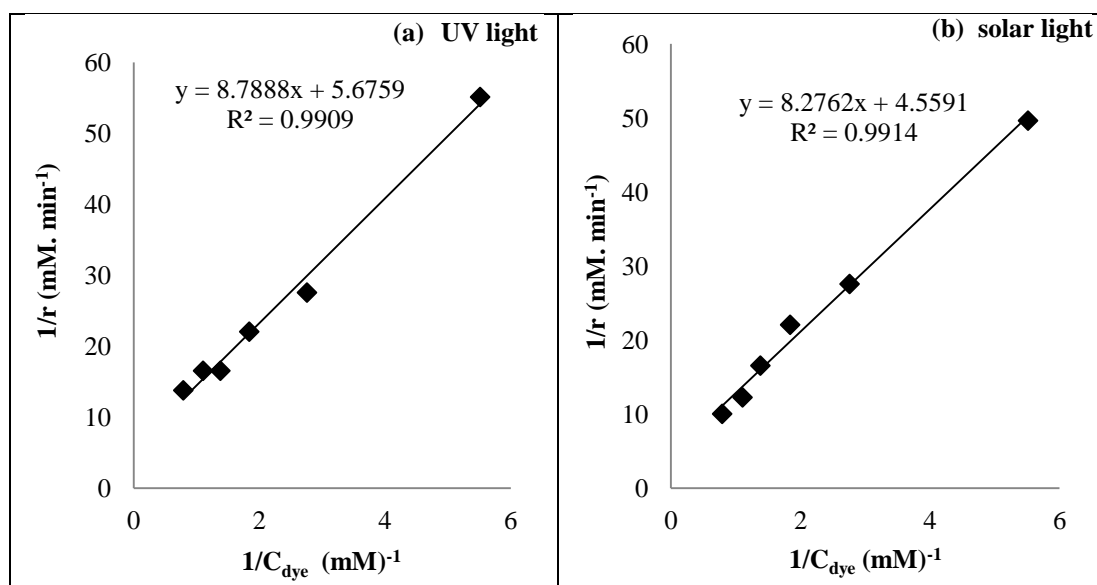
Figure 4.68 Plot of linear form of L-H kinetic model for AY-17 dye.
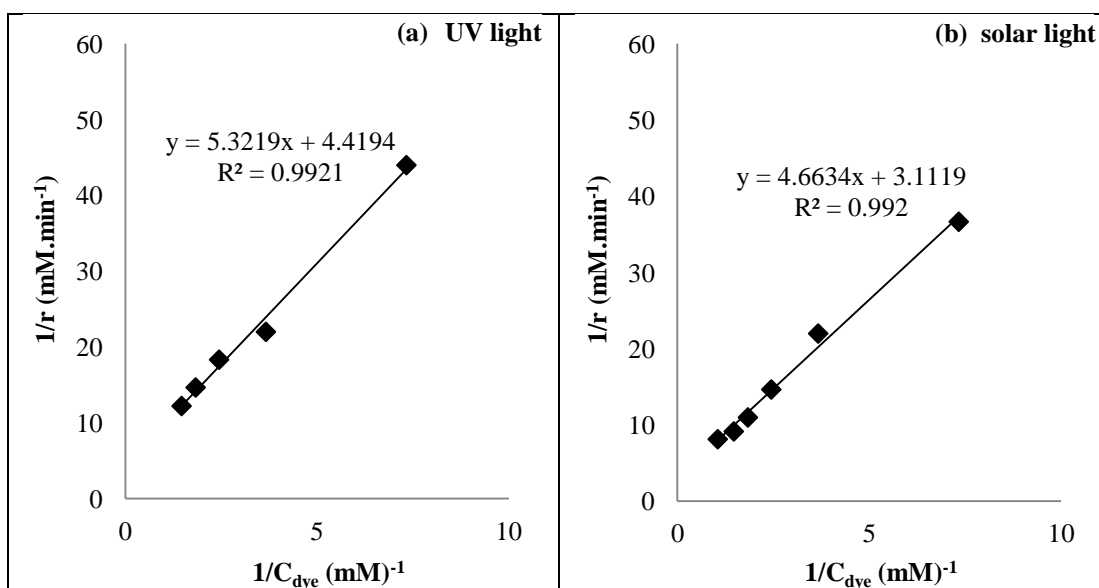
Figure 4.69 Plot of linear form of L-H kinetic model for RB-220 dye.

4.11 Effect of light intensity on the photocatalytic degradation of AY-17 and RB-220

Light intensity is a very important parameter in photocatalysis, as the light is to be absorbed by catalyst to initiate the reaction. The rate of initiation step in photocatalysis that is generation of electron and holes is dependent on the light intensity. The pollutant conversion and degradation efficiency depends on the

distribution of light intensity in the reactor (Ollis et al. 1991). So effect of UV and solar light intensity was studied on the photocatalytic degradation of AY-17 and RB-220 dyes. All the experiments were conducted with crude optimized conditions as obtained from Section 4.6.

a) Under UV light

Batch photocatalysis experiments were carried out in an immersion well reactor to study the effect of light intensity on photocatalysis of AY-17 and RB-220 dyes using Ag@TiO$_2$ core shell structured nanoparticles as a photocatalyst under UV light irradiation with medium pressure mercury vapor lamps of 80 W and 125 W power. These experiments were conducted with crude optimized condition and air at flow rate of 2 LPM was used as the oxidant. In these experiments ammonium persulfate was not used as an oxidant, but air was supplied as a source of oxidant. Addition of ammonium persulfate was found not necessary, as air itself was found sufficient due to high power of UV lamps. The rate of photocatalysis with air itself was very rapid. The effect of UV radiation power on the photocatalytic degradation of AY-17 and RB-220 dyes was studied at initial dye concentration of 100 mg/L, pH=3 and with catalyst loading of 3 g/L for AY-17 and 2 g/L for RB-220. The results with lamps of 80 W and 125 W powers are presented in Figure 4.70. The average UV light intensities measured at the surface of immersion well reactor with 80 and 125 W are 11.2 and 13.5 mW/cm^2 respectively. Time course variations of AY-17 and RB-220 dye concentrations obtained with different average UV light intensities are shown in Table 4.57 for UV photocatalysis. Figure 4.70 clearly shows that the rate of removal increases with increasing UV light intensity for both the dyes. As UV power increases from 80 to 125 W, UV light radiation intensity also increases from 11.2 to 13.5 mW/cm^2 which increases the degradation of AY-17 from 74.83 to 92.3 % and RB-220 from 79.22 to 94.55 % (in 5 min irradiation). Almost complete degradation of both the dyes was achieved in 10 min with 125 W lamp, whereas with 80W lamp it took around 20 min for the same degradation. When the experiments were conducted in batch stirred reactor illuminated from outside by two UV lamps of 36 W each (UV light intensity= 5.85 mW/cm^2), under same set of conditions used in the immersion

well reactor, around 66 % degradation of AY-17 and 91 % degradation of RB-220 was achieved in 360 and 240 min of UV irradiation respectively as presented in Section 4.6.3. It clearly indicates that higher light intensity enhances the rate of photocatalysis.

UV light intensity determines the amount of photon absorbed by the catalyst. More photons are absorb by the catalyst surface with increase of UV light intensity as a result more formation of electron–hole pairs occurs on the catalyst surface which further increase concentration of hydroxyl radicals and consequently increases the rate of photocatalysis. Previous studies (Oliveira et al. 1990; Inel and Okte 1996; Muruganandham and Swaminathan 2006b) on the effect of light intensity have shown the following relationship between intensity and degradation rate: (i) at low light intensities, with increase in radiation intensity the rate of degradation increases linearly, (ii) at intermediate light intensities, the rate of degradation depends on the square root of the radiation intensity and (iii) at high light intensities, the rate is independent of radiation intensity. The transition points between these regimes will vary with pollutant and photocatalyst species. According to Daneshvar et al. (2004) the linear relation indicates that saturation of the catalyst by the incident photons was not reached and electron–hole pairs are consumed more rapidly by chemical reactions than by recombination, therefore the rate of formation of the electron–hole pairs is directly proportional to the light intensity. Since light intensity used in present study is below 20 mW/cm^2 and it is reported in literature that, below this intensity, rate follows linear relationship hence it was assumed that the rate and intensity to have linear relation. The initial rates obtained were 0.04 mM.min^{-1} and 0.05 mM.min^{-1} for AY-17 and 0.03 mM.min^{-1} and 0.04 mM.min^{-1} for RB-220 with light intensities of 11.2 and 13.5 mW/cm^2. The relationship between the rate of degradation of the dyes with UV light intensity are given by Eq.(4.8).

$$rate = K_I.I \qquad\qquad\qquad\qquad (4.8)$$

where I is the light intensity and K_I is the constant of proportionality. K_I values were found to be 33×10^{-4} (mM.cm^2).(mW.min)$^{-1}$ for AY-17 degradation and 28×10^{-4} (mM.cm^2).(mW.min)$^{-1}$ for RB-220 degradation. Muruganandham and Swaminathan (2006b) and Ollis et al. (1991) have reported linear increase in rate with increase in radiation intensity, at lower light intensity of < 20 mW/cm^2. The intensities used in

the present study are less than 20 mW/cm^2 and hence the linear increase in rate with increase in UV light intensity is justified.

Table 4.57 Time course variation of concentration of AY-17 and RB-220 obtained with different average light intensies during UV photocatalysis. Conditions: C$_0$= 100 mg/L; pH=3; Ag@TiO$_2$ loading= 3 g/L (AY-17) and 2 g/L (RB-220).

Time (min)	C$_{AY-17}$ (mg/L)		C$_{RB-220}$ (mg/L)	
	Average light intensity		Average light intensity	
	11.2 mW/cm^2	13.5 mW/cm^2	11.2 mW/cm^2	13.5 mW/cm^2
0	100	100	100	100
5	25.17	7.72	20.78	5.45
10	6.6	2.9	5.75	2.58
15	3.87	1.9	2.59	1.65
20	1.98	0.95	1.13	0.67
25	0.82	0.3	0.59	0.38
30	0.44	0.19	0.28	0.19
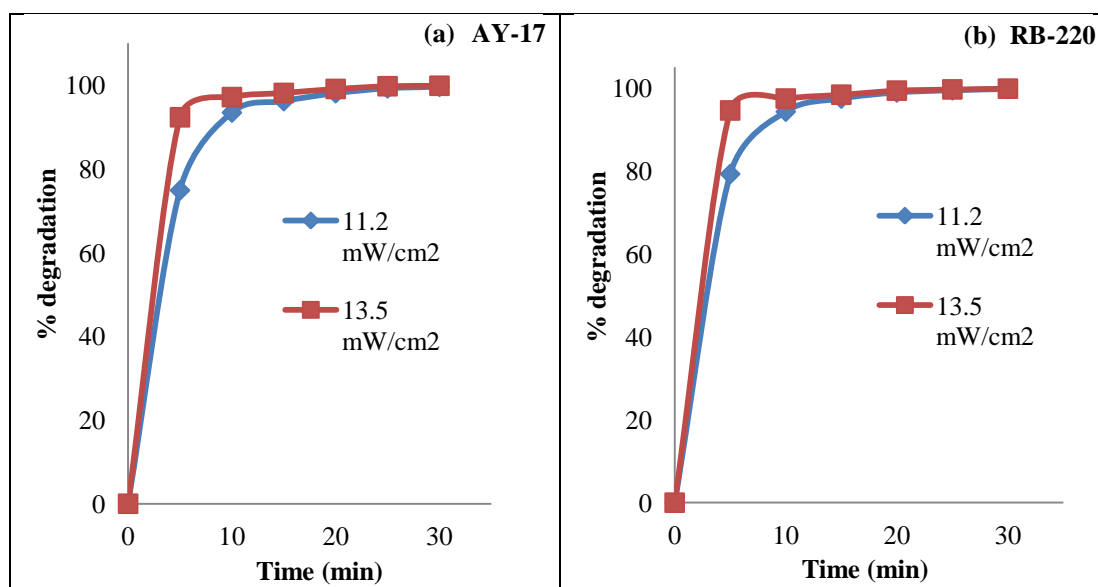
Figure 4.70 Effect of UV light intensity on the photocatalytic degradation of dyes a) AY-17 b) RB-220. Conditions: C$_0$= 100 mg/L; pH=3; Ag@TiO$_2$ loading= 3 g/L (AY-17) and Ag@TiO$_2$ loading= 2 g/L (RB-220).

b) Solar light

Batch photocatalysis experiments were carried out in a batch stirred reactor to study the effect of light intensity on solar photocatalysis of AY-17 and RB-220 dyes using Ag@TiO$_2$ core shell structured nanoparticles as a photocatalyst on a sunny day, semi cloudy day and a cloudy day. These experiments were conducted with crude optimized condition and no additional oxidant was used in this study. Dissolved and atmospheric oxygen itself acted as an oxidant. The effect of solar light intensity on photocatalytic degradation of AY-17 and RB-220 dyes were studied at initial concentration of 100 mg/L, pH=3 and with catalyst loading of 1 g/L. Three experiments were performed at different conditions of illumination; one on a full sunny day (clear sky), another on a semi cloudy day, and the other on full cloudy day as shown in Figure 4.71. The average UV and Visible light intensities on a full sunny, semi and full cloudy day are presented in Table 4.58. Visible light intensity was measured in terms of lux which is a measure of illuminance. The lux is one lumen per square meter (lm/m^2), and the corresponding radiometric unit, which measures intensity, is the watt per square meter (W/m^2). There is no single conversion factor between lux and W/m^2; there is a different conversion factor for every wavelength, and it is not possible to make a conversion unless one knows the spectral composition of the light. The peak of the luminosity function is at 555 nm (green). For monochromatic light of this wavelength, the irradiance needed to make one lux is the minimum, at 1.464×10^{-4} mW/cm^2. So the visible light intensity of solar light was calculated in terms of mW/cm^2 by assuming wavelength at 555 nm (as reference). The values are presented in Table 4.58. Time course variations of AY-17 and RB-220 dye concentrations obtained with different average solar light intensity are shown in Table 4.59 for UV and solar photocatalysis. It could be noticed from Figure 4.71a, around 60 % degradation of AY-17 occurred on a full sunny day and around 39 % and 15 % degradation of AY-17 was observed on semi and full cloudy day after 60 min of irradiation time. As seen from Figure 4.71a, degradation increased with increase in irradiation time and around 97 %, 84 %, and 62 % degradation of AY-17 took place in 360 min on a full sunny, semi and full cloudy day respectively. Since the UV and

visible light intensities on full cloudy day are much less as compared to full sunny day, the degradation of AY-17 dye was not completed on a full cloudy day.

Figure 4.71b shows that, during photocatalysis of RB-220 around 69 % degradation occurred on a full sunny and around 39 % and 16 % degradation was observed on semi and full cloudy day after 60 min of irradiation time. As observed from Figure 4.71b, degradation increased with increase in irradiation time and around 100 %, 90 %, and 67 % degradation of RB-220 took place with a full sunny, semi and full cloudy day respectively. Due to lower UV and visible light intensities on full cloudy day as compared to full sunny day, the degradation of RB-220 dye was not completed on a full cloudy day.

This suggests that when the light intensity is much less, hydroxyl and oxygen radicals could not be generated properly and constantly on a full cloudy day (Ali et al. 1996). Such an effect was expected as light intensity determines the amount of photon absorbed by the catalyst. Under the higher intensity of light illumination, the degradation was considerably higher because the electron-hole formation and storage of electron in Ag core is predominant and, hence, electron-hole recombination is negligible. However, at lower light intensity such as on full cloudy day, rate of electron-hole pair generation and storage in the Ag core may be much lesser than the rate of recombination which in turn decreases the formation of free radicals, causing reduction in the photocatalytic degradation of AY-17 and RB-220 dye.

The initial rates of degradation of dyes were calculated using the tangents drawn at t=0, on concentration - time data obtained with photocatalysis of AY-17 and RB-220 on full sunny day, semi cloudy day and cloudy day. Rate versus average UV and Visible light intensity of sunlight on these days were plotted for AY-17 and RB-220 dyes as shown in Figure 4.72 and Figure 4.73 respectively and the values of K_I were estimated from the slope. The rate of degradation of AY-17 and RB-220 were found to increase linearly with UV and visible light intensity and the corresponding K_I values are presented in Table 4.58 for AY-17 and RB-220 degradation under solar light irradiation. Linear nature of Figure 4.72 and Figure 4.73 confirms that rate increases linearly with UV and Visible light intensity. Similar result was reported in earlier studies (Muruganandham and Swaminathan 2006b; Ollis et al. 1991) and as explained in Section 4.11.1 it was reported that at lower light intensity of 0-20

mW/cm^2, the rate increases linearly with increasing radiation intensity. The rate of degradation of AY-17 under a sunny day was about two and three times higher than that of photocatalytic degradation under a semi cloudy and full cloudy day, respectively. The rate of degradation of RB-220 under a full sunny day was about two and three times higher than that of photocatalytic degradation under a semi cloudy and full cloudy day, respectively.

Table 4.58 Variation of solar light intensity and K_I values for three different irradiation conditions

	Full Sunny day		Semi cloudy day		Full cloudy day	
	UV	**Visible**	**UV**	**Visible**	**UV**	**Visible**
Average light intensity	3.56 (mW/cm^2)	13×10^4 (lux) 17.93 (mW/cm^2)	2.65 (mW/cm^2)	92×10^3 (lux) 13.39 (mW/cm^2)	1.25 (mW/cm^2)	45×10^3 (lux) 6.51 (mW/cm^2)
K_I $(mM.cm^2)$ $(mW.min)^{-1}$ for AY-17			5×10^{-4} (UV)	1×10^{-4} (Visible)		
K_I $(mM.cm^2)$ $(mW.min)^{-1}$ for RB-220			7×10^{-4} (UV)	1×10^{-4} (Visible)		

Table 4.59 Time course variation of concentration of AY-17 and RB-220 obtained under three different conditions of the day during solar photocatalysis. Conditions: C_0= 100 mg/L; pH=3; Ag@TiO$_2$= 1 g/L.

Time (min)	C_{AY-17} (mg/L)			C_{RB-220} (mg/L)		
	Full Sunny day	Semi cloudy day	Full cloudy day	Full Sunny day	Semi cloudy day	Full cloudy day
0	100	100	100	100	100	100
60	39.95	61.45	85.21	10.28	45.21	74.93
120	23.88	42.58	74.77	0.63	30.00	65.35
180	14.32	30.65	63.13	0.63	21.83	57.89
240	8.55	24.67	51.6	0.42	16.06	49.58
300	5.85	20.5	43.18	0.28	11.55	41.69
360	3.1	16.2	37.64	0.21	10.00	34.37
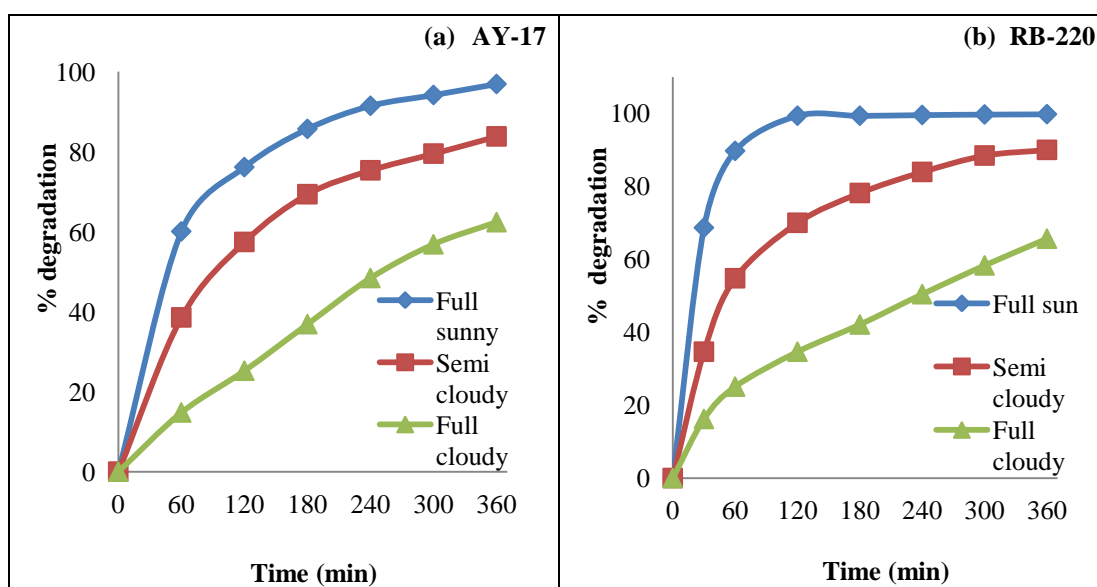
Figure 4.71 Effect of solar light intensity on the photocatalytic degradation of dyes a) AY-17 b) RB-220. Conditions: C_0= 100 mg/L; pH=3; Ag@TiO$_2$ loading= 1 g/L.
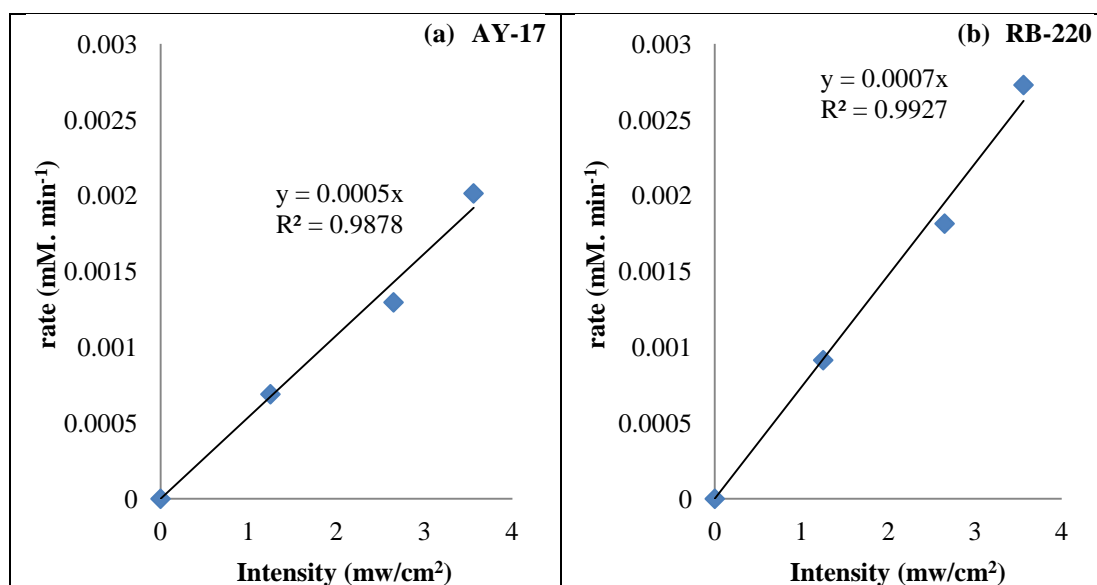
Figure 4.72 Linear relationship of rate versus UV light intensity during solar photocatalysis of a) AY-17 b) RB-220.
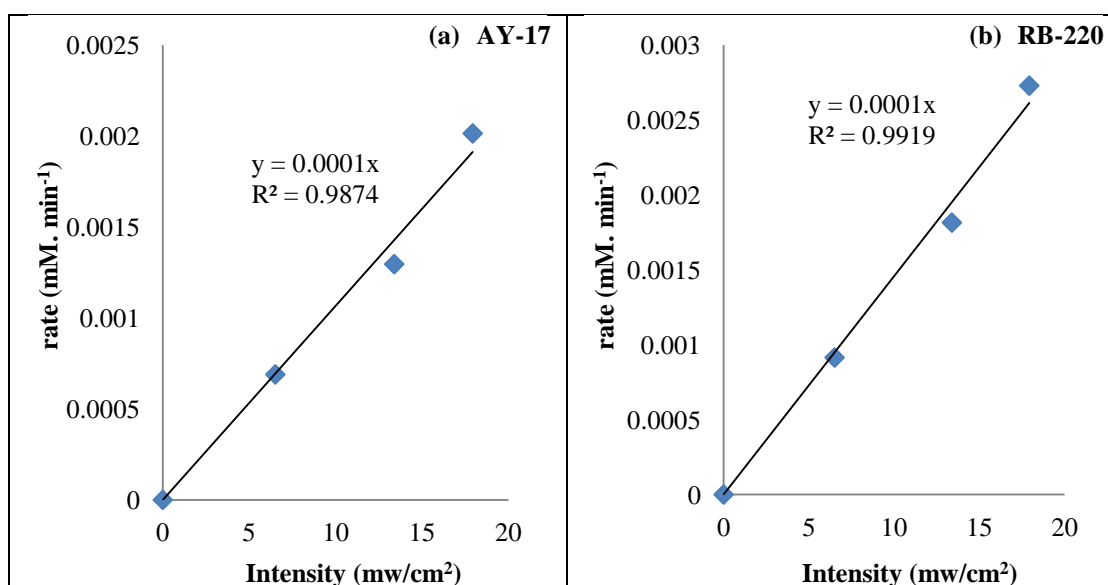
Figure 4.73 Linear relationship of rate versus visible light intensity during solar photocatalysis of a) AY-17 b) RB-220.

4.12 Effect of presence of NaCl and Na_2CO_3 on the photocatalytic degradation of AY-17 and RB-220 under UV and solar light irradiation

In the dyeing process, the other auxiliary chemicals such as sodium carbonate (Na_2CO_3) and sodium chloride (NaCl) are used. To adjust the pH of dye bath, Na_2CO_3

is added which plays a significant role in fastness of colour and dye fixation on the fabrics dye on the fabrics. NaCl is also added during dying process for the transfer of dyes to fabric. The dye industry wastewater contains a considerable amount of carbonate and chloride ions. Presence of these chemicals in wastewater may alter the rate of photocatalysis. So, the effect of presence of NaCl and Na_2CO_3 on the photocatalytic degradation of AY-17 and RB-220 under UV and solar light at RSM based methodically optimized conditions were studied in a batch stirred reactor. RSM based methodically optimized conditions for the photocatalytic degradation of AY-17 and RB-220 at initial concentration of 100 mg/L under UV and solar light irradiation are presented in Table 4.47.

(a) UV light irradiation

The time course variations of dye concentrations during the UV photocatalysis of AY-17 and RB-220 dye with different concentrations of NaCl are presented in Table 4.60-4.61 respectively. The influence of Cl^- ion on the photocatalytic degradation of AY-17 and RB-220 was studied by conducting experiments in the presence and absence of NaCl and the results are presented in Figure 4.74a and 4.74b respectively. As seen from Figure 4.74, in the absence of NaCl rate of degradation is more as compared to that in the presence of NaCl. Addition of NaCl has tremendously reduced the rate of degradation of the dyes. Increased addition of NaCl from 25 mg/L to 100 mg/L to the reaction mixture decreases the degradation (after 60 min) of AY-17 from 96.44 to 77.40 % and RB-220 from 98.38 to 85.63 %. The degradation (after 120 min of irradiation) decreased from 99.02 to 92.56 % for AY-17 as the NaCl concentration was increased from 25 mg/L to 100 mg/L. Similarly addition of NaCl from 25 mg/L to 100 mg/L has decreased the degradation (at 120 min irradiation time) of RB-220 from 99.23 to 96.41 %. Rate of degradation has decreased with the increased addition of NaCl. The hole and hydroxyl radical scavenging property of Cl^- results in the decrease in photocatalytic degradation efficiency (Wenhua et al. 2000). The chloride radical anions formed can also block the reactive sites of the catalyst surface.

The effect of presence of CO_3^{2-} ion on the photocatalytic degradation of AY-17 and RB-220 was studied by conducting experiments with and without the presence of Na_2CO_3 and the results are shown in Figure 4.75. The time course variations of AY-17 and RB-220 dye concentrations during the UV photocatalysis of AY-17 and RB-220 dyes with different concentrations of Na_2CO_3 are presented in Table 4.62. Addition of 25 to 50 mg/L of Na_2CO_3 decreases the degradation (after 60 min) of AY-17 from 92.74 to 82.91 % and RB-220 from 92.25 to 83.38 %. As seen from Figure 4.75, in the absence of Na_2CO_3, rate of degradation is more as compared to that in the presence of Na_2CO_3 and the rate decreases with the increase in Na_2CO_3 concentration. The hydroxyl radical scavenging property of carbonate ion results in decrease in the degradation efficiency of the dye. Thus, the primary oxidant hydroxyl radical decreases gradually with the increase in carbonate ion and consequently there is a significant decrease in photocatalytic oxidation.

(b) Solar light irradiation

The time course variations of dye concentrations during the solar photocatalysis of AY-17 and RB-220 dye with different concentrations of NaCl are presented in Table 4.63 and Table 4.64 respectively. The influence of Cl^- ion on the solar photocatalytic degradation of AY-17 and RB-220 was studied and the results are shown in Figure 4.76. Increased addition of NaCl from 25 mg/L to 100 mg/L to the reaction mixture decreases the degradation (after 60 min) of AY-17 from 97.81 to 87.91 % and RB-220 from 98.73 to 91.41 %. The degradation of AY-17 decreased from 99.26 to 96.56 % as the NaCl concentration was increased from 25 mg/L to 100 mg/L. Similarly addition of NaCl from 25 mg/L to 100 mg/L has decreased the degradation (at 120 min irradiation time) from 99.86 to 98.66 % for RB-220. As seen from Figure 4.76, in the absence of NaCl rate of degradation is more as compared to that in the presence of NaCl. Rate of degradation has decreased with the increased addition of NaCl. The reason for decrease in the degradation of the dye in the presence of NaCl is as explained in Section 4.12a.

The effect of presence of CO_3^{2-} ion on the photocatalytic degradation of AY-17 and RB-220 were also studied and the time course variations of AY-17 and RB-

220 dye concentrations during the solar photocatalysis of AY-17 and RB-220 dye with different concentrations of Na_2CO_3 are presented in Table 4.65. Addition of 25 to 50 mg/L of Na_2CO_3 decreases the degradation (after 60 min) of AY-17 from 97.56 to 90.72 % and RB-220 from 97.61 to 92.32 %. As seen from Figure 4.77, in the absence of Na_2CO_3 rate of degradation is more as compared to that in the presence of Na_2CO_3 and the rate decreases with the increase in Na_2CO_3 concentration. The reason for decrease in the degradation of the dye by the presence of Na_2CO_3 is as explained in Section 4.12a.

So it may be concluded that the presence of salts *viz.* NaCl and Na_2CO_3 affect the photocatalytic activity of $Ag@TiO_2$ nanoparticles during UV and solar photocatalysis of AY-17 and RB-220. So it is important to take salt concentration in the effluent into consideration while designing the photoreactor for treatment of dyeing wastewater.

Table 4.60 Time course variation of concentration of AY-17 obtained with different initial concentration of NaCl (mg/L) during UV photocatalysis. Conditions: C_0= 100 mg/L; pH=2.9; Catalyst loading= 3.4 g/L; $(NH_4)_2S_2O_8$= 2.25 g/L.

Time (min)	C_{AY-17} (mg/L) obtained with different initial concentrations of NaCl				
	C_{NaCl}=0 mg/L	C_{NaCl}=25 mg/L	C_{NaCl}=50 mg/L	C_{NaCl}=75 mg/L	C_{NaCl}=100 mg/L
0	100	100	100	100	100
15	1.22	37.81	52.50	67.72	80.19
30	0.28	16.19	26.37	38.01	53.21
45	0.23	7.12	12.37	20.43	33.86
60	0.03	3.56	5.78	12.45	22.60
90	0.03	2.02	3.09	5.21	12.65
120	0.03	0.98	1.87	2.69	7.44

Table 4.61 Time course variation of concentration of RB-220 obtained with different initial concentration of NaCl (mg/L) during UV photocatalysis. Conditions: C_0= 100 mg/L; pH=3.2; Catalyst loading= 1.8 g/L; $(NH_4)_2S_2O_8$= 1.3 g/L.

Time (min)	C_{RB-220} (mg/L) obtained with different initial concentrations of NaCl				
	C_{NaCl}=0 mg/L	C_{NaCl}=25 mg/L	C_{NaCl}=50 mg/L	C_{NaCl}=75 mg/L	C_{NaCl}=100 mg/L
0	100	100	100	100	100
15	4.33	31.34	43.10	59.23	71.27
30	0.46	15.77	21.97	30.63	41.69
45	0.08	6.83	11.76	16.69	24.72
60	0.06	1.62	3.66	8.59	14.37
90	0.06	1.20	1.76	3.17	8.73
120	0.04	0.77	0.11	1.55	3.59

Table 4.62 Time course variation of concentration of AY-17 and RB-220 obtained with different initial concentrations of Na_2CO_3 (mg/L) during UV photocatalysis. Conditions: C_0= 100 mg/L; pH=2.9; Catalyst loading= 3.4 g/L; $(NH_4)_2S_2O_8$ = 2.25 g/L (AY-17) and pH=3.2, Catalyst loading= 1.8 g/L, $(NH_4)_2S_2O_8$= 1.3 g/L (RB-220).

Time (min)	Concentration of dye obtained with different initial concentration of Na_2CO_3					
	AY-17			RB-220		
	C_{Na2CO3}= 0 mg/L	C_{Na2CO3}=25 mg/L	C_{Na2CO3}=50 mg/L	C_{Na2CO3}= 0 mg/L	C_{Na2CO3}=25 mg/L	C_{Na2CO3}=50 mg/L
0	100	100	100	100	100	100
15	1.22	47.02	66.77	4.33	48.24	72.54
30	0.28	23.93	45.07	0.46	25.07	45.49
45	0.23	13.81	26.86	0.08	14.44	26.34
60	0.03	7.26	17.09	0.06	7.75	16.62
90	0.03	2.72	9.14	0.06	3.38	9.23
120	0.03	1.26	3.98	0.04	1.48	4.01

Table 4.63 Time course variation of concentration of AY-17 obtained with different initial concentration of NaCl (mg/L) during solar photocatalysis. Conditions: C_0= 100 mg/L; pH=2.1; Catalyst loading= 1.8 g/L; $(NH_4)_2S_2O_8$= 2.71 g/L.

Time (min)	C_{AY-17} (mg/L) obtained with different initial concentrations of NaCl				
	$C_{NaCl}=0$ mg/L	$C_{NaCl}=25$ mg/L	$C_{NaCl}=50$ mg/L	$C_{NaCl}=75$ mg/L	$C_{NaCl}=100$ mg/L
0	100	100	100	100	100
15	0.66	17.05	31.12	47.58	65.58
30	0.16	6.84	14.58	23.93	39.44
45	ND	3.44	8.51	12.91	20.56
60	ND	2.19	4.47	7.26	12.09
90	ND	1.33	2.02	3.77	6.42
120	ND	0.74	0.98	1.67	3.44

Table 4.64 Time course variation of concentration of RB-220 obtained with different initial concentration of NaCl (mg/L) during solar photocatalysis. Conditions: C_0= 100 mg/L; pH=3.3, Catalyst loading= 1.11 g/L, = $(NH_4)_2S_2O_8$= 1.36 g/L.

Time (min)	C_{RB-220} (mg/L) obtained with different initial concentrations of NaCl				
	$C_{NaCl}=0$ mg/L	$C_{NaCl}=25$ mg/L	$C_{NaCl}=50$ mg/L	$C_{NaCl}=75$ mg/L	$C_{NaCl}=100$ mg/L
0	100	100	100	100	100
15	0.09	14.79	29.01	44.65	59.30
30	0.02	6.62	14.58	20.28	31.34
45	ND	3.94	6.20	10.49	17.39
60	ND	1.27	2.61	4.01	8.59
90	ND	0.56	0.85	1.55	3.17
120	ND	0.14	0.35	0.99	1.34

Table 4.65 Time course variation of concentration of AY-17 and RB-220 obtained with different initial concentration of Na$_2$CO$_3$ (mg/L) during solar photocatalysis. Conditions: C$_0$= 100 mg/L; pH=2.1; Catalyst loading= 1.8 g/L; (NH$_4$)$_2$S$_2$O$_8$= 2.71 g/L (AY-17) and pH=3.3, Catalyst loading= 1.11 g/L, = (NH$_4$)$_2$S$_2$O$_8$= 1.36 g/L (RB-220).

Time (min)	Concentration of dye obtained with different initial concentration of Na$_2$CO$_3$					
	AY-17			RB-220		
	C$_{Na2CO3}$= 0 mg/L	C$_{Na2CO3}$=25 mg/L	C$_{Na2CO3}$=50 mg/L	C$_{Na2CO3}$= 0 mg/L	C$_{Na2CO3}$=25 mg/L	C$_{Na2CO3}$=50 mg/L
0	100	100	100	100	100	100
15	0.66	30.47	65.28	0.09	36.06	57.25
30	0.16	13.26	33.86	0.02	15.21	28.03
45	ND	6.10	18.64	ND	6.69	15.56
60	ND	2.44	9.28	ND	2.39	7.68
90	ND	1.16	4.56	ND	1.06	2.89
120	ND	0.76	1.87	ND	0.28	0.99
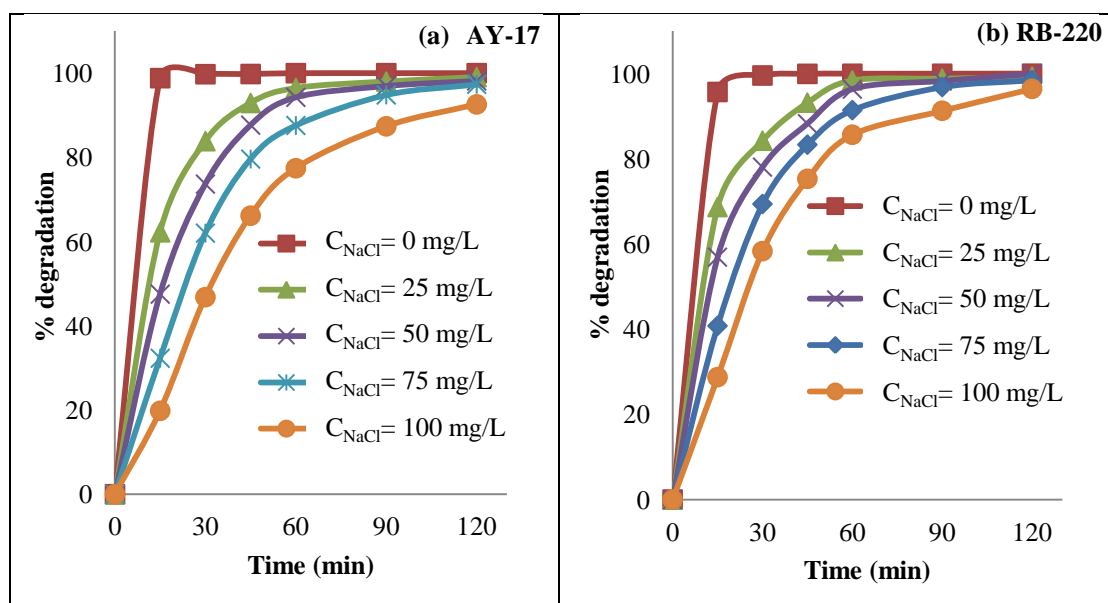
Figure 4.74 Effect of presence of NaCl on time course variation of UV photocatalytic degradation of dyes (a) AY-17. Conditions: C$_0$=100 mg/L; pH=2.9; Catalyst loading= 3.4 g/L; (NH$_4$)$_2$S$_2$O$_8$= 2.25 g/L (b) RB-220. Conditions: C$_0$=100 mg/L; pH=3.2, Catalyst loading= 1.8 g/L, (NH$_4$)$_2$S$_2$O$_8$= 1.3 g/L.
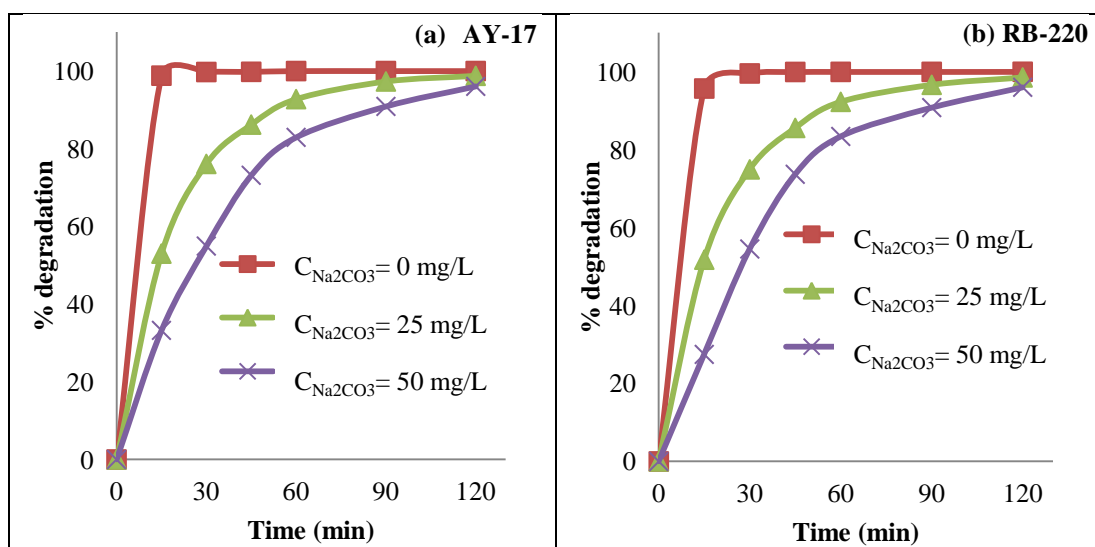
Figure 4.75 Effect of presence of Na$_2$CO$_3$ on time course variation of UV photocatalytic degradation of dyes (a) AY-17. Conditions: C$_0$=100 mg/L; pH=2.9; Catalyst loading= 3.4 g/L; (NH$_4$)$_2$S$_2$O$_8$= 2.25 g/L (b) RB-220. Conditions: C$_0$=100 mg/L; pH=3.2, Catalyst loading= 1.8 g/L, (NH$_4$)$_2$S$_2$O$_8$= 1.3 g/L.
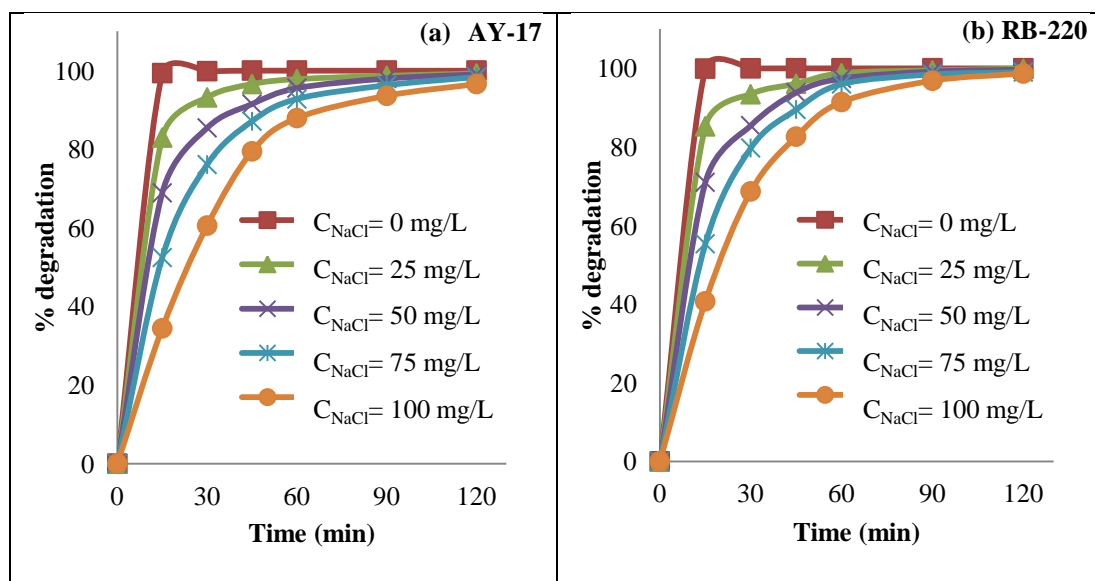
Figure 4.76 Effect of presence of NaCl on time course variation of solar photocatalytic degradation of dyes a) AY-17 b) RB-220. Conditions: pH=2.1; Catalyst loading= 1.8 g/L; (NH$_4$)$_2$S$_2$O$_8$= 2.71 g/L; average UV and visible light intensity of solar light= 3.62 mW/cm^2 and 1224×100 lux respectively from 11 a.m. to 1 p.m. (AY-17) and pH=3.3, Catalyst loading= 1.11 g/L, = (NH$_4$)$_2$S$_2$O$_8$= 1.36 g/L; average UV and visible light intensity of solar light= 3.58 mW/cm^2 and 1217×100 lux respectively from 11 a.m. to 1 p.m. (RB-220).
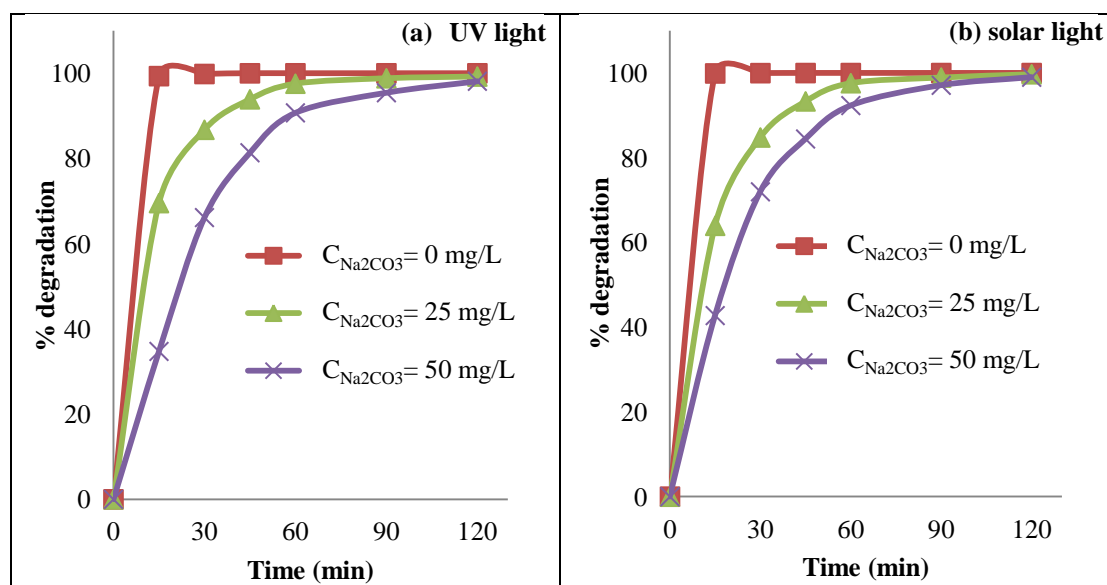
Figure 4.77 Effect of presence of Na$_2$CO$_3$ on time course variation of solar photocatalytic degradation of dyes a) AY-17 b) RB-220. Conditions: pH=2.1; Catalyst loading= 1.8 g/L; (NH$_4$)$_2$S$_2$O$_8$= 2.71 g/L; average UV and visible light intensity of solar light= 3.58 mW/cm^2 and 1205×100 lux respectively from 11 a.m. to 1 p.m. (AY-17) and pH=3.3; Catalyst loading= 1.11 g/L; = (NH$_4$)$_2$S$_2$O$_8$= 1.36 g/L; average UV and visible light intensity of solar light= 3.53 mW/cm^2 and 1221×100 lux respectively from 11 a.m. to 1 p.m. (RB-220).

4.13 Degree of mineralization of dyes during UV and solar photocatalysis

In order to assess the degree of dye mineralization achieved during the photocatalytic treatment, the formation of CO$_2$ and the inorganic ions (Bianco-Prevot et al. 2001; Zhang et al. 1998; Liu et al. 1999; Stylidi et al. 2003; Tanaka et al. 2000; Spadaro et al. 1994) is generally determined. However, in real wastewaters the monitoring of inorganic ions and CO$_2$ gives only a global estimation on the well-functioning of the treatment, but does not provide information on the real decay of the contaminant. In such cases the determination of total organic carbon (TOC) and/or the measurement of the chemical oxygen demand (COD) or the biological oxygen demand (BOD) of the photocatalytically treated water is generally used for monitoring the mineralization of the dyes (Neppolian et al. 2002a; Zhang et al. 1998; Sakthivel et al. 2003; So et al. 2002; Tanaka et al. 2000; Hu et al. 2003; Chun and Yizhong 1999). So

photocatalytic mineralization of dyes (AY-17 and RB-200) under UV and solar light irradiation was studied by measuring TOC and COD of the dye solution. Batch experiments were performed under UV and solar light at corresponding RSM based methodically optimized conditions for the dyes (AY-17 or RB-220). Optimum conditions for the photocatalytic degradation of AY-17 and RB-220 at initial concentration of 100 mg/L under UV and solar light irradiation are presented in Table 4.47. For solar photocatalysis of AY-17 and RB-220 dye, average UV and visible light intensity of solar light= 3.61 mW/cm^2 and 1215×100 lux respectively from 11 a.m. to 1 p.m.

Figure 4.78 presents the time course variation of percentage removal of TOC during photocatalytic degradation of the dyes (AY-17 and RB-220) under UV and solar light. As shown in Figure 4.78, percentage removal of TOC of AY-17 and RB-220 increases as the irradiation time increases. As it can be seen from Figure 4.78a, within 60 min of irradiation time TOC removal of around 88 % and 89 % occurred under UV and solar light respectively during the photocatalytic degradation of AY-17. There is no much variation in TOC removal occurred after, even upto 120 min of irradiation time. Figure 4.78b clearly shows that within 60 min of irradiation time TOC removal of around 76 % and 79 % occurred under UV and solar light respectively during the photocatalytic degradation of RB-220 and around 87 % and 90 % TOC removal was observed after 120 min of irradiation respectively.

TOC removal in solar photocatalysis is slightly higher than UV photocatalysis for RB-220 dye, but for AY-17 dye the TOC removal is similar for both UV and solar photocatalysis.

Figure 4.79 shows the COD removal during UV and solar photocatalysis of AY-17 and RB-220 dyes. As irradiation time increases, percentage COD removal during photocatalysis of the dyes increases. It can be seen from Figure 4.79a, within 60 min of irradiation time COD removal of around 78 % and 84 % occurred under UV and solar light respectively during the photocatalytic degradation of AY-17. Around 83 % and 88 % COD removal was observed for AY-17 after 120 min of UV and solar irradiation respectively. As observed from Figure 4.79b, within 60 min of irradiation time COD removal of around 70 % and 75 % occurred under UV and solar light respectively during the photocatalytic degradation of RB-220. Around 85 % and

89 % COD removal was observed for RB-220 after 120 min of UV and solar irradiation respectively. However, mineralization was not complete probably due to presence of intermediate compounds which were resistant to UV/solar photocatalytic degradation by the Ag@TiO$_2$ nanoparticles or more irradiation time is needed for mineralization of these intermediates.

Table 4.66 shows the comparison of percentage colour, TOC, and COD removal by photocatalysis of AY-17 and RB-220 obtained with Ag@TiO$_2$ nanoparticles in the present work, with those obtained by photocatalysis of different dyes in aqueous solutions using different catalysts reported in literature. As observed from Table 4.66 with other catalysts, even though almost 100 % colour removal occurred for most of the dyes, the extent of mineralization and hence the rate of COD and TOC removal were found to be much less than those obtained with Ag@TiO$_2$ nanoparticles. Ag@TiO$_2$ nanoparticles exhibited better and high rate of mineralization of AY-17 and RB-220 dyes as compared to TiO$_2$, which shows the potential of Ag@TiO$_2$ nanoparticles as effective catalysts for the degradation of dyes in waste water.

Table 4.66 Comparison of percentage colour, TOC and COD removal from water contaminated with different dyes as obtained by various researchers.

Name of dye	Catalyst used	Irradiation source	Irradiation time	C_0 (mg/L)	% colour removal	% COD removal	% TOC removal	Reference
Reactive Brilliant Red	TiO$_2$	Solar	4 h	20	≈100	-	80	Wang (2000)
Reactive Brilliant Red	TiO$_2$	Solar	4 h	20	≈100	-	61	Wang (2000)
Reactive Brilliant Red	TiO$_2$	Solar	4 h	20	≈100	-	70	Wang (2000)
Reactive Brilliant Red	TiO$_2$	Solar	4 h	20	≈100	-	55	Wang (2000)
Acid Yellow-17	TiO$_2$	UV	1 h	55	≈100	-	75	Tanaka et al. (2000)
Acid Orange-7	TiO$_2$	Solar	10 h	298	≈100	35	-	Stylidi et al. (2003)
Acid Orange-7	TiO$_2$	Vis	120 h	100	≈100	45	-	Stylidi et al. (2004)
Acid Yellow-17	TiO$_2$	UV	9 h	50	≈100	73	-	Liu et al. (2006)
Maxilon Navy Blue	TiO$_2$	Solar	4 h	100	99	-	75	Ghaly et al. (2007)
Reactive Blue-220	**Ag@TiO$_2$**	**UV**	**2 h**	100	**≈100**	**85**	**87**	**Present study**
Reactive Blue-220	**Ag@TiO$_2$**	**Solar**	**2 h**	100	**≈100**	**89**	**90**	**Present study**
Acid Yellow-17	**Ag@TiO$_2$**	**UV**	**2 h**	100	**≈100**	**87**	**89**	**Present study**
Acid Yellow-17	**Ag@TiO$_2$**	**Solar**	**2 h**	100	**≈100**	**90**	**90**	**Present study**
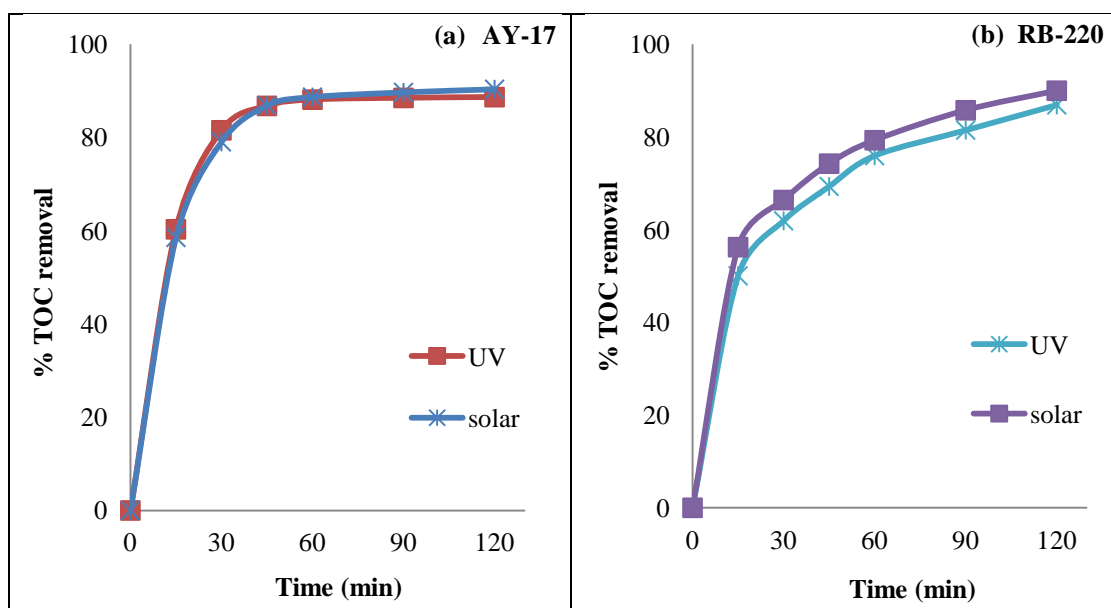
Figure 4.78 TOC removal of dyes during the UV and solar photocatalytic degradation under RSM based methodically optimized conditions (presented in Table 4.47) a) AY-17 b) RB-220. Conditions: C_0= 100 mg/L.
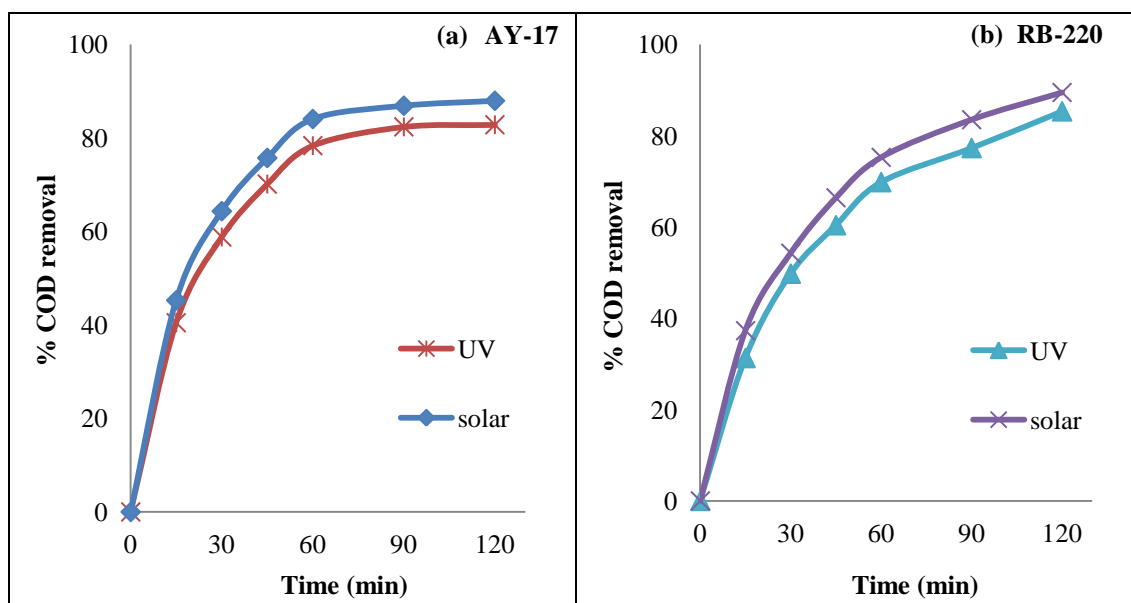
Figure 4.79 COD removal of dyes during the UV and solar photocatalytic degradation under RSM based methodical optimized conditions (presented in Table 4.47) a) AY-17 b) RB-220. Conditions: C_0= 100 mg/L.

In order to further understand if there are inorganic ions released during mineralization of AY-17 and RB-220 dyes by UV and solar photocatalysis in the presence of Ag@TiO$_2$ catalyst, the levels of inorganic ions produced during photocatalysis were monitored by spectrophotometric method as described in Section 3.6. The mineralization leads to conversion of organic carbon into harmless CO$_2$ and conversion of sulphur and nitrogen heteroatoms into inorganic ions such as sulphate, nitrate ions respectively (Houas et al. 2001). Figure 4.80 to 4.83 show the time course variation of inorganic ions formed (sulphate, nitrate, nitrite and chloride respectively) during photocatalytic degradation of the dyes (AY-17 and RB-220 respectively under UV and solar light.

As shown in Figure 4.80a, concentration of sulphate ions has increased as the irradiation time increased and around 211 mg/L and 196 mg/L sulphate ions formation occurred within 60 min of irradiation time during UV and solar photocatalysis of AY-17 respectively. After 120 min of irradiation, around 214 mg/L and 224 mg/L sulphate formation was observed during UV and solar photocatalysis of AY-17 dye respectively. Similar observations have been reported by other researchers during the degradation of AY-17 dye using TiO$_2$ (Tanaka et al. 2000; Liu et al. 2006). As seen from Figure 4.80b in case of RB-220, sulphate ion levels increase as irradiation time is increased and around 115 mg/L and 118 mg/L of sulphate ion formation occurred within 60 min; around 204 mg/L and 207 mg/L in 120 min of UV and solar light irradiation respectively. Similar observations have been reported by Mahmoodi et al. (2006) during the degradation of RB-220 dye using TiO$_2$. Formation of high concentrations of sulphate ions was observed, which may be due to the use of ammonium persulphate as oxidant in the reaction mixture. Muruganandham and Swaminathan, (2004, 2006 a,b) have reported that, when persulphate was used as an oxidant it lead to the formation of sulphate ions as described below:

(i) Persulphate ion can trap the conduction band electron and results in the formation of (SO$_4$$^{\bullet-}$ and sulphate ion SO$_4$$^{2-}$)

$$S_2O_8^{2-} + e^-_{(CB)} \rightarrow SO_4^{\bullet-} + SO_4^{2-} \tag{4.9}$$

The sulphate radical ion (SO$_4$$^{\bullet-}$) produced can add hydrogen to the unsaturated carbon, subtracts hydrogen from the saturated carbon or it can remove electrons from

the carboxylate anion and from certain neutral molecules of dye. In addition, it can trap the conduction band electrons and/or generate hydroxyl radical and sulphate ion

$$SO_4^{\bullet -} + e^-_{(CB)} \rightarrow SO_4^{2-} \tag{4.10}$$

$$SO_4^{\bullet -} + H_2O \rightarrow {}^{\bullet}OH + SO_4^{2-} + H^+ \tag{4.11}$$

The unique nature of the $SO_4^{\bullet -}$ also increases the fragmentation of the dye molecules by attacking at various position and result in the formation of sulphate ion

$$SO_4^{\bullet -} + dye \rightarrow SO_4^{2-} + dye^{+\bullet} \text{ (intermediates)} \tag{4.12}$$

$$SO_4^{\bullet -} + dye^{+\bullet} \text{ (intermediates)} \rightarrow SO_4^{2-} + CO_2 + HNO_3 + \text{other inorganics} \tag{4.13}$$

Since formation of sulphate ions increased with the irradiation time, it is proposed that the SO_3Na group would break from the dye molecule and be mineralized in the solution in the form of sulphate ion during the photocatalytic degradation of AY-17 and RB-220 under UV and solar light irradiation.

Figure 4.81 shows the time course variation of formation of nitrate ion during photocatalytic degradation of the dyes (AY-17 and RB-220) under UV and solar light. As seen from Figure 4.81a, concentration of nitrate ions during photocatalysis of AY-17 dye increases, as the irradiation time increases and 1.51 mg/L and 1.7 mg/L nitrate ion formation occurred within 60 min of irradiation time under UV and solar light respectively. After 120 min of UV and solar irradiation, 1.64 mg/L and 1.9 mg/L nitrate formation was observed during photocatalysis of AY-17 dye respectively. Similar observations have been reported by other researchers during degradation of AY-17 dye using TiO_2 (Tanaka et al. 2000; Liu et al. 2006). As seen from Figure 4.81b, in case of photocatalysis of RB-220, nitrate ion levels increase as irradiation time increases both under UV and solar light irradiation. 1.14 mg/L and 1.4 mg/L nitrate levels were observed within 60 min of irradiation time under UV and solar light respectively. After 120 min of UV and solar irradiation, nitrate levels reached to 1.4 mg/L and 1.71 mg/L respectively by photocatalysis of RB-220 dye. Similar observations have been reported by Mahmoodi et al. (2006) in degradation of RB-220 dye using TiO_2. Since formation of nitrate ions increased with the irradiation time, it is proposed that the azo group would break from the dye molecule and be mineralized

in the solution in the form of nitrate ion during the photocatalytic degradation of AY-17 and RB-220 under UV and solar light irradiation.

Figure 4.82 shows the time course variation of formation of chloride ion during photocatalytic degradation of AY-17 dye under UV and solar light. The result presented in Figure 4.82 shows that chloride levels increase as the reaction time increases during photocatalytic degradation of AY-17 under UV and solar light. Around 6 mg/L and 8 mg/L of chloride ion formation occurred within 60 min of irradiation time during photocatalysis of AY-17 under UV and solar light respectively. The chloride levels increased to 10 mg/L and 12 mg/L after 120 min of UV and solar irradiation respectively, during the photocatalysis of AY-17 dye. Wang, (2000) in their study on eight dyes with sunlight mediated photocatalytic treatment, proposed that the chlorine atom would break from the dye molecule and be released into the solution depending on the bonding position. The chlorine would break most easily if it is bonded in straight chain of the dye molecule followed by the site bonded in benzene ring; the chemical stability of the chlorine bonding structure is the key. Similar observations have been reported by other researchers during degradation of AY-17 dye using TiO_2 (Tanaka et al. 2000; Liu et al. 2006). No chloride ion formation occurs during photocatalytic degradation of RB-220 under UV and solar light irradiation as RB-220 has no chlorine atom in its molecule.

Figure 4.83 shows time course variation of the formation of nitrite ion during photocatalytic degradation of RB-220 dye under UV and solar light. The concentration of nitrite ions increased as the irradiation time increased, during the photocatalysis of RB-220. Around 38 mg/L and 48 mg/L of nitrite ions were formed within 60 min of irradiation time under UV and solar light respectively. The nitrite levels increased to around 50 mg/L and 61 mg/L after 120 min of UV and solar light irradiation respectively during the photocatalysis of RB-220. Since formation of nitrite ions increased with the irradiation time, it is proposed that the azo group in RB-220 would break from the dye molecule and be mineralized in the solution in the form of nitrite ion during the photocatalytic degradation of RB-220 under UV and solar light irradiation.

No nitrite formation occurred during photocatalytic degradation of AY-17 under UV and solar light irradiation. Similar observations have been reported by

Tanaka et al. (2000) during the degradation of AY-17 dye using TiO_2 as a photocatalyst.

So, formation of inorganic ions (sulphate, nitrate, nitrite and chloride) during photocatalysis of dyes using $Ag@TiO_2$ indicates that the non-biodegradable organic part of the dyes AY-17 and RB-220 were destroyed, decomposed and even mineralized during the UV and solar photocatalytic process. High TOC and COD removal indicates that AY-17 and RB-220 degrade to simpler and easily biodegradable organic compounds by photocatalysis with $Ag@TiO_2$.
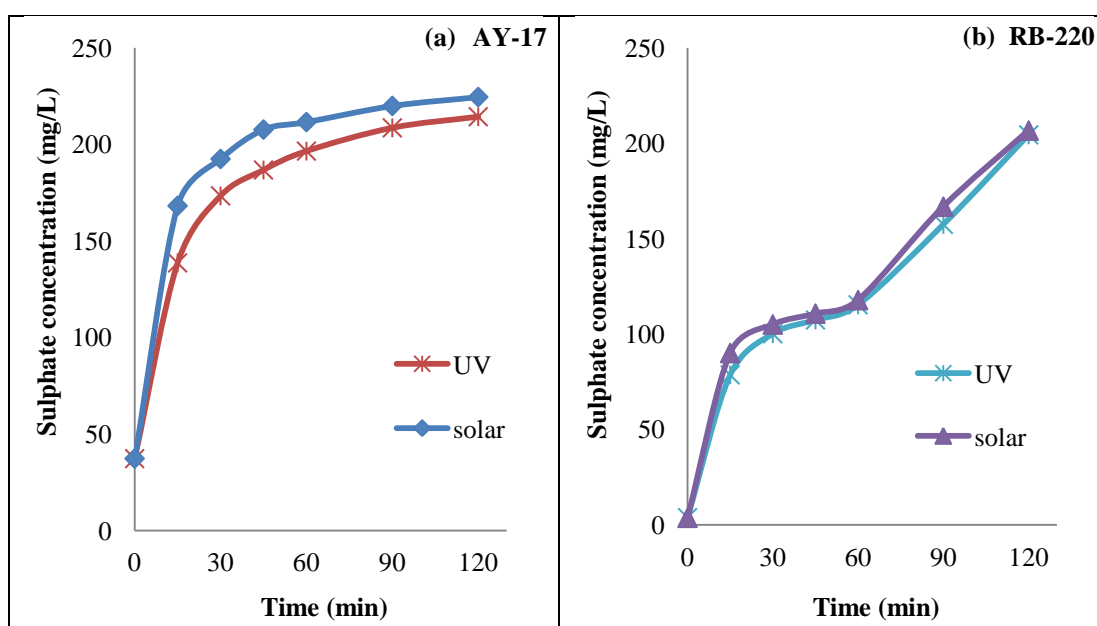
Figure 4.80 Formation of sulphate ion during the UV and solar photocatalytic degradation of dyes under RSM based methodical optimized conditions (presented in Table 4.47 a) AY-17 b) RB-220. Conditions: C_0= 100 mg/L.
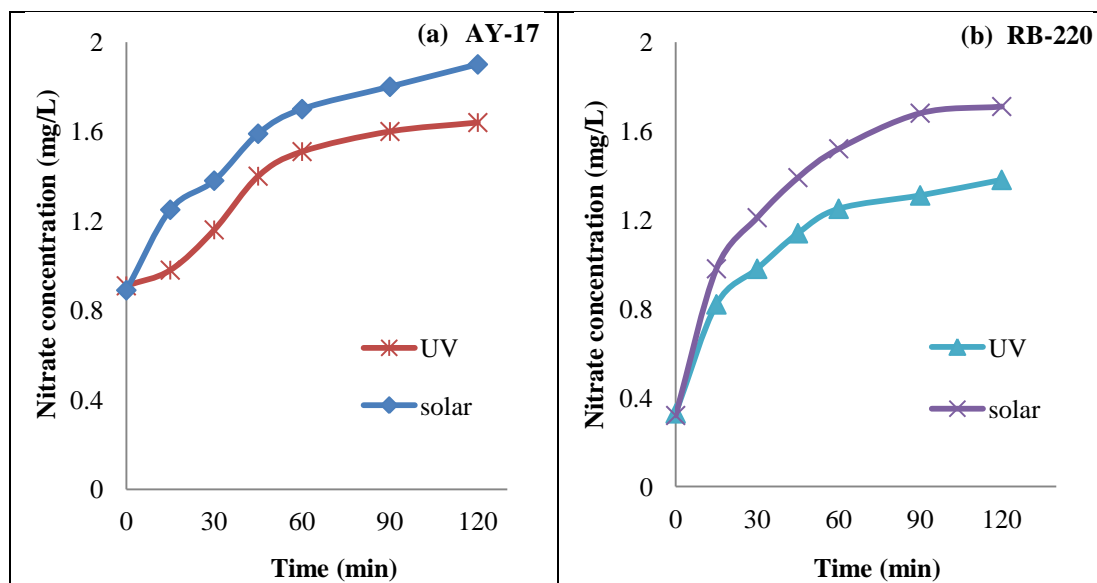
Figure 4.81 Formation of nitrate ion during the UV and solar photocatalytic degradation of dyes under RSM based methodical optimized conditions (presented in Table 4.47 a) AY-17 b) RB-220. Conditions: C_0= 100 mg/L.
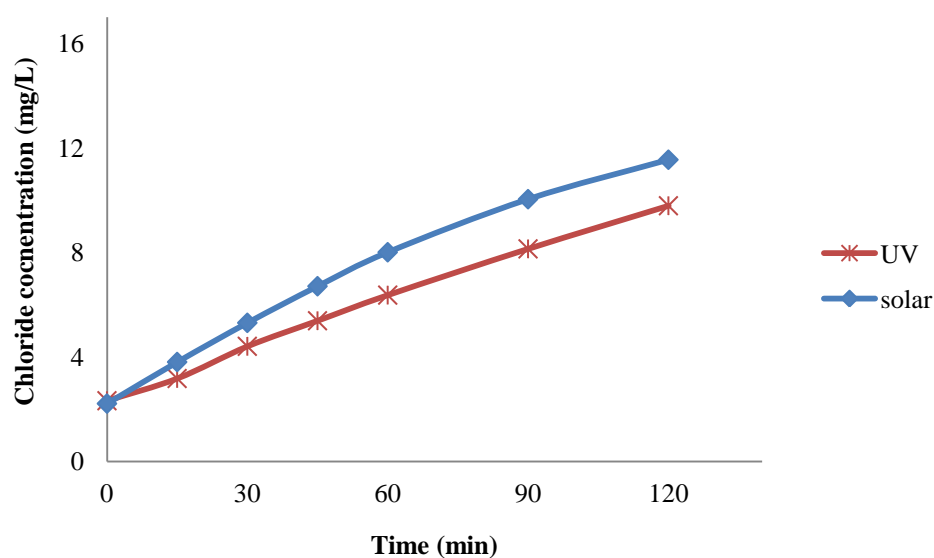
Figure 4.82 Formation of chloride ion during the UV and solar photocatalytic degradation of AY-17 under RSM based methodical optimized conditions (presented in Table 4.47. Conditions: C_0= 100 mg/L.
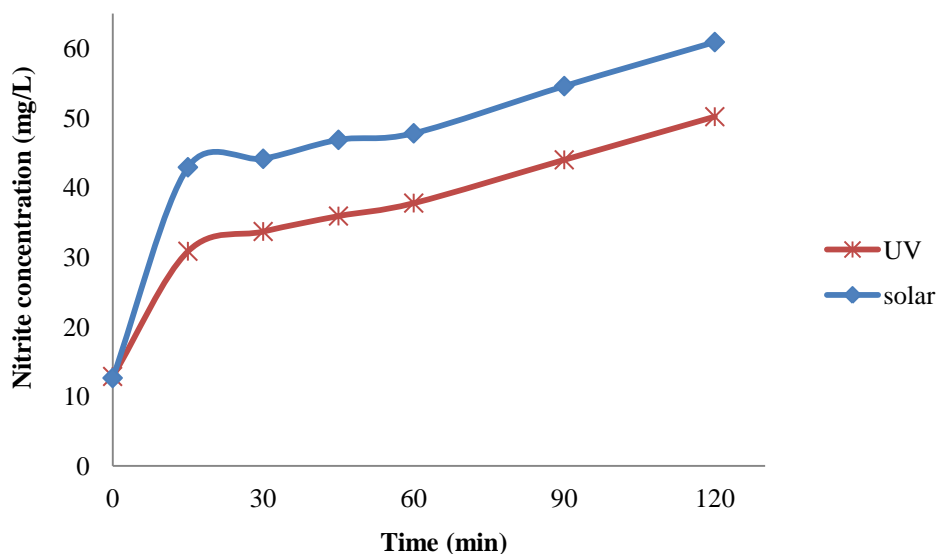
Figure 4.83 Formation of nitrite ion during the UV and solar photocatalytic degradation of RB-220 under RSM based methodical optimized conditions (presented in Table 4.47. Conditions: C_0= 100 mg/L.

4.14 Treatment of mixture of dyes in contaminated water at RSM based methodically optimized conditions for single dye solution (AY-17 or RB-220) by UV and solar photocatalysis

Wastewater from textile industries may contain mixture of dyes and the presence of other dye may interfere with the degradation of a specific dye. If the wastewater treatment process is operated at optimum conditions derived for one of the dyes and if the photocatalytic reactor is also designed based on kinetics at optimum conditions for one of the dyes, then the degradation of the other dye may not be complete, as these optimum conditions may not favor the degradation of the other dye. So the photocatalysis of mixture of the two dyes in solution were tested for the degradation of both the dyes under optimum conditions devised for each of the dyes, so as to test the applicability of optimized conditions for the treatment of water contaminated with mixture of dyes. Photocatalysis with mixture of dyes has been hardly reported so far. In the present work, the experiments were carried out on the photocatalytic degradation of mixtures of two azo dyes AY-17 and RB-220, by using the Ag@TiO$_2$ nanoparticles as catalysts under UV and solar light irradiation at RSM based

306

methodically optimized conditions obtained for each of the dyes when present as single dye system, as reported in Section 4.8. Optimum conditions for the photocatalytic degradation of AY-17 and RB-220 in single dye system, under UV and solar light irradiation are shown in Table 4.47. Batch photocatalytic experiments were conducted with 100 mL of the dye solution and with the dye concentration combination as specified in Section 3.14.

4.14.1 Treatment of mixture of dyes in contaminated water at RSM based methodically optimized conditions for AY-17 dye and RB-220 by UV photocatalysis

Batch photocatalysis experiments were performed with different dye concentration combination of AY-17 and RB-220 in aqueous mixed dye solution as specified in Table 3.7. under UV light irradiation and at the RSM based methodical optimized conditions obtained for each of the dyes The optimum conditions for AY-17 degradation by UV photocatalysis were: pH=2.9, catalyst loading= 3.4 g/L and ammonium persulfate= 2.25 g/L for AY-17 under UV light. Similarly the optimum conditions for RB-220 degradation by UV photocatalysis were: pH=3.2, catalyst loading= 1.8 g/L and ammonium persulfate= 1.3 g/L. The optimized conditions chosen in these experiments were the optimum values as obtained by RSM based methodical optimization. In all the experiments 100 mL volume of aqueous dye solution was used. Table 4.67 shows the percentage degradation of each of the dyes in the mixed dye solution, obtained at the end of 180 min, at optimum conditions for AY-17 dye and RB-220 dye with different concentration combinations of the dyes. Table 4.67 also presents the percentage degradation of AY-17 and RB-220 under optimum conditions for their degradation, when they are present in a single dye system.

It can be observed from Table 4.67, under optimized conditions for AY-17 dye, degradation of RB-220 is higher than that which occurred at optimized conditions for RB-220 itself. More than 99.5 % of degradation of RB-220 could be achieved at all the initial dye concentration combinations and the percentage degradation of RB-220 was found to be higher at optimized conditions of AY-17 dye

as compared to the optimized conditions for RB-220 dye. But under optimized conditions for RB-220 dye, the degradation of AY-17 in the mixed dye solution is much lesser at all the dye concentration combinations. It is also observed, the percentage degradation of AY-17 dye in mixed dye solution is lesser than the percentage degradation in single dye system, even though the concentrations of AY-17 are the same both in mixed and single dye solution. Similarly the percentage degradation of RB-220 dye in mixed dye solution is lesser than the percentage degradation in single dye system, even though the concentrations of RB-220 are the same both in mixed and single dye solution. The rate of degradation of each of the dyes in a mixture was found to be inhibited by the presence of the other dye. This shows that the presence of one dye in the mixture reduces the rate of degradation of other dye and it is due to competitive nature of both the dyes for the reactive site (Ong et al. 2013) on Ag@TiO$_2$ surface.

In the mixed dye solution, when the AY-17 concentration was 100 mg/L and when the RB-220 concentration was increased from 100 mg/L to 400 mg/L, the percentage degradation of both RB-220 and AY-17 have decreased. This shows that, the competitive nature of inhibition increases with the increase in the concentration of the other dye. It also indicates that increase in initial concentration of a particular dye leads to decrease in its percentage degradation. It may be because the optimum catalyst loading used in these experiments were for initial dye concentration of 100 mg/L. If the initial concentration of the dye increases, then the available active sites on the catalyst may not be adequate for increased number of dye molecules and more of dye molecules compete for the active sites. Due to large number of dye molecules being present, the rate of achievement of successful collisions on to the active sites may reduce and hence leading to lower rate of degradation.

4.14.2 Treatment of mixture of dyes in contaminated water at RSM based methodical optimized conditions for AY-17 dye and RB-220 by solar photocatalysis

Batch photocatalysis experiments were performed with different dye concentration combination of AY-17 and RB-220 in aqueous mixed dye solution as

specified in Table 3.7, under solar light irradiation and at the RSM based methodical optimized conditions obtained for each of the dyes The optimum conditions for AY-17 degradation by solar photocatalysis were: pH=2.1, catalyst loading= 1.8 g/L and ammonium persulfate= 2.71 g/L under solar light. Similarly the optimum conditions for RB-220 degradation by solar photocatalysis were: pH=3.3, catalyst loading= 1.11 g/L and ammonium persulfate= 1.36 g/L. For solar photocatalysis of AY-17 and RB-220 dye, average UV and visible light intensity of solar light= 3.64 mW/cm^2 and 1223×100 lux respectively from 11 a.m. to 2 p.m. The optimized conditions chosen in these experiments were the optimum values as obtained by RSM based methodical optimization. In all the experiments 100 mL volume of aqueous dye solution was used. Table 4.68 shows the percentage degradation of each of the dyes in the mixed dye solution, obtained at the end of 180 min, at optimum conditions for AY-17 dye and RB-220 dye with different concentration combinations of the dyes. Table 4.68 also presents the percentage degradation of AY-17 and RB-220 under optimum conditions for their degradation, when they are present in a single dye system. The results obtained in solar photocatalysis of mixed dye solution are similar to those obtained with UV photocatalysis, as evident from Table 4.68.

Studies on mixture of dyes showed that the optimum conditions for AY-17 were more favorable for the degradation of both the dyes in mixed dye solution, as compared to optimum conditions for RB-220 dye, both in UV and solar photocatalysis. The optimum conditions for RB-220 are suboptimal for AY-17, as the molecular structure of AY-17 is more complex as compared with the RB-220. Hence the optimized conditions obtained for RB-220 degradation are milder than those for AY-17. The milder optimum conditions for RB-220 dye are suboptimal for the degradation of the complex AY-17 dye. So, when mixtures of dyes are present in wastewater, it is recommended to use optimum conditions of the most complex dye for photocatalysis.

Table 4.67 Percentage degradation of each of the dyes in the mixed dye solution and in a single dye system obtained at the end of 180 min, at RSM based methodical optimized conditions for UV photocatalysis of AY-17 dye and RB-220 dye with different concentration combinations of the dyes.

	At optimum conditions for AY17			At optimum conditions for RB-220		
	Dyes in mixed dye solution		Dye in single dye solution	Dyes in mixed dye solution		Dye in single dye solution
	AY-17	RB-220	AY-17	RB-220	AY-17	RB-220
C_0 (mg/L)	100	100	100	100	100	100
% degradation	99.37	99.93	99.53	96.14	99.88	$\approx$100
C_0 (mg/L)	400	100	400	400	100	100
% degradation	90.69	99.93	91.69	86.91	99.83	$\approx$100
C_0 (mg/L)	300	200	300	300	200	200
% degradation	96.63	99.94	97.31	90.44	99.07	99.51
C_0 (mg/L)	200	300	200	200	300	300
% degradation	98.38	99.75	97.92	93.5	96.2	97.21
C_0 (mg/L)	100	400	100	100	400	400
% degradation	99.29	99.68	99.53	95.65	94.19	94.75

Table 4.68 Percentage degradation of each of the dyes in the mixed dye solution and in a single dye system obtained at the end of 180 min, at RSM based methodical optimized conditions for solar photocatalysis of AY-17 dye and RB-220 dye with different concentration combinations of the dyes.

| | At optimum conditions for AY17 | | | At optimum conditions for RB-220 | | |
| | Dyes in mixed dye solution | | Dye in single dye solution | Dyes in mixed dye solution | | Dye in single dye solution |
	AY-17	RB-220	AY-17	RB-220	AY-17	RB-220
C_0 (mg/L)	100	100	100	100	100	100
% degradation	99.52	99.99	99.72	98.07	99.99	≈100
C_0 (mg/L)	400	100	400	400	100	100
% degradation	93.95	99.98	95	88.16	99.99	≈100
C_0 (mg/L)	300	200	300	300	200	200
% degradation	97.02	99.99	97.83	93.81	99.58	≈100
C_0 (mg/L)	200	300	200	200	300	300
% degradation	98.07	99.96	98.98	96.1	99.31	99.93
C_0 (mg/L)	100	400	100	100	400	400
% degradation	99.35	99.98	99.72	96.98	99.15	99.95

4.15 Determination of colour in Hazen unit

According to Central Pollution Control Board (CPCB 2010) of India, colour of the dye contaminated water is specified in terms of Hazen unit and maximum permissible limit is set at 400 HU. To check for whether the colour of water contaminated with the dyes under study were reduced by photocatalysis and meet specified colour

311

standard, batch UV and solar photocatalysis experiments were conducted with single and mixed dye solutions at RSM based methodically optimized conditions for each of the dyes and the colour was measured in terms of Hazen unit. Table 4.69 shows the colour of single dye solution (AY-17 or RB-220) in terms of Hazen unit after treatment by UV and solar photocatalysis at their corresponding RSM based methodically optimized conditions after 15 min of irradiation. The RSM based methodically optimized conditions for the dyes are shown in Table 4.47. The colour of water contaminated with any single dye, after treatment by UV and solar photocatalysis were found to be much less than the specified permissible limit of 400 HU.

Table 4.70 shows the time course variation of colour of the mixed dye solution with AY-17 and RB-220 each at 100 mg/L concentration in terms of Hazen unit (HU) at RSM based methodical optimized conditions for AY-17 by UV photocatalysis. After 180 min of UV irradiation, the colour of the treated water containing mixture of dyes was found to be 2.97 HU which is much lesser than the specified permissible limit. It is also observed in Table 4.71, which presents the time course variation of colour of the mixed dye solution with AY-17 and RB-220 (AY-17+RB-220= 400 and 100 mg/L) in terms of Hazen unit (HU) at optimized conditions for AY-17 by UV photocatalysis, that after 180 min of UV irradiation, the colour of the treated water containing mixture of dyes was found to be 271.74 HU which is less than the specified permissible limit. Similar observations were made during the treatment of mixed dye solution containing 100 mg/L of AY-17 and 400 mg/L of RB-220 dyes by UV photocatalysis, as presented in Table 4.72.

Table 4.73 to Table 4.75 show the time course variation of colour of the solution in terms of HU during solar photocatalysis of the mixed dye solution at different concentrations of (i) 100 mg/L each (ii) 400 mg/L AY-17 and 100 mg/L RB-220 (iii) 100 mg/L AY-17 and 400 mg/L RB-220, respectively under RSM based methodical optimized conditions for AY-17. After 180 min of solar irradiation, the colour of the treated water containing mixture of dyes was found to be less than the specified permissible limit, in all the cases.

Table 4.76 and Table 4.78 show the time course variation of colour of the solution in terms of HU during UV photocatalysis of the mixed dye solution at

different concentrations of (i) 100 mg/L each (ii) 400 mg/L AY-17 and 100 mg/L RB-220 (iii) 100 mg/L AY-17 and 400 mg/L RB-220, respectively under RSM based methodically optimized conditions for RB-220 dye. After 180 min of solar irradiation, colour of the treated water containing mixture of dyes was found to be less than the specified permissible limit, in all the cases. Table 4.79-4.81 shows the time course variation of colour of the solution in terms of HU during solar photocatalysis of the mixed dye solution at different concentrations of (i) 100 mg/L each (ii) 400 mg/L AY-17 and 100 mg/L RB-220 (iii) 100 mg/L AY-17 and 400 mg/L RB-220, respectively under RSM based methodically optimized conditions. As observed from these Tables, the colour of the treated water containing mixture of dyes is less than the specified permissible limit of 400 HU. It can also observed from Tables 4.70 and Table 4.71, in mixed dye solution containing 400 mg/L of AY-17 and 100 mg/L of RB-220 the colour is 3226.56 HU and in mixed dye solution with 100 mg/L of AY-17 and 400 mg/L of RB-220, the colour is 1333.7. It shows that AY-17 dye contributes largely to the colour of contaminated water as compared to RB-220 dye. Rate of decolourization by solar photocatalysis was found to be faster than that with UV photocatalysis, as observed from Table 4.70 to Table 4.80. This study showed that at optimum conditions for both the dyes, colour of the treated water with single dye and mixture of dyes was found to be less than the permissible limit of 400 HU, specified by Central Pollution Control Board (CPCB 2010) of India, even at the high concentration of the dyes. Ag@TiO$_2$ nanoparticles were found to be efficient photocatalysts for treatment of wastewaters contaminated with dyes by UV and solar photocatalysis and they can be effectively utilized for decolourization of wastewater to meet the stipulated standards.

Table 4.69 Dye concentration and colour in HU during UV and solar photocatalysis of AY-17 and RB-220 dyes in single dye solutions at their corresponding optimized conditions for degradation.

Time (min)	AY-17 dye in single dye solution (at RSM based methodically optimized conditions for AY-17)				RB-220 in single dye solution (at RSM based methodically optimized conditions for RB-220)			
	UV photocatalysis		Solar photocatalysis		UV photocatalysis		Solar photocatalysis	
	C_{AY-17} (mg/L)	Colour (HU)	C_{AY-17} (mg/L)	Colour (HU)	C_{RB-220} (mg/L)	Colour (HU)	C_{RB-220} (mg/L)	Colour (HU)
0	100	739.33	100	739.33	100	144	100	144
15	1.46	6.81	1.22	5.93	1.38	0.51	1.68	0.66

Table 4.70 Time course variation of colour of mixed dye solution (AY-17 and RB-220 at 100 mg/L each) in terms of Hazen unit (HU) at RSM based methodically optimized conditions for AY-17 dye during UV photocatalysis.

S. No.	Time (min)	Concentration of dyes (mg/L)		Colour (HU)
		AY-17	RB-220	
1	0	100	100	806.64
2	60	1.11	0.34	6.21
3	120	0.78	0.14	3.72
4	180	0.63	0.07	2.97

Table 4.71 Time course variation of colour of mixed dye solution (AY-17 and RB-220 at 400 and 100 mg/L each) in terms of Hazen unit (HU) at RSM based methodically optimized conditions for AY-17 dye during UV photocatalysis.

S. No.	Time (min)	Concentration of dyes (mg/L)		Colour (HU)
		AY-17	RB-220	
1	0	400	100	3226.56
2	120	43.31	0.15	343.38
3	180	38.24	0.07	271.74

Table 4.72 Time course variation of colour of mixed dye solution (AY-17 and RB-220 at 100 and 400 mg/L each) in terms of Hazen unit (HU) at RSM based methodically optimized conditions for AY-17 dye during UV photocatalysis.

S. No.	Time (min)	Concentration of dyes (mg/L)		Colour (HU)
		AY-17	RB-220	
1	0	100	400	1333.7
2	120	0.86	2.94	7.24
3	180	0.71	1.27	4.25

Table 4.73 Time course variation of colour of mixed dye solution (AY-17 and RB-220 at 100 mg/L each) in terms of Hazen unit (HU) at RSM based methodically optimized conditions for AY-17 dye during solar photocatalysis

S. No.	Time (min)	Concentration of dyes (mg/L)		Colour (HU)
		AY-17	RB-220	
1	0	100	100	806.64
2	45	0.95	0.02	5.26
3	120	0.62	0.01	3.16
4	180	0.48	0.01	1.89

Table 4.74 Time course variation of colour of mixed dye solution (AY-17 and RB-220 at 400 and 100 mg/L each) in terms of Hazen unit (HU) at RSM based methodically optimized conditions for AY-17 dye during solar photocatalysis.

S. No.	Time (min)	Concentration of dyes (mg/L)		Colour of (HU)
		AY-17	RB-220	
1	0	400	100	3226.56
2	120	34.08	0.02	246.24
3	180	24.22	0.02	167.89

Table 4.75 Time course variation of colour of mixed dye solution (AY-17 and RB-220 at 100 and 400 mg/L each) in terms of Hazen unit (HU) at RSM based methodically optimized conditions for AY-17 dye during solar photocatalysis.

S. No.	Time (min)	Concentration of dyes (mg/L)		Colour (HU)
		AY-17	RB-220	
1	0	100	400	1333.7
2	120	0.8	0.14	3.87
3	180	0.65	0.08	3.11

Table 4.76 Time course variation of colour of mixed dye solution (AY-17 and RB-220 at 100 mg/L each) in terms of Hazen unit (HU) at RSM based methodically optimized conditions for RB-220 dye during UV photocatalysis.

S. No.	Time (min)	Concentration of dyes (mg/L)		Colour (HU)
		AY-17	RB-220	
1	0	100	100	806.64
2	60	14.78	0.31	120.32
3	120	5.05	0.18	31.42
4	180	3.86	0.12	29.87

Table 4.77 Time course variation of colour of mixed dye solution (AY-17 and RB-220 at 400 and 100 mg/L each) in terms of Hazen unit (HU) at RSM based methodically optimized conditions for RB-220 dye during UV photocatalysis.

S. No.	Time (min)	Concentration of dyes (mg/L)		Colour (HU)
		AY-17	RB-220	
1	0	400	100	3226.56
2	120	62.35	0.25	460.47
3	180	52.35	0.17	387.89

Table 4.78 Time course variation of colour of mixed dye solution (AY-17 and RB-220 at 100 and 400 mg/L each) in terms of Hazen unit (HU) at RSM based methodically optimized conditions for RB-220 dye during UV photocatalysis.

S. No.	Time (min)	Concentration of dyes (mg/L)		Colour (HU)
		AY-17	RB-220	
1	0	100	400	1333.7
2	120	6.78	25.81	71.04
3	180	4.35	23.25	58.14

Table 4.79 Time course variation of colour of mixed dye solution (AY-17 and RB-220 at 100 mg/L each) in terms of Hazen unit (HU) at RSM based methodically optimized conditions for RB-220 dye during solar photocatalysis

S. No.	Time (min)	Concentration of dyes (mg/L)		Colour (HU)
		AY-17	RB-220	
1	0	100	100	806.64
2	60	7.67	0.1	50.45
3	120	2.89	0.03	14.46
4	180	1.93	0.01	7.85

Table 4.80 Time course variation of colour of mixed dye solution (AY-17 and RB-220 at 400 and 100 mg/L each) in terms of Hazen unit (HU) at RSM based methodically optimized conditions for RB-220 dye during solar photocatalysis

S. No.	Time (min)	Concentration of dyes (mg/L)		Colour (HU)
		AY-17	RB-220	
1	0	400	100	3226.56
2	120	60.41	0.04	440.21
3	180	47.37	0.01	331.22

Table 4.81 Time course variation of colour of mixed dye solution (AY-17 and RB-220 at 100 and 400 mg/L each) in terms of Hazen unit (HU) at RSM based methodically optimized conditions for RB-220 dye during solar photocatalysis

S. No.	Time (min)	Concentration of dyes (mg/L)		Colour (HU)
		AY-17	RB-220	
1	0	100	400	1333.7
2	120	4.25	4.82	33.14
3	180	3.02	3.41	19.87

4.16 Possible reaction mechanism and degradation pathway of solar photocatalysis of AY-17 and RB-220 dye

As the studies presented in earlier Sections revealed that solar photocatalysis using Ag@TiO$_2$ is more effective than UV photocatalysis, the mechanism of photocatalysis and the reaction pathway of degradation of AY-17 and RB-220 were proposed through identification of intermediates formed during solar photocatalysis of these dyes by LC-MS analysis. The possible intermediates were identified by interpretation of their fragment ions mass to charge (m/z) ratio in the mass spectra. The LC-MS analysis of the samples collected for every 15 min during solar photocatalysis of AY-17 and RB-220 conducted under RSM based methodically optimized conditions was performed. The mass spectra of intermediates formed are shown in Appendix VII.

The possible reaction mechanisms for solar photocatalysis of AY-17 and RB-220 are proposed on the basis of the experimentally identified intermediate species.

Highly reactive hydroxyl and superoxide anion radicals are produced during photocatalysis and are found to be responsible for the degradation of the dyes into simpler compounds (e.g., water-soluble organic acids). In some cases, complete mineralization into ions (NO_3^-, and SO_4^{2-}) also occurred. Although OH radicals are indiscriminate, nonspecific oxidants, LC-MS studies of dye-degradation products have revealed distinct patterns in the degradation process. The following Sections discuss the possible mechanisms that are proposed for splitting of AY-17 and RB-220 organic-dye molecules into simpler components and the loss of small entities.

4.16.1 Generation and attack of •OH radical

When Ag@TiO_2 nanoparticle is exposed to light, electrons are promoted from the valence band to conduction band and result in the formation of an electron–hole pair. Further electron can migrate to the Ag core and get discharged when an oxidant such as O_2 is supplied (Hirakawa and Kamat 2005). As shown in Figure 4.84 (Eqs. (1) and (2)), the photo excited electrons are penetrated or transferred quickly through TiO_2 shell into the Ag nano core until the Fermi level charge equilibrium is attained between the shell and core systems, after which the electrons are facilitated to quickly transfer from excited TiO_2, initiating the redox reactions at the interface of TiO_2 shell and dye solution (Abdulla-Al-Mamun et al. 2010). Further electrons can easily react with O_2 and form active species H_2O_2, $O_2^{\bullet-}$, $HO_2^{\bullet}$ (Sung-Suh et al. 2004) which considerably advance the photocatalytic degradation of dyes. These active species further react and produce hydroxyl radical ($^{\cdot}$OH). In addition, it was reported that holes react with adsorbed water molecules, leading to the production of $^{\bullet}$OH as shown in equations (3)–(4) (Jaeger and Bard 1979; Cai et al. 1992). On the photoexcitation of Ag@TiO_2, reactive oxygen species such as hydroxyl radicals and hydrogen peroxide etc. are formed which are highly oxidizable species and expected to be responsible for the photocatalytic degradation of dyes (Abdulla-Al-Mamun et al. 2010). Redox potential of $^{\bullet}$OH radical is very high ($E\circ$ + 2.8 V) thus it is a powerful

oxidizing agent and attacks the dye molecules present at or near the surface of TiO_2 to oxidize it.

4.16.2 Degradation pathway of AY-17

Based on LC-MS analysis and the mass to charge ratio obtained from mass spectra, the intermediate compounds were identified and the possible degradation pathway of AY-17 was proposed. The proposed pathway is shown in Figure 4.85. The process of degradation of AY-17 dye is initiated by either removal of SO_3Na or removal of sodium sulphate from the AY-17 dye. Next step in AY-17 dye degradation is then initiated by attack of hydroxyl radicals. The AY-17 dye later may undergo cleavage of C–N bond or symmetrical cleavage of azo bond.

Cleavage of C-N bond

The first pathway involves the cleavage of C–N bond between benzene ring and azo bond and resulting in formation of intermediates A and E shown in Table 4.82. The compound A having benzene ring intact undergoes cleavage of azo bond to form the intermediate B.

Reductive symmetrical cleavage of azo bond of AY-17

The presence of Π-bonds in the azo groups makes them the preferred site of OH radical attack (Karkmaz et al. 2004; Ozen et al. 2004; Chen et al. 2008b; Erdemoglu et al. 2008). The addition products of hydroxyl radicals to N=N are among the first intermediates to be detected during the progress of an OH radical-mediated degradation. The addition can occur on either of the two nitrogen atoms. However, it has been reported that there is a preferential attack on electron-deficient nitrogen, as exemplified by Meetani et al. (2010). So the second degradation pathway involves the reduction and symmetrical cleavage of azo bond and results in formation of intermediate B, C, D, F, G, and H shown in Table 4.82. The intermediates may further be mineralized to form simpler inorganic compounds on prolonged irradiation. The

complete degradation pathway of Ag@TiO$_2$ mediated solar photocatalysis of AY-17 is shown in Figure 4.85 and can be briefly summarized as follows:

$AY - 17\ dye \rightarrow smaller\ aliphatic\ and\ aromatic\ compounds$

$\rightarrow H_2O, CO_2, SO_4{}^{2-}, NO_3{}^{2-}, Cl^-$

4.16.3 Degradation pathway of RB-220

The process of degradation of RB-220 dye is initiated by decomplexation of co-ordination bond from the dye which further may undergo cleavage of C–N bond as shown in Figure 4.86 (Scheme 1). This pathway results in formation of intermediates A, B, and C and their chemical names are given in Table 4.83.

Decomplexation and cleavage of C-N bond

This pathway involves the decomplexation of coordination bond and cleavage of C-N bond resulting in formation of intermediates A, B, and C as shown in Scheme 1. The compounds A and B further undergo oxidation which leads to formation of different intermediates as shown in Figure 4.87 and Figure 4.88 (scheme 2 and 3). Table 4.83 shows the chemical names of intermediates produced during the photocatalytic degradation of RB-220 dye.

Devinylsulphonation

The pathway involves the removal of vinylsulfone group leading to the formation of intermediate compound D. Similar observation was reported by Bansal and Sud, (2013) during the photocatalytic degradation of Reactive Red 35. The intermediates may further be mineralized to form simpler inorganic compounds on prolonged irradiation. The complete degradation pathway of Ag@TiO$_2$ mediated solar photocatalysis of RB-220 can be briefly summarized as follows:

$RB - 220\ dye \rightarrow smaller\ aliphatic\ and\ aromatic\ compounds$

$\rightarrow H_2O, CO_2, SO_4{}^{2-}, NO_3{}^{2-}, NO_2{}^-$

Table 4.82 The chemical names of degradation intermediates of AY-17 dye.

Compounds	Molecular weight	Name of degradation products
A	197	(E)-3-methyl-4-(phenyldiazenyl)-1H-pyrazol-5-ol radical
B	113	4-amino-3-methyl-1H-pyrazol-5-ol radical
C	180	Sodium benzenesulfonate
D	191	1-(4-hydroxyphenyl)-3-methyl-1H- pyrazol-5-ol
E	189	4-3-methyl-1-H- pyrazol-1-yl)benzenethiol radical
F	328	3,4-dimethyl-1-phenyl-1H-pyrazol-5-ol compound with 1-hydroxy-2-phenylhydrzine (1:1)
G	123	1-hydroxy-2-phenylhydrzine radical
H	224	1-(3-chloro-4-hydroxylphenyl)-3-methyl-1H-pyrazol-5-ol
I	100	3-methyl-1H-pyrazol-5-ol
J	194	Sodium 4-aminobenzenesulfonate radical

Table 4.83 The chemical names of degradation intermediates of RB-220 dye.

Compounds	Molecular weight	Name of degradation products
A	361	Sodium2-((3-carboxy-4-hydrazinylphenyl)sulfonyl)ethyl sulphate anion
B	551	Disodium mono((E)-2-(2-(3-sulfonatobenzylidene)hydrazinyl)-5-((2-(sulfonatooxy)ethyl)sulfonyl)benzoate) anion
C	121	2-Diazenylphenol radical
D	122	Benzoic acid
E	280	2-((4-Aminophenyl)sulfonyl)ethyl hydrogen sulphate
E	189	2-Hydrosulfonylethylsulphate
F	329	Sodium2-((4-amino-3-formylphenyl)sulfonyl)ethyl sulfate radical
G	216	2-((4-Hydrzinylphenyl)sulfonyl)ethanol
H	103	Monosodium monosulfite
I	276	Sodium2-((4-amino-3-methylphenyl)sulfonyl)ethyl hydrogen sulfate radical
J	189	2-Hydrosulfonylethylsulphate
K	196	(E)-1-Benzylidene-2-phenylhydrazine
L	122	Benzoic acid
M	216	3-(4-Mercaptobenzyl) phenol radical
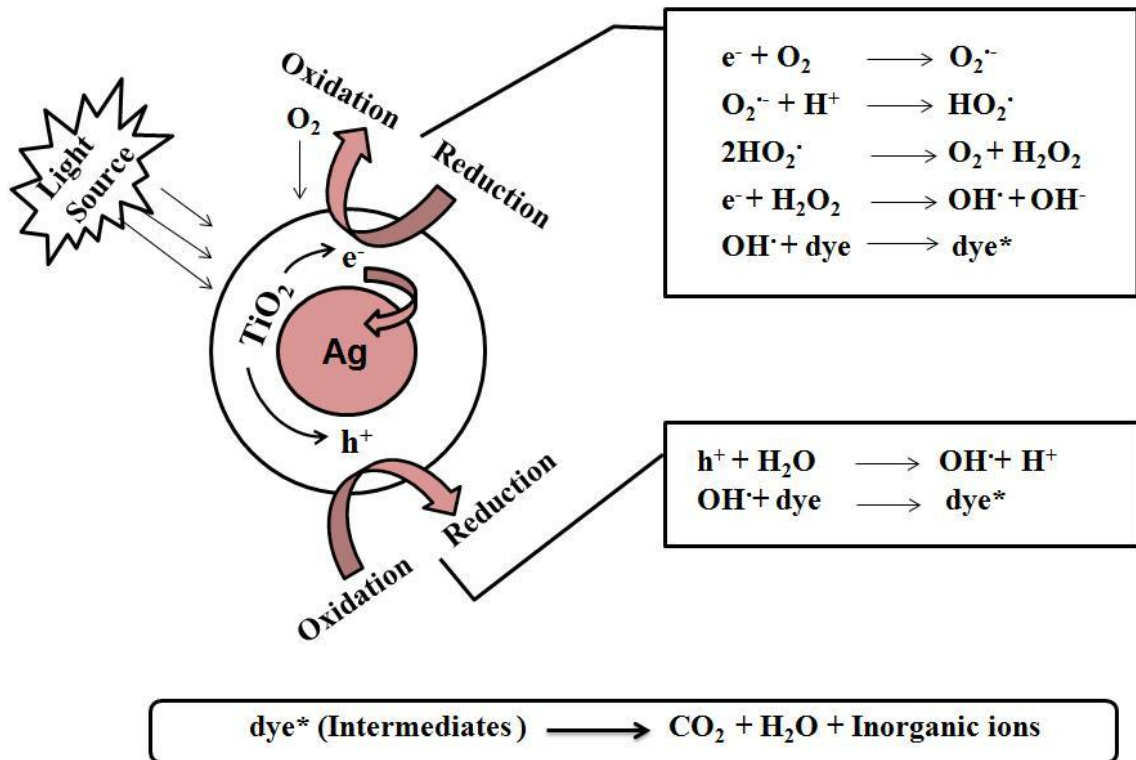
Figure 4.84 Proposed mechanism of photocatalytic degradation of dyes using Ag@TiO$_2$ nanoparticles.
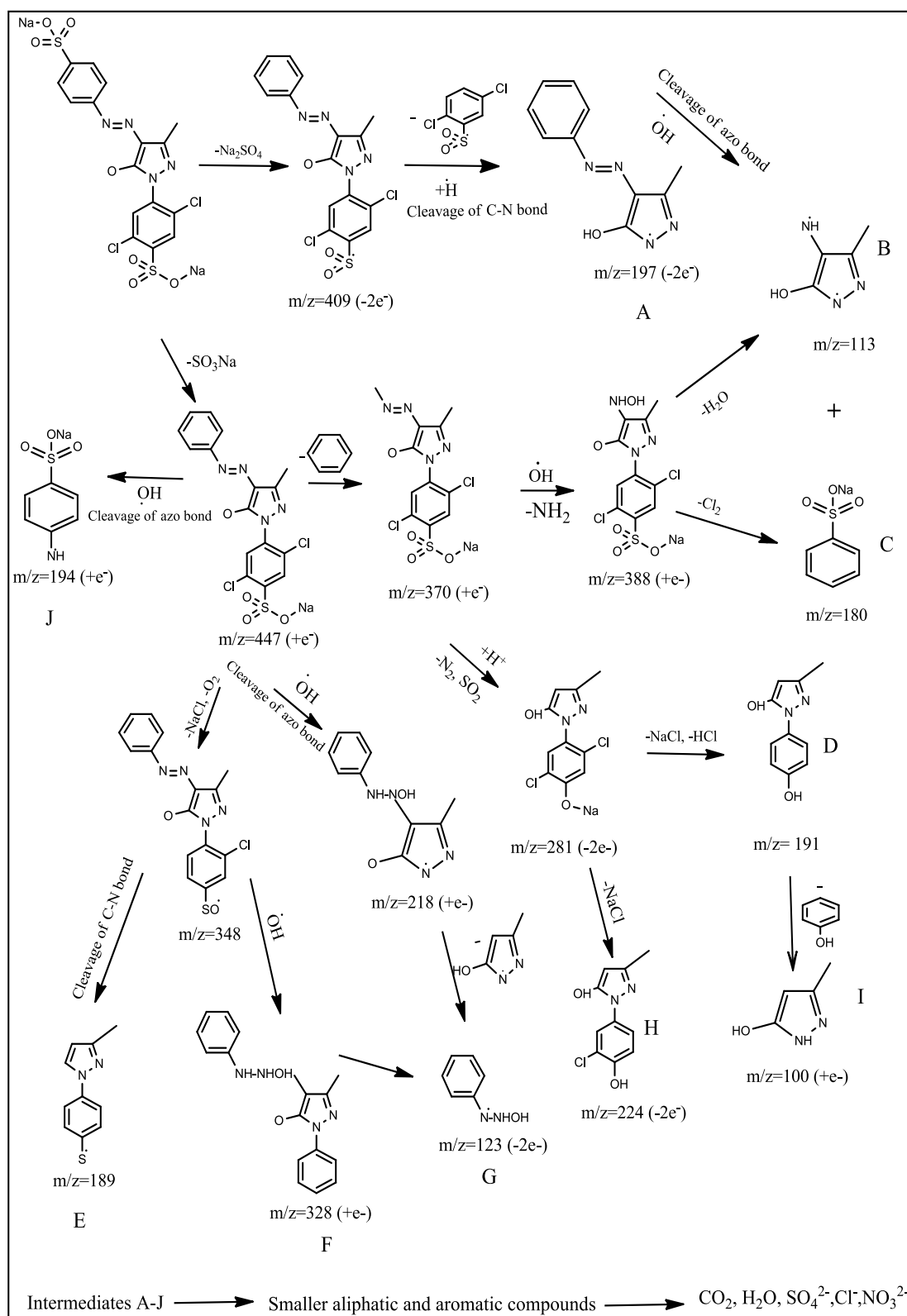
Figure 4.85 Proposed degradation pathways of AY-17 dye.
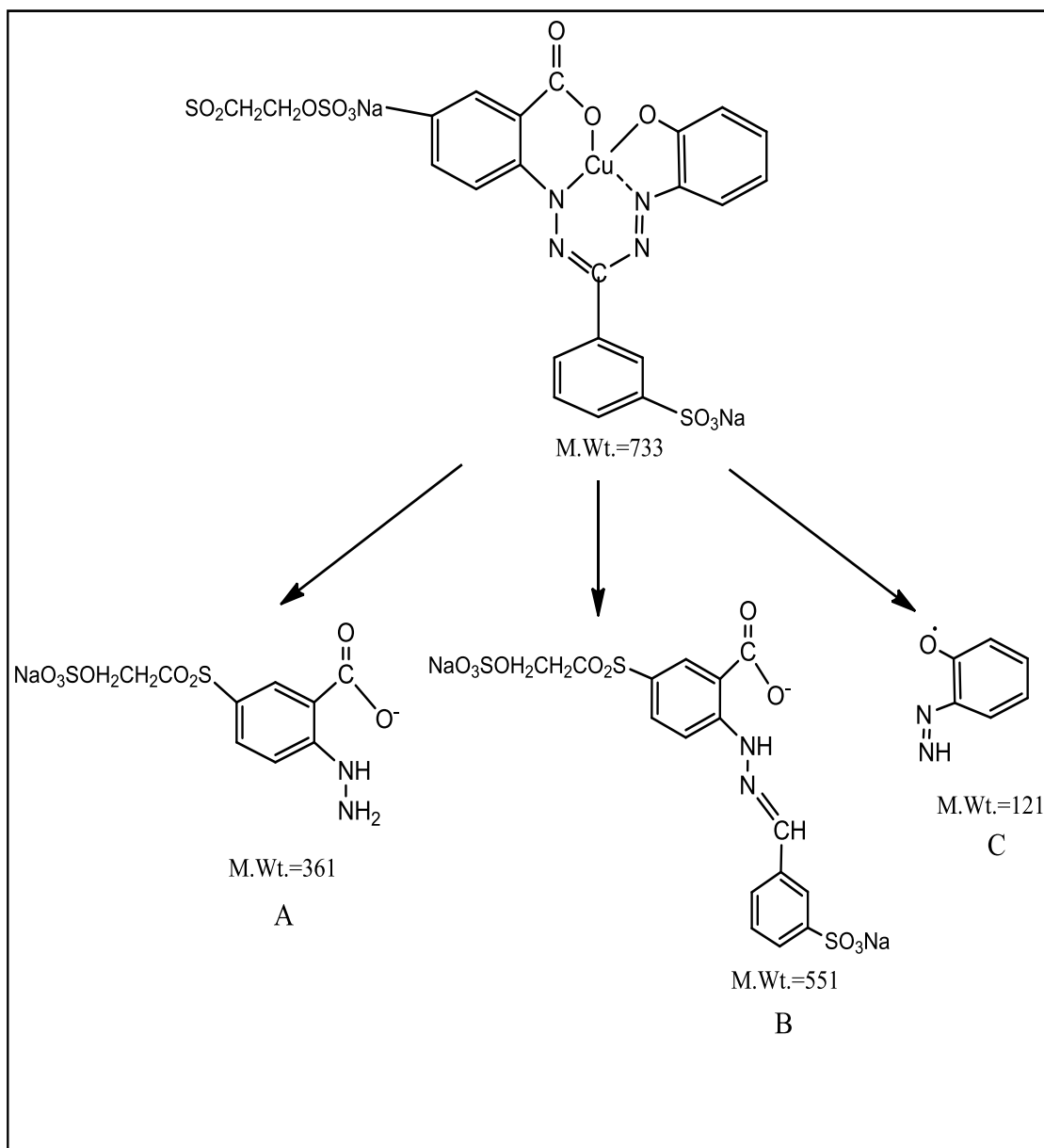
Figure 4.86 Proposed degradation pathways of (RB-220) dye (Scheme 1).
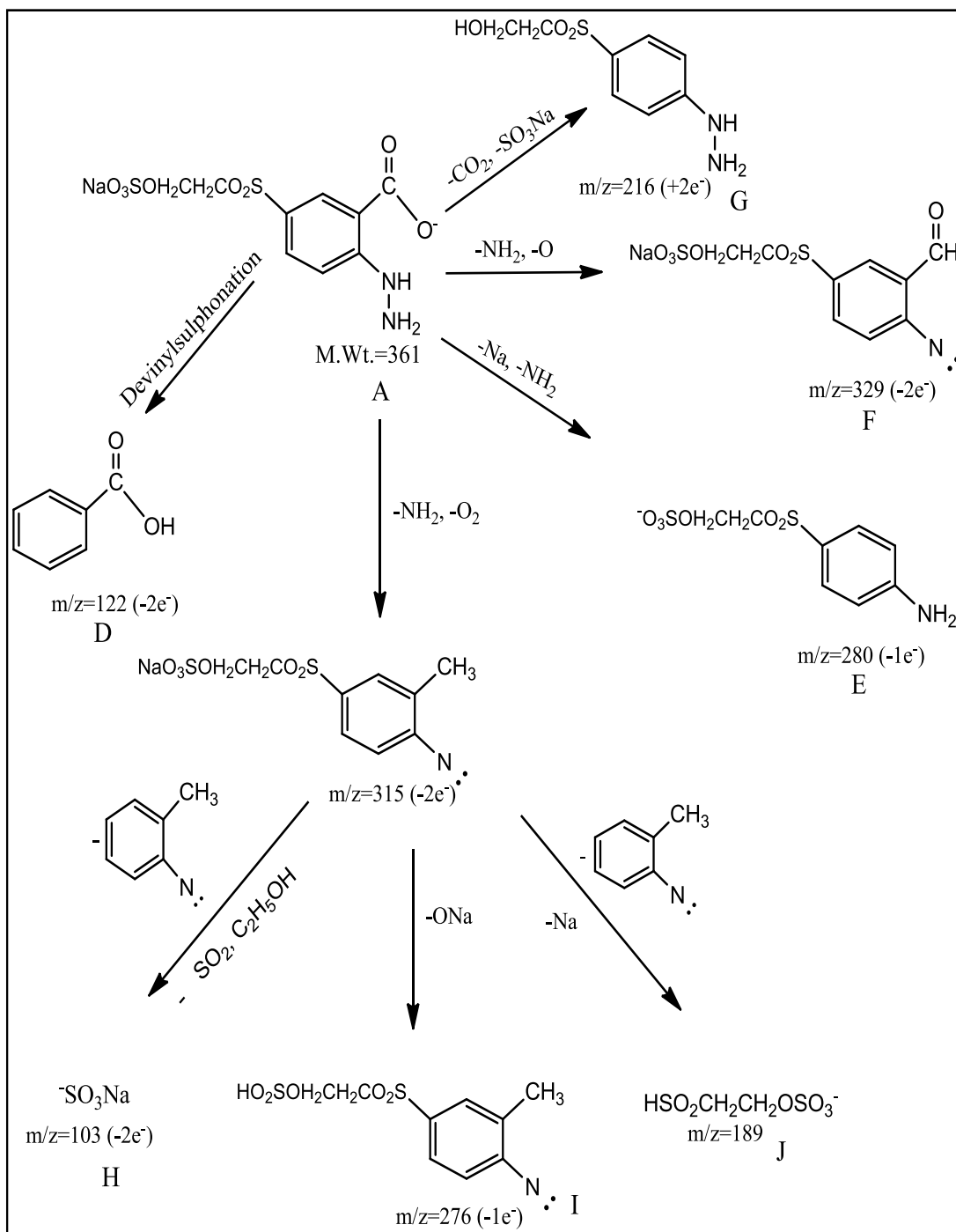
Figure 4.87 Proposed degradation pathways of (RB-220) dye (Scheme 2).
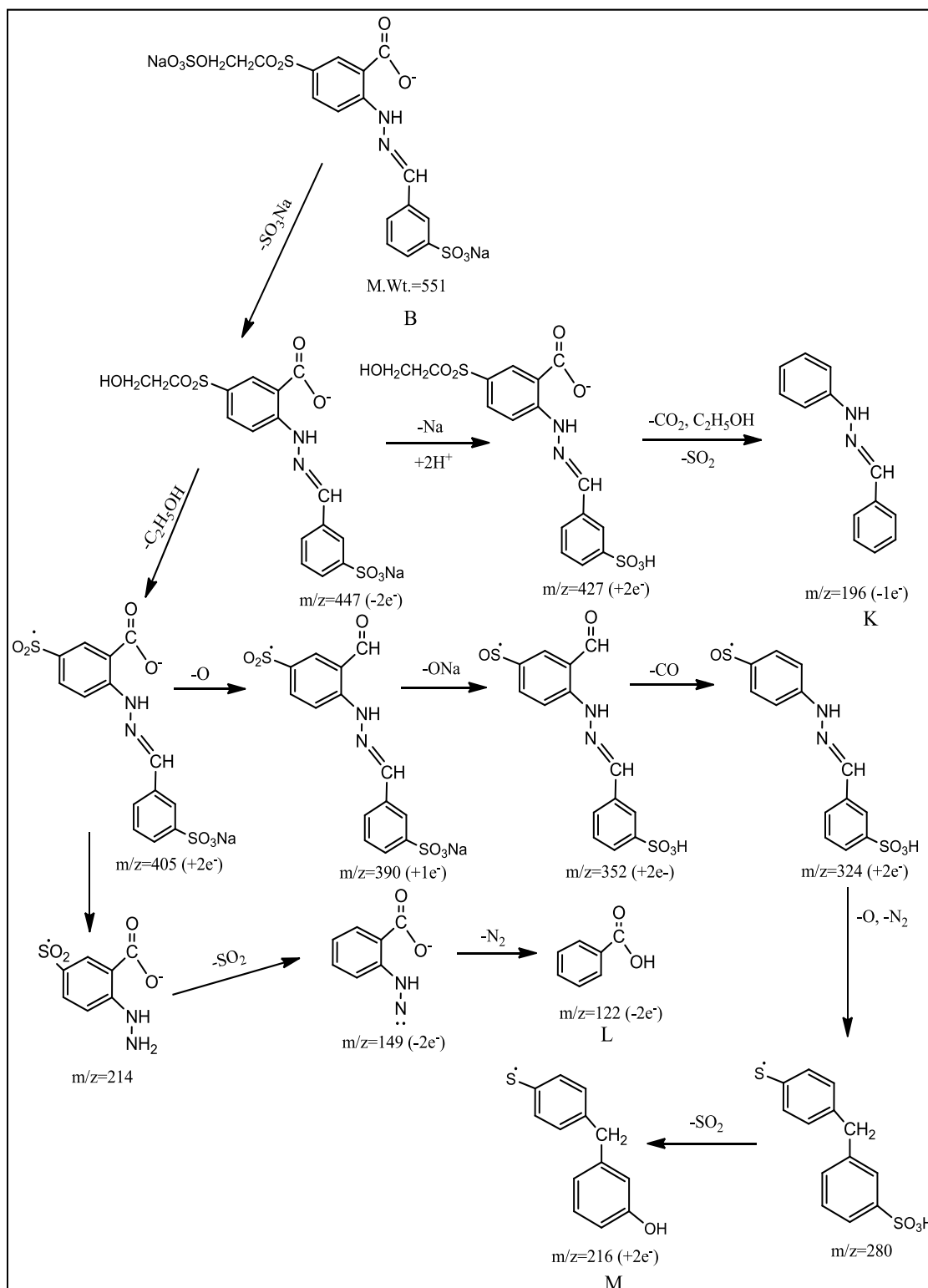
Figure 4.88 Possible degradation pathways of (RB-220) dye (Scheme 3).

4.17 Photocatalytic degradation of AY-17 and RB-220 using immobilized Ag@TiO$_2$ nanoparticles

4.17.1 Comparison of photocatalytic activity of free Ag@TiO$_2$ with immobilized nanoparticles for photocatalysis of AY-17 and RB-220

When catalyst used in the form of powder slurries, the major problems are: (a) the need for separation or filtration steps, (b) problems of particle wash out in continuous flow systems and (c) the particles aggregation, especially at high concentrations (Fujishima et al. 2000). To overcome these drawbacks, nanoparticles can be immobilized on supports in photocatalytic reactors. In the present study, Ag@TiO$_2$ nanoparticles were immobilized on two polymer supports that are chitosan and cellulose acetate for the photocatalytic degradation of AY-17 and RB-220. It was found that compared to UV, under solar light rate of photocatalysis was very high, as discussed in Section 4.3, 4.5, 4.6 and 4.8. Catalyst loading required for solar photocatalysis is much lesser than that used in UV photocatalysis for both the dyes as shown in Table 4.47 and in Section 4.8. This showed higher efficacy of Ag@TiO$_2$ for solar photocatalysis. Hence the efficacy of immobilized Ag@TiO$_2$ nanoparticles was tested in terms of degradation of AY-17 and RB-220 by solar photocatalysis. The solar photocatalysis experiments were conducted using RSM based methodical optimized conditions of both dyes (AY-17 and RB-220) as shown in Table 4.47. The average UV and visible light intensity of solar light= 3.59 mW/cm^2 and 1220×100 lux respectively from 11 a.m. to 1 p.m. Experiments were also conducted with only chitosan beads and cellulose acetate films in order to confirm that the degradation of AY-17 and RB-220 from contaminated water, in the presence of light is due to photocatalysis. It was observed from the results, no adsorption of dyes on chitosan beads and cellulose acetate film took place. Figure 4.89 shows the time course variation of immobilized Ag@TiO$_2$ nanoparticles with chitosan and cellulose acetate for the degradation of AY-17 and RB-220 under solar light. As observed from Figure 4.89, the rate of photocatalysis with immobilized Ag@TiO$_2$ nanoparticles is lesser than that with the free catalyst. The photocatalytic process is a surface phenomenon, so easy access to light irradiation and dye is essential for successful photocatalytic

degradation. Immobilized system offers diffusional limitations for the transfer of dye molecules on to the catalyst surface. Light absorption by Ag@TiO$_2$ is hindered due to immobilization. So as compared to free Ag@TiO$_2$ nanoparticles, low initial rate of degradation of AY-17 and RB-220 dye was observed with immobilized nanoparticles. Though the amount of nanoparticles used with chitosan beads and cellulose acetate films were the same, the number of cellulose acetate film particles supporting the catalyst was more than the number of chitosan beads supporting the catalyst. Higher number of support particles in the reactor system, would have lead to hindrance to light penetration in case of cellulose acetate, hence leading to lower rate of degradation as compared to that with chitosan beads as the support. Also it was observed during experimentation, Chitosan-Ag@TiO$_2$ beads were more transparent as compared to Cellulose Acetate-Ag@TiO$_2$ films. Lower transparency of cellulose Acetate-Ag@TiO$_2$ films may hinder the light penetration and compactness of the film may decrease the intraparticle diffusion of the dyes in the polymer matrix and hence reducing the ease with which the dye molecules reach the nanoparticles embedded in the matrix. Almost complete degradation of AY-17 and RB-220 could be achieved within 60 min of irradiation time with both free and immobilized nanoparticles. It depicts that the efficacy of immobilized Ag@TiO$_2$ nanoparticles are comparable with free catalyst, in spite of the diffusional and light penetration limitations of immobilized system. From the results of investigations carried out in the present study, it can be concluded that the immobilized Ag@TiO$_2$ nanoparticles have similar efficacy as free nanoparticles for to act as photocatalysts in degradation of AY-7 and RB-220 dyes and Chitosan-Ag@TiO$_2$ beads are the better immobilization matrix as compared to Cellulose Acetate-Ag@TiO$_2$ films.
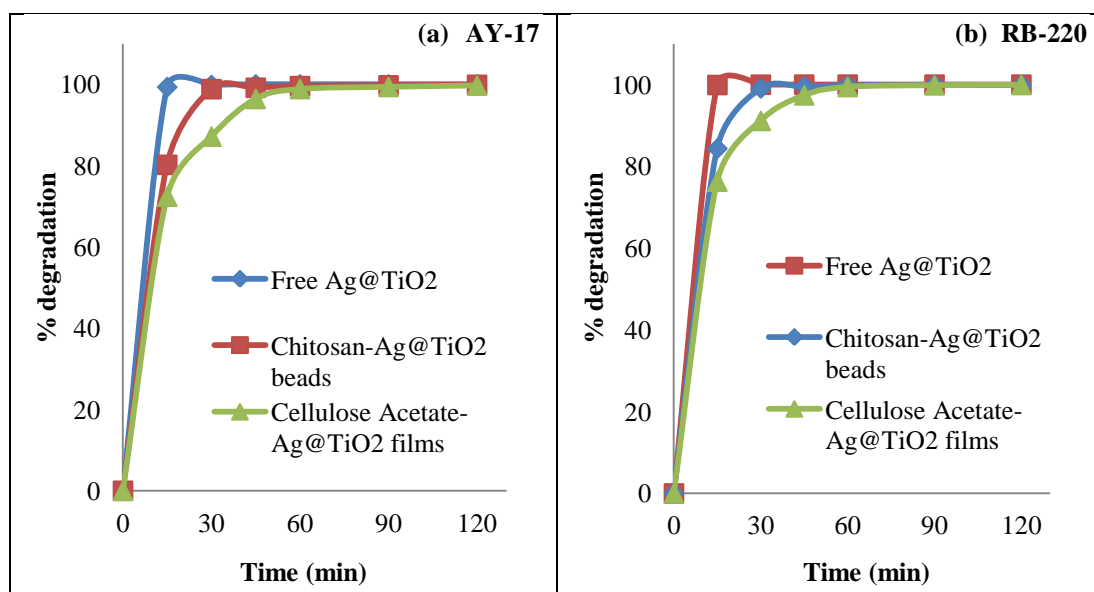
Figure 4.89 Immobilization of Ag@TiO$_2$ nanoparticles with chitosan and cellulose acetate at RSM based methodical optimized conditions for the solar photocatalysis of (a) AY-17. Conditions: pH=2.1; Catalyst loading= 1.8 g/L; (NH$_4$)$_2$S$_2$O$_8$= 2.71 g/L; C$_0$= 100 mg/L. (b) RB-220. Conditions: pH=3.3; Catalyst loading= 1.11 g/L; (NH$_4$)$_2$S$_2$O$_8$= 1.36 g/L; C$_0$= 100 mg/L.

4.17.2 Recycling of immobilized Ag@TiO$_2$

In order to check for any loss of activity of the immobilized catalyst and feasibility of their reuse for repeated photocatalysis, similar experiments were carried out as discussed previously under solar light irradiation. After an experiment with a fresh immobilized catalyst, the nanoparticles were reused twice for degradation experiments. So totally the nanoparticles were used for three cycles, out of which the first cycle was with the fresh immobilized catalyst and the remaining two cycles were with the recycled immobilized catalysts. Before the use of immobilized catalyst in the next cycle of experiment, the immobilized catalyst was separated from the treated water by filtration and then washed thrice with distilled water. After filtration, the immobilized particles were dried in room temperature for 2 h and then used for the next cycle of batch experiments. For all the three cycles same experimental conditions were used. Figure 4.90 to 4.91 present the time course variation of % degradation of AY-17 and RB-220 dyes achieved with fresh immobilized particles (Cycle I),

immobilized particles of single prior use (Cycle II), and immobilized particles of two prior uses (Cycle III) under solar light irradiation. As seen from Figure 4.90, after three cycles of reuse of Chitosan-Ag@TiO_2 beads, decrease in photocatalytic activity of AY-17 from 99.89 to 93.46 % and for RB-220 from 99.93 to 95.12 % was observed after 120 min of solar light irradiation. As it can be observed from Figure 4.91, after three cycles of reuse of Cellulose Acetate-Ag@TiO_2 film, decrease in photocatalytic activity of AY-17 from 99.72 to 87.43 % and for RB-220 from 99.92 to 91.36 % was observed after 120 min of solar light irradiation. Also it was observed, initial rate of photocatalysis of AY-17 and RB-220 slightly decreased after three cycle of reuse of immobilized particles which may be due to the adsorption of dye molecule on the immobilized support (chitosan and cellulose acetate). Not much reduction in activity was found after three cycles of reuse. So it can be concluded that Ag@TiO_2 immobilized on chitosan or cellulose acetate can be recycled without much decline in activity.
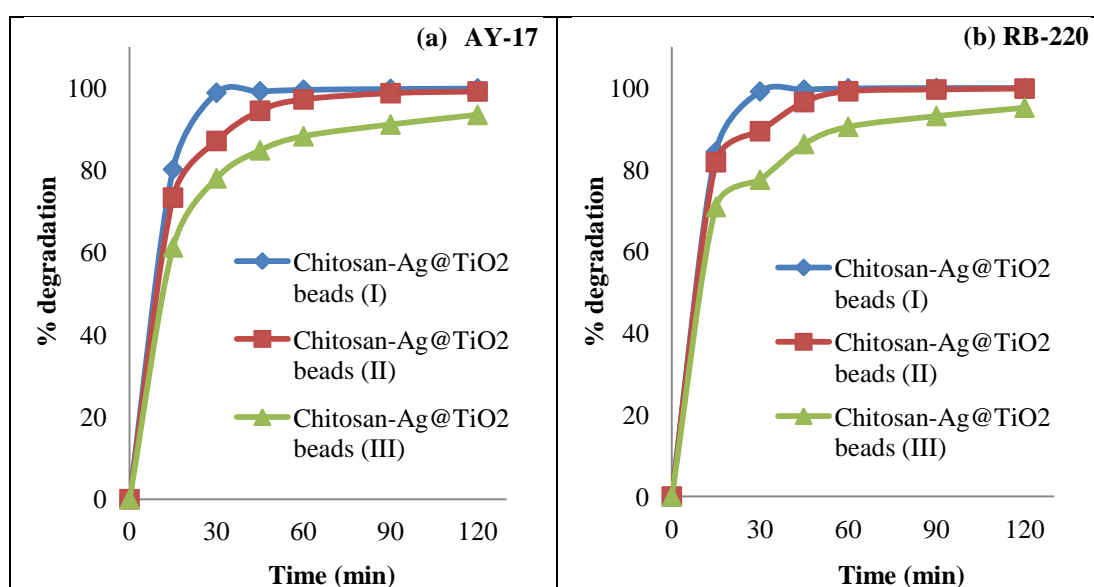
Figure 4.90 Effect of recycling of Ag@TiO_2 immobilized in chitosan, at RSM based methodical optimized conditions for the solar photocatalysis of (a) AY-17. Conditions: pH=2.1; Catalyst loading= 1.8 g/L; $(NH_4)_2S_2O_8$= 2.71 g/L; C_0= 100 mg/L. (b) RB-220. Conditions: pH=3.3; Catalyst loading= 1.11 g/L; $(NH_4)_2S_2O_8$= 1.36 g/L; C_0= 100 mg/L.
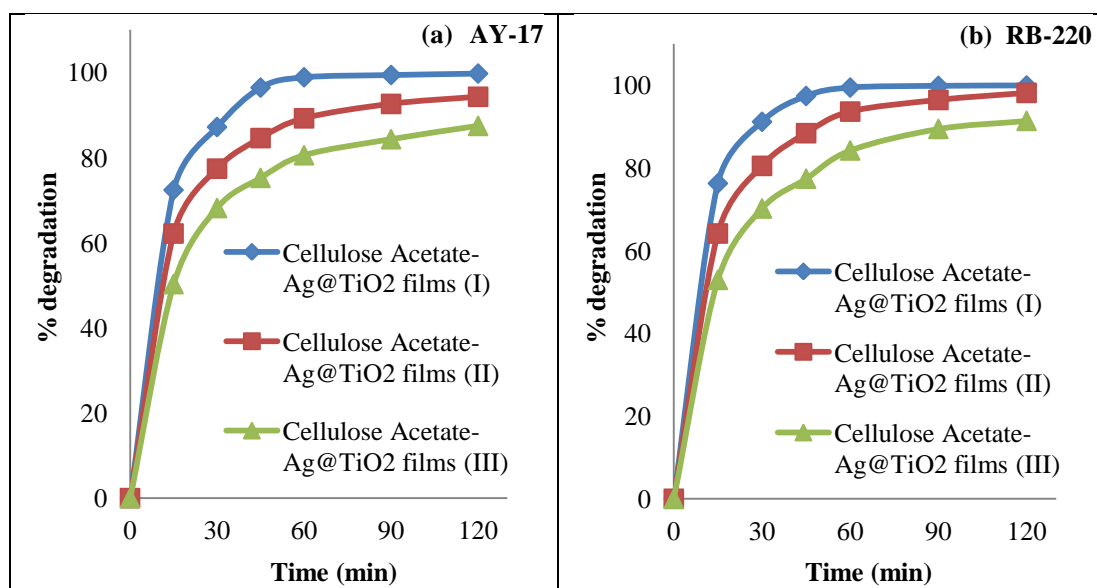
Figure 4.91 Effect of recycling of Ag@TiO$_2$ immobilized with cellulose acetate at RSM based methodical optimized conditions for the solar photocatalysis of (a) AY-17. Conditions: pH=2.1; Catalyst loading= 1.8 g/L; (NH$_4$)$_2$S$_2$O$_8$= 2.71 g/L; C$_0$= 100 mg/L. (b) RB-220. Conditions: pH=3.3; Catalyst loading= 1.11 g/L, = (NH$_4$)$_2$S$_2$O$_8$= 1.36 g/L; C$_0$= 100 mg/L.

4.18 Efficacy of Ag@TiO$_2$ as a photocatalyst for degradation of other class of dyes under solar light irradiation

Batch experiments were performed in order to check the photocatalytic efficacy of Ag@TiO$_2$ nanoparticles for the degradation of other dyes belonging to different classes, like : Basic Blue-41 (basic azo dye), Malachite Green (triarylmethane dye), Acid Blue-129 (anthraquinone dye), Congo Red (diazo dye), Reactive Red-120 (reactive diazo dye), Methyl Orange (acid azo dye), Methyl Red (acid azo dye), and Methylene Blue (thi- azine dye). Experiments were performed under solar light with catalyst loading=100 mg/L and initial dye concentration=10 mg/L. The average UV and visible light intensity of solar light= 3.59 mW/cm^2 and 1220×100 lux respectively from 11 a.m. to 2 p.m. Experiments were done at different initial pH, depending upon the nature of dyes. pH of 3 was used for acidic dyes and 9 for basic dyes. Experiments were done at different initial pH due to the amphoteric character of TiO$_2$. The point of zero charge (pzc) of TiO$_2$ is 6.8 (pH$_{pzc}$), so the surface of the particles is positively

charged when pH < pH_{pzc}. Above this value it is negatively charged (pH > pH_{pzc}) whereas it is neutral when pH = pH_{pzc} (Chiou et al. 2008). As anionic dye molecules will be negatively charged at lower pH hence more degradation of dye will occur due to the charge difference between negatively charged dye molecule and positively charged catalyst. Similarly for cationic dye, molecules will be positively charged at higher pH hence more degradation of dye will occur due to the charge difference between positively charged dye molecule and negatively charged catalyst. Table 4.84 shows the conditions used for the photocatalysis and the percentage degradation of the dyes. Results showed almost complete degradation of all the dyes under solar light irradiation. It can be seen from Table 4.84, with in 60 min of solar irradiation almost complete degradation of Congo Red, Methyl Orange and Methyl Red were observed whereas for Basic Blue-41, Malachite Green, Reactive Red-120 (reactive diazo dye) and Methylene Blue (thi- azine dye) it took around 180 min for almost complete degradation of dyes. Almost complete degradation of Acid Blue-129 was observed within 150 min of solar irradiation. Ag@TIO_2 was found be an efficient photocatalyst not only for the degradation of azo dyes such as AY-17 and RB-220, but also for the degradation of other class of dyes. The difference in efficacy of Ag@TiO_2 for degradation of different dyes, as indicated by varied time of irradiation to achieve greater than 98 % degradation depicting the variations in the rate of photocatalysis, may be due the varied degree of complexity of dye structures. However, this study proves the ability of Ag@TiO_2 nanoparticles to degrade almost all class of dyes and hence can be exploited efficiently for treatment of textile wastewater and other industrial effluents contaminated with dyes.

Table 4.84 The efficacy of Ag@TiO$_2$ as a photocatalyst for degradation of other class of dyes.

Name of the dye	Initial pH	Ag@TiO$_2$ loading (mg/L)	Initial Concentration of dye (mg/L)	Irradiation time in min	% degradation of dye
Acid Blue -129	3	100	10	150	98.5
Basic Blue-41	9	100	10	180	98.72
Congo Red	3	100	10	60	99.24
Malachite Green	3	100	10	180	99.42
Methyl Orange	3	100	10	60	98.76
Methyl Red	3	100	10	60	99.23
Methylene Blue	9	100	10	180	98.69
Reactive Red-120	3	100	10	180	97.45

CHAPTER 5

SUMMARY
AND
CONCLUSIONS

SUMMARY AND CONCLUSIONS

The research work presented in this report, shows the efficacy of Ag@TiO$_2$ core shell structured nanoparticles as a photocatalyst, for the removal of two azo dyes: AY-17 and RB-220 from contaminated water by batch photocatalytic degradation. The nanoparticles were synthesized by one pot synthesis route and the Ag to Ti molar ratio used in the synthesis mixture during the synthesis Ag@TiO$_2$ core shell structured nanoparticles, calcination temperature and calcination time for the photocatalysts were optimized to impart and enhance UV and solar photocatalytic activity to these nanoparticles in terms of photocatalytic degradation of AY-17 and RB-220 dyes. These nanoparticles were assessed for their suitability as photocatalyst for degradation of AY-17 and RB-220 dyes by photocatalysis under UV and solar light irradiation. The nanoparticles were characterized for their size, structure, morphology, composition, crystallinity, thermal characteristics and light absorption characteristics and an attempt has been made to explain their UV and solar photocatalytic behavior. The efficacy of Ag@TiO$_2$ core shell nanoparticles as photocatalyst was tested and compared with those of other commercial and synthesized catalysts. Effects of operational factors were investigated and optimization of operational factors for UV and solar photocatalysis of AY-17 and RB-220 dyes were carried out using RSM through experiments designed as per CCD. Studies on kinetics of degradation, effect of presence of salts, effect of light intensity, mineralization of the dyes, degradation pathway, the treatment of water contaminated with mixture of dyes, degradation with immobilized nanoparticles, reuse of free and immobilized nanoparticles for repeated photocatalysis were carried out. Efficacy of Ag@TiO$_2$ nanoparticles for the degradation of other class of dyes was also studied.

Based on the investigation reported in this report, following conclusions were drawn.

- Ag@TiO$_2$ core-shell nanoparticles synthesized by one pot synthesis route were engineered to impart and enhance UV and solar photocatalytic activity and those synthesized with Ag to Ti molar ratio of 1:1.7 in the synthesis mixture and calcined at 450˚C for 3 h were found to exhibit maximum solar and UV photocatalytic activity in terms of degradation of AY-17 and RB-220 dyes and hence these synthesis and calcination conditions were considered as the optimum.

- The removal of AY-17 and RB-220 dyes from contaminated water, in the presence of Ag@TiO$_2$ core-shell nanoparticles and under UV or solar light irradiation was attributed to photocatalysis of the dyes. Hence these core-shell nanoparticles are considered as the effective photocatalyst for the degradation of azo dyes such as AY-17 and RB-220 by UV and solar photocatalysis. These nanoparticles are hence suitable for treatment of water contaminated with these dyes.

- The engineered Ag@TiO$_2$ nanoparticles were characterized by TEM and AFM, which revealed the formation of Ag core and TiO$_2$ shell. Ag core and TiO$_2$ shell were found to be crystalline in nature as confirmed by XRD and SAED results. The average crystallite size calculated by Scherrer's formula being 39.40 nm, was in close agreement with the average particle size of 37.33 nm obtained by TEM and showed reasonable match with the average particle size obtained by particle size analysis with AFM. The EDS spectrum showed the presence of O, Ti and Ag elements.

- TG-DTA analysis indicated the possible phase conversion from amorphous to anatase TiO$_2$ at around 350 °C, surface hydroxyl groups dissociation in the range of 350–600 °C and conversion from anatase to rutile phase of TiO$_2$ at around 514 °C.

- DRS indicated that Ag@TiO$_2$ is able to absorb both UV light and visible light, maximum visible light absorption being at 509 nm. Band gap energy of Ag@TiO$_2$ nanoparticles was calculated with DRS using Kubelka-Munk model and found to be around 1.85eV. It is much lesser than the band gap energy for TiO$_2$ (3.2eV), indicating that the nanoparticles have all the potential to be excited by longer wavelength radiations in visible range and hence can be used effectively for solar photocatalysis.

- Ag@TiO$_2$ nanoparticles were found to be more efficient in degradation of AY-17 and RB-220 dyes as compared to other catalysts such as Degussa P25, synthesized TiO$_2$ and Ag doped TiO$_2$ both under UV and solar irradiation.

- Solar photocatalysis was found to be more efficient as compared to UV photocatalysis with Ag@TiO$_2$ catalyst. High photocatalytic activity of

Ag@TiO$_2$ is due to its affinity to absorb both UV and visible light radiation and low band gap energy of 1.85eV.

- Initial solution pH, catalyst loading, initial dye concentration, type and concentrations of oxidants added; were found to affect the rate of photocatalysis of AY-17 and RB-220 under UV and solar light irradiation.

- The optimum conditions of pH, catalyst loading and oxidant concentrations were obtained from crude optimization by "One factor at a time approach". pH of 3 was the optimum for the degradation of both the dyes under UV and solar light irradiation using Ag@TiO$_2$ nanoparticles as catalyst. The optimum catalyst loading for the photocatalysis of AY-17 and RB-220 under UV and solar light were obtained and the optimum dye to catalyst ratio for degradation of AY-17 under UV and solar light irradiation using Ag@TiO$_2$ core-shell structured nanoparticles were 1:30 and 1:10 (g/g) respectively. Similarly the optimum dye to catalyst ratio for degradation of RB-220 under UV and solar light irradiation using Ag@TiO$_2$ core-shell structured nanoparticles were 1:20 and 1:10 (g/g) respectively.

- Initial dye concentration acted as an independent factor affecting the rate of photocatalysis, even when the dye to catalyst ratio was the optimum.

- Addition of oxidants such as H$_2$O$_2$, KBrO$_3$ and (NH$_4$)$_2$S$_2$O$_8$ improved the photocatalytic degradation of dyes and (NH$_4$)$_2$S$_2$O$_8$ was found to be the effective oxidant as compared to others.

- It was found feasible to recycle Ag@TiO$_2$ nanoparticles at least thrice for repeated photocatalysis, without much decline in efficiency.

- Optimum conditions for UV and solar photocatalysis of AY-17 and RB-220 were obtained using RSM, based on experiments designed as per CCD. Rate of degradation was found to be enhanced tremendously with the RSM based methodically optimized conditions as compared to crude optimized conditions. Statstically significant multiple regression models were developed to predict the percentage degradation of dyes as a function of pH, catalyst loading and ammonium persulfate concentration. Interaction effects between these factors (pH, catalyst loading and ammonium persulfate concentration) were observed.

- Studies on effect of initial dye concentration showed the effectiveness of the catalyst to degrade the dye solution at high concentrations, with conditions optimized for photocatalysis of 100 mg/L of dye. Greater than 95 % degradation of AY-17 could be achieved at the end of 360 min irradiation time, with upto 400 mg/L dye concentration, both under UV and solar photocatalysis. In the case of RB-220 dye, greater than 99 % degradation could be achieved with upto 500 mg/L initial dye concentration in 120 min of solar light irradiation and greater than 95% of degradation was achieved with upto 400 mg/L initial dye concentration in 240 min of UV light irradiation. It is always advisable to design the reactor based on most probable maximum dye concentration in the industrial effluent and its corresponding optimum catalyst loading, so that the treated effluent quality will always meet the standard.

- Kinetics of UV and solar photocatalysis of dyes with $Ag@TiO_2$ nanoparticles obeyed modified Langmuir-Hinshelwood model and the kinetic parameters for photocatalysis of AY-17 and RB-220 dyes were reported. This indicates that the rate of degradation of these dyes is determined mainly by the reaction occurring on the surface of $Ag@TiO_2$.

- Presence of salts like sodium chloride and sodium carbonate inhibited the rate of UV and solar photocatalysis of AY-17 and RB-220. So it is important to take salt concentration in the effluent into consideration while designing the photoreactor for treatment of dyeing wastewater

- Rate of degradation of AY-17 and RB-220 by photocatalysis, increased with increase in UV light intensity.

- Rate of degradation increased linearly with increase in UV and visible light radiation intensity of solar light.

- High TOC and COD removal indicated that AY-17 and RB-220 dyes degrade to simpler and easily biodegradable organic compounds by photocatalysis with $Ag@TiO_2$.

- Formation of inorganic ions (sulphate, nitrate, nitrite and chloride) indicated that the non-biodegradable organic part of AY-17 and RB-220 were destroyed,

decomposed and even mineralized during the UV and solar photocatalytic process.

- Studies on mixture of dyes showed that the optimum conditions for AY-17 were more favorable for the degradation of both the dyes in mixtures as compared to optimum conditions for RB-220 dye, both under UV and solar photocatalysis. RB-220 could be degraded easily under both the optimum conditions, but AY-17 could not be degraded easily under optimum conditions for RB-220. The difficulty in degradation of AY-17 as compared to that of RB-220 is owing to complexity of AY-17 dye structure and optimum conditions of RB-220 dye is sub optimal for AY-17 degradation. So, when mixtures of dyes are present in wastewater, it is recommended to use optimum conditions of the most complex dye for photocatalysis.

- Colour of the dye contaminated water was also measured in terms of Hazen unit during UV and solar photocatalysis of single and binary dye solution under optimum conditions and the colour of the treated water were found to be less than the permissible limit of 400 HU, specified by Central Pollution Control Board (CPCB, 2010) of India, for the range of initial concentrations used in the current study.

- The intermediates and products of photocatalytic degradation of AY-17 and RB-220 were identified through LC-MS analysis and the complete degradation pathway of Ag@TiO_2 mediated solar photocatalysis of AY-17 and RB-220 was proposed. The pathway are briefly summarized as follows:

$$AY - 17 \: dye \rightarrow smaller \: aliphatic \: and \: aromatic \: compounds \rightarrow$$
$$H_2O, CO_2, SO_4{}^{2-}, NO_3{}^{2-}, Cl^-$$
$$RB - 220 \: dye \rightarrow smaller \: aliphatic \: and \: aromatic \: compounds \rightarrow$$
$$H_2O, CO_2, SO_4{}^{2-}, NO_3{}^{2-}, NO_2{}^-$$

- Almost complete degradation of AY-17 and RB-220 could be achieved with both free and immobilized nanoparticles which depicted the nearly comparable efficacy of immobilized Ag@TiO_2 nanoparticles with the free photocatalyst.

- The activity of Ag@TiO$_2$ immobilized on chitosan and cellulose acetate as support matrices, were found almost unaltered after repeated uses. So it can be recycled without much decline in activity.
- Ag@TiO$_2$ core-shell structured nanoparticles were also found suitable for photocatalysis of other classes of dyes.

Hence Ag@TiO$_2$ core-shell structured nanoparticles may be considered as effective catalysts for the photocatalytic degradation of dyes/textile wastewater by being more effective than TiO$_2$ or Ag doped TiO$_2$ nanoparticles, due to their ability of prevention of electron-hole recombination by storage of electrons in the Ag core, and band gap excitation resulting in effective utilization of solar energy for environmental remediation strategies. Solar energy utilization and fast kinetics feature of this process makes it an economical and favorable option for large scale treatment of dye/textile wastewater. However, implementation of the process on a large scale for industrial scale applications in industrial wastewater treatment needs further research on continuous reactors and live effluents.

SCOPE FOR FUTURE STUDIES

Based on the results of present studies the following suggestions are made for future research as a logical continuation of the present work

- Immobilization of Ag@TiO$_2$ nanoparticles on various supports and to check for their batch photocatalytic efficacy at the optimum conditions.
- Characterization of immobilized Ag@TiO$_2$ nanoparticles.
- To design suitable reactor to increase the solar photocatalytic efficacy of Ag@TiO$_2$ nanoparticles for dye degradation.
- To study the artificial visible light photocatalytic efficacy of Ag@TiO$_2$ nanoparticles.
- Continuous reactor studies for the degradation of dye in single and binary solution using immobilized Ag@TiO$_2$ nanoparticles.
- To device reaction and inhibition mechanism during the photocatalysis of solutions containing mixture of dyes.
- Treatment of industrial dye effluent using Ag@TiO$_2$ nanoparticles
- To test the efficacy of Ag@TiO$_2$ nanoparticles as a catalyst for the degradation of other organic pollutants such as phenol, pesticide, herbicide and pharmaceuticals etc.

REFERENCES

REFERENCES

Aarthi, T., Narahari, P. and Madras, G. (2007). "Photocatalytic degradation of Azure and Sudan dyes using nano TiO_2." *J. Hazard Mater*., 149, 725–734.

Abdulla-Al-Mamun, M., Kusumoto, Y., Ahmmad, B. and Islam, M.S. (2011). "Synergistic cell-killing by photocatalytic and plasmonic photothermal effects of Ag@TiO_2 core–shell composite nanoclusters against human epithelial carcinoma (HeLa) cells." *Appl. Catal. A*., 398, 134-142.

Abdulla-Al-Mamun, M., Kusumoto, Y., Ahmmad, B. and Islam, M.S., (2010). "Photocatalytic cancer (hela) cell-killing enhanced with Cu–TiO_2 nanocomposite." *Top. Catal*., 53, 571–577.

Abo-Farha, S.A. (2010). "Photocatalytic degradation of monoazo and diazo dyes in wastewater on nanometer-sized TiO_2." *J. Am. Sci*., 6(11), 130-142.

Addamo, M., Augugliaro, V., Paola, A.D., Garcia, L.E., Loddo, V., Marci, G., Molinari, R., Palmisano, L. and Schiavello, M. (2004). " Preparation, characterization and photoactivity of polycrystalline nanostructured TiO_2 catalysts." *J. Phys. Chem. B*, 108:3303–3310.

Adesina (2004). "Industrial exploitation of photocatalysis: progress, perspectives and prospects". *Catal. Surv. Asia*, 8(4), 265–273.

Ahmed, S., Rasul, M.G., Martens, W.N., Brown, R. and Hashib, M.A. (2011). "Advances in heterogeneous photocatalytic degradation of phenols and dyes in Wastewater: A Review." *Water Air Soil Poll*., 215, 3–29.

Akbari, B., Tavandashti, M.P. and Zandrahimi, M. (2011). "Particle size characterization of nanoparticles – a practical approach." *Iran. J. Mater. Sci. Eng*., 8, 48-56.

Akpan, U.G. and Hameed, B.H. (2009). "Parameters affecting the photocatalytic degradation of dyes using TiO_2-based photocatalysts: A review". *J. Hazard. Mater.*, 170, 520–529.

Akpan, U.G. and Hameed, B.H. (2011). "Enhancement of the photocatalytic activity of TiO_2 by doping it with calcium ions". *J. Colloid Interface Sci.*, 357, 168–178.

Aksu, Z. (2005). "Application of biosorption for the degradation of organic pollutants: A review." *Process Biochem.*, *40*, 997–1026.

Akyol, A., Yatmaz, H.C. and Bayramoglu, M. (2004). "Photocatalytic decolorization of Remazol Red RR in aqueous ZnO suspensions." *Appl. Catal. B: Environ.*, 54, 19–24.

Al-Bastaki, N., (2004). "Removal of methyl orange dye and Na_2SO_4 salt from synthetic waste water using reverse osmosis." *Chem. Eng. Process.*, 43, 1561–1567.

Al-Ekabi, H. and Serpone, N. (1988). "Kinetic studies in heterogeneous photocatalysis.1. Photocatalytic degradation of chlorinated phenols in aerated aqueous solution over TiO_2 supported on a glass matrix." *J. Phys. Chem.*, 92, 5726–5731.

Ali, S.A., Bolton, J.R. and Cater, S.R. (1996). "Ferrioxalate-mediated solar degradation of organic contaminants in water." *Sol. Energy,* 56 (5), 439–443.

Andreozzi, R., Caprio, V., Insola, A and Martota, R. (1999). "Advanced oxidation processes (AOP) for water purification and recovery." *Catal. Today*, 53, 51-59.

Angkaew, S. and Limsuwan, P. (2012). "Preparation of silver-titanium dioxide core-shell ($Ag@TiO_2$) nanoparticles: Effect of Ti-Ag mole ratio." *Procedia Eng.*, 32, 649-655.

Anliker, R. (1979). "Ecotoxicology of dyestuffs a joint effort by industry." *Ecotox. Environ. Safe.,* 3, 59- 74.

APHA (American Public Health Association), (1995). "Standard methods for examination of water and wastewater", 20th edition. American Public Health Association, American Water Works Association and Water pollution Control Federation, Washington DC, USA.

Arami. H., Mazloumi, M., Khalifehzadeh, R and Sadrnezhaad, S. K. (2007). "Sonochemical preparation of TiO_2 nanoparticles." *Mater. Lett.*, 6, 4559–4561.

Arslan, I. A., Balcioglu, T. and Tuhkanen, S. (1999). "Advanced oxidation synthetic dye house effluent by O_3, H_2O_2/O_3 and H_2O_2/UV processes." *Environ. Technol.*, 20, 921-931.

Bahadir, K., Korbahti, M.A. and Rauf (2008). "Application of response surface analysis to the photolytic degradation of Basic Red 2 dye." *Chem. Eng. J.*, 138, 166–171.

Bahnemann, D. (2004). "Photocatalytic water treatment: solar energy applications." *Sol. Energy*, 77, 445–459.

Bahnemann, W., Muneer, M. and Haque, M. M. (2007). "Titanium dioxide-mediated photocatalysed degradation of few selected organic pollutants in aqueous suspensions." *Catal. Today*, 124, 133–148.

Baiocchi, C., Brussino, M. C., Pramauro, E., Bianco-Prevot, A., Palmisano, L and Marci, G. (2002). "Characterization of methyl orange and its photocatalytic degradation products by HPLC/UV-VIS diode array and atmospheric pressure ionization quadrupole ion trap mass spectrometry." *Int. J. Mass Spectrom.*, 214, 247-256.

Bandara. J, Mielczarski. J. A. and Kiwi, J. (1999). "Photosensitized Degradation of Azo Dyes on Fe, Ti, and Al Oxides. Mechanism of Charge Transfer during the Degradation." *Langmuir*, 15(22), 7680-7687.

Bansal, P. and Sud, D. (2011). "Photodegradation of commercial dye, Procion Blue HERD from real textile wastewater using nanocatalysts." *Desalination,* 267, 244–249.

Bansal, P. and Sud, D. (2012). "Photodegradation of commercial dye, CI Reactive Blue 160 using ZnO nanopowder:Degradation pathway and identification of intermediates by GC/MS. *Sep. Purif. Technol.*, 85, 112-119.

Bansal, P. and Sud, D. (2013). "Photocatalytic degradation of commercial dye, CI reactive red 35 in aqueous suspension: Degradation pathway and identification of intermediates by LC/MS." *J. Mol. Catal A: Chem.*, 374–375, 66 –72.

Bansal, P., Singh, D. and Sud, D. (2010). "Photocatalytic degradation of azo dye in aqueous TiO_2 suspension: Reaction pathway and identification of intermediates products by LC/MS." *Sep. Purif. Technol.*, 72, 357-365.

Behar, D., Czapki, G. and Duchovny, I. (1970). "Carbonate radical in flash photolysis and pulse." *J. Phy. Chem.*, 74(10), 2206-2210.

Behnajady, M. A., Modirshahla, N., Shokri, M. and Rad, B. (2008). "Enhancement of photocatalytic activity of TiO_2 nanoparticles by silver doping: photodeposition versus liquid impregnation methods." *Global Nest J.*, 10, 1-7.

Behnajady, M.A., Modirshahla, N., Daneshvar, N. and Rabbani, M. (2007). "Photocatalytic degradation of an azo dye in a tubular continuous-flow photoreactor with immobilized TiO_2 on glass plates." *Chem. Eng. J.*, 127, 167-176.

Behpour. M, Ghoreishi, S.M. and Razavi, F. S. (2010). "Photocatalytic activity of TiO_2 /Ag nanoparticle on degradation of water pollutions." *Dig. J. Nanomater. Bios.*, 5, 467 − 475.

Belhekar, A. A., Awate, S. V. and Anand, R. (2002). "Photocatalytic Activity of Titania Modified Mesoporous Silica for Pollution Control." *J. Catal. Commun.*, 3(10), 453−458.

Benitez, F.J., Beltran, H.J., Gonzalez, T. and Real, F. (1995). "Photooxidation of carbofuran by a polychromatic UV irradiation without and with hydrogen peroxide." *Ind. Eng. Chem. Res.*, 34, 4099-4105.

Bianco-Prevot, A., Baiocchi, C., Brussino, M.C., Pramauro, E., Savarino, P., Augugliaro, V., Marci, G. and Palmisano, L. (2001). "Photocatalytic degradation of acid blue 80 in aqueous solutions containing TiO_2 suspensions." *Environ. Sci. Technol.*, 35, 971–976.

Bickley, R.I., Gonzalez-carreno, T. and Lees, J.S. (1991). "A structural investigation of titanium dioxide photocatalysts." *J. Solid State Chem.*, 92 (1), 178-190.

Binnie, C., Kimber, M. and Smethurst, G. (2002). "Basic Water Treatment", third ed., *Thomas Telford,* 150-165.

Bockelmann, D., Linder, D. and Bahnemann. (1996). "From nanosized particles to commercial products, the search for novel photocatalysis (E. Pelizzetti, Ed.), Fine particles science and technology." *Kulwer Academic Publishers.*, Netherlands, 675–689.

Bokare, A., Pai, M. and Athawale, A. A. (2013). "Surface modified Nd doped TiO_2 nanoparticles as photocatalysts in UV and solar light irradiation." *Sol. Energy*, 91, 111–119.

Bonnell, D. (2001). Scanning Probe Microscopy and spectroscopy, Wiley-VCH, 16-128.

Bottcher, H., Mahltig, B., Sarsour, J. and Stegmaier, T. (2010). "Qualitative investigations of the photocatalytic dye destruction by TiO_2-coated polyester fabrics." *J. Sol-Gel Sci. Technol.*, 55, 177-185.

Bouanimba, N., Laid, N., Zouaghi, R. and Sehili, T. (2013). "Effect of pH and inorganic salts on the photocatalytic decolorization of methyl orange in the presence of TiO_2 P25 and PC500." *Desalination Water Treat.*, 1-15.

Bouanimba, N., Zouaghi, R., Laid, N. and Sehili T. (2011). "Factors influencing the photocatalytic decolorization of Bromophenol blue in aqueous solution with different types of TiO2 as photocatalysts." *Desalination*, 275, 224-230.

Box, G. E.P., Hunter, J. S. and Hunter, W. G. (1978). "Statistics for experiments." New York *Wiley*, 25- 32.

Boye. B, Dieng. M, M. and Brillas, E. (2002). "Degradation of herbicide 4-Chlorophenoxyacetic acid by advanced electrochemical oxidation methods." *Environ. Sci. Tech.*, 36, 3030-3035.

Bras. R., Gomes, A., Ferra, M. I. A., Pinheiro, H. M. and Goncalves, I. C. (2005) Monoazo and diazo dye decolourisation studies in a methanogenic UASB reactor. *J. Biotechnol.*, 115: 57–66

Byrappa, K., Subramani, A. K., Ananda, S., Rai, L. K. M., Dinesh, R. and Yoshimura, M. (2006). "Photocatalytic Degradation Of Rhodamine B Dye Using Hydrothermally Synthesized Zno." *Bull. Mater. Sci.*, *29* (5), 433–438.

Byrappa, K., Lokanatha, K.M. and Yoshimura, M. (2000). "Hydrothermal preparation of TiO$_2$ and photocatalytic degradation of hexachlorocyclohexane and dicholorodiphenyltrichloromethane". *Env.Technol.*, 21, 1085-1090.

Cai, R., Kubota, Y., Shuin, T., Sakai, H., Hashimoto, K. and Fujishima, A., (1992). "Increment of photocatalytic killing of cancer cells using TiO$_2$ with the aid of superoxide dismutase." *Chem. Lett.*, 3, 427–430.

Cangcang, C. and Dewan, H. (1998). "Application of fixed bed reactor to photodegradation of soluble dye 4BS (Red) with solar light." *Korean J. Chem. Eng.*, 20(4), 17-19.

Carlos, A. K., Gouveaa, F. W., Sandra, G.M., Nelson, D., Noemi, N. and Peralta-Zamoraa, P. (2000). "Semiconductor-assisted photocatalytic degradation of reactive dyes in aqueous solution". *Chemosphere*, 40, 433-440.

Carmen, Z. and Daniela, S. (2012). "Textile organic dyes, characteristics, polluting effects, and separation/elimination procedures from industrial effluents-A critical overview." Chapter 3 in: Organic Pollutants Ten Years after the Stockholm Convention. *Environmental and Analytical Update*, ISBN 978-953-307-917-2, 2012.02

Carp, O., Huisman, C. L. and Reller, A. (2004). "Photoinduced reactivity of titanium dioxide." *Prog. Solid State Chem.*, 32: 33-177.

Casero, I., Sicilia, D., Rubio, S. and Bendito, P. D. (1997). "Chemical degradation of aromatic amines by fenton's reagent." *Water Res.*, 31, 1985-1995.

Cassano, A. E. and Alfano, O. M. (2000). "Reaction engineering of suspended solid heterogenous photocatalytic reactors." *Catal. Today*, 58, 167–197.

Chai, Y. S., Lee. J, C. and Kim, B. W. (2000). "Photocatalytic Disinfection of E. coli in a Suspended TiO$_2$/UV Reactor." *Korean J. Chem. Eng.*, 17(6), 633-637.

Chan, S.C. and Barteau, M. A. (2005). "Preparation of highly uniform Ag/TiO$_2$ and Au/TiO$_2$ supported nanoparticle catalysts by photodeposition." *Langmuir*, 21, 5588−5595.

Chen, J.Q., Wang, D., Zhu, M.X. and Gao, C. J. (2006). "Study on degradation of methyl orange using pelagite as Photocatalyst". *J. Hazard. Mater.*, 138, 182–186.

Chen, C.C.,Lu, C.S., Chung, Y.C. and Jan, J.L. (2007). "UV light induced photodegradation of malachite green on TiO_2 nanoparticles." *J. Hazard. Mater.*, 141, 520-528.

Chen, C-Y., Cheng, M-C. and Chen, A-H. (2012). "Photocatalytic decolorization of Remazol Black 5 and Remazol Brilliant Orange 3R by mesoporous TiO_2." *J. Environ. Manage.*, 102, 125-133.

Chen, D. and Ray, A. K. (1998). "Photodegradation kinetics of 4-nitrophenol in TiO_2 suspension." *Water Res.*, 32, 3223–3234.

Chen, T., Zheng, Y., Lin, J. and Chen, G., (2008b). "Study on the photocatalytic degradation of methyl orange in water using Ag/ZnO as catalyst by liquid chromatography electrospray ionization ion–trap mass spectrometry." *J. Am. Soc. Mass Spectrom.*, 19, 997–1003.

Chen, X., Du, W. and Liu, D. (2008a). "Response surface optimization of biocatalytic biodiesel production with acid oil." *Biochem. Eng. J.*, 40, 423–429.

Chen, X., Lou, Y. and Burda, C. (2004). "Prepration of gold titanium dioxide nanoparticles." *Int. J. Nanotech.*, 1, 105-109.

Cheng, B., Le, Y. and Yu, J., (2010). "Preparation and enhanced photocatalytic activity of Ag@TiO_2 core–shell nanocomposite nanowires." *J. Hazard. Mater.*, 177, 971–977.

Cheng, M. M., Ma, W. H., Li, J., Huang, Y.P. and Zhao, J.C. (2004). "Visible-light-assisted degradation of dye pollutants over Fe(III)-loaded resin in the presence of H_2O_2 at neutral pH values." *Environ. Sci. Technol.*, 38, 1569–1575.

Chin,S. S., Lim, T. M., Chiang, K. and Fane, A. G. (2007). "Factors affecting the performance of a low-pressure submerged membrane photocatalytic reactor." *Chem. Eng. J.*, 130, 53–63.

Chin. S. S., Lim, T. M., Chiang, K. and Fane, A. G. (2006). "Hybrid low-pressure submerged membrane photoreactor for the removal of bisphenol A." *Desalination*, 202, 253–261.

Chiou, C-H., Wu, C-Y. and Juang, R-S. (2008). "Influence of operating parameters on photocatalytic degradation of phenol in UV/TiO$_2$ process." *Chem. Eng. J.*, 139, 322–329.

Cho, I.-H. and Zoh, K. D. (2007). "Photocatalytic degradation of azo dye (Reactive Red 120) in TiO$_2$/UV system: optimization and modeling using a response surface methodology (RSM) based on the central composite design." *Dyes Pigment*, 75, 533–543.

Chun, H. and Yizhong, W. (1999). "Decolorization and biodegradability of photocatalytic treated azo dyes and wool textile wastewater." *Chemosphere*, 39 (12), 2107-2115.

Chun, H. D., Kim, J. S., Yoon, S. M. and Kim, C. G. (2001). "Physical Properties and Photocatalytic Performance of TiO$_2$ Coated Stainless Steel Plate." *Korean J. Chem. Eng.*, 18(6), 908-913.

Chung, Y. C. and Chen, C. Y. (2009). "Degradation of azo dye reactive violet 5 by TiO$_2$ photocatalysis." *Environ Chem. Lett.*, 7, 347–352.

Clark, J. H. and Macquarrie, D. (2002). "Handbook of Green Chemistry and Technology." *Black-well Publishing*, Oxford.

Coleman, H. M., Chiang, K. and Amal, R. (2005). "Effects of Ag and Pt on photocatalytic degradation of endocrine disrupting chemicals in water." *Chem. Eng. J.*,113, 65-72.

Comparelli, R., Cozzoli, P.D., Curri, M.L., Agostiano, A., Mascolo and Lovecchio, G. (2004). "Photocatalytic degradation of methyl-red by immobilized nanoparticles of TiO$_2$ and ZnO." *Water Sci. Technol.*, 49(4), 183-188.

CPCB report (2010). "Ministry of Environment and Forests." http://www.cpcb.nic.in/dye.pdf (January 9, 2011).

Crittender, J.C., Rominder., Suri P.S., David, P.L. and Hand, D. W. (1997). "Decontamination of water using adsorption and photocatalysis". *Water Res.*, 31, 411-418.

Dalrymple, O.K., Stefanakos, E., Trotz, M.A. and Goswami, D.Y. (2010). "A review of the mechanisms and modeling of photocatalytic disinfection." *Appl. Catal. B*, 98, 27-38.

Damodar, R.A., Swaminathan, T. and You, S-J. (2009). "Degradation of synthetic dyes in a novel immobilized rotating tube photocatalytic reactor (IRTPR)." *J. Environ. Eng. Manage.*, 19(2), 107-112.

Daneshvar, N., Rasoulifard, M. H., Khataee, A.R. and Hosseinzadeh, F. (2007). "Removal of C.I. Acid Orange 7 from aqueous solution by UV irradiation in the presence of ZnO nano powder." *J. Hazard. Mater.,* 143, 95–101.

Daneshvar, N., Salari, D. and Khataee, A.R. (2004). "Photocatalytic degradation of azo dye acid red 14 in water on ZnO as an alternative catalyst to TiO$_2$." *J. Photochem. Photobiol. A: Chem.*, 162, 317–322.

Daneshvar, N., Salari, D. and Khataee, A. R. (2003). "Photocatalytic degradation of azo dye Acid Red 14 in water: Investigation of the effect of operational parameters." J. *Photochem. Photobiol. A*, 157, 111–116.

Daneshvar, N., Salari, D., Niaei, A. and Khataee, A. R. (2006). "Photocatalytic degradation of the herbicide erioglaucine in the presence of nanosized titanium dioxide: comparison and modeling of reaction kinetics." *J. Environ. Sci. Health., Part B.*, 41, 1273–1290.

Dang Z-M., You, S-S., Zha, J-W., Song, H-T. and Li, S-T. (2010). "Effect of shell-layer thickness on dielectric properties in Ag@TiO$_2$ core@shell nanoparticles filled ferroelectric poly (vinylidene fluoride) composites. "*Phys. Status Solidi A*, 207, 739–742.

Davis, E.A. and Mott, N.F. (1970). "Conduction in non-crystalline systems V. conductivity, optical absorption and photoconductivity in amorphous semiconductors." *Philos. Mag.*, 22, 903-922.

Davis, M.E. and Davis, R.J. (2003). "Fundamentals of chemical reaction engineering." McGraw-Hill, New York, 147-149.

Davis, R.J., Gainer, J.L., Neal, G.O. and Wu, I.W. (1994). "Photocatalytic decolorization of wastewater dyes." *Water Environ. Res.,* 66, 50-53.

Davydov, L., France, P. A. and Smirniotis, P. G. (2003). *US20036585863*.

Dawson, A. and Kamat, P. V. (2001). "Semiconductor-metal nanocomposites. Photoinduced fusion and photocatalysis of gold-capped TiO_2 (TiO_2/Gold) nanoparticles". *J. Phy. Chem. B.*, 105,960–966.

Delee, W., O'Neill, C., Hawkes, F.R. and Pinheiro, H.M. (1998). "Anaerobic treatment of textile effluents: a review." *J. Chem. Technol. Biotechnol.*, 73, 323–335.

Department of Chemicals and Petrochemicals, Ministry of Chemicals and Petrochemicals, Government of India (2013). *Annual Report 2012-2013*, http://chemicals.nic.in/AR_2012-2013_(1-94).pdf (October 26, 2013).

Dijkstra, M.F.J., Buwalda, H., de Jong, A.M., Michorius, A. and Winkelman, J.G.M. (2001). "Photocatalytic degradation of methyl orange by TiO_2". *Chem. Eng. Sci.*, 56, 547-555.

Ding, Z., Hu, X., Yue, P.L., Lu, G.Q. and Greenfield, P.F. (2001). "Synthesis of anatase TiO_2 supported solids by chemical vapor deposition." *Catal. Today*, 68, 173–182.

Di-Paola, A., Garcia-Lopex, E., Ikeda S., Marci G., Othani, B. and Palmisano, L. (2002). "Photocatalytic degradation of organic compounds in aqueous system by transition metal doped polycrystalline TiO_2." *Catal. Today*, 75, 87-93.

Dostanić, J. , Lončarević, D., Rožić, L., Petrović, S., Mijin, D. and Jovanović, D.M. (2013). "Photocatalytic degradation of azo pyridone dye: Optimization using response surface methodology." *Desalination Water Treat.*, 51, 2802–2812.

Dror, S. (1994). "Scanning force microscopy: with applications to electric, magnetic and atomic forces." *Oxford University Press*, 224- 230.

Du, J.M., Zhang, J.L., Liu, Z.M. and Ha. (2006). "Controlled synthesis of Ag/TiO$_2$ core-shell nanowires with smooth and bristled surfaces via a one-step solution route". *Langmuir*, 22, 1307-1312.

El-Guendi, M.S., Ismail, H.M. and Attyia, K.M.E. (1995). "Activated clay as an adsorbent for cationic dyestuffs." *Adsorpt. Sci. Technol.*, 12, 109–117.

Erdemoglu, S., Aksu, S., Sayilkan, F., Izgi, B., Asilturk, M., Sayilkan, H., Frimmel, F.and Gucer, S., (2008). "Photocatalytic degradation of Congo Red by hydrothermally synthesized nanocrystalline TiO$_2$ and identification of degradation products by LC–MS." *J. Hazard. Mater.*, 55, 469–476.

Fabbri, D., Calza, P. and Prevot, A.B. (2010). "Photoinduced transformations of Acid Violet 7 and Acid Green 25 in the presence of TiO$_2$ suspension. "*J. Photochem. Photobiol. A Chem.*, 213, 14-22.

Faisal, M., Tariq, M.A. and Muneer, M. (2007). "Photocatalysed degradation of two selected dyes in UV-irradiated aqueous suspensions of titania." *Dyes Pigments*, 72, 233–239.

Fathinia, M., Khataee, A.R., Zarei, M. and Aber, S. (2010). "Comparative photocatalytic degradation of two dyes on immobilized TiO$_2$ nanoparticles: Effect of dye molecular structure and response surface approach." *J. Mol. Catal. A-Chem.*, 333, 73-84.

Fernandes-Machado, N.R.C and Santana, V.S. (2005). "Influence of thermal treatment on the structure and photocatalytic activity of TiO$_2$ P25." *Catal. Today*, 107, 595–601.

Fernandez, G., Lassaletta, V. M., Jimenez, A., Justo, A. R., Gonzalez-Elipe, H.J. M., Tahiri, H. and Ait-Ichou, Y. (1995). "Preparation and characterization of TiO$_2$ photocatalyst supported on various rigid supports (glass, quartz and stainless steel). Comparative studies of photocatalytic activity in water purification." *J. App. Catal. B: Environ.*, 7, 49–63.

Fernandez, J., Kiwi, J., Baeza, J., Freer, J., Lizama, C. and Mansilla, H. D. (2004). "Orange II photocatalysis on immobilized TiO_2. Effect of the pH and H_2O_2." *Appl. Catal. B Environ*., 48(3), 205-211.

Fox, A. (1992). "Photocatalysis: Decontamination with sunlight." *Chemtech.*, 22, 680–685.

Fox, M. A. and Dulay, M. T. (1993). "Heterogeneous photocatalysis." *Chem. Rev*., 93, 341–357.

Fu, J. and Wu, Q. (2008). "Statistical designs of experiments for photocatalytic process of Acid Blue 7 dye wastewater by nano TiO_2." *Taiyangneng Xuebao/Acta Energiae Solaris Sinica,* 29, 152–157.

Fu, J., Zhao, Y. and Wu, Q. (2007). "Optimising photoelectrocatalytic oxidation of fulvic acidusing response surface methodology." *J. Hazard. Mater*., 144, 499–505.

Fu, X., Zeltner, W. A. and Anderson, M. A. (1996). "Semiconductor Nanoclusters Studies in Surface Science and Catalysis." Edited by Kamat PV, Meisel D. *Elsevier Science*, Amsterdam, 445–461.

Fujishima, A. and Tryk, D. A. (1999). "Photoelectrochemical Conversion". Ed. Honda K. (*Springer-Verlag*, Tokyo). Functionality of Molecular Systems, 2, 196.

Fujishima, A., Rao, T.N. and Tryk, D.A. (2000). "Titanium dioxide Photocatalysis." *J. Photochem. Photobiol. C: Photochem. Rev*., 1, 1-21.

Gahr, F., Hermanutz, F. and Opperman, W. (1994). "Ozonation an important technique to comply with new German law for textile wastewater treatment." *Water Sci. Technol.*, 30, 255-263.

Galindo, C., Jacques, P. and Kalt, A. (2000). "Photodegradation of the aminoazo benzene Acid Orange 52 by three advanced oxidation processes: UV/H_2O_2, UV/TiO_2 and VIS/TiO_2 comparative mechanistic and kinetic investigations". *J. Photochem, Photobiol. A: Chem*., 130, 35-47.

Galindo, C., Jacques, P. and Kalt, A. (2001). "Photochemical and photocatalytic degradation of an Indigoid dye: a case study of acid blue 74 (AB 74)." *J. Photochem. Photobiol. A: Chem*., 141, 47-56.

Ghaly, M.Y., Farah, J.Y. and Fathy, A.M. (2007). "Enhancement of decolorization rate and COD removal from dyes containing wastewater by the addition of hydrogen peroxide under solar photocatalytic oxidation." *Desalination*, 217, 74-84.

Gogate, P.R. and Pandit, A.B. (2004). "A review of imperative technologies for wastewater treatment. I: Oxidation technologies at ambient conditions." *Adv. Environ. Res.*, 8, 501–551.

Gonçalves, M.S.T., Ana M.F., Oliveira-Campos, Elisa, M.M., Paula, M.S., Plasência, M. and Maria João, R.P. (1999). "Photochemical treatment of solutions of azo dyes containing TiO_2". *Chemosphere*, 39, 781-786.

Gopalakrishnan, A.N. and Mohan, V. (1997). "Solar photo sensitizer technology for dyeing waste reclamation." *Indian J. Environ. Prot.*, 17, 268-271.

Gouvea, C.A.K., Wypych, F., Moraes, S.G., Duran, N., Nagata, N. and Peralta-Zamora, P. (2000). "Semiconductor-assisted photocatalytic degradation of reactive dyes in aqueous solution." *Chemosphere*, 40, 433-440.

Gratzel, C. K., Jirousek, M. and Gratzel, M. (1990). "Decomposition of organophosphorus compounds on photoactivated TiO_2 surfaces." *J. Mol. Catal.,* 60, 375–387.

Grzechulska, J. and Morawski, A. W. (2002). "Photocatalytic decomposition of azo-dye acid black 1 in water over modified titanium dioxide." *Appl. Catal. B: Environ.*, 36, 45-51.

Guillard, C., Lachheb, H., Honas, A., Ksibi, M. and Hermann, J.M. (2003). "Influence of chemical structure of dyes, of pH and of inorganic salts on their photo- catalytic degradation by TiO_2 comparison of the efficiency of powder and supported TiO_2." *J. Photochem. Photobiol. A: Chem.*, 158, 27-36.

Gumus, D. and Akbal, F (2011). "Photocatalytic Degradation of Textile Dye and Wastewater." *Water Air Soil Pollut.*, 216, 117–124.

Gupta, A. K., Pal, A. and Sahoo, C. (2006). "Photocatalytic degradation of a mixture of Crystal Violet (Basic Violet 3) and Methyl Red dye in aqueous suspensions using Ag^+ doped TiO_2." *Dyes Pigments*, 69, 224-232.

Gupta, G.S., Prasad, G. and Singh, V.H., (1990). "Removal of chrome dye from aqueous solutions by mixed adsorbents: ash and coal." *Water Res.*, 24, 45-50.

Gupta, G.S., Singh, A.K., Tayagi, B.S., Prasad, G. and Singh, V. N. (1992). "Treatment of carpet and metallic effluent by China clay." *J. Chem. Technol. Biotechnol.*, 55, 227–283.

Gupta, V.K. and Suhas, (2009). "Application of low-cost adsorbents for dye removal—a review." *J. Environ. Manage.*, 90, 2313–2342.

Gupta, V.K., Jain, R., Agarwal, S., Nayak, A. and Shrivastava, M. (2012a). "Photodegradation of hazardous dye quinoline-yellow catalyzed by TiO_2." *J. Colloid Interface Sci.*, 366, 135–140.

Gupta, V.K., Jain, R., Mittal, A., Mathur, M. and Sikarwar, S. (2007). "Photochemical degradation of the hazardous dye Safranin-T using TiO_2 catalyst." *J. Colloid Interface Sci.* 309, 464–469.

Gupta, V.K., Jain, R., Mittal, A., Saleh, T.A., Nayak, A., Agarwal, S. and Sikarwar, S. (2012b). "Photo-catalytic degradation of toxic dye amaranth on TiO_2/UV in aqueous suspensions." *Mater. Sci. Eng. C*, 32, 12–17.

Gupta, V.K., Jain, R., Nayak, A., Agarwal, S. and Shrivastava, M. (2011). "Removal of the hazardous dye-Tartrazine by photodegradation on titanium dioxide surface." *Mater. Sci. Eng. C*, 31, 1062–1067.

Habibi, M.H., Hassanzadeh, A. and Mahdavi, S. (2005). "The effect of operational parameters on the photocatalytic degradation of three textile azo dyes in aqueous TiO_2 suspensions." *J. Photochem. Photobiol. A: Chem.*, 172, 89–96.

Hai, F.I., Yamamoto, K. and Fukushi, K., (2007). "Hybrid treatment systems for dye wastewater." *Crit. Rev. Env. Sci. Technol.*, 37, 315–377.

Hameed, B.H., Ahmad, A.A. and Aziz, N. (2007). "Isotherms, kinetics and thermodynamics of acid dye adsorption on activated palm ash." *Chem. Eng. J.*, 133, 195-203.

Harizanov, O. and Harizanova, A. (2000). "Development and investigation of sol-gel solutions for the formation of TiO_2 coatings." *Sol. Energy Mater. Sol. Cells*, 63, 185–195.

Harold, P. K. and Leroy, E. (1974). "X-ray diffraction procedures: for polycrystalline and amorphous materials." 2nd edition, *Wiley-VCH*, 44-51.

Hasnat, M.A., Siddiquey, I.A. and Nuruddin, A. (2005). "Comparative photocatalytic studies of degradation of a cationic and an anionic dye." *Dyes Pigments*, 66, 185-188.

Hegfeldt, A. and Gratzel, M. (1995). "Light-induced redox reactions in nanocrystalline systems." *Chem. Rev.*, 95, 49–68.

Heglin, A. (1989). "TiO_2-assisted photodegradation of dye pollutants. II.Adsorption and degradation kinetics of eosin in TiO_2 dispersions under visible light irradiation." *Chem. Rev.*, 89, 1861–1873.

Heller, A. (1995). "Chemistry and applications of photocatalytic oxidation of thin organic films." *Adv. Chem. Res.*, 28, 503–508.

Herrmann, J. M. (1999). "Heterogeneous photocatalysis: fundamentals and applications to the removal of various types of aqueous pollutants." *Catal. Today*, 53, 115–129.

Hidaka, H., Honjo, H., Horikoshi, S. and Serpone, N. (2007). "Photoinduced Ag on cluster deposition. Photoreduction of Ag+ ions on a TiO_2-coated quartz crystal microbalance monitored in real time." *Sens. Actuators B*, 123, 822–828.

Hirakawa, T. and Kamat, P. V. (2004). "Photoinduced Electron Storage and Surface Plasmon Modulation in Ag@TiO_2 Clusters." *Langmuir*, 20, 5645–5647.

Hirakawa, T. and Kamat, P.V. (2005). "Charge separation and catalytic activity of Ag@TiO_2 core-shell composite clusters under UV-irradiation." *J. Am. Chem. Soc.*, 127, 3928-3934.

Hisaindee, S., Meetani, M.A. and Rauf, M.A. (2013). "Application of LC-MS to the analysis of advanced oxidation process (AOP) degradation of dye products and reaction mechanisms." *Trends Anal. Chem.*, 49, 31–44.

Hoffmann, M. R., Martin, S. T. Choi, W. and D. W.Bahnemann, D. (1995). "Environmental Applications of Semiconductor Photocatalysis." *Chem. Rev.,* 95, 69-96.

Hosono. M., Arai. H., Aizana, M., Yamameta, I., Shimizu, R. and Augiyama, M. (1993). "Decolouration and degradation of azo dye in aqueous solution supersaturated with oxygen by irradiation of high energy electron beams." *Appl. Radiat. Iso.*, 44, 1199–1203

Houas, A., Lachheb, H., Ksibi, M., Elaloui, E., Guillard, C. and Herrmann, J.M. (2001). "Photocatalytic degradation pathway of methylene blue in water." *Appl. Catal. B:Environ.*, 31, 145-157.

Hu, C., Yu, J. C., Hao, Z. and Wong, P. K. (2003). "Effects of acidity and inorganic ions on the photocatalytic degradation of different azo dyes." *Appl. Catal. B.*, 46, 35–47.

Hua, D.S., Kunfeng, Z., Daorong, L., Qiya, Y. and Changwen, H. (2009). "Synthesis, characterization and photocatalytic activity of Co^{2+}-doped titania." *8th China International Nanoscience and Technology Symposium* (CINSTS09). J. Phys.: Conference Series 188. 012018.

Huang, M., Xu, C., Wu, Z., Huang, Y., Lin, J. and Wu, J. (2008). "Photocatalytic discolorization of Methyl Orange solution by Pt modified TiO_2 loaded on natural zeolite". *Dyes Pigments*, 77, 327–334.

Hufschmidt, D. and Bahnemann, D. W. (2002). "Enhancement of the photocatalytic activity of various TiO_2 materials by platinisation." *J. Photochem. Photobiol*. A, 148, 223-231.

Hunger, K. (2003). "Industrial Dyes: Chemistry, Properties, Applications." *Wiley-VCH*, 2-590.

Hurum, D.C., Agrios, A.G., Gray, K.A., Rajh, T. and Thurnauer, M.C. (2003). "Explaining the enhanced photocatalytic activity of Degussa P25 mixed-phase TiO_2 using EPR." *J. Phys. Chem. B.*, 107, 4545–4549.

Hyun-Woo, K., Young, M. L., Suraj, K.T., Byoung, G.K., Min. S.L. and Yeon, T. Y. (2007). "Synthesis of Au/TiO$_2$ Core–Shell Nanoparticles from Titanium Isopropoxide and Thermal Resistance Effect of TiO$_2$ Shell." *Jpn. J. Appl. Phys.*, 46, 2567-2570.

Ilinoiu, E.C., Pode, R., Manea, F. Colar, L.A., Jakab, A., Orha, C., Ratiu, C., Lazau, C. and Sfarloaga, P. (2013). "Photocatalytic activity of a nitrogen-doped TiO$_2$ modified zeolite in the degradation of Reactive Yellow 125 azo dye." *J. Taiwan Inst. Chem. Eng.*, 44, 270–278.

Ince, N.H. and Gonenc, D.T. (1997). "Treatability of a textile azo dye by UV/H$_2$O$_2$." *Environ. Technol.*, 18, 179-185.

Inel, Y. and Okte, A. (1996). "Photocatalytic degradation of malonic acid in aqueoussuspensions of titanium dioxide: an initial kinetic investigation of CO$_2$ photogeneration." *J. Photochem. Photobiol. A: Chem.*, 96, 175–180.

International Standard Organization (1984). "Water quality -- Determination of nitrite – Molecular absorption spectrometric method." ISO 6777. International Organization for Standardization, Case Postale 56, CH-1211, Geneva 20 Switzerland.

Irmak, S., Kusvuran, E. and Erbatur, O. (2004) "Degradation of 4-chloro-2-methyl phenol in aqueous solution by UV irradiation in the presence of titanium dioxide."*Appl. Catal. B Environ.*, 54, 85–91.

Jaeger, C.D. and Bard, A.J., (1979). "Spin trapping and electron spin resonance detection of radical intermediates in the photodecomposition of water at TiO$_2$ paniculate systems." *J. Phys. Chem.*, 93, 3146–3152.

Jeni, J. and Kanmani, S. (2011). "Solar nano photocatalytic decolorisation of reactive dyes using titanium dioxide." *Iran. J. Environ. Health. Sci. Eng.*, 8, 15-24.

Jeonga, E. D., Borseb, P. H., Jangb, J. S., Leeb, J. S., Jungc, O.S., Changd, H., Jina, J. S., Wona, M. S. and Kima, H. G. (2008). "Hydrothermal synthesis of Cr and Fe co-doped TiO$_2$ nanoparticle photocatalyst." *J. Ceram. Process. Res.*, 9(3), 250-253.

Jian-Hua, L. and Hai-Jun, W. (2009). "Treating dye wastewater by TiO$_2$ coated on coal cinder." *J. Chongqing Uni.*, 8(3), 165-169.

Jing, L., Qu, Y., Wang, B., Li, S., Jiang, B., Yang, L., Fu, W. and Fu, H (2006). "Review of photoluminescence performance of nano-sized semiconductor materials and its relationships with photocatalytic activity." *Sol. Energy Mater. Sol. Cells.*, 90, 1773–1787.

Jing, M.X., Jiang, X.Q., Li, W.X., Li, D.H. and Zhou, W. (2009). "Preparation and Photocatalytic Activity of Mesoporous TiO_2 Microspheres." *Micro Nanosyst.*, 1, 12-16.

Joice, J.A.I., Sivakumar, T., Ramakrishnan,R., Ramya,G., Prasad,K.P.S. and Selvan, D.A. (2012). "Visible active metal decorated titania catalysts for the photocatalytic degradation of Amidoblack-10B." *Chem. Eng. J.*, 210, 385-397.

Jung, J-T., Kim, J-O. and Choi, J-Y. (2009). "Effect of various oxidants in a photocatalysis/filtration system for the treatment of contaminants." *Res. Chem. Intermed.*, 35, 243–248.

Jung, K.Y. and Park, S.B. (2001)." Effect of calcinations temperature and addition of Silica, Zirconia, Alumina on the photocatalytic activity of titania." *Korean J. Chem. Eng.*, 18, 879–888.

Jung, K.Y., Park, S.B. and Anpo, M. (2005). "Photoluminescence and photoactivity of titania particles prepared by the sol-gel technique: Effect of calcination temperature". *J. Photochem. Photobiol. A.*, 170, 247–252.

Kalsoom, U. ,Ashraf, S.S., Meetani, M.A., Rauf, M.A. and Bhatti, H.N. (2012). "Degradation and kinetics of H_2O_2 assisted photochemical oxidation of Remazol Turquoise Blue.**" *Chem. Eng. J.*, 373, 200–202.

Kamat, P.V. (1993). "Photochemistry on nonreactive and reactive (semiconductor) surfaces." *Chem. Rev.*, 93, 267–300.

Kang, J.W. and Hoffmann, M.R. (1998)."Kinetics and mechanism of the sonolytic destruction of MTBE by ultrasonic irradiation in the presence of ozone." *Environ. Sci. Tech.* 32, 3194-3199.

Kansal, S. K., Singh, M. and Sud, D. (2008). "Effluent quality at kraft/soda agro-based paper mills and its treatment using a heterogeneous photocatalytic system." *Desalination*, 228 (1-3), 183-190.

Kansal, S.K., Ali, A.H. and Kapoor, S. (2010). "Photocatalytic decolorization of biebrich scarlet dye in aqueous phase using different nanophotocatalysts." *Desalination*, 259, 147–155.

Kansal, S.K., Kaur, N. and Singh, S. (2009). "Photocatalytic degradation of two commercial reactive dyes in aqueous phase using nanophotocatalysts." *Nanoscale Res Lett*., 4,709–716.

Kansal, S.K., Singh, M. and Sud, D. (2006). "Studies on photodegradation of two commercial dyes in aqueous Phase Using Nanophotocatalysts." *Nanoscale Res. Lett*., 4, 709–716.

Karcher, S., Kornmuller, A. and Jekel, M. (1999a). "Eects of alkaline-earth cations on the removal of reactive dyes with cucurbituril." *Acta hydrochim.*, 27, 38-42.

Karcher, S., Kornmuller, A. and Jekel, M., (1999b). "Removal of reactive dyes by sorption/complexion with cucurbituril." *Water Sci. Technol*., 40, 425-433.

Karkmaz, M., Puzenat, E., Guillard, C. and Herrmann, J.M. (2004). "Photocatalytic degradation of the alimentary azo dye amaranth mineralization of the azo group to nitrogen." *Appl. Catal. B: Environ*., 51, 183-194

Karthikeyan, J. (1990). "A study on colour removal from textile dye waste by chemical treatment." Ph.D., thesis IIT, Kanpur

Kasiri, M.B. and Khatee, A.R. (2011). "Photooxidative decolorization of two organic dyes with different chemical structures by UV/H_2O_2 process: Experimental design." *Desalination,* 270, 151-159.

Kasiri, M.B., Aleboyeh, H. and Aleboyeh, A. (2008). "Modeling and optimization of heterogeneous photo-Fenton process with response surface methodology and artificial neural networks." *Environ. Sci. Technol*., 42, 7970–7975.

Khataee, A.R., Pons, M.N. and Zahraa, O. (2009). "Photocatalytic degradation of three azo dyes using immobilized TiO_2 nanoparticles on glass plates activated by UV

light irradiation: Influence of dye molecular structure." *J. Hazard. Mater.*, 168, 451–457.

Khezrianjoo, S. and Revanasiddappa, H.D. (2012). "Langmuir-Hinshelwood kinetic expression for the photocatalytic degradation of metanil yellow aqueous solutions by ZnO catalyst." *Chem. Sci. J.*, 2012, 1-7.

Khodja, A. A., Sehili, T., Pilichowski, J. F. and Boule, P. (2001). "Photocatalytic degradation of 2-phenylphenol on TiO_2 and ZnO in aqueous suspensions." *J. Photochem. Photobiol. A: Chem.*, 141, 231-239.

Kim, H. Hong, H-J., Jung, J., Kim, S-H. and Yang, J-W. (2010). "Degradation of trichloroethylene (TCE) by nanoscale zero-valent iron (nZVI) immobilized in alginate bead." *J. Hazard. Mater.*, 176, 1038–1043.

Kim, Y.H., Kang, Y.S. and Jo, B.G. (2004). "Preparation and characterization of Ag-TiO_2 core–shell type nanoparticles." *J. Ind. Eng. Chem.*, 10, 739–744.

Kiriakidou, F., Kondarides, D.I. and Verykios X.E.(1999). "The effect of operational parameters and TiO_2-doping on the photocatalytic degradation of azo-dyes". *Catal. Today*, 54, 119-130.

Klare, M., Scheen, J., Vogelsang, K., Jacobs, H. and Broekaert, J. A. C. (2000). "Degradation of Short-Chain Alkyl- and Alkanolamines by TiO_2 and Pt/TiO_2-assisted Photocatalysis." *Chemosphere*, 41, 353-362.

Klug, H.P. and Alexander, L.E. (1974). "X-Ray diffraction procedures: For polycrystalline and amorphous materials." *Wiley*, 168-347.

Kominami, H., Kato, J., Murakami, S., Ishii, Y., Kohno, M., Yabutani, K. and Yamamoto, T. (2003). "Solvothermal syntheses of semiconductor photocatalysts of ultra-high activities." *Catal. Today*, *84*, 181–189.

Kondo, M. M. and Jardim, W. F. (1991). "Photodegradation of chloroform and urea using Ag-loaded titanium dioxide as catalyst." *Water Res.*, 25, 823-827.

Konstantinou, I. and Albanis, T.A. (2004). "TiO_2-assisted photocatalytic degradation of azo dyes in aqueous solution: kinetic and mechanistic investigations." *Appl. Catal. B: Environ.*, 49, 1–14.

Kreibig, U. and Vollmer, M. (1995). "Optical Properties of Metal Clusters; Springer Series in Materials Science." ed. J. P. Toennies, *Springer-Verlag*: Verlag Berlin Heidelberg New York.

Ku. Y., Wang, L. C., Ma, C.M. and Chou, Y.C. (2011). "Photocatalytic Oxidation of Reactive Red 22 in Aqueous Solution Using $La_2Ti_2O_7$ Photocatalyst." *Water Air Soil Pollut.*, 215, 97-103.

Kumar, S.A., Lo, P.H. and Chen, S.M. (2008). "Electrochemical synthesis and characterization of TiO_2 nanoparticles and their use as a platform for flavin adenine dinucleotide immobilization andefficient electrocatalysis." *Nanotechnol.*, 19, 1-7.

Kusvuran, E., Samil, A., Atanur , O. M. and Erbatur, O. (2005). "Photocatalytic degrada-tion of di- and tri-substituted phenolic compounds in aqueous solution by TiO_2/UV." *Appl. Catal. B: Environ.*, 58, 211-216.

Lackey, L.W., Mines, R.O. and Mc Creanor, P.T. (2006). "Ozonation of acid yellow 17 dye in a semi-batch bubble column." *J. Hazard. Mater.*, 138, 357–362.

Lahiri, D., Subramanian, V., Shibata, T., Wolf, E.E., Bunker, B.A. and Kamat, P.V. (2003). "Photoinduced transformations at semiconductor/metal interfaces: X-ray absorption studies of titania/gold films." *J. Appl. Phys.*, 93, 2575-2583.

Langlet, M., Kim, A., Audier, M. and Herrmann, J.M. (2002). "Sol-Gel Preparation of Photocatalytic TiO_2 Films on Polymer Substrates." *J. Sol-Gel Sci. Tech.*, 25, 233–234.

Lathasree, S., Nageswara, R., Sivasankar, B., Sadasivam, V. and Rengaraj, K. (2004). "Heterogeneous photocatalytic mineralization of phenols in aqueous solutions." *J. Mol. Catal. A: Chem.*, 223, 101-105.

Lee, S.M., Kim, Y.G. and Cho, I.H. (2005). "Treatment of dyeing wastewater by TiO_2/H_2O_2/UV process: experimental design approach for evaluating total organic carbon (TOC) removal efficiency." *J. Environ. Sci. Health Part A: Toxic/Hazard. Subst. Environ. Eng.*, 40, 423–436.

Legrini, O., Oliveros, E. and Braun, A.M. (1993). "Photochemical process for water treatment." *Chem. Rev.*, 93, 671-698

Lei, L., Chu, H.P., Hu, X. and Yue, P.L. (1999). "Preparation of heterogeneous photocatalyst (TiO$_2$/alumina) by metallo-organic chemical vapour deposition." *Ind. Eng. Chem.*, 38, 3381-3385.

Lei, P., Wang, F., Gao, X., Ding, Y., Zhang, S., Zhao, J., Liu, S. and Yang, M. (2012). "Immobilization of TiO$_2$ nanoparticles in polymeric substrates by chemical bonding for multi-cycle photodegradation of organic pollutants." *J. Hazard. Mater.*, 227-228, 185-194.

Levenspiel, O. (1972). "Chemical reaction engineering." New York: *Wiley*.

Levin, L., Herrmann, C. and Papinutti, V.L. (2008). "Optimization of lignocellulolytic enzyme production by the white-rot fungus Trametes trogii in solid-state fermentation using response surface methodology." *Biochem. Eng. J.*, 39, 207–214.

Li Y, Niu J, Yin L, 2011. Photocatalytic degradation kinetics and mechanism of pentachlorophenol based on superoxide radicals. *J. Environ. Sci.*, 23, 1911-1918.

Li, C., Goswami, Y. and Stefanakos, E. (2013). "Solar assisted sea water desalination: A review." *Renew. Sust. Energy Rev.*, 19, 136–163.

Li, D., Haneda, H., Hishita, S. and Ohashi, N. (2005). "Visible-light driven nitrogen-doped TiO$_2$ photocatalysts: effect of nitrogen precursors on their photocatalysis for decomposition of gas-phase organic pollutants." *Mater. Sci. Eng. B*, 117, 67–75.

Li, H., Duan, X., Liu, G. and Liu, X., (2008). "Photochemical synthesis and characterization of Ag/TiO$_2$ nanotube composites." *J. Mater. Sci.*, 43, 1669–1676.

Li, Y., Niu, J. and Yin, L. (2011). "Photocatalytic degradation kinetics and mechanism of pentachlorophenol based on superoxide radicals." *J. Environ. Sci.*, 23, 1911-1918.

Lim, T.H. and Kim, S. D. (2005). "Photocatalytic degradation of trichloroethylene (TCE) over TiO$_2$/silica gel in a circulating fluidized bed (CFB) photoreactor." *J. Chem. Eng. Process.* 44, 327–334.

Lindner, M., Bahnemann, D.W., Hirthe, B. and Griebler, W. D. (1997). "Solar water detoxification: novel TiO_2 powders as highly active photocatalysts." *J. Sol. Energy Eng.*, 119, 120-125.

Linesbigler, A. L., Lu, G. and Yates, J. L. (1995). "Photocatalysis on TiO_2 surfaces: principles, mechanisms and selected results." *Chem. Rev.*, 95, 735–758.

Liu, C.C., Hsieh, Y.H., Lai, P.F., Li, C. H. and Kao, C.L. (2006). "Photodegradation treatment of azo dye wastewater by UV/TiO_2 process." *Dyes Pigments*, 68, 191-195.

Liu, G., Li, X. and Zhao, J. (2000). "Photo-oxidation pathway of Sulforhodamine-B dependence on the adsorption mode on TiO_2 exposed to visible light radiation." *Environ. Sci. Technol.*, 34, 3982-3990.

Liu, G., Wu, T., Zhao, J., Hidaka, H. and Serpone, N. (1999). "Photoassisted degradation of dye pollutants. 8. Irreversible degradation of alizarin red under visible light radiation in air-equilibrated aqueous TiO_2 dispersions." *Environ. Sci. Technol.*, 33, 2081.

Liu, H.-L. and Chiou, Y.-R. (2005a). "Optimal decolorization efficiency of Reactive Red 239 by UV/TiO_2 photocatalytic process coupled with response surface methodology." *Chem. Eng. J.*, 112, 173–179.

Liu, J., Xing, J., Ghang, T., Zhiya, M.A., Liu, H. (2005b). "Optimization of nutritional conditions for nattokinase production by *Bacillus natto* NLSSE using statistical experimental methods." *Process Biochem.*, 40(8), 2757-2762.

Liu, S. X., Qu, Z. P., Hanb, X.W. and Sun, C. L. (2004). "A mechanism for enhanced photocatalytic activity of silver-loaded titanium dioxide." *Catal. Today*, 93–95, 877–884.

Liu, Y., Liu, C-Y., Rong, Q-H. and Zhang, Z. (2003). "Characteristics of the silver-doped TiO_2 nanoparticles." *Appl. Surf. Sci.*, 220, 7–11.

Lizama, C., Freer, J., Baeza, J. and Mansilla, H.D. (2002). "Optimized photodegradation of reactive blue 19 on TiO_2 and ZnO suspensions." *Catal. Today*, 76, 235–246.

Liz-Marzan, L. M. and Mulvaney, P. (2003). "The Assembly of Coated Nanocrystals." *J. Phys. Chem. B., 107, 7312-7326.

Lopes, C. N., Carlos, J., Petrus, C. and Riella, H.G. (2005). "Color and COD retention by nanofiltration membranes." *Desalination*, 172, 77–83.

Lorimer, J.P., Mason, T.J., Plattes, M., Phull, S.S. and Walton, D.J. (2001). "Degradation of dye effluent." *Pure Appl. Chem.* 12, 1957-1968.

Lucarelli. L., Nadtochenko, V. and Kiwi, J. (2000). "Environmental photochemistry: quantitative adsorption and FTIR studies during the TiO_2-photocatalyzed degradation of Orange II." *Langmuir*, 16, 1102-1108.

Mahmoodi, N.M. (2013). "Photocatalytic degradation of dyes using carbon nanotube and titania nanoparticle." *Water Air Soil Pollut*., 224, 1612-1620.

Mahmoodi, N.M., Arami, M., Limaee, N.Y. and Tabrizi, N.S. (2006). "Kinetics of heterogeneous photocatalytic degradation of reactive dyes in an immobilized TiO_2 photocatalytic reactor." *J. Colloid Interface Sci.*, 295, 159-164.

Malato, S., Blanco, J., Vidal, A., Alarco´ n, D., Maldonado, M.I., Caceres, J. and Gernjak, W. (2003). "Applied studies in solar photocatalytic detoxification: an overview." *Sol. Energy*, 75, 329–336.

Mangal, V.P., (2010). "The Future of Indian Dyes & Dye Intermediates." *Textile Review. August 23.* http://www.fibre2fashion.com/industry-article/29/2887/the-future-of-indian-dyes-and-dye-intermediates1.asp. (October 26, 2013).

Marcucci, M., Nosenzo, G., Capannelli, G., Ciabatti, I., Corrieri, D. and Ciardelli, G., (2001). "Treatment and reuse of textile effluents based on new ultrafiltration and other membrane technologies." *Desalination*, 138, 75-82.

Masten, S.J. and Davies, S.H. (1994). "The use of ozonation to degrade organic contaminants in wastewaters." *Environ. Sci. Technol*., 28, 180-185

Masuda, H., Hiqasitani, K. and Yoshida, H. (2007). "Powder technology handbook." *Taylor and Francis*, 351.

Matatov-Meytal, Y. I. and Sheintuch, M. (1998)." Catalytic abatement of water pollutants." *Ind. Eng. Chem. Res*., 37(2), 309–326.

Matthews, R.W. (1987). "Photooxidation of organic impurities in water using thin films of titanium dioxide." *J. Phys. Chem.*, 91, 3328–3333.

Mbuligwe, S. E. (2003). "Assessment of performance and potential of wetland systems in wastewater treatment and resource recovery in Tanzania." Research Report, Department of Environmental Engineering, University college of Lands and Archtectural Studies, Dar Es Salaam, Tanzania.

Mbuligwe, S. E. (2005). "Comparative treatment of dye-rich wastewater in engineered wetland systems (EWSs) vegetated with different plants." *Water Res.*, 39, 271–280.

Meetani, M.A., Hisaindee, S.M., Abdullah, F., Ashraf, S.S. and Rauf, M.A. (2010). "Liquid chromatography tandem mass spectrometry analysis of photodegradation of a diazo compound: A mechanistic study." *Chemosphere*, 80, 422–427.

Merabet, S., Schneider, M., Robert, D., Benkhanouche, S., Bouhelassa, M. and Weber, J.V. (2008). "Optimization of the indole photodegradation on supported TiO_2: influences of temperature, concentration, TiO_2 amount and flow rate." *Water Sci. Technol.*, 58, 549–554.

Mercuri, R.A. (2007). *US20070037701.*

Miller, L. W., Tejedor, M. I. and Anderson, M. A. (1999). "Titanium dioxide coated waveguides for the photocatalytic oxidation of formic acid in water." *Environ. Sci. Technol.*, 33, 2070-2075.

Miller, R. M., Singer, G. M., Rosen, J.D. and Bartha, R. (1988). "Sequential degradation of chlorophenols by photolytic and microbial treatment." *Environ. Sci. Technol.*, 22, 1215-1219.

Mills, A. and Le Hunte, S. (1997). "An overview of semiconductor photocatalysis." *Journal of J. Photochem. Photobiol. A.*, 108, 1-35.

Mills, A., Davis, R.H. and Worsley, D. (1993). "Water purification by semiconductor photocatalysis". *Chem. Soc. Rev.,* 22, 413-417.

Mills, A., Elliott, N., Parkin, I. P., Neill, S.A.O. and Clark, R.J. (2002). "Novel TiO$_2$ CVD films for semiconductor photocatalysis." *J. Photochem. and Photobio. A: Chem.*, 151, 171–179.

Minero, C., Pelizzetti, E., Malato, S. and Blanco, J. (1993). "Larger solar plant photocatalytic water decontamination: degradation of pentachlorophenol." *Chemosphere*, 26, 2103–2119.

Mirkhani, V., Tangestaninejad, S., Moghadam, M., Habibi, M. H. and Rostami, V. A. (2009). "Photodegradation of Aromatic Amines by Ag-TiO$_2$ Photocatalyst." *J. Iran. Chem. Soc., 6*, 800-807.

Mishra, G. and Tripathy, M. (1993). "A critical review of the treatments for decolourization of textile e.uent." *Colourage*, 40, 35-38.

Montgomery, D.C. (1997). "Design and Analysis of Experiments" (fourth ed.), *Wiley*, New York, USA

Morikawa, T., Shiga, T., Asahi, R., Ohwaki, T. and Taga, Y. (2004). *US20046743749.*

Mozia S. (2008). "Effect of calcination temperature on photocatalytic activity of TiO$_2$. Photodecomposition of mono- and polyazo dyes in water." *Polish J. chem. Tech.*, 10(3), 42-49.

Mrowetz, M., Balcerski, W., Colussi, A.J. and Hoffmann, M.R. (2004). "Oxidative power of nitrogen-doped TiO$_2$ photocatalysts under visible illumination." *J. Phys. Chem. B.* 108, 17269–17273.

Mulvaney, P. (1996). "Surface plasmon spectroscopy of nanosized metal particles."*Langmuir,* 12, 788-800.

Muneer, M., Theurich, J. and Bahnemann, D. (1991). "Formation of toxic intermediates upon the photocatalytic degradation of the pesticide Diuron." *Res. Chem. Intermed.*, 25, 667-683.

Muneer, M. and Bahnemann, D. (2001). "Semiconductor mediated photocatalysed degradation of two-selected pesticide Terbacil and 2, 4, 5, Tribromoimidazole." *Water Sci. Technol.*, 144, 331-337.

Muneer, M., Theurich, J. and Bahnemann, D. (2001). **"**Titanium dioxide mediated Photocatalytic degradation of 1, 2-diethyl phthalate." *J. Photochem. Photobiol. A Chem.*, 143, 213-219.

Murphy, A.B. (2001). "Band-gap determination from diffuse reflectance measurements of semiconductor films, and application to photoelectrochemical water-splitting." Sol. *Energy Mater. Sol. Cells*, 91, 1326–1337.

Murthy, M.S.R.C., Swaminathan, T., Rakshit, S.K. and Kosugi, Y., (2000). "Statistical optimization of lipase catalyzed hydrolysis of methyloleate by response surface methodology." *Bioprocess Eng.*, 22, 35–39.

Muruganandham, M. and Swaminathan, M. (2004). "Solar photocatalytic degradation of a reactive azo dye in TiO_2-suspension." *Sol. Energy Mater. Sol. Cells*, 81, 439–457.

Muruganandham, M. and Swaminathan, M. (2006a)."Photocatalytic decolourisation and degradation of Reactive Orange 4 by TiO_2-UV process." *Dyes Pigments*, 68, 133–142.

Muruganandham, M. and Swaminathan, M. (2006b). "TiO_2–UV photocatalytic oxidation of Reactive Yellow 14: Effect of operational parameters." *J. Hazard. Mater B.* 135, 78–86.

Muruganandham, M., Sobana N. and Swaminathan, M. (2006c). "Solar assisted photocatalytic and photochemical degradation of Reactive Black 5." *J. Hazard. Mater.* 137, 1371-1376.

Murzin D.Y. (2006). "Heterogeneous photocatalytic kinetics: beyond the adsorption/desorption equilibrium concept." *React. Kinet. Catal. Lett.*, 89, 277-284.

Myers, R.H., Montgomery, D.C., Vining, G.G., Borror, C.M. and Kowalski, S.M. (2004). "Response surface methodology: a retrospective and literature survey." *J. Quality Tech.* 36, 53-77.

Na, Y., Song, S. and Park, Y. (2005). "Photocatalytic Decolorization of Rhodamine B by Immobilized TiO_2/UV in a Fluidized-bed Reactor." *Korean J. Chem. Eng.*, 22(2), 196-200.

Nagaveni, K., Sivalingam, G., Hedge, M. S. and Madras, G. (2004). "Solar photocatalytic degradation of dyes: high activity of combustion synthesized nano TiO$_2$." *Appl. Catal. B Environ.*, 48, 83-93.

Namasivayam, C. and Kadirvelu, K.K. (1998). "Carbonised coirpith as an adsorbent for the removal of toxic ions dyes and pesticides from wastewaters." *Indian J. Chem. Technol.*, 5, 334–336.

Namasivayam, C., Prabha, D. and Kumutha, M. (1998). "Removal of direct red and acid brilliant blue by adsorption on to banana pith." *Bioresour. Technol.,* 64, 77–79.

Namboodri, C.G. and Walsh, W.K. (1996). "Ultraviolet light/hydrogen peroxide system for decolorizing spent reactive dye bath waste water." *Am. Dyes. Rep.*, 15-25.

Namboodri, C.G., Perkins, W.S. and Walsh, W.K., (1994a). "Decolorizing dyes with chlorine and ozone: Part I." *Am. Dyestuff Rep.*, 83, 17–22.

Namboodri, C.G., Perkins, W.S. and Walsh, W.K., (1994b). "Decolorizing dyes with chlorine and ozone: Part II." *Am. Dyestuff Rep.*, 83, 17–26.

Nansheng, D., Tao, F. and Shizhong, T. (1996). "Photodegradation of dyes in aqueous solutions containing Fe (III) hydroxy complex I. Photodegradation kinetics." *Chemosphere.*, 33, 547-557.

Nasr, C., Vinodgopal, K., Hotchandani, S., Chattopadhyay, A.K. and Kamat, P.V. (1997). "Photocatalytic reduction of azo dyes naphthol blue black and disperse blue 79." *Res. Chem. Interm.*, 23, 219-231.

Natarajan, T.S., Thomas, M., Natarajan, K. Bajaj, H.C. and Tayade, R.J. (2011). "Study on UV-LED/TiO$_2$ process for degradation of Rhodamine B dye." *Chem. Eng. J.*, 169, 126–134.

Neppolian, B., Choi, H.C., Sakthivel, Arabindoo, B. and Murugesan, V. (2002a). "Solar/UV-induced photocatalytic degradation of three commercial textile dyes." *J. Hazard. Mater. B.*, 89, 303-317.

Neppolian, B., Choi, H.C., Sakthivel, S., Arabindoo, B. and Murugesan, V. (2002b). "Solar light induced and TiO$_2$ assisted degradation of textile dye reactive blue 4." *Chemosphere*, 46, 1173–1181.

Neppolian, B., Kanel, S.R ., Choi, H.C., Shankar, M.V., Arabindoo, B. and Murugesan, V. (2003). "Photocatalytic Degradation of Reactive Yellow 17 Dye in Aqueous Solution in the Presence of TiO_2 with Cement Binder". *Int. J. Photoenergy*, 5, 45-49.

Nigam, P., Armour, G., Banat, I.M., Singh, D. and Marchant, R. (2000). "Physical removal of textile dyes and solid state fermentation of dyeadsorbed agricultural residues." *Bioresour. Technol.*, 72, 219-226.

Nikazara, M., Gholivandb, K. and Mahanpoorc, K. (2007). "Using TiO_2 Supported on Clinoptilolite as a Catalyst for Photocatalytic Degradation of Azo Dye Disperse Yellow 23 in Water." *Kinet. Catal.*, 48(2), 214–220.

Nohara, K., Hidaka, H., Pelizzetti, E. and Serpone, N. (1997). "Processes of formation of NH_4^+ and NO_3^- ions during the photocatalysed oxidation of N-containing compounds at the titania/ water interface*J. Photochem. Photobiol. A: Chem.*, 102, 265-272.

Noorjahan, M., DurgaKumari, V. and Subramanyam, M. (2002). "Photocatalytic degradation of Orange-G". *Indian J. Environ. Prot.*, 22, 1162-1167.

Noorjahan, M., Reddy, M. P., Kumari, V. D., Lavedrine, B., Boule, P. and Subrahmanyam, M. (2003). "Photocatalytic degradation of H-acid over a novel TiO_2 thin film fixed bed reactor and in aqueous suspensions." *J. Photochem. Photobiol. A: Chem.*, 156, 179-187.

Ogutveren, U.B. and Kaparal, S. (1994). "Colour removal from textile effluents by electrochemical destruction." *J. Environ. Sci. Health.,* A29, 1-16.

Ohko, Y., Tatsuma, T. and Fujishima, A. (2001). "Characterization of TiO_2 Photocatalysis in the Gas Phase as a Photoelectrochemical System: Behavior of Salt-Modified Systems." *J. Phys. Chem. B.*, 105, 10016- 10021.

Okuya, M., Nakade, K. and Kaneko, S. (2002). "Porous TiO_2 thin films synthesized by a spray pyrolysis deposition (SPD) technique and their application to dye-sensitized solar cells." *Sol. Energy Mater. Sol. Cells*, 70, 425-435.

Oliveira, J.C., Al-sayyed, G. and Pichat, P. (1990). "Photodegradation of 2- and 3-chlorophenol in titanium dioxide aqueous suspensions." *Environ. Sci. Technol.*, 24, 990–996.

Ollis, D. F. and Serpone, N. (1989). *"Heterogeneous Photocatalysis in the Environment: Application to Water Purification. Photocatalysis: Fundamentals and Applications."* John Wiley and sons, 650- 655.

Ollis, D.F., Pelizzetti, E. and Serpone, N. (1991). "Photocatalyzed destruction of water contaminants." *Environ. Sci. Technol.*, 25(9), 1522–1529.

Ong, S-A., Min, O-M., Ho, L-N. and Wong, Y-S. (2013). "Solar photocatalytic degradation of mono azo methyl orange and diazo reactive green 19 in single and binary dye solutions: adsorbability vs photodegradation rate." *Environ. Sci. Pollut. Res.*, 20, 3405-3413.

Ovenstone, J. (2001). "Synthesis of TiO_2 by sol-gel methods." *J. Mater. Sci.*, 36, 1325–1329.

Ovenstone, J. and Yanagisawa, K. (1999). "Effect of hydrothermal treatment of amorphous titania on the phase change from anatase to rutile during calcination". *Chem. Mater.*, 11 (10), 2770-2774.

Ozawa, T., Iwasaki, M. and Tada, H. (2005). "Low-temperature synthesis of anatase–brookite composite nanocrystals: the junction effect on photocatalytic activity". *J. Colloid Interface Sci.*, 281(2), 510-513.

Ozen, A.S., Aviyente, V., Proft, F.D. and Geerlings, P., (2004). "Modeling the substituent effect on the oxidative degradation of azo dyes." *J. Phys. Chem. A,* 108, 5990–6000.

Pagga, U. and Brown, D. (1986). "The degradation of dyestuffs: Part II. Behaviour of dyestuffs in aerobic biodegradation tests." *Chemosphere*, 15, 479–491.

Pak, D. and Chang, W. (1999). "Decolorizing dye wastewater with low temperature catalytic oxidation." *Water Sci. Technol.*, 40, 115-121.

Paola, A. D., Marci, G., Palmisano, L., Schiavello, M., Uosaki, K., Ikeda, S. and Ohtani, B. (2002). "Preparation of polycrystalline TiO_2 photocatalysts impregnated

with various transition metal ions: characterization and photocatalytic activity for the degradation of 4-nitrophenol." *J. Phys. Chem. B*, 106, 637–645.

Pare, B., Jonnalagadda, S.B., Tomar, H., Singh, P. and Bhagwat, V.W. (2008). "ZnO assisted photocatalytic degradation of Acridine Orange aqueous solution using visible irradiation". *Desalination*, 232, 80–90.

Pareek, V., Chong, S., Tade, M. and Adesina, A. (2008). "Light intensity distribution in heterogeneous photocatalytic reactors." *Asia-Pacific J. Chem. Eng.*, 3, 171–201.

Park , O.H. and Na, H. Y. (2008). "Photocatalytic degradation of toluene vapour using fixed bed multichannel photoreactors equipped with TiO_2-coated fabrics." *J. Environ. Technol.*, 29(9), 1-7.

Park, J-H., Cho, I-H. and Kim, Y-G. (2004). "Solar light induced degradation of reactive dye using photocatalysis." *J. Environ. Sci. Health Part A,* 39, 159-171.

Pastoriza-Santos, I., Koktysh, D.S., Mamedov, A.A., Giersig, M., Kotov, N. A. and Liz-Marzan, L. M. (2000). "One-pot synthesis of Ag@TiO_2 core-shell nanoparticles and their layer-by-layer assembly." *Langmuir*, 16, 2731−2735.

Peill, N. J., Borne, L. and Hoffmann, M. R. (1997). "Iron (III),-doped Q-sized TiO_2 coatings in fiber-optic cable reactor." *J. Photochem. Photobio. A: Chem.*, 108, 221–228.

Pelegrini, R., Peralto-Zamora, P., de Andrade, A.R., Reyers, J. and Duran, N. (1999). "Electrochemically assisted photocatalytic degradation of reactive dyes." *App. Catal B-Environ.*, 22, 83-90.

Pelizzetti, E., Carlin, V., Minero, C. and Gratzel, M. (1991). "Enhancement of the rate of photocatalytic degradation on TiO_2 of 2-chlorophenol, 7-dichlorobibenzodioxin and trazine by inorganic oxidising species." *New J. Chem.*, 15, 351–359.

Pereira, L. and Alves, M. (2012). "Dyes-environmental impact and remediation." Environmental Protection Strategies for Sustainable Development, Springer, Dordrecht, 111-162, Springer, (ISBN: 978-94-007-1590-5).

Periyat, P., McCormack, D.E., Hinder, S. J. and Pillai, S.C. (2009). "One-Pot Synthesis of Anionic (Nitrogen) and Cationic (Sulfur) Codoped High-Temperature

Stable, Visible Light Active, Anatase Photocatalysts." *J. Phys. Chem. C*, 113, 3246–3253.

Peyton, G.R., Huang, F.Y., Burleson, J.L. and Glaze, W.H., (1982). "Destruction of pollutants in water with ozone in combination with ultraviolet radiation 1. General principles and oxidation of tetrachloroethylene." *Environ. Sci. Technol.*, 16, 449-453.

Pichat, P., Guillard, C., Amalric, L., Renard, A. and Plaidy, O. (1995). "Assessment of the importance of the role of H_2O_2 and $O_2^{\bullet-}$ in the photocatalytic degradation of 1,2-dimethoxybenzene." *Sol. Energy Mater. Sol. Cells*, 38, 391–399.

Poon, C.P.C. and Vittimberga, B.M. (1981). "UV photodecomposition of color in dyeing wastewater in: Industrial Waste." Proceedings 13th Mid-Atlantic *Industrial Waste Conference*, Huang C P (Ed), Ann Arbor, MI, 427-433.

Poulios, I. and Aetopoulon, I. (1999). "Photocatalytic degradation of the textile dye Reactive Orange 16 in the presence of TiO_2 suspensions". *Environ. Tech.*, 20, 479-488.

Poulios, I. and Tsachpinis, I. (1999). "Photodegradation of the textile dye reactive Black 5 in the presence of semiconducting oxides." *J. Chem. Technol. Biotechnol.*, 74, 349–357.

Pourahmad, A., Sohrabnezhad, S. and Radaee, E. (2010). "Preparation of Fe doped TiO_2 with sol-gel method." *J Porous Mater.*, 17, 367–375.

Pouretedal, H.Z. and Hosseini, M. (2010). "Bleaching kinetic and mechanism study of congo red catalyzed by zro_2 nanoparticles prepared by using a simple precipitation method." *Acta Chim. Slov.,* 57, 415–423.

Pradeep T. (2007). "Nano: The essentials. Understanding Nanoscience and Nanotechnology." *Tata McGraw-Hill*, New Delhi. 652- 660.

Puttamraju, P. K. and Ray, M. B. (2008). "Performance improvement of TiO_2 supported on adsorbents for photocatalytic degradation of MEK in air." *Int. J. Environ. Technol. Manage.*, 9,105 – 124.

Puzenat, E., Lacheb, H., Karkmaz, M., Houas, A., Guillard, C. and Hermann, J.M. (2003). "Fate of nitrogen atoms in the photocatalytic degradation of industrial (congo red) and alimentary (amaranth) azo dyes. Evidence for mineralization into gaseous dinitrogen." *Int. J. Photoenergy*., 5, 51-58.

Qamar, M. (2010). "Photodegradation of acridine orange catalyzed by nanostructured titanium dioxide modified with platinum and silver metals." *Desalination*, 254, 108–113.

Qamar, M. and Muneer, M. A. (2009). **"A comparative photocatalytic activity of titanium dioxide and zinc oxide by investigating the degradation of vanillin."** *Desalination*, *249*, 535–540.

Qamar, M., Saquib, M. and Muneer, M. (2005a)."Photocatalytic degradation of two selected dye derivatives, chromotrope 2B and Amido Black 10B, in aqueous suspensions of titanium dioxide." *Dyes Pigments*, 6, 1–9.

Qamar, M., Saquib, M. and Muneer, M. (2005b). "Titanium dioxide mediated photocatalytic degradation of two selected azo dye derivatives, chrysoidine R and acid red 29 (chromotrope 2R), in aqueous suspensions." *Desalination,* 186, 255–271.

Qamar, M., Saquib, M., and Muneer, M. (2004). "Semicondcutor mediated photocatalytic degradation of an azo dye, chrysoidine Yin aqueous suspensions." *Desalination*, 171, 185–193.

Raghavacharya, C. (1997). "Colour removal from industrial effluents a comparative review of available technologies." *Chem. Eng. World*, 32, 53-54.

Rai, H.S., Bhattacharyya, M.S., Singh, J., Bansal, T.K., Vats, P. and Banerjee, U.C., (2005). "Removal of dyes from the effluent of textile and dyestuff manufacturing industry: a review of emerging techniques with reference to biological treatment." *Crit. Rev. Env. Sci. Technol.*, 35, 219–238.

Rajeshwar, K., Osugi, M.E., Chanmanee, W., Chenthamarakshan, C.R., Zanoni, M.V.B., Kajitvichyanukul, P. and Krishnan-Ayer, R. (2008). "Heterogeneous photocatalytic treatment of organic dyes in air and aqueous media." *J. Photoch. Photobio. C:Photochem. Rev*., 9, 171-192.

Rao, K.L.L.N., Krishnaiah, K. and Ashutush, (1994). "Colour removal from a dye stuff industry effluent using activated carbon." *Indian J. Chem. Technol.*, 1, 13-19.

Rao, K.V.S., Rachel, A., Subramanyam, M. and Boule P, (2003). Immobilization of TiO_2 on pumice stone for the photocatalytic degradation of dyes and dye industry pollutants. *Appl. Catal. B: Environ.*, 46(1), 77-85.

Rashed, M.N. and El-Amin, A.A. (2007). "Photocatalytic degradation of methyl orange in aqueous TiO_2 under different solar irradiation sources." *Int. J. Phy. Sci.*, 2 (3), 73-81.

Ratnamala, G.M., Shetty, V.K. and Srinikethan, G. (2012). "Removal of remazol brilliant blue dye from dye-contaminated water by adsorption using red mud: Equilibrium, kinetic, and thermodynamic studies." *Water Air Soil Pollut.*, 223, 6187–6199.

Rayford, C. E., Schatz, G. and Shuford, K. (2005). "Optical Properties of Gold Nanospheres." *Nanoscape*, 2(1), 27-33.

Reddy, E. P., Davydov, L. and Smirniotis, P. (2003). "TiO_2-loaded Zeolites and Mesoporous Materials in the Sonophotocatalytic Decomposition of Aqueous Organic Pollutants. The Role of the Support." *J. Appl. Catal. B: Environ.*, 42 (1), 1−11.

Reddy, K.M., Manorama, S.V. and Reddy, A. R. (2002). "Bandgap studies on anatase titanium dioxide nanoparticles." *Mater. Chem. Phys.*, 78, 239–245.

Reid, R. and Soc. J. Dyers. (1996). "Colour. Go green – a sound business decision." *J. Soc. Dyers Colour,* 112, 103–105.

Reife, A., and Fremann, H.S., (1996). "Environmental Chemistry of Dyes and Pigments." *Wiley*, New York, 368-375.

Robert, D. and Malato, S. (2002). "Solar photocatalysis: A clean process for water detoxification". *Sci. Total Environ.*, 291, 85-97.

Robert, D., Piscopo, A., Heintz, O. and Weber, J. V. (1999). "Photocatalytic detoxification with TiO_2 supported on glass fibre by using artifical and natural light." *Catal. Today*, 54, 291-296.

Robinson, T., McMullan, G., Marchant, R. and Nigam, P., (2001). "Remediation of dyes in textile effluent: a critical review on current treatment technologies with a proposed alternative." *Bioresour. Technol.*, 77, 247–255.

Rodriguez-Gattorno, G., Diaz, D., Rendon, L. and Hernandez-Segura, G.O. (2002). "Metallic nanoparticles from spontaneous reduction of silver (I) in DMSO. Interaction between nitric oxide and silver nanoparticles." *J. Phys. Chem. B*, 106, 2482–2487.

Roselin, L. S., Rajarajeswari, G.R., Selvin, R., Sadasivan, V., Sivasankar, B. and Rengaraj, K. (2002). "Sunlight/ZnO-mediated photocatalytic degradation of Reactive Red 22 using thin film flat bed flow photoreactor." *Sol. Energy*, 73(4), 281-285.

Rothenberger, G., Moser, J., Gratzel, M., Serpone, N. and Sharma, D.K. (1985). "Charge carrier trapping and recombination dynamics in small semiconductor particles." *J. Am. Chem. Soc.*, 107, 8054–8059.

Rupa, A. V., Manikandan, D., Divakar, D. and Sivakumar, T. (2007). "Effect of deposition of Ag on TiO$_2$ nanoparticles on the photodegradation of Reactive Yellow-17." *J. Hazard. Mater.,* 147, 906-913.

Rupa, A.V., Divakar, D. And Sivakumar, T. (2009). "Titania and noble metals deposited titania catalysts in the photodegradation of tartazine." *Catal. Lett.*, 132, 259–267.

Saepurahman, Abdullah, M.A. and Chong, F.K. (2010). "Preparation and characterization of tungsten-loaded titanium dioxide photocatalyst for enhanced dye degradation." *J. Hazard. Mater.*, 176, 451-458.

Sahel, K., Perol, N., Dappozze, F., Bouhent, M. Derriche, Z. and Guillard, C. (2010). "Photocatalytic degradation of a mixture of two anionic dyes: Procion Red MX-5B and Remazol Black 5 (RB5)." *J. Photochem. Photobiol., A:Chem.*, 212, 107–112.

Sahoo, C. and Gupta, A.K. (2012). "Optimization of photocatalytic degradation of methyl blue using silver ion doped titanium dioxide by combination of experimental design and response surface approach." *J. Hazard. Mater.*, 215–216, 302–310.

Sahoo, C. and Gupta, A.K. (2013). "Application of statistical experimental design to optimize the photocatalytic degradation of a thiazin dye using silver ion-doped

titanium dioxide." *J. Environ. Sci. Health Part A: Toxic/Hazard. Subst. Environ. Eng.*, 48, 694–705.

Sahoo, C., Gupta, A. K. and Pal, A. (2005). "Photocatalytic degradation of Crystal Violet (C.I. Basic Violet 3) on silver ion doped TiO$_2$." *Dyes Pigments,* 66, 189-196.

Sajjad, A. K., Shamaila, S., Tian, B., Chen, F. and Zhang J.(2010) Comparative studies of operational parameters of degradation of azo dyes in visible light by highly efficient WOx/TiO$_2$ photocatalyst. *J. Hazard. Mater.*, 177, 781-91.

Sakkas, V.A. Islam, M.A., Stalikas, C. and Albanis, T.A. (2010). "Photocatalytic degradation using design of experiments: A review and example of the Congo red degradation." *J. Hazard. Mater.*, 175, 33–44.

Sakthivel, S. and Kish, H. (2003). "Photocatalytic and photo electrochemical properties of nitrogen-doped titanium dioxide." *Chem. Phys. Chem.*, 4, 487–490

Sakthivel, S., Neppolian, B., Shankar, M.V., Arabindoo, B., Palanichamy, M.P. and Murugesan, V. (2003) Solar photocatalytic degradation of azo dye: comparison of photocatalytic efficiency of ZnO and TiO$_2$. *Sol. Energy Mater. Sol. Cells*, 77, 65–82.

Sakthivel, S., Shankar, M. V., Palanichamy, M., Arabindoo, B., Bahnemann, D. W. and Murugesan, V. (2004). "Enhancement of photocatalytic activity by metal deposition: characterisation and photonic efficiency of Pt, Au and Pd deposited on TiO$_2$ catalyst." *Water Res.*, 38, 3001-3008.

San, N., Hatipoglu, A., Kocturk, G. and Cinar, Z. (2002). "Photocatalytic degradation of 4-nitrophenol in aqueous TiO$_2$ suspensions: Theoretical prediction of the intermediates". *J. Photochem. Photobiol.*, *A*, 146, 189–197.

Sanchez, L., Peral, J. and Domenech, X. (1998). "Aniline degradation by combined photocatalysis and ozonation." *Appl. Catal. B: Environ.*, 19, 59–65.

Saquib, M. and Muneer, M. (2002). "Semiconductor mediated photocatalysed degradation of an anthraquinone dye, Remazol Brilliant Blue R under sunlight and artificial light source". *Dyes Pigments*, 53, 237–249.

Saquib, M. and Muneer, M. (2003a). "Titanium dioxide mediated photocatalyzed degradation of a textile dye derivative, Acid Orange 8, in aqueous suspensions." *Desalination*, 155, 255–263.

Saquib, M. and Muneer, M. (2003b). "TiO$_2$-mediated photocatalytic degradation of a triphenylmethane dye (gentian violet), in aqueous suspensions." *Dyes Pigments*, 56, 37–49.

Saquib, M., Tariq, M. A., Faisal, M. and Muneer, M. (2008). "Photocatalytic degradation of two selected dye derivatives in aqueous suspensions of titanium dioxide". *Desalination*, 219, 301-311.

Sarthy, S.R. and Mohseni, M. (2006). "An Overview of UV-based Advanced Oxidation Processes for Drinking Water Treatment." *IUVA News,* 8(2), 16-27.

Sathish, M., Viswanathan, B. and Viswanath, R.P. (2007). "Characterization and photocatalytic activity of N-doped TiO$_2$ prepared by thermal decomposition of Ti-melamine complex." *Appl. Catal. B.*, *Environ., 74*, 307–312.

Schiavello (Ed.) (1988). Photocatalysis and Environment: Trends and Applications, *Kluwer Academic Publishers*, Dordecht, 368- 396.

Schiavello, M. (1997). "Heterogeneous Photocatalysis". Wiley Series in Photoscience and Photoengineer ing. Vol. 3. *Wiley*, New York, 245- 256.

Sclafani, J. and Herrmann, M. (1998). "Influence of metallic silver and of platinum-silver bimetallic deposits on the photocatalytic activity of titania (anatase and rutile) in organic and aqueous media." *J. Photochem. Photobiol. A.*, 113, 181-188.

Serpone, N. and Pelizzetti, E. (Eds.) (1989). "Photocatalysis Fundamentals and Applications." *Wiley* Interscience, New York, 456-466.

Serpone, N., Marimuthu, P., Pichat, P., Pelizzati, E. and Hidaka, H. (1995). "Exploiting the interparticle electron transfer process in the photocatalysed oxidation of phenol, 2-chlorophenol and pentachlorophenol: chemical evidence for electron and hole transfer between coupled semiconductors." *J. Photochem. Photobiol. A: Chem.*, 85, 247–255.

Sharma, M., Jain, T., Singh, S. and Pandey, O.P. (2012). "Photocatalytic degradation of organic dyes under UV–Visible light using capped ZnS nanoparticles." *Sol. Energy*, 86, 626–633.

Shchukin, D. G., Sviridov, D.V. and Kulak, A.I. (1999). "Magneto rheological photocatalytic systems." *Int. J. Photoenergy*, 1, 65-67.

Siemon,U., Bahnemann, D. W., Testa, J. J. , Rodriguez, D., Litter, M.I. and Bruno. N. (2002). "Heterogeneous photocatalytic reactions comparing TiO_2 and Pt/TiO_2." *J. Photochem. Photobiol. A,* 148, 247-255.

Silva, C.G. and Faria, J.L. (2003). "Photochemical and Photocatalytic degradation of an azo dye in aqueous solution by UV irradiation." *J. Photochem. Photobiol. A: Chem*., 155, 133–143.

Silva, J.P., Sousa, S., Rodrigues, J., Antunes, H., Porter, J.J., Gonc¸alves, I. and Dias, S.F. (2004). "Adsorption of acid orange 7 dye in aqueous solutions by spent brewery grains." *Sep. Purif. Technol*., 40, 309–315.

Singh, A.N., Singh, S., Suthar, N. and Dubey, V.K. (2011b). "Glutaraldehyde-activated chitosan matrix for immobilization of a novel cysteine protease, procerain B." *J. Agric. Food Chem*., 59(11), 6256-6262.

Singh, C., Chaudhary, R. and Thakur, R. S. (2011a). "Performance of advanced photocatalytic detoxification of municipal wastewater under solar radiation - A mini review." *Int. J. Energy Environ*., 2, 337–350.

Sirisuk, A., Hill, C.G.J. and Anderson, M.A. (1999). "Photocatalytic degradation of ethylene over thin films of titania supported on glass rings." *Catal. Today*, 54,159-164.

Sivalingam, G., Nagaveni, K., Hegde, M. S. and Madras, G. (2003). "Photocatalytic degradation of various dyes by combustion synthesized nano anatase TiO_2." *Appl. Catal. B: Environ*. 45 (1), 23-38.

Skoog, D.A., Holler, F.J. and Crouch S.R. (2003). "Principles of instrumental analysis." 6th edition, *Thomson*, 213-650.

Sleiman, M., Vildozo, D., Ferronato, C. and Chovelon, J.-M. (2007). "Photocatalytic degradation of azo dye Metanil Yellow: optimization and kinetic modeling using a chemometric approach." *Appl. Catal. B: Environ.*, 77, 1–11.

Slokar, Y.M. and Le Marechal, A.M. (1998). "Methods of decoloration of textile wastewaters." *Dyes Pigments*, 37, 335-356.

So, C. M., Cheng, M. Y., Yu, J. C. and Wong, P. K. (2002). "Degradation of azo dye Procion Red MX-5B by photocatalytic oxidation." *Chemosphere*, 46, 905–912.

Sobana, N. and Swaminathan, M. (2007). "The effect of operational parameters on the photocatalytic degradation of acid red 18 by ZnO." *Sep. Purif. Technol.,* 56,101–107.

Sobana, N., Muruganadham, M. and Swaminathan, M. (2006). "Nano-Ag particles doped TiO_2 for efficient photodegradation of Direct azo dyes." *J. Mol. Catal. A*, 258, 124-132.

Sobana, N., Selvam, K. and Swaminathan, M. (2008). "Optimization of photocatalytic degradation conditions of Direct Red 23 using nano-Ag doped TiO_2." *Sep. Purif. Technol.*, 62, 648–653.

Sohrabi, M. R. and Ghavami, M. (2008). "Photocatalytic degradation of Direct Red 23 dye using UV/TiO_2: Effect of operational parameters." *J. Hazard. Mater.,* 153, 1235–1239.

Sohrabi, M.R. and Ghavami, M. (2010). "Comparison of Direct Yellow 12 dye degradation efficiency using UV/semiconductor and UV/H_2O_2/semiconductor systems." *Desalination*, 252, 157–162.

Sohrabi, M.R., Davallo, M. and Miri, M. (2009). "Influence of operational parameters on eliminating azo dyes from wastewater by advanced oxidation technology." *Int. J. Chem. Tech. Res*. 1(3), 446-451.

Song, Y.L., Li, J.T. and Bai, B. (2010) TiO_2-assisted photodegradation of direct blue 78 in aqueous solution in sunlight." *Water Air Soil Pollut.*, 213, 311-317.

Sostar-Turk, S., Simonic, M. and Petrinic, I. (2005). "Wastewater treatment after reactive printing." *Dyes Pigments*, 64, 147–152.

Soutsas, K., Karayannis,V., Poulios, I., Riga, A., Ntampegliotis, K. and Spiliotis, X. (2010). "Decolorization and degradation of reactive azo dyes via heterogeneous photocatalytic processes." *Desalination*, 250, 345-350.

Spadaro, J.T, Isabelle, L. and Renganathan, V. (1994). "Hydroxyl radical mediated degradation of azo dyes: evidence for benzene generation." *Environ. Sci. Technol.*, 28, 1389–1393.

Spurr R.A. and Myers H. (1957). "Quantitative analysis of anatase-rutile mixtures with an x-ray diffractometer." *Anal. Chem.*, 29 (5), 760–762.

Stasinakis, A. S. (2008). "Use of selected advanced oxidation processes (AOPs) for wastewater treatment – a mini review." *Global NEST J.*, 10, 376-385.

Stylidi, M., Kondarides, D.I. and Verykios, X.E. (2003). "Pathways of solar light-induced photocatalytic degradation of azo dyes in aqueous TiO_2 suspentions." *Appl. Catal. B: Environ.,* 40, 271–286.

Stylidi, M., Kondarides, D.I. and Verykios, X.E. (2004). "Visible light-induced photocatalytic degradation of Acid Orange 7 in aqueous TiO_2 suspensions." *Appl. Catal. B: Environ.*, 47, 189-201.

Su, Y., Liping, D., Zhang, N.,Wang, X. and Zhu, X. (2009). "Photocatalytic degradation of C.I. Acid Blue 80 in aqueous suspensions of titanium dioxide under sunlight." *React. Kinet. Catal. Lett.*, 98, 227–240.

Subba Rao, K. V., Lavédrine, B. and Boule, P. (2003). "Influence of metallic species on TiO_2 for the photocatalytic degradation of dyes and dye intermediates." *J Photochem. Photobiol. A.*, 154, 189-193.

Subrahmanyam, M., Rao, K.V.S., Babu, M.R. and Srinivas, B. (1998). "Photocatalytic degradation of textile dyes using TiO_2 based catalysts." *Ind. J. Environ. Protect.*, 18, 266-272.

Subramanian, V., Wolf, E. E. and Kamat, P. V. (2003) "Influence of metal/metal ion concentration on the photocatalytic activity of TiO_2-Au composite nanoparticles." *Langmuir*, 19, 469-474.

Subramanian, V., Wolf, E.E. and Kamat, P. V. (2001). "Semiconductor−Metal Composite Nanostructures. To What Extent Do Metal Nanoparticles Improve the Photocatalytic Activity of TiO$_2$ Films." *J. Phys. Chem. B*., 105, 11439-11446.

Sung-Suh, H.M., Choi, J.R., Hah, H.J. and Koo, S.M. (2004). "Comparison of Ag deposition effects on the photocatalytic activity of nanoparticulate TiO$_2$ under visible and UV light irradiation." *J. Photochem. Photobiol. A*, 163, 37–44.

Takeda, S., Suzuki, H. and Odaka, H. H. (2001). "Photocatalytic TiO$_2$ thin film deposition onto glass by DC magnetron sputtering." *J. Thin Solid Films*, 392, 338–344.

Tanaka, K., Padermpole, K. and Hisanaga, T. (2000). "Photocatalytic Degradation of Commercial Azo Dyes." *Water Res*., 34, 327-333.

Tang, W.Z. and An, H. (1995). "UV/TiO$_2$ photocatalytic oxidation of commercial dyes in aqueous solutions." *Chemospehre*, 31, 4157-4170.

Tao, H. J., Tao, J. and Wang, T. (2005). "Fabrication of selforganized TiO$_2$ nanotubes by anodic oxidation and their photocatalysis". *J. Trans. Nonferrous Met. Soc. China*., 15(S3), 462-467.

Tariq, M.A., Faisal, M. and Muneer, M. (2005). "Semiconductormediated photocatalysed degradation of two selected azo dye derivatives, amaranth and bismarck brown in aqueous suspension." *J. Hazard. Mater. B*, 127, 172–179.

Tariq, M.A., Faisal, M., Saquib, M. and Muneer, M. (2008). "Heterogeneous photocatalytic degradation of an anthraquinone and a triphenylmethane dye derivative in aqueous suspensions of semiconductor." *Dyes Pigments*, 76, 358–365.

Tauc, J. (F. Abeles ed.) (1972). "Optical Properties of Solids", North-Holland, Amsterdam, 277.

Tauc, J., Grigorovici, R. and Vancu, A. (1966). *Phys. Status Solidi*., 15, 627.

Tiede, K., Boxall, A.B., Tear, S.P., Lewis J., David, H. and Hassellov, M. (2008) "Detection and characterization of engineered nanoparticles in food and the environment." *Food Addit Contam*., 25, 795-821.

Tom, R.T., Sreekumaran, N.A., Singh, N., Aslam, M., Nagendra, C.L., Philip, R., Vijayamohanan, K. and Pradeep, T. (2003). "Freely Dispersible Au@TiO$_2$, Au@ZrO$_2$, Ag@TiO$_2$, and Ag@ZrO$_2$ Core−Shell Nanoparticles: One-Step Synthesis, Characterization, Spectroscopy, and Optical Limiting Properties." *Langmuir,* 19, 3439-3445.

Toor, A.P., Verma, A., Jotshi, C.K., Bajpai, P.K. and Singh, V. (2006). "Photocatalytic degradation of Direct Yellow 12 dye using UV/TiO$_2$ in a shallow pond slurry reactor." *Dyes Pigments*, 68, 53-60.

Torimoto, T., Okawa, Y. and Takeda, N. (1997). "Effect of Activated Carbon Content in TiO$_2$-loaded Activated Carbon on Photodegradation Behaviors of Dichloromethane." *J. Photochem. Photobiol. A: Chem.*, 103, 153−157.

Tran, H., Scott, J., Chiang, K. and Amal, R. (2006). "Clarifying the role of silver deposits on titania for the photocatalytic mineralisation of organic compounds." *J. Photochem. Photobiol., A*, 183, 41−52.

Tributsch, H., Serpone, N. and Pelizzetti, E. (1989). "Photocatalysis: Fundamentals and Applications." *Wiley*, New York, USA, 324-345.

Ubonchonlakat, K., Sikong, L. and Phochanugoon, S. (2008). "Photocatalytic activity of Titanium dioxide coating on diatomite by sol-gel method." *Technol. Innovation Sustainable Dev. Conference* (TISD2008), 500-503.

Ung, T., Liz-Marzan, L. M. and Mulvaney, P. (2001). "Optical properties of thin films of Au@SiO$_2$ particles." *J. Phys. Chem. B.*, 105:3441−3452.

USEPA (United States Environmental Protection Agency), (2013). "Secondary Drinking Water Regulations: Guidance for Nuisance Chemicals." http://water.epa.gov/drink/contaminants/secondarystandards.cfm (October 26, 2013).

Vaidya, S., Patra, A. and Ganguli, A.K. (2010). "Core-shell nanostructures and nanocomposites of Ag@TiO$_2$: Effect of capping agent and shell thickness on the optical properties". *J. Nanopart. Res.*, 12, 1033-1044.

Vamathevan, A., Amal, R. and Beydoun, D. (2002). "Photocatalytic oxidation of organics in water using pure and silver-modified titanium dioxide particles." *J. Photochem. Photobiol A*., 148, 233-245

Vıctor, M., Menendez-Flores, D. F. and Bahnemann, D. W. (2008). "Durability of Ag-TiO$_2$ photocatalysts assessed for the degradation of Dichloroacetic acid*." Int. J. Photoenergy*, 2008, 1-11.

Vineetha, M.N., Matheswaran, M. and Sheeba, K.N. (2013). "Photocatalytic colour and COD removal in the distillery effluent by solar radiation." *Sol. Energy*, 91, 368–373

Wang, C.C., Lee, C.K., Lyu, M.D. and Juang, L.C. (2008d). "Photocatalytic degradation of C.I. Basic Violet 10 using TiO$_2$ catalysts supported by Y zeolite: An investigation of the effects of operational parameters." *Dyes Pigments*, *76*, 817-824.

Wang, H., Wu, Y., Xu, B. Q., Wang, H., Wu, Y. and Xu, B.Q. (2005). "Preparation and characterization of nanosized anatase TiO$_2$ cuboids for photocatalysis," *Appl. Catal*., *59*, 139–146.

Wang, J., Li, J., Xie, Y., Li, C., Han, G., Zhang, L., Xu, R. and Zhang, X. (2010). "Investigation on solar photocatalytic degradation of various dyes in the presence of Er^{3+}:YAlO$_3$/ZnO–TiO$_2$ composite." *J. Environ. Manage.*, 91, 677–684.

Wang, J., Li, J., Zhang, L., Li, C., Xie, Y., Liu, B., Xu, R. and Zhang, X. (2009). "Photocatalytic Degradation of Organic Dyes by a High Efficient TiO$_2$-Based Catalysts Under Solar Light Irradiation." *Catal Lett* ., 130, 551–557.

Wang, P., Wang, D., Xie, T., Li, H., Yang, M. and Wei, X., (2008a). "Preparation of monodisperse Ag/Anatase TiO$_2$ core–shell nanoparticles." *Mater. Chem. Phys*., 109,181–183.

Wang, W. and Ku, Y. (2003). "The Light Transmission and Distribution in an Optical Fiber Coated with TiO$_2$ Particles." *Chemosphere*, 50, 999-1006.

Wang, W., Zhang, J., Chen, F., He, D. and Anpo, M., (2008b). "Preparation and photocatalytic properties of Fe^{3+}-doped Ag@TiO$_2$ core–shell nanoparticles." *J. Colloid Interface Sci*., 323, 182–186.

Wang, Y. (2000). "Solar photocatalytic degradation of eight commercial dyes in TiO_2 suspension." *Water Res.,* 34, *990*–994.

Wang, Y., Wang, Y., Meng, Y., Ding, H., Shan, Y., Zhao, X. and Tang, X.A. (2008c). "Highly efficient visible-light-activated photocatalyst based on bismuth- and sulfur-codoped TiO_2." *J. Phys. Chem. C*, 112 (17), 6620-6626.

Wan-Ngah, W.S., Kamari, A., Fatinathan, S. and Ng, P.W. (2006) "Adsorption of chromium from aqueous solution using chitosan beads." *Adsorpt.* 12, 249–257.

Wardman, P. (1989). "Reduction potentials of one-electron couples involving free radicals in aqueous solution." *J. Phys. Chem. Ref. Data*, 18, 1637–1755.

Wei, T.Y. and Wan, C.C. (1991). "Heterogeneous Photocatalytic Oxidation of Phenol with. Titanium Dioxide Powders". *Ind. Eng. Chem. Res.* 30, 1293-1300.

Wenhua, L., Hong, L. Suo'an, C., Jianqing Z. and Chunan, C. (2000). "Kinetics ofphotocatalytic degradation of aniline in water over TiO_2 supported on porous nickel." *J. Photochem. Photobiol. A: Chem.*, 131, 125–132.

Wu, C. H. (2004). "Comparison of azo dye degradation efficiency using UV/single semiconductor and UV/coupled semiconductor systems." *Chemosphere*, 57, 601-608.

Wu, L., Shamsuzzoha, M. and Ritchie, S.M.C. (2005). "Preparation of cellulose acetate supported zero-valent iron nanoparticles for the dechlorination of trichloroethylene in water." *J. Nanopart. Res.*, 7, 469–476.

Xu, Y. and Langford. C, H. (1997). "Photoactivity of Titanium Dioxide Supported on MCM41, Zeolite X, and Zeolite Y." *J. Phys. Chem. B*, 101, 3115-3121.

Xu, Y. and Lebrun, R. E. (1999). "Treatment of textile dye plant effluent by nanofiltration membrane." *Separ. Sci. Technol.*, 34, 2501–2519

Yamashita, H., Harada, M. and Tanii, A. (2000). "Preparation of efficient titanium oxide photocatalysts by an ionized cluster beam (ICB) method and their photocatalytic reactivities for the purification of water." *Catal. Today*, 63(1), 63-69.

Yang, X., Wang, Y., Xu, L., Yu, X. and Guo, Y. (2008). "Silver and indium oxide codoped tio_2 nanocomposites with enhanced photocatalytic activity." *J. Phys. Chem. C,* 112, 11481–11489.

Yoshida, M.M., Martinez, V.C., Madrid, P.A. and Elguezabal, A. A. (2002). "Thin films of photocatalytic TiO_2 and ZnO deposited inside tubing by spray pyrolysis." *Thin Solid Films*, 419, 60-64.

You, X., Chen, F. and Zhang, J. (2005). "Effects of Calcination on the physical and photocatalytic properties of TiO_2 powders prepared by sol–gel template method." J. Sol-Gel Sci. Technol., 34, 181–187.

You, Y.S., Chung, K.H., Kim, J.H. and Seo, G. (2001). "Photocatalytic Oxidation of Toluene over TiO_2 Catalysts Supported on Glass Fiber." *Korean J. Chem. Eng.*, 18(6), 924-929.

Young, H. K., Young, S. K. and Beong, G. J. (2004). "Preparation and Characterization of Ag-TiO_2 Core-Shell-Type Nanoparticles." *J. Ind. Eng. Chem.*, 10, 739- 744.

Yu, H. G., Yu, J.G., Cheng, B. and Lin, J. (2007a). "Synthesis, characterization and photocatalytic activity of mesoporous titania nanorod/titanate nanotube composites." *J. Hazard. Mater.,* 147, 581–587.

Yu, J. G., Wang, G. H., Cheng, B. and Zhou, M.H. (2007b). "Effects of hydrothermal temperature and time on the photocatalytic activity and microstructures of bimodal mesoporous TiO_2 powders." *Appl. Catal.,* 69, 171–180.

Yu, J. G., Xiong, J. F., Cheng, B. and Liu, S.W. (2005). "Fabrication and characterization of Ag–TiO_2 multiphase nanocomposite thin films with enhanced photocatalytic activity." *Appl. Catal. B: Environ., 60*, 211–221.

Yu, J. G., Yu, H. G., Cheng, B., Zhao, X. J., Yu, J. C., Ho, W. K., Yu, J. G., Yu, H.G., Cheng, B., Zhao, X.J., Yu, J.C. and Ho, W.K. (2003). "The effect of calcination temperature on the surface microstructure and photocatalytic activity of TiO_2 thin films prepared by liquid phase deposition." *J. Phys. Chem. B,* 107, 13871–13879.

Yu, L., Lei, T., Ren, X., Pei, X. and Feng Y. (2008). "Response surface optimization of l-(+)-lactic acid production using corn steep liquor as an alternative nitrogen source by Lactobacillus rhamnosus CGMCC 1466." *Biochem. Eng. J.*, 39, 496–502.

Zainudin, N. F., Abdullah, A. Z. and Mohamed, A. R. (2008). "Development of Supported TiO$_2$ Photocatalyst Based Adsorbent For Photocatalytic Degradation Of Phenol." *Int. Conference on Environ., (ICENV 2008)*.

Zang, F., Zhao, J., Shen, T., Hidaka, H., Pelizzeti, H.E. and Serpone, N. (1998). "TiO$_2$- assisted photodegradation of dye pollutants. II. Adsorption and degradation kinetics of eosin in TiO$_2$ dispersions under visible light irradiation." *Appl. Catal. B: Environ.*, 15, 147–156.

Zeena, S. P. and Kamat, P.V. (2004). "What Factors Control the Size and Shape of Silver Nanoparticles in the Citrate Ion Reduction Method?." *J. Phys. Chem. B*, 108, 945-951.

Zhang Y and Reller A (2002). Phase transformation and grain growth of doped nanosized titania. *Mater. Sci. Eng.,* 19, 323-326.

Zhang, D., Song, X., Zhang, R., Zhang, M and Liu, F. (2005). "Preparation and Characterization of Ag@TiO$_2$ Core-Shell Nanoparticles in Water-in-Oil Emulsions." *Eur. J. Inorg. Chem.*, 1643–1648.

Zhang, F., Guan, N., Li, Y., Zhang, X., Chen, J. and Zeng, H. (2003). "Control of morphology of silver clusters coated on titanium dioxide during photocatalysis." *Langmuir*, 19, 8230–8234.

Zhang, F., Zhao, J., Shen, T., Hidaka, H., Pelizzetti, E. and Serpone, N. (1998). "TiO$_2$ assisted photodegradation of dye pollutants II. Adsorption and degradation kinetics of eosin in TiO$_2$ dispersions under visible light irradiation." *Appl.Catal. B: Environ.*, 15, 147-156.

Zhang, L., Xia, D. and Shen, Q. (2006). "Synthesis and characterization of Ag@TiO$_2$ core-shell nanoparticles and TiO$_2$ nanobubbles." *J. Nanopart. Res.*, 8, 23–28.

Zhang, L.C., Cai, K.F. and Yao, X. (2008). "Preparation, characterization and photocatalytic performance of Co/Ni Co-doped TiO$_2$ nanopowders." *J. Electroceram.*, 21, 512-515.

Zhao, J. and Yang, X. (2003). "Photocatalytic oxidation for indoor air purification: a literature review." *Build. Environ.*, 38645–38654.

APPENDICES

1 Preparation of dye stock solution

100 mg/L of AY-17 dye stock solution was prepared by dissolving 0.0166 g (purity 60%) of AY-17 in 100 mL of distilled water. 100 mg/L of RB-220 solution was prepared by dissolving 0.011g (90% pure) of RB-220 in 100 mL of distilled water.

1.1 Calibration of UV spectrophotometer for analysis AY-17 and RB-220 dyes in aqueous solutions

Standard solutions of the dyes in the range of 1 to 10 mg/L in increments of 1 mg/L were prepared by taking 1 to 10 mL of dye stock solution in increments of 1 mL in a 100 mL standard flask and making it up to the mark with distilled water. The standard solutions of the dyes were transferred to a glass cuvette and the absorbance was read against distilled water blank at 418 nm for AY-17 and at 609 nm for RB-220 using Hitachi UV-160A spectrophotometer. The values of absorbance and concentrations for AY-17 and RB-220 in standard solutions are presented in the Table 1.1. Figure 1.1a and Figure 1.1b presents the calibration graph for AY-17 and RB-220 dyes respectively. Linear equations for calibration are also presented in Figure 1.1a and Figure 1.1b.

Table 1.1 Calibration Table for AY-17 and RB-220.

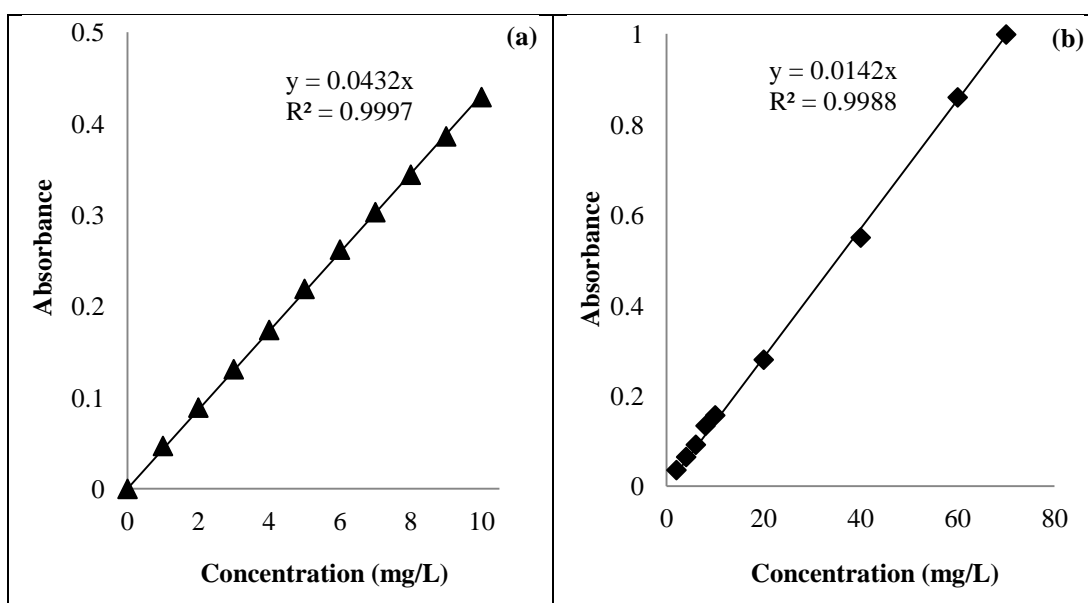| S. No.	Concentration of AY-17 (mg/L)	Absorbance	Concentration of RB-220 (mg/L)	Absorbance
0	0	0	2	0.036
1	1	0.047	4	0.065
2	2	0.089	6	0.092
3	3	0.131	8	0.0134
4	4	0.174	10	0.157
5	5	0.219	20	0.28
6	6	0.262	40	0.55
7	7	0.303	60	0.86
8	8	0.344	70	0.999
9	9	0.386	-	-
10	10	0.429	-	-

Figure 1.1 Calibration plot for a) AY-17 b) RB-220.

APPENDIX II

1 Calibration curve for estimation of nitrate in aqueous dye solutions

1.1 Preparation of nitrate stock solution

100 mg/L of potassium nitrate (KNO_3) stock solution was prepared by dissolving 0.07218 g of KNO_3 in 1000 mL of distilled water.

1.2 Calibration of UV spectrophotometer for nitrate estimation

Standard solutions of the nitrate in the range of 0.5 to 2 mg/L were prepared by taking 0.5 to 2 mL of nitrate stock solution in increments of 0.5 mL in a 100 mL standard flask and making it up to the mark with distilled water. The standard solutions of the nitrate were transferred to a quartz cuvette and the absorbance was read against distilled water containg 1 mL HCl at 220 nm using Hitachi UV-160A spectrophotometer. The value of absorbance and concentrations in standard solution is presented in the Table 1.1. Figure 1.1 presents the calibration graph and linear equations for calibration.

Table 1.1 Calibration Table for nitrate estimation.

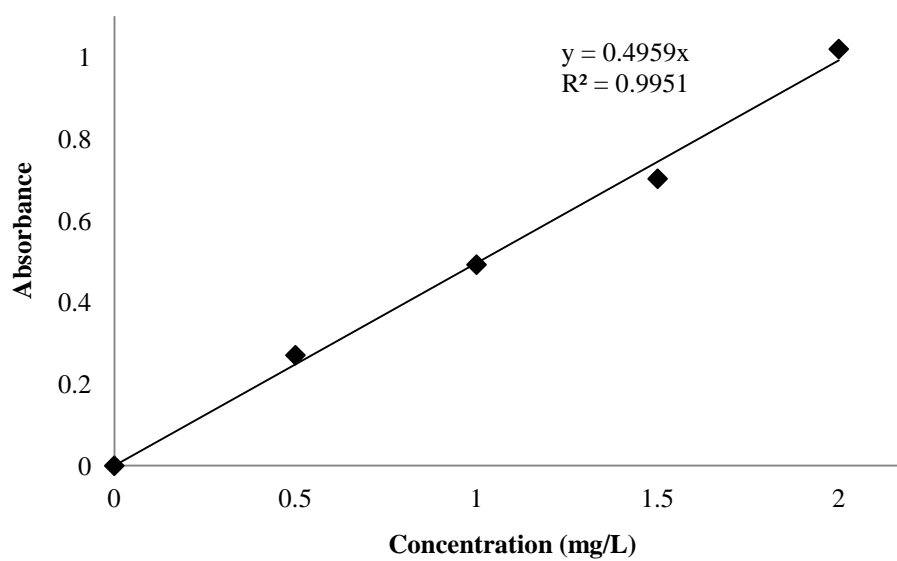| S. No.	Concentration of nitrate (mg/L)	Absorbance
0	0	0
1	0.5	0.2704
2	1	0.4919
3	1.5	0.7021
4	2	1.0194

$y = 0.4959x$
$R^2 = 0.9951$

Figure 1.1 Calibration plot for nitrate estimation.

APPENDIX III

1 Calibration curve for estimation of nitrite in aqueous dye solutions

1.1 Preparation of nitrite stock solution

100 mg/L of sodium nitrite ($NaNO_2$) stock solution was prepared by dissolving 54.3 mg of $NaNO_2$ in 100 mL of distilled water.

1.2 Calibration of UV spectrophotometer for nitrite estimation

Standard solutions of the nitrite in the range of 0.5 to 2 mg/L were prepared by taking 0.5 to 2 mL of nitrite stock solution in increments of 0.5 mL in a 100 mL standard flask and making it up to the mark with distilled water. In the standard solution, 1 mL of sulfanilamide was added and made upto mark. After 2-8 min, NEDA was added and mixed. The standard solutions of the nitrate were transferred to a quartz cuvette and the absorbance was read against distilled water containg sulfanilamide and NEDA at 540 nm using Hitachi UV-160A spectrophotometer. The value of absorbance and concentrations in standard solution is presented in the Table 1.1. Figure 1.1 presents the calibration graph and linear equations for calibration.

Table 1.1 Calibration Table for nitrite estimation.

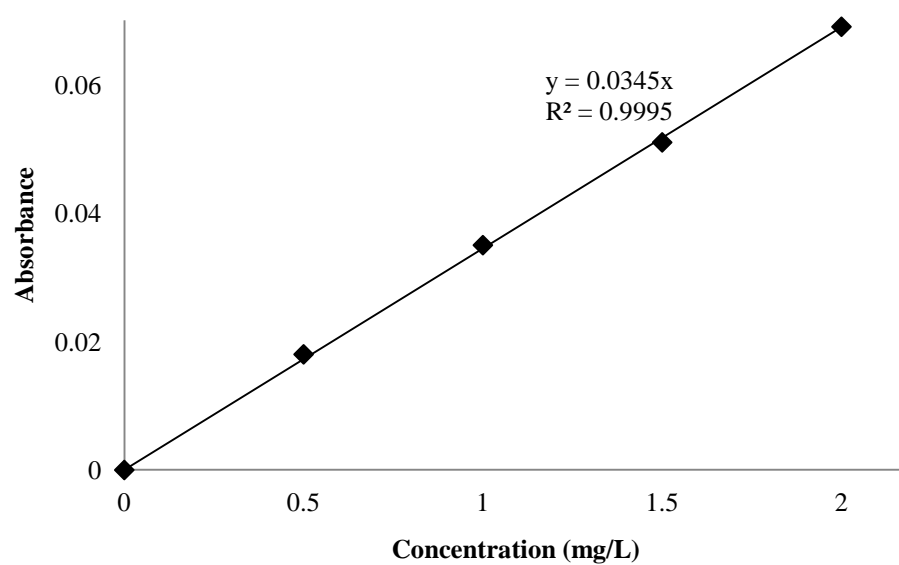| S. No.	Concentration of nitiite (mg/L)	Absorbance
0	0	0
1	0.5	0.018
2	1	0.035
3	1.5	0.051
4	2	0.069

Figure 1.1 Calibration plot for nitrite estimation.

APPENDIX IV

1 Calibration curve for estimation of sulphate in aqueous dye solutions

Preparation of sulphate stock solution

100 mg/L of anhydrous sodium sulphate (Na_2SO_4) stock solution was prepared by dissolving 0.1479 mg of Na_2SO_4 in 100 mL of distilled water.

1.2 Prepartation of conditioning agent

Conditiong agent was preoared by dissolving 75 g of NaCl, 30 mL of HCl and 100 mL 95% of ethyl alcohol in 300 mL of idtilled water. Then 50 mL of glycerol was added to the above solution and mixed well.

1.3 Calibration of UV spectrophotometer for sulphate estimation

Standard solutions of the sulphate in the range of 5 to 20 mg/L were prepared by taking 5 to 20 mL of sulphate stock solution in increments of 5 mL in a 100 mL standard. In the standard solution, 10 mL of conditioning agent was added and made upto mark. 10 mL of 10 % $BaCl_2$ was added to above solution and mixed. The standard solutions of the sulpahte were transferred to a quartz cuvette and the absorbance was read against distilled water containg conditioning agent and $BaCl_2$ at 420 nm using Hitachi UV-160A spectrophotometer. The value of absorbance and concentrations in standard solution is presented in the Table 1.1. Figure 1.1 presents the calibration graph and linear equations for calibration.

Table 1.1 Calibration Table for sulphate estimation.

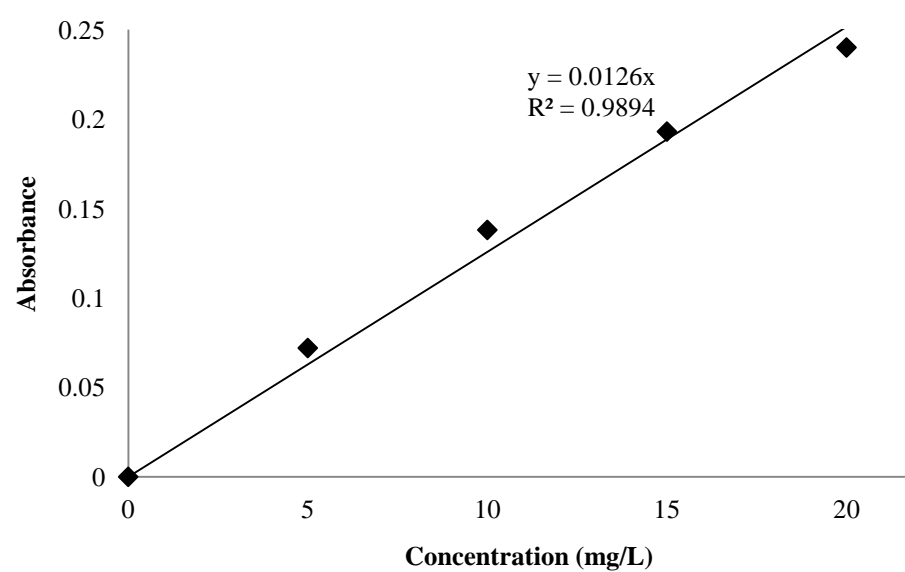| S. No.	Concentration of sulphate (mg/L)	Absorbance
0	0	0
1	5	0.072
2	10	0.138
3	15	0.193
4	20	0.24

Figure 1.1 Calibration plot for sulphate estimation.

APPENDIX V

Calibration curve for analysis of mixture of dyes (AY-17 and RB-220) solution

1 Preparation of dyes stock solution

100 mg/L of AY-17 dye stock solution was prepared by dissolving 0.0166 g (purity 60%) of AY-17 in 100 mL of distilled water. 100 mg/L of RB-220 solution was prepared by dissolving 0.011g (90% pure) of RB-220 in 100 mL of distilled water.

1.1 Calibration of UV spectrophotometer for analysis AY-17 and RB-220 dyes in aqueous solutions

Standard solutions of the dyes in the range of 1 to 10 mg/L in increments of 1 mg/L were prepared by taking 1 to 10 mL of dye stock solution in increments of 1 mL in a 100 mL standard flask and making it up to the mark with distilled water. The standard solutions of the dyes were transferred to a glass cuvette and the absorbance was read against distilled water blank at 418 nm for AY-17 and at 609 nm for RB-220 using Hitachi UV-160A spectrophotometer. The values of absorbance and concentrations for AY-17 and RB-220 in standard solutions are presented in the Table 1.1. Figure 1.1 presents the calibration graph for AY-17 and RB-220 dye. Linear equations for calibration are also presented in Figure 1.1.

Table 1.1 Calibration Table for mixture of dyes (AY-17 and RB-220).

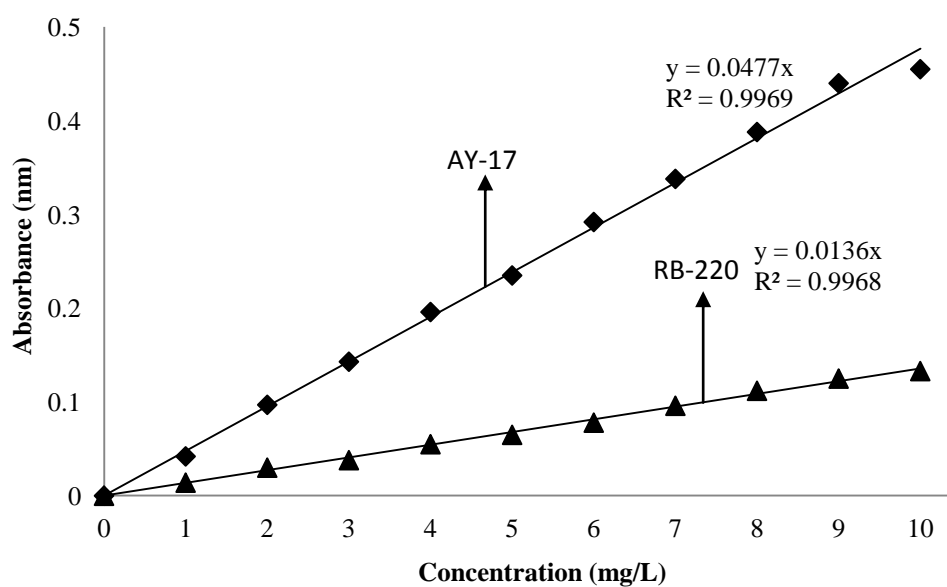| S. No.	Concentration	Absorbance	Absorbance
0	0	0	0
1	1	0.042	0.014
2	2	0.097	0.03
3	3	0.143	0.038
4	4	0.196	0.055
5	5	0.235	0.065
6	6	0.292	0.078
7	7	0.338	0.096
8	8	0.388	0.112
9	9	0.44	0.125
10	10	0.455	0.133

Figure 1.1 Calibration plot for mixture of dyes (AY-17 and RB-220).

APPENDIX VI

Calibration curve for Hazen colour analysis

The values of absorbance and Hazen colour in standard solutions are presented in the Table 1.1. Figure 1.1 presents the calibration graph for Hzaen colour analysis. Linear equations for calibration are also presented in Figure 1.1.

Table 1.1 Calibration Table for Hazen colour analysis.

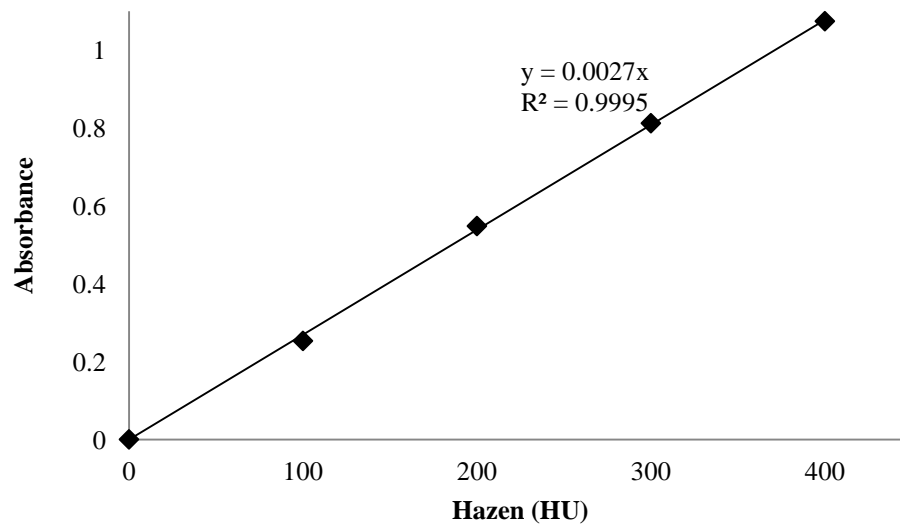| S. No.	Hazen (HU)	Absorbance
0	0	0
1	100	0.253
2	200	0.548
3	300	0.812
4	400	1.074

$y = 0.0027x$
$R^2 = 0.9995$

Figure 1.1 Calibration plot for Hazen colour analysis.

The mass spectra of formed intermediates

To propose the reaction pathway of degradation of AY-17 and RB-220 dyes, samples collected after every 15 min were sent to IISc, Bangalore for LC-MS analysis. The mass spectra of intermediates formed are presented in Figure 1.1 to 1.6 for AY-17 and Figure 1.7 to 1.12 for RB-220 dye respectively.
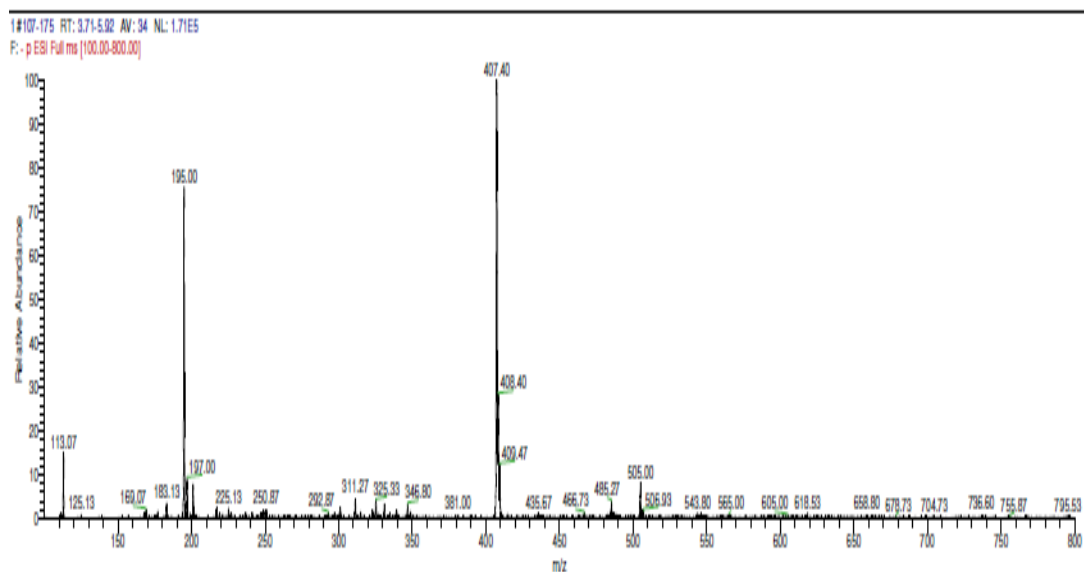

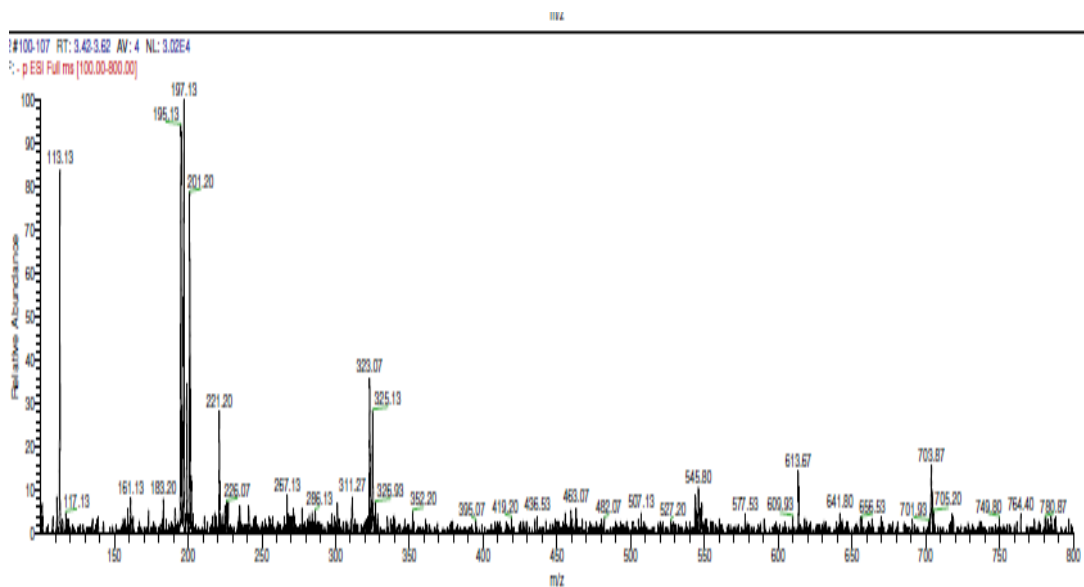**Figure 1.1 Mass spectrum of AY-17 after 15 min of solar irradiation.**

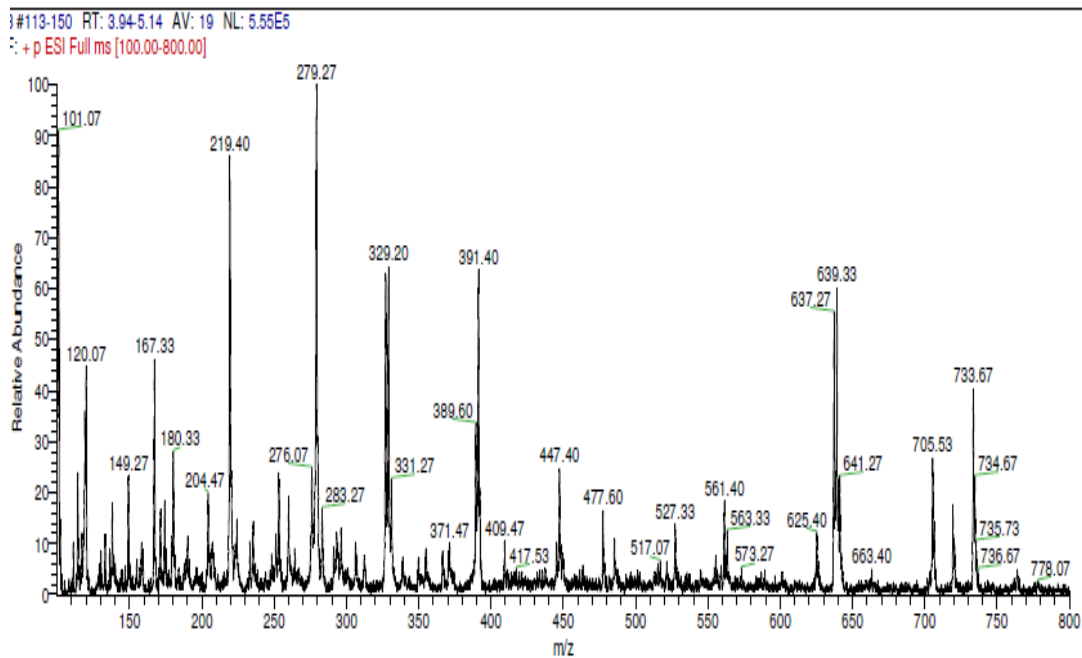**Figure 1.2 Mass spectrum of AY-17 after 30 min of solar irradiation.**

Figure 1.3 Mass spectrum of AY-17 after 45 min of solar irradiation.

Figure 1.4 Mass spectrum of AY-17 after 60 min of solar irradiation.

5 #256-287 RT: 8.55-9.55 AV: 16 NL: 7.38E6
F: + p ESI Full ms [100.00-800.00]

Figure 1.5 Mass spectrum of AY-17 after 90 min of solar irradiation.

6 #141-148 RT: 4.84-5.04 AV: 4 NL: 3.40E6
F: + p ESI Full ms [100.00-800.00]

Figure 1.6 Mass spectrum of AY-17 after 120 min of solar irradiation.

Figure 1.7 Mass spectrum of RB-220 after 15 min of solar irradiation.

Figure 1.8 Mass spectrum of RB-220 after 30 min of solar irradiation.

Figure 1.9 Mass spectrum of RB-220 after 45 min of solar irradiation.

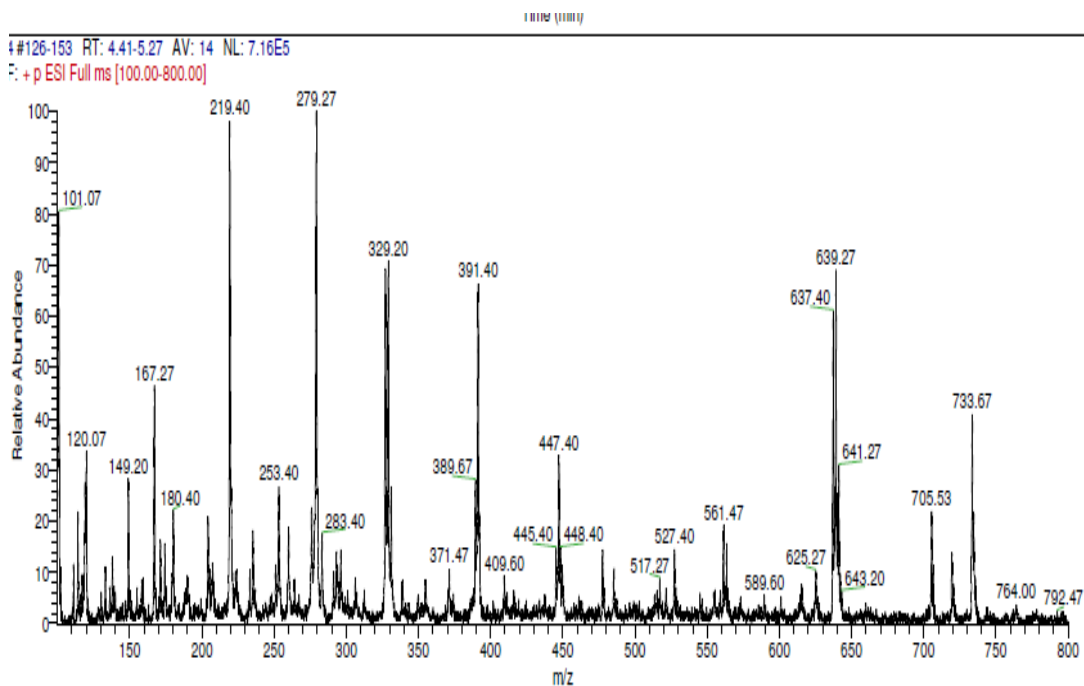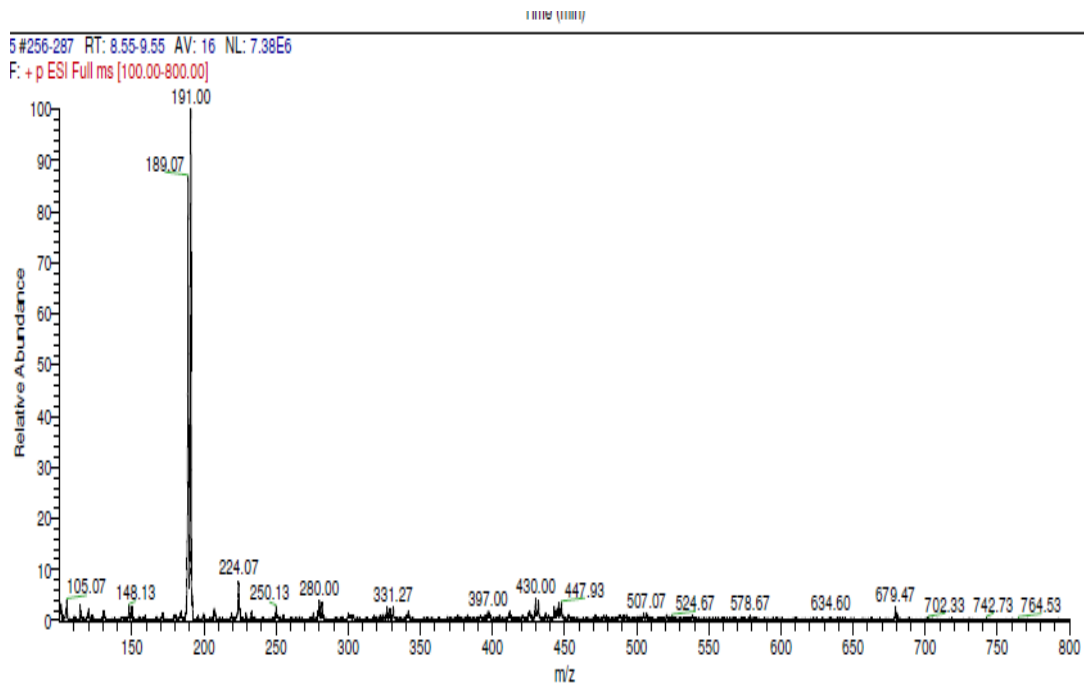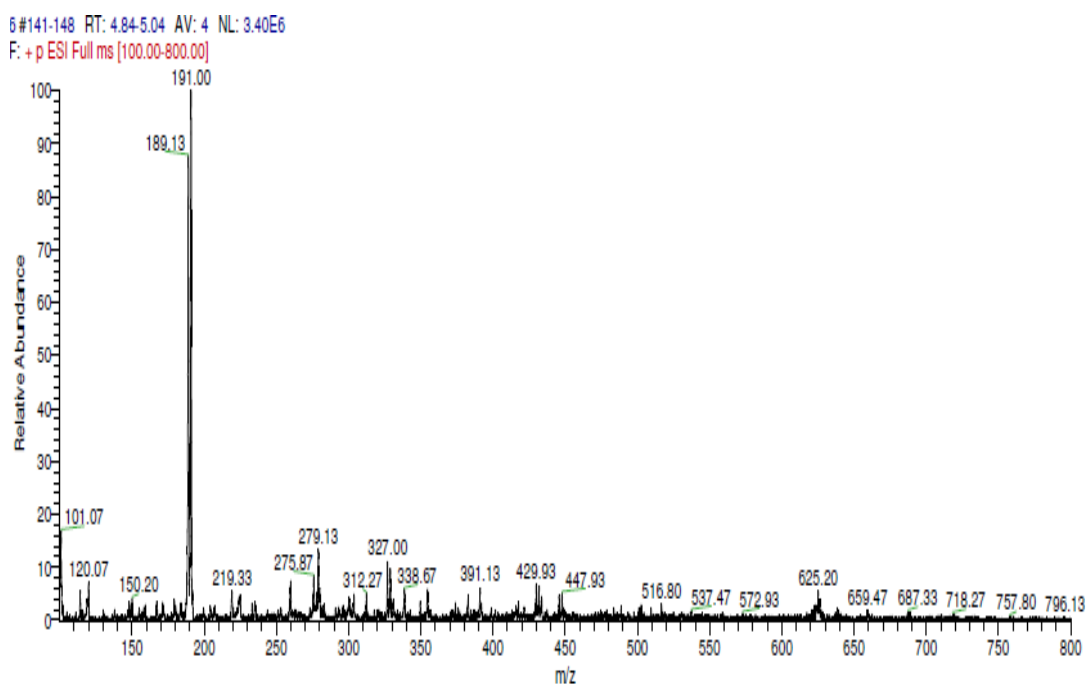**Figure 1.10 Mass spectrum of RB-220 after 60 min of solar irradiation.**

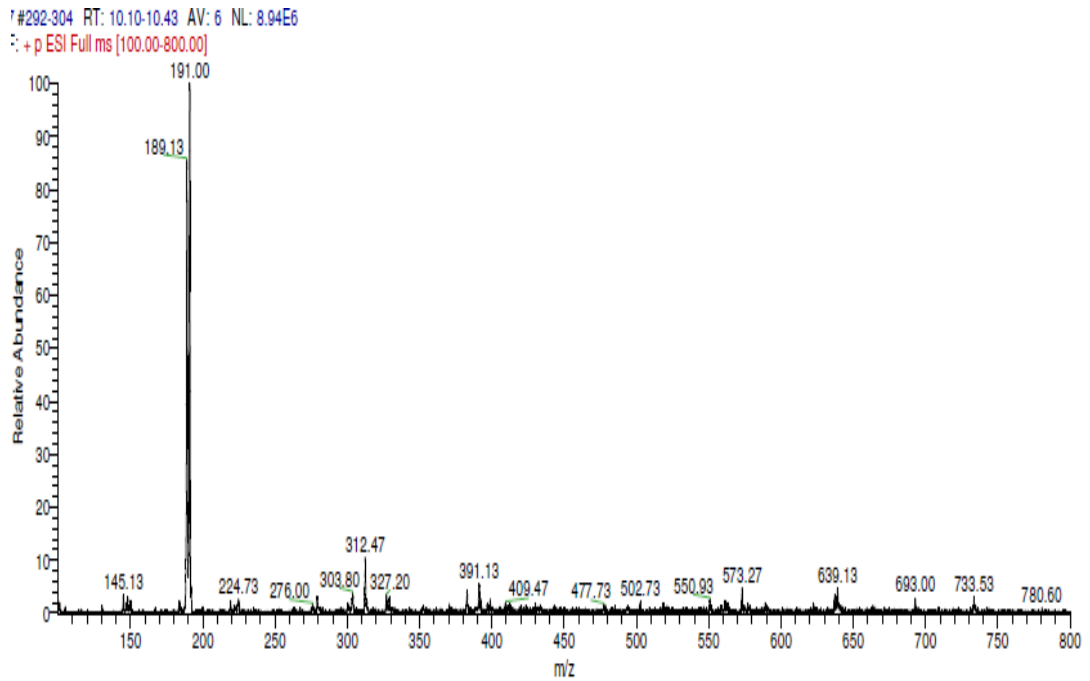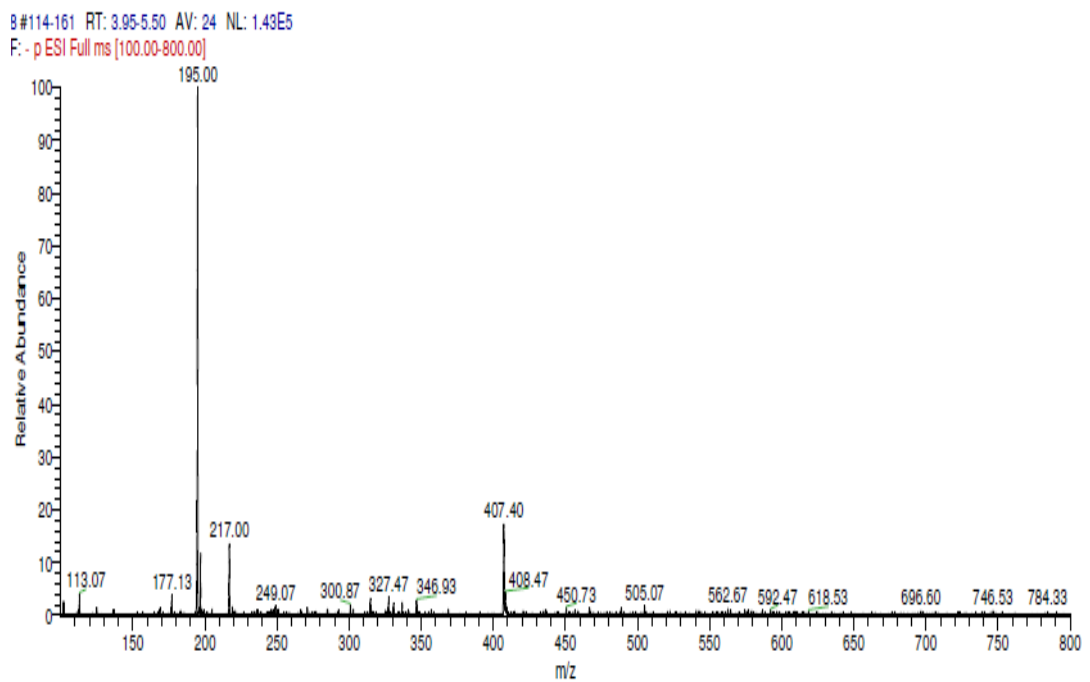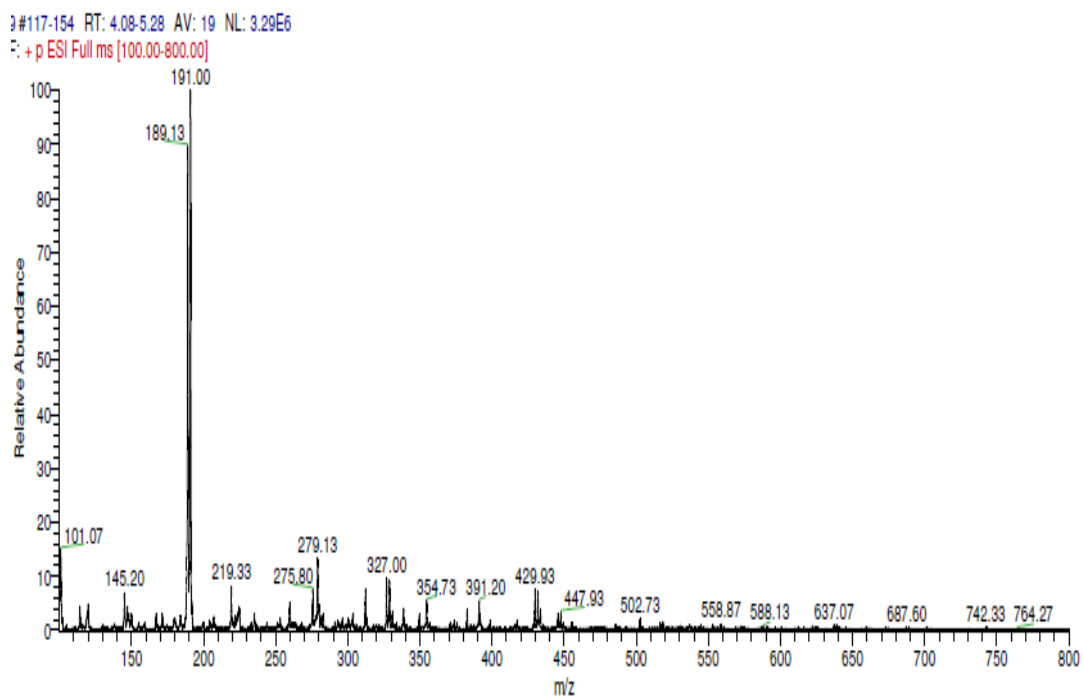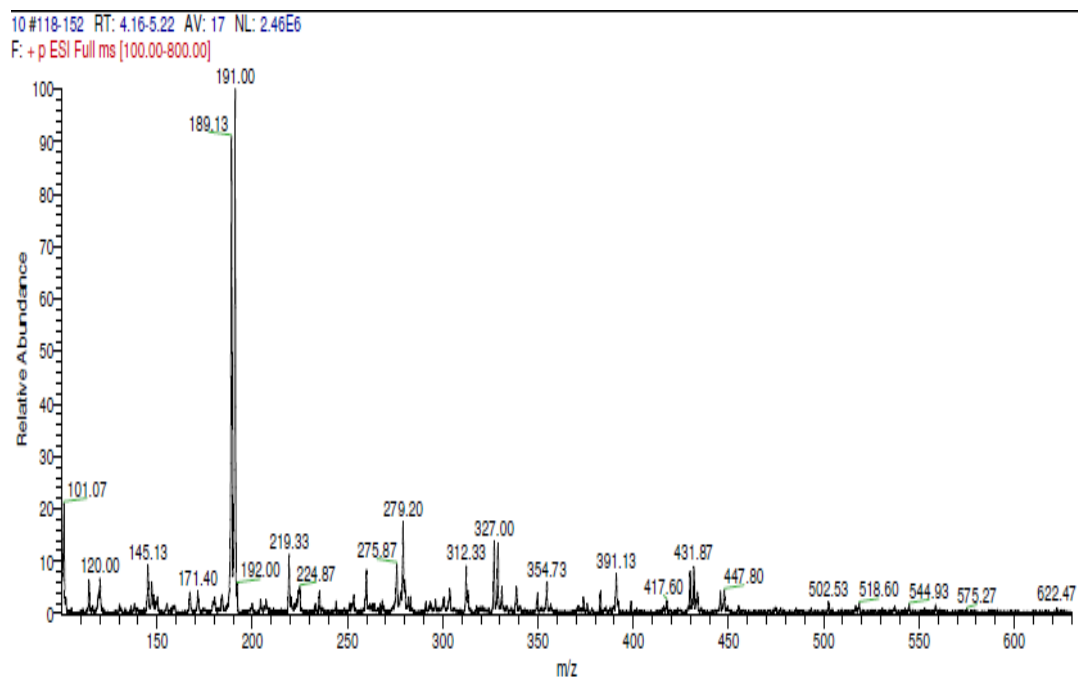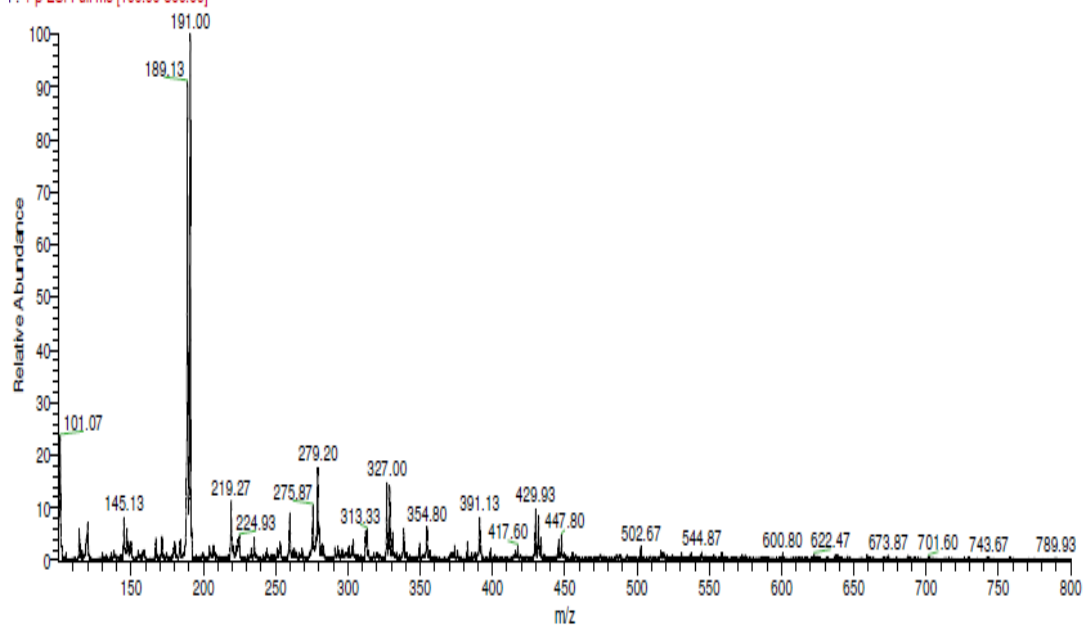**Figure 1.11 Mass spectrum of RB-220 after 90 min of solar irradiation.**

Figure 1.12 Mass spectrum of RB-220 after 120 min of solar irradiation.

PAPERS BASED ON THIS RESEARCH WORK

PAPERS IN PEER REVIEWED INTERNATIONAL JOURNALS
Published

1. Khanna, A., Shetty, V.K., (2013) **"Solar photocatalysis for treatment of Acid Yellow-17 (AY-17) dye contaminated water using Ag@TiO₂ core–shell structured nanoparticles**" *Environmental Science and Pollution Research.* 20, 5692–5707. (Springer) [**IF:2.651**]

2. Khanna, A., Shetty, V.K., (2014) **"Solar Light Induced Photocatalytic Degradation of Reactive Blue 220 (RB-220) Dye with Highly Efficient Ag@TiO₂ Core-Shell Nanoparticles: A Comparison with UV Photocatalysis"** *Solar Energy.* 99, 67-76 (Elsevier) [**IF: 2.952**]

3. Khanna, A., Shetty, V.K., (2014) **"Solar light driven photocatalytic degradation of Anthraquinone dye contaminated water by engineered Ag@TiO₂ core–shell nanoparticles"** *Desalination and Water Treatment.* 2014, 1-14 *(Taylor and Francis)* [**IF: 0.852**]

RESEARCH PAPERS IN INTERNATIONAL CONFERENCES

1. Khanna, A., Shetty, V.K., (2012) **"Photocatalytic application of Ag@TiO₂ core-shell nanoparticles for dye degradation under solar light"** Proceedings of the Second International Conference on Nanomaterials: Synthesis, Characterization and Applications (ICN-2012), Mahatma Gandhi University, Kottayam, 12-15th January 2012, pp. 22. The paper was awarded with **The Best Paper Award.**
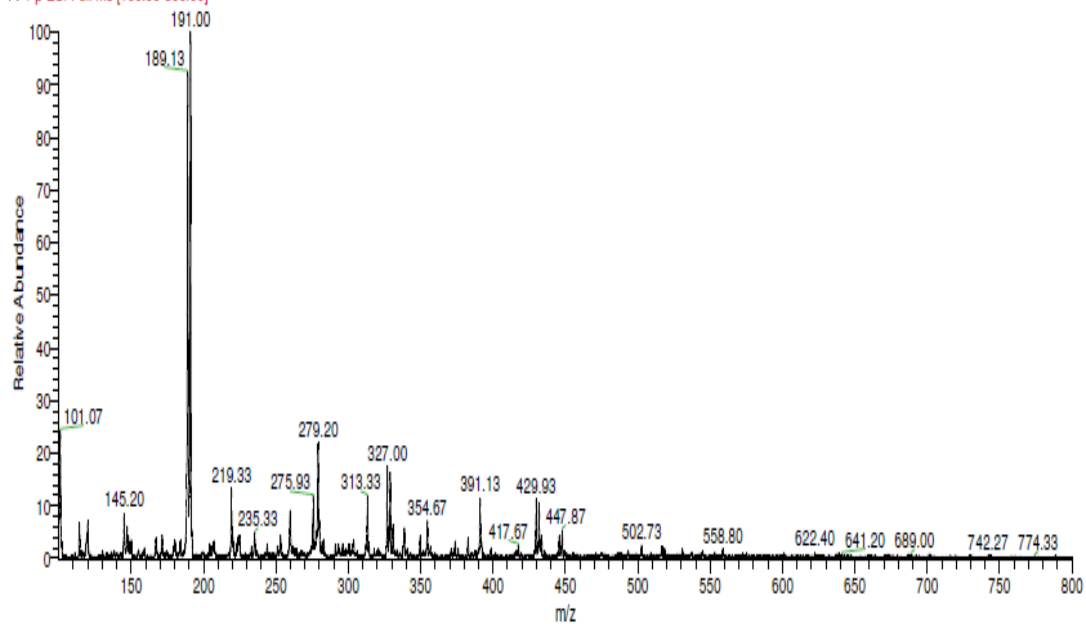
2. Khanna, A., Shetty, V.K., (2012) **"Efficacy of Ag@TiO₂ Core -Shell Structured Nanocatalysts for the Photocatalytic Degradation of Reactive Blue 220 dye under UV Light Irradiation"** Proceedings of the First International Conference on Functional materials for Defense (ICFMD-2012), Defense Institute of Advanced Technology, Pune, 17-19th May 2012, pp. 139.

3. Khanna, A., Shetty, V.K., (2013) **"Effect of Calcination Conditions on the Solar Photocatalytic Efficacy of Ag@TiO₂ for the degradation of an Azo Dye"** Proceedings of First International Conference on Water Desalination, Treatment and Management (InDACON-2013), Malaviya National Institute of

Technology Jaipur, India, 21-22nd February 2013, pp. 1-6. The paper was awarded with **The Best Paper Award.**

4. Khanna, A., Shetty, V.K., (2013) **"Solar Applicability of Ag@TiO$_2$ Core–Shell Nanoparticles for Photocatalytic Degradation of an Anthraquinone Dye (Acid Blue-129)"** Proceedings of Fourth International Conference on Advancements in Polymeric Materials (APM-2013), Central Institute of Plastics Engineering and Technology Lucknow, India, 1-3rd March 2013, pp. 261.

RESEARCH PAPERS IN NATIONAL CONFERENCES

1. Khanna, A., Shetty, V.K., (2011) **"Effect of molar ratio & Calcination temperature on the photocatalytic degradation of azo dye using Ag@TiO$_2$ core-shell nanoparticles under UV light"** Proceedings of the Indo-UK Workshop-2011 on Current Advances in water and waste water treatment, National Institute of Technology Trichy, 29-31st August 2011.

2. Khanna, A., Shetty, V.K., (2011) **"Effect of composition, calcination temperature & time on the photocatalytic degradation of azo dye using Ag@TiO$_2$ core-shell nanoparticles under sunlight"** National Conference on Current Advances in water and waste water treatment, MVJ College of Engineering, Bangalore, 7-8th September 2011, pp. 21 and won **"Third prize"**.

3. Khanna, A., Shetty, V.K., (2011) **"Efficacy of Ag@TiO$_2$ core-shell structured Nanocatalysts for the photocatalytic degradation of Acid Yellow-17 under UV light irradiation"** CHEMCON-2011, M.S. Ramaiah Institute of Technology, Bangalore, 27-29th December 2011, pp. 441-442.

4. Khanna, A., Shetty, V.K., (2012) **"Solar photocatalytic efficacy of Ag@TiO$_2$ core-shell nanoparticles for the degradation of dye"** Chemference-2012, Indian Institute of Technology, Bombay and Institute of Chemical Technology, Mumbai, India, 10-11th December 2012, pp. 25.

BIODATA

ANKITA KHANNA

Email ID: ankitakhanna1987@gmail.com

Contact no: +91-9945842765

Personal details:

Name	: Ankita Khanna
Father's name	: Suresh Khanna
Date of birth	: 01 October 1987
Marital status	: Single
Gender	: Female
Nationality	: Indian
Permanent address	: Ankita Khanna, C/O Suresh Khanna, # 177, Ward No. 1, Power House Road Saproon District –Solan, Himachal Pradesh– 173211

Educational qualification:

Ph.D., Department of Chemical Engineering, NITK, Surathkal, Mangalore, Karnataka (2009 Onward).

Academic background:

COURSE	INSTITUTION	BOARD	MARKS OBTAINED	YEAR OF PASSING
Ph. D. (Chemical Engineering)	National Institute of Technology Karnataka, Surathkal (NITK)	National Institute of Technology Karnataka, Surathkal (NITK)	7.67 CGPA	2014
M.Sc. (Industrial Chemistry)	University Institute of Chemical Engineering (UICET), PU Chandigarh	Panjab University (PU), Chandigarh	74.59 %	2009
B.Sc. (Industrial Chemistry)	GGDSD College, Chandigarh	Panjab University (PU), Chandigarh	71.75 %	2007
XII (H.S.C)	GGSS School, Solan	Himachal Pradesh School Education Board (HPSEB), Dharamshala	68.6 %	2004
X (Matric.)	GGSS School, Solan	Himachal Pradesh School Education Board (HPSEB), Dharamshala	75.57 %	2002

Projects Executed:

1) **Preparation and Characterization of Starch/Clay Bio nanocomposites by solvent casting method.**

   S. S. Bhatnagar University Institute of Chemical Engineering (UICET), Chandigarh, 2007-2009.

2) **Photocatalytic degradation of azo dyes using Ag@TiO$_2$ core shell structured nanoparticles.**

   National Institute of Technology Karnataka, Surathkal (NITK) 2009-2014.

PAPER IN PEER REVIEWED INTERNATIONAL JOURNALS

Published

1) Khanna, A., Shetty, V.K., (2013) **"Solar photocatalysis for treatment of Acid Yellow-17 (AY-17) dye contaminated water using Ag@TiO$_2$ core–shell structured nanoparticles***"* *Environmental Science and Pollution Research.* 20, 5692–5707. (Springer) [**IF: 2.651**]

2) Khanna, A., Shetty, V.K., (2014) **"Solar Light Induced Photocatalytic Degradation of Reactive Blue 220 (RB-220) Dye with Highly Efficient** Ag@TiO$_2$ **Core-Shell Nanoparticles: A Comparison with UV Photocatalysis"** *Solar Energy.* 99, 67-76 (Elsevier) [**IF: 2.952**]**.**

3) Khanna, A., Shetty, V.K., (2014) **"Solar light driven photocatalytic degradation of Anthraquinone dye contaminated water by engineered Ag@TiO$_2$ core–shell nanoparticles"** *Desalination and Water Treatment. 2014, 1-14. (Taylor and Francis)* [**IF: 0.852**]**.**

RESEARCH PAPERS IN INTERNATIONAL CONFERENCES

1. Khanna, A., Shetty, V.K., (2012) **"Photocatalytic application of Ag@TiO$_2$ core-shell nanoparticles for dye degradation under solar light"** Proceedings of the Second International Conference on Nanomaterials: Synthesis, Characterization and Applications (ICN-2012), Mahatma Gandhi University, Kottayam, 12-15th January 2012, pp. 22. The paper was awarded with **The Best Paper Award.**

2. Khanna, A., Shetty, V.K., (2012) **"Efficacy of Ag@TiO$_2$ Core -Shell Structured Nanocatalysts for the Photocatalytic Degradation of Reactive Blue 220 dye under UV Light Irradiation"** Proceedings of the First International Conference on Functional materials for Defense (ICFMD-2012), Defense Institute of Advanced Technology, Pune, 17-19th May 2012, pp. 139.

3. Khanna, A., Shetty, V.K., (2013) **"Effect of Calcination Conditions on the Solar Photocatalytic Efficacy of Ag@TiO$_2$ for the degradation of an Azo Dye"** Proceedings of First International Conference on Water Desalination, Treatment and Management (InDACON-2013), Malaviya National Institute of Technology Jaipur, India, 21-22nd February 2013, pp. 1-6. The paper was awarded with **The Best Paper Award.**

4. Khanna, A., Shetty, V.K., (2013) **"Solar Applicability of Ag@TiO$_2$ Core–Shell Nanoparticles for Photocatalytic Degradation of an Anthraquinone Dye (Acid Blue-129)"** Proceedings of Fourth International Conference on Advancements in Polymeric Materials (APM-2013), Central Institute of Plastics Engineering and Technology Lucknow, India, 1-3rd March 2013, pp. 1-3.

RESEARCH PAPERS IN NATIONAL CONFERENCES

1. Khanna, A., Shetty, V.K., (2011) **"Effect of molar ratio & Calcination temperature on the photocatalytic degradation of azo dye using Ag@TiO$_2$ core-shell nanoparticles under UV light"** Proceedings of the Indo-UK Workshop-2011 on Current Advances in water and waste water treatment, National Institute of Technology Trichy, 29-31st August 2011.

2. Khanna, A., Shetty, V.K., (2011) **"Effect of composition, calcination temperature & time on the photocatalytic degradation of azo dye using Ag@TiO$_2$ core-shell nanoparticles under sunlight"** National Conference on Current Advances in water and waste water treatment, MVJ College of Engineering, Bangalore, 7-8th September 2011, pp. 21 and won **"Third prize"**.

3. Khanna, A., Shetty, V.K., (2011) **"Efficacy of Ag@TiO$_2$ core-shell structured Nanocatalysts for the photocatalytic degradation of Acid Yellow-17 under UV light irradiation"** CHEMCON-2011, M.S. Ramaiah Institute of Technology, Bangalore, 27-29th December 2011, pp. 441-442.

4. Khanna, A., Shetty, V.K., (2012) **"Solar photocatalytic efficacy of Ag@TiO₂ core-shell nanoparticles for the degradation of dye"** Chemference-2012, conducted by Indian Institute of Technology, Bombay and Institute of chemical Technology, Mumbai, India, 10-11th December 2012, pp. 25.

5. Khanna, A., Sharma A., (2009) **"Preparation and Characterization of Starch/Clay Bio nanocomposites by solvent casting method"** 24th Indian Engineering Congress, conducted by National Institute of Technology, Karnataka, India, 11-13th December 2009, pp.41.

6. Khanna, A., Sharma A., (2009) "**Thermoplastic Starch-Clay Nanocomposites prepared by High Shear Homogenizer with improved Barrier Properties**" Polymer Congress 'APA-2009' Polymer Science and Technology: Vision and Scenario, conducted by Indian Institute of Technology, Delhi, India, 17-20th December 2009, pp.422.

Technical Skills:

- Having hands on experience in synthesis of nanomaterials like $Ag@TiO_2$, TiO_2 nanoparticles using different methods and nanocomposites like starch-clay nanocomposites.

- Characterization of nanomaterials.

- Design of experiments like central composite design (CCD), Box–Behnken design and Doehlert design.

- Proficient in handling equipments and instruments like Centrifuges, Sonicator, UV-Vis spectrophotometer, pH meter, DO meter, light intensity meter, muffle furnace, high shear mixer, Thermogravmetric analysis (TG-DTA), Total organic carbon analyzer.

- Proficient in analysis of pollutant like dyes, phenols, heavy metal, organic pollutant, COD, BOD, TOC, Hazen unit etc.

Computer Expertise:

Microsoft office, Origin, Minitab, Design expert, and Chem draw.

Achievements:

- ✓ Secured 3rd position in State Science Model Competition at state level in 10th.
- ✓ Secured 96th position in 10th (Matriculation).
- ✓ Secured 2nd position in B.Sc. (III) in Industrial Chemistry.

Extra Curricular Activities:

- ✓ I have been the School pupil leader.
- ✓ I served as a volunteer in many functions organized at NITK.

Training:

- ✓ Undergone 4 weeks summer training in Mohan Meakin Ltd during summer vacation of B.Sc. (I) year at Brewery, Distt- Solan.
- ✓ Undergone 4 weeks summer training in JM Remedies during summer vacation of B.Sc. (II) year at Solan.
- ✓ Undergone 6 weeks summer training in HPMC during summer vacation of M.Sc. (I) year at Jabli, Distt-Solan.

Declaration:

I hereby declare that the above written particulars are true to the best of my knowledge and I bear the responsibility for the correctness of the above-mentioned particulars.

Place: Surathkal, India   **ANKITA KHANNA**

Date: